Epigenetic control of the ovarian transcriptome in Drosophila melanogaster

Daniela Torres Campana

N°d'ordre NNT :2021LYSE1176

THESE de DOCTORAT DE L'UNIVERSITE DE LYON
opérée au sein de
l'Université Claude Bernard Lyon 1

Ecole Doctorale N° 340
Biologie Moléculaire, Intégrative et Cellulaire

Spécialité de doctorat : Biologie moléculaire et cellulaire
Discipline : Épigénétique

Soutenue publiquement le 28/09/2021, par :
Daniela TORRES CAMPANA

Contrôle épigénétique du transcriptome ovarien chez *Drosophila melanogaster*

Devant le jury composé de :

VIEIRA-HEDDI, Cristina Professeure des Universités, Université Lyon 1, Lyon	Présidente
DI STEFANO, Luisa, Chargée de recherche CNRS, Centre de Biologie Intégrative, Toulouse	Rapporteure
MARTINEZ, Anne-Marie, Professeure des Universités, Université de Montpellier, Montpellier	Rapporteure
DOSTATNI, Nathalie, Professeure des Universités, Sorbonne Université, Paris	Examinatrice
LOPPIN Benjamin, Directeur de Recherche CNRS, Laboratoire de Biologie et Modélisation de la Cellule, Lyon	Directeur de thèse
ORSI Guillermo, Chargé de recherche, INSERM Laboratoire de Biologie et Modélisation de la Cellule, Lyon	Co-directeur de thèse

Université Claude Bernard – LYON 1

Président de l'Université	M. Frédéric FLEURY
Président du Conseil Académique	M. Hamda BEN HADID
Vice-Président du Conseil d'Administration	M. Didier REVEL
Vice-Président du Conseil des Etudes et de la Vie Universitaire	M. Philippe CHEVALLIER
Vice-Président de la Commission de Recherche	M. Petru MIRONESCU
Directeur Général des Services	M. Pierre ROLLAND

COMPOSANTES SANTE

Département de Formation et Centre de Recherche en Biologie Humaine	Directrice : Mme Anne-Marie SCHOTT
Faculté d'Odontologie	Doyenne : Mme Dominique SEUX
Faculté de Médecine et Maïeutique Lyon Sud - Charles Mérieux	Doyenne : Mme Carole BURILLON
Faculté de Médecine Lyon-Est	Doyen : M. Gilles RODE
Institut des Sciences et Techniques de la Réadaptation (ISTR)	Directeur : M. Xavier PERROT
Institut des Sciences Pharmaceutiques et Biologiques (ISBP)	Directrice : Mme Christine VINCIGUERRA

COMPOSANTES & DEPARTEMENTS DE SCIENCES & TECHNOLOGIE

Département Génie Electrique et des Procédés (GEP)	Directrice : Mme Rosaria FERRIGNO
Département Informatique	Directeur : M. Behzad SHARIAT
Département Mécanique	Directeur M. Marc BUFFAT
Ecole Supérieure de Chimie, Physique, Electronique (CPE Lyon)	Directeur : Gérard PIGNAULT
Institut de Science Financière et d'Assurances (ISFA)	Directeur : M. Nicolas LEBOISNE
Institut National du Professorat et de l'Education	Administrateur Provisoire : M. Pierre CHAREYRON
Institut Universitaire de Technologie de Lyon 1	Directeur : M. Christophe VITON
Observatoire de Lyon	Directrice : Mme Isabelle DANIEL
Polytechnique Lyon	Directeur : Emmanuel PERRIN
UFR Biosciences	Administratrice provisoire : Mme Kathrin GIESELER
UFR des Sciences et Techniques des Activités Physiques et Sportives (STAPS)	Directeur : M. Yannick VANPOULLE
UFR Faculté des Sciences	Directeur : M. Bruno ANDRIOLETTI

Remerciements

Après une explosion, un déménagement et une pandémie, elle est là cette thèse et je tiens à remercier les personnes qui ont fait ça possible.

Tout d'abord je veux remercier mon directeur, Benjamin Loppin, de m'avoir ouvert les portes de l'équipe Épigénétique et Formation du Zygote pour la réalisation de ma thèse. Je le remercie de m'avoir proposé un projet si intéressant qui m'a passionné du début à la fin.

Ensuite, je tiens à remercier mon co-directeur, Guille. (El gracias se queda corto para todo lo que hiciste por mí durante estos años). Merci pour ton encadrement de qualité, ton soutien, ta patience, ta pédagogie et ta bonne humeur. Ce fût une expérience très enrichissante d'avoir travaillé à tes côtés. Je te souhaite le meilleur pour le #OrsiLab.

Je veux également remercier Béa qui, pour l'anecdote, fût la première personne à m'avoir parlé d'épigénétique quand j'étais une jeune étudiante en première année de licence. Merci pour ton accompagnement, tes conseils et ton aide au cours de ces années. Merci également à Raphaëlle d'avoir pris le temps de répondre à mes questions, d'avoir passé mes commandes etc. Enfin, merci à vous deux de m'avoir intégré dans cette belle équipe.

Je remercie également les anciens membres de l'équipe. Plus particulièrement Daniel qui est arrivé au bon moment pour m'aider à démarrer cette aventure qu'est la thèse et qui s'est converti en un grand ami. Merci aussi à Fabiola, qui a rajouté une dose de bonne humeur aux journées au labo. J'ai mangé des bons burgers avec cette Latino Team mais j'ai surtout vécu des moments inoubliables avec vous.

Mes chers collègues du M4 RdC, merci d'avoir créé une super ambiance au labo. Je parle, en partie, des gens qui sont venus envahir mon bureau, Marion, Jérôme, Agnès, mais avec qui, malgré la pandémie, j'ai partagé de très bons moments. Merci Jérôme pour avoir égayé les longues journées au labo et pour les nombreuses conversations pouvant aller du fruit préféré jusqu'aux questions les plus philosophiques. Merci Marion, déjà, pour avoir été notre guide LBMC et surtout pour lâcher des phrases mythiques que je ne retranscrirais pas. Merci Victor pour ton soutien et ta patience surtout pendant la rédaction de ce manuscrit.

Quiero por supuesto agradecer a mi familia y amigos quienes, de cerca o de lejos, siempre me han brindado su apoyo.

Agradezco a mis padres por su incondicional apoyo, por enseñarme a perseguir mis sueños y por no dejar que un océano les impida estar siempre a mi lado.

Finalmente, quiero agradecer a la persona que ha estado siempre a mi lado apoyándome, aguantándome, consolándome, ayudándome y un sinnúmero mas de cosas: mi hermana. Gracias por ser mi hogar durante todos estos años y por demostrarme lo que es la valentía.

La thèse, comme la transcription, est un processus complexe, nécessitant de plusieurs étapes et acteurs et rencontrant souvent des obstacles à contourner. Néanmoins ça reste une période riche en créations et en rencontres. Pour moi, la thèse, fût non seulement une période d'intense apprentissage scientifique mais également de croissance personnelle qui m'a laissé beaucoup de leçons. C'est une période qui nous met à l'épreuve et qui n'est pas simple mais qu'avec les bonnes personnes (mentionnées ci-dessus) peut devenir une expérience épanouissante comme elle le fût pour moi.

¡ Gracias totales!

To my sister,
It got better.

« La curiosité est nécessaire à la nature humaine, sans elle, on croupirait dans l'ignorance » -Le Taureau Blanc, Voltaire

Résumé :

La régulation dynamique de l'épigenome est à la base de la plasticité cellulaire et permet aux cellules de répondre aux programmes développementaux et de différenciation. Les effecteurs épigénomiques entraînent des changements tels que la modification des queues des histones, le positionnement des histones ou l'incorporation de variants d'histones, ce qui impacte la structure de la chromatine et donc l'expression génique. Cependant, les mécanismes moléculaires sous-jacents restent, en grande partie, inconnus. Un défi majeur du domaine est l'établissement de liens fonctionnels directs entre modificateurs épigénétiques, qui ont tendance à avoir un effet global sur le génome, et expression de gènes effecteurs.

Mon projet de thèse s'est justement basé sur la découverte d'une connexion fonctionnelle entre une série d'effecteurs épigénomiques et un effecteur de la formation du zygote chez *Drosophila melanogaster* : la thiorédoxine maternelle Deadhead (Dhd). Dhd est cruciale pour le remodelage de la chromatine paternelle à la fécondation et donc pour la formation du zygote.

Tout d'abord, un crible génétique basé sur l'expression de shRNAs dans la lignée germinale femelle m'a permis d'identifier : (i) l'histone demethylase Lid/dKDM5 (ii) les membres du complexe déacétylase Sin3A et Rpd3 (iii) la sous-unité Snr1du remodeleur de la chromatine Swi/Snf et (iv) le facteur chromatinien Mod(mdg4), comme étant essentiels pour l'expression de *dhd*. Pour la suite des analyses je me suis focalisée sur Lid, Sin3A, Snr1 et Mod(mdg4). Des analyses transcriptomiques ont montré que *dhd* est parmi les gènes les plus exprimés dans les ovaires et que cette expression est abolie lors du *knockdown* dans la lignée germinale femelle de *lid*, *sin3a*, *snr1* ou *mod(mdg4)*. De façon remarquable la quantité de gènes dérégulés dans les ovaires *knockdown* est limitée. Ceci suggère que ces complexes ubiquitaires et conservés sont dédiés à la régulation de *dhd* dans ce tissu. Ce cas paradigmatique m'a donc offert une opportunité pour disséquer les mécanismes moléculaires agissant sur le contrôle épigénomique de l'établissement de programmes transcriptionnels spécifiques, comme c'est le cas lors de l'ovogénèse.

Ensuite, en utilisant la méthode de profilage de la chromatine Cut&Run et une stratégie d'analyse de données dédiée, j'ai trouvé que *dhd* est intégré dans un mini-domaine enrichi en marques hétérochromatiques H3K27me3/H3K9me3 et délimité par des éléments régulateurs.

De plus, l'élément régulateur à proximité du promoteur de *dhd* s'est avéré essentiel pour son expression. De façon surprenante, Lid, Sin3A, Snr1 et Mod(mdg4) ont des effets différents sur H3K27me3 et sur ces éléments régulateurs. Néanmoins, j'ai mis en évidence que ces effecteurs activent *dhd* de façon indépendante de H3K27me3/H3K9me3. De plus, j'ai trouvé que ces marques ne sont pas nécessaires pour réprimer *dhd* dans les tissus adultes.

Mes travaux de thèse ont donc révélé plusieurs caractéristiques inhabituelles, au niveau génomique et épigénomique, au locus *dhd.* Cependant je n'ai pas établi un trait unique qui conduise à l'hyperactivation de *dhd* dans la lignée germinale femelle. La régulation de *dhd* dépendrait non pas d'une seule caractéristique mais plutôt d'une combinaison de traits particuliers.

À travers l'exemple de *dhd*, mes travaux démontrent la complexité des processus qu'implique l'activation d'un gène au bon endroit, au bon moment et en bonne quantité. Ils illustrent également la difficulté d'établir des règles générales sur les mécanismes de régulation transcriptionnelle médiés par la chromatine, qui sont très souvent contexte-spécifique.

Mots clés: épigénetique, épigénomique, régulation transcriptionnelle, ovogénèse, *Drosophila melanogaster,* Deadhead, transition ovocyte-zygote

Summary:

Dynamic regulation of the epigenome underlies cellular plasticity and allows cells to respond to developmental and differentiation programs. Epigenomic effectors can mediate changes such as modification of histone tails, nucleosome positioning or the incorporation of specific histone variants, altering chromatin structure and thus gene expression. Yet, the molecular mechanisms underpinning these processes remain largely unknown. A major challenge in the field is to establish direct functional connections between upstream chromatin factors, which generally have broad impact on chromatin, and the controlled expression of specific cellular effectors.

My PhD project was precisely based on the discovery of a specific functional link between a series of epigenomic effectors and the highly regulated terminal effector of zygote formation in *Drosophila melano*gaster: the maternal thioredoxin Deadhead (Dhd). Dhd is critical to ensure paternal chromatin remodeling at fertilization, and thus zygote formation.

First, an shRNA-based genetic screen in the female germline led me to identify (i) the H3K4me3 demethylase Lid, (ii) the members of the deacetylase complex Sin3A and Rpd3, (iii) the Snr1 subunit of the chromatin remodeler Swi/Snf and (iv) the chromatin factor Mod(mdg4), as essential for the expression of *dhd*. For further analyses I focused on Lid, Sin3A, Snr1 and Mod(mdg4). Transcriptomic analyses showed that *dhd* is among the most highly expressed genes in ovaries and this expression is completely abolished when I deplete Lid, Sin3A, Snr1 or Mod(mdg4) specifically in the female germline. Remarkably, there is a paucity of misregulated genes in *knockdown* ovaries. This suggested that these broadly conserved, ubiquitous complexes are mostly dedicated to regulation of *dhd* in this tissue. This paradigmatic case presented the opportunity to dissect the mechanisms at play in the epigenomic control of the establishment of specific transcriptional programs, as is the one set during oogenesis.

Next, using Cut&Run chromatin profiling with a dedicated data analysis strategy, I found that *dhd* is embedded in a heterochromatic H3K27me3/H3K9me3-enriched mini-domain flanked by DNA regulatory elements, including a *dhd* promoter-proximal element essential for its expression. Surprisingly, Lid, Sin3A, Snr1 and Mod(mdg4) impact H3K27me3 and this regulatory element in distinct manners. However, I showed that these effectors activate *dhd*

independently of H3K27me3/H3K9me3 and that these marks are not required to repress *dhd* in adult tissues.

Altogether, my work uncovered multiple unusual genomic and epigenomic characteristics at the *dhd* locus, but did not identify a single feature that was truly defining ovarian hyperactivation. The dramatic regulation of *dhd* may rely not on an individual trait but rather on a unique combination of such rare features.

Through the example of *dhd*, my work demonstrates the puzzling process that is gene activation in the right place, at the right time and in the right amount. It also illustrates the difficulty to establish general rules on chromatin-based regulatory systems, which are very often context-dependent.

Keywords: epigenetics, epigenomics, transcriptional regulation, oogenesis, *Drosophila melanogaster,* Deadhead, oocyte-to-zygote transition

Table of Contents

INTRODUCTION

RESULTS &DISCUSSION

Abbreviations

CDS: CoDing sequence

ESCs: Embryonic Stem Cells

GSC: Germ Stem Cell

GTF: General Transcription Factors

HAT: Histone Acetyltransferase

HDAC: Histone DeAcetylase

HDMT: Histone DeMethylase

HMT: Histone Methyltransferase

HP1: Heterochromatin Protein 1

IBP: Insulator Binding Protein

NDR: Nucleosome Depleted Region

PcG: Polycomb Group

piRNA: piwi-RNA

PRC: Polycomb Repressive Complex

PRE: Polycomb Response Element

PTM: PostTranslational Modification

RNA Pol: RNA Polymerase

shRNA: short hairpin RNA

siRNA: small interference RNA

SNBPs: Sperm Nuclear Basic Proteins

TAD: Topologically Associated Domain

TE: Transposable Element

TF: Transcription Factor

TrxG: Trithorax Group

TSS: Transcription Start Site

INTRODUCTION

Germ cells retain the potential to reproduce an entire organism upon fertilization. Gametogenesis represents thus an extreme cellular differentiation process where complex transcriptional programs must be tightly regulated. Chromatin-based regulation of gene expression and thus epigenomic effectors are crucial in the establishment of specific transcriptional programs in the female germline. Yet, the molecular mechanisms underpinning this regulation remain largely unknown. A major challenge in the field is to establish direct functional connections between upstream chromatin factors, which generally have a broad impact on chromatin, and the controlled expression of highly specialized terminal effectors. My PhD project was precisely based on the discovery of a specific functional connection between a series of epigenomic effectors and the highly regulated terminal effector of zygote formation in *Drosophila melanogaster*: the maternal thioredoxin Deadhead (Dhd). In this introduction I will first describe the mechanisms of eukaryotic transcription followed by the presentation of chromatin-based regulatory mechanisms of gene expression. Next, I will focus on the importance of transcriptional regulation during oogenesis. I will finish by the presentation of the maternal thioredoxin Deadhead and its epigenomic regulators.

I. PART I: Mechanisms of eukaryotic transcription

The DNA molecule carries the genetic information necessary for an organism's development and functioning. Yet, in multicellular organisms, each cell has specific features that define its identity and function. Therefore, information stored in the DNA molecule needs to be used at the right place at the right time. Indeed, gene expression is temporarily, spatially and quantitively regulated. Various factors affect gene expression and regulation can be exerted at transcriptional, post transcriptional and post translational levels. My case study, the *dhd* gene, is a hyperactivated gene, it is thus important to put it in perspective the mechanisms of transcription, which is the focus of these paragraphs.

1. The process of eukaryotic transcription

Globally, the process of transcription can be divided into three main steps: initiation, elongation and termination. During initiation, the RNA polymerase (RNA Pol) complex is formed on the gene's promoter with the help of general transcription factors (GTFs), resulting in the assembly of the Pre-initiation complex (PIC), which begins transcription and can go into pause. Next, throughout the elongation step, the RNA Pol moves along the template strand, synthesizing the RNA molecule. The polymerase continues transcribing until it reaches the terminator sequence. Finally, the nascent mRNA and the RNA Pol II are released constituting the termination step (Fig1). Transcription is thus a multistep process and all these steps can undergo regulatory control that depends on the gene, the cell type, as well as internal and external signaling.

In eukaryotes not all genes are transcribed by the same polymerase. Three RNA polymerases (RNA Pol I-III) have been identified, differing in their subunit composition and targeting different classes of genes (Sentenac, 1985) RNA Pol I transcribes ribosomal RNAs, RNA Pol II transcribes protein coding genes and some non-coding RNAs and finally, RNA Pol III transcribes small ribosomal 5S RNA, tRNAs and other small non-coding RNAs. On the contrary, prokaryotes use the same RNA Pol to transcribe all their genes. This reflects the increased complexity that is regulation of gene expression in eukaryote systems. Why develop different enzymes? Differences in the structure and composition of the three RNA Pol are linked to the genes they transcribe. For example, to abundantly synthesize tRNAs, RNA Pol III must efficiently terminate and re-initiate transcription on the short genes it targets. Structural analysis of this enzyme revealed that specific subunits permit a loose binding of the RNA:DNA hybrid thereby allowing a fast termination of transcription (Arimbasseri and Maraia, 2016; Hoffmann et al., 2015). Also, two RNA Pol I-specific subunits are needed for the high polymerase loading rate and enhancement of the rRNA gene transcription cycle (Albert et al., 2011). At last, RNA Pol II targets a large set of differently regulated genes, including protein-encoding genes, which is why it has been of particular interest for the study of the regulation of gene expression and will be the main focus of the next paragraph.

RNA Pol II is composed of 12 subunits Rpb1-12 (RNA polymerase B) and is conserved from yeast to human. The largest subunit Rpb1 has a C-terminal domain (CTD) containing a repeat sequence of 7 amino acids (Tyr1–Ser2–Pro3–Thr4–Ser5–Pro6–Ser7) necessary for the proper functioning of RNA Pol II (Hsin and Manley, 2012). Specific residues in the CTD repeats can be phosphorylated and these post-translational modifications (PTM) play an important

role in the regulation of RNA Pol II activity during the transcription cycle (Fig1) (Buratowski, 2009; Hsin and Manley, 2012). Deletion of the RNA Pol II's CTD, negatively affects mRNA processing, including capping, cleavage/polyadenylation and splicing (S. McCracken et al., 1997; Susan McCracken et al., 1997), indicating thus a crucial role in mRNA processing. First, phosphorylation of serine 5 (Ser5P) is found concomitant with transcription initiation and it has been shown that this modification recruits and stimulates capping machinery at the nascent pre-mRNA. This mark is also important for initial RNA Pol II progression through DNA by the unbinding of the specific proteins that recruited it. During elongation Ser5P undergoes progressive dephosphorylation coincident with the release of 5′ processing factors. Next, phosphorylation of Ser2 marks the elongation phase of transcription and is increasingly enriched towards the ends of genes. It has been observed that Ser2P is required for the recruitment of polyadenylation factors to the 3′ end of genes in vivo (Ahn et al., 2004). Additionally, genome-wide ChIP experiments showed that peaks of 3′ processing factors followed Ser2P peaks, consistent with the view that CTD Ser2P contributes to the recruitment of the polyadenylation complex (Mayer et al., 2012, 2010). Also, Ser7 phosphorylation is found early in transcription initiation and retained until transcription termination in all RNA Pol II-dependent genes. However, this mark has been found to be particularly required for expression of a sub-class of genes encoding small nuclear (sn)RNAs, where it facilitates recruitment of the gene-specific Integrator complex (Egloff et al., 2012, 2007). Finally, hypophosphorylation of the CTD is a prerequisite for RNA pol II to enter the preinitiation complex therefore at the end of the transcription cycle, the regeneration of the hypophosphorylated state of the CTD is critical for RNA Pol II recycling. In conclusion, the CTD "code" allows the coupling of transcription with co-transcriptional RNA processing through the timely recruitment of the appropriate factors at the right point of the transcription cycle. Transcription dynamics, efficiency and rate can thus be regulated, in part, by modifying the enzyme that synthesizes the RNA molecule.

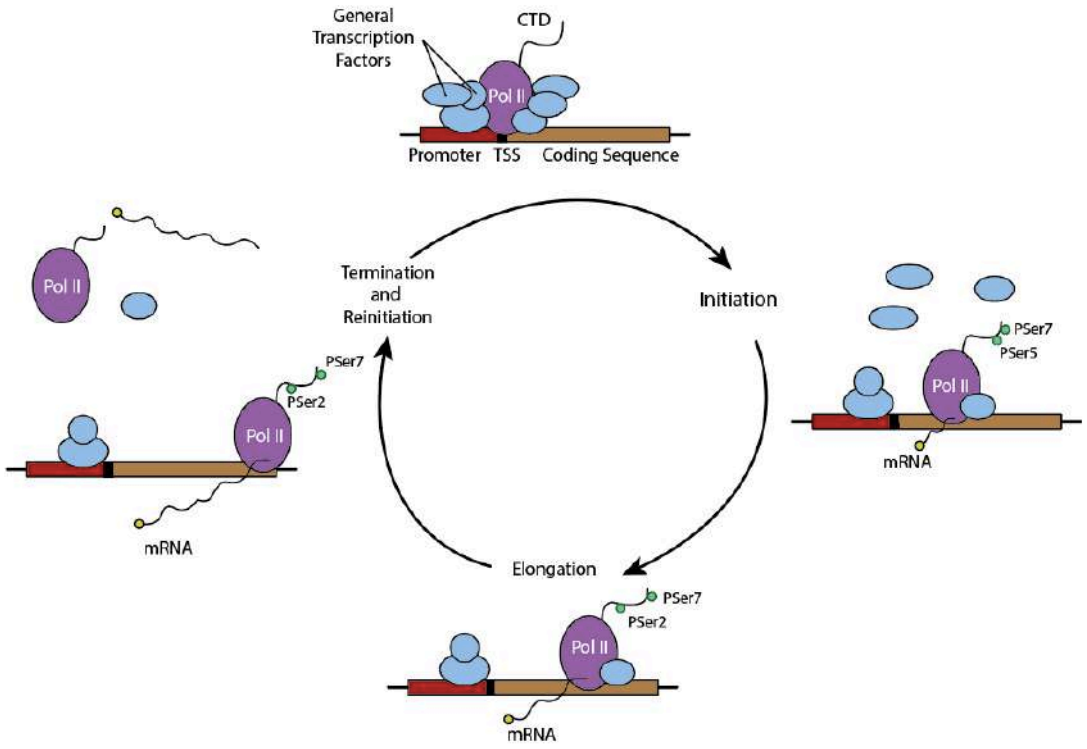

Fig1-Schematic representation of the main steps of the RNA Pol II transcription cycle.
The main steps of the transcription cycle: initiation elongation and termination. Phosphorylations of Serines 2, 5 and 7 on the RNA Pol II C-terminal domain (CTD) are shown. RNA Pol II binds the gene promoter assisted by general transcription factors (GTFs). The polymerase is released and begins active RNA synthesis throughout the elongation phase. Finally, polymerase is dephosphorylated and released along with the mRNA and can be recruited for a new cycle (inspired from Chang Hongh, 2016).

2. Promoter-Enhancer interactions regulate transcription

Promoters are DNA sequences that define where transcription of a gene by the RNA Pol begins. Indeed, transcription initiates at a defined positioned, the transcription start site (TSS) located at the 5' end of a gene. The TSS is embedded within a core promoter which is the minimal stretch of contiguous DNA sequence sufficient to direct transcription initiation. The core promoter serves as a binding platform for the assembly of the transcription machinery. Indeed, general transcription factors (GTFs) bind DNA sequences at the core promoter elements and subsequently recruit the RNA Pol II to form the preinitiation complex (Matsui et al., 1980; Orphanides et al., 1996). However, core promoters generally have low basal activity that can be activated by enhancers (Banerji et al., 1981; Shlyueva et al., 2014). Enhancers are segments of DNA that enable transcriptional regulation in a spatio-temporal

manner. Central to the communication between enhancer and promoters are transcription factors (TFs) and cofactors (Haberle and Stark, 2018). TFs are DNA binding proteins, recognizing specific sequence motifs on promoters and enhancers which in turn recruit cofactors having a variety of biochemical functions. These are thus central effectors of transcriptional regulation. Therefore, to better understand transcriptional regulation it is important to gain insight on all these regulatory elements and their interactions.

Computational analyses of core promoters in fly (Ohler et al., 2002) and human (FitzGerald et al., 2006) have revealed a series of over-represented sequence motifs in these regions. For example, the TATA-box is a core promoter element recognized by one of the GTFs that mediates RNA Pol II recruitment. It has a well-defined position and might thereby determine the choice of TSS at a fixed downstream position. Although it is a well conserved element from yeast to human it is found only at a minority of core promoters, in flies they correspond to ~5% of core promoters (FitzGerald et al., 2006; Ohler et al., 2002). A more widely used element is the initiator (Inr) motif. Although its consensus sequence differs between flies and humans, this element, as the TATA-box, has a well-defined position, that in this case, overlaps with the TSS (FitzGerald et al., 2006). In promoters that lack a TATA-box, the Inr motif is often accompanied by another motif, the downstream promoter element (DPE), which is positioned downstream of the TSS (Burke and Kadonaga, 1996) and functions cooperatively with the Inr for GTFs binding. Increasing or decreasing of one nucleotide the spacing between the Inr and DPE results in reduced binding of GTFs and decrease in transcriptional activity (Kutach and Kadonaga, 2000), indicating thus the importance of a strict Inr–DPE spacing. In addition to these three most abundant core promoter motifs, other motifs either with defined positions relative to the TSS or not, have been identified showing the variety of core promoters.

Interestingly, TATA-box and DPE rarely co-occur in flies, they were thus suggested to be associated with functionally distinct groups of genes (FitzGerald et al., 2006; Ohler et al., 2002). This raised thus the question of the association of core promoters and gene function. Integrating data of sequence composition and motifs with other properties including transcription initiation pattern (focused or dispersed), chromatin configuration and gene function revealed three main types of core promoter in metazoa (Fig2) (Haberle and Stark, 2018; Vo ngoc et al., 2017). First, promoters found at adult tissue-specific genes and differentiated cell-specific genes, characterized by TATA-box and Inr motifs, sharp initiation

patterns and imprecisely positioned nucleosomes (see section II-3). Second, promoters of broadly expressed housekeeping genes, in flies were enriched for the motifs DRE (DNA replication-related element) and ohler 1/6 and in mammals they overlapped with CpG islands. They were also associated with dispersed transcription initiation and a well-defined nucleosome-depleted region. Third, core promoters of developmental TFs, in mammals they resemble to housekeeping gene core promoters. In flies, they tend to contain a DPE motif and focused initiation of transcription. There is thus a correlation between features of core promoters and gene function. Notably, a bias between gene function and specificity of promoter-enhancer interaction has also been observed. Zabidi and colleagues studied this specificity on a genome-wide scale, by high-throughput genome-wide screening of enhancer activity in housekeeping and developmental core promoters (Arnold et al., 2013; Zabidi et al., 2015). Their study revealed different motif enrichment in both core promoters and enhancers between housekeeping and developmental genes (summarized in Table1). Developmental and housekeeping core promoter enhancer elements also show proximity bias. Enhancer sequences activating developmental core promoters appeared to be gene promoter-distal while enhancers activating housekeeping core promoters were generally found proximal to the gene promoter (Arnold et al., 2013). This suggests that some transcriptional enhancers exhibit preferences for certain core promoter elements. Overall, these data show that specific features of cis regulatory elements are linked to gene function. However, the mechanisms of how these features can influence a specific transcription pattern are yet to be elucidated.

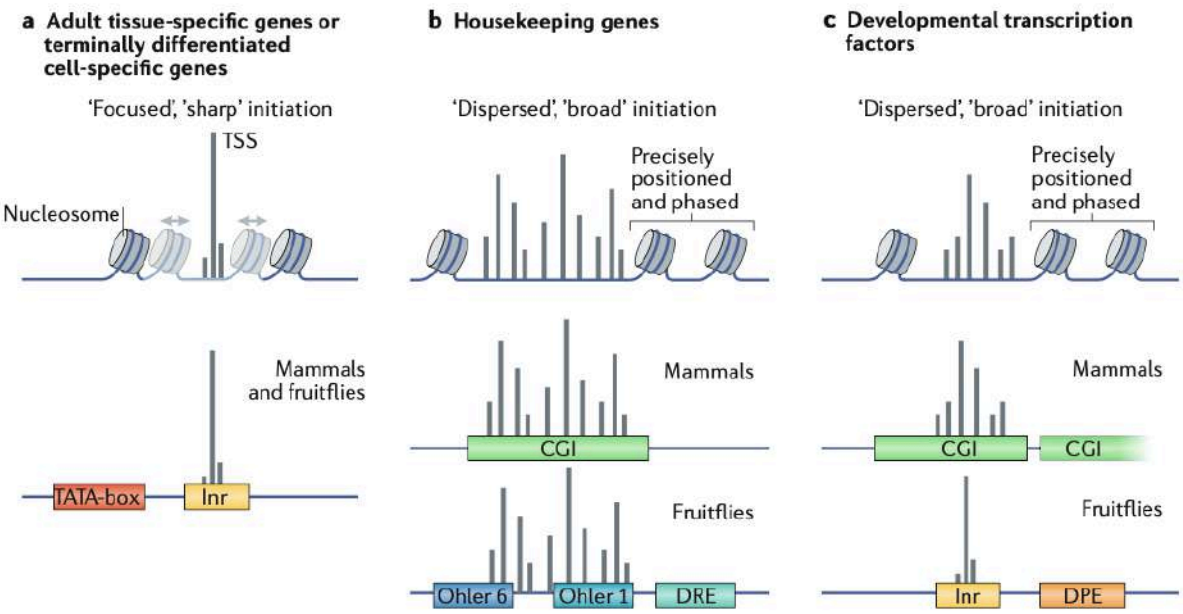

Fig2-Three types of core promoters in metazoa

Main categories of core promoters in *Drosophila* and mammals based on different properties, including initiation pattern (focused or dispersed), sequence composition motifs and gene function (Haberle and Stark, 2018).

	dCP enhancers	hkCP enhancers
Target gene function	Signaling, patterning, morphogenesis	House-keeping
Enhancer location	Distal or intronic	Promoter-proximal
Target gene promoter motifs	TATA, Inr, MTE, DPE	DRE, TCT, others
Enhancer motifs	GAGA (GAGAG)	DRE (TATCGATA)
Transcription factors	Trithorax-like (Trl) / GAF	DRE binding factor (Dref)

Table 1: Summary of differences between developmental and housekeeping core promoters and their enhancers.

(From Lorberbaum and Barolo 2015 based on the result by Zabidi et al., 2015).

Enhancers can be located near the promoter of their cognate gene or be distally positioned. Distances can vary from a few kb to several megabases. Active promoters however, are often in spatial proximity to their enhancer and the establishment of these contacts are tightly linked to 3D organization of DNA in the nucleus (mechanisms to achieve genome folding will be detailed in section II-9).

The regulatory input that core promoters receive from enhancers is mediated by TF binding both of these elements and by transcriptional cofactors, which are recruited by TFs through protein–protein interactions (Fig3). Importantly, cofactors often have enzymatic activities and can post-translationally modify components of the transcription machinery and the surrounding nucleosomes. It has been observed that the Mediator complex, a cofactor, recruited to enhancers and interacting with core promoters can increase RNA Pol II recruitment and PIC assembly (Eychenne et al., 2016), thereby increasing transcription rate. Mediator in yeast can stimulate phosphorylation of Ser5 at the CTD of RNA Pol II (Esnault et al., 2008), which is important for mRNA processing and RNA Pol II progression through the transcription cycle. The interaction between bound TFs and recruited cofactors can thus lead to transcription activation.

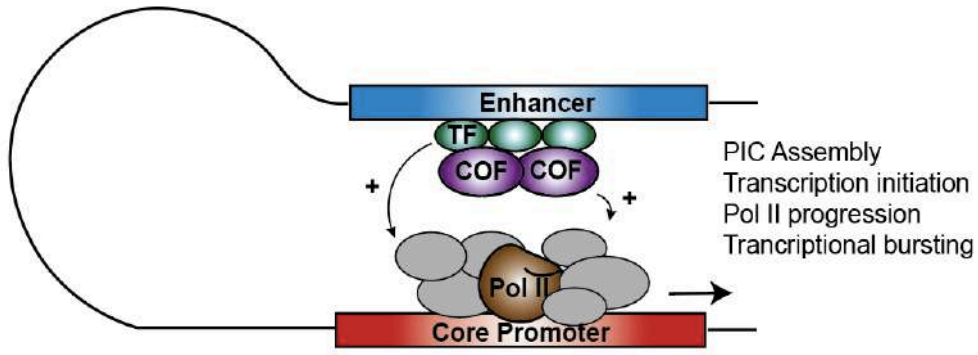

Fig 3-Enhancers communicate with promoters through transcription factors and cofactors. Enhancers and promoters can bind transcriptional factors (TF) which in turn bind cofactors (COF) thereby mediating enhancer-promoter communication. This communication results in stimulation of transcription via different mechanisms such as PIC assembly, transcription initiation, stimulation of RNA Pol II progression or modulation of transcriptional bursts.

Another mechanism through which enhancers can regulate promoter activation is by modulating transcription bursts. Transcription is episodic consisting on short but intense

"bursts", which comprise initiation events separated by periods of inactivity (Chubb et al., 2006; Raj et al., 2006). Patterns of these bursts can have important roles in development. For example, when visualizing transcription in living fly embryos, it was observed that lengthening of transcriptional activity periods is important for the establishment of boundaries during embryo patterning (Lucas et al., 2013). It is therefore important to understand how these "bursts" are regulated. Another study in living *Drosophila* embryos revealed that the levels of gene activity depend on the frequency of transcriptional bursts and that this frequency can be regulated by enhancers (Fukaya et al., 2016). The authors evaluated the effect of different developmental enhancers on transcriptional bursting of a reporter gene. and observed that enhancers produced transcriptional bursts with similar amplitudes and duration but generated different bursting frequencies, with strong enhancers producing more bursts than weak enhancers. This result suggests thus that regulation of bursting frequencies by enhancers can be a parameter of gene control. Moreover, it was observed that mutations in the TATA-box led to a decrease in burst size, that is the number of transcribing RNA Pol II molecules per burst (Hornung et al., 2012), suggesting that burst size is a promoter-specific property. These data show that several factors can influence transcription bursts, either in frequency or in amplitude and thereby regulate the transcriptional output. Further research will be needed to fully understand the mechanisms regulating transcriptional bursts.

3. Regulation of gene expression by untranslated regions

Additional sequences within the gene can also provide a regulatory point for transcription. Majority of eukaryotic genes contain introns. The process of removing introns is energy and time-consuming, however, these elements have been evolutionary conserved which is indicative of a biological functional role. The most obvious advantage they confer is increasing the repertoire of proteins through alternative splicing, meaning that a single gene can produce multiple isoforms of a protein depending on cell type and environment (Nilsen and Graveley, 2010). Additional research in the field has associated introns to a variety of functions such as protection against environmental stress, or as the source of non-coding RNAs (Dwyer et al., 2021). A third role for introns, well established in the literature, is their function in regulating gene expression. It has been observed in yeast that in a physiological

context, genes require promoter proximal introns for full transcriptional output (Furger et al., 2002). Additionally, a quantitative analysis of constructs containing a human intron in the open reading frame of a reporter gene, revealed that its presence increased not only the accumulation of mature mRNA but also the efficiency of their translation (Nott, 2003). The capacity of introns to increase gene expression has been observed in many eukaryotes including mammals, plants, yeast, and insects (Shaul, 2017), however the underlying mechanisms are not fully elucidated. Studies in budding yeast have started to provide hints for the mechanisms at play. It was observed that the presence of an intron within a gene results in formation of a multi-looped gene architecture. When looping is defective, these interactions are abolished and there is no enhancement of transcription despite normal splicing (Agarwal and Ansari, 2016). Introns are thus important players in the regulation of gene expression.

Furthermore, the 5' and 3' untranslated regions (UTR) located at the extremities of a given gene have also been involved in the regulation of expression. A study investigated the role of alternative 5'UTRs of the same gene on mRNA translation efficiency with an in vivo reporter assay (McClelland et al., 2009). They observed that among the 5'UTRs tested, three enhanced translation while two had repressive effects. Modeling of the mRNA secondary structure in the 5'UTR revealed the presence of compact structures around the start codon in the repressive 5'UTRs. Translational efficiency was also found inversely correlated to 5'UTR length. Additionally, genome-wide studies in human revealed differences in structure and nucleotide content of 5'UTRs of housekeeping and developmental genes (Ganapathi et al., 2005). *In silico* comparisons of genes with low and high levels of protein output showed that 5'UTRs that enable efficient translation are short, have low GC content, are relatively unstructured, and do not contain upstream AUG codons (Kochetov et al., 1999). Although mechanisms describing how 5'UTR sequence can influence transcription are not well understood, these data suggest a correlation between this gene element and regulation of transcription. The 3'UTR, situated downstream of the protein coding sequence, has also been involved in the regulation of gene expression. Indeed, the poly(A) tail at the 3' end mRNAs provide a binding platform for poly(A) binding proteins (PABP) that have roles in mRNA export, stability, decay and translation(Gorgoni, 2004; Mangus et al., 2003). For example, PABP mRNAs can bind poly(A) tracts in their own 5'UTRs, resulting in translational repression. Moreover, in human, it was observed that the generation of alternative 3′ UTR isoforms is a characteristic of ubiquitously transcribed genes that are involved in diverse gene

regulatory processes and are distinct from the classical housekeeping genes that generate single UTRs (Lianoglou et al., 2013). These ubiquitously transcribed multi-UTR genes use different 3′ UTR isoforms to achieve tissue- and context-dependent expression. Changes in the 3'UTR isoform expression represents thus a component of gene expression programs. Altogether, these data shows that untranslated regions can have an important role in transcriptional regulation but mechanisms are yet to be elucidated.

To conclude, transcription is a complex process that can be modulated by regulatory elements encoded within the DNA molecule and by the binding of specific proteins. However, DNA is not naked in the nucleus but wrapped around histone proteins. This structure represents thus a major point of transcriptional regulation.

II. Part II: Shaping of the chromatin regulates gene transcription

1. The Nucleosome: the basic unit of chromatin

The basic unit of organization of chromatin is the nucleosome, formed of 146 bp of DNA that wrap around an octamer of histones. This octamer is composed of two copies of the four "core histones": H2A, H2B, H3 and H4. Additionally, linker DNA between two nucleosome cores is bound by the linker histone H1 (Fig4). Histones have positively charged surfaces formed by basic amino acid side chains which allow them to interact with the negatively charged DNA backbone forming thus a highly tight bound.

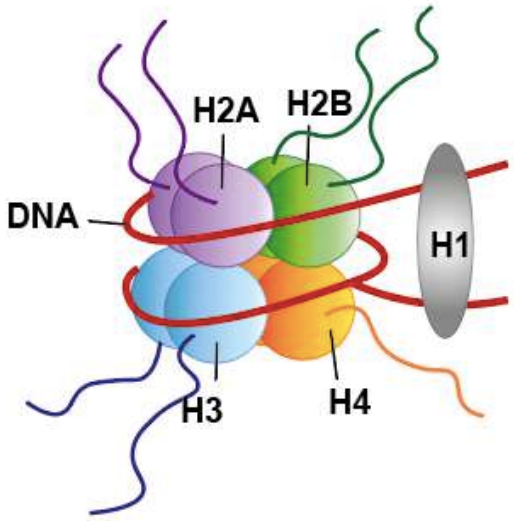

Fig4-Schematic representation of the nucleosome.
The nucleosome core is composed of 146 bp of DNA wrapped around a histone octamer containing two H2A-H2B dimers and two H3-H4 dimers. Linker DNA between two nucleosome cores is bound by the linker histone H1.

The amino acid sequences of the core histones (H2A, H2B, H3 and H4) are extremely well conserved in evolution. Histones are small proteins (10-15 kDa) that share a globular domain with a α-helical arrangement called histone fold, implicated in histone dimerization (Arents et al., 1991; Luger et al., 1997). Importantly, core histones possess flexible N-terminal regions, called histone tails, that associate more loosely with the nucleosome and remain accessible for posttranslational modifications. The most well-studied histone modifications include acetylation, phosphorylation, methylation, and ubiquitylation, although many other modifications have been reported. These modifications play a central role in the regulation of gene expression as well as many other DNA processes such as repair, replication and recombination (Bannister and Kouzarides, 2011). Notably, these histone modifications are reversible by specific enzymes giving the possibility of a dynamic and fine regulation of transcription.

Nucleosome composition can be altered by the insertion of histone variants (Martire and Banaszynski, 2020; Talbert and Henikoff, 2017). These are encoded by a different set of genes and show slight variations in the amino acid sequence. Different variants of histones can be incorporated. Variations of histone H3 and histone H2A are common while histones H2B and H4 appear to be predominantly canonical.

To date, the H2A family contains the greatest sequence diversity of identified variants. The variant H2A.Z, H2Av in *Drosophila*, is present in almost all organisms and has been associated to diverse transcriptional states. Indeed, several studies have shown that H2A.Z nucleosome occupancy at promoters is inversely correlated with transcription (Guillemette et al., 2005; Zhang et al., 2005). However, it has also been observed that H2A.Z is required for activation of heat shock genes during heat shock responses (Zhang et al., 2005) and that it can promote the recruitment of the RNA Pol II (Adam et al., 2001). Additionally, in Drosophila, the presence of H2Av, the homolog of H2A.Z (van Daal et al., 1988), correlates with paused RNA Pol II (Mavrich et al., 2008). It was later observed that H2Av occupies the promoter in absence of gene expression but it decreases upon gene induction (Kusch et al., 2014). Together, these results suggest that the role of H2A.Z may be to recruit Pol II and poise genes for activation.

Histone H3 possesses two universal variants. First, CENP-A, who is found at chromosome centromeres and is important for cohesin recruitment at these regions (Santaguida and Musacchio, 2009). Second, H3.3 enriched at gene bodies and regulatory elements such as promoters and enhancers (Ahmad and Henikoff, 2002; Mito et al., 2007), suggesting an association with active transcription. Although, absence of H3.3 in Drosophila led to transcriptional defects, the latter could be compensated by increased expression of variant H3.1 (Sakai et al., 2009). This suggests that transcription was affected by lack of histone replacement rather than by the variant of H3. Additionally, H3.3 has also been found at transcriptionally silent regions such as telomeres and centromeres (Goldberg et al., 2010; Szenker et al., 2012). These data suggests thus that the link of H3.3 with transcription is more complex that initially thought. Overall, even though the mechanisms are not fully elucidated, histone variants can influence transcription and have thus functional roles in the genome.

Dynamic histone PTMs and variants contribute to the complexity of epigenetic regulation of the genome. Chromatin dynamics is mediated by epigenomic effectors it is thus crucial to understand how these factors work.

2. Diversity of epigenomic effectors

The chromatin is highly dynamic and can be shaped to respond to the needs of the cells through a wide variety of mechanisms that will be detailed throughout this manuscript. Accordingly, the molecular actors behind chromatin shaping are also very varied. They can essentially be classified in three main categories: histone modifiers, nucleosome remodelers and histone chaperones. During my PhD I also focused on insulator binding proteins, that even though they do not interact with histones, they are also important for the organization of the chromatin landscape. I will thus also describe this category.

Histone modifiers: Histone PTMs play vital roles in regulating both gene activation and repression. These modifications are reversible which helps fine-regulate gene transcription according to specific cues. Over the years a plethora of histone modifiers i.e., enzymes catalyzing changes in histone PTMs have been identified. These epigenetic players have been categorized as writers: that introduce various chemical modifications on histones, readers: the specialized domain containing proteins that identify and interpret those modifications and erasers: the dedicated group of enzymes proficient in removing these chemical tags. Writers and erasers are divided into classes on the basis of the specific PTM they effect (Fig5) (Bannister and Kouzarides, 2011; Biswas and Rao, 2018). The corresponding enzymatic activities are referred to as histone acetyltransferases (HATs), histone methylases (HMTs), histone kinases and histone ubiquitin-transferases. Analogously, erasers comprise histone deacetylases (HDACs) histone demethylases (HDMs, or KDMs for lysine demethylases) phosphatases and deubiquitinating enzymes. In general, HDACs have relatively low substrate specificity by themselves, a single enzyme being capable of deacetylating multiple sites within histones. HKMTs and HKDMs on the contrary possess a high level of substrate specificity with respect to their target lysine.

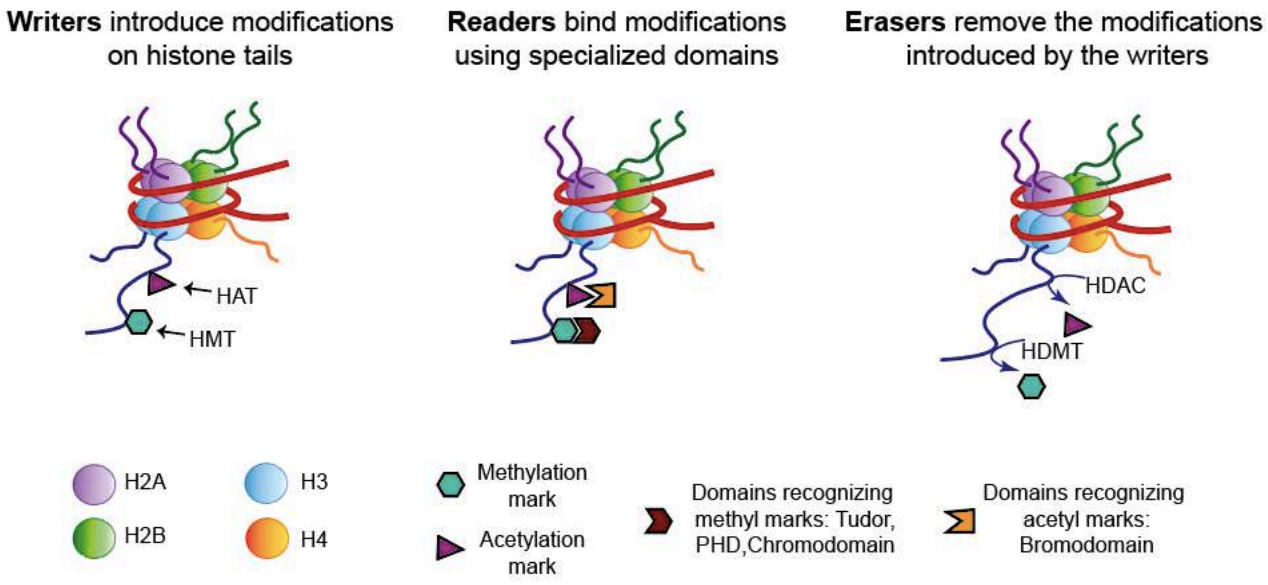

Fig 5-Actions of epigenetic writers, readers and erasers.

Enzymes and proteins capable of adding, binding or removing posttranslational modifications on histone tails are known as writers, readers and erasers respectively. Examples for methylation and acetylation are represented. HAT: histone acetyltransferase, HMT: histone methyltransferase, HDAC: histone deacetylase, HDMT: histone demethylase (modified from Biswas and Rao, 2018).

Nucleosome remodelers are a category of enzymes capable of altering DNA-histone interactions at target nucleosomes, thereby locally and differentially regulating access to DNA. Remodelers can (i) mediate nucleosome sliding i.e., the translational movement of a nucleosome in either direction to expose a region that was previously occluded, (ii) exchange a core histone for a variant histone and (iii) induce eviction of a nucleosome to expose the associated DNA (Fig6). A conserved feature among remodelers is the use of the energy from ATP hydrolysis to achieve these reconfigurations (Becker and Workman, 2013; Clapier and Cairns, 2009).

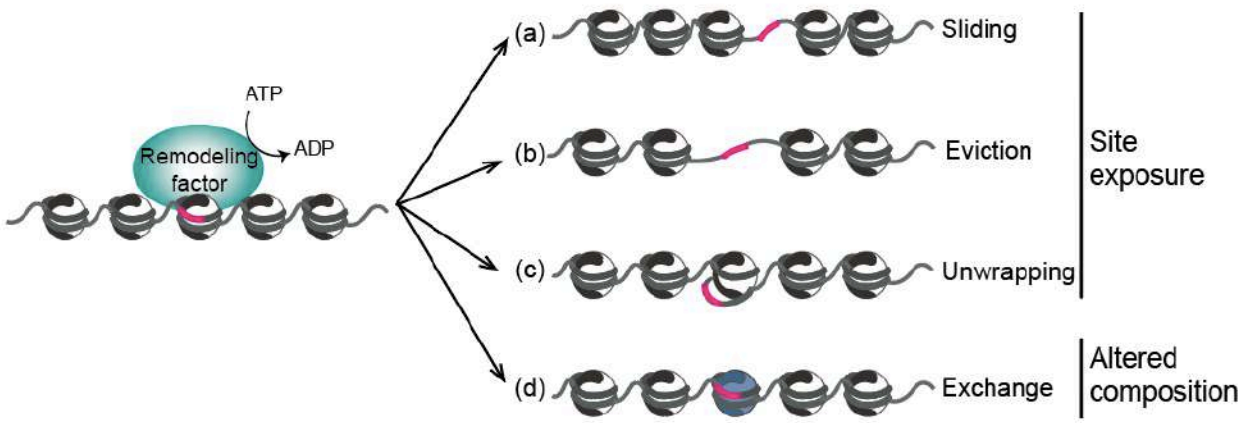

Fig6-Outcomes of nucleosome remodeling

Models for nucleosome remodeling. Remodelers (green) alter nucleosome-DNA interactions in an ATP-dependent manner. They mediate: (a) nucleosome sliding, the translational movement of a nucleosome, (b) nucleosome eviction, (c) localized unwrapping or (d) nucleosome exchange. Processes (a) to (c) lead to DNA site exposure while (d) results in altered composition of the nucleosome (modified from Clapier and Cairns, 2009).

Histone chaperones are proteins that handle non-nucleosomal histones *in vivo*. They accompany and safeguard histones throughout their cellular life. Histone chaperones escort histones, preventing them from aggregating or from spurious interactions with DNA (Hammond, 2017). Importantly, histone chaperones are necessary for deposition of canonical histones as well as of histone variants into particular places in the genome thereby participating in the regulation of chromatin processes. Interestingly, the conserved histone chaperone CAF-1 complex involved in the assembly of H3-H4 histone dimers on newly synthesized DNA, has also been found to participate in the maintenance of heterochromatin trough interaction with heterochromatin effectors in fly (Roelens et al., 2017). Overall, this shows the importance of chromatin dynamics regulation by histone chaperones.

Insulators are conserved DNA elements that help organize eukaryotic genomes into physically and functionally regions through diverse mechanisms. They are thought to act by recruiting specific Insulator Binding Proteins (IBPs). The first IBP to be discovered was the CCCTC-binding factor (CTCF). To date, CTCF remains the major protein implicated in insulation in vertebrates (Lobanenkov et al., 1990). On the contrary, in flies, various insulator sequences have been identified and classified according to the proteins they bind. Experiments in *Drosophila* have identified a dozen or more IBPs binding specific DNA

sequences (Melnikova et al., 2020; Özdemir and Gambetta, 2019). They were identified based on their ability to bind to characterized insulators and mediate their function or in genetic screens as being required for the function of a specific insulator. Interestingly, most of these proteins are also classified as transcription factors, such as the conserved dCTCF/CTCF or the GAGA factor (GAF). While most IBPs exhibit direct DNA binding, additional proteins were identified as necessary for insulator activity. This is particularly the case for the cofactors CP190 and Mod(mdg4) which are required along with the DNA-binding protein Su(Hw) at the gypsy transposon for proper insulator function (Georgiev and Gerasimova, 1989; Gerasimova et al., 1995; Pai et al., 2004). Subsequently, studies have shown that CP190 is common to almost all insulators (Ahanger et al., 2013). At least one of the roles of these co-factors is to mediate homotypic and heterotypic protein-protein interactions bridging thus contacts between distant genomic regions. Initially, insulators were defined as having either an enhancer blocker role or a barrier role between euchromatin and heterochromatin. However, extensive research has now associated insulators to broader functions in nuclear biology, such as nuclear organization.

Chromatin dynamics enables the cell to tightly regulate fundamental activities of the genome. It is thus the concerted activity of epigenomic effectors (modifiers, remodelers, chaperones) along with nuclear organizing proteins (insulators), that achieve fine gene regulation. Malfunctioning of these machineries is tightly linked to diseases such as cancer or intellectual disability. It is thus crucial to understand the molecular mechanisms mediated by epigenomic effectors to modulate transcription.

3. Nucleosome dynamics impact transcription

An unavoidable side effect of the structural organization of chromatin is the occlusion of DNA sequences and thus of its regulatory elements and binding sites. Nucleosomes represent a barrier for RNA Pol II progression, therefore, the coordination of histones sliding, leaving, recycling, depositing and positioning together with RNA Pol II passage is crucial in defining transcriptional activity (Fig7).

Nucleosome positioning and composition are regulated processes that can reflect DNA-related activities such as transcription. Genome-wide analyses of nucleosome landscapes have revealed a general feature of eukaryotic promoters. Two well-positioned nucleosomes, designated ‘‘+1’’ and ‘‘-1’’, separated by a nucleosome-depleted region (NDR) of variable length, demarcate the site of transcription initiation (Jiang and Pugh, 2009). In yeast, a nucleosome is part of the TSS [Albert et al., 2007] while in higher metazoans the TSS does not overlap with a nucleosome, but there is one just downstream (Mavrich et al., 2008).

What determines nucleosome positioning? Some DNA sequences like poly(dA:dT) stretches are unfavorable to DNA wrapping around histones *in vitro* and AT-rich sequences are good predictors of nucleosome-depleted regions *in vivo* (Segal and Widom, 2009). Additionally, DNA-binding activator proteins can recruit nucleosome remodelers and generate nucleosome-depleted regions (Schwabish and Struhl, 2007). Importantly, elongation by RNA Pol II needs cycles of disassembly/reassembly of nucleosomes in coding regions. This complex process implies nucleosome disruption, mobilization and reassembly after the RNA Pol II passage. As a result, a decrease on nucleosomal density can be observed at highly transcribed genes (Lee et al., 2004; Schwabish and Struhl, 2004). Additionally, high rates of histone turnover have been observed at active genes while repressed regions showed low histone turnover in ESCs and *Drosophila* cells (Deal et al., 2010; Deaton et al., 2016). A recent study has shown that transcription is the major cause of old histones eviction, with a more pronounced effect on the variant H3.3 than on the canonical H3.1 (Torné et al., 2020).The authors also described a mechanism ensuring histone recycling and new deposition dependent on the histone chaperone HIRA during transcription. Overall, these data show the complex processes around nucleosome dynamics which are crucial for transcriptional activity.

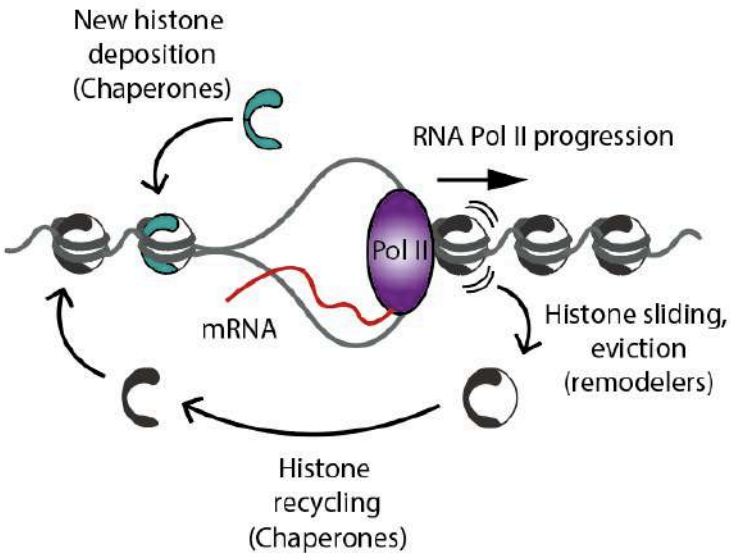

Fig7-Nucleosome dynamics during transcription.
Examples of nucleosomes dynamics during transcription. To allow RNA Pol II progression and reassemble chromatin after, histones are evicted and can then be recycled or a *de novo* histone deposition can take place. These processes are mediated by epigenomic effectors (inspired from Torné et al., 2020).

Despite showing a stereotypical nucleosomal landscape around TSS, not all genes have the same nucleosome stability. At these regions the occupancy of nucleosomes containing the histone variants H3.3/H2A.Z was observed in *Drosophila* and yeast (Henikoff et al., 2008; Xi et al., 2011) and it was shown that these are highly unstable nucleosomes. Although why these nucleosomes are unstable remains unclear, this could provide a mean to achieve NDR regions and promote transcription. Additionally, genome-wide characterization of *in vivo* promoter nucleosome landscapes in yeast revealed two types of promoters. One type is characterized by the presence of dynamic, unstable nucleosomes and is found at highly expressed genes. The other type, contains well-known stable nucleosomes and is found at less frequently expressed genes. Current hypothesis is that the presence of dynamic nucleosomes at highly expressed genes helps to rapidly unwind DNA and as often as necessary, resulting in an increased access of transcriptional machinery to the promoter (Kubik et al., 2015). Accordingly, TSSs of many constitutively expressed housekeeping promoters are usually depleted of nucleosomes and so depend less on nucleosome remodeling (Cairns, 2009; Ganapathi et al., 2005; Rach et al., 2011). In contrast, tightly regulated genes, depend more on remodeling factors to clear their promoters. These data highlight the importance of nucleosome positioning in transcription activity.

To achieve nucleosome depleted regions necessary for transcription, a specific interplay between different categories of epigenomic effectors can take place. Nucleosome remodelers play a crucial role in generating NDRs but they are not the only actors in this process. Indeed, acetylation of histone tails can eliminate positive charges on this residue, decreasing thus their interaction with the negative charged DNA and result in chromatin decompaction (Bannister and Kouzarides, 2011). Many chromatin remodeling enzymes contain protein motifs that recognize modified histones, opening thus the possibility of an interaction between these epigenomic effectors. Interestingly, two *in vitro* studies using budding yeast enzymes showed such interaction. First, Carey and colleagues observed that histone acetylation is sufficient to recruit the remodeler Rsc to nucleosomes (Carey et al., 2006). In turn, Rsc facilitated the passage of RNA Pol II in an ATP-hydrolysis dependent manner, resulting in stimulation of transcription elongation. Second, a study using several yeast nucleosome remodelers showed that specific patterns of histone acetylation resulted in increased rate of nucleosome repositioning or eviction (Ferreira et al., 2007). Notably, a single histone mark combined with different remodelers had different outcomes. This was observed for histone H4 tetra-acetylation, which increased nucleosome transfer by the Rsc complex but reduced the activity of two other remodelers, Chd1 and Isw2. These data show how histone PTMs can recruit remodelers and/or alter their activity impacting thus nucleosome dynamics. In budding yeast, the cooperation between the remodeler complex Swi/Snf and the histone deacetylase complex Saga was found necessary for induction of the stress response transcriptional program (Sanz et al., 2016). Upon cell wall stress, the TF Rlm1 is activated by phosphorylation and interacts with the Swi/Snf complex. It was then observed that Saga subunits are recruited to the promoter of cell wall stress-responsive genes, in a Rlm1 and Swi/Snf-dependent manner, where it acetylates histone H3 at promoters. Interestingly, both Swi/Snf and Saga complexes were necessary for H3 eviction, Rlm1 recruitment and subsequent gene expression. This data suggests thus a cooperation between epigenomic effectors in order to create a favorable chromatin environment for transcriptional activity. Nonetheless, further *in vivo* studies are required to investigate if this is a more general mechanism for the establishment of basal transcriptional programs, to identify the actors at play and assess the impact on transcription

A relationship between nucleosome density and transcription level was also observed in mouse ESCs (Fig8). The comparison of nucleosome density profiles for genes with

varying levels of transcriptional activity showed that patterns emerge from a featureless profile as transcription level elevates. Interestingly, the qualitative trends observed in mouse ESCs are conserved across multi-cellular organisms (Jiang and Zhang, 2021). A correlation between nucleosome positioning and transcription has been observed for a while but how positioning is determined has not been entirely elucidated. Recently, a "tug-of-war" model was proposed based on stochastic simulations. On one hand, enzymes that regulate and reduce inter-nucleosome spacing tend to drive the nucleosome array away from the transcription start site (TSS). On the other hand, positioning enzymes help to align nucleosomes towards the TSS. Competition between these enzymes results in two types of density profiles with well- and ill- positioned +1 nucleosome that qualitatively reproduce in vivo results from both yeast and mouse ESC (Jiang and Zhang, 2021). This results show how the coordinated activity of enzymes could potentially achieve a specific nucleosome positioning.

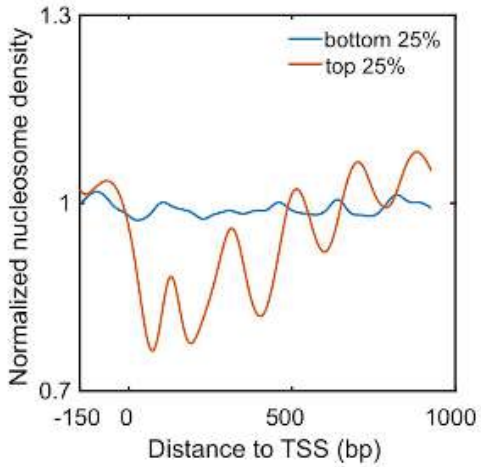

Fig8-Nucleosome density is correlated to transcription level.
Normalized nucleosome density profile in mouse embryonic stem cells near the transcription start site (TSS). Genes were separated depending on levels of transcription activity. Bottom 25% corresponds to the quartile of most inactive genes and top 25% corresponds to the quartile of most active genes (from Jiang & Zhang, 2021).

Overall, these data show the tight link between nucleosome dynamics and the process of transcription. Complex mechanisms and numerous actors determine nucleosome positioning, composition and movements. Further research will be thus necessary to continue to elucidate these mechanisms and their impact on transcription.

4. The heterochromatic H3K9me3/HP1 pathway

Heterochromatin is an architectural feature of eukaryotic chromosomes. It corresponds to tightly packed chromatin and refers to molecular subtypes of transcriptionally repressed domains. One type of heterochromatin has been named "constitutive heterochromatin" since it's found at structural chromosomal elements such as telomeres and pericentromeres, as well as transposable elements (TEs) and virus-derived sequences (Allshire and Madhani, 2018). This chromatin is distinguished by the formation of heterochromatin blocks characterized by histone hypoacetylation, methylation of histone H3 at lysine 9 (H3K9me) and the presence of the protein HP1 (Heterochromatin Protein 1).

Loss of H3K9me3 following depletion of silencing guides or effectors is associated with transcriptional upregulation of normally silenced regions decorated with this mark (Karimi et al., 2011; Matsui et al., 2010; Smolko et al., 2018). Additionally, artificial recruitment of H3K9 histone methyltransferases or other silencing factors such as HP1 to euchromatin regions result in transcriptional silencing of reporter genes (Ayyanathan, 2003; Ivanov et al., 2007). These data suggest thus, that repressive mechanisms use H3K9me3 and HP1 to achieve this transcriptional state.

Chromatin-based silencing can be achieved by a denser chromatin structuring process that results in efficient exclusion of RNA polymerases or other nuclear enzymes. To create this structure, di- and tri-methylation of H3K9 act as molecular anchors to recruit proteins that either directly modify chromatin or recruit others that do so (see below). Additionally, HP1 proteins can also serve as platforms to establish a repressive chromatin structure. For example, the two HP1 proteins in S. pombe, Swi6 and Chp2 are associated with histone deacetylases (HDACs) (Fischer et al., 2009; Yamada et al., 2005). Swi6, Chp2 and their associated HDACs were found to limit RNA Pol II occupancy at centromeric repeats. Furthermore studies *in vitro* and *in vivo* showed that the Swi6 protein can promote repression by capturing transcripts and direct them to the RNA degradation machinery (Keller et al., 2012). Finally, recent work has indicated roles of human and *Drosophila* HP1 in regulating higher-order chromatin structure through the formation of liquid-liquid phase-separated compartments (Larson et al., 2017; Strom et al., 2017). These studies suggest that heterochromatin-mediated gene silencing occurs in part, through sequestration of compacted

chromatin in specific nuclear compartments. These compartments can isolate repressed chromatin from transcription factors and machinery while maintaining a high concentration of factors required for heterochromatin formation, such as HP1 and H3K9 methyltransferases.

How is H3K9me3 chromatin targeted to specific genomic territories? Two main mechanisms have been described relying: (i) on an RNA-based recognition system to appropriately localize histone modification enzymes and HP1 proteins and initiate the heterochromatin formation cascade or (ii) on protein recognition of specific DNA sequences (Fig9).

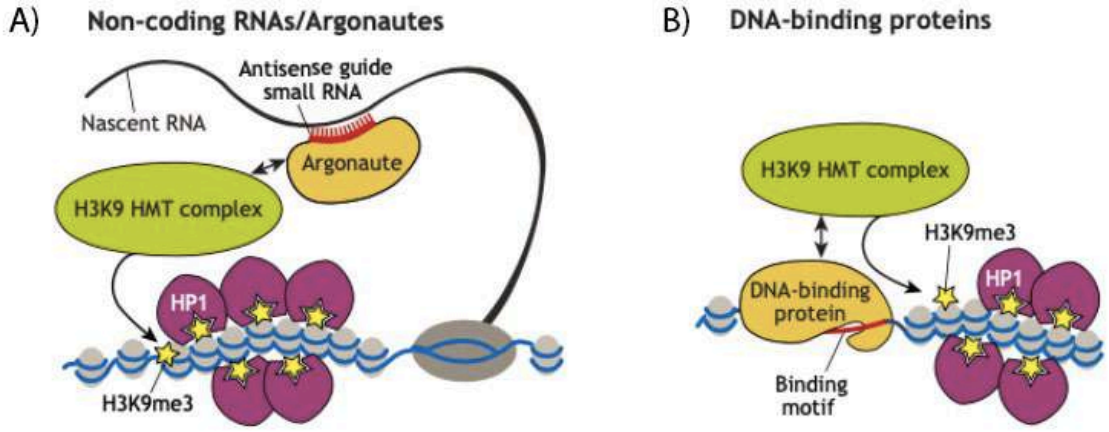

Fig 9-Recruitment of the H3K9me3 machinery

H3K9 methyltransferases can be recruited to specific genomic targets by (A) small non coding RNAs associated with Argonaute proteins or (B) by sequence specific DNA-binding proteins. (Adapted from Ninova et al., 2019)

Studies mainly in *S. pombe* helped elucidate the mechanisms of heterochromatin nucleation. It was observed that the deletion of *argonaute* (*ago*), *dicer* (*dcr*) and *RNA-dependent RNA polymerase* gene homologs resulted in loss of H3K9 methylation and derepression of transgenes at centromeres (Volpe, 2002). The depleted genes belong to the RNA interference (RNAi) machinery hinting thus on a mechanism involving this pathway. Additionally, induced double-stranded RNA (dsRNA) in fission yeast was sufficient to generate synthetic small interfering RNAs (siRNAs) and direct H3K9me-heterochromatin formation at the locus producing the dsRNAs [Simmer et al., 2010]. Verdel and colleagues purified indeed a nuclear Ago complex, the RITS (RNA-induced initiation of transcriptional gene silencing) complex,

which uses Dcr-generated siRNAs to localize to heterochromatic domains (Verdel, 2004). Indeed, when cells lack Dcr, the loss of siRNAs is accompanied by delocalization of RITS from centromeric regions. Further research revealed that the RITS complex can associate with the Clr4 complex, which contains the Clr4 enzyme, the sole H3K9 methyltransferase in fission yeast (Zhang et al., 2008). This interaction promotes thus nucleation of heterochromatin at determined regions. The RITS complex associates also with the RNA-dependent RNA polymerase complex (RDRC). RDRC uses primary transcripts as templates for synthesis of dsRNA, which is subsequently processed into siRNAs, thereby increasing siRNA production and amplifying the system of heterochromatin formation (Allshire and Madhani, 2018). The established model proposes thus that RNA Pol II transcribes RNAs from heterochromatin repeats which are then processed into siRNAs. These siRNAs are next bound by the Ago1 protein and are used to target homologous nascent repeat transcripts, resulting in the recruitment of silencing factors such as H3K9 methyltransferases. In metazoans, RNAi-based targeting and silencing mechanism involve another class of small non coding RNAs, piwi-interacting RNAs (piRNAs). This system of silencing is used for transposable elements in most Metazoa, particularly in the female germline and will be detailed in section III-3-A.

RNA independent mechanisms to target heterochromatin nucleation involve DNA binding proteins. In mammalian systems, the KRAB-containing zinc finger proteins (KRAB-ZFPs) have been found to induce H3K9me3-dependent silencing at endogenous retrovirus targets (Wolf et al., 2015) and TEs (Ecco et al., 2016; Imbeault et al., 2017), presumably by recruitment of H3K9 methyltransferases. Additionally, a high concordance between heterochromatic repeat regions and some transcription factor-binding sites in mouse has been observed. For example, paired box 3 (Pax3) and Pax9 have binding sites in pericentric heterochromatin and depletion of these factors results in derepression of satellite transcripts and impairment of heterochromatic marks (Bulut-Karslioglu et al., 2012). The data points to a model where specific DNA-binding proteins could attract silencing effectors to their DNA-bound region. Interestingly, in some cases, binding of specific transcription factors to euchromatic sites appears to trigger the formation of small blocks of heterochromatin to achieve silencing. In *Drosophila*, phosphorylated Hers (Histone gene-specific Epigenetic Repressor in late S phase) binds to histone gene regulatory regions and anchors HP1a and the H3K9 methyltransferase Su(var)3-9 to induce silencing of this repeated gene cluster (Ito et al., 2012). Similarly, the corepressor TIF1b/KAP1 (Transcription Intermediary Factor 1-

beta/KRAB-associated protein 1) targets HP1 to specific loci in the euchromatic arms to silence those genes (Cammas, 2004; Schultz, 2002). Importantly, in contrast to pericentric heterochromatin, there is little spreading (see below) of the silencing marks in these cases, suggesting a silencing state that differs in some key characteristics from classic heterochromatin formation. Unfortunately, there has been little study of this process to date.

Once established, histone methylation serves as a molecular anchor. In *Drosophila*, di- or tri-methylation of H3K9 by the HMT Su(var)3-9 provides binding sites for HP1a resulting in a stable interaction (Eskeland et al., 2007; Jacobs et al., 2001). Chromatin-bound HP1 in turn mediates the recruitment of more HMTs Su(var)3-9, either directly or through the bifunctional binding partner, Su(var)3-7 (Delattre et al., 2000). Su(var)3-9 is the main producer of H3K9 methylation and as long as it carries out this reaction on an adjacent histone, the heterochromatin assembly process continues. By recognizing both the histone modification and the enzyme responsible for that modification, HP1a provides a mechanism for heterochromatin spreading and maintenance (Fig10). Similarly, in fission yeast, nucleated heterochromatin repeat elements can spread in a Swi6/HP1-dependent manner (Hall, 2002). A key feature of heterochromatin is thus its ability to propagate, thereby influencing gene expression in a region-specific, sequence-independent manner.

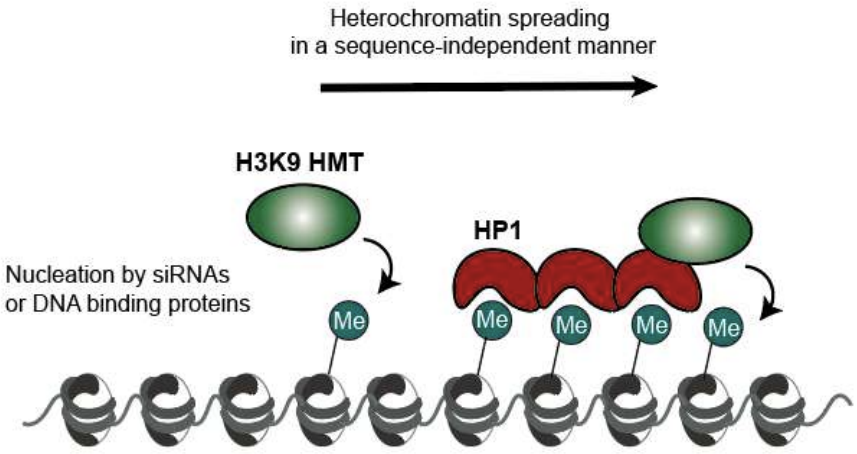

Fig 10-H3K9me3/HP1 heterochromatin spreading

Once nucleated, di-and tri-methylated H3K9 provide a binding platform for HP1 proteins. In turn HP1 can recruit H3K9 methyltransferases and the process is repeated, thereby spreading heterochromatin structure in a region-specific manner. Abbreviations: HMT= histone methyltransferase, Me= methyl mark.

Because heterochromatin can spread, mechanisms to restrict its expansion are necessary to avoid erroneous and potentially deleterious gene silencing. tRNA genes are a class of heterochromatin-spreading barrier conserved from yeast to human (Raab et al., 2012; Scott et al., 2006). Binding sites for transcription factors associated to the RNA Pol III can function as heterochromatin barriers independent of tRNA genes, revealing their role in barrier function. Another mechanism to restrain heterochromatin spreading is the generation of nucleosome depleted regions. This is observed at the silent mating type region in fission yeast which contains large nucleosome free regions that form a 'gap' in chromatin over which some reader–writer machineries cannot cross (Garcia et al., 2010). The existence of multiple mechanisms to limit heterochromatin spreading highlights the importance of proper chromatin organization in maintaining genome homeostasis.

Interestingly, HP1a can also have a role in transcription of genes residing in heterochromatin. In *Drosophila*, two genes, *light* and *rolled*, found within a heterochromatin domain show a loss of expression upon depletion of HP1a (Lu et al., 2000; Wakimoto and Hearn, 1990). There is a loss of silencing marks at the TSS of active genes in these domains although the usual heterochromatic marks, including H3K9me2/3, are still present upstream and across the gene body. The TSSs are occupied by RNA Pol II and are flanked downstream by nucleosomes with euchromatic marks. This data shows that the presence of H3K9 methylation on the gene body, but not on the TSS, is compatible with transcription. Further work will be required to determine if the specific localization of these marks has a role on active transcription.

Furthermore, a non-repressive role for H3K9me3 was described in a recent study by the Torres-Padilla laboratory. Immediately after fertilization, the paternal pronucleus of mammalian embryos acquires *de novo* H3K9me3 via catalysis by the methyltransferase SUV39H2 which in turn is negatively regulated by satellite RNAs transcribed from the paternal pericentromere. *De novo* H3K9me3 is initially non-repressive for gene expression, but instead bookmarks promoters for compaction later during development, suggesting that the mark is not repressive per se (Burton et al., 2020). This study provides an illustration of the complex role of heterochromatin and demonstrates that heterochromatin function can vary depending on the cellular and developmental context.

In conclusion, H3K9/HP1 heterochromatin is a potent silencing mechanism. However, the actors involved in this pathway seem to have a more complex role in transcriptional regulation than just promote transcriptional repression.

5. Polycomb effectors mediate gene silencing…and more?

The Polycomb group (PcG) genes were first discovered in Drosophila as crucial epigenetic repressors of homeotic (*Hox*) genes. They have since then been discovered to control hundreds of genes in insects, mammals and many other branches. Indeed, PcG genes and targets are conserved in evolution and their study has allowed unveiling regulation of a plethora of cellular processes.

The PcG machinery is mainly composed of two biochemical complexes: Polycomb Repressive Complex 1 (PRC1) and PRC2. PRC1 contains the E3 ligase activity for monoubiquitylation of H2A at Lys 118 in Drosophila and Lys 119 in mammals (Wang et al., 2004). PRC2 contains histone methyltransferase activity specifically targeting H3K27 (Cao et al., 2002; Czermin et al., 2002; Kassis et al., 2017; Kuzmichev, 2002; Müller et al., 2002; Schuettengruber et al., 2017). H3K27me3 is found on many silenced regions in a cell-specific manner (Beuchle et al., 2001; Plath, 2003; Ringrose and Paro, 2004). This mark is deposited by the histone methyltransferase E(z)/EZH2, a subunit of the PRC2 complex and its catalytic activity is required for *Hox* gene repression (Czermin et al., 2002; Müller et al., 2002). Additionally, it was observed that flies carrying a point mutation in lysine 27 of H3 fail to repress PRC2-target genes demonstrating thus the need of this mark for PcG- mediated repression (Pengelly et al., 2013). Contrariwise, it was observed that the mark catalyzed by the PRC1 complex is dispensable for repression of canonical PcG targets during *Drosophila* embryogenesis (Kahn et al., 2016; Pengelly et al., 2015). H2AK118ub is carried out by the PRC1subunit Sce in Drosophila. Flies with catalytically inactive Sce or with pointmutated H2A were generated and it was observed that H2Aub-deficient animals fully maintain repression of PRC1 target genes. These data suggest thus that catalytic activity of PRC2, *i.e.*, H3K27 methylation, is necessary for repression however PRC1 represses canonical targets independently of its catalytic activity.

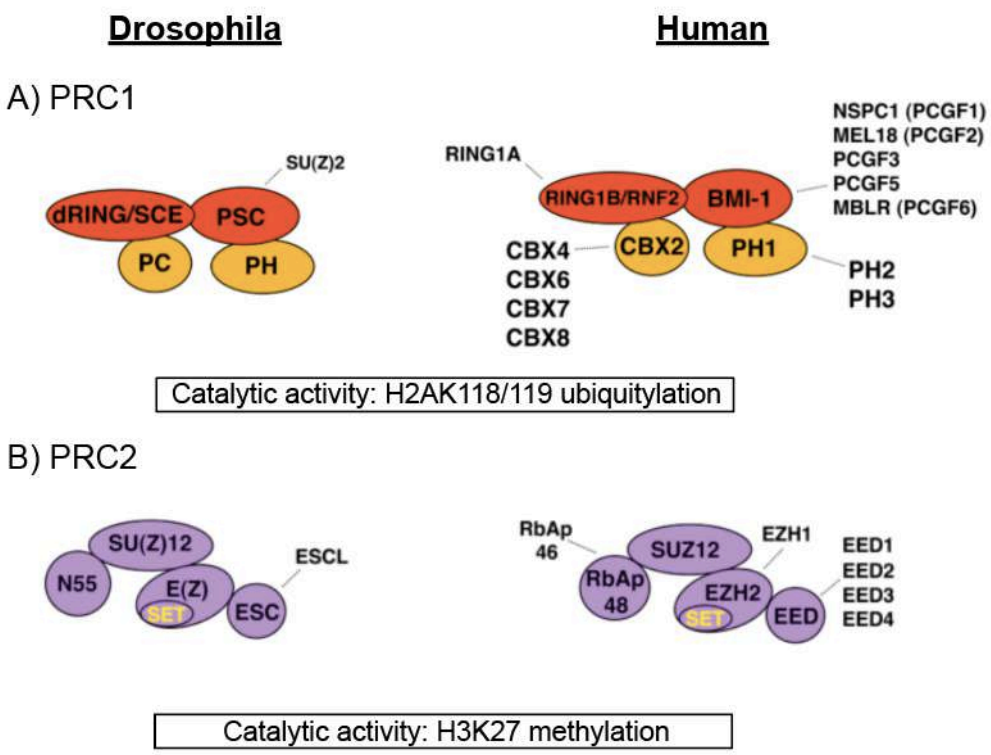

Fig 11-Composition of Polycomb Repressive Complexes (PRC) in *Drosophila* and Human. (A) PRC1 complex contains four core subunits. Its catalytic activity is ubiquitylation of H2AK118 in *Drosophila* and H2AK119 in mammals, conferred by the dRING/RING subunit. (B) PRC2 complex contains four core subunits. Its catalytic activity is methylation of H3K27 conferred by the subunit E(z)/EZH2. Dashed lines indicate alternative subunits (Simon and Kingston, 2013).

What is then the role of H3K27me3? It has been suggested that H3K27me3 stabilizes interactions between DNA-bound PcG complexes and the surrounding chromatin. It was observed that abolishing H3K27me3 within a promoter or transcriptional unit of a target gene impairs the interactions of DNA-anchored PcG complexes with these gene elements (Kahn et al., 2016). By promoting interaction stability with these gene regions, H3K27me3 would deliver PcG complexes that can interfere with transcription. Stable loops could also contribute to spreading and maintenance of H3K27me3 from its anchor points, thereby reinforcing the system. Additionally, a bulk tri-methylation of H3K27 may contribute to the repression directly by competing with acetylation of H3K27, a mark involved in gene activation. Furthermore, PRC1 subunit Pc/CBX can inhibit the acetyltransferase activity of dCBP/CBP (Tie et al., 2016, 2009). Even if the importance of H3K27me3 for polycomb-

mediated silencing has been shown, the precise mechanism by which it allows gene repression is not fully understood.

Initially, it was observed that PcG proteins and H3K27me3 marked histones accumulate in discrete nuclear foci: “Polycomb bodies” (Buchenau et al., 1998; Messmer et al., 1992), indicating that nuclear compartmentalization could play a functional role in Polycomb-mediated repression. Interestingly, interactions with elements of the nuclear periphery seem to be important for the formation of these compartments and for gene repression. Indeed, the knock-down of lamin A/C causes the dispersion of Polycomb bodies and leads to impaired PcG-mediated transcriptional silencing in both mammalian and *Drosophila* cell lines (Cesarini et al., 2015; Marullo et al., 2016). Nuclear compartmentalization could thus play an important role in PcG-mediated silencing.

Although targets and PcG proteins are well conserved, the mechanisms to recruit them at target sequences vary between species. The *Drosophila* genome is equipped with, Polycomb Response Elements (PREs), these are discrete DNA elements to which PRC1 and PRC2 are targeted. These elements contain binding sites for many different DNA-binding proteins such as Pho, GAF/Psq, Dsp1, Spps, Zeste, Grh, Adf1, Cg and many others (Blastyák et al., 2006; Brown and Kassis, 2010; Déjardin et al., 2005; Orsi et al., 2014; Ray et al., 2016). These TFs play an important role in PcG recruitment however none of them is sufficient to recruit PcG complexes on their own. Initially, a hierarchical recruitment model was proposed in which TFs recruit PRC2, which subsequently recruits PRC1 via the interaction of the Pc subunit with the PRC2-deposited mark, H3K27me3. Accumulating evidence has challenged this model (Dorafshan et al., 2017). For instance, it has been observed that PRC1 can bind PREs in the absence of PRC2 but at many PREs, PRC2 requires PRC1 to be targeted (Kahn et al., 2016). Additionally, PRC1-bound regions devoid of H3K27me3 exist in both *Drosophila* and human cultured cells (Loubiere et al., 2016; Schwartz et al., 2006). Moreover, none of the histone marks deposited by PRCs complexes are required for their targeting at PREs, suggesting that PREs work upstream to histone mark deposition (Kahn et al., 2016). The relationship among TFs, PRC1, and PRC2 seems thus cooperative rather than hierarchical. Whilst PRE characterization in flies is well advanced, their mammalian counterpart has not been clearly identified. In mammals it has been shown that CpG islands can recruit PcG proteins (Lynch et al., 2012; Mendenhall et al., 2010; Reddington et al., 2013), a genomic feature (CpG islands) that has not been found in flies. Nonetheless, similarly to *Drosophila*, *de novo* PRC2 recruitment is independent of

H3K27me3 and H2AK118ub in ESCs (Lavarone et al., 2019). Some mammalian PREs have binding sites for TF important at *Drosophila* PREs (Kassis and Brown, 2013). For example, a homolog of the Drosophila protein Polycomb-like, can bind DNA and recruit PRC2 in mouse ESCs. It selectively binds regions with high density of unmethylated CpGs which discriminate target from non-target CpG islands (Li et al., 2017; Perino et al., 2018). The quest for mammalian PREs is still a field of active ongoing research that will shed light into the specific targeting PcG proteins in mammals.

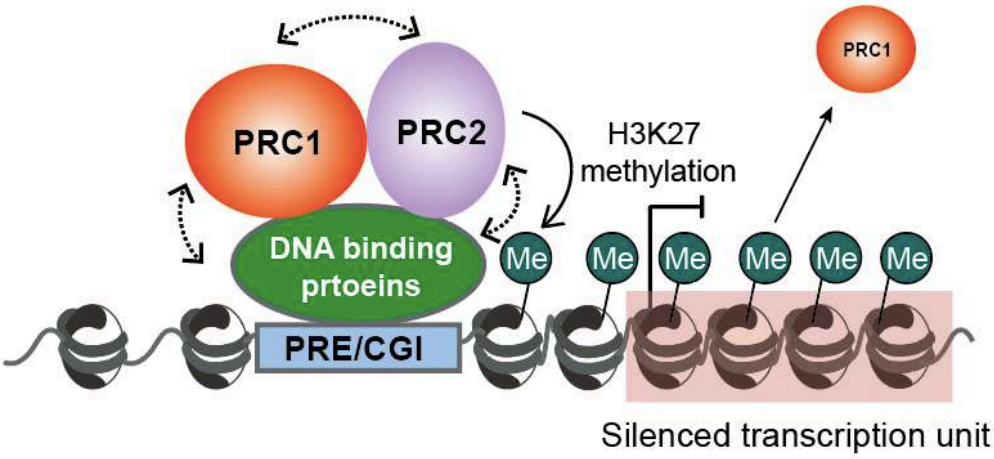

Fig 12-Polycomb Repressive Complex recruitment

PcG proteins are recruited to specific DNA sequences, in flies these are Polycomb Response Element (PREs). In mammals CpG islands have been found capable of recruiting PcG proteins. PREs contain binding sites for numerous DNA binding proteins important for Polycomb Repressive complexes (PRC) recruitment. Dashed arrows represent a cooperative relationship between DNA binding proteins and PRCs to target them at PREs/CGIs. PRC2 catalyzes H3K27me3 necessary for transcriptional silencing and PRC1 is capable of binding this modification thereby stabilizing their recruitment to chromatin.

Although many elements required for targeting and establishment of PcG-mediated repression are known, more and more evidence are revealing other roles for the actors involved. Firstly, fragments of DNA that contain PREs have been shown to mediate gene activation in transgenes under certain conditions and at some chromosomal insertion sites (Kassis and Brown, 2013), suggesting that these regulatory elements can have dual regulatory functions. Indeed, during *Drosophila* embryogenesis, some classic PREs can recruit tissue-

specific TFs and function as developmental enhancers *in vivo*, activating spatio-temporal expression of a reporter gene (Erceg et al., 2017). Conversely, a subset of developmental enhancers binds the PcG complex, Pho-RC, resulting in polycomb-dependent transcriptional silencing. This dual activity of *cis*-regulatory elements may help fine-tune gene expression and ensure the timely maintenance of cell identities. The same *cis*-regulatory element can thus have opposite outcomes on gene transcription in a context-dependent manner. Furthermore, the characterization of the *in vivo* role of the two PREs near the *vestigial* (*vg*) gene, reported a promoter that requires a PRE for expression during development (Ahmad and Spens, 2019). On one hand, the PRE near the *vg* promoter is required for its activation and not for repression. On the other hand, the distal PRE, located in the middle of the chromatin domain, is required for high-level of H3K27me3 in the domain. Surprisingly, removal of both PREs does not completely eliminate H3K27me3 across the *vg* domain and this residual methylation is similar to that in cells where the *vg* gene is active. These data confirms that PREs can also have a role in gene activation and the definition of their roles might depend on the factors they bind.

Interestingly, the binding of factors implicated in PcG silencing are not incompatible with transcription. PRC1 components were found to bind actively transcribed genes in *Drosophila* larval imaginal discs and human cultured cells (Loubiere et al., 2016). Strikingly, despite the proven need of H3K27me3 for polycomb-mediated repression, its presence was not incompatible with transcription of the *vg* gene (Ahmad and Spens, 2019). Normal transcription of the *vg* gene occurs concomitantly with a basal enrichment of H3K27me3 at the endogenous locus. This shows the complexity of the roles of the PcG proteins.

We also mentioned that PRC1 can be recruited independently of H3K27me3, suggesting that it might have functions independently of PRC2. It was observed in *Drosophila* that PRC1 components are targeted to a distinct set of genes that lack H3K27me3 during larval development (Loubiere et al., 2016). The redeployment of PRC1 was also observed in human differentiated cells when compared to embryonic stem cells. In both species PRC1-only gene targets were involved in regulation of cell proliferation, polarity and signaling. Mutations in PRC1, but not PRC2 resulted in the upregulation of a majority of these new target genes, suggesting that PRC1 has a role dampening a specific subset of genes independently of PRC2. Moreover, RNAi depletion of PRC1 subunits in *Drosophila* cell culture alters phosphorylation of RNA Pol II at most active genes and enhancers (Pherson et al., 2017). These effects coincide with changes in nascent RNA density indicating altered transcriptional

elongation and RNA processing. Although the mechanisms by which PRC1 can alter gene transcription are not fully elucidated, these findings describe a role for PRC1 components beyond epigenetic silencing.

Overall, these data reveal the complexity of the Polycomb system showing that factors and DNA regulatory elements involved can play different roles in a context-dependent manner, hence the inability to establish absolute rules for its role in transcriptional regulation.

6. Counteracting repression to promote activation

Gene repression can be accomplished by creating a chromatin configuration that blocks access to the large number of proteins required for transcription. A way to promote gene activation is thus to counteract silencing mechanisms.

There is a regulatory interplay between epigenomic effectors that supposes a balance between their activities in order to ensure the proper transcriptional outcome. One of the most well-studied epigenetic regulatory systems is the Polycomb group (PcG) and Trithorax groug (TrxG) genes. These two groups of genes were discovered in *Drosophila* by their opposing effects on homeotic gene (*Hox*) expression. PcG proteins exert a negative effect on transcription while TrxG are positive regulators. Given the complexity of factors required for gene expression, the biochemical nature of TrxG proteins is a very heterogeneous group that includes remodelers and histone modifiers, acting at different levels of gene transcription (Kassis et al., 2017; Kingston and Tamkun, 2014; Schuettengruber et al., 2017).

How can regulators of these groups achieve antagonistic effects at their targets? One proposed mechanism by which TrxG can promote activation is by counteracting Polycomb-mediated repression. This was proposed for the TrxG histone methyltransferases Trx and Ash1. Indeed, genetic studies in *Drosophila* showed that the removal of PcG complexes reactivates genes even in the absence of Trx and Ash1, suggesting that these proteins function as PcG antirepressors rather than direct activators (Klymenko and Müller, 2004). Trx and Ash1 methyltransferases target H3K4 and H3K36 respectively, both of which are considered active marks (see section II-7). In agreement with genetic studies, *in vitro* assays using

engineered methylated histones showed that H3K4me3 or H3K36me2/3 can inhibit H3K27 methylation on the same histone by fly or human PRC2 complex (Schmitges et al., 2011). Therefore, these data suggest mechanistic antagonism between these two groups could be mediated by histone PTMs.

As mentioned, the TrxG encompasses a great diversity of biochemical activities indicating that mechanisms involving other type of epigenomic effectors could also be at play. Several subunits of the nucleosome remodeler SWI/SNF complex, including the catalytic subunit, have been classified as TrxG proteins. The opposition between PRCs and the SWI/SNF complex has been the focus of extensive research especially because of its implication in development and disease such as cancer (Kadoch and Crabtree, 2015). Recent studies have unveiled the mechanisms for the interaction between these two groups of regulators. It was observed in cultured cells, that recruitment of the mammalian SWI/SNF complex leads to a rapid, ATP-dependent eviction of both PRC1 and PRC2 (Kadoch et al., 2017). The reversal of this process results in reassembly of Polycomb-mediated heterochromatin. This study proposes thus a mechanism in which a TrxG remodeler opposes Polycomb complexes by their active removal, resulting in chromatin accessibility (Fig13). Interestingly, a recent study reported that degradation of the SWI/SNF ATPase subunit in mouse ESCs resulted in derepression of genes highly occupied by Polycomb, such as *Hox* genes, suggesting also a role for SWI/SNF in promoting PcG-based repression (Weber et al., 2021). Upon rapid depletion of the catalytic SWI/SNF subunit, PRC1 and PRC2 are redistributed away from sites where they usually accumulate, like *Hox* clusters. Collectively, these findings reveal the complexity of the regulatory interplay of the Polycomb-Trithorax axis to achieve proper gene espression.

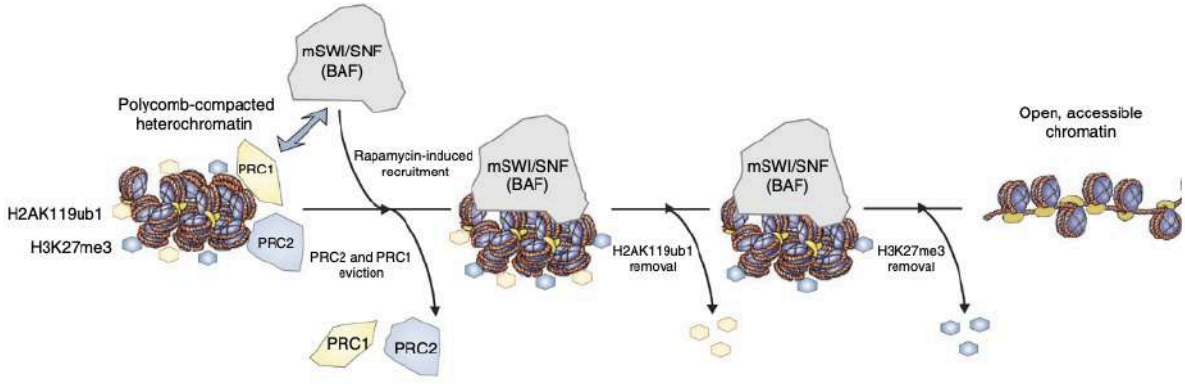

Fig 13-Model for opposition between mSWI/SNF and Polycomb

Recruitment of the mSWI/SNF complex to Polycomb-repressed regions leads to an ATP-dependent eviction of PRC1 and PRC2 complexes, followed by H2AK119 and H3K27me3 removal resulting in an increase of DNA accessibility (modified from Kadoch et al., 2017)

Another mechanism used to counteract repression is to create a boundary between regions of different transcriptional activities. In fly embryos, insulators and their insulator binding proteins (IBPs) can be found at borders between different chromatin landscapes and block the spreading of histone modifications at *Hox* genes (Bowman et al., 2014; Fujioka et al., 2013; Kahn et al., 2006). Additionally, the IBPs, Beaf-32, CP190, dCTCF and Mod(mdg4) can be found enriched at promoter pairs of differentially expressed genes (Nègre et al., 2010) suggesting that insulators and their binding proteins can indeed separate different transcriptional states. However, in *Drosophila* cultured cells, knock-downs of the mentioned IBPs led to changes of the repressive mark H3K27me3 within the chromatin domain rather than spreading outside of it (Van Bortle et al., 2012). IBPs can indeed be found enriched at borders of H3K27me3 domains but only a fraction of these sites can actually restrict the mark's spreading (Schwartz et al., 2012). One possibility is that additional co-factors are necessary to inhibit the repressive mark spreading. Such example was described in *Drosophila* embryonic cells, where the IBP Beaf-32 is capable of recruiting the H3K36 histone methyltransferase dMes-4 to promote transcription of flanking genes by antagonizing the spread of H3K27 methylation from nearby regions (Lhoumaud et al., 2014). More work is needed to identify this type of co-factors and their role at heterochromatin/euchromatin borders. Nonetheless, these data suggest a cooperation between epigenomic effectors to maintain appropriate transcriptional states.

Altogether, this suggests that repression counteracting is the result of an interplay between epigenomic effectors. Although this can contribute to promote gene expression, activation of a gene requires numerous steps and actors and thus many other mechanisms involved.

7. Histone PTMs in active transcription

As for a silenced state of transcription, histone modifications can also be associated to an active state of transcription. For example, genome-wide studies have found H3K27ac and

H3K4me1 at active enhancers, H3K4me3 and H3/H4 acetylation are found at promoters of active genes, H2Bub1 at promoters and gene bodies and finally high levels of H3K79me3 and increasing H3K36me3 towards the 3' end are found at actively transcribing genes (Fig14) (Gates et al., 2017). While these correlations have been widely described, determining which modifications are causal drivers and by which mechanisms they promote transcription is not completely understood. Nonetheless, roles for histone marks, particularly during the elongation step, have been described.

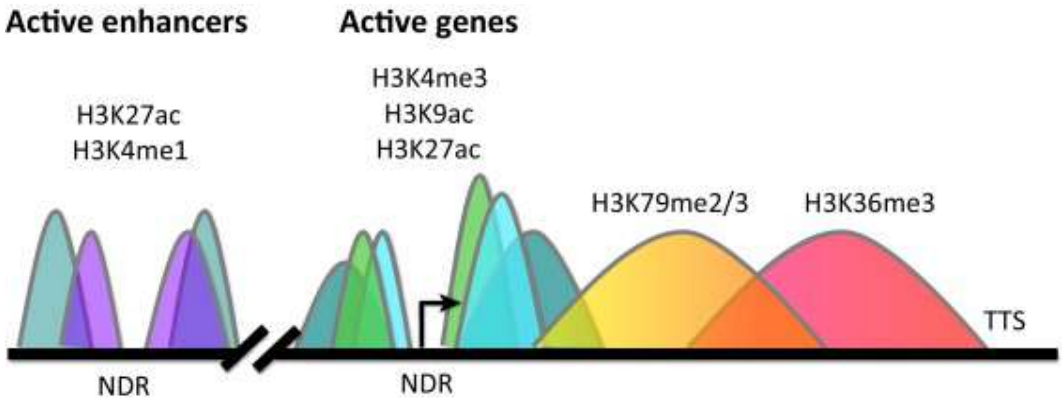

Fig 14-Histone marks at active genes.

Non-exhaustive illustration of the distribution of histone modifications at active genes and enhancers. Regions in color represent ChIP-signal at eukaryotic genes. H3K4me3 and H3K9ac are associated with transcriptionally active gene promoter regions while H3K36me3 and H3K79me3 are localized at gene bodies. H3K27ac localizes to both active gene promoters and enhancer regions, and H3K4me1 is predominantly enriched at enhancers. Abbreviations: NDR= nucleosome depleted region, TTS = transcription termination site, the transcription start site is shown by an arrow (adapted from Gates et al., 2017).

A. Histone PTMs during transcription elongation

Trimethylation of H3K36me3 during elongation has been found important for maintaining transcription fidelity. Studies in budding yeast have indeed investigated the function of H3K36 methylation during transcription. Successive transcription may cause histone hyperacetylation in gene bodies leading to cryptic transcription initiation. The RNA Pol II phosphorylated on the Serine 2 *i.e.*, the elongating Pol II, recruits the histone methyltransferase Set2 to deposit H3K36me3 which serves as a docking site for the Rpd3S

histone deacetylase complex to actively transcribed genes. In turn, Rpd3S catalytic activity, ensures that coding regions remain hypoacetylated, which is important to suppress cryptic transcription initiation (Carrozza et al., 2005; Drouin et al., 2010). Additionally, it was later observed that longer genes and genes transcribed at lower frequency had a stronger dependency on the Set2-Rpd3S pathway to suppress spurious transcription (Li et al., 2007). Transcription elongation-coupled SETD2 recruitment and H3K36me3 deposition are conserved in mammals, as well as the role of H3K36me3 to prevent aberrant transcription initiation [Huang and Zhu, 2018]. However, in mouse embryonic cells it was observed that this depended on the recruitment of DNA methyltransferases to the gene body by H3K36me3 (Neri et al., 2017). Although mechanisms to prevent spurious transcription may be different, these data highlight the importance of H3K36me3 in maintaining transcription fidelity.

Another mark associated with transcription elongation is the monoubiquitination on histone H2B (H2Bub1). This mark has been found enriched at promoters and open reading frames of actively transcribed genes (Kao, 2004; Minsky et al., 2008), suggesting thus a role in gene activation. *In vitro* experiments showed that H2B monoubiquitination by the ubiquitin ligase RNF20/40 jointly with the ubiquitin-conjugating enzyme UbcH6 facilitates displacement of the H2A/H2B dimer from the core nucleosome, facilitating RNA Pol II passage and enhancing transcript elongation rates on chromatin templates (Pavri et al., 2006). This effect was observed while H2ub1 remained in the chromatin but *in vivo* observations in yeast showed that both ubiquitination and deubiquitination are important for full transcription activation at the *Gal1* promoter (Henry, 2003). Further research is needed to understand the full extent of this histone mark on transcription initiation and elongation.

These data show the implication of histone PTMs in elongation and reflects how the epigenome can regulate gene expression at different points of the transcription process.

B. Is H3K4me3 instructive for transcription activation?

A connection between H3K4 methylation and transcriptional activity was first evoked when this mark was observed to decorate the transcriptionally active macronucleus but not the transcriptionally inert micronucleus in the single-celled eukaryote *Tetrahymena*. (Strahl et al., 1999). When mapped in genome-wide experiments, the histone mark H3K4me3 was

found at TSSs of transcriptionally active genes in various organisms and the levels of this mark were strongly correlated to nascent transcripts (Bernstein et al., 2005; Guenther et al., 2007; Heintzman et al., 2007; Howe et al., 2017; Nojima et al., 2015). This led to the classification of H3K4me3 as a hallmark of active promoters resulting in the use of it as a marker of active transcription. Supporting this view, studies in human cultured cells showed that H3K4me3 interacts with TAF3, a subunit of the general transcription factor TFIID, facilitating thereby the formation of the transcriptional pre-initiation complex (Lauberth et al., 2013). This resulted in the enhancement of specific p53-dependent transcription in response to genotoxic stress. A more recent study, again in human cells, employed epigenome editing to investigate the role of H3K4me3 in transcriptional activation (Cano-Rodriguez et al., 2016). They used the methyltransferase PRDM9 to locally induce H3K4me3 and observed re-expression of silenced targets. However, maintenance of this re-expression was dependent on chromatin environment, particularly on hypomethylated DNA and H3K79me. Indeed, when H3K4me was targeted to a hypermethylated locus, re-activation was only transient. Yet, the precise contribution of these genomic features are to be determined. Although this study links H3K4me3 to gene (re-)activation, the chosen HMT possesses other targets on histones linked to transcription, for example H3K36 *in vivo*, and H3K9 at least *in vitro* [Koh-Stenta et al., 2014, Powers et al., 2016], none of which were examined. Further studies are required to elucidate if these observations are reproducible at other targets and organisms, particularly in those without DNA methylation like *Drosophila*.

Why is it difficult to study the impact of H3K4me3 on transcription? In yeast the Set1 complex is in charge of mono-, di- and trimethylation of H3K4, therefore altering this enzyme would also impact histone marks other than H3K4me3 (Gu and Lee, 2013). In contrast, human possesses several enzymes catalyzing H3K4 methylation, six Set1 homologs (SET1A, SET1B, MLL1 to 4) but also other enzymes non-related to Set1 (MLL5, SET7 (also called SET9), SMYD1-3, SETMAR, and PRDM9). In *Drosophila*, three Set1 homologs have been identified dSet1, Trithorax (Trx), and Trithorax-related (Trr). Deletion of any of their genes results in lethality in flies, indicating that their target genes may not be redundant. Additionally, loss of *dSet1*, but not *Trx* or *Trr*, leads to a global reduction of H3K4me2/3, suggesting that *Trx* and *Trr* have more specialized functions (Ardehali et al., 2011; Mohan et al., 2011). This diversity complexifies the study of the direct implication of only the H3K4me3 mark due to possible overlapping functions and/or indirect effects on other marks. Indeed, the field is still lacking a conserved model mechanism to support causality between

H3K4me3 and transcriptional activity and accumulating evidence has challenged this causal link.

Several studies in yeast revealed that absence of H3K4me3 has little effect on gene transcription even at genes where H3K4me3 is highly enriched (Margaritis et al., 2012; Ramakrishnan et al., 2016; Weiner et al., 2012). Accumulating evidence in *Drosophila* has also questioned the relevance of H3K4 methylation in transcriptional activation. One of *Drosophila*'s H3K4 HMT, Trx can be cleaved into two proteins Trx-C and Trx-N. Trx-N lacks methyltransferase activity and is associated with broad regions of active genes (Schuettengruber et al., 2009; Schwartz et al., 2010), suggesting that it activates transcription via mechanisms other than histone methylation. Furthermore, the replacement of H3K4 with a non-methylable arginine, revealed that despite the absence of H3K4 methylation, transcriptional activation was still possible and only minimal changes in developmental gene expression were observed (Hödl and Basler, 2012). Methylation of H3K4 is thus dispensable for transcriptional activation and this mark is likely to have a more complex role in chromatin regulation. Furthermore, a recent study in mouse ESCs showed that gene reactivation can occur without reacquisition of H3K4me3 (Douillet et al., 2020). These findings showed thus an uncoupling between transcriptional activation and the histone mark H3K4me3.

Overall, these data show that the role of H3K4me3 cannot be exclusively reduced to that of transcriptional activation.

8. Bivalent promoters

A peculiar class of promoters, known as bivalent promoters, were originally identified in ES cells and are characterized by the simultaneous enrichment of both H3K27me3, associated to gene repression and H3K4me3, commonly associated to gene activation (Berstein et al., 2006, Mikkelsen et al., 2007). The enrichment of these opposing modifications correlates with a low-level expression or no expression (Bernstein et al., 2006). During cell differentiation, these bivalent regions are resolved as they undergo either full transcriptional activation, in which case they preserve H3K4me3 and lose H3K27me3, or stable silencing where they preserve H3K27me3 and lose H3K4me3 (Gaertner et al., 2012; Mikkelsen et al., 2007; Pan et al., 2007; Zhao et al., 2007). Interestingly, in more committed cells, neural progenitors and embryonic fibroblasts, bivalent domains were still present in

different proportions, 8% and 43% respectively (Mikkelsen et al., 2007). To explain this difference the authors proposed that the high number of bivalent domains in embryonic fibroblasts may reflect a less differentiated state and/or heterogeneity in the population analyzed. Nevertheless, at least in neural progenitors, genes where bivalent domains were not resolved, continued to be repressed. These data suggest thus a functional role for bivalent domains.

Genome-wide mapping of bivalent chromatin revealed it is frequently found within promoter regions of developmentally important genes (Bernstein et al., 2006; Lesch et al., 2013), providing a silencing system for these genes while keeping them poised for activation. Like this, during development, certain genes become active in a tissue-specific manner leading to cell lineage specification. These regions have been suggested to "safeguard differentiation" and their malfunction might have a profound impact on the cell (Voigt et al., 2013). Indeed, bivalent domains identified in human tumors, such as ovarian cancer, colon cancer, and glioblastomas, coincide with genomic regions decorated with H3K4me3/H3K27me3 in ESCs (Curry et al., 2018; Hall et al., 2018; Rodriguez et al., 2008). However, the extent of this overlap and the biological significance of these recovered bivalent domains in cancerous cells remains to be investigated.

Despite its apparent importance, bivalency is functionally and mechanistically not well understood. A study in ESCs revealed however that nucleosomes carrying H3K4me3 along with H3K27me3 did so on opposite H3 tails. PRC2-mediated methylation of H3K27 was inhibited when nucleosomes contained symmetrically, but not asymmetrically, positioned H3K4me3, showing that the location of the "active" mark can be decisive for establishment of bivalency (Voigt et al., 2012). Further studies should elucidate the requirements for establishment of these chromatin domains.

Until recently, bivalent domains had not been identified in *Drosophila*. Akmammedov and colleagues used re-ChIP to confirm the co-occurrence of H3K27me3 and H3K4me3 in fly embryos, leading to the uncovering of such bivalent domains (Akmammedov et al., 2019). However, only a handful of endogenous sites, all members of the *Hox* genes, were tested. More studies will be needed to see if these domains are present across the genome of Drosophila at key developmental genes and if their state of bivalency changes during differentiation.

9. Genome folding and transcription

DNA and its associated proteins are confined within the nucleus. This is a topologically constrained and a highly crowded environment. The 3D folding of the eukaryotic genome compatible with all the activities described above is thus a major requirement.

The study of a functional link between higher-order chromatin arrangements and transcription has greatly increased thanks to the rapid development on new techniques. In the mid-2000s, FISH experiments in human fibroblasts, showed the existence of chromosome territories (Bolzer et al., 2005). These territories segregate in regions rich in active genes, typically located in the interior of the nucleus, and regions rich in inactive genes, found at the nuclear periphery. The rapid development of chromosome capture techniques, namely C-based techniques, now allow to assay contact frequency at a genome-wide level. At large scales, Hi-C confirmed two major types of structural domains: A and B compartments. The A compartment corresponds to active chromatin, presents transcriptional activity, higher chromatin accessibility and H3K36me3 deposition. Compartment B contains repressed chromatin in a more compacted state, with low transcriptional activity, associated with the nuclear lamina and presenting H3K27me3 deposition (Lieberman-Aiden et al., 2009; Rao et al., 2014). At a lower scale, chromosomes fold into domains of 100kb-1Mb, with preferential intradomain interactions compared to interdomain interactions. These contact domains are partitioned by boundaries between them and are referred to as topologically associating domains (TADs) (Fig15) (Dixon et al., 2012). The presence of TADs has been confirmed across cell lines and species, indicating that they may represent a conserved feature of genome organization. Importantly, a conserved characteristic across species, is the relationship between gene activity and genome folding (Szabo et al., 2019). Overall, these observations point towards a functional implication of chromosomal organization within the nucleus.

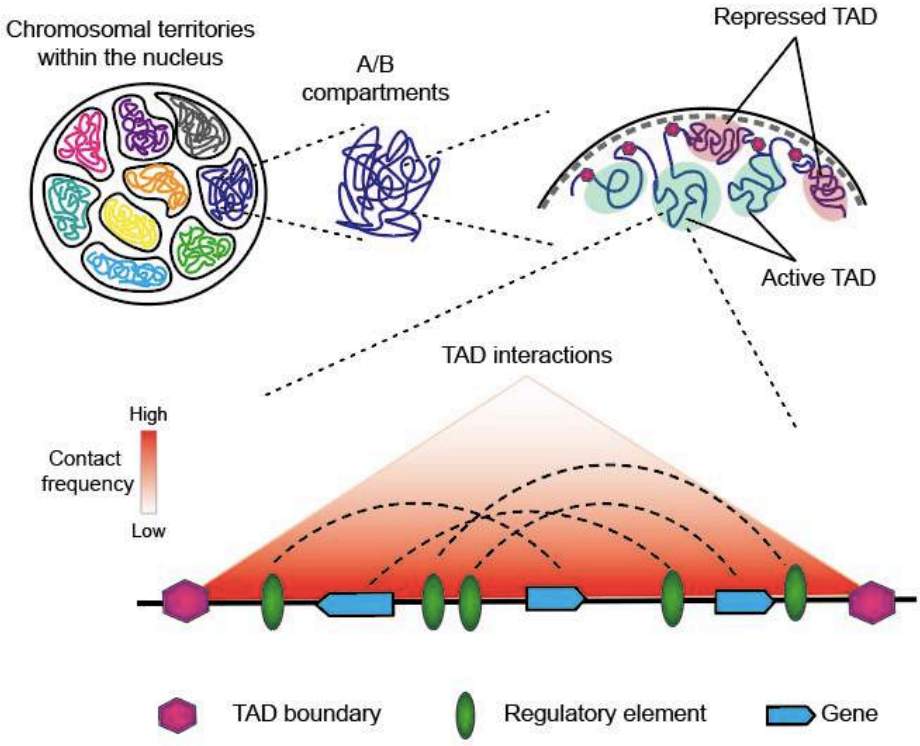

Fig15-Hierarchical organization of the eukaryotic genome

Individual chromosomes occupy specific nuclear spaces, forming chromosomes territories, shown schematically in different colors. At the chromosomal scale, chromatin is segregated into active "A" and repressed "B" compartments. At a finer scale the chromatin fibers are partitioned into higher-order domains of preferential internal interactions defined by boundaries referred to as Topologically Associated Domains (TADs). An example of an active TAD with several interactions between distal regulatory elements and genes within it is shown (Matharu and Ahituv, 2015).

Studies in mammalian cells have shown that disruption of TADs can lead to *de novo* interactions between regulatory elements, such as enhancers, and promoters, resulting in gene misexpression and disease (Flavahan et al., 2016; Franke et al., 2016; Lupiáñez et al., 2015). To fully understand the role of TADs in transcriptional regulation it is thus necessary to understand their formation and maintenance. Notably, TAD boundaries in mammals are frequently enriched in both the transcription factor and insulator CTCF and the structural maintenance of chromosomes (SMC) cohesin complex (Dixon et al., 2012; Phillips-Cremins et al., 2013; Rao et al., 2014) Hi-C maps indicate a strong contact between the CTCF- and cohesin-bound TAD boundaries *i.e*, "corner peaks", suggesting a model wherein CTCF binds its cognate sites and recruits cohesin, which then folds the in-between chromatin into a loop structure. Interestingly, removal or change in orientation of a single CTCF site can abolish or

shift the position of the TAD boundary (de Wit et al., 2015; Guo et al., 2015; Lupiáñez et al., 2015), suggesting that not only the presence of CTCF but also a convergent orientation is important for TAD boundaries in mammals. A loop extrusion model has been proposed (Fig16), in which extruding factors, the engaged cohesin SMC complex, progressively forms larger chromatin loops until it encounters boundary proteins, including CTCF, or until the complex is dissociated (Fudenberg et al., 2017, 2016). This model has been reinforced by recent studies that show that depletion of CTCF, cohesin or its loading factor disrupt loop domains while depletion of the cohesin release factor reinforces the strength of the loops at TAD borders (Nora et al., 2017; Rao et al., 2017; Wutz et al., 2017), suggesting a determinant role for cohesion in loop formation.

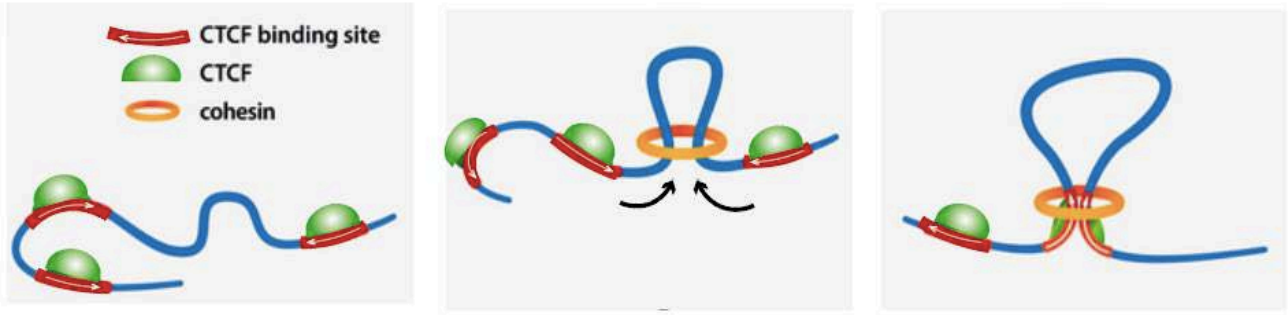

Fig16-Model for loop extrusion

Cohesin binds to chromatin, extrudes a chromatin loop and stalls upon encountering CTCF bound at convergently oriented CTCF sites (Wutz et al., 2017).

TADs are also present in the *Drosophila* genome; however, differences have been observed compared to mammalian TADs. Cohesin is also enriched at TAD borders but there are no interaction loops at these borders and enrichment of dCTCF is minor (Van Bortle et al., 2014). Nonetheless, various insulator proteins have been found enriched at boundaries, including Beaf-32, CP190, Pita, M1BP and Chromator (Cubeñas-Potts et al., 2017; Ramírez et al., 2018; Sexton et al., 2012). Also, combinations of these proteins such as Beaf-32/Chromator or Beaf-32/CP190 are good predictors of boundaries (Wang et al., 2018). Surprisingly, siRNA-mediated depletion of Beaf-32 does not abolish boundaries nor has a significant effect on chromatin interactions (Ramírez et al., 2018). A possibility evoked by the authors is that the transcription factor Dref, who binds almost the exact motif as Beaf-32,

could also play a role in chromatin organization. However, no data to support this hypothesis was presented. It is also possible that depletion of a combination of factors is required to disrupt TAD boundaries in *Drosophila*. Further work is thus needed to determine the role of insulator proteins and of other proteins, such as Dref, at *Drosophila* TAD boundaries.

Other mechanisms could also be responsible for 3D organization of chromosomes. Indeed, in mammals even though a majority of TAD boundaries were associated to CTCF, a fraction turned out to be resistant to CTCF loss (Nora et al., 2017). It was observed in mammals and *Drosophila* that TAD borders were enriched for housekeeping genes (Cubeñas-Potts et al., 2017; Dixon et al., 2012; Rennie et al., 2018; Ulianov et al., 2016), those are zones of active transcription hinting thus on a possible role for this process at TAD boundaries. Furthermore, modeling of chromatin fibers proposes that transcription-associated supercoiling could be involved in driving loop extrusion (Racko et al., 2018), suggesting a role for transcription in TAD formation. Based on Hi-C and RNA-seq data in four fly cell lines of various origins, Ulianov and colleagues proposed that inactive TADs are separated by active chromatin regions (Ulianov et al., 2016). In agreement, super-resolution analysis of immunolabeled repressive H3K27me3 or "active" H3K4me3 marks showed active domains at the borders of repressed ones (Boettiger et al., 2016; Cattoni et al., 2017). Moreover, a recent study observed that the degree of transcriptional activity correlates with the strength of TAD insulation (Luzhin et al., 2019). However, inhibition of transcription in mammals and *Drosophila*, does not abolish TAD boundaries (Du et al., 2017; Hug et al., 2017; Ke et al., 2017) nor its induction is sufficient to create TAD boundaries *de novo* (Bonev et al., 2017). It is therefore likely that additional factors are necessary for TAD formation.

Interestingly, polymer simulations using as single input the experimentally derived epigenome from *Drosophila* embryonic cells, agreed with the folding patterns observed in chromosome conformation capture experiments (Ghosh and Jost, 2018; Jost et al., 2014). Additionally, Ulianov and colleagues proposed a "self-assembly" model where nonacetylated nucleosomes from inactive chromatin aggregate whereas acetylated nucleosomes in inter-TADs and TAD boundaries are less prone to interact (Ulianov et al., 2016). These data suggests that the epigenome is a primary driver of chromosome folding in *Drosophila*. Various factors including, transcription, insulator/architectural proteins, epigenetic marks seem to have a role in TAD formation. Further study is thus necessary to determine which

elements are required to form and maintain these compartments separating transcriptional states. This will also help to understand the transition from one domain to another.

As mentioned before, at a larger scale, chromatin in the nucleus is also segregated according to its transcriptional state. Recent research suggests that liquid-liquid phase separation can result in these non-membrane bound compartments in cells. These studies propose that the nucleus is a phase separated compartment containing several different immiscible liquid-like sub-compartments. Segregation of heterochromatin is driven by phase separation mediated, at least in part, by multivalent hydrophobic interactions of HP1a (Larson et al., 2017; Strom et al., 2017). Additionally, clusters of enhancers, regulating cooperatively gene expression can undergo phase separation by transcriptional coactivators suggesting that active domains may also generate phase-separated compartments (Sabari et al., 2018). Together, these physical forces may account at least in part for the compartmentalization of the nucleus.

Importantly, most data gathered from C-based techniques come from a large number of cells and therefore, only averages are observed. To overcome this, chromatin conformation capture-based techniques have been extended to single cell analysis. These studies have revealed heterogeneity in contacts at the TAD scale from cell to cell, with domains appearing as tendencies that become more visible when averaged over a population of cells (Nagano et al., 2013; Stevens et al., 2017; Szabo et al., 2019). This raises the question of the physical reality of TADs rather than just the result of statistical averages. Also, of their functional relevance if such heterogeneity between cells is confirmed. Further single-cell studies are required to elucidate the conservation of TADs at this scale.

There is still much we do not know about nuclear compartments formation and their role in genomic functions. Nonetheless, data gathered in the last few years indicate that these compartments correspond to a functional subdivision of the genome. However, the need of partition the genome into domains to ensure proper gene regulation is still a mystery that hopefully the combination and continuous improvement of new technologies (single-cell omics, super resolution microscopy, modeling of the chromatin fiber…) will be able to elucidate.

In conclusion, eukaryotic transcription is a complex multistep process subject to numerous modes of regulation. This regulation involves the controlled interaction between regulatory elements in the DNA sequence and proteins with a variety of biochemical activities. Interestingly, regulatory elements in the DNA sequence seem to correlate with gene function, however the molecular mechanisms underlying this apparent specificity are yet to be elucidated. In the nucleus, DNA is organized as a chromatin fiber. Therefore, the structure, composition and folding of chromatin represent a major point of control of gene expression. These chromatin features can be dynamically regulated by the concerted action of epigenomic effectors to achieve specific transcriptional outcomes. Indeed, the establishment of specific and highly regulated transcriptional programs determines cell identity and function. During my PhD I particularly focused in the epigenetic control of the *Drosophila melanogaster* ovarian transcriptome. In the next part I will thus describe this particular system.

III. Part III Epigenomic regulation during *D. melanogaster* oogenesis

Fertilization involves the union of two highly different gametes followed by the formation of a totipotent embryo. This implicates a series of complex nuclear and cellular events (Loppin et al., 2015). Remarkably, this occurs in the absence of zygotic transcription which means that these processes are almost entirely controlled by factors already present in the mature oocyte (Avilés-Pagán and Orr-Weaver, 2018; Stitzel and Seydoux, 2007). This developmental strategy is used by a nearly every animal and requires thus the accumulation and deposition of maternal stores during oogenesis. Maternal stockpiles include mRNAs, proteins, and nutrients which permit early embryogenesis to occur in the absence of zygotic transcription.

Preparation of the fertilized oocyte includes profound changes such as completion of female meiosis, formation of male and female pronuclei and the selective translation of

maternal RNAs. The ensemble of events required for the transition from mature oocyte to developing embryo are collectively known as egg activation. Great efforts have been deployed to identify the factors needed for the oocyte-to-zygote transition. (Avilés-Pagán et al., 2020; Avilés-Pagán and Orr-Weaver, 2018; Horner and Wolfner, 2008; Stitzel and Seydoux, 2007). For example, maternal mRNAs synthesized during oogenesis and loaded into the oocyte need to be stably maintained for prolonged periods yet not translated until the right time. Dynamic changes of the poly(A) tail have been involved in the translational control of maternal mRNAs (Eichhorn et al., 2016; Lim et al., 2016; Tadros et al., 2007). These changes depend at least on the kinase Png, the RNA binding protein Smaug and the noncanonical poly(A) polymerase Wispy. However, translational control has not been fully elucidated indicating that more factors are involved. Overall, the oocyte-to-zygote transition requires complex regulation to link developmental signals with profound changes in mRNA translation, cell cycle control, and metabolism. These are complex processes that depend therefore on a wide range of factors with different biochemical properties.

The control of the oocyte-to-embryo transition in *Drosophila* parallels that of other animals, but *Drosophila* offers experimental advantages as a model. In addition to the numerous genetic tools available, the oocyte is the single largest cell and a single ovary contains every stage of oocyte maturation, from stem cell to mature oocyte, and each stage is morphologically distinct (Bastock and St Johnston, 2008; McLaughlin and Bratu, 2015).

1. Main steps of Drosophila oogenesis

Oogenesis denominates the process of female gamete formation. In insects, this process occurs in the ovarioles of an ovary. *Drosphila melanogaster* females have two ovaries, each containing 16 to 20 autonomous ovarioles, each composed of their own stem cell populations and egg chambers at varying developmental stages (Fig17-A). Each egg chamber gives rise to a single egg. The process of oogenesis has been arbitrarily divided into 14 stages based on morphological criteria (Fig17-B) (King, RC, 1970; Spradling, 1993).

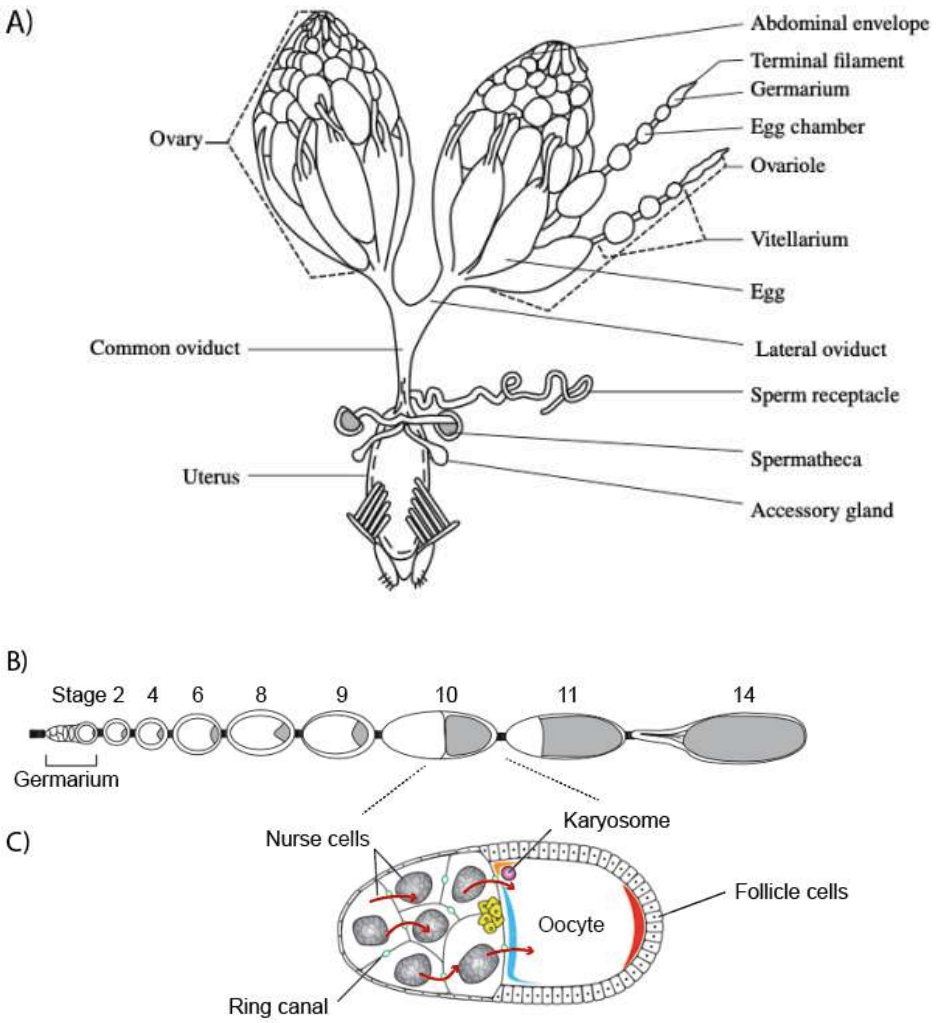

Fig 17-Oogenesis process in *D. melanogaster*

(A) Organization of the reproductive system in a mature *D. melanogaster* female. The two ovaries are composed of ovarioles each composed of the germarium and egg chambers at varying developmental stages. (B) Scheme of the ovariole with all stages of oogenesis. Egg chambers are formed at the anterior tip, in the germarium and bud at stage 2. The egg chamber grows until stage 10 where the nurse cells empty their content into the oocyte (dumping). Finally at stage 14, the mature egg is enveloped by the vitelline membrane and the chorion and is ready for fertilization. The oocyte is in gray. (C) Detail of an egg chamber at stage 10 where the process of dumping occurs indicated by red arrows (McLaughlin and Bratu, 2015; Ogienko et al., 2007).

Oogenesis progresses from the anterior to the posterior of the ovariole (McLaughlin and Bratu, 2015; Ogienko et al., 2007). The latter can be divided into three regions: a terminal filament, a germarium and a vitellarium. The germarium contains somatic and

germline stem cells (GSC). From there, egg chambers bud off and mature as they pass down the ovariole. Processes like vitellogenesis and choriogenesis are completed in the vitellarium. These constitute the synthesis of protective layers around the egg: the vitelline membrane and the chorion to jointly form the eggshell (Pascucci et al., 1996). Finally, mature eggs reach the posterior part of the ovariole competent for fertilization.

At the anterior tip of the germarium GSCs divide asymmetrically to produce a cystoblast and a new stem cell. Next, the cystoblast undergoes a total of four divisions, producing a 16-cell cyst. Each mitotic division is accompanied by incomplete cytokinesis, forming inter-cellular cytoplasmic bridges known as ring canals. One out of the 16 cells of the cyst becomes the oocyte and the other 15 cells differentiate into nurse cells (Fig18). The oocyte and nurse cells enveloped by somatic follicle cells constitute an egg chamber. Before the egg chamber leaves the germarium, DNA in the oocyte condenses into a compact structure called karyosome. Additionally, meiosis is arrested in prophase I and it will not be continued until late oogenesis, at which point meiosis progresses to metaphase I and is arrested again until egg activation.

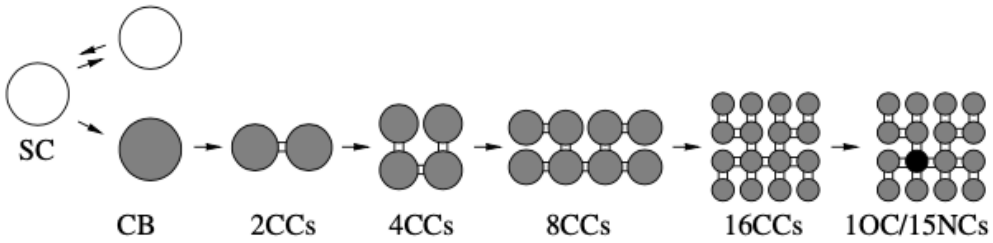

Fig18-Scheme of germline cell division from a stem cell to a 16-cell cyst.
Abbreviations: SC= stem cell, CB= cystoblast; CC= cystocyte; OC= oocyte; NC= nurse cell (Ogienko et al., 2007).

The egg chamber buds from the germarium to the vitellarium, marking stage 1 of oogenesis. Developing egg chambers move along the ovariole to the posterior end. The oocyte and nurse cells grow while follicle cells undergo active mitotic divisions. Both nurse cells and follicle cells undergo several rounds of endocycles to synthesize nutrients, mRNAs and proteins essential for oocyte growth and development (see next section). By the end of stage 10, nurse cells empty their content into the oocyte (Fig17-B,C), only nuclei, some actin filaments and a minor amount of cytoplasm remains in the nurse cell. This process is known as “dumping”. It ends with the formation of mature egg, ready for fertilization. Simultaneously, follicle cells

secrete the chorion and the vitelline membrane to protect the mature oocyte. Finally, both nurse cells and follicle cells experience apoptosis at the end of egg chamber development.

2. Transcriptional programs of nurse and follicle cells are essential for oocyte nutrition and maturation

In *Drosophila*, germ line transcriptional activity is ensured by the nurse cells, directly connected to the oocyte by cytoplasmic junctions to provide it with large amounts of mRNAs, proteins and other cellular material (Bastock and St Johnston, 2008; Spradling, 1993). This strategy ensures gene expression while maintaining chromosome condensation in the oocyte (Davidson, E, 1986). During early development of egg chamber, certain mRNAs, proteins, and organelles are preferentially transported from nurse cells into the oocyte, in a process known as selective transport. This is a slow and highly selective transport and is essential for oocyte determination and polarity. This process is dependent on the microtubule network and leads to the asymmetric distribution of proteins and mRNAs (Ogienko et al., 2007). After stage 10, rapid transport starts and nonselective dumping of the nurse cell content takes place. This substantial supply is possible thanks to the massive RNA synthesis occurring in the nurse cells. In these cells DNA undergoes 10 to 12 rounds of endoreplication cycles (Dej and Spradling, 1999) and as a result, polyploidy reaches 2048C in cells adjacent to the oocyte. Interestingly, genomic intervals are differentially replicated during the endocycle S phase such that some regions are under-replicated, while others can be amplified (Royzman and Orr-Weaver, 1998). For example, during polyploidization of the nurse cell nuclei, satellite DNA is differentially lost and ribosomal DNA increases in content in their genome (Hammond and Laird, 1985). This bias certainly reflects the needs of the mature oocyte, where great amounts of translation of maternal mRNAs will be needed.

Follicle cells surround the developing oocyte and are also essential for oocyte maturation. Until stage 6 of oogenesis, these cells proliferate by mitosis giving rise to a maximum number of ~1000 cells surrounding the egg chamber (Deng et al., 2001). At stage 6, follicle cells stop a normal mitotic cycle and enter several rounds of endocycles (Nordman and Orr-Weaver, 2012). At stage 10, follicle cells exit the endocycle and begin gene amplification cycles. this event is known as E/A switch. During this amplification, four specific genomic loci, encoding genes involved in chorion and vitelline membrane synthesis,

are amplified from 4 to 80-fold. The four amplified loci are known as a *Drosophila* amplicon in the follicle cells (Claycomb and Orrweaver, 2005). Amplification of two clusters of chorion protein genes allows the production of high-levels of chorion-related proteins, required for egg maturation. Egg chambers are composed of morphologically, genetically and functionally different cells and transcriptional regulation of each of them is important for correct oogenesis.

In conclusion, DNA endoreplication and gene amplification constitute an effective strategy to supply the high demand that represents nourishment and maturation of the oocyte.

3. Mechanisms of epigenomic regulation in the female germline

A. Silencing of bulk chromatin by the piRNA system

Additional to the silencing of bulk chromatin (described in section II-4) mediated by the H3K9me3/HP1 pathway, the metazoan germline developed the piRNA (PIWI-interacting RNA) system. This is a small RNA silencing system that acts in animal gonads and protects the genome against the deleterious influence of transposable elements (TEs). Indeed, TEs are DNA pieces that can move within the genome potentially compromising faithful transmission of the genetic information in the germline. Loss of piRNAs is associated with significant over expression of retrotransposons (Aravin et al., 2001; Malone et al., 2009), suggesting thus that the mechanism silencing them is piRNA-dependent.

Two types of silencing can be achieved with this pathway, transcriptional silencing mediated by the nuclear Piwi protein in *Drosophila*, or post-transcriptional silencing mediated by cytoplasmic proteins such as Aubergine and Argonaute3. One of the prevalent models for Piwi-mediated transcriptional silencing proposes that the Piwi-piRNA complex binds to the nascent transposon transcript and recruits several proteins ultimately tethering the H3K9 histone methyltransferase Eggless/dSETDB1. This results in the establishment of a repressive chromatin state, silencing thus transposon expression (Fig19). Alternatively, it has also been proposed that Piwi can directly recruit HP1a to initiate the heterochromatinization process. These models are not mutually exclusive and share two features, the binding of a Piwi-piRNA complex at the target site to recruit chromatin factors and transcriptional

repression mediated by chromatin structure modification. Post-transcriptional silence takes place in the cytoplasm where a Piwi-piRNA complex binds the complementary transposon RNA and the latter is cleaved by the Piwi protein. This also promotes piRNA biogenesis and amplifies the system (Ozata et al., 2019; Wang and Lin, 2021), maintaining thereby a solid repression.

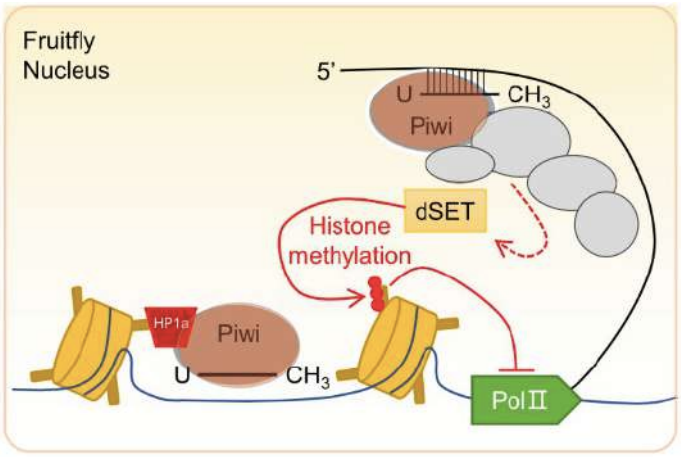

Fig19-Model for Piwi-mediated transcriptional silencing of transposons in *D. melanogaster* nucleus.

Piwi-piRNA complex binds to a nascent transposon transcript ultimately recruiting to the vicinity of the target chromatin region the H3K9 methyltransferase Eggless/dSetDB1 which establishes a repressive chromatin state to suppress transposon expression. Alternative model proposes that Piwi can directly recruit HP1a (Wang and Lin, 2021).

piRNA biogenesis can be divided into two stages. First, long RNA precursors are transcribed in the nucleus and exported into the cytoplasm. In the cytoplasm, piRNA precursors are further processed to generate mature piRNAs that get loaded into Piwi proteins. In flies, piRNA precursors come from heterochromatic loci. In the germline, majority of piRNAs are produced in “dual-strand” clusters. They produce sense and antisense piRNAs regardless of transposon orientation and their transcription requires both the repressive chromatin mark H3K9me3 and the transcriptional silencing protein Piwi (Akkouche et al., 2017; Rangan et al., 2011). Dual-strand clusters give rise to piRNA precursor RNAs via non-canonical transcription facilitated by the Rhino protein, a germline-specific HP1 variant (Klattenhoff et al., 2009). Rhino binds H3K9me3 and tethers a specific transcription factor initiator, Moonshiner, on both strands of DNA. In turn, Moonshiner forms an alternative pre-initiation complex, allowing RNA Pol II to initiate transcription from many

sites on both DNA strands. Rhino is thus able to bypass the need of specific DNA regulatory sequences such as promoters (Andersen et al., 2017). To conclude, the piRNA-Piwi silencing system provides a potent chromatin-based defense against potential deleterious effects from TEs, thereby guarding genome integrity in the future gametes.

B. The importance of fine transcriptional regulation during oogenesis

The products contained in the oocyte ensure a successful oocyte-to-zygote transition and early embryogenesis. However, most of our knowledge of this process is centered on the post-transcriptional regulation of gene expression (Kronja et al., 2014). Polyploid nurse cells are capable of mass-producing the necessary factors for the onset of development. Yet, transcriptional regulation during oogenesis has been largely overlooked. Focus on the fundamental importance of proper regulation of transcriptional programs during oogenesis has just recently emerged.

a. Targeted silencing is essential for female germline determination

In part II of this introduction, I described a series of mechanisms to ensure fine gene regulation based on chromatin-related mechanisms. Nonetheless, knowledge on how these mechanisms are used in the female germline is very limited. As said before, a unique germ stem cell (GSC) gives rise to different lineages of the germline, the nurse cells and the oocyte. This unique cell must thus undergo major changes in gene expression and chromatin organization.

New insights underlying epigenomic changes during oogenesis came from a recent study, from the Spradling lab, where they used *Drosophila* oogenesis to study Polycomb repression. Implication of Polycomb proteins in gene regulation during *Drosophila* oogenesis had already been observed. A mutation in E(z), the catalytic subunit of the PRC2 complex, impairs gene silencing of *Cyclin E* and *dacapo*, a cyclin-dependent kinase inhibitor. This results in the oocyte-to-be entering a nurse cell-like endoreplicative program and failing to be determined as the oocyte (Iovino et al., 2013). In the new study by DeLuca *et al*., authors unveiled a role for Polycomb silencing in the transition from GSC to nurse cell (DeLuca et

al., 2020). They first noticed that the patterns of H3K27me3 between these two cell types were different. Indeed, nurse cell progenitors lack silencing and H3K27me3 shows a broad distribution, referred to by the authors as non-canonical H3K27me3 pattern. As nurse cells differentiate, the H3K27me3 pattern becomes focused on common PcG domains. The authors proposed a model where association of PRC2 with the PcG protein Pcl, prevents it from sampling at many sites, resulting in infrequent and stochastic silencing. As differentiation occurs, Pcl levels drop and core-PRC2 is freed to sample and silence more sites. This study shows how Polycomb-mediated reshaping of chromatin is essential for female germline development in *Drosophila*.

Interestingly, it was also observed that female germ cell fate is maintained by an epigenetic regulatory pathway depending on H3K9me3/HP1a silencing of key spermatogenesis genes (Smolko et al., 2018). Female germ line specific knockdown of the H3K9 methyltransfearse *eggless/dSETDB1* and its partners *HP1a* and *windei* results in ectopic expression of testis-specific genes. Mapping of H3K9me3 revealed the accumulation of this mark on 21 of the ectopically expressed genes. Remarkably, and contrary to the general vision of H3K9me3 as broad heterochromatin blocks, the mark was highly localized and did not spread into neighboring loci. A striking example the authors described was the *phf7* gene, where in ovaries, H3K9me3 is restricted to the region surrounding the silent testis-specific TSS. The mechanisms through which H3K9me3 is targeted and restricted in such a specific manner are not fully elucidated. Nevertheless, this study provides a non-common usage of the H3K9me3/HP1a silencing pathway in the female germline.

Overall, these data emphasize the importance of fine chromatin-based regulation of transcription in the female germline for correct gamete production.

b. *Histone modifiers play an important role in transcription activation during oogenesis*

Different studies found an important role for histone modifiers during oogenesis, pointing out the importance of an epigenetic mode of regulation during this process. The importance of the H3K4me3 histone demethylase Lid/dKDM5 during oogenesis was observed by two different groups in addition to ours (see Results). Zhaunova and colleagues observed that absence of Lid/dKDM5 in the female germline leads to a series of defects in meiotic chromatin organization in oocytes, including instability of the recombination

machinery (Zhaunova et al., 2016). Oocytes remain arrested in prophase I of meiosis for a significant amount of time. They are transcriptionally silent throughout this arrest but they reactivate transcription prior to the resumption of meiosis (Mahowald and Tiefert, 1970). Navarro-Costa and colleagues characterized the epigenome of the prophase I-arrested oocyte and found that it is highly dynamic and contains both euchromatic and heterochromatic marks that vary during oocyte quiescence and reactivation (Navarro-Costa et al., 2016). Female germ-line depletion of Lid/dKDM5, led to a significant increase in the levels of H3K4me3 and to precocious transcriptional reactivation of the quiescent prophase I-arrested oocytes. On the contrary, no changes in H3K27me3 levels were detected. Importantly, the demethylase activity of Lid/dKDM5 was required for correct transcriptional reactivation of the oocyte and meiotic progression, suggesting a role of this histone demethylase in the regulation of the oocyte epigenome. These data support the hypothesis that correct reactivation of the dormant primary oocyte is epigenetically regulated. They also observed that loss of Lid/dKDM5 severely affects meiotic completion and accordingly, most fertilized eggs fail to initiate mitotic divisions.

Furthermore, a recent study identified the H3K4 methyltransferase Trr as essential for the oocyte-to-zygote transition. Interestingly, in the absence of Trr, oocytes develop normally but fail to complete maternal meiosis and to form the paternal pronucleus. The proposed model is that during oocyte development, Trr promotes the expression of a subset of genes that are not required during oogenesis but their presence in the mature oocyte is critical for proper zygote formation (Fig20). One of the identified genes under direct control of Trr and necessary for the oocyte-to-zygote transition coded for the IDGF4 glycoprotein (Prudêncio et al., 2018) but its specific role at zygote formation is yet to be determined. Overall, these data emphasize the important role of chromatin regulation during female gametogenesis.

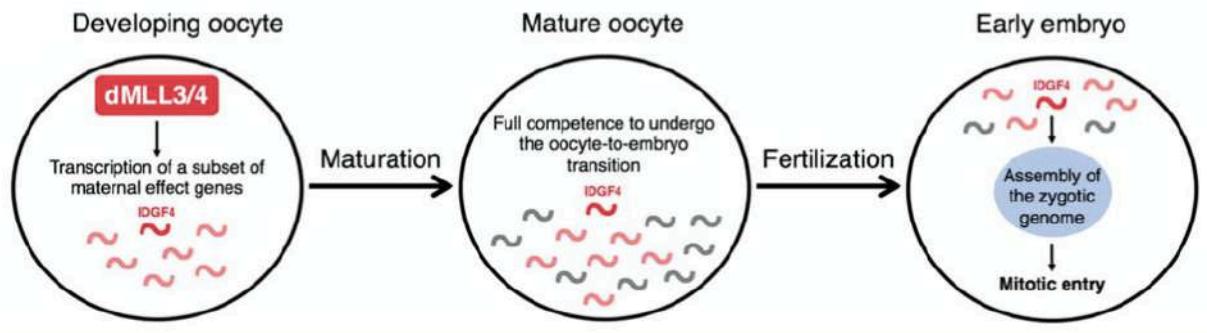

Fig20-Proposed model for Trr-regulated acquisition of embryo fate at fertilization. During oocyte maturation, Trr promotes the expression of a subset of genes, which products are not required for normal oogenesis but will be indispensable for zygotic genome assembly at fertilization (Prudêncio et al., 2018).

Emergent evidence suggests that transcriptional regulation during oogenesis is mediated, at least in part, by epigenetic mechanisms that define specific gene expression modules. This allows the establishment of the molecular basis of the crucial and complex oocyte-to-zygote transition.

IV. Part IV The peculiar case of *dhd* regulation

My PhD project was based on the discovery of a specific functional connection between a series of epigenomic effectors and the highly regulated terminal effector of zygote formation, the maternal thioredoxin Deadhead (Dhd). The different effectors involved are: the histone demethylase Lid/dKDM5, the histone deacetylase complex scaffold Sin3A, the Brahma chromatin remodeler sub-unit Snr1 and the insulator component Mod(mdg4). The case of *dhd* represented thus an opportunity to study the molecular mechanisms underneath transcriptional regulation by chromatin factors. I will first introduce the role of Dhd at fertilization and the specific features of this protein and of the gene that encodes it. This will be followed by a state-of-the art on the epigenomic effectors that regulate this singular gene.

1. The essential role of Deadhead at fertilization

The *dhd* gene encodes an egg specific thioredoxin required for female fertility and development of viable embryos (Emelyanov and Fyodorov, 2016; Salz et al., 1994; Tirmarche et al., 2016). Thioredoxins are small, highly conserved redox proteins that catalyze the reduction of disulfide bonds on target proteins (Arnér and Holmgren, 2000). At fertilization, Dhd is critically required for sperm chromatin remodeling. DNA in the sperm nucleus is highly compacted due to the almost total replacement of histones by sperm nuclear basic proteins (SNBPs), including protamines (Miller et al., 2010). This level of compaction is incompatible with basic nuclear activities such as transcription, replication or repair. One of the first key events at fertilization is thus remodeling of this nucleus so that paternal chromosomes can be integrated into the zygote (Fig21-A) (Loppin et al., 2015). This process depends on Dhd reducing disulfide bonds between protamines thus allowing sperm nuclear decondensation. Indeed, in eggs laid by *dhd* null mutant females, the sperm nucleus retains protamines and remains needle-shaped, reminiscent of its ultra-compacted DNA (Fig21-B,C) (Emelyanov and Fyodorov, 2016; Tirmarche et al., 2016). A catalytic mutant is unable to rescue the dhd mutant phenotype showing that this process depends on Dhd catalytic reducing activity (Emelyanov and Fyodorov, 2016; Tirmarche et al., 2016). Dhd has also been involved in the redox balance at the oocyte-to-embryo transition (Petrova et al., 2018). The study of redox state changes during this process revealed that early embryos have a more oxidized state than mature oocytes. It was observed that *dhd* mutant oocytes are prematurely oxidized and exhibit meiotic delay. A highly specific list of Dhd substrates was established and a major fraction of Dhd's interactors are ribosomes or ribosome-associated. These data show that Dhd has crucial roles during the oocyte-to-zygote transition.

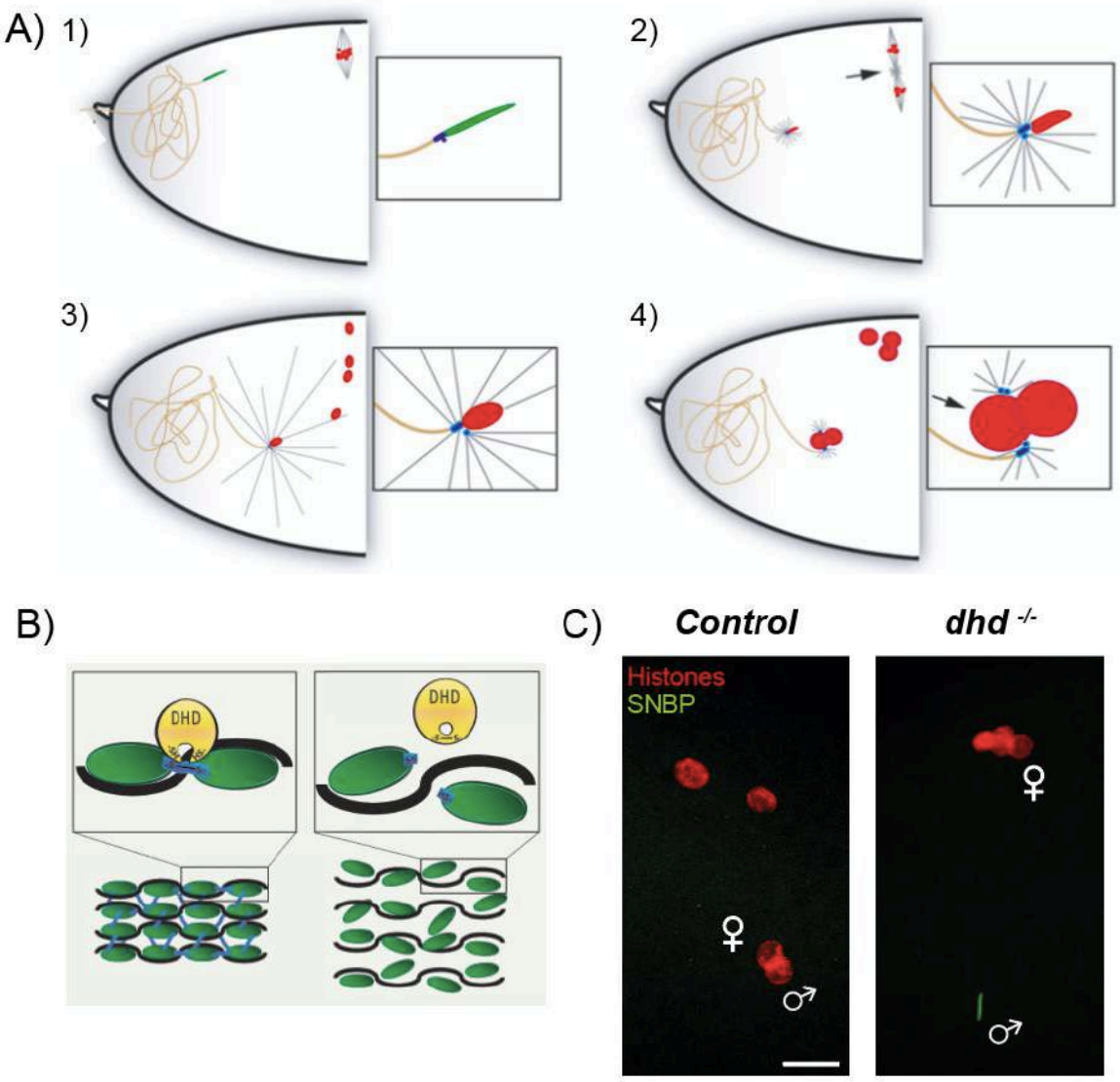

Fig 21: The essential role of Deadhead at fertilization.

(A) First steps of zygote formation in *Drosophila melanogaster*. (1) Sperm enters the egg. At fertilization, maternal chromosomes are arrested in metaphase I of meiosis I. Sperm nucleus is ultra-compacted and packed with sperm nuclear basic proteins (SNBPs) (green). (2) Maternal chromosomes progressed to metaphase of meiosis II. Remodeling of the sperm chromatin took place: SNBPs were replaced by maternally provided histones (red) and the nucleus is decondensed. (3) Pronuclei migration. The inner most product of female meiosis migrates towards its male counterpart. (4) Apposition of female and male pronuclei. The first zygotic replication begins (Loppin et al., 2015). (B) Schematic representation of the role of Deadhead at fertilization. The thioredoxin DHD reduces disulfide bonds between SNBPs (left) allowing their eviction and chromatin decondensation (right) (Horard and Loppin, 2017). (C) Confocal images of eggs at the apposition stage, laid by control (left) and *dhd* null (right) mutant females. In control eggs both male and female pronuclei are round and

contain only histones. In *dhd* mutant eggs, the sperm nucleus retains SNBPs and is needle-shaped, reminiscent of compacted DNA. Scale bar 10 µm.

Dhd is exclusively found in ovaries, its levels increase during oocyte maturation and start decreasing at egg activation (Kronja et al., 2014; Tirmarche et al., 2016). At fertilization, Dhd is abundant and homogeneously distributed throughout the egg cytoplasm. Strikingly, it becomes rapidly undetectable after completion of the first zygotic cycle (Fig22) (Tirmarche et al., 2016). This indicates that likely Dhd plays no other role after zygote formation and it is possible that its continued presence is detrimental to embryogenesis.

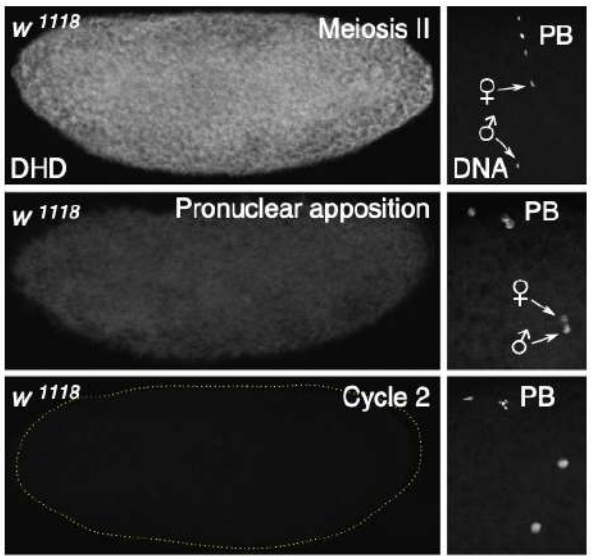

Fig22-Deadhead is rapidly degraded after fertilization
Confocal images of control eggs stained for DHD (left) and DNA (right). DHD is abundant and homogeneously distributed at fertilization but is rapidly undetectable (Tirmarche et al., 2016).

The role of Dhd is thus essential for the oocyte-to-zygote transition and the onset of embryonic development. Interestingly, *dhd* stands out for a series of unusual features at the protein level as well as at its genomic locus.

2. Dhd, a thioredoxin not like the others

As mentioned before, Dhd is a thioredoxin. Thioredoxins constitute a family of small thiol proteins that are present in all organisms studied so far, and are characterized by the sequence of their conserved active site (WCGPC). In addition to their role maintaining redox homeostasis in the cell, they have been implicated in DNA synthesis, regulation of transcription factors or programmed cell death (Arnér and Holmgren, 2000), indicating a wide variety of roles for these proteins.

Drosophila melanogaster possesses three true thioredoxins, the testis-specific TrxT, the ovary-specific Dhd and the ubiquitous Trx2. Alignment of the protein sequences revealed that Dhd is less related to Trx2 than TrxT (J. Svensson and Larsson, 2007). Accordingly, *in vitro* Trx2 is not able to substitute Dhd's role in reducing protamine disulfide bonds (Emelyanov and Fyodorov, 2016; Tirmarche et al., 2016). Interestingly, a recent characterization of the structure of the *Drosophila melanogaster* thioredoxins revealed that Dhd has an atypical structure for a thioredoxin (Freier et al., 2021). In contrast to the negatively charged surfaces commonly found in most thioredoxins, it was observed that Dhd has positively charged patches on its surface. Dhd is in charge of reducing protamine disulfide bonds in sperm chromatin and was found associated with ribosomes (Petrova et al., 2018; Tirmarche et al., 2016). The unusual positive patches on its surface might thus help Dhd in selecting proteins and DNA/RNA partners by complementarity with their negatively charged backbone. This distinctive charge distribution helps to define the initial encounter with DNA/RNA complexes that will lead to final specific interactions with cofactors to promote chromatin remodeling (Freier et al., 2021). Specific and unusual features of the Dhd thioredoxin are thus important for its role at fertilization.

3. The intricate *dhd* locus

Dhd protein is present exclusively in ovaries (Salz et al., 1994; Tirmarche et al., 2016). Accordingly, RNA *in situ* hybridization experiments show that the gene is transcribed in nurse cells and the transcript is highly present at stage 10 and then deposited in the oocyte (Salz et al., 1994; Svensson et al., 2003; Tirmarche et al., 2016).

Data from Flybase (http://flybase.org), and our own RNA-seq analyses, indicate that *dhd* is among the most highly expressed genes in ovaries (Fig23-A). This is all the more

surprising due to the genomic context of this gene. *dhd* is a small, intronless gene located in the middle of a cluster of fifteen densely packed genes spanning about 40 kb of genomic DNA (Fig23-B). Commonly, *Drosophila* genes with tissue-, temporally-biased expression patterns have been shown to be concentrated in neighborhoods of contiguous genes (Parisi et al., 2004; Spellman and Rubin, 2002). However, the *dhd* gene lies within a 1.4 kb region that is immediately flanked by two genes with testis-specific expression, the thioredoxin *Trx-T* and the *CG4198* gene of unknown function. *TrxT* and *dhd* are arranged as a gene pair, transcribed in opposite directions separated by 282 bp. These two genes have thus closely spaced promoters and are differentially regulated by a short common control region. A transgene including the *TrxT-dhd* region and an additional 2 kb and 1 kb downstream of *TrxT* and *dhd* respectively (*P[w^{+} snf^{+} TrxT^{+} dhd^{+}]*) (Fig23-B), inserted at the X chromosome or at an autosome was able to recreate the expression pattern of *TrxT* and *dhd*. This shows that the endogenous X chromosome location of *TrxT-dhd* is not essential for tissue-specific transcription (Svensson et al., 2007). Furthermore, an even smaller transgene spanning only *Trx-T*, *dhd* and part of *CG4198 (pW8-attB-dhd^{WT})* (Fig23-B), fully rescues *dhd* maternal effect embryonic lethal phenotype (Tirmarche et al., 2016), showing that this 4.3 kb region is capable of recapitulating *dhd* expression. The necessary regulatory signals for *dhd* activation are thus contained within this restricted region.

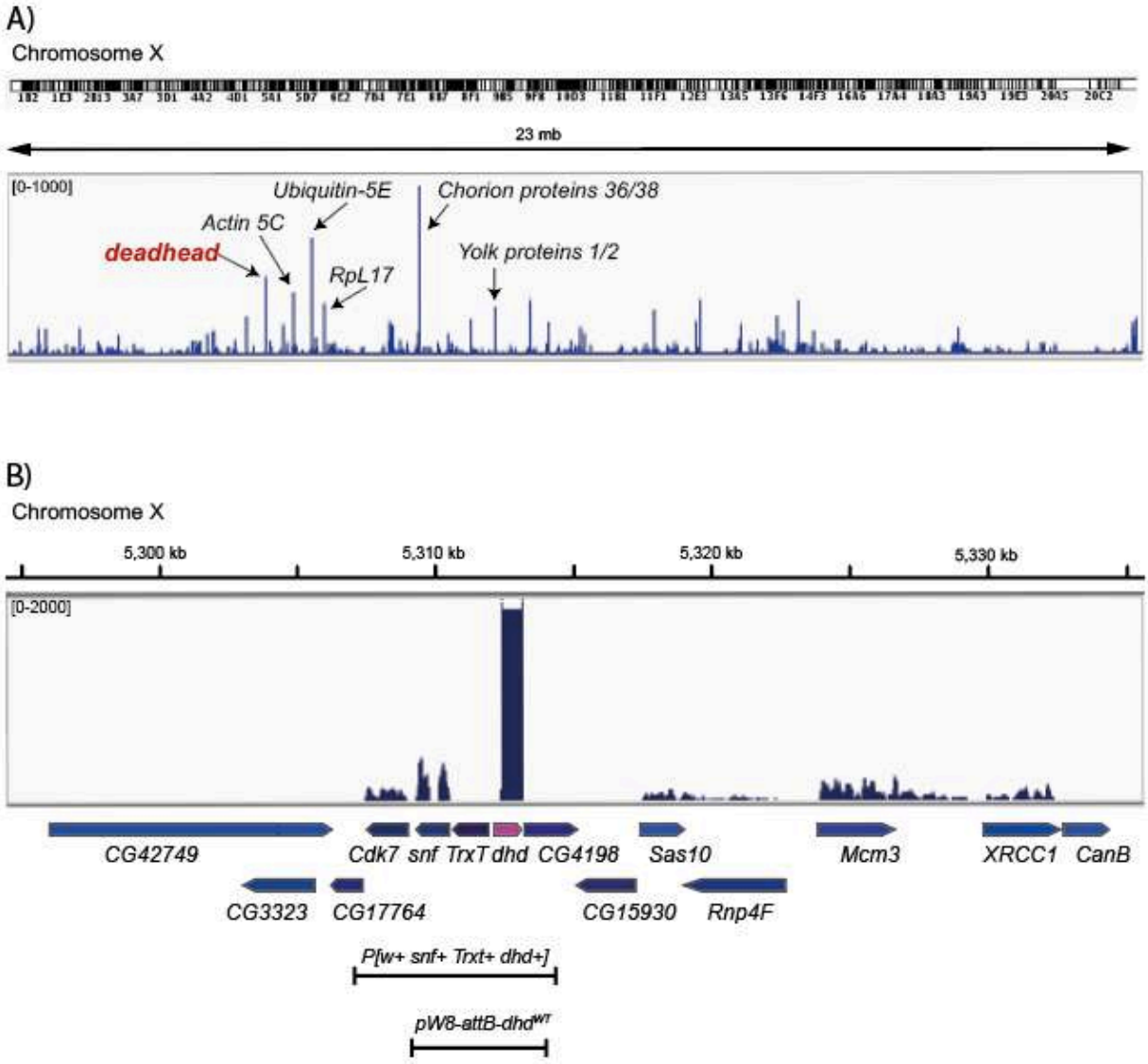

Fig 23-*deadhead* is massively expressed in ovaries

dhd is amongst the highest expressed genes in ovaries. (A) Genome browser view of control ovarian RNA-seq signal of the X-chromosome showing the high level of transcription of *dhd*. Examples of other highly expressed genes are indicated by arrows. (B) Genome browser view of control ovarian RNA-seq signal at the *dhd* region. Signal coming from the *dhd* locus was truncated for readability. The genomic region covered by two different transgenes are shown: (i) the *P[w+ snf+ Trxt+ dhd+]* transgene, capable of recreating *dhd* expression pattern (Svensson et al., 2003) and (ii) the pW8-attB-dhd^{WT}transgene, capable of restoring *dhd* expression and rescue female sterility [Tirmarche et al., 2016].

Svensson and colleagues did a thorough analysis of the organization of the *TrxT* and *dhd* locus across several *Drosophilid* species (Svensson et al., 2007). The intriguing gene organization and regulation of *TrxT* and *dhd* is remarkably well conserved. For both of these

genes, the lack of introns in the coding region is conserved across species. Additionally, predictions of TSSs for *dhd* and *TrxT* in different *Drosophilid* species revealed that the closer to the transcription start sites, the higher the conservation level of the sequence. Conserved motif analysis within 150 bp upstream of the predicted TSSs revealed 9 different motifs however, none of them had obvious similarities with known common target sequences for transcription factors. The motifs identified were also compared to the 5' flanking regions of ovary- and testis-specific genes. They were detected in less than 1% of the genes in both ovary and testes sets indicating that they are neither ovary- nor testis-specific. Finally, the search for gene pairs including a testis-specific gene and an ovary- specific gene transcribed in opposite directions and separated by no more than 1000 bp, showed only 8 additional gene pairs in this configuration. None of the nine motifs previously identified were found in the 5′ flanking regions of any of the other gene pairs. Importantly, none had such extreme ovary- or testes-specific expression as *dhd* and *TrxT* when expressed as a ratio, showing thus the rareness of this organization.

In conclusion, the genomic organization and regulation of *TrxT* and *dhd* is unique and well conserved in evolution. Strikingly, the *dhd* locus accumulates a series of counterintuitive features when considering its high expression.

4. State-of-the art of dhd regulators in transcription regulation

My PhD project focused on the epigenetic regulation of the *dhd* singular gene which led me to focus on the role of particular epigenomic effectors so in this section I will more precisely lay out the current literature on their roles in transcription regulation.

A. The histone demethylase Lid/dKDM5

Lid/dKDM5 is the sole member of the KDM5 histone demethylases in *Drosophila*. It specifically targets H3K4me3 *in vivo* (Secombe et al., 2007). Lid/dKDM5 has been found enriched at promoter regions in embryonic cells, whole adults and wing discs (Gajan et al., 2016; Liu and Secombe, 2015; Lloret-Llinares et al., 2012; Zamurrad et al., 2018), hinting about a role in transcriptional regulation.

Since H3K4me3 has long been associated with transcriptional activation and Lid/dKDM5 removes this mark, this enzyme could have been expected to have a role in global repression rather than activation. Nonetheless, RNA-seq analyses in mutants and Lid/dKDM5-depleted cultured cells, show equivalent up-regulated and down-regulated genes (Drelon et al., 2018; Gajan et al., 2016; Liu and Secombe, 2015). A global increase in H3K4me3 is consistently observed upon Lid/dKDM5 depletion or mutation, however the impact on transcription has been found mild (Drelon et al., 2018; Liu et al., 2014; Lloret-Llinares et al., 2012; Zamurrad et al., 2018). This reinforces the enigmatic role of H3K4me3 in transcriptional activation discussed in section II-7-B.

The impact of H3K4me3 on transcription is not clear however Lid/dKDM5 possesses additional domains with other functions. Indeed, the family of KDM5 proteins contain the following domains: JmjN domain (unknown function), JmjC domain (H3K4me3 demethylase activity), ARID (implicated in DNA binding), C5HC2 zinc finger and two or three PHD domains (protein-protein interaction). Interestingly, null *lid* mutants are lethal but can be rescued with a demethylase-dead transgene (Drelon et al., 2018; Li et al., 2010; Liu and Secombe, 2015), showing thus that Lid/dKDM5 has catalytic-independent crucial roles. Indeed, in whole adults, Lid/dKDM5 proved to be a critical regulator of genes associated with mitochondrial structure and function. This regulation was independent from its demethylase JmjC domain however the C-terminal PHD motif, capable of binding di- and trimethylated H3K4 was essential (Liu and Secombe, 2015). Nonetheless, in a study where only fly brains where analyzed, it was observed that Lid/dKDM5 can directly activate or repress transcription in a demethylase-dependent manner (Zamurrad et al., 2018). These data indicates thus that Lid/dKDM5 regulates genes involved in different cellular processes and that this regulation can depend or not on its demethylase activity.

An extra layer of complexity comes from the fact that Lid/dKDM5 can act with different partners, probably due to its different protein domains. These interactions can lead to different outcomes on gene transcription. In *Drosophila* embryos, Lid/dKDM5 was found in a complex with the histone deacetylase Rpd3, the scaffold Sin3A, the histone chaperones (Asf1 or Nap-1) and other proteins. The resulting complexes acted as repressors of Notch target genes (Moshkin et al., 2009). However, in embryonic fly cells, Lid/dKDM5 interaction with the transcription factor Foxo and the histone deacetylase dHDAC4 leads to the activation of a subset of Foxo target genes (Liu et al., 2014), showing the versatility of Lid/dKDM5 on transcriptional outcomes. It has been also observed that Lid/dKDM5

genetically interacts with the H3K4me1/2 demethylase dLsd1 (Di Stefano et al., 2011). Lid/dKDM5 opposes the functions of dLsd1 and the H3K9 methyltransferase Su(var)3–9 in promoting heterochromatin spreading at heterochromatin–euchromatin boundaries. However, Lid/dKDM5 cooperates with dLsd1 in regulating certain Notch target genes in euchromatic contexts, illustrating that the activity of histone demethylases is context-dependent. Lid/dKDM5 has thus a complex and intricate role in gene transcription regulation that depends on several factors such as cell-type and interactors.

B. The Sin3-HDAC complex

The Sin3 protein is highly conserved from yeast to mammals and has different isoforms in metazoans (Chaubal and Pile, 2018). Sin3, through its interaction with DNA-binding factors, acts as a scaffold protein that recruits histone deacetylases (HDACs) and other chromatin-modifying enzymes onto target promoters (Silverstein and Ekwall, 2005).

Classically, Sin3-HDAC complexes have been associated with transcriptional repression via direct recruitment of transcriptional repressors mediated by Sin3 and nucleosome deacetylation (Kadamb et al., 2013; McDonel et al., 2009; van Oevelen et al., 2008; Sahu et al., 2008). Accumulating evidence, however, points to a dual role of the SIN3 complex in transcriptional regulation. The Sin3A protein in *Drosophila* was found to bind promoters at euchromatic regions, preferentially at TSSs (Das et al., 2013; Saha et al., 2016). The transcriptional profile of a Sin3-deleted yeast strain showed both gene upregulation (173) and downregulation (269), suggesting thus a dual role of this protein in transcription (Bernstein et al., 2000). This tendency was also observed in *Drosophila* cultured cells upon depletion of Sin3A (Gajan et al., 2016; Saha et al., 2016). Sin3 can then positively or negatively influence transcription.

Studies integrating transcriptome and genome-wide binding data in human kidney and fly embryonic cells provided evidence of a direct role of SIN3A in gene transcription. For human SIN3A, 42% of activated genes and 61% of repressed genes were directly bound by this protein (Williams et al., 2011). In *Drosophila* embryonic cells, 92 % and 46 % of the genes repressed and activated by Sin3A, respectively, are direct targets (Saha et al., 2016).

These results suggest thus a direct role of SIN3A both in activation and repression and at least for *Drosophila*, repressed genes are more likely to be direct targets. The corepressor activity of Sin3A is commonly attributed to its association with histone deacetylases. However, the mechanisms through which Sin3A could mediate gene activation are not known. One possibility is that the deacetylase component of the SIN3 complex could act on transcription factors thereby altering DNA-binding capability or protein interactions. For example, it has been observed that acetylation of the transcription factor FoxO1 reduces DNA-binding affinity (Brent et al., 2008). These data show that at least a subset of genes can be direct targets of Sin3A, however the Sin3A-dependent molecular mechanisms regulating transcription are fully understood. Much work remains to determine the network of interactors of Sin3 proteins which will help elucidate how a single complex can have opposite effects on transcription.

C. The nucleosome remodeler subunit Snr1

The conserved SWI/SNF family contains multi-subunit chromatin-remodeling complexes. These are large protein complexes usually formed around Brm (Brahma) in *Drosophila* or BRG1 in Humans, which confer the ATP-hydrolysis catalytic activity. In *Drosophila*, two Swi/Snf compleCxes exist: the BRM-associated protein complex (BAP) and the polybromo-containing BAP complex (PBAP). These complexes share a common core and differ by signature subunits (Mohrmann et al., 2004). Snr1 is part of the common core of the BAP/PBAP complexes and was found essential for fly viability (Dingwall et al., 1995).

First indications that *snr1* might have a role in gene expression came from its genetic interaction with the TrxG genes *brahma* and *trithorax* (Dingwall et al., 1995). Furthermore, staining in polytene chromosomes showed that a subset of Snr1 overlaps with a fraction of RNA Pol II, suggesting a wide array of potential *in vivo* targets for gene regulation (Zraly et al., 2003). Additionally, an upregulation of the clustered *Ecdysone induced genes* (*Eig*) was observed in loss of function *snr1* mutants and *snr1*-depleted cultured cells. The proposed model by the authors was that upon Snr1 loss, nucleosome accessibility increases and minimizes barriers to transcription. Like this, RNA Pol II proceeds elongation with little or no stalling (Zraly et al., 2006; Zraly and Dingwall, 2012). This suggests thus a function for Snr1 within remodeler activities.

Moreover, it was observed that Snr1 is not required or expressed in all tissues dependent on BAP/PBAP complex activities (Zraly et al., 2003). Snr1 is thus not necessary for all BAP/PBAP functions. Since Snr1 is essential for viability it likely has regulatory functions independent from the BAP/PBAP complexes. RNA-seq analysis in control and Snr1-depleted tumorigenic wing imaginal discs revealed hundreds of misregulated genes upon *snr1* loss and most of them (336 vs 57) were upregulated (Xie et al., 2017). In contrast to *Eig* genes, in this case Snr1, mostly had a repressive role. Strikingly, this study also described a cytoplasmic localization of Snr1 in wing disc cells and salivary gland cells contrary to other core subunits of the BAP/PBAP complexes. This location was required for its tumor-suppressor role. Overall, these data show that Snr1 has gene regulatory functions within and outside the BAP/PBAP complexes. These functions can favor or repress transcription depending on the targets.

D. The multifaceted protein Mod(mdg4)

Between 1993 and 1997, the *mod(mdg4)* gene was cloned three separate times, each time by a different laboratory and was associated to different functions. First, as an enhancer of position-effect variegation, a protein involved in establishing and/or maintaining an open chromatin conformation (Dorn et al., 1993). Next, as a chromatin insulator by directing the repressive effect of Su(Hw) (Gerasimova et al., 1995). Finally, as a protein that induces apoptosis (Harvey et al., 1997). Around the same time, it was also observed that in *mod(mdg4)* mutant larvae, expression of some homeotic genes was decreased, suggesting a positive role for Mod(mdg4) in their regulation (Gerasimova and Corces, 1998). The multifaceted character of Mod(mdg4) could be due to the wide variety of isoforms that come from the single gene. Indeed, at least 31 isoforms sharing a common N-terminal region have been identified from the *mod(mdg4)* gene (Büchner et al., 2000). To date, the most well-studied isoform is the 67.2 for its essential role along with Su(Hw) and CP190 at the *gypsy* insulator (Gerasimova et al., 1995; Melnikova et al., 2017, 2004). However, polytene chromosome staining and ChIP experiments of the 67.2 isoform do not account for all Mod(mdg4) recruitment to DNA (Büchner et al., 2000; Melnikova et al., 2019; Van Bortle et al., 2012). Additionally, a null allele of *mod(mdg4)* showed that this gene is essential but mutations disrupting only the 67.2 isoform are viable (Savitsky et al., 2016) indicating that the roles of Mod(mdg4) go beyond its insulator function.

Little is known about the mechanisms of action of Mod(mdg4) and its influence on gene transcription but mapping of the protein revealed its enrichment at gene promoters in fly embryos (Nègre et al., 2010). Mod(mdg4) does not have sequence specificity and may not be able to bind DNA directly but can mediate homotypic and heterotypic protein–protein interactions via its BTB/POZ domain. This in turn could support pairing between distant regions in the chromosomes (Gurudatta and Corces, 2009; Kyrchanova and Georgiev, 2014). Studies of the role of Mod(mdg4) at the BX-C complex revealed that it promotes *Abd-B* expression in the posterior abdominal segments (Büchner et al., 2000; Dorn et al., 1993; Savitsky et al., 2016) but no mechanism has been proposed. It was observed that *mod(mdg4)* mutations enhance transformations caused by dCTCF deficiency. Also, dCTCF and Mod(mdg4) share many sites at the bithorax complex and genome-wide (Nègre et al., 2010; Savitsky et al., 2016; Van Bortle et al., 2012), favoring a scenario where these two proteins are part of the same molecular pathway. One possibility is that Mod(mdg4) and dCTCF promote the interaction of *Abd-B* promoter with the corresponding enhancers. Since both proteins bind the vicinity of some of the *Abd-B* TSSs, a direct role promoting transcription is also worth considering (Savitsky et al., 2016). Mod(mdg4) has also been found at the borders of H3K27me3 domains. Its depletion led to a decrease of the mark within the domain. Surprisingly, there was no significant effect on expression at genes flanking the domain nor at those embedded in the domain (Schwartz et al., 2012; Van Bortle et al., 2012). However, this was only assessed at a limited number of genes, a genome-wide study would help to evaluate the impact of Mod(mdg4) depletion on transcription. It is well-documented that Mod(mdg4) can affect gene expression when it is part of an insulator complex. However, there is limited data concerning the roles that other isoforms may have in gene transcriptional regulation. Further work is needed to clarify this potential role and to unveil the molecular mechanisms underneath it.

The accumulation of specific features makes Deadhead truly unique. The *dhd* locus is located in an unfavorable genomic environment but achieves high ovary-specific expression, which makes its regulation even more intriguing. Additionally, the epigenomic effectors at play have been shown capable of favoring repression as well as activation of transcription in a context-dependent manner. The *dhd* locus represents thus a paradigmatic gene exquisitely

regulated by chromatin factors and offering a unique opportunity to study the molecular mechanisms at play in epigenetic transcriptional regulation.

RESULTS & DISCUSSION

I. An shRNA screen identifies maternal chromatin factors required for the oocyte-to-zygote transition

1. Article presentation

This first article published in PLOS Genetics presents an shRNA-based genetic screen designed to identify maternal chromatin factors required for the integration of paternal chromosomes into the zygote. This consisted on expressing shRNAs specifically in the female germline and identify embryos that lost paternal chromosomes and developed as gynohaploids. Like this, we identified the histone demethylase Lid/dKDM5 and the members of the HDAC complex Sin3A and Rpd3 as essential for the activation of a critical effector of the oocyte-to-zygote transition: the maternal thioredoxin Deadhead.

To investigate the mechanism underneath this regulation, we focused mainly on Lid/dKDM5. As mentioned in the introduction, H3K4me3 is a hallmark of active transcription and is also the target of the demethylase Lid/dKDM5, therefore we assessed the impact of depletion of *lid* on this mark in ovaries.

Finally, we tested to what extent the phenotype observed in eggs laid by Lid-depleted females was caused by *dhd* loss.

PLOS GENETICS

RESEARCH ARTICLE

The Lid/KDM5 histone demethylase complex activates a critical effector of the oocyte-to-zygote transition

Daniela Torres-Campana[1☯*], Shuhei Kimura[2☯¤], Guillermo A. Orsi[1], Béatrice Horard[1], Gérard Benoit[1], Benjamin Loppin[1*]

1 Laboratoire de Biologie et de Modélisation de la Cellule, CNRS UMR5239, Ecole Normale Supérieure de Lyon, University of Lyon, France, **2** Laboratoire de Biométrie et Biologie Evolutive, Université Lyon 1, CNRS, UMR 5558, Villeurbanne F-69622, France

☯ These authors contributed equally to this work.
¤ Current address: Seto Hospital, Kanayama-cho, Tokorozawa-shi, Saitama-ken, Japan
* benjamin.loppin@ens-lyon.fr

Citation: Torres-Campana D, Kimura S, Orsi GA, Horard B, Benoit G, Loppin B (2020) The Lid/KDM5 histone demethylase complex activates a critical effector of the oocyte-to-zygote transition. PLoS Genet 16(3): e1008543. https://doi.org/10.1371/journal.pgen.1008543

Editor: Giovanni Bosco, Geisel School of Medicine at Dartmouth, UNITED STATES

Received: June 28, 2019

Accepted: November 26, 2019

Published: March 5, 2020

Data Availability Statement: The DNA sequencing data from this publication have been deposited to the Gene Expression Omnibus database [https://www.ncbi.nlm.nih.gov/geo/] and assigned the identifier GSE133064 (RNA-Seq) and GSE133202 (ChIP-Seq).

Funding: SK was supported by a fellowship from the Agence Nationale de la Recherche (https://anr.fr) (ZygoPat ANR-12-BSV5-0014). The funders had no role in study design, data collection and

Abstract

Following fertilization of a mature oocyte, the formation of a diploid zygote involves a series of coordinated cellular events that ends with the first embryonic mitosis. In animals, this complex developmental transition is almost entirely controlled by maternal gene products. How such a crucial transcriptional program is established during oogenesis remains poorly understood. Here, we have performed an shRNA-based genetic screen in *Drosophila* to identify genes required to form a diploid zygote. We found that the Lid/KDM5 histone demethylase and its partner, the Sin3A-HDAC1 deacetylase complex, are necessary for sperm nuclear decompaction and karyogamy. Surprisingly, transcriptomic analyses revealed that these histone modifiers are required for the massive transcriptional activation of *deadhead* (*dhd*), which encodes a maternal thioredoxin involved in sperm chromatin remodeling. Unexpectedly, while *lid* knock-down tends to slightly favor the accumulation of its target, H3K4me3, on the genome, this mark was lost at the *dhd* locus. We propose that Lid/KDM5 and Sin3A cooperate to establish a local chromatin environment facilitating the unusually high expression of *dhd*, a key effector of the oocyte-to-zygote transition.

Author summary

Nuclear enzymes that add or remove epigenetic marks on histone tails potentially control gene expression by affecting chromatin structure and DNA accessibility. For instance, members of the KDM5 family of histone demethylases specifically remove methyl groups on the lysine 4 of histone H3, a mark generally correlated with gene expression. Lid (Little imaginal discs), the *Drosophila* KDM5, is essential for viability but is also required for female fertility. In this paper, we have found that the specific removal of Lid in developing oocytes perturbs the decompaction of the sperm nucleus at fertilization and the integration of paternal chromosomes in the zygote. Sperm nuclear decompaction normally requires the presence of a small redox protein called Deadhead (Dhd), which is massively

analysis, decision to publish, or preparation of the manuscript.

Competing interests: The authors have declared that no competing interests exist.

expressed at the end of oogenesis. Strikingly, our analyses of ovarian transcriptomes revealed that the absence of Lid completely abolishes the expression of *dhd*. This direct functional link between a general histone modifier and the expression of an essential terminal effector gene represents a rare finding. We hope that our work will help understanding how histone demethylases function in controlling complex developmental transitions as well as cancer progression.

Introduction

In sexually reproducing animals, fertilization allows the formation of a diploid zygote through the association of two haploid gametes of highly different origins and structures. Generally, the spermatozoon delivers its compact nucleus within the egg cytoplasm, along with a pair of centrioles, while the egg provides one haploid meiotic product and all resources to sustain zygote formation [1]. In some species, this maternal control extends to early embryo development, as in *Drosophila melanogaster*, where the initial amplification of embryo cleavage nuclei occurs without significant zygotic transcription [2]. Instead, the bulk of transcriptional activity takes place in the fifteen interconnected large polyploid germline nurse cells that deposit gene products in the cytoplasm of the growing oocyte [3]. The developmental potential of the egg is thus initially dependent on the establishment of a highly complex transcriptional program in female germ cells.

One of the earliest events of the oocyte-to-zygote transition is the rapid transformation of the fertilizing sperm nucleus into a functional male pronucleus. In *Drosophila*, the needle-shaped, highly compact sperm nucleus is indeed almost entirely organized with non-histone, Sperm Nuclear Basic Proteins (SNBPs) of the protamine-like type [4,5]. Male pronucleus formation begins with the genome-wide replacement of SNBPs with maternally supplied histones, a process called sperm chromatin remodeling, which is followed by extensive pronuclear decondensation [1]. Finally, zygote formation involves the coordinated migration and apposition of male and female pronuclei and the switch from meiotic to mitotic division within the same cytoplasm.

Here, we report the results of a genetic screen specifically designed to find new genes required for the oocyte-to-zygote transition in *Drosophila*. Our screen identified two histone modifiers, the Lid/KDM5 histone H3K4me3 demethylase and the Sin3A-HDAC1 histone deacetylase complex, which are both required for the integration of paternal chromosomes into the zygote. These interacting epigenetic factors are known to regulate the expression of hundreds of genes in somatic tissues but their role in the establishment of the ovarian transcriptome is unknown. Strikingly, RNA-Sequencing analyses revealed that, despite the modest impact of their depletion on ovarian transcripts, Lid and Sin3A are critically required for the massive expression of *deadhead* (*dhd*), a key effector of the oocyte-to-zygote transition [6,7]. Furthermore, we demonstrate that germline knock-down of these histone modifiers specifically prevent sperm chromatin remodeling through a mechanism that depends on the DHD thioredoxin.

Results & discussion

A maternal germline genetic screen for gynohaploid embryo development

We performed an *in vivo* RNA interference screen in the female germline to identify genes required for the integration of paternal chromosomes in the zygote. In *Drosophila*, failure to

form a male pronucleus following fertilization is generally associated with the development of haploid embryos that possess only maternally-derived chromosomes (gynohaploid embryos) and that never hatch [8]. We chose to screen transgenic lines from the TRiP collection that express small hairpin RNAs (shRNAs) under the control of the Gal4 activator [9]. We selected shRNA lines that targeted genes with known or predicted chromatin-related function and that show adult ovarian expression (Flybase). Among the 374 tested TRiP lines, 157 (41.9%) induced female sterility or severely reduced fertility when induced with the germline-specific *P{GAL4::VP16-nos.UTR}* ^{MVD1} Gal4 driver (*nos*-Gal4), thus underlying the importance of chromatin regulation for oogenesis and early embryo development (S1 Table). We then specifically searched for shRNAs that induced a maternal effect embryonic lethal phenotype associated with gynohaploid development (Fig 1A). Gynohaploid embryos can be efficiently identified by scoring the zygotic expression of a paternally-transmitted *Pfg-GFP::cid]* transgene at the gastrulation stage or beyond [10]. Among the sterile lines with late developing embryos (class 4 in Fig 1A and S1 Table) that were identified, four shRNA lines (GLV21071, GL00612, HMS00359 and HMS00607) produced embryos that were negative for GFP::CID (Fig 1B). Note that none of these shRNAs induced complete female sterility and about 1 to 4% of embryos hatched and were thus diploid (Table 1).

Two of the identified lines (GLV21071 and GL00612) express the same shRNA against the *little imaginal disc (lid)* gene, which encodes the single fly member of the KDM5/JARID1A family of histone demethylases [11,12]. KDM5 demethylases specifically target the trimethylation of lysine 4 of histone H3 (H3K4me3), a mark typically enriched around the Transcriptional Start Site (TSS) of transcriptionally active genes [13,14]. The two other shRNAs (HMS00359 and HMS00607) target the *Sin3A* and *HDAC1/rpd3* genes, respectively. The conserved Sin3A protein scaffold interacts with the histone lysine deacetylase HDAC1 to form the core SIN3 histone deacetylase complex, which is generally considered as a transcriptional repressor [15]. The SIN3 complex regulates the expression of genes involved in a number of metabolic and developmental processes [16–19]. Interestingly, Lid and the largest Sin3A isoform were previously shown to physically and functionally interact [16,17,20,21], thus opening the possibility that these histone modifiers could control the same pathway leading to the formation of a diploid zygote.

Lid and SIN3 are required for sperm chromatin remodeling at fertilization

The Lid demethylase has been previously shown to be required in the female germline for embryo viability [22,23]. Both studies reported a dual phenotype for eggs produced by *lid* KD females (hereafter called *lid* KD eggs): while a majority of eggs fail to initiate development, a variable but significant fraction developed but died at later stages. Our own observations confirmed that about 15% of *lid* KD embryos reach or develop beyond the blastoderm stage (S1 Fig). Furthermore, our analysis of *Pfg-GFP::cid]* expression (Fig 1B) indicates that most of these late, non viable KD embryos are haploid and develop with maternal chromosomes. To follow the fate of paternal chromosomes in *lid* KD eggs, we crossed *lid* KD females with males expressing the sperm chromatin marker Mst35Ba::GFP (ProtA::GFP) [24]. In *Drosophila*, protamine-like proteins such as Mst35Ba are rapidly removed from sperm chromatin at fertilization [1] and, accordingly, ProtA::GFP is never observed in the male nucleus of control eggs. In striking contrast, the vast majority of fertilized *lid* KD eggs contained a needle-shaped sperm nucleus that was still positive for ProtA::GFP, indicating that sperm chromatin remodeling was compromised (Fig 1C and 1D). Anti-histone immunostaining indeed revealed that the replacement of SNBPs with maternally supplied histones was variable in KD eggs, ranging from complete absence of histones in the sperm nucleus to the coexistence of variable amounts

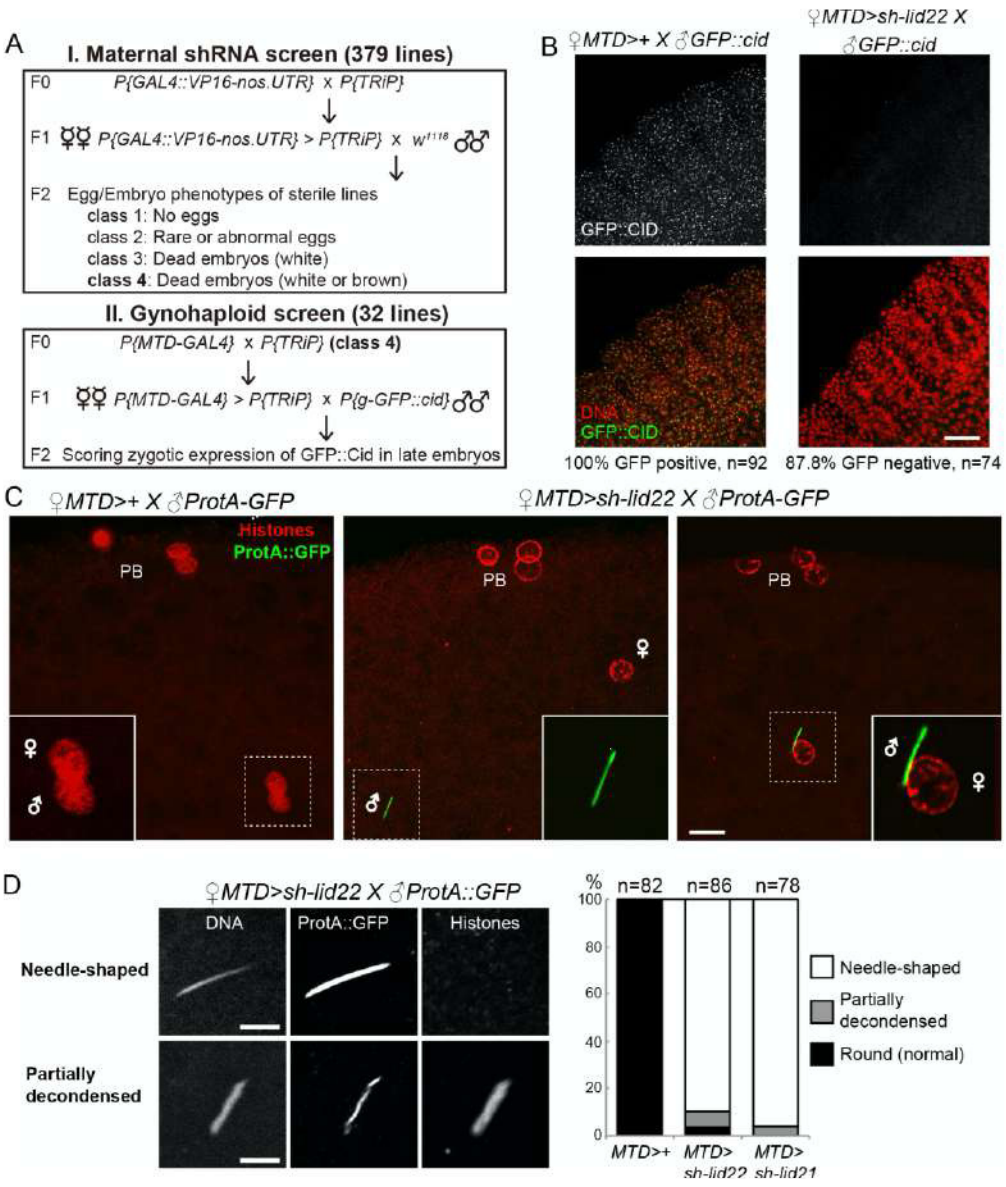

Fig 1. Lid is required for sperm nuclear decompaction at fertilization. A—Scheme of shRNA screen in the female germline. B—Left: Zygotic expression of a paternally-derived *P{g-GFP::cid}* transgene in a control embryo. GFP::Cid marks centromeric chromatin and is visible as nuclear dots. Right: *lid* KD females produce embryos that fail to express the paternally-inherited transgene. Scale bar: 25 μm. C—Maternal Lid is required for SNBP removal and sperm nuclear decompaction at fertilization. Left: a control egg at pronuclear apposition. Both pronuclei (inset) appear similar in size and shape and the SNBP marker ProtA::GFP is not detected. Middle: A representative *lid* KD egg containing a needle-shaped sperm nucleus (inset) still packaged with ProtA::GFP. Right: A fertilized *lid* KD egg with the sperm nucleus apposed to the female pronucleus. Scale bar: 10 μm. D—SNBP replacement with histones is impaired in *lid* KD eggs. Left: Confocal images of representative sperm nuclei in *lid KD* eggs. Partially decondensed nuclei are positive for histones. Scale bar: 5 μm. Right: Quantification of sperm nuclear phenotype in control and *lid* KD eggs.

https://doi.org/10.1371/journal.pgen.1008543.g001

Table 1. Embryo hatching rates.

Female genotype	Male genotype	Number of eggs	Hatch. rate (%)
w^{1118}	w^{1118}	344	97.67
dhd^{J5}	w^{1118}	375	0.00
dhd^{J5}/FM7c	w^{1118}	573	78.36
MTD>+	w^{1118}	1561	98.27
MTD>sh-lid22	w^{1118}	1403	2.14
MTD>sh-lid21	w^{1118}	1144	1.05
MTD>sh-Sin3A	w^{1118}	1221	0.25
MTD>sh-rpd3	w^{1118}	521	4.03
MTD>sh-Hira	w^{1118}	315	0.00
Rescue with *P[dhd^{WT}]* genomic transgene			
dhd^{J5}; *P[dhd]*	w^{1118}	663	85.67
dhd^{J5}; *P[dhd]/TM2*	w^{1118}	884	94.57
MTD>sh-lid22, P[dhd]	w^{1118}	1159	4.57
Rescue with *P[gnu-dhd^{WT}]* transgene			
dhd^{J5}; *P[gnu-dhd]*	w^{1118}	331	7.25
dhd^{J5}; *P[gnu-dhd]/TM2*	w^{1118}	1059	3.40
MTD>sh-lid22, P[gnu-dhd]/+	w^{1118}	695	7.48
Rescue with *P[UASP-dhd]* inducible transgenes			
nos>+	w^{1118}	711	95.36
nos>P[UASP-dhd]/+	w^{1118}	450	97.33
dhd^{J5}; *nos>P[UASP-dhd]*	w^{1118}	1163	99.28
dhd^{J5}; *nos>P[UASP-dhd^{XXXS}]*	w^{1118}	702	0.00
MTD>sh-lid22, P[UASP-dhd]	w^{1118}	1343	28.44
MTD>sh-lid22, P[UASP-dhd^{XXXS}]	w^{1118}	315	14.60
nos>sh-lid21	w^{1118}	1508	1.92
nos>P[UASP-dhd]/sh-lid21	w^{1118}	383	19.32
nos>sh-Sin3a	w^{1118}	542	2.03
nos>P[UASP-dhd]/sh-Sin3a	w^{1118}	621	8.86
nos>sh-Rpd3	w^{1118}	919	2.94
nos>P[UASP-dhd]/sh-Rpd3	w^{1118}	395	7.59
nos>sh-Hira	w^{1118}	514	0.00
nos>P[UASP-dhd]/sh-Hira	w^{1118}	380	0.00

https://doi.org/10.1371/journal.pgen.1008543.t001

of histones and ProtA::GFP (Fig 1D). Notably, we noticed that partially decondensed sperm nuclei in *lid* KD eggs were systematically positive for histones. Taken together, our observations indicate that sperm chromatin remodeling is severely impaired in *lid* KD eggs, thus explaining the absence of paternal chromosomes in most developing embryos.

Germline depletion of Lid was previously shown to affect karyosome morphology and chromosome positioning in metaphase I oocytes [25]. In contrast, another study had previously reported that meiotic progression was not affected in *lid* KD oocytes [22]. Interestingly, although our own observations indeed confirmed the aberrant karyosome structure in *lid* KD oocytes, we observed that the second meiotic division appeared to resume normally in a vast majority of *lid* KD eggs (S2 Fig). We noted, however, that, following meiosis, the female pronucleus frequently (62%, n = 76) failed to appose to the sperm nucleus in *lid* KD eggs (Fig 1C). Thus, we propose that defective pronuclear migration largely accounts for the previously reported failure of *lid* KD embryos to initiate cleavage divisions [23]. Like Navarro-Costa

et al., we noted that the rosette of polar body chromosomes was frequently abnormal in morphology, but this phenotype appeared independent of meiosis *per se*.

Remarkably, we found that germline KD of *Sin3A* also induced a highly penetrant sperm nuclear phenotype with all scored fertilizing sperm nuclei retaining a needle-like shape (100%, n = 19) (S3 Fig). Finally, a similar but less penetrant phenotype was also observed in *rpd3 KD* eggs (S3 Fig). As this low penetrance could result from less efficient gene knock-down, we chose to mainly focus on *lid and Sin3A* in the rest of this study.

Transcriptomic analysis of *lid* KD and *Sin3A* KD ovaries identifies *deadhead* as a common and major target gene

In eggs from wild-type females, anti-Lid immunostaining failed to detect Lid protein in the male or female pronucleus, thus suggesting that its implication in sperm chromatin remodeling was indirect. In fact, Lid was not detected in embryos before the blastoderm stage (S4 Fig). We thus turned to RNA sequencing (RNA Seq) to analyze the respective impact of *lid* KD and *Sin3A* KD on the ovarian transcriptome.

We compared transcriptomes obtained from *lid* KD or *Sin3A* KD ovaries (using the maternal triple driver MTD-Gal4) with control transcriptomes (MTD-Gal4 only). Globally, our analyses revealed a relatively modest impact of *lid* KD and *Sin3A* KD on ovarian gene expression, with more genes downregulated in both cases (Fig 2B and S5 Fig; S2 Table). Note that these changes are expected to reflect the activity of Lid and Sin3A in germ cells, as ovarian somatic cells (see Fig 2A) do not express the targeting shRNAs. In their transcriptome analysis (based on microarrays) of *lid* KD wing imaginal discs, Azorin and colleagues found a similar number of differentially-expressed genes, most of them being downregulated [14]. However, RNA Seq analyses recently published by Drelon *et al.* in contrast found 1630 genes (FDR<0.05) dysregulated in wing discs from a null *lid* mutant [26]. Moreover, Liu and Secombe [27] found 8,056 genes differentially expressed (60% were down-regulated) in *lid* adult mutant flies (FDR<0.05), a number which could reflect the greater cell type complexity involved in this analysis.

We found that only 29% (139) of the 473 differentially-expressed genes in *lid* KD were also differentially-expressed in *Sin3A* KD, and only 100 genes (21%) were dysregulated in the same direction in both KD (Fig 2B). As a matter of comparison, Gajan *et al.* found a 65% overlap in *Drosophila* S2 cells [17]. As the *Sin3A* shRNA that we used targets all predicted alternatively spliced mRNAs, this suggests that the knock-down affects Sin3A isoforms with Lid-independent functions [16].

Remarkably, however, we noticed that the *deadhead (dhd)* gene was by far the most severely impacted gene, downregulated by more than two orders of magnitude in both *lid* KD and *Sin3A* KD transcriptomes (Fig 2C, S6 Fig). The implication of *dhd* appeared particularly interesting because we and others have recently established that this germline-specific gene is critically required for sperm nuclear decompaction at fertilization [6,28]. *dhd* indeed encodes a specialized thioredoxin that cleaves disulfide bonds on SNBPs, thus facilitating their removal from sperm chromatin [6,28]. RT-PCR and Western-blot analyses confirmed the severe down-regulation of *dhd* in *lid* KD and *Sin3A* KD (S5 Fig).

dhd is a small, intronless gene located in the middle of a cluster of fifteen densely packed genes spanning about 40 kb of genomic DNA. Interestingly, the *dhd* gene lies within a 1.4 kb region that is immediately flanked by two genes with testis-specific expression (*Trx-T* and *CG4198*) (Fig 2D). Despite this apparently unfavorable genomic environment, *dhd* is one of the most highly-expressed genes in ovaries [29], as confirmed by our RNA Seq profiles (Fig 2C and S6 Fig). Interestingly, although this 40 kb region contains six additional genes expressed

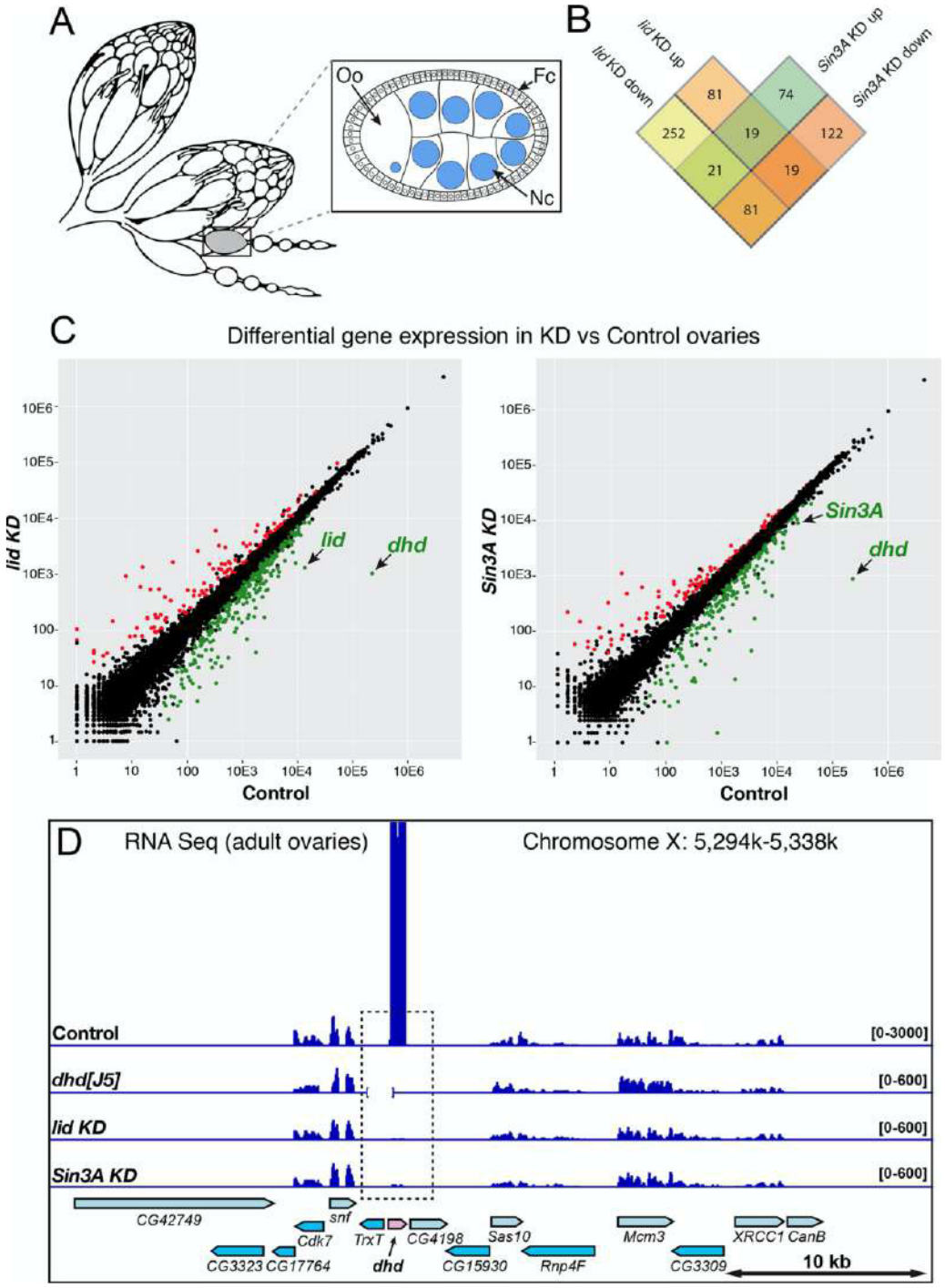
A
Oo
Fc
Nc
B
lid KD up
lid KD down
Sin3A KD up
Sin3A KD down
81
74
252
19
122
21
19
81
C
Differential gene expression in KD vs Control ovaries
lid KD
Control
lid
dhd
Sin3A KD
Sin3A
dhd
D
RNA Seq (adult ovaries)
Chromosome X: 5,294k-5,338k
Control
dhd[J5]
lid KD
Sin3A KD
[0-3000]
[0-600]
[0-600]
[0-600]
CG42749
snf
Cdk7
TrxT
CG4198
Sas10
Mcm3
XRCC1
CanB
CG3323
CG17764
dhd
CG15930
Rnp4F
CG3309
10 kb

Fig 2. *deadhead* is strongly downregulated in *lid* KD and *Sin3A* KD ovaries. A—Scheme of a pair of adult ovaries with two isolated ovarioles and an egg chamber (inset). Germline nuclei are in blue. Oo: Oocyte, Nc: Nurse cells, Fc: Follicle cells. B—Venn diagram showing the number of differentially expressed genes in *lid* KD and *Sin3A* KD ovarian transcriptomes (FDR<0.001). C—Comparison of RNA seq normalized reads per gene (DESeq2) are shown for *lid* KD vs Control (left) and *Sin3A* KD vs Control (right). Genes with a negative foldchange (downregulated in KD) are in green (FDR<0.001). Genes with a positive foldchange (upregulated in KD) are in red (FDR<0.001). D—Integrative Genomics Viewer (igv) view of Control, dhd^{Df5}, *lid* KD and *Sin3A* KD ovarian RNA Seq signal on the *dhd* region. The *Df(1)5* deficiency is indicated as an interrupted baseline on the dhd^{Df5} track.

https://doi.org/10.1371/journal.pgen.1008543.g002

in ovaries, *dhd* is the only one affected by *lid* KD or *Sin3A* KD (Fig 2D). Thus, Lid and the SIN3 complex exert a critical and surprisingly specific control on the transcriptional activation of *dhd* in female germ cells.

Impact of Lid depletion on the distribution of H3K4me3 in ovaries

To evaluate the impact of *lid* KD on the distribution of its target histone mark in the female germline, we performed chromatin immunoprecipitation and sequencing (ChIP-Seq) analyses of H3K4me3 in ovaries from control and *lid* KD females. Consistent with earlier reports of a global increase of H3K4me3 in *lid* mutant tissues [14,23,25,30], we observed that H3K4me3 ChIP peaks in *lid* KD ovaries were globally more pronounced compared to control ovaries (Fig 3A). Our analysis actually revealed that about 10% (1528) of H3K4me3 identified peaks in control ovaries were significantly increased in *lid* KD ovaries (S3 Table; FDR<0.05). For those peaks that were associated with genes, the relative enrichment of H3K4me3 in *lid* KD ovaries mainly affected the promoter region and gene body (Fig 3B). A similar effect was previously observed in *lid* depleted wing imaginal discs, with H3K4me3 abundance specifically increased at the TSS of Lid direct target genes [14]. We nevertheless found 46 H3K4me3 peaks that were significantly decreased in *lid* KD ovaries compared to control ovaries (S3 Table; FDR<0.05). Among these, the H3K4me3 peak on the *dhd* gene was the second most severely affected (S3 Table and Fig 3C). Furthermore, only ten of the negatively affected peaks covered genes that were downregulated in *lid* KD ovaries, including *dhd*. Remarkably, the prominent H3K4me3 peak on *dhd* was almost completely lost in *lid* KD ovaries while other peaks within the *dhd* region remained essentially unchanged. *CG4198*, which lies immediately downstream of *dhd* is a notable exception, as this gene also shows a decrease of H3K4me3 (Fig 3C). In this case, however, it is interesting to note that the presence of the mark is not correlated with transcriptional activity.

At first, the paradoxical loss of H3K4me3 enrichment on the *dhd* gene upon Lid depletion suggests that the demethylase activity of Lid is not locally responsible for this regulation. In fact, it has been established that *lid* mutant females with a catalytic dead JmjC^{-} *lid* rescue transgene are viable and at least partially fertile [23,26,31], thus suggesting that the catalytic activity of Lid is not absolutely required to form a viable zygote. To directly test the implication of the Lid demethylase domain in *dhd* regulation, we measured *dhd* expression in JmjC^{-} rescued females. Surprisingly, *dhd* transcripts were severely reduced in these females compared to control females rescued with a wild-type *lid* transgene (S7 Fig). We thus conclude that the demethylase activity of Lid is important for *dhd* expression. At least two hypotheses could reconcile this conclusion with our ChIP-Seq results. First, it is possible that the demethylase activity of Lid is only transiently required at the *dhd* locus, perhaps to switch on its transcription at mid-oogenesis, while later, massive *dhd* expression would no longer require this activity. Alternatively, Lid could exert a control on *dhd* transcription by restricting the level of H3K4me3 at an enhancer element, similarly to what was previously reported for KDM5 demethylases in different model organisms [32–34]. Although our ChIP-Seq analyses failed to identify any

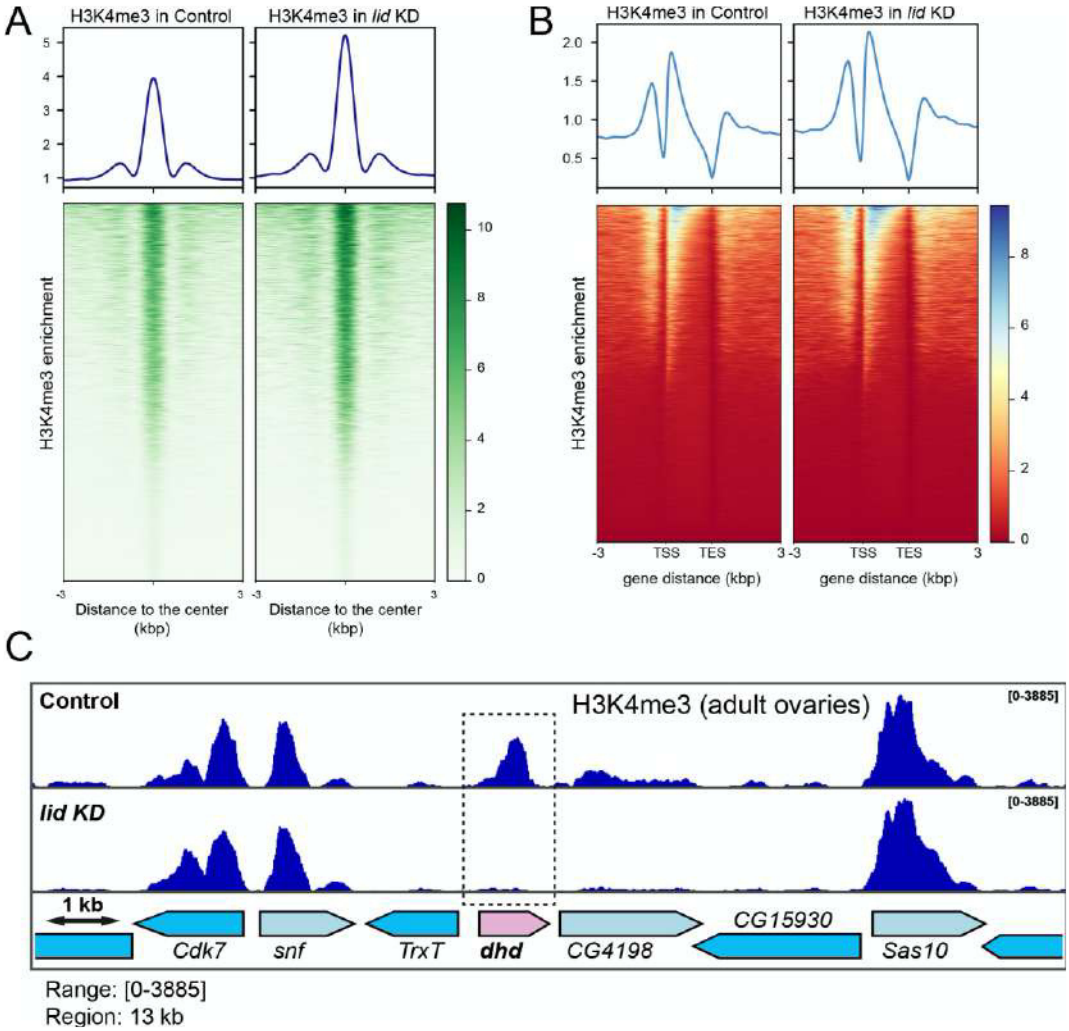

Fig 3. H3K4me3 ovarian ChIP-Seq analysis. A–H3K4me3 enrichment around peak center for Control and *lid* KD ovaries. Upper panels show the average profile around detected peak centers. Lower panels show read density heatmaps around the detected peak centers. B—H3K4me3 enrichment around gene loci for Control and *lid* KD ovaries. Upper panels show the average signal profile on genomic loci defined as 3kb upstream of annotated TSS to 3kb downstream of annotated TES. Lower panels show read density heatmaps around the same genomic loci. C—igv view of H3K4me3 occupancy on the *dhd* genomic region in Control and *lid* KD ovaries.

https://doi.org/10.1371/journal.pgen.1008543.g003

obvious candidate enhancer element in the vicinity of the *dhd* gene region, we cannot exclude this possibility.

Besides its JmjC demethylase domain, Lid/KDM5 possesses a conserved C-terminal PHD motif capable of binding H3K4me2/3. This binding motif is required for the recruitment of Lid at the promoter of target genes, where it could promote their activation [27]. The local recruitment of Lid, either through its C-terminal PHD motif or through its DNA binding ARID (AT-rich interaction domain) motif, or both, could thus establish a chromatin

environment permissive to *dhd* massive expression in late oogenesis. In this context, the role of the Sin3A/HDAC1 complex also remains to be clarified. The Sin3A histone deacetylase complex is generally considered as a transcriptional repressor [15], but it also functions as a transcriptional activator in *Drosophila* S2 cells [17]. Lacking an intrinsic DNA binding ability [15], the recruitment of this complex to chromatin requires an additional factor. It is thus tempting to propose that Lid itself could recruit Sin3A/HDAC1 locally to activate *dhd* expression in female germ cells.

Forced *dhd* expression in *lid* KD ovaries partially restores sperm chromatin remodeling at fertilization

Taken together, our cytological and transcriptomic analyses strongly suggest that the loss of *dhd* expression in *lid* KD ovaries at least contributes to the observed fertilization phenotype. To directly test this possibility, we attempted to restore *dhd* expression in *lid* KD female germ cells through the use of transgenic constructs. A genomic transgene (P[*dhd*]) that fully rescued the fertility of *dhd* mutant females [6] only had a very limited impact on the hatching rate of *lid* KD embryos (Table 1) but quantitative RT-PCR analyses revealed that P[*dhd*] remained essentially silent in *lid* KD ovaries (Fig 4A). This result indicates that the 4.3 kb genomic region present in this transgene is sufficient to recapitulate the endogenous control exerted by Lid on *dhd* transcription. We then designed another transgene expressing *dhd* under the control of the *giant nuclei* (*gnu*) regulatory sequences. Like *dhd*, *gnu* is specifically expressed during oogenesis and is functionally required during zygote formation [35]. In addition, our RNA Seq data indicated that its expression is not controlled by Lid. We observed that the P[*gnu-dhd*] transgene indeed restored fertility to *dhd* homozygous mutant females albeit to modest level (about 7% embryo hatching rate; Table 1). In fact, rescued females only produced about 10% of the normal amount of *dhd* mRNA in their ovaries and the DHD protein remained almost undetectable in Western-blot (Fig 4A). Interestingly, when introduced into *lid* KD females, the P[*gnu-dhd*] transgene also slightly increased embryo hatching rate (Table 1). Furthermore, cytological examination of eggs laid by these females revealed a limited but clear improvement of sperm nuclear decondensation (Fig 4B and 4C). These results thus indicate that forced expression of *dhd* can improve the survival of *lid* KD eggs through its positive impact on sperm chromatin remodeling. Finally, we tried to further increase the level of expression of *dhd* by using a Gal4 inducible transgene, P[UAS-dhd^{WT}]. Indeed, induction of this transgene in the germline of dhd^{P5} mutant females fully restored their fertility (Table 1). We also observed a strong effect on the hatching rate of embryos laid by *lid* KD, P[UAS-dhd^{WT}] females (about 28%; Table 1). However, a P[UAS-dhd^{sons}] transgene expressing a catalytic mutant DHD with no rescuing potential also improved the fertility of *lid* KD females. This effect suggests that Gal4 becomes limiting in the presence of two UAS transgenes, with a negative impact on knock-down efficiency. The fertility of P[UAS-dhd^{WT}] rescued females was nevertheless doubled compared to P[UAS-dhd^{sons}] control females (Table 1), thus supporting the idea that partial *dhd* re-expression in *lid* KD ovaries significantly improved the probability of these eggs to form a viable, diploid zygote. Besides its already established roles in controlling the oocyte epigenome and the architecture of meiotic chromosomes, we show that the transcriptional regulation of *dhd* (and possibly additional early acting genes) is indeed a critical function of Lid and associated factors in female germ cells.

Trr controls sperm chromatin remodeling through a DHD-independent pathway

Intriguingly, germline KD of the Trithorax group protein Trithorax-related (Trr, also known as dMLL3/4), a histone methyltransferase responsible for monomethylation of H3K4 [36], was

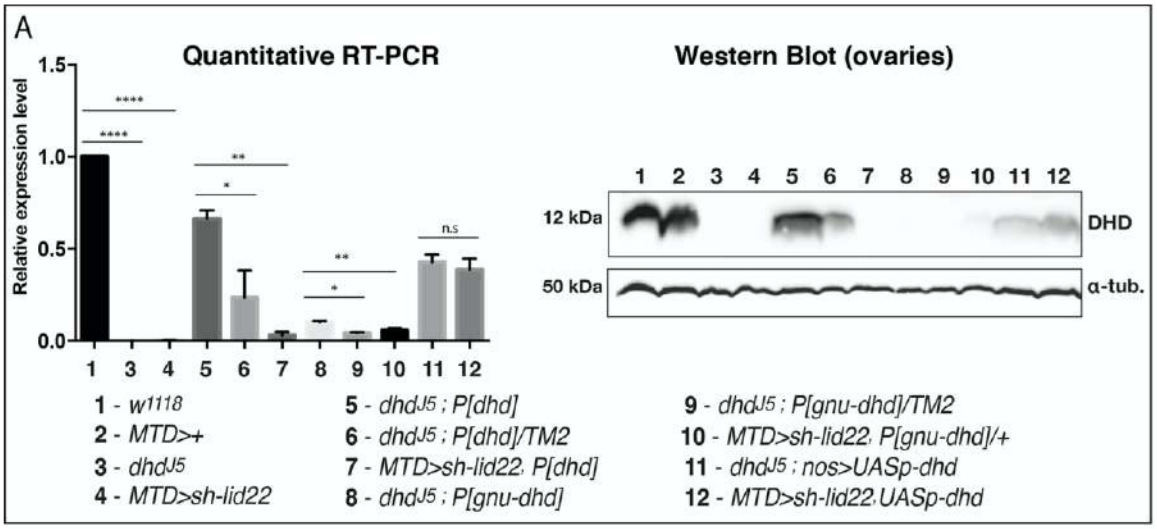
A
Quantitative RT-PCR
Relative expression level
1.5
1.0
0.5
0.0
****
****
**
*
**
*
n.s
1 3 4 5 6 7 8 9 10 11 12
Western Blot (ovaries)
1 2 3 4 5 6 7 8 9 10 11 12
12 kDa
DHD
50 kDa
α-tub.
1 - w1118
2 - MTD>+
3 - dhdJ5
4 - MTD>sh-lid22
5 - dhdJ5 ; P[dhd]
6 - dhdJ5 ; P[dhd]/TM2
7 - MTD>sh-lid22, P[dhd]
8 - dhdJ5 ; P[gnu-dhd]
9 - dhdJ5 ; P[gnu-dhd]/TM2
10 - MTD>sh-lid22, P[gnu-dhd]/+
11 - dhdJ5 ; nos>UASp-dhd
12 - MTD>sh-lid22,UASp-dhd

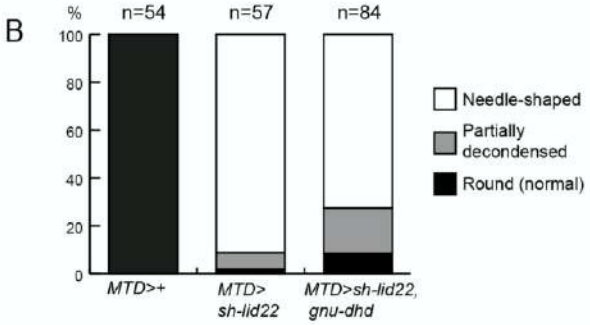
B
%
n=54
n=57
n=84
100
80
60
40
20
0
MTD>+
MTD> sh-lid22
MTD>sh-lid22, gnu-dhd
Needle-shaped
Partially decondensed
Round (normal)

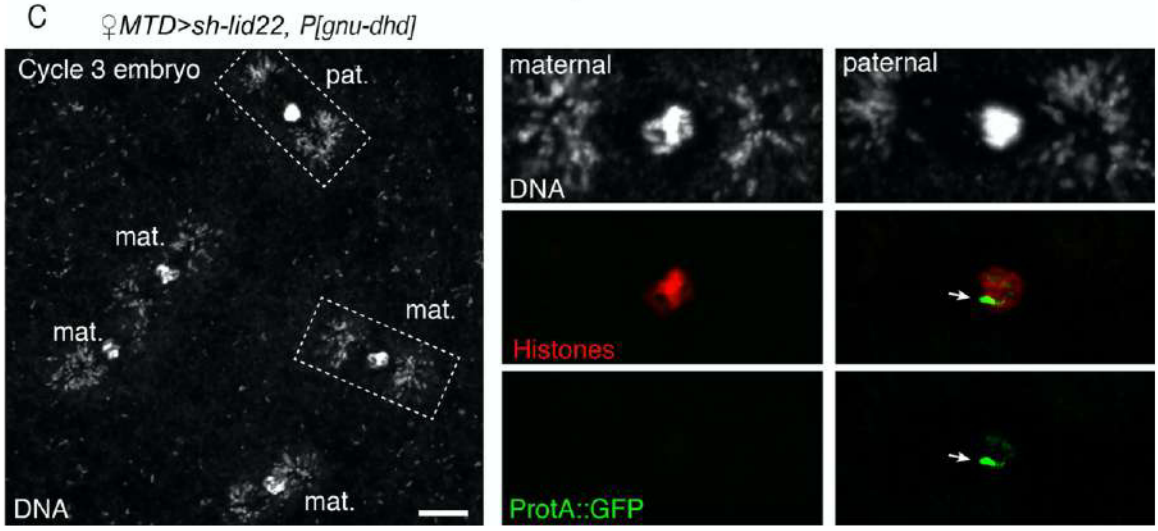
C
♀MTD>sh-lid22, P[gnu-dhd]
Cycle 3 embryo
pat.
mat.
mat.
mat.
mat.
DNA
maternal
paternal
DNA
Histones
ProtA::GFP

Fig 4. Forced expression of *dhd* partially rescues the *lid* KD phenotype. A—Left: RT-qPCR quantification of *dhd* mRNA levels in ovaries of indicated genotypes (normalized to *rp49* and relative to expression in w^{1118}). Data are presented as mean ± SD of 2 biological replicates. P values indicate one-way ANOVA with Dunnett's multiple comparisons test to a control (****: $P < 0.0001$; **: $P < 0.01$; *: $P < 0.03$; n.s = not significant). Right: Western blot analysis of DHD expression in ovaries of indicated genotypes. Alpha-tubulin detection is used as a loading control in Western-blotting. B—Quantification of sperm nuclear phenotype in eggs laid by females of indicated genotypes. C—Confocal images of a *MTD>lid22, P{gtu-dhd}* haploid embryo during the third nuclear division with incompletely remodeled male nucleus. Karyogamy has failed and the embryo contains four haploid nuclei of presumably maternal origin. The paternal nucleus (inset) still contains a region packaged with ProtA::GFP (arrow). Note that DNA positive dots at the spindle poles are *Wolbachia* endosymbionts. Scale bar: 10 μm.

https://doi.org/10.1371/journal.pgen.1008543.g004

recently shown to induce a sperm decondensation defect at fertilization similar to the one reported here for *lid*, *Sin3a* and *rpd3* KD [37]. In their study, however, Prudêncio *et al.* did not find any significant change in *dhd* mRNA level in *trr* KD early embryos. To more directly exclude any implication of DHD in the *trr* KD phenotypes, we stained control and KD eggs with an anti-DHD antibody. At fertilization, maternally-expressed DHD is abundant throughout the egg cytoplasm (100%, n = 41) but is rapidly degraded after pronuclear apposition. As expected, DHD protein remained undetectable in most *lid* KD eggs (92%, n = 50), including those that were fixed before the end of meiosis II (S8 Fig). In sharp contrast, DHD protein was normally detected in a majority of *trr* KD eggs, even though these eggs indeed contained a needle-shaped sperm nucleus still packaged with SNBPs (S8 Fig). This result thus confirms that Trr/dMLL3/4 controls sperm nuclear remodeling through a yet unknown, DHD-independent mechanism. Conversely, Trr was shown to control meiosis progression through the activation of *Idgf4* [37], a gene that is not affected by *lid* or *Sin3a* KD (this study). Thus Trr and Lid/Sin3A respectively activate a distinct repertoire of genes important for the oocyte-to-zygote transition and sperm chromatin remodeling.

Conclusion

Our maternal germline genetic screen has unveiled a complex and remarkably specific transcriptional regulation of the *dhd* gene by Lid/KDM5 and the Sin3A/HDAC1 complex. In addition to its crucial role in sperm protamine removal at fertilization, DHD was recently involved in the establishment of a redox state balance at the oocyte-to-zygote transition with a number of identified target proteins [7]. This important DHD-dependent thiol proteome remodeling is thus ultimately controlled by Lid and the SIN3 complex, underlying the critical contribution of these transcriptional regulators to this delicate developmental transition. Future work will aim at dissecting the chromatin mechanisms at play in setting up *dhd* specific activation in female germ cells.

Materials & methods

Drosophila strains

Flies were raised at 25˚C on standard medium. The w^{1118} strain was used as a wild-type control. shRNAs lines used in this study (see S1 Table) were established by the Transgenic RNAi Project (TRiP) at Harvard Medical School and were obtained from the Bloomington Drosophila Stock Center at Indiana University. The *lid* and *Sin3A* shRNA lines target all predicted isoforms of their respective target genes. Additional stocks were *EGFP-Cid* [38], *P{otu-GAL4::VP16.R}1*; *P{GAL4-nos.NGT}40*; *P{GAL4::VP16-nos.UTR}MVD1* ("MTD-Gal4"), *P{GAL4::VP16-nos.UTR}MVD1* ("nos-Gal4"), *P{Mst35Ba-EGFP}* [24] and *Df(1)J5/FM7c* [39]. The *pUASP-dhd{WT}* and *pUASP-dhd{SXXS}* transgenic flies were a gift from C. Gonzalez and C. Molnar. The *PattB{gLid-WT-HA}* and *PattB{gLid-ΔMIC-HA}* transgenic flies were kindly provided by P. Navarro-Costa [23].

Germline knock-down and fertility tests

To obtain *KD* females, virgin shRNA transgenic females were mass crossed with transgenic Gal4 males at 25˚C and females of the desired genotype were recovered in the F1 progeny. To measure fertility, virgin females of different genotypes were aged for 2 days at 25˚C in the presence of males and were then allowed to lay eggs on standard medium for 24 hours. Embryos were counted and then let to develop for at least 36 hours at 25˚C. Unhatched embryos were counted to determine hatching rates.

Immunofluorescence and imaging

Early (0–30 min) and late (about 6 hours) embryos laid by randomly selected females were collected on agar plates. Embryos were dechorionated in bleach, fixed in a 1:1 heptane:methanol mixture and stored at -20˚C. Embryos were washed three times (10 min each) with PBS1X 0.1%, Triton X-100 and were then incubated with primary antibodies in the same buffer on a wheel overnight at 4˚C. They were then washed three times (20 min each) with PBS 0.1%, Triton X-100. Incubations with secondary antibodies were performed identically. Embryos were mounted in Dako mounting medium containing DAPI.

Ovaries were dissected in PBS-Triton 0.1% and fixed at room temperature in 4% formaldehyde in PBS for 25 minutes. Immunofluorescence was performed as for embryos except for secondary antibodies that were incubated four hours at room temperature. Ovaries were then mounted as described above.

Primary antibodies used were mouse monoclonal anti-histones (Sigma #MABE71; 1:1000), rabbit polyclonal anti-DHD (1:1000) [6], rat polyclonal anti-Lid (1:500) [14], mouse monoclonal anti-GFP (Roche #118144600001; 1:200) and Rat monoclonal anti alpha-tubulin (Abcam #ab6160; 1:50). Secondary antibodies were goat anti-rabbit antibodies (ThermoFisher Scientific, 1:500), goat anti-mouse or anti-rat antibodies (Jackson ImmunoResearch, 1:500) conjugated to AlexaFluor. Images were acquired on an LSM 800 confocal microscope (Carl Zeiss). Images were processed with Zen imaging software (Carl Zeiss) and Photoshop (Adobe).

Western blotting

Ovaries from 30 females were collected and homogenized in lysis buffer (20mM Hepes pH7.9, 100mM KCl, 0.1mM EDTA, 0.1mM EGTA, 5% Glycerol, 0.05% Igepal and protease inhibitors (Roche)). The protein extracts were cleared by centrifugation and stored at -80˚C.

Eggs were collected every 30 min, dechorionated in bleach and quickly frozen in liquid nitrogen. Protein extracts were prepared from ca. 10 μl of embryos. Protein samples were run on 15% SDS polyacrylamide gel and transferred to Immun-Blot® PVDF membrane (Bio-Rad) for 1h at 60V. Membranes were blocked for 1h at room temperature in 5% non-fat milk in PBS 1X-Tween20 0.05%, followed by an overnight incubation with the primary antibody at 4˚C in 5% non-fat milk in PBS1X-Tween20 0.05%. Secondary antibodies used were added and incubated for 2 hours at room temperature. Protein detection was performed using ECL solution according manufacturer's instruction (GE Healthcare). Antibodies used were: rabbit polyclonal anti-DHD (1/1000) [6], mouse monoclonal anti-α-Tubulin (Sigma Aldrich #T9026, 1:500), HRP-conjugated goat anti-mouse (Biorad #170–5047; 1:50 000) and peroxidase-conjugated goat anti-rabbit (Thermoscientific #32460; 1:20 000).

Gene expression analysis by RT-QPCR

Total RNA was extracted from ovaries of 3-day-old females using the NucleoSpin® RNA isolation kit (Macherey-Nagel), following the instructions of the manufacturer. Duplicates were

processed for each genotype. cDNAs were generated from 1μg of purified RNA with oligo (dT) primers using the SuperScript™ II Reverse Trancriptase kit (Invitrogen).

Generated cDNAs were diluted to 1/5 and were used as template in a real time quantitative PCR assay using SYBR® Premix Ex TaqTM II (Tli RNaseH Plus) (Takara). All qRT-PCR reactions were performed in duplicate using Bio-Rad CFX-96 Connect system with the following conditions: 95˚C for 1 min followed by 40 cycles of denaturation at 95˚C for 10 s, annealing at 59˚C for 30 s and extension at 72˚C for 30 s. Relative fold change in gene expression was determined by the comparative quantification ΔΔCT method of analysis [40]. The housekeeping gene *rp49* was used to normalize cDNA amounts in the comparative analysis. The primer sets used in the PCR reactions were: dhd-forward 5'- TCTATGCGACATGGTGTGGT -3' and dhd-reverse 5'- TCCACATCGATCTTGAGCAC -3'; lid-forward 5'- ATTGGTTTCACGAGGATTGC-3' and lid-reverse 5'- CATAGCCACTTGGGTCGATT -3'; Rp49-forward 5'- AAGATCGTGAAGAA GCGCAC -3' and Rp49-reverse 5'- GATACTGTCCCTTGAAGCGG -3'. Statistical tests were performed using GraphPad Prism version 6.00 for Mac OS X (GraphPad Software).

Ovarian RNA sequencing and analysis

For each samples, 8 pairs of ovaries were dissected from 6 day-old virgin females and total RNA were extracted using the NucleoSpin® RNA isolation kit (Macherey-Nagel), following the instructions of the manufacturer. Extracted RNAs were treated with Turbo™DNAse (Ambion #AM2238). After DNase inactivation, RNAs were purified using the NucleoSpin® RNA Clean-up XS kit (Macherey-Nagel) according to manufacturer's instructions. Sequencing was completed on two biological replicates of each genotype:

Control KD *(MTD-Gal4>+)*

P{w[+mC] = otu-GAL4::VP16.R}1, w[*]/y[1] v[1]; P{w[+mC] = GAL4-nos.NGT}40/+; P{w[+mC] = GAL4::VP16-nos.UTR}CG6325[MVD1]/P{y[+t7.7] = CaryP}attP2

lid KD *(MTD-Gal4>shRNA lid)*

P{w[+mC] = otu-GAL4::VP16.R}1, w[*]/y[1] sc[*] v[1]; P{w[+mC] = GAL4-nos.NGT}40/+; P{w[+mC] = GAL4::VP16-nos.UTR}CG6325[MVD1]/P{y[+t7.7] v[+t1.8] = TRiP.GLV21071}attP2

Sin3A KD *(MTD-Gal4>shRNA Sin3A)*

P{w[+mC] = otu-GAL4::VP16.R}1, w[*]/y[1] sc[*] v[1];P{w[+mC] = GAL4-nos.NGT}40/+; P{w[+mC] = GAL4::VP16-nos.UTR}CG6325[MVD1]/P{y[+t7.7] v[+t1.8] = TRiP.HMS00359}attP2

Sequencing libraries for each sample were synthesized using TruSeq Stranded mRNA kit (Illumina) following supplier recommendations (Sample Preparation Guide—PN 15031047, version Rev.E Oct 2013) and were sequenced on Illumina Hiseq 4000 sequencer as Single-Reads 50 base reads following Illumina's instructions (GenomEast platform, IGBM, Strasbourg, France). Image analysis and base calling were performed using RTA 2.7.3 and bcl2fastq 2.17.1.14. Adapter dimer reads were removed using DimerRemover. Sequenced reads were mapped to the *Drosophila melanogaster* genome assembly dm6 using TopHat (version 2.1.1) with default option. The aligned reads were assigned to genes by FeatureCounts, run with default options on the dmel-all-r6.15 version of the *Drosophila melanogaster* genome annotation. Differentially expressed genes were identified using the R-package DESeq2 (version 1.14.1). The annotated genes exhibiting an adjusted-P < 0.001 were considered differentially expressed compared to Control.

Chromatin immunoprecipitation, sequencing and analysis

ChIP assays were performed as previously described [41]. Two biological replicates for *control* KD and *lid* KD ovaries (same genotypes as for RNA Seq) were processed and analyzed. For

each biological replicate, eighty ovary pairs were dissected from 2 day-old females and flash frozen. Dissected ovaries were fixed in 1.8% formaldehyde at room temperature for 10 minutes. Chromatin was sonicated using a Diagenod Bioruptor (18 cycles, high intensity, 30s on/30s off) to generate random DNA fragments from 100 to 800 base pairs. Sheared chromatin was incubated overnight at 4˚C with H3K4me3 antibody (ab8580 Abcam). Immunoprecipitated samples were treated with RNAse A, proteinase K and DNA purified using the ChIP DNA Purification kit (Active Motif #58002) following the manufacturer's instructions. Quantification assessment of purified DNA was done using Qbit dsDNA HS Assay on the Qbit fluorometer (Invitrogen). Immunoprecipited DNA quality was evaluated on a Bioanalyzer 2100 (Agilent).

Sequencing libraries for each sample were synthesized using Diagenode MicroPlex Library Preparation kit according to supplier recommendations (version 2.02.15) and were sequenced on Illumina Hiseq 4000 sequencer as Paired-End 50 base reads following Illumina's instructions (GenomEast platform, IGBM, Strasbourg, France). Image analysis and base calling were performed using RTA 2.7.3 and bcl2fastq 2.17.1.14. Adapter dimer reads were removed using DimerRemover. Sequenced reads were mapped to the *Drosophila melanogaster* genome assembly dm6 using Bowtie (version 2.3.3) with default option. Only uniquely aligned reads have been retained for further analyses. Duplicated reads were removed using picard-tools (version 2.17.10). Peak calling was performed for each individual samples and on merged biological replicates using MACS algorithm (version 2.1.1) with default option and a relaxed q-value cut-off of 0.1. Consistent peaks between biological replicates were identified using irreproducible discovery rate (IDR version 2.0.3) with a 0.05 cut-off. Differentially modified H3K4me3 peaks between Control and *lid* Knock-down ovaries were identified using the R-package DiffBind (version 2.2.12) with a 0.05 FDR cut-off.

Data visualization

The Deeptools software was used to convert alignment files to bigwig (bamCoverage) and to generate H3K4me3 heatmap and density profiles (computeMatrix and plotHeatmap). The generated bigwig files were visualized using IGV software.

Supporting information

S1 Fig. Developmental defects of *lid* KD embryos. Embryos were collected for four hours and aged for another four hours at 25˚C before DAPI staining and examination in fluorescent microscopy. More than 85% of *lid* KD embryos arrest development before the blastoderm stage. In contrast, 100% of control embryos had reached gastrula or later stages.
(TIF)

S2 Fig. Meiosis II is not visibly affected in eggs from *lid* KD females. A—Representative confocal images of eggs in metaphase of meiosis II stained for DNA (blue), alpha-tubulin (red) and ProtA::GFP (green). The tandem of meiotic spindles is shown on the left, the corresponding male nucleus from the same egg is on the right. Bars: 5 μm. B—Quantification of meiosis II phenotypes (normal or abnormal chromosome segregation).
(TIF)

S3 Fig. Phenotype of *Sin3A* KD and *rpd3* KD eggs/embryos. A—Confocal images of *Sin3A* KD eggs stained for DNA at the indicated stages. The sperm nucleus in the left panel is indicated (arrow). Bar: 10 μm. PB: Polar bodies. B—Confocal images of *rpd3* KD early embryos (from ProtA::GFP fathers) stained for DNA and anti-GFP. The sperm nucleus is indicated

(arrows). Bar: 10 μm. PB: Polar bodies.
(TIF)

S4 Fig. Lid is not directly invoved in sperm chromatin remodeling at fertilization. A—Top row: confocal images of stage 10 egg chambers from control (left) and lid KD (right) females stained for DNA (red) and anti-Lid (green). Middle row: detail of a nurse cell nucleus. Bottom row: detail of the oocyte germinal vesicle (oocyte nucleus). Bar: 20 μm. B—Confocal images of the male pronucleus and the female pronucleus from a control egg in meiosis II stained for DNA and anti-Lid. Bar: 10 μm. Quantification of Lid positive nuclei is indicated. C—Confocal images of a control (left) and lid KD (right) blastoderm embryo with same staining as in B. Bar: 10 μm. Quantifications of embryos with a positive/negative nuclear Lid staining are indicated for each genotype.
(JPG)

S5 Fig. Lid and Sin3A control *dhd* expression in female germ cells. A—Principal Component Analysis of Control, *lid* KD and *Sin3A* KD ovarian transcriptomes (two biological replicates for each genotype). B—Volcano plot representations of Differentially-Expressed genes in Control vs *lid* KD (left) and Control vs *Sin3A* KD (right). C—RT-qPCR quantification of *dhd* mRNA levels in ovaries of indicated genotypes. mRNA levels were normalized to rp49 and shown as relative expression in MTD>+ control. Error bars represent SD (Dunnett's multiple comparisons test to the control MTD>+, **** $P < 0.0001$). D—Western blot analysis of DHD in adult ovaries (left) and 0-30min postfertilization embryos (right). α-tubulin was used as a loading control. E—Western blot analysis of DHD in adult ovaries of indicated genotypes. α-tubulin was used as a loading control.
(TIF)

S6 Fig. Top twelve most downregulated and upregulated genes in *lid* KD and *Sin3A* KD transcriptomes.
(TIF)

S7 Fig. The JmjC domain of Lid is required for normal *dhd* expression. A—Embryo hatching rates from females of indicated genotypes. B—RT-qPCR quantification of *dhd* (left) and *lid* (right) mRNA levels in ovaries of indicated genotypes. mRNA levels were normalized to rp49 and shown as relative expression in w^{1118} control. Error bars represent SD (Dunnett's multiple comparisons test to the control (** $P < 0.01$; **** $P = 0.0002$). C—Analysis of paternal GFP::Cid expression in late embryos from indicated females (as in Fig 1B).
(TIF)

S8 Fig. *trr* KD does not affect *dhd* expression. A—Confocal images of representative embryos of the indicated genotypes stained for DNA and anti-DHD. The fertilizing sperm nucleus is magnified in insets. Bar: 20 μm. B—Details of maternal chromosomes (top row) and sperm nucleus (bottow row) from a representative *trr* KD egg stained for ProtA::GFP and histones.
(JPG)

S1 Table. Haploid TRiP genetic screen.
(XLSX)

S2 Table. Differentially expressed genes in *lid* KD and *Sin3A* KD ovaries.
(XLSX)

S3 Table. Quantitative analysis of H3K4me3 differential enrichment in Control vs *lid* KD ovarian ChIP-Seq.
(XLSX)

Acknowledgments

We thank Ferran Azorin, Cayetano Gonzalez, Cristina Molnar and Paulo Navarro-Costa for sharing fly stocks and antibodies. We are grateful to the TRiP projects and Bloomington Drosophila Stock Center for shRNA stocks. The authors would like to thank the members of the IGBMC GenomEast platform for their help. We also thank Raphaëlle Dubruille for her helpful comments on the manuscript.

Author Contributions

Conceptualization: Daniela Torres-Campana, Shuhei Kimura, Guillermo A. Orsi, Benjamin Loppin.

Data curation: Guillermo A. Orsi, Gérard Benoit.

Formal analysis: Gérard Benoit.

Funding acquisition: Benjamin Loppin.

Investigation: Daniela Torres-Campana, Shuhei Kimura, Béatrice Horard, Benjamin Loppin.

Methodology: Gérard Benoit.

Supervision: Béatrice Horard, Benjamin Loppin.

Validation: Daniela Torres-Campana, Guillermo A. Orsi, Béatrice Horard, Gérard Benoit, Benjamin Loppin.

Writing – original draft: Benjamin Loppin.

Writing – review & editing: Daniela Torres-Campana, Guillermo A. Orsi, Béatrice Horard, Gérard Benoit, Benjamin Loppin.

References

1. Loppin B, Dubruille R, Horard B (2015) The intimate genetics of Drosophila fertilization. Open Biol 5: 150076. https://doi.org/10.1098/rsob.150076 PMID: 26246493
2. Hamm DC, Harrison MM (2018) Regulatory principles governing the maternal-to-zygotic transition: insights from Drosophila melanogaster. Open Biol 8: 180183. https://doi.org/10.1098/rsob.180183 PMID: 30977698
3. Spradling AC (1993) Developmental genetics of oogenesis. The Development of Drosophila melanogaster—Cold Spring Harbor Laboratory Press. 1–69.
4. Eirín-López JM, Ausió J (2009) Origin and evolution of chromosomal sperm proteins. Bioessays 31: 1062–1070. https://doi.org/10.1002/bies.200900050 PMID: 19708021
5. Rathke C, Baarends WM, Awe S, Renkawitz-Pohl R (2014) Chromatin dynamics during spermiogenesis. Biochim Biophys Acta 1839: 155–168. https://doi.org/10.1016/j.bbagrm.2013.08.004 PMID: 24091090
6. Tirmarche S, Kimura S, Dubruille R, Horard B, Loppin B (2016) Unlocking sperm chromatin at fertilization requires a dedicated egg thioredoxin in Drosophila. Nature Commun 7: 13539. https://doi:10.1038/ncomms13539
7. Petrova B, Liu K, Tian C, Kitaoka M, Freinkman E, Yang J, et al. (2018) Dynamic redox balance directs the oocyte-to-embryo transition via developmentally controlled reactive cysteine changes. Proc Natl Acad Sci USA 115: E7978–E7986. https://doi.org/10.1073/pnas.1807918115 PMID: 30082411
8. Horard B, Sapey-Triomphe L, Bonnefoy E, Loppin B (2018) ASF1 is required to load histones on the HIRA complex in preparation of paternal chromatin assembly at fertilization. Epigenetics Chromatin 11: 19. https://doi.org/10.1186/s13072-018-0189-x PMID: 29751847
9. Ni J-Q, Zhou R, Czech B, Liu L-P, Holderbaum L, Yang-Zhou D, et al. (2011) A genome-scale shRNA resource for transgenic RNAi in Drosophila. Nat Meth 8: 405–407. https://doi.10.1038/nmeth.1592
10. Delabaere L, Orsi GA, Sapey-Triomphe L, Horard B, Couble P, Loppin B (2014) The Spartan Ortholog Maternal Haploid Is Required for Paternal Chromosome Integrity in the Drosophila Zygote. Curr Biol 24: 2281–2287. https://doi.org/10.1016/j.cub.2014.08.010 PMID: 25242033

11. Gildea JJ, Lopez R, Shearn A (2000) A screen for new trithorax group genes identified little imaginal discs, the Drosophila melanogaster homologue of human retinoblastoma binding protein 2. Genetics 156: 645–663. PMID: 11014813

12. Secombe J, Li L, Carlos L, Eisenman RN (2007) The Trithorax group protein Lid is a trimethyl histone H3K4 demethylase required for dMyc-induced cell growth. Genes & Dev 21: 537–551. https://doi.10.1101/gad.1523007

13. Lloret-Llinares M, Carr CM, Vaquero A, de Olano N, Azorin F (2008) Characterization of Drosophila melanogaster JmjC+N histone demethylases. Nucleic Acids Res. 36: 2852–2863. https://doi.org/10.1093/nar/gkn098 PMID: 18375980

14. Lloret-Llinares M, Perez-Lluch S, Rossell D, Moran T, Ponsa-Cobas J, Auer H, et al. (2012) dKDM5/LID regulates H3K4me3 dynamics at the transcription-start site (TSS) of actively transcribed developmental genes. Nucleic Acids Res. 40: 9493–9505. https://doi.org/10.1093/nar/gks773 PMID: 22904080

15. Grzenda A, Lomberk G, Zhang J-S, Urrutia R (2009) Sin3: Master scaffold and transcriptional corepressor. Biochim Biophys Acta 1789: 443–450. https://doi.org/10.1016/j.bbagrm.2009.05.007 PMID: 19505602

16. Spain MM, Caruso JA, Swaminathan A, Pile LA (2010) Drosophila SIN3 Isoforms Interact with Distinct Proteins and Have Unique Biological Functions. J Biol Chem 285: 27457–27467. https://doi.org/10.1074/jbc.M110.130245 PMID: 20566628

17. Gajan A, Barnes VL, Liu M, Saha N, Pile LA (2016) The histone demethylase dKDM5/LID interacts with the SIN3 histone deacetylase complex and shares functional similarities with SIN3. Epigenetics Chromatin 9:4 https://doi.org/10.1186/s13072-016-0053-9 PMID: 26848313

18. Liu M, Pile LA (2017) The Transcriptional Corepressor SIN3 Directly Regulates Genes Involved in Methionine Catabolism and Affects Histone Methylation, Linking Epigenetics and Metabolism. J Biol Chem 292: 1970–1976. https://doi.org/10.1074/jbc.M116.749754 PMID: 28028175

19. Barnes VL, Bhat A, Unnikrishnan A, Heydari AR, Arking R, Pile LA (2014) SIN3 is critical for stress resistance and modulates adult lifespan. Aging 6: 645–660. https://doi.org/10.18632/aging.100684 PMID: 25133314

20. Moshkin YM, Kan TW, Goodfellow H, Bezstarosti K, Maeda RK, Pilyugin M, et al. (2009) Histone Chaperones ASF1 and NAP1 Differentially Modulate Removal of Active Histone Marks by LID-RPD3 Complexes during NOTCH Silencing. Mol Cell 35: 782–793. https://doi.org/10.1016/j.molcel.2009.07.020 PMID: 19782028

21. Lee N, Erdjument-Bromage H, Tempst P, Jones RS, Zhang Y (2009) The H3K4 Demethylase Lid Associates with and Inhibits Histone Deacetylase Rpd3. Mol Cell Biol 29: 1401–1410. https://doi.org/10.1128/MCB.01643-08 PMID: 19114561

22. Kronja I, Yuan B, Eichhorn SW, Dzeyk K, Krijgsveld J, Bartel DP, et al. (2014) Widespread Changes in the Posttranscriptional Landscape at the Drosophila Oocyte-to-Embryo Transition. Cell Reports 7: 1495–1508. https://doi.org/10.1016/j.celrep.2014.05.002 PMID: 24882012

23. Navarro-Costa P, McCarthy A, Prudêncio P, Greer C, Guilgur LG, Becker JORD, et al. (2016) Early programming of the oocyte epigenome temporally controls late prophase I transcription and chromatin remodelling. Nature Commun 7: 1–15. https://doi:10.1038/ncomms12331

24. Manier MK, Belote JM, Berben KS, Novikov D, Stuart WT, Pitnick S (2010) Resolving Mechanisms of Competitive Fertilization Success in Drosophila melanogaster. Science 328: 354–357. https://doi.org/10.1126/science.1187096 PMID: 20299550

25. Zhaunova L, Ohkura H, Breuer M (2016) Kdm5/Lid Regulates Chromosome Architecture in Meiotic Prophase I Independently of Its Histone Demethylase Activity. PLoS Genet. 12 e1006241. https://doi.org/10.1371/journal.pgen.1006241 PMID: 27494704

26. Drelon C, Belalcazar HM, Secombe J. The Histone Demethylase KDM5 Is Essential for Larval Growth in Drosophila (2018) Genetics 209 773–787. https://doi.org/10.1534/genetics.118.301004 PMID: 29764901

27. Liu X, Secombe J (2015) The Histone Demethylase KDM5 Activates Gene Expression by Recognizing Chromatin Context through Its PHD Reader Motif. Cell Reports 13: 2219–2231. https://doi.org/10.1016/j.celrep.2015.11.007 PMID: 26673323

28. Emelyanov AV, Fyodorov DV (2016) Thioredoxin-dependent disulfide bond reduction is required for protamine eviction from sperm chromatin. Genes & Dev 30: 2651–2656. https://doi:10.1101/gad.290916.116

29. Sandler JE, Stathopoulos A (2016) Quantitative Single-Embryo Profile of Drosophila Genome Activation and the Dorsal-Ventral Patterning Network. Genetics 202: 1575–1584. https://doi.org/10.1534/genetics.116.186783 PMID: 26896327

30. Zamurrad S, Hatch HAM, Drelon C, Belalcazar HM, Secombe J (2018) A Drosophila Model of Intellectual Disability Caused by Mutations in the Histone Demethylase KDM5. Cell Reports 22: 2359–2369. https://doi.org/10.1016/j.celrep.2018.02.018 PMID: 29490272

31. Li L, Greer C, Eisenman RN, Secombe J (2010) Essential functions of the histone demethylase lid. PLoS Genet. 6: e1001221. https://doi.org/10.1371/journal.pgen.1001221 PMID: 21124823

32. Lussi YC, Mariani L, Friis C, Peltonen J, Myers TR, Krag C, et al. (2016) Impaired removal of H3K4 methylation affects cell fate determination and gene transcription. Development 143: 3751–3762. https://doi.org/10.1242/dev.139139 PMID: 27578789

33. Kidder BL, Hu G, Zhao K (2014) KDM5B focuses H3K4 methylation near promoters and enhancers during embryonic stem cell self-renewal and differentiation. Genome Biol 15: R32. https://doi.org/10.1186/gb-2014-15-2-r32 PMID: 24495580

34. Outchkourov NS, Muiño JM, Kaufmann K, van Ijcken WFJ, Koerkamp MJG, van Leenen D, et al. (2013) Balancing of Histone H3K4 Methylation States by the Kdm5c/SMCX Histone Demethylase Modulates Promoter and Enhancer Function. Cell Reports 3: 1071–1079. https://doi.org/10.1016/j.celrep.2013.02.030 PMID: 23545502

35. Freeman M, Nüsslein-Volhard C, Glover DM (1986) The dissociation of nuclear and centrosomal division in gnu, a mutation causing giant nuclei in Drosophila. Cell 46: 457–468. https://doi.org/10.1016/0092-8674(86)90666-5 PMID: 3089628

36. Herz HM, Mohan M, Garruss AS, Liang K, Takahashi YH, Mickey K, et al. (2012) Enhancer-associated H3K4 monomethylation by Trithorax-related, the Drosophila homolog of mammalian Mll3/Mll4. Genes & Dev. 26: 2604–2620. https://doi:10.1101/gad.201327.112

37. Prudêncio P, Guilgur LG, Sobral J, Becker JD, Martinho RG, Navarro-Costa P (2018) The Trithorax group protein dMLL3/4 instructs the assembly of the zygotic genome at fertilization. EMBO Rep 19: e45728. https://doi.org/10.15252/embr.201845728 PMID: 30037897

38. Schuh M, Lehner CF, Heidmann S (2007) Incorporation of Drosophila CID/CENP-A and CENP-C into centromeres during early embryonic anaphase. Curr Biol 17: 237–243. https://doi.org/10.1016/j.cub.2006.11.051 PMID: 17222555

39. Salz HK, Flickinger TW, Mattendorf E, Pellicena-Palle A, Petschek JP, Brown Albretch E (1994) The Drosophila Maternal Effect Locus deadhead Encodes a Thioredoxin Homolog Required for Female Meiosis and Early Embryonic Development. Genetics 136: 1075–1086. PMID: 7516301

40. Livak KJ, Schmittgen TD (2001) Analysis of Relative Gene Expression Data Using Real-Time Quantitative PCR and the 2−ΔΔCT Method. Methods 25: 402–408. https://doi.org/10.1006/meth.2001.1262 PMID: 11846609

41. Grentzinger T, Armenise C, Brun C, Mugat B, Serrano V, Pelisson A, et al. (2012) piRNA-mediated transgenerational inheritance of an acquired trait. Genome Res 22: 1877–1888. https://doi.org/10.1101/gr.136614.111 PMID: 22555593

Supplemental data:

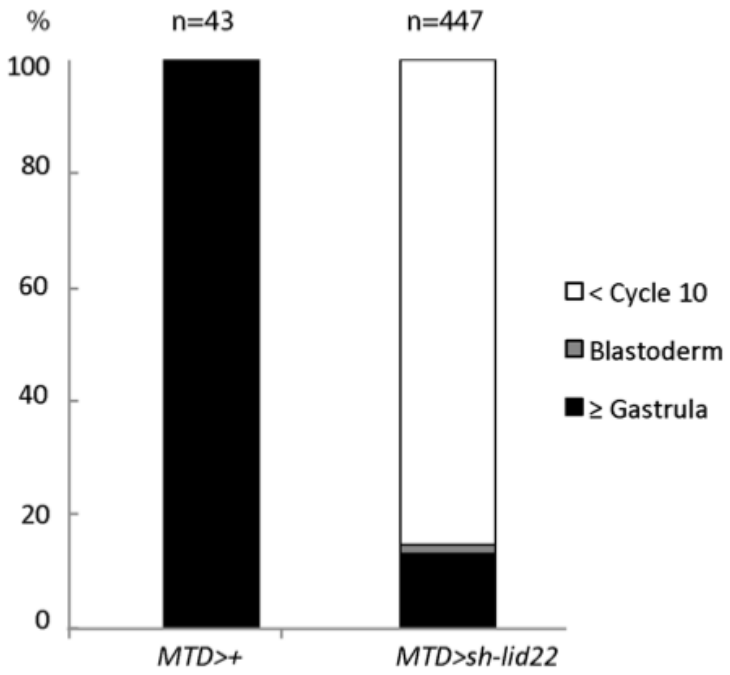

Fig S1. Developmental defects of *lid* KD embryos.
Embryos were collected for four hours and aged for another four hours at 25°C before DAPI staining and examination in fluorescent microscopy. More than 85% of *lid* KD embryos arrest development before the blastoderm stage. In contrast, 100% of control embryos had reached gastrula or later stages.

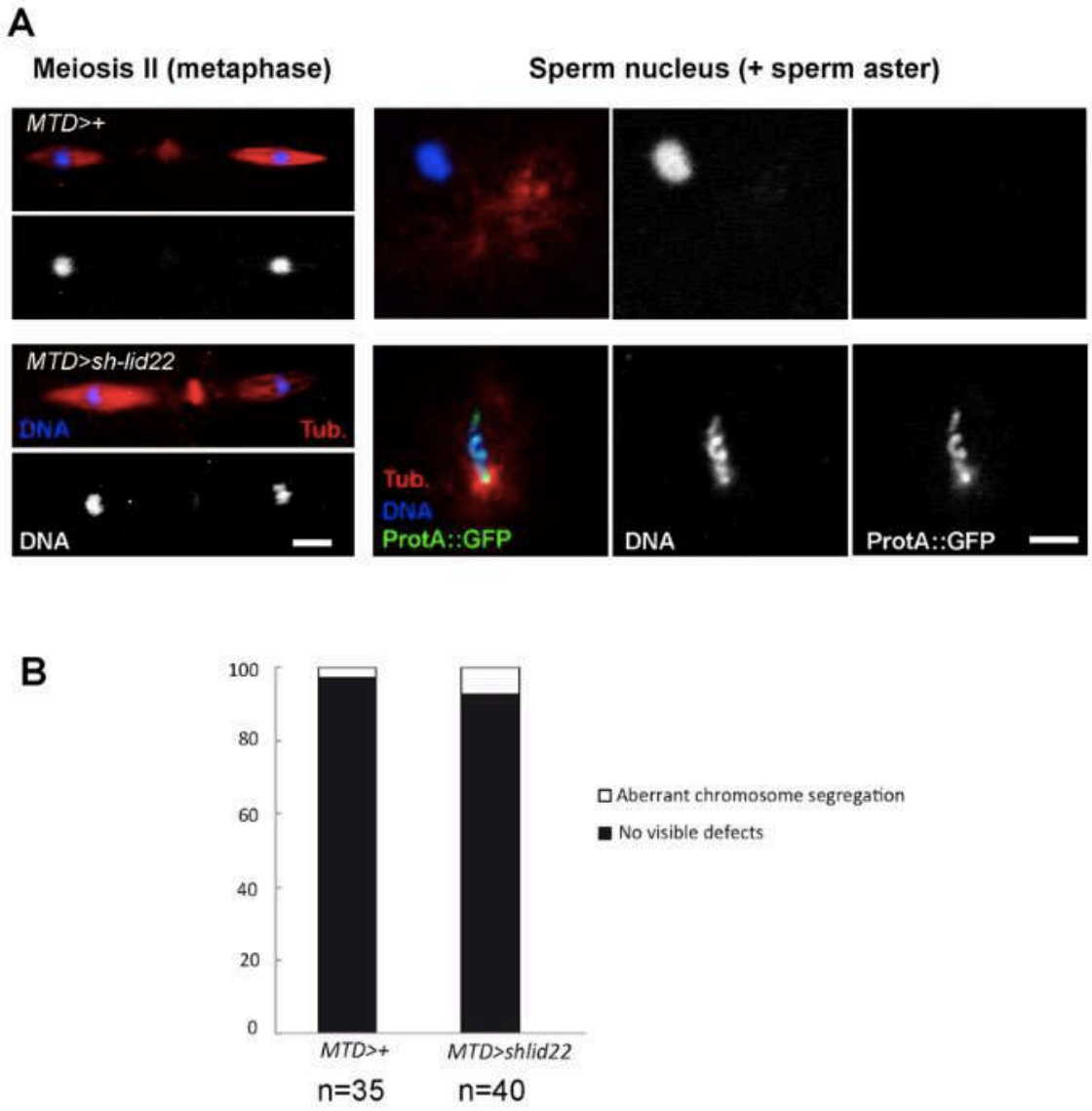

Fig S2. Meiosis II is not visibly affected in eggs from *lid* KD females.

A-Representative confocal images of eggs in metaphase of meiosis II stained for DNA (blue), alpha-tubulin (red) and ProtA::GFP (green). The tandem of meiotic spindles is shown on the left, the corresponding male nucleus from the same egg is on the right. Bars: 5 µm. B-Quantification of meiosis II phenotypes (normal or abnormal chromosome segregation).

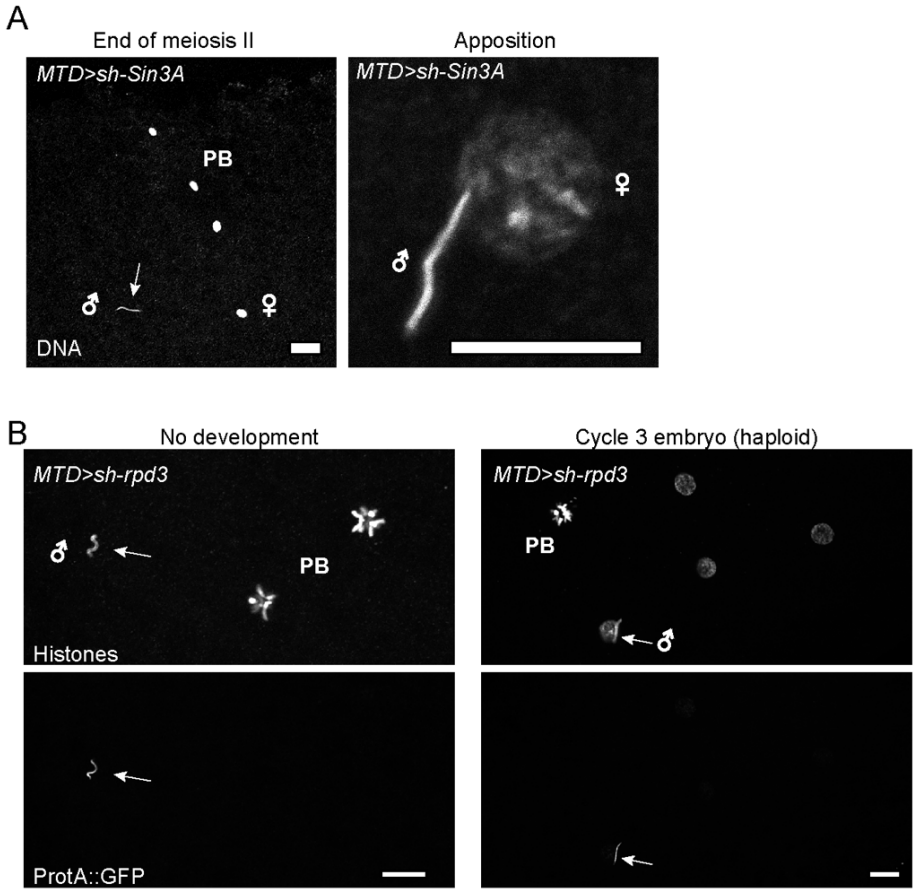

Fig S3. Phenotype of *Sin3A* KD and *rpd3* KD eggs/embryos.
A-Confocal images of *Sin3A* KD eggs stained for DNA at the indicated stages. The sperm nucleus in the left panel is indicated (arrow). Bar: 10 µm. PB: Polar bodies. B-Confocal images of *rpd3* KD early embryos (from ProtA::GFP fathers) stained for DNA and anti-GFP. The sperm nucleus is indicated (arrows). Bar: 10 µm. PB: Polar bodies.

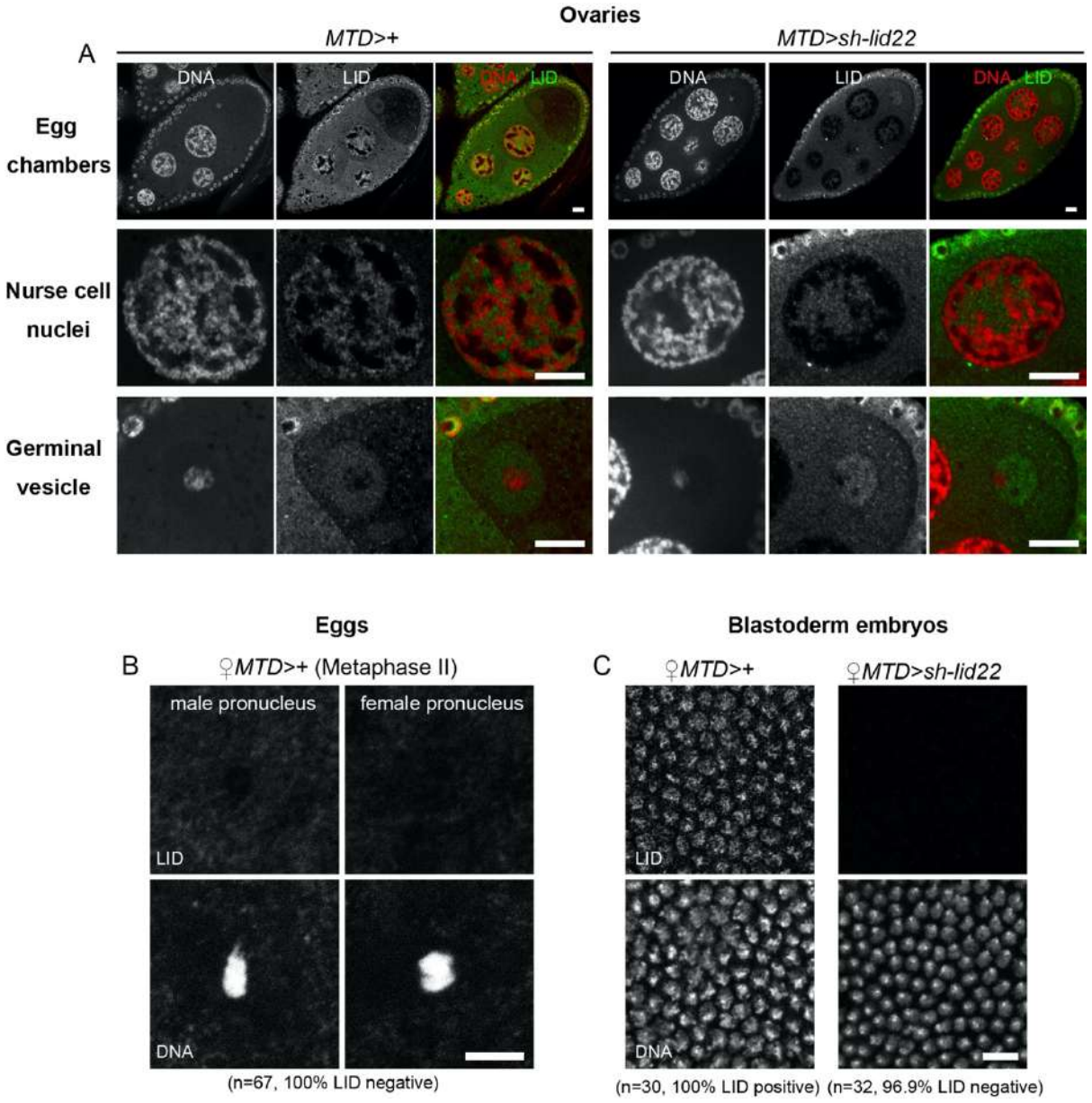

Fig S4. Lid is not directly invoved in sperm chromatin remodeling at fertilization.

A-Top row: confocal images of stage 10 egg chambers from control (left) and lid KD (right) females stained for DNA (red) and anti-Lid (green). Middle row: detail of a nurse cell nucleus. Bottom row: detail of the oocyte germinal vesicle (oocyte nucleus). Bar: 20 µm. B-Confocal images of the male pronucleus and the female pronucleus from a control egg in meiosis II stained for DNA and anti-Lid. Bar: 10 µm. Quantification of Lid positive nuclei is indicated. C-Confocal images of a control (left) and lid KD (right) blastoderm embryo with same staining as in B. Bar: 10 µm. Quantifications of embryos with a positive/negative nuclear Lid staining are indicated for each genotype.

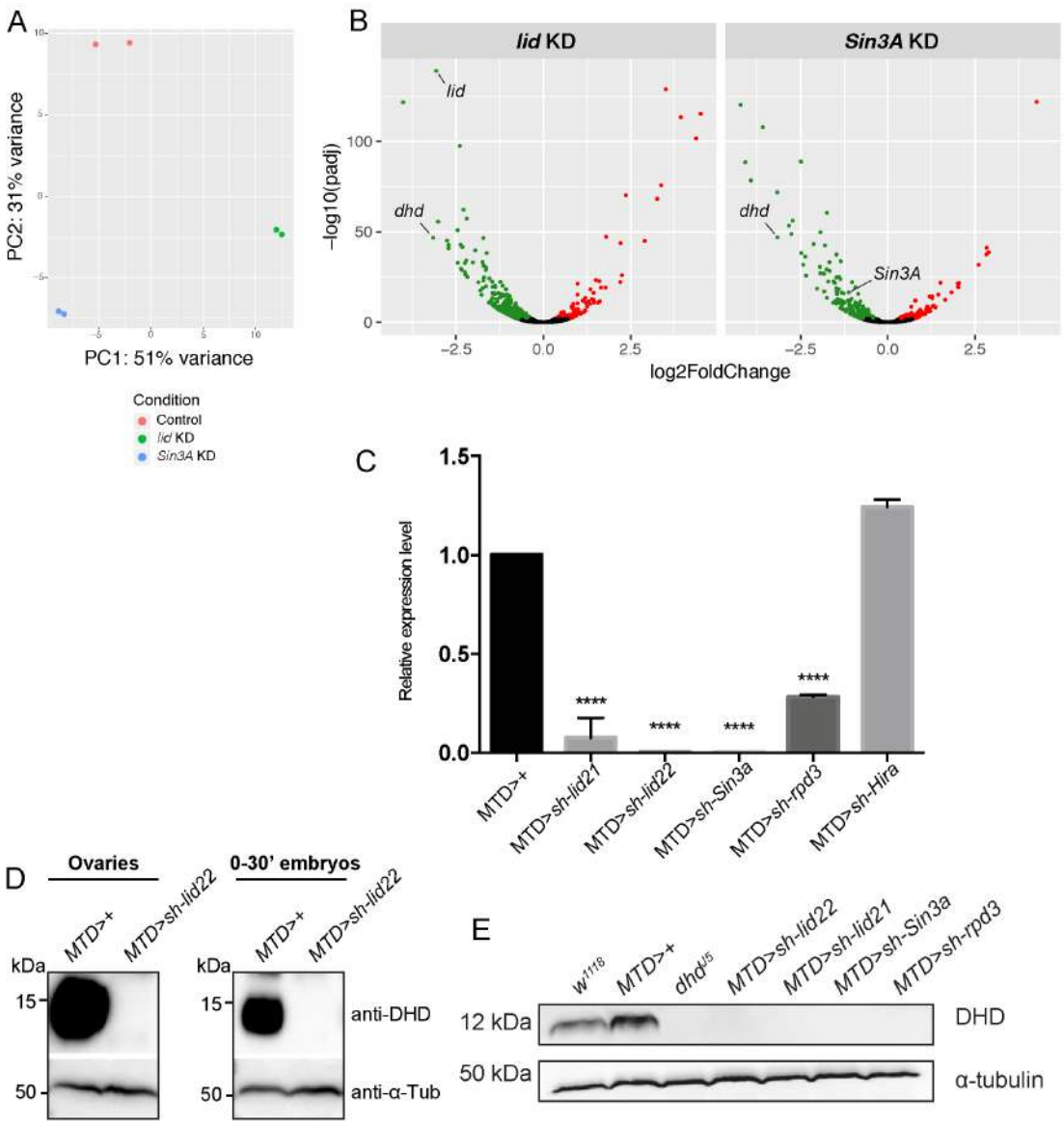

Fig S5. Lid and Sin3A control *dhd* expression in female germ cells.

A-Principal Component Analysis of Control, *lid* KD and *Sin3A* KD ovarian transcriptomes (two biological replicates for each genotype). B-Volcano plot representations of Differentially-Expressed genes in Control vs *lid* KD (left) and Control vs *Sin3A* KD (right). C-RT-qPCR quantification of *dhd* mRNA levels in ovaries of indicated genotypes. mRNA levels were normalized to rp49 and shown as relative expression in MTD>+ control. Error bars represent SD (Dunnett's multiple comparisons test to the control MTD>+, **** P < 0.0001). D—Western blot analysis of DHD in adult ovaries (left) and 0-30min postfertilization embryos (right). α-tubulin was used as a loading control. E—Western blot analysis of DHD in adult ovaries of indicated genotypes. α-tubulin was used as a loading control.

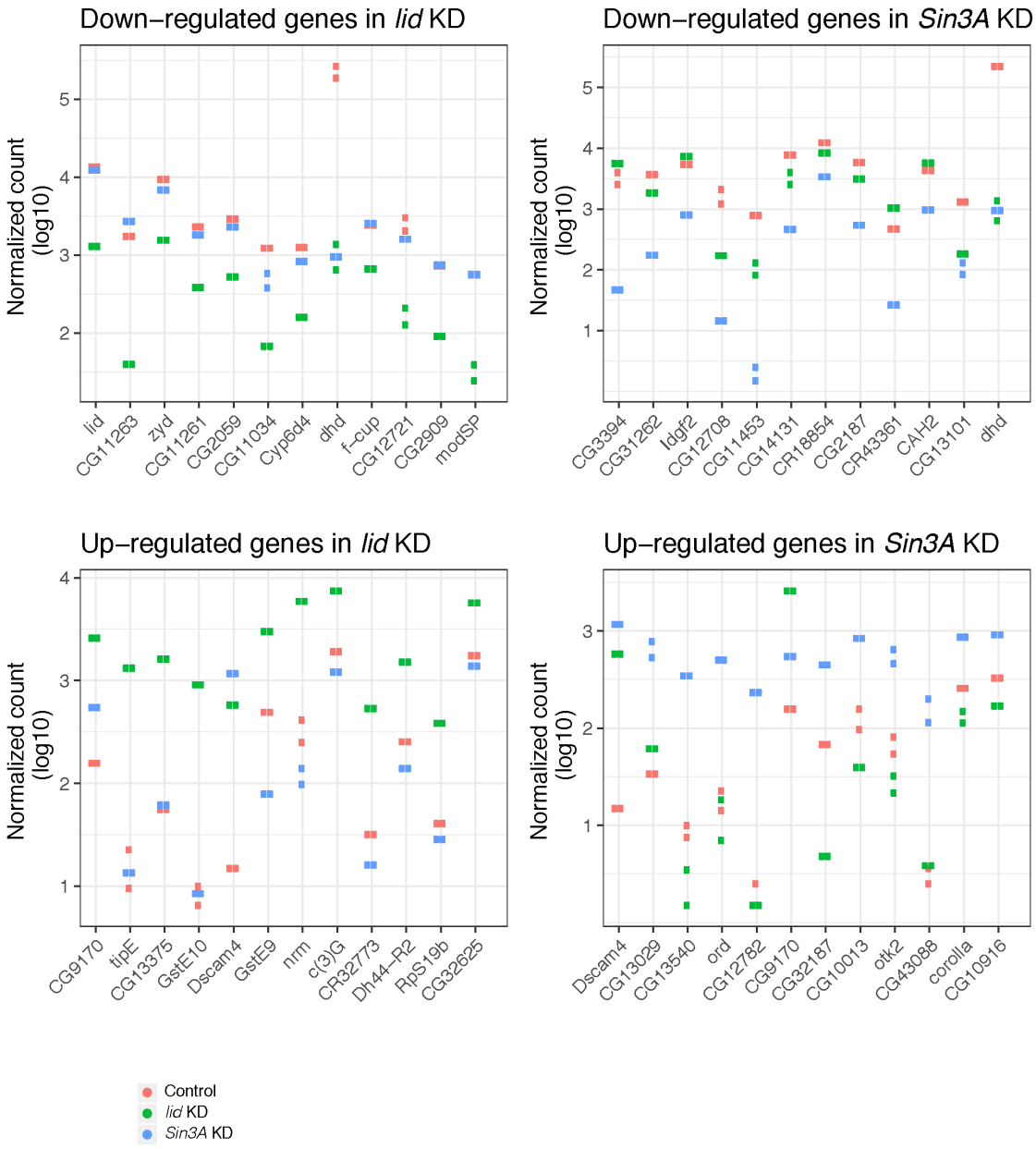

Fig S6. Top twelve most downregulated and upregulated genes in *lid* KD and *Sin3A* KD transcriptomes.

A

Female Genotype	No. eggs	Hatching rate
w^{1118}	330	97.2
lid^{10424}/lid^{K06801}; $gLid^{WT}$-HA/TM2	921	63.4
lid^{10424}/lid^{K06801}; $gLid^{JmjC}$-HA/TM2	117	16.2

B

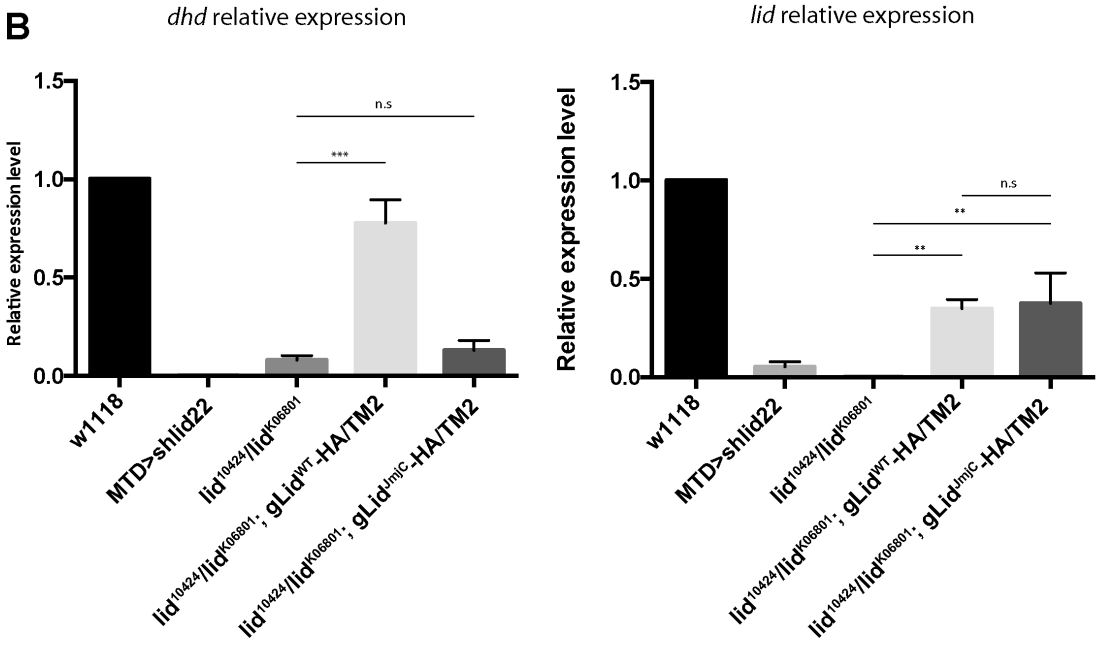

C

Female Genotype	No. eggs	Gastrula or beyond	GFP neg.	GFP pos.
lid^{10424}/lid^{K06801}; $gLid^{WT}$-HA/TM2	53	34	0	34
lid^{10424}/lid^{K06801}; $gLid^{JmjC}$-HA/TM2	14	6	3	3

Fig S7. The JmjC domain of Lid is required for normal *dhd* expression.

A-Embryo hatching rates from females of indicated genotypes. B-RT-qPCR quantification of *dhd* (left) and *lid* (right) mRNA levels in ovaries of indicated genotypes. mRNA levels were normalized to rp49 and shown as relative expression in w^{1118} control. Error bars represent SD (Dunnett's multiple comparisons test to the control (** P <0.01; *** P = 0.0002). C-Analysis of paternal GFP::Cid expression in late embryos from indicated females (as in Fig 1B).

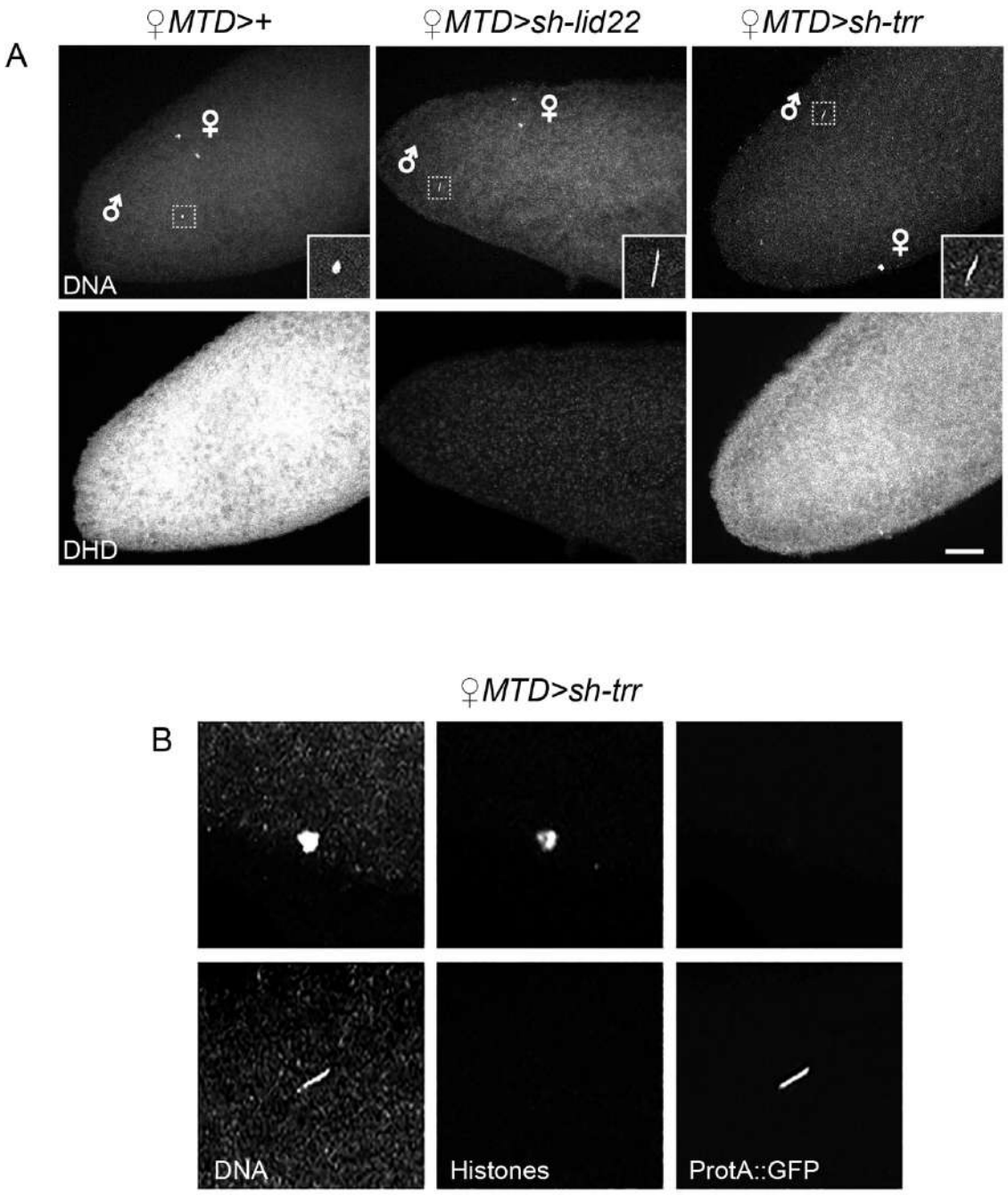

Fig S8. *trr* KD does not affect *dhd* expression.

A-Confocal images of representative embryos of the indicated genotypes stained for DNA and anti-DHD. The fertilizing sperm nucleus is magnified in insets. Bar: 20 µm. B-Details of maternal chromosomes (top row) and sperm nucleus (bottow row) from a representative *trr* KD egg stained for ProtA::GFP and histones.

S1 Table - Haploid TRiP screen

Fertile

Sterile, class 1: No egg laying.

Sterile, class 2: Few abnormal eggs, no hatching.

Sterile, class 3: Eggs do not hatch (HR<5%) and remain white.

Sterile, class 4: Eggs do not hatch (HR<5%), some turn brown.

"dhd-like": needle-shaped sperm nucleus, as in *dhd[J5]* mutant.

"ssm-like": small, round male nucleus, as in *Hira[ssm]* mutant.

BDSC#	TRiP#	CG#	Gene Symbol	Vector	Female fertility	GFP::Cid expression	Sperm nuclear phenotype
35334	GL00243	CG9638	Ada2b	pVALIUM22	Fertile	Not tested	Not tested
35232	GL00117	CG40300	AGO3	pVALIUM22	Fertile	Not tested	Not tested
36803	GL01012	CG8887	ash1	pVALIUM22	Fertile	Not tested	Not tested
32503	HMS00507	CG4303	Bap60	pVALIUM20	Fertile	Not tested	Not tested
36781	GL00127	CG6046	Bin1	pVALIUM22	Fertile	Not tested	Not tested
43174	GL01516	CG2009	bip2	pVALIUM22	Fertile	Not tested	Not tested
42502	HMJ02067	CG1845	Br140	pVALIUM20	Fertile	Not tested	Not tested
42658	HMS02494	CG14514	Brd8	pVALIUM20	Fertile	Not tested	Not tested
35623	GL00467	CG31256	Brf	pVALIUM22	Fertile	Not tested	Not tested
35211	GL00090	CG5942	brm	pVALIUM22	Fertile	Not tested	Not tested
35163	GL00031	CG7597	Cdk12	pVALIUM22	Fertile	Not tested	Not tested
33701	HMS00578	CG10133	CG10133	pVALIUM20	Fertile	Not tested	Not tested
43137	GL01475	CG10445	CG10445	pVALIUM22	Fertile	Not tested	Not tested
41847	GL01275	CG11329	CG11329	pVALIUM22	Fertile	Not tested	Not tested
36834	GL01075	CG12877	CG12877	pVALIUM22	Fertile	Not tested	Not tested
33731	HMS00614	CG13900	CG13900	pVALIUM20	Fertile	Not tested	Not tested
36914	GL01123	CG14352	CG14352	pVALIUM22	Fertile	Not tested	Not tested
36812	GL01030	CG1815	CG1815	pVALIUM22	Fertile	Not tested	Not tested
42488	HMJ02050	CG2051	CG2051	pVALIUM20	Fertile	Not tested	Not tested
35803	GL00427	CG32772	CG32772	pVALIUM22	Fertile	Not tested	Not tested
35475	GL00403	CG33694,CG33695	cana,CG33695	pVALIUM22	Fertile	Not tested	Not tested
38211	GL00652	CG3509	CG3509	pVALIUM22	Fertile	Not tested	Not tested
34077	HMS00584	CG4049	CG4049	pVALIUM20	Fertile	Not tested	Not tested
32973	HMS00770	CG4078	CG4078	pVALIUM20	Fertile	Not tested	Not tested
41976	HMS02374	CG4203	CG4203	pVALIUM20	Fertile	Not tested	Not tested
34606	HMS00577	CG43320	CG43320	pVALIUM20	Fertile	Not tested	Not tested
42533	HMJ02100	CG4400	CG4400	pVALIUM20	Fertile	Not tested	Not tested
33696	HMS00568	CG4747	CG4747	pVALIUM20	Fertile	Not tested	Not tested
42833	HMS02525	CG4854	CG4854	pVALIUM20	Fertile	Not tested	Not tested
32441	HMS00439	CG6418	CG6418	pVALIUM20	Fertile	Not tested	Not tested
42552	HMJ02125	CG6506	CG6506	pVALIUM20	Fertile	Not tested	Not tested
41824	GL01252	CG6937	CG6937	pVALIUM22	Fertile	Not tested	Not tested
32485	HMS00488	CG7200	CG7200	pVALIUM20	Fertile	Not tested	Not tested
35229	GL00113	CG7878	CG7878	pVALIUM22	Fertile	Not tested	Not tested
35593	GL00430	CG7911	CG7911	pVALIUM22	Fertile	Not tested	Not tested
41874	GL01305	CG8223	CG8223	pVALIUM22	Fertile	Not tested	Not tested
33361	HMS00233	CG8289	CG8289	pVALIUM20	Fertile	Not tested	Not tested
41649	GL01231	CG9272	CG9272	pVALIUM22	Fertile	Not tested	Not tested
42766	GL00722	CG9418	CG9418	pVALIUM22	Fertile	Not tested	Not tested
35807	GL00455	CG9576	CG9576	pVALIUM22	Fertile	Not tested	Not tested
35652	GLV21017	CG10890,CG13399	mus201,Chrac-14	pVALIUM21	Fertile	Not tested	Not tested
36084	GL00503	CG10712	Chro	pVALIUM22	Fertile	Not tested	Not tested
35387	GL00306	CG2714	crm	pVALIUM22	Fertile	Not tested	Not tested
35354	GL00266	CG8591	CTCF	pVALIUM22	Fertile	Not tested	Not tested
34732	HMS01212	CG7405	CycH	pVALIUM20	Fertile	Not tested	Not tested
35168	GL00037	CG6292	CycT	pVALIUM22	Fertile	Not tested	Not tested
32451	HMS00450	CG7098	dik	pVALIUM20	Fertile	Not tested	Not tested
32397	HMS00391	CG42799	dikar	pVALIUM20	Fertile	Not tested	Not tested
33410	HMS00290	CG7143	DNApol-eta	pVALIUM20	Fertile	Not tested	Not tested
36648	GL00608	CG7602	DNApol-iota	pVALIUM22	Fertile	Not tested	Not tested
35353	GL00265	CG32346	E(bx)	pVALIUM22	Fertile	Not tested	Not tested
32346	HMS00337	CG12238	e(y)3	pVALIUM20	Fertile	Not tested	Not tested
33904	HMS00846	CG12756	Eaf6	pVALIUM20	Fertile	Not tested	Not tested
37017	HMS01255	CG6755	EloA	pVALIUM20	Fertile	Not tested	Not tested
36906	GL01110	CG10215	Ercc1	pVALIUM22	Fertile	Not tested	Not tested
43285	HMS02657	CG1474	Es2	pVALIUM20	Fertile	Not tested	Not tested
33891	HMS00829	CG5899	Etl1	pVALIUM20	Fertile	Not tested	Not tested
35805	GL00442	CG4274	fzy	pVALIUM22	Fertile	Not tested	Not tested
42787	GL01157	CG10670	Gen	pVALIUM22	Fertile	Not tested	Not tested
41893	GL01325	CG42803	gpp	pVALIUM22	Fertile	Not tested	Not tested
33705	HMS00582	CG8887	ash1	pVALIUM20	Fertile	Not tested	Not tested
34817	HMS00127	CG2995	G9a	pVALIUM20	Fertile	Not tested	Not tested
34727	HMS01206	CG6662	GstO1	pVALIUM20	Fertile	Not tested	Not tested
34033	HMS01004	CG4976	NSD	pVALIUM20	Fertile	Not tested	Not tested
33703	HMS00580	CG8651	trx	pVALIUM20	Fertile	Not tested	Not tested
40931	HMS02179	CG40351	Set1	pVALIUM20	Fertile	Not tested	Not tested
35276	GL00176	CG40080	Haspin	pVALIUM22	Fertile	Not tested	Not tested
42620	HMS02455	CG5825	His3.3A	pVALIUM20	Fertile	Not tested	Not tested
36639	GL00599	CG13363	Hmt4-20	pVALIUM22	Fertile	Not tested	Not tested
32401	HMS00396	CG7041	HP1b	pVALIUM20	Fertile	Not tested	Not tested
33962	HMS00919	CG6990	HP1c	pVALIUM20	Fertile	Not tested	Not tested
37473	GL00616	CG31212	Ino80	pVALIUM22	Fertile	Not tested	Not tested
35819	GL00286	CG5247	Irbp	pVALIUM22	Fertile	Not tested	Not tested
37545	GLV21092	CG13201	ix	pVALIUM21	Fertile	Not tested	Not tested
40855	HMS02022	CG3654	Jarid2	pVALIUM20	Fertile	Not tested	Not tested
35438	GL00363	CG4029	jumu	pVALIUM22	Fertile	Not tested	Not tested
33699	HMS00574	CG11033	Kdm2	pVALIUM20	Fertile	Not tested	Not tested
34629	HMS01304	CG15835	Kdm4A	pVALIUM20	Fertile	Not tested	Not tested
34912	HMS01260	CG10080	mahj	pVALIUM20	Fertile	Not tested	Not tested
33709	HMS00587	CG3753	Marcal1	pVALIUM20	Fertile	Not tested	Not tested
34012	HMS00978	CG5465	MED16	pVALIUM20	Fertile	Not tested	Not tested
42634	HMS02470	CG14802	MED18	pVALIUM20	Fertile	Not tested	Not tested
33710	HMS00588	CG5546	MED19	pVALIUM20	Fertile	Not tested	Not tested
34577	HMS01051	CG18780	MED20	pVALIUM20	Fertile	Not tested	Not tested
34573	HMS01047	CG3034	MED22	pVALIUM20	Fertile	Not tested	Not tested

33755	HMS01097	CG7999	MED24	pVALIUM20	Fertile	Not tested	Not tested
42501	HMJ02066	CG12254	MED25	pVALIUM20	Fertile	Not tested	Not tested
32459	HMS00458	CG5121	MED28	pVALIUM20	Fertile	Not tested	Not tested
34697	HMS01176	CG8609	MED4	pVALIUM20	Fertile	Not tested	Not tested
35371	GL00284	CG4252	mei-41	pVALIUM22	Fertile	Not tested	Not tested
36605	GL00565	CG11301	Mes4	pVALIUM22	Fertile	Not tested	Not tested
36870	GL01011	CG3025	mof	pVALIUM22	Fertile	Not tested	Not tested
35241	GL00128	CG6363	MRG15	pVALIUM22	Fertile	Not tested	Not tested
35737	HMS01479	CG7003	Msh6	pVALIUM20	Fertile	Not tested	Not tested
35345	GL00256	CG10385	msl-1	pVALIUM22	Fertile	Not tested	Not tested
35272	GL00170	CG8631	msl-3	pVALIUM22	Fertile	Not tested	Not tested
42906	HMS02599	CG10692	Mt2	pVALIUM20	Fertile	Not tested	Not tested
34905	HMS01251	CG2244	MTA1-like	pVALIUM20	Fertile	Not tested	Not tested
32941	HMS00735	CG8274	Mtor	pVALIUM20	Fertile	Not tested	Not tested
35430	GL00354	CG18543	mtrm	pVALIUM22	Fertile	Not tested	Not tested
35732	GLC01346	CG4644	mtRNApol	pVALIUM22	Fertile	Not tested	Not tested
43244	GLC01431	CG11156	mus101	pVALIUM22	Fertile	Not tested	Not tested
32446	HMS00444	CG12124	mxc	pVALIUM20	Fertile	Not tested	Not tested
34741	HMS01221	CG42279	Nedd4	pVALIUM20	Fertile	Not tested	Not tested
36682	HMS01570	CG15319	nej	pVALIUM20	Fertile	Not tested	Not tested
35328	GL00235	CG17256	Nek2	pVALIUM22	Fertile	Not tested	Not tested
32897	HMS00686	CG5874	Nelf-A	pVALIUM20	Fertile	Not tested	Not tested
42547	HMJ02119	CG32721	NELF-B	pVALIUM20	Fertile	Not tested	Not tested
32835	HMS00525	CG5994	Nelf-E	pVALIUM20	Fertile	Not tested	Not tested
35595	GL00432	CG33554	Nipped-A	pVALIUM22	Fertile	Not tested	Not tested
32837	HMS00527	CG4453	Nup153	pVALIUM20	Fertile	Not tested	Not tested
32391	HMS00385	CG4738	Nup160	pVALIUM20	Fertile	Not tested	Not tested
33707	HMS00585	CG3736	okr	pVALIUM20	Fertile	Not tested	Not tested
35447	GL00372	CG7467	osa	pVALIUM22	Fertile	Not tested	Not tested
43263	GLC01452	CG11237	Oseg6	pVALIUM22	Fertile	Not tested	Not tested
39009	HMS01926	CG5581	Ote	pVALIUM20	Fertile	Not tested	Not tested
35792	GL00229	CG40411	Parp	pVALIUM22	Fertile	Not tested	Not tested
33972	HMS00929	CG1800	pasha	pVALIUM20	Fertile	Not tested	Not tested
34667	HMS01144	CG5208	Patr-1	pVALIUM20	Fertile	Not tested	Not tested
36070	GL00488	CG32443	Pc	pVALIUM22	Fertile	Not tested	Not tested
35601	GL00439	CG4107	Pcaf	pVALIUM22	Fertile	Not tested	Not tested
33946	HMS00897	CG5109	Pcl	pVALIUM20	Fertile	Not tested	Not tested
34690	HMS01169	CG3291	pcm	pVALIUM20	Fertile	Not tested	Not tested
35632	GL00479	CG17509	pds5	pVALIUM22	Fertile	Not tested	Not tested
35206	GL00082	CG17743	pho	pVALIUM22	Fertile	Not tested	Not tested
35724	GLV21089	CG3941	pita	pVALIUM21	Fertile	Not tested	Not tested
35178	GL00049	CG7001	Pk17E	pVALIUM22	Fertile	Not tested	Not tested
32840	HMS00531	CG11375	polybromo	pVALIUM20	Fertile	Not tested	Not tested
35322	GL00228	CG3307	pr-set7	pVALIUM22	Fertile	Not tested	Not tested
34622	HMS01297	CG8877	Prp8	pVALIUM20	Fertile	Not tested	Not tested
35297	GL00199	CG3886	Psc	pVALIUM22	Fertile	Not tested	Not tested
33700	HMS00576	CG5383	PSR	pVALIUM20	Fertile	Not tested	Not tested
35269	GL00167	CG32133	ptip	pVALIUM22	Fertile	Not tested	Not tested
34784	HMS00093	CG7138	r2d2	pVALIUM20	Fertile	Not tested	Not tested
32882	HMS00670	CG9862	Rae1	pVALIUM20	Fertile	Not tested	Not tested
33005	HMS00805	CG5252	Ranbp9	pVALIUM20	Fertile	Not tested	Not tested
32466	HMS00466	CG4879	RecQ5	pVALIUM20	Fertile	Not tested	Not tested
36654	GL00614	CG12189	Rev1	pVALIUM22	Fertile	Not tested	Not tested
34684	HMS01162	CG30149	rig	pVALIUM20	Fertile	Not tested	Not tested
43259	GLC01448	CG18145	Ripalpha	pVALIUM22	Fertile	Not tested	Not tested
32472	HMS00472	CG5422	Rox8	pVALIUM20	Fertile	Not tested	Not tested
34587	HMS01061	CG9273	RPA2	pVALIUM20	Fertile	Not tested	Not tested
36800	GL01005	CG7471	Rpd3	pVALIUM22	Fertile	Not tested	Not tested
43282	HMC02681	CG3180	RpII140	pVALIUM20	Fertile	Not tested	Not tested
35420	GL00343	CG3178	Rrp1	pVALIUM22	Fertile	Not tested	Not tested
42604	HMS02437	CG7292	Rrp6	pVALIUM20	Fertile	Not tested	Not tested
38914	GL00686	CG4385	S	pVALIUM22	Fertile	Not tested	Not tested
35446	GL00371	CG5595	Sce	pVALIUM22	Fertile	Not tested	Not tested
36637	GL00597	CG30390	Sgf29	pVALIUM22	Fertile	Not tested	Not tested
34630	HMS01305	CG9936	skd	pVALIUM20	Fertile	Not tested	Not tested
34949	HMS00313	CG18271	slx1	pVALIUM20	Fertile	Not tested	Not tested
36598	GL00558	CG6057	SMC1	pVALIUM22	Fertile	Not tested	Not tested
35477	GL00406	CG5263	smg	pVALIUM22	Fertile	Not tested	Not tested
34087	HMS00842	CG4013	Smr	pVALIUM20	Fertile	Not tested	Not tested
36125	HMS01540	CG4494	smt3	pVALIUM20	Fertile	Not tested	Not tested
36881	GL01045	CG31755	SoYb	pVALIUM22	Fertile	Not tested	Not tested
38898	GL00669	CG7948	spn-A	pVALIUM22	Fertile	Not tested	Not tested
43158	GL01500	CG3325	spn-B	pVALIUM22	Fertile	Not tested	Not tested
35148	GL00016	CG3169	Spt3	pVALIUM22	Fertile	Not tested	Not tested
35437	GL00362	CG8396	Ssb-c31a	pVALIUM22	Fertile	Not tested	Not tested
38344	HMS01811	CG14216	Ssu72	pVALIUM20	Fertile	Not tested	Not tested
34996	HMS01406	CG11268	ste14	pVALIUM20	Fertile	Not tested	Not tested
36867	GL01006	CG17149	Su(var)3-3	pVALIUM22	Fertile	Not tested	Not tested
33402	HMS00280	CG8013	Su(z)12	pVALIUM20	Fertile	Not tested	Not tested
33403	HMS00281	CG3905	Su(z)2	pVALIUM20	Fertile	Not tested	Not tested
36893	GL01080	CG7869	SuUR	pVALIUM22	Fertile	Not tested	Not tested
42770	GL00726	CG9874	Tbp	pVALIUM22	Fertile	Not tested	Not tested
35429	GL00353	CG3710	TfIIS	pVALIUM22	Fertile	Not tested	Not tested
42931	HMS02624	CG9984	TH1	pVALIUM20	Fertile	Not tested	Not tested
41843	GL01271	CG1981	Thd1	pVALIUM22	Fertile	Not tested	Not tested
35603	GL00443	CG10387	tos	pVALIUM22	Fertile	Not tested	Not tested
35790	GL00397	CG10897	tou	pVALIUM22	Fertile	Not tested	Not tested
35794	GL00258	CR34649	tre-1	pVALIUM22	Fertile	Not tested	Not tested
41582	GL00699	CG33261,CG42507	Trl,CG42507	pVALIUM22	Fertile	Not tested	Not tested
36116	HMS01492	CG42595	uex	pVALIUM20	Fertile	Not tested	Not tested
34076	HMS00575	CG5640	Utx	pVALIUM20	Fertile	Not tested	Not tested
35468	GL00394	CG12701	vfl	pVALIUM22	Fertile	Not tested	Not tested
36877	GL01036	CG10728	vls	pVALIUM22	Fertile	Not tested	Not tested
36616	GL00576	CG3707	wapl	pVALIUM22	Fertile	Not tested	Not tested

32469	HMS00469	CG4448	wda	pVALIUM20	Fertile	Not tested	Not tested
33363	GLC01357	CG9226	WDR79	pVALIUM20	Fertile	Not tested	Not tested
35680	GLV21045	CG4148	wek	pVALIUM21	Fertile	Not tested	Not tested
32894	HMS00683	CG4548	XNP	pVALIUM20	Fertile	Not tested	Not tested
35208	GL00084	CG7803	z	pVALIUM22	Fertile	Not tested	Not tested
35228	GL00112	CG12314	zuc	pVALIUM22	Fertile	Not tested	Not tested
34846	HMS00164	CG7471	Rpd3	pVALIUM20	Fertile	Not tested	Not tested
32853	HMS00638	CG17149	Su(var)3-3	pVALIUM20	Fertile	Not tested	Not tested
33726	HMS00608	CG17149	Su(var)3-3	pVALIUM20	Fertile	Not tested	Not tested
38285	HMS01738	CG7467	osa	pVALIUM20	Fertile	Not tested	Not tested
33954	HMS00909	CG4303	Bap60	pVALIUM20	Fertile	Not tested	Not tested
34520	HMS00050	CG5942	brm	pVALIUM20	Fertile	Not tested	Not tested
41857	GL01285	CG4193	dhd	pVALIUM22	Fertile	Not tested	Not tested
36867	GL01006	CG17149	Su(var)3-3	pVALIUM22	Fertile	Not tested	Not tested
32993	HMS00793	CG3143	foxo	pVALIUM20	Fertile	Not tested	Not tested
32427	HMS00422	CG3143	foxo	pVALIUM20	Fertile	Not tested	Not tested
34774	HMS00083	CG1770	HDAC4	pVALIUM20	Fertile	Not tested	Not tested
44103	HMS02823	CG44132	mamo	pVALIUM20	Fertile	Not tested	Not tested
37486	GLV21091	CG44132	mamo	pVALIUM21	Fertile	Not tested	Not tested
40850	HMS02017	CG8591	CTCF	pVALIUM20	Fertile	Not tested	Not tested
42536	HMJ02105	CG6384	Cp190	pVALIUM20	Fertile	Not tested	Not tested
33944	HMS00895	CG6384	Cp190	pVALIUM20	Fertile	Not tested	Not tested
33903	HMS00845	CG6384	Cp190	pVALIUM20	Fertile	Not tested	Not tested
35642	GLV21006	CG10159	BEAF-32	pVALIUM21	Fertile	Not tested	Not tested
34006	HMS00970	CG8573	su(Hw)	pVALIUM20	Fertile	Not tested	Not tested
33906	HMS00848	CG8573	su(Hw)	pVALIUM20	Fertile	Not tested	Not tested
34351	HMS01340	CG6057	SMC1	pVALIUM20	Fertile	Not tested	Not tested
33431	HMS00318	CG9802	Cap	pVALIUM20	Fertile	Not tested	Not tested
33622	HMS00016	CG32443	Pc	pVALIUM20	Fertile	Not tested	Not tested
33964	HMS00921	CG32443	Pc	pVALIUM20	Fertile	Not tested	Not tested
42926	HMS02619	CG17743	pho	pVALIUM20	Fertile	Not tested	Not tested
38261	HMS01706	CG3886	Psc	pVALIUM20	Fertile	Not tested	Not tested
40940	HMS02188	CG33261,CG42507	Trl,CG42507	pVALIUM20	Fertile	Not tested	Not tested
43962	GL01314	CG10798	dm	pVALIUM22	Fertile	Not tested	Not tested
36126	HMS01541	CG6376	E2f	pVALIUM20	Fertile	Not tested	Not tested
33669	HMS00082	CG18412	ph-p	pVALIUM20	Fertile	Not tested	Not tested
35207	GL00083	CG18412	ph-p	pVALIUM22	Fertile	Not tested	Not tested
36720	HMS01610	CG1772	dap	pVALIUM20	Fertile	Not tested	Not tested
32890	HMS00678	CG10414	Atac2	pVALIUM20	Sterile, class 1	N/A	N/A
36624	GL00584	CG10726	barr	pVALIUM22	Sterile, class 1	N/A	N/A
35185	GL00057	CG9748	bel	pVALIUM22	Sterile, class 1	N/A	N/A
36067	GL00485	CG10480	Bj1	pVALIUM22	Sterile, class 1	N/A	N/A
33421	HMS00304	CG31132	BRWD3	pVALIUM20	Sterile, class 1	N/A	N/A
32989	HMS00789	CG7581	Bub3	pVALIUM20	Sterile, class 1	N/A	N/A
35199	GL00073	CG3319	Cdk7	pVALIUM22	Sterile, class 1	N/A	N/A
34857	HMS00175	CG10333	CG10333	pVALIUM20	Sterile, class 1	N/A	N/A
43205	GL01550	CG10565	CG10565	pVALIUM22	Sterile, class 1	N/A	N/A
42810	GL01184	CG3430	CG3430	pVALIUM22	Sterile, class 1	N/A	N/A
35020	HMS01433	CG5033	CG5033	pVALIUM20	Sterile, class 1	N/A	N/A
43254	GLC01443	CG5290	CG5290	pVALIUM22	Sterile, class 1	N/A	N/A
32334	HMS00325	CG5589	CG5589	pVALIUM20	Sterile, class 1	N/A	N/A
43206	GL01551	CG5800	CG5800	pVALIUM22	Sterile, class 1	N/A	N/A
34565	HMS01037	CG6015	CG6015	pVALIUM20	Sterile, class 1	N/A	N/A
34804	HMS00113	CG7185	CG7185	pVALIUM20	Sterile, class 1	N/A	N/A
36609	GL00569	CG8142	CG8142	pVALIUM22	Sterile, class 1	N/A	N/A
36589	GL00549	CG9253	CG9253	pVALIUM22	Sterile, class 1	N/A	N/A
41679	HMS02243	CG9422	CG9422	pVALIUM20	Sterile, class 1	N/A	N/A
34564	HMS01036	CG5602	DNA-ligI	pVALIUM20	Sterile, class 1	N/A	N/A
34827	HMS00142	CG9696	dom	pVALIUM20	Sterile, class 1	N/A	N/A
35149	GL00017	CG1828	dre4	pVALIUM22	Sterile, class 1	N/A	N/A
35271	GL00169	CG7776	E(Pc)	pVALIUM22	Sterile, class 1	N/A	N/A
32345	HMS00336	CG6474	e(y)1	pVALIUM20	Sterile, class 1	N/A	N/A
35764	HMS01512	CG8648	Fen1	pVALIUM20	Sterile, class 1	N/A	N/A
41716	HMS02281	CG5148	cal1	pVALIUM20	Sterile, class 1	N/A	N/A
33666	HMS00076	CG7269	Hel25E	pVALIUM20	Sterile, class 1	N/A	N/A
41988	HMS02387	CG33882,CG33880,CG33876,C	His2B	pVALIUM20	Sterile, class 1	N/A	N/A
35299	GL00202	CG6620	ial	pVALIUM22	Sterile, class 1	N/A	N/A
34552	HMS01024	CG10850	ida	pVALIUM20	Sterile, class 1	N/A	N/A
35366	GL00279	CG12165	Incenp	pVALIUM22	Sterile, class 1	N/A	N/A
41916	HMS02313	CG6189	l(1)1Bi	pVALIUM20	Sterile, class 1	N/A	N/A
43981	GL01591	CG10563	l(2)37Cd	pVALIUM22	Sterile, class 1	N/A	N/A
33002	GLC01635	CG8426	l(2)NC136	pVALIUM22	Sterile, class 1	N/A	N/A
34024	HMS02950	CG5931	l(3)72Ab	pVALIUM20	Sterile, class 1	N/A	N/A
34575	HMS01049	CG12031	MED14	pVALIUM20	Sterile, class 1	N/A	N/A
34664	HMS01141	CG7957	MED17	pVALIUM20	Sterile, class 1	N/A	N/A
34731	HMS01211	CG17397	MED21	pVALIUM20	Sterile, class 1	N/A	N/A
33743	HMS01081	CG9473	MED6	pVALIUM20	Sterile, class 1	N/A	N/A
34926	HMS01275	CG13867	MED8	pVALIUM20	Sterile, class 1	N/A	N/A
35398	GL00318	CG8103	Mi-2	pVALIUM22	Sterile, class 1	N/A	N/A
35150	GL00018	CG13778	Mnn1	pVALIUM22	Sterile, class 1	N/A	N/A
34990	HMS01400	CG12202	Nat1	pVALIUM20	Sterile, class 1	N/A	N/A
37482	GL00625	CG9938	Ndc80	pVALIUM22	Sterile, class 1	N/A	N/A
33694	HMS00564	CG7421	Nopp140	pVALIUM20	Sterile, class 1	N/A	N/A
32836	HMS00526	CG34407	Not1	pVALIUM20	Sterile, class 1	N/A	N/A
34710	HMS01189	CG4579	Nup154	pVALIUM20	Sterile, class 1	N/A	N/A
33897	HMS00837	CG3820	Nup214	pVALIUM20	Sterile, class 1	N/A	N/A
33003	HMS00803	CG11856	Nup358	pVALIUM20	Sterile, class 1	N/A	N/A
35695	GLV21060	CG6251	Nup62	pVALIUM21	Sterile, class 1	N/A	N/A
32409	GLC01628	CG2917	Orc4	pVALIUM22	Sterile, class 1	N/A	N/A
32838	HMS00528	CG8241	pea	pVALIUM20	Sterile, class 1	N/A	N/A
41997	HMS02398	CG7769	pic	pVALIUM20	Sterile, class 1	N/A	N/A
43984	GLC01465	CG6375	pit	pVALIUM22	Sterile, class 1	N/A	N/A
32865	HMS00652	CG5519	Prp19	pVALIUM20	Sterile, class 1	N/A	N/A
41912	HMS02306	CG4320	raptor	pVALIUM20	Sterile, class 1	N/A	N/A

32415	HMS00410	CG9750	rept	pVALIUM20	Sterile, class 1	N/A	N/A
41861	GL01291	CG11979	Rpb5	pVALIUM22	Sterile, class 1	N/A	N/A
36830	GL01068	CG1554	RpII215	pVALIUM22	Sterile, class 1	N/A	N/A
34567	HMS01040	CG7885	RpII33	pVALIUM20	Sterile, class 1	N/A	N/A
32363	HMS00354	CG2173	Rs1	pVALIUM20	Sterile, class 1	N/A	N/A
38531	HMS01744	CG9198	shtd	pVALIUM20	Sterile, class 1	N/A	N/A
35602	GL00440	CG10212	SMC2	pVALIUM22	Sterile, class 1	N/A	N/A
38371	HMS01840	CG13570	spag	pVALIUM20	Sterile, class 1	N/A	N/A
33914	HMS00857	CG9809	Spargel	pVALIUM20	Sterile, class 1	N/A	N/A
35466	GL00392	CG11451	Spc105R	pVALIUM22	Sterile, class 1	N/A	N/A
32896	HMS00685	CG12372	spt4	pVALIUM20	Sterile, class 1	N/A	N/A
34837	HMS00153	CG7626	Spt5	pVALIUM20	Sterile, class 1	N/A	N/A
32373	HMS00364	CG12225	Spt6	pVALIUM20	Sterile, class 1	N/A	N/A
38948	HMS01862	CG6238	ssh	pVALIUM20	Sterile, class 1	N/A	N/A
41648	GL01230	CG8592	stil	pVALIUM22	Sterile, class 1	N/A	N/A
35415	GL00337	CG3836	stwl	pVALIUM22	Sterile, class 1	N/A	N/A
38255	HMS01699	CG12864	Su(var)2-HP2	pVALIUM20	Sterile, class 1	N/A	N/A
35314	GL00219	CG17603	Taf1	pVALIUM22	Sterile, class 1	N/A	N/A
35367	GL00280	CG7704	Taf5	pVALIUM22	Sterile, class 1	N/A	N/A
35428	GL00352	CG10281	TfIIFalpha	pVALIUM22	Sterile, class 1	N/A	N/A
35462	GL00388	CG3278	Tif-IA	pVALIUM22	Sterile, class 1	N/A	N/A
36307	GL00491	CG1782	Uba1	pVALIUM22	Sterile, class 1	N/A	N/A
35806	GL00452	CG7528	Uba2	pVALIUM22	Sterile, class 1	N/A	N/A
42642	HMS02478	CG7989	wcd	pVALIUM20	Sterile, class 1	N/A	N/A
32952	HMS00746	CG17437	wds	pVALIUM20	Sterile, class 1	N/A	N/A
38297	HMS01758	CG7670	WRNexo	pVALIUM20	Sterile, class 1	N/A	N/A
36123	HMS01538	CG10798	dm	pVALIUM20	Sterile, class 1	N/A	N/A
51454	HMC03189	CG10798	dm	pVALIUM20	Sterile, class 1	N/A	N/A
34069	HMS00051	CG4236	Caf1	pVALIUM20	Sterile, class 1	N/A	N/A
35139	GL00006	CG2252	fs(1)h	pVALIUM22	Sterile, class 1	N/A	N/A
52111	HMC03356	CG4039	Mcm6	pVALIUM20	Sterile, class 1	N/A	N/A
41842	GL01270	CG4039	Mcm6	pVALIUM22	Sterile, class 1	N/A	N/A
36092	GL00511	CG3938	CycE	pVALIUM22	Sterile, class 1	N/A	N/A
38902	GL00673	CG3938	CycE	pVALIUM22	Sterile, class 1	N/A	N/A
41693	HMS02257	CG2252	fs(1)h	pVALIUM20	Sterile, class 1	N/A	N/A
41943	HMS02340	CG2252	fs(1)h	pVALIUM20	Sterile, class 1	N/A	N/A
44009	HMS02723	CG2252	fs(1)h	pVALIUM20	Sterile, class 1	N/A	N/A
35388	GL00307	CG6677	ash2	pVALIUM22	Sterile, class 2	N/A	Not tested
34390	HMS01384	CG13192	CG13192	pVALIUM20	Sterile, class 2	N/A	Not tested
33704	HMS00581	CG40351	Set1	pVALIUM20	Sterile, class 2	N/A	Not tested
35460	GL00386	CG2161	Rga	pVALIUM22	Sterile, class 2	N/A	Not tested
32473	HMS00473	CG16975	Sfmbt	pVALIUM20	Sterile, class 2	N/A	Not tested
35454	GL00379	CG4735	shu	pVALIUM22	Sterile, class 2	N/A	Not tested
35303	GL00206	CG3158	spn-E	pVALIUM22	Sterile, class 2	N/A	Not tested
35592	GL00429	CG42373,CG31917	Tfb5,CG31917	pVALIUM22	Sterile, class 2	N/A	Not tested
32926	HMS00718	CG17293	Wdr82	pVALIUM20	Sterile, class 2	N/A	Not tested
35240	GL00126	CG3733	Chd1	pVALIUM22	Sterile, class 2	N/A	Not tested
36068	GL00486	CG6502	E(z)	pVALIUM22	Sterile, class 2	N/A	Not tested
35323	GL00230	CG5179	Cdk9	pVALIUM22	Sterile, class 2	N/A	Not tested
35201	GL00076	CG6137	aub	pVALIUM22	Sterile, class 3	N/A	Not tested
35443	GL00368	CG10542	Bre1	pVALIUM22	Sterile, class 3	N/A	Not tested
36783	GL00518	CG9802	Cap	pVALIUM22	Sterile, class 3	N/A	Not tested
35324	GL00231	CG10572	Cdk8	pVALIUM22	Sterile, class 3	N/A	Not tested
36899	GL01093	CG14222	CG14222	pVALIUM22	Sterile, class 3	N/A	Not tested
36916	HMS01019	CG3848	trr	pVALIUM20	Sterile, class 3	N/A	Not tested
32517	HMS00522	CG4184	MED15	pVALIUM20	Sterile, class 3	N/A	Not tested
32995	HMS00795	CG32491	mod(mdg4)	pVALIUM20	Sterile, class 3	N/A	Not tested
35630	GL00477	CG18740	mor	pVALIUM22	Sterile, class 3	N/A	Not tested
38190	GL00629	CG12047	mud	pVALIUM22	Sterile, class 3	N/A	Not tested
34580	HMS01054	CG2158	Nup50	pVALIUM20	Sterile, class 3	N/A	Not tested
43215	GL01560	CG3041	Orc2	pVALIUM22	Sterile, class 3	N/A	Not tested
42803	GL01176	CG9183	plu	pVALIUM22	Sterile, class 3	N/A	Not tested
42482	GL01341	CG1404	ran	pVALIUM22	Sterile, class 3	N/A	Not tested
35171	GL00041	CG10683	rhi	pVALIUM22	Sterile, class 3	N/A	Not tested
36794	GL00534	CG3423	SA	pVALIUM22	Sterile, class 3	N/A	Not tested
32372	HMS00363	CG1064	Snr1	pVALIUM20	Sterile, class 3	N/A	Not tested
36095	GL00514	CG13109	tai	pVALIUM22	Sterile, class 3	N/A	Not tested
36786	GL00522	CG17436	vtd	pVALIUM22	Sterile, class 3	N/A	Not tested
43141	GL01482	CG15737	wisp	pVALIUM22	Sterile, class 3	N/A	Not tested
32845	HMS00628	CG8625	Iswi	pVALIUM20	Sterile, class 3	N/A	Not tested
33907	HMS00849	CG32491	mod(mdg4)	pVALIUM20	Sterile, class 3	N/A	Not tested
33395	HMS00272	CG3423	SA	pVALIUM20	Sterile, class 3	N/A	Not tested
33659	HMS00066	CG6502	E(z)	pVALIUM20	Sterile, class 3	N/A	Not tested
33654	HMS00060	CG3938	CycE	pVALIUM20	Sterile, class 3	N/A	No tested
33739	HMS01075	CG5451	Smu1	pVALIUM20	Sterile, class 4	Yes	WT
32889	HMS00677	CG7583	CtBP	pVALIUM20	Sterile, class 4	Yes	WT
35242	GL00129	CG7055	dalao	pVALIUM22	Sterile, class 4	Yes	WT
43185	GL01529	CG2207	Df31	pVALIUM22	Sterile, class 4	Yes	WT
35488	GL00417	CG15433	Elp3	pVALIUM22	Sterile, class 4	Yes	WT
33706	HMS00583	CG1716	Set2	pVALIUM20	Sterile, class 4	Yes	WT
35399	GL00319	CG42245,CG1244	CG42245,MEP-1	pVALIUM22	Sterile, class 4	Yes	WT
35759	HMS01506	CG8384	gro	pVALIUM20	Sterile, class 4	Yes	WT
34778	HMS00087	CG2128	Hdac3	pVALIUM20	Sterile, class 4	Yes	WT
35238	GL00123	CG11990	hyx	pVALIUM22	Sterile, class 4	Yes	WT
36597	GL00557	CG3696	kis	pVALIUM22	Sterile, class 4	Yes	WT
34980	HMS01389	CG2684	lds	pVALIUM20	Sterile, class 4	Yes	WT
36652	GL00612	CG9088	lid	pVALIUM22	Sterile, class 4	**No**	**dhd-like**
35152	GL00020	CG10895	lok	pVALIUM22	Sterile, class 4	Yes	WT
36829	GL01067	CG1793	MED26	pVALIUM22	Sterile, class 4	Yes	WT
39028	HMS01947	CG16928	mre11	pVALIUM20	Sterile, class 4	Yes	WT
36614	GL00574	CG17704	Nipped-B	pVALIUM22	Sterile, class 4	Yes	WT
33985	HMS00945	CG4118	nxf2	pVALIUM20	Sterile, class 4	Yes	WT
37483	GL00626	CG6122	piwi	pVALIUM22	Sterile, class 4	Yes	WT
35419	GL00342	CG2368	psq	pVALIUM22	Sterile, class 4	Yes	WT

36632	GL00592	CG12352	san	pVALIUM22	Sterile, class 4	Yes	WT
35389	GL00308	CG9495	Scm	pVALIUM22	Sterile, class 4	Yes	WT
32368	HMS00359	CG8815	Sin3A	pVALIUM20	Sterile, class 4	**No**	**dhd-like**
40881	HMS02049	CG4413	trem	pVALIUM20	Sterile, class 4	Yes	WT
36835	GL01076	CG18009	Trf2	pVALIUM22	Sterile, class 4	Yes	WT
35706	GLV21071	CG9088	lid	pVALIUM21	Sterile, class 4	**No**	**dhd-like**
33725	HMS00607	CG7471	Rpd3	pVALIUM20	Sterile, class 4	**No**	**dhd-like**
Control	GL00257	CG12153	Hira	pVALIUM22	Sterile, class 4	No	ssm-like
Control	MTD>attP2				Fertile	Yes	WT
Control	*w[1118]*				Fertile	Yes	WT
					Female fertility	**GFP::Cid expression**	**Sperm nuclear phenotype**

S2 Table - Differentially expressed genes in *lid* KD and *Sin3A* KD ovaries

		lid KD		
gene_ID	Flybase_record	log2FC	pvalue	fdr
FBgn0031759	lid	-3,0712584	1,19E-143	1,09E-139
FBgn0036330	CG11263	-4,0238806	8,08E-126	2,47E-122
FBgn0265767	zyd	-2,3911626	2,14E-101	2,80E-98
FBgn0036332	CG11261	-2,289144	6,93E-66	5,77E-63
FBgn0029942	CG2059	-2,1961104	5,04E-61	3,85E-58
FBgn0031741	CG11034	-3,0166023	2,50E-59	1,76E-56
FBgn0039006	Cyp6d4	-2,4571248	1,69E-54	1,11E-51
FBgn0011761	dhd	-3,1639711	2,36E-50	1,35E-47
FBgn0028487	f-cup	-1,7169953	4,48E-50	2,42E-47
FBgn0030373	CG12721	-2,759553	1,23E-48	6,24E-46
FBgn0030189	CG2909	-2,3738814	2,85E-46	1,24E-43
FBgn0051217	modSP	-2,7201402	4,00E-46	1,67E-43
FBgn0010549	l(2)03659	-2,3208622	5,27E-45	2,10E-42
FBgn0031157	CG1503	-2,7196155	2,06E-44	7,85E-42
FBgn0030757	CG9902	-1,9505708	4,17E-43	1,53E-40
FBgn0037205	BoYb	-1,6205084	1,34E-41	4,72E-39
FBgn0030799	CG4872	-2,2114932	1,87E-37	6,33E-35
FBgn0032449	CG17036	-1,7420374	1,28E-36	4,18E-34
FBgn0034270	PIG-A	-2,0221889	2,63E-36	8,03E-34
FBgn0030666	CG12708	-2,4559175	3,98E-36	1,18E-33
FBgn0032084	CG13101	-2,2464821	6,86E-36	1,96E-33
FBgn0034179	CG6805	-1,718645	1,81E-34	5,04E-32
FBgn0029831	CG5966	-1,6877179	2,77E-34	7,47E-32
FBgn0038115	CG7966	-1,6351573	2,76E-33	7,22E-31
FBgn0264676	CR43961	-2,3616771	7,97E-33	2,03E-30
FBgn0039941	CG17167	-2,3378925	3,56E-32	8,82E-30
FBgn0037617	nom	-1,6497844	4,41E-32	1,06E-29
FBgn0003950	unc	-2,2472133	8,29E-31	1,95E-28
FBgn0029710	CG3568	-2,2292889	1,66E-29	3,80E-27
FBgn0038734	CG11453	-2,1747893	3,40E-28	7,42E-26
FBgn0033051	Stnica	-1,6975548	6,51E-28	1,39E-25
FBgn0035955	CG5194	-1,5455268	2,56E-27	5,33E-25
FBgn0051075	CG31075	-1,7191968	3,57E-26	7,11E-24
FBgn0031814	retm	-1,4618361	1,84E-25	3,45E-23
FBgn0030421	CG3812	-1,2307055	2,69E-25	4,93E-23
FBgn0040964	CG18661	-1,8630762	3,82E-25	6,73E-23
FBgn0020379	Rfx	-1,1649689	3,12E-23	5,30E-21
FBgn0035102	CG7049	-1,3835219	3,70E-23	6,16E-21
FBgn0034706	CG11275	-1,6436042	6,46E-23	1,06E-20
FBgn0015714	Cyp6a17	-1,4470292	1,14E-22	1,84E-20
FBgn0264745	CR44003	-1,3760264	2,39E-22	3,77E-20
FBgn0052243	CG32243	-1,7389495	7,42E-22	1,11E-19
FBgn0261859	CG42788	-1,0677649	3,11E-21	4,60E-19
FBgn0036324	CG12520	-1,8023267	1,57E-20	2,25E-18
FBgn0038296	CG6752	-1,4303478	4,08E-19	5,58E-17
FBgn0028746	CG18508	-1,2806776	4,03E-19	5,58E-17
FBgn0047199	CG31517	-1,4214417	4,55E-19	6,14E-17
FBgn0023094	cyc	-1,4563032	4,75E-19	6,31E-17
FBgn0032820	fbp	-1,4464475	1,14E-18	1,50E-16
FBgn0038190	CG9926	-1,3835824	1,75E-18	2,26E-16
FBgn0035151	CG17129	-1,1841525	1,99E-18	2,53E-16
FBgn0260932	cuff	-1,3874404	2,38E-18	2,98E-16
FBgn0050440	CG30440	-1,0217497	4,41E-18	5,39E-16
FBgn0032382	Mal-B2	-1,0646868	4,70E-18	5,66E-16
FBgn0031313	CG5080	-1,7721223	5,47E-18	6,51E-16
FBgn0037838	CG4089	-1,1250484	1,95E-17	2,29E-15
FBgn0037921	CG6808	-1,226594	1,99E-17	2,30E-15
FBgn0038815	CG5466	-0,9670653	2,51E-17	2,88E-15
FBgn0085245	CG34216	-1,2301847	1,39E-16	1,57E-14
FBgn0032343	CG6201	-1,0192506	4,46E-16	4,92E-14
FBgn0001224	Hsp23	-1,4714794	5,23E-16	5,70E-14
FBgn0022702	Chi2	-1,4310409	7,08E-16	7,63E-14
FBgn0261393	alpha-Est5	-1,3211846	1,68E-15	1,77E-13
FBgn0011770	Gip	-0,9263151	2,95E-15	3,07E-13
FBgn0035641	CG5568	-0,988897	9,04E-15	9,10E-13
FBgn0037583	CG9684	-1,0702856	1,24E-14	1,23E-12
FBgn0033917	SmydA-1	-0,943787	1,57E-14	1,53E-12
FBgn0029137	Patsas	-1,5041647	1,94E-14	1,88E-12
FBgn0034262	swi2	-1,509625	2,73E-14	2,55E-12
FBgn0000346	comt	-1,3234813	3,14E-14	2,91E-12
FBgn0029866	CG3842	-1,076243	3,26E-14	2,99E-12
FBgn0036843	Sbzn2	-0,9270425	5,61E-14	5,09E-12
FBgn0051320	HEATR2	-1,1200264	9,20E-14	8,26E-12
FBgn0029753	CG4198	-1,5619893	1,28E-13	1,13E-11
FBgn0027865	Tsp96F	-0,9262642	2,08E-13	1,76E-11
FBgn0025739	pan	-1,0767554	2,19E-13	1,84E-11
FBgn0037186	CG11241	-1,390111	2,65E-13	2,21E-11
FBgn0044020	Roc2	-0,9693241	3,79E-13	3,13E-11
FBgn0003210	rb	-0,7951324	4,49E-13	3,67E-11
FBgn0051373	CG31373	-1,1418253	5,61E-13	4,51E-11
FBgn0014342	mia	-1,4117988	1,53E-12	1,20E-10
FBgn0010194	Wnt5	-0,9969608	1,95E-12	1,51E-10
FBgn0050046	CG30046	-1,4641854	2,18E-12	1,68E-10
FBgn0037696	GstZ1	-1,1641738	2,95E-12	2,25E-10
FBgn0036501	CG7272	-1,1433254	4,51E-12	3,42E-10
FBgn0030883	CG7772	-1,1675829	4,84E-12	3,63E-10
FBgn0052187	CG32187	-1,4297304	5,92E-12	4,41E-10
FBgn0037661	Ada	-1,0613728	7,97E-12	5,89E-10
FBgn0052485	CG32485	-1,0521644	8,19E-12	5,99E-10
FBgn0036906	CG14102	-0,8096291	8,23E-12	5,99E-10
FBgn0040089	meso18E	-1,3685324	8,50E-12	6,14E-10
FBgn0039226	Ude	-1,2586048	1,36E-11	9,76E-10

		Sin3A KD		
gene_ID	Flybase_record	log2FC	pvalue	fdr
FBgn0034999	CG3394	-4,2202683	1,06E-124	4,49E-121
FBgn0051262	CG31262	-3,585744	5,36E-112	1,51E-108
FBgn0020415	Idgf2	-2,4924243	6,00E-93	1,27E-89
FBgn0030666	CG12708	-4,091286	1,57E-92	2,65E-89
FBgn0038734	CG11453	-3,9323184	2,36E-82	3,32E-79
FBgn0036205	CG14131	-3,1718177	1,08E-75	1,30E-72
FBgn0042174	CR18854	-1,7444457	2,48E-64	2,61E-61
FBgn0017448	CG2187	-2,7282585	6,16E-60	5,77E-57
FBgn0263093	CR43361	-2,8379209	4,08E-57	3,44E-54
FBgn0027843	CAH2	-1,9318723	2,16E-53	1,66E-50
FBgn0032084	CG13101	-2,7702721	1,67E-52	1,17E-49
FBgn0011761	dhd	-3,1714692	1,39E-50	8,99E-48
FBgn0063491	GstE9	-2,1322519	9,01E-47	5,43E-44
FBgn0264385	CR43837	-1,8051528	5,23E-46	2,94E-43
FBgn0038098	CG7381	-2,4840253	8,69E-42	4,07E-39
FBgn0028516	Zn135C	-1,4720133	7,88E-41	3,32E-38
FBgn0003285	rst	-2,3689615	1,14E-39	4,57E-37
FBgn0016054	phn6-4	-1,3532928	3,77E-37	1,44E-34
FBgn0036824	CG3902	-1,6753711	1,50E-36	5,48E-34
FBgn0259224	CG42324	-2,4297305	3,97E-35	1,34E-32
FBgn0034270	PIG-A	-1,9494089	7,37E-34	2,39E-31
FBgn0010039	GstD3	-1,7549245	1,77E-32	5,54E-30
FBgn0029866	CG3842	-1,6741608	1,07E-31	3,23E-29
FBgn0031894	CG4496	-1,9342072	2,22E-30	6,46E-28
FBgn0265810	CR44599	-1,827715	4,24E-30	1,19E-27
FBgn0050046	CG30046	-2,3477317	5,95E-29	1,62E-26
FBgn0263607	l(3)72Dp	-1,4039175	2,14E-28	5,64E-26
FBgn0034406	Jheh3	-1,4772969	5,73E-28	1,47E-25
FBgn0000251	cad	-1,3652224	4,24E-27	1,05E-24
FBgn0260388	CG42514	-1,5594298	9,97E-26	2,40E-23
FBgn0010549	l(2)03659	-1,7120513	1,18E-25	2,76E-23
FBgn0037203	slif	-1,0254701	2,49E-25	5,67E-23
FBgn0025739	pan	-1,5225974	6,70E-25	1,45E-22
FBgn0016034	mael	-0,9278028	2,30E-22	4,51E-20
FBgn0250785	vari	-1,4747975	7,39E-22	1,42E-19
FBgn0265203	CR44263	-2,032906	1,25E-21	2,34E-19
FBgn0262524	ver	-1,4075366	1,84E-21	3,38E-19
FBgn0028369	kirre	-1,8269137	5,43E-20	9,74E-18
FBgn0029881	pigs	-1,465781	6,39E-20	1,12E-17
FBgn0022764	Sin3A	-1,1227377	1,72E-19	2,90E-17
FBgn0015714	Cyp6a17	-1,3288249	2,14E-19	3,53E-17
FBgn0032891	Oseg5	-1,2772665	6,30E-19	1,02E-16
FBgn0033232	CG12159	-0,8479804	1,22E-18	1,94E-16
FBgn0034706	CG11275	-1,4584788	1,85E-18	2,89E-16
FBgn0063923	Kaz1-ORFB	-1,7465855	2,41E-16	3,50E-14
FBgn0035517	CG1265	-1,0430897	7,24E-16	1,02E-13
FBgn0036821	CG3961	-1,4377702	8,61E-16	1,19E-13
FBgn0004396	CrebA	-1,3364748	5,14E-15	6,88E-13
FBgn0033978	Cyp6a23	-1,141044	7,33E-15	9,65E-13
FBgn0085212	CG34183	-1,0941979	9,69E-15	1,24E-12
FBgn0028523	CG5888	-1,4984311	1,42E-14	1,79E-12
FBgn0013995	Calx	-0,7936823	3,03E-14	3,76E-12
FBgn0034262	swi2	-1,4987164	3,95E-14	4,82E-12
FBgn0036369	CG10089	-1,2616404	6,11E-14	7,36E-12
FBgn0010225	Gel	-0,9302227	9,01E-14	1,07E-11
FBgn0263492	CR43481	-1,3214228	1,01E-13	1,19E-11
FBgn0260435	CR42530	-1,5741372	1,16E-13	1,35E-11
FBgn0034126	jtb	-1,2521974	1,26E-13	1,44E-11
FBgn0036765	CG7408	-1,4021843	1,42E-13	1,60E-11
FBgn0033979	Cyp6a19	-0,8188227	3,12E-13	3,46E-11
FBgn0034322	CG18536	-1,4809179	3,86E-13	4,23E-11
FBgn0035084	CG15861	-1,1101584	6,72E-13	7,26E-11
FBgn0034729	CG10344	-0,8888346	1,75E-12	1,86E-10
FBgn0025628	CG4199	-0,9498517	1,92E-12	2,02E-10
FBgn0036620	CG4842	-1,3062619	2,41E-12	2,51E-10
FBgn0050440	CG30440	-0,8206139	3,28E-12	3,38E-10
FBgn0030968	CG7322	-1,1011257	5,10E-12	5,12E-10
FBgn0003353	sei	-0,8772684	5,09E-12	5,12E-10
FBgn0029723	Proc-R	-1,0504156	1,19E-11	1,17E-09
FBgn0031182	Cyp6t1	-1,0634995	1,31E-11	1,27E-09
FBgn0024194	rasp	-0,7121256	1,39E-11	1,33E-09
FBgn0037664	CG8420	-0,9313398	2,16E-11	2,02E-09
FBgn0262987	CG43295	-1,0673364	5,73E-11	5,20E-09
FBgn0026263	bip1	-0,8522921	6,42E-11	5,70E-09
FBgn0030598	CG9503	-1,0489086	8,19E-11	7,19E-09
FBgn0033079	Fmo-2	-1,3682329	1,11E-10	9,66E-09
FBgn0039099	GlLT2	-0,7327631	4,47E-10	3,85E-08
FBgn0029114	Trillo	-1,1827078	4,82E-10	4,10E-08
FBgn0029603	CG14053	-1,2936781	6,45E-10	5,38E-08
FBgn0034351	rswl	-0,6549448	8,01E-10	6,55E-08
FBgn0250907	Chl10	-1,2916825	9,00E-10	7,30E-08
FBgn0038099	CG7091	-0,5724301	1,01E-09	8,15E-08
FBgn0031435	Elba2	-0,8698732	1,04E-09	8,30E-08
FBgn0032034	Rod4	-0,8422531	1,71E-09	1,33E-07
FBgn0031741	CG11034	-1,0844981	2,10E-09	1,62E-07
FBgn0024984	CG3457	-1,0010634	2,43E-09	1,86E-07
FBgn0034321	CG14502	-1,2292823	3,16E-09	2,34E-07
FBgn0264979	CG4267	-0,8221925	3,14E-09	2,34E-07
FBgn0037617	nom	-0,813118	3,09E-09	2,34E-07
FBgn0040529	COX7A	-0,6038853	3,14E-09	2,34E-07
FBgn0266347	nAChRalpha4	-1,0453241	5,78E-09	4,20E-07
FBgn0041182	Tep2	-0,7714701	5,96E-09	4,30E-07

FBgn0029881	pigs	-1,0651714	2,06E-11	1,45E-09
FBgn0052641	CG32641	-1,2247928	2,38E-11	1,67E-09
FBgn0260874	Ir76a	-1,0911372	2,74E-11	1,90E-09
FBgn0050414	CG30414	-1,2153351	3,13E-11	2,14E-09
FBgn0001987	Gli	-0,9659603	3,59E-11	2,44E-09
FBgn0035833	CG7565	-0,8088702	4,12E-11	2,78E-09
FBgn0033257	sand	-1,3823352	5,66E-11	3,79E-09
FBgn0034117	CG7997	-0,763632	5,86E-11	3,89E-09
FBgn0033903	CG8323	-1,1131696	7,96E-11	5,21E-09
FBgn0036764	CG5535	-0,7545567	8,88E-11	5,77E-09
FBgn0266619	CR45126	-1,2911846	1,32E-10	8,52E-09
FBgn0034321	CG14502	-1,3268889	1,64E-10	1,05E-08
FBgn0037031	CG11456	-0,7363562	2,42E-10	1,53E-08
FBgn0026315	Ugt35a	-0,8958298	2,86E-10	1,80E-08
FBgn0037999	CG4860	-0,914685	2,89E-10	1,80E-08
FBgn0037717	CG8301	-0,7261462	2,98E-10	1,84E-08
FBgn0026263	big1	-0,8163696	3,82E-10	2,35E-08
FBgn0031961	CG7102	-1,2412474	3,92E-10	2,39E-08
FBgn0031488	CG17265	-1,059634	5,31E-10	3,22E-08
FBgn0014395	tilB	-1,3194748	5,85E-10	3,53E-08
FBgn0051119	HDAC11	-1,205338	6,74E-10	4,03E-08
FBgn0003087	pim	-0,8624825	7,25E-10	4,28E-08
FBgn0038243	CG8066	-0,8549971	1,04E-09	6,10E-08
FBgn0037819	CG14688	-0,721363	1,05E-09	6,16E-08
FBgn0015558	tty	-1,2965917	1,14E-09	6,60E-08
FBgn0035904	GstO3	-1,1528477	1,30E-09	7,47E-08
FBgn0037960	mthl5	-1,0338692	1,39E-09	7,97E-08
FBgn0031419	CG15390	-0,8367551	1,50E-09	8,51E-08
FBgn0040551	CG11686	-1,0442442	1,64E-09	9,30E-08
FBgn0264561	Glg1	-0,6445743	1,78E-09	9,99E-08
FBgn0036205	CG14131	-1,0276741	1,85E-09	1,04E-07
FBgn0029588	CG14798	-1,0967802	2,18E-09	1,21E-07
FBgn0030968	CG7322	-0,949729	2,50E-09	1,38E-07
FBgn0030347	CG15739	-1,2401826	2,76E-09	1,51E-07
FBgn0030357	Scip	-1,0122455	3,06E-09	1,67E-07
FBgn0034322	CG18536	-1,2110539	3,50E-09	1,90E-07
FBgn0030187	lpod	-1,2385667	5,95E-09	3,15E-07
FBgn0030745	CG4239	-0,8448908	6,13E-09	3,23E-07
FBgn0039525	CG5646	-1,2155351	7,04E-09	3,69E-07
FBgn0037092	M6	-0,963899	7,52E-09	3,90E-07
FBgn0002778	rnd	-0,806747	9,72E-09	5,00E-07
FBgn0031530	pgant2	-1,1444054	9,96E-09	5,10E-07
FBgn0264494	CG17646	-0,9205579	1,05E-08	5,33E-07
FBgn0034371	SP2637	-0,6113293	1,33E-08	6,72E-07
FBgn0030457	CG12096	-0,894159	1,59E-08	7,98E-07
FBgn0035356	CG16986	-0,9019828	1,61E-08	8,03E-07
FBgn0031031	CG14218	-1,0942315	1,62E-08	8,04E-07
FBgn0036689	CG7730	-0,6978042	1,73E-08	8,50E-07
FBgn0040259	Ugt86Da	-0,6475277	1,88E-08	9,24E-07
FBgn0024179	wit	-0,9130951	2,02E-08	9,85E-07
FBgn0051262	CG31262	-0,861913	2,33E-08	1,12E-06
FBgn0032452	CG15484	-1,0295249	2,48E-08	1,19E-06
FBgn0264744	CG44002	-0,8415038	2,53E-08	1,21E-06
FBgn0035957	CG5144	-1,0227201	2,87E-08	1,36E-06
FBgn0036463	Reck	-1,1572904	3,73E-08	1,76E-06
FBgn0029648	CG3603	-0,745846	4,08E-08	1,91E-06
FBgn0052512	CG32512	-0,6016979	4,21E-08	1,96E-06
FBgn0027070	CG17322	-0,7492832	4,28E-08	1,98E-06
FBgn0041182	Tep2	-0,7242566	4,63E-08	2,12E-06
FBgn0039250	Mink	-0,639282	5,95E-08	2,70E-06
FBgn0039098	GILT3	-0,7013264	6,00E-08	2,71E-06
FBgn0035167	Gr61a	-1,1497859	6,74E-08	3,03E-06
FBgn0031245	CG3625	-0,971262	7,57E-08	3,39E-06
FBgn0033274	CG14757	-1,090869	7,70E-08	3,39E-06
FBgn0037623	CG9801	-0,6974149	7,67E-08	3,39E-06
FBgn0031484	CG3165	-0,6795141	7,67E-08	3,39E-06
FBgn0038047	CG5245	-0,7751217	7,74E-08	3,39E-06
FBgn0031678	CG31918	-0,8319058	7,94E-08	3,47E-06
FBgn0031968	CG7231	-0,6421679	8,08E-08	3,51E-06
FBgn0037654	CG11983	-1,0667257	8,28E-08	3,58E-06
FBgn0028504	CG12182	-0,6690131	8,84E-08	3,80E-06
FBgn0036777	CG7341	-0,6764114	1,15E-07	4,92E-06
FBgn0036333	MICAL-like	-0,6050858	1,27E-07	5,37E-06
FBgn0033174	CG11125	-0,744251	1,54E-07	6,47E-06
FBgn0030749	Arad11	-0,6167345	1,74E-07	7,25E-06
FBgn0023531	CG32809	-0,8578439	1,77E-07	7,33E-06
FBgn0262987	CG43295	-0,8451577	1,91E-07	7,87E-06
FBgn0031227	CG3709	-0,766059	2,02E-07	8,31E-06
FBgn0042174	CR18854	-0,5297378	2,27E-07	9,31E-06
FBgn0010039	GstD3	-0,7605547	2,48E-07	1,01E-05
FBgn0035770	pst	-0,5961126	2,54E-07	1,03E-05
FBgn0037215	beta-Man	-0,4990579	3,24E-07	1,30E-05
FBgn0037203	slif	-0,5000146	3,72E-07	1,48E-05
FBgn0038381	EndoU	-0,5336266	3,99E-07	1,57E-05
FBgn0026570	CG5704	-0,6871541	4,23E-07	1,66E-05
FBgn0030876	CG6762	-1,0198113	4,43E-07	1,73E-05
FBgn0265362	CG44303	-0,9489117	4,64E-07	1,80E-05
FBgn0263746	CR43671	-1,0550132	5,30E-07	2,04E-05
FBgn0033234	MFS12	-0,6970743	6,29E-07	2,41E-05
FBgn0034523	Nrf1a	-0,8203413	6,64E-07	2,54E-05
FBgn0038016	MBD-R2	-0,716337	6,71E-07	2,55E-05
FBgn0040321	GNBP3	-1,0545182	6,84E-07	2,59E-05
FBgn0033079	Fmo-2	-1,048226	7,44E-07	2,80E-05
FBgn0034312	CG10916	-0,7803511	7,47E-07	2,80E-05
FBgn0040778	CG17977	-0,6999545	7,70E-07	2,88E-05
FBgn0086909	CG31751	-0,8017727	8,31E-07	3,10E-05

FBgn0033233	Kdm4A	-0,6829652	1,01E-08	7,14E-07
FBgn0030187	lpod	-1,204368	1,53E-08	1,06E-06
FBgn0031948	CG7149	-1,0429932	1,63E-08	1,12E-06
FBgn0031645	CG30036	-0,8406185	2,05E-08	1,38E-06
FBgn0034046	tun	-0,55626	2,04E-08	1,38E-06
FBgn0002736	mago	-0,5731716	2,58E-08	1,70E-06
FBgn0039914	mav	-0,7934145	2,68E-08	1,75E-06
FBgn0039251	Trl4-2	-0,7011303	2,87E-08	1,86E-06
FBgn0058006	CG40006	-0,7958262	3,01E-08	1,94E-06
FBgn0031434	insv	-0,6828101	5,73E-08	3,64E-06
FBgn0261016	clos	-0,8133906	7,24E-08	4,56E-06
FBgn0041629	Hexa2	-0,8525238	9,62E-08	6,01E-06
FBgn0036857	CG9629	-1,0935355	1,27E-07	7,83E-06
FBgn0058298	CG40298	-1,0896436	1,33E-07	8,12E-06
FBgn0051999	CG31999	-1,0118804	1,68E-07	1,02E-05
FBgn0039094	CG10184	-0,8494729	1,89E-07	1,13E-05
FBgn0031263	Tspo	-0,8185505	1,95E-07	1,16E-05
FBgn0262509	nrm	-0,9612758	2,34E-07	1,37E-05
FBgn0037186	CG11241	-0,9780927	2,48E-07	1,44E-05
FBgn0264822	CR44030	-1,0195041	2,95E-07	1,70E-05
FBgn0069969	CG40458	-1,0623555	3,45E-07	1,97E-05
FBgn0040260	Ugt36Bc	-0,8753219	4,38E-07	2,45E-05
FBgn0266319	CR44984	-1,0737286	4,51E-07	2,50E-05
FBgn0038803	CG5191	-0,6495903	4,67E-07	2,58E-05
FBgn0040823	dpr6	-0,70335	6,86E-07	3,73E-05
FBgn0035999	CG3552	-0,6534192	7,51E-07	4,06E-05
FBgn0037578	CG9601	-0,6525109	8,02E-07	4,31E-05
FBgn0036294	CG10654	-0,73282	8,44E-07	4,51E-05
FBgn0032645	CG15142	-0,9543489	1,07E-06	5,68E-05
FBgn0261794	lac	-0,5784062	1,12E-06	5,89E-05
FBgn0050005	GstT2	-0,655386	1,33E-06	6,85E-05
FBgn0000246	e(3)G	-0,5895323	1,3619E-06	6,9605E-05
FBgn0031117	GstT3	-0,6273411	1,65E-06	8,3189E-05
FBgn0031031	CG14218	-0,9280998	1,73E-06	8,63E-05
FBgn0035151	CG17129	-0,6414527	1,91E-06	9,48E-05
FBgn0039938	Sox102F	-0,8740615	2,3254E-06	0,00011401
FBgn0020908	Scp1	-0,9771089	2,64E-06	1,28E-04
FBgn0026593	CG5707	-0,8438915	2,65E-06	1,28E-04
FBgn0038331	Corn3	-0,5150585	2,67E-06	1,29E-04
FBgn0035186	CG13912	-0,987372	3,11E-06	1,47E-04
FBgn0050000	GstT1	-0,523767	3,10E-06	1,47E-04
FBgn0032249	TBC1D16	-0,7023452	3,35E-06	1,56E-04
FBgn0031814	retm	-0,64624	3,35E-06	1,56E-04
FBgn0265362	CG44303	-0,8715818	3,66E-06	1,69E-04
FBgn0001987	Gli	-0,6662484	4,66E-06	2,14E-04
FBgn0063492	GstE8	-0,727191	4,75E-06	2,17E-04
FBgn0266982	CR45433	-0,9637767	5,92E-06	2,63E-04
FBgn0046776	CR14033	-0,7082347	8,32E-06	0,00035889
FBgn0003205	Ras85D	-0,4664327	8,34E-06	3,59E-04
FBgn0032775	CG17544	-0,7910398	8,46E-06	3,62E-04
FBgn0040262	Ugt36Ba	-0,8297009	1,03E-05	4,34E-04
FBgn0035082	CG2811	-0,5063722	1,11E-05	4,60E-04
FBgn0263746	CR43671	-0,9226564	1,17E-05	0,00048167
FBgn0028400	Syt4	-0,69069	1,18E-05	0,00048695
FBgn0028499	CG7985	-0,7328768	1,43E-05	5,81E-04
FBgn0031032	CG14204	-0,7709141	1,44E-05	5,83E-04
FBgn0029975	spidey	-0,4900255	1,64E-05	6,57E-04
FBgn0266096	CR44833	-0,8551666	1,71E-05	0,00067917
FBgn0038047	CG5245	-0,618797	1,75E-05	6,89E-04
FBgn0001224	Hsp23	-0,7763302	1,79E-05	6,97E-04
FBgn0027865	Tsp96F	-0,5401966	1,79E-05	6,97E-04
FBgn0033258	CG8712	-0,4730603	1,81E-05	7,00E-04
FBgn0028743	Dhit	-0,7528332	2,00E-05	7,67E-04
FBgn0032620	CG12288	-0,553131	2,02E-05	7,73E-04
FBgn0036927	Gabat	-0,428105	2,17E-05	8,12E-04
FBgn0033744	Dh44-R2	-0,6829629	2,32E-05	8,62E-04
FBgn0035243	CG13926	-0,5272733	2,74E-05	9,93E-04
FBgn0036152	CG6175	-0,4987982	2,74E-05	9,93E-04
FBgn0263219	Dscam4	4,26575635	1,54E-126	1,30E-122
FBgn0036670	CG13029	2,83424902	1,19E-44	6,28E-42
FBgn0034839	CG13540	2,89163461	3,44E-42	1,70E-39
FBgn0003009	ord	2,82783356	5,85E-41	2,60E-38
FBgn0034838	CG12782	2,60654219	3,33E-35	1,17E-32
FBgn0030716	CG9170	1,50784841	4,94E-25	1,10E-22
FBgn0052187	CG32187	2,04105356	7,36E-25	1,55E-22
FBgn0038012	CG10013	2,0095881	1,55E-24	3,20E-22
FBgn0267728	otk2	2,02130435	1,56E-22	3,12E-20
FBgn0262534	CG43088	1,82971272	1,54E-19	2,65E-17
FBgn0267967	corolla	1,44841679	3,13E-18	4,80E-16
FBgn0036196	CG11658	1,20258103	3,60E-17	5,37E-15
FBgn0034312	CG10916	1,2776931	3,63E-17	5,37E-15
FBgn0032899	CG9338	1,27676094	4,27E-16	6,10E-14
FBgn0052364	tut	1,64735177	2,53E-15	3,44E-13
FBgn0085370	Pde11	0,79023517	9,19E-15	1,19E-12
FBgn0014342	mia	1,31881784	6,68E-12	6,63E-10
FBgn0039941	CG17167	1,29442172	1,58E-11	1,50E-09
FBgn0085638	CG41378	1,13276183	2,51E-11	2,33E-09
FBgn0262169	magu	0,67550554	3,20E-11	2,93E-09
FBgn0031999	CG8419	1,36819061	6,11E-11	5,49E-09
FBgn0037229	CG9766	1,206099	5,42E-10	4,57E-08
FBgn0029588	CG14798	1,10208561	6,63E-10	5,48E-08
FBgn0284435	tyn	0,93076393	1,59E-09	1,2519E-07
FBgn0033521	CG12896	1,14951467	3,86E-09	2,83E-07
FBgn0040001	FASN3	1,21906851	9,86E-09	7,04E-07
FBgn0026255	clumsy	1,18782244	1,19E-08	8,35E-07
FBgn0039124	tbrd-1	1,20998769	1,34E-08	9,36E-07

FBgn0260027	CG42495	-0,968787	8,35E-07	3,10E-05
FBgn0030598	CG9503	-0,7904792	8,51E-07	3,14E-05
FBgn0031998	SLC5A11	-0,7290666	9,82E-07	3,615E-05
FBgn0031589	CG3714	-0,522241	1,01E-06	3,71E-05
FBgn0033205	CG2064	-0,7867165	1,04E-06	3,79E-05
FBgn0037581	CG7352	-0,8753558	1,08E-06	3,92E-05
FBgn0028468	rtet	-0,6723628	1,43E-06	5,16E-05
FBgn0015569	alpha-Est10	-0,8392161	1,44E-06	5,18E-05
FBgn0031117	GstT3	-0,6298817	1,48E-06	5,2882E-05
FBgn0265761	CR44568	-0,9108888	1,88E-06	6,72E-05
FBgn0030668	CG8128	-0,6943842	1,92E-06	6,81E-05
FBgn0053005	GstT2	-0,6438248	2,01E-06	7,11E-05
FBgn0034032	CG8195	-0,5408707	2,05E-06	7,22E-05
FBgn0030925	Hayan	-0,9826592	2,15E-06	7,55E-05
FBgn0037000	Zn877C	-0,6746768	2,26E-06	7,89E-05
FBgn0004108	Nrt	-0,6964366	2,36E-06	8,20E-05
FBgn0032249	TBC1D16	-0,7115413	2,42E-06	8,36E-05
FBgn0259224	CG42324	-0,8959483	2,45E-06	8,44E-05
FBgn0033233	Kdm4A	-0,5605395	2,53E-06	8,70E-05
FBgn0262902	CR43257	-0,957284	2,61E-06	8,94E-05
FBgn0038012	CG10013	-0,9437117	2,77E-06	9,36E-05
FBgn0039094	CG10184	-0,7620824	2,77E-06	9,36E-05
FBgn0033875	CG6357	-0,8296114	2,97E-06	9,98E-05
FBgn0011660	Prns2	-0,6191626	4,01E-06	1,33E-04
FBgn0023540	CG3630	-0,7750882	4,38E-06	1,44E-04
FBgn0040260	Upt36Bc	-0,7920914	4,55E-06	1,49E-04
FBgn0032744	Tfc19	-0,7666045	4,63E-06	1,52E-04
FBgn0034399	CG15083	-0,6891411	4,71E-06	1,54E-04
FBgn0031161	CG15445	-0,5597491	5,16E-06	1,66E-04
FBgn0034569	dgt3	-0,5100777	5,16E-06	1,66E-04
FBgn0031011	CG8034	-0,5605182	5,44E-06	0,00017485
FBgn0027499	wde	-0,4701503	5,51E-06	1,77E-04
FBgn0053170	CG33170	-0,7056534	5,85E-06	0,00018566
FBgn0000152	Axs	-0,6035714	5,84E-06	1,86E-04
FBgn0017448	CG2187	-0,7509568	5,90E-06	1,86E-04
FBgn0024222	IKKbeta	-0,5333447	6,15E-06	1,94E-04
FBgn0011642	Zyx	-0,6685735	6,47E-06	0,00020304
FBgn0034928	CG13562	-0,9576823	6,71E-06	2,10E-04
FBgn0025702	Srpk79D	-0,9076152	6,96E-06	2,17E-04
FBgn0032210	CYLD	-0,6022837	8,33E-06	2,58E-04
FBgn0035160	hng3	-0,7523256	8,55E-06	2,63E-04
FBgn0040384	CG32795	-0,5216919	8,89E-06	2,72E-04
FBgn0030683	CG8239	-0,5479759	1,16E-05	3,53E-04
FBgn0038704	CG5316	-0,5674446	1,19E-05	3,59E-04
FBgn0261794	lcc	-0,5170776	1,31E-05	3,96E-04
FBgn0267967	comilla	-0,7468133	1,40E-05	4,20E-04
FBgn0034985	CG3328	-0,9088474	1,42E-05	4,23E-04
FBgn0058160	CG40160	-0,5573892	1,44E-05	0,00042856
FBgn0263001	CR43309	-0,9140864	1,55E-05	4,59E-04
FBgn0035264	Oseg4	-0,8324113	1,58E-05	4,66E-04
FBgn0030467	CG1764	-0,6086858	1,68E-05	4,94E-04
FBgn0031224	CG11454	-0,6511044	1,79E-05	5,23E-04
FBgn0261363	PPO3	-0,908642	1,87E-05	5,43E-04
FBgn0036765	CG7408	-0,8043628	1,92E-05	5,57E-04
FBgn0038966	pinta	-0,6002371	1,93E-05	5,57E-04
FBgn0264979	CG4267	-0,5921441	1,95E-05	5,62E-04
FBgn0031974	CG12560	-0,6468851	2,10E-05	5,99E-04
FBgn0030349	CG10353	-0,5110312	2,26E-05	6,42E-04
FBgn0046685	Wsck	-0,554038	2,39E-05	6,80E-04
FBgn0036196	CG11658	-0,6157453	2,51E-05	7,08E-04
FBgn0002932	neur	-0,5215054	2,55E-05	7,16E-04
FBgn0038490	CG5285	-0,6202791	2,59E-05	7,25E-04
FBgn0027535	botv	-0,5633173	2,64E-05	7,39E-04
FBgn0011676	Nos	-0,882868	2,73E-05	7,61E-04
FBgn0052109	CG32109	-0,6631842	2,96E-05	0,00082025
FBgn0266211	CR44906	-0,84417	3,08E-05	8,49E-04
FBgn0032079	CG31886	-0,7657233	3,21E-05	8,78E-04
FBgn0086898	dgo	-0,6488394	3,30E-05	9,01E-04
FBgn0036331	CG14117	-0,7419989	3,32E-05	9,02E-04
FBgn0033715	CG8490	-0,565824	3,39E-05	9,17E-04
FBgn0034578	CG15653	-0,6741581	3,52E-05	9,50E-04
FBgn0033261	uddl	-0,5640484	3,64E-05	0,00097761
FBgn0085212	CG34183	-0,5802033	3,68E-05	0,00098506
FBgn0030716	CG9170	3,51543874	2,73E-133	1,25E-129
FBgn0003710	tipE	4,51536274	2,28E-119	5,23E-116
FBgn0040370	CG13375	3,94270954	2,25E-117	4,12E-114
FBgn0063499	GstE10	4,38522941	1,29E-105	1,96E-102
FBgn0263219	Dscam4	3,38390085	1,29E-79	1,48E-76
FBgn0063491	GstE9	2,37209129	5,43E-74	5,53E-71
FBgn0262509	nrm	3,26989536	5,19E-72	4,76E-69
FBgn0000246	o(3)G	1,80256044	7,60E-51	4,64E-48
FBgn0052773	CR32773	2,91153609	2,21E-48	1,06E-45
FBgn0033744	Dh44-R2	2,21228708	3,41E-47	1,56E-44
FBgn0004034	y	2,3656636	1,46E-36	4,63E-34
FBgn0039129	Rpl19b	2,25634285	4,45E-29	9,94E-27
FBgn0052625	CG32625	1,50639584	1,75E-26	3,56E-24
FBgn0003965	v	2,2137325	8,01E-26	1,56E-23
FBgn0028400	Syt4	1,60413573	8,45E-26	1,61E-23
FBgn0035086	CG12851	2,20739805	3,06E-25	5,51E-23
FBgn0014417	CG13397	0,9799056	2,34E-24	4,05E-22
FBgn0052373	CG32373	1,65820956	3,79E-22	5,89E-20
FBgn0039883	RhoGAP100F	1,78355414	4,14E-22	6,32E-20
FBgn0052816	CG32816	1,34949326	3,29E-21	4,78E-19
FBgn0036369	CG10089	1,43828569	3,97E-19	5,58E-17
FBgn0035083	Tina-1	0,97905168	3,91E-18	4,84E-16
FBgn0031645	CG3036	1,20681255	3,21E-16	3,59E-14

FBgn0283427	FASN1	0,86975756	2,30E-08	1,52E-06
FBgn0050401	dany	1,11817354	2,28E-08	1,52E-06
FBgn0263705	Myo10A	0,98315534	3,45E-08	2,20E-06
FBgn0025676	Cldialpha-i3	0,67693092	1,26E-07	7,83E-06
FBgn0039927	CG11155	0,90203488	1,71E-07	1,03E-05
FBgn0037623	CG9801	0,6640328	2,35E-07	1,37E-05
FBgn0031157	CG1503	0,93002568	3,29E-07	1,88E-05
FBgn0004895	Fmd-1	1,0757224	4,27E-07	2,42E-05
FBgn0266710	hng	0,83815038	4,39E-07	2,45E-05
FBgn0000038	nAChRbeta1	1,04459491	6,48E-07	3,55E-05
FBgn0039118	CG10208	0,80995118	1,20E-06	6,26E-05
FBgn0033458	CG18446	0,58308966	1,28E-06	6,64E-05
FBgn0033520	Prx2540-1	0,74375135	1,29E-06	6,66E-05
FBgn0031689	Cyp28d1	0,80053352	1,58E-06	8,04E-05
FBgn0032729	L2HGDH	0,52320052	1,72E-06	8,62E-05
FBgn0037717	CG8301	0,54410035	1,94E-06	9,55E-05
FBgn0033205	CG2064	0,73749684	3,06E-06	1,47E-04
FBgn0027621	Pfrx	0,72002681	3,25E-06	1,53E-04
FBgn0050460	CG30460	0,62944429	3,81E-06	1,76E-04
FBgn0035094	CG9380	0,93844635	4,81E-06	0,00021789
FBgn0051793	CG31793	0,65755611	4,93E-06	2,23E-04
FBgn0025885	Imps	0,61521329	5,50E-06	2,47E-04
FBgn0037326	CG14669	0,84098198	5,58E-06	2,49E-04
FBgn0032719	CG17321	0,73961713	6,03E-06	2,66E-04
FBgn0037606	CG8032	0,48037173	6,10E-06	2,68E-04
FBgn0026417	Hus1-like	0,61835828	6,46E-06	2,82E-04
FBgn0001085	fz	0,60208374	6,78E-06	2,95E-04
FBgn0267347	sqh	0,60195776	8,58E-06	3,66E-04
FBgn0033257	sand	0,9250535	8,99E-06	3,81E-04
FBgn0003071	Pfk	0,57585055	9,37E-06	3,95E-04
FBgn0261041	stj	0,81342642	1,07E-05	4,47E-04
FBgn0051676	CG31676	0,89263646	1,42E-05	5,81E-04
FBgn0038296	CG6752	0,66542534	1,56E-05	6,28E-04
FBgn0022709	Adk1	0,55981758	1,65E-05	6,58E-04
FBgn0032161	CG4594	0,57432263	1,75E-05	6,89E-04
FBgn0023535	arg	0,90279534	1,76E-05	6,89E-04
FBgn0033246	ACC	0,51387976	1,98E-05	7,62E-04
FBgn0017482	l(3)dh	0,78501069	2,08E-05	7,91E-04
FBgn0014417	CG13397	0,40998593	2,1026E-05	0,00079514
FBgn0031703	CG12512	0,55306249	2,15E-05	8,08E-04
FBgn0264816	lmko	0,43906737	2,28E-05	8,50E-04
FBgn0037742	Rpl3R	0,90083167	2,34E-05	8,66E-04
FBgn0033815	CG4676	0,88304551	2,39E-05	8,80E-04
FBgn0085339	CG34310	0,71342358	2,46E-05	9,03E-04
FBgn0263665	CR43656	0,67340873	2,72E-05	9,93E-04

FBgn0028743	Dhit	1,400557	1,35E-15	1,44E-13
FBgn0264439	CR43857	1,44206442	3,80E-15	3,91E-13
FBgn0029723	Proc-R	1,16467501	8,98E-15	9,10E-13
FBgn0036368	CG10738	1,12952567	1,06E-14	1,05E-12
FBgn0267733	CR46064	1,30463417	2,70E-14	2,55E-12
FBgn0266258	CR44953	1,61734556	2,70E-14	2,55E-12
FBgn0038204	CG14357	1,45024866	1,17E-13	1,04E-11
FBgn0039900	Syt7	1,57434289	1,36E-13	1,18E-11
FBgn0031275	GABA-B-R3	1,56925587	1,55E-13	1,34E-11
FBgn0039118	CG10208	1,225912	1,70E-13	1,45E-11
FBgn0267347	squ	0,97779595	4,75E-13	3,85E-11
FBgn0003866	tsh	1,33447888	7,38E-13	5,88E-11
FBgn0033458	CG18446	0,8595366	9,18E-13	7,25E-11
FBgn0050403	CG30403	0,83287764	1,55E-11	1,10E-09
FBgn0032645	CG15142	1,25685861	2,82E-11	1,94E-09
FBgn0264385	CR43837	0,80630682	7,48E-11	4,93E-09
FBgn0038038	CG5167	0,86009134	2,30E-10	1,46E-08
FBgn0263093	CR43361	0,98968277	7,16E-10	4,26E-08
FBgn0284435	tyn	0,90935674	3,67E-09	1,9771E-07
FBgn0259229	CG42329	0,99577599	4,2094E-09	2,2561E-07
FBgn0035317	Oseg2	1,2035749	4,82E-09	2,57E-07
FBgn0030723	dpr18	1,20750721	7,53E-09	3,90E-07
FBgn0266005	CR44779	0,91939442	1,40E-08	7,03E-07
FBgn0283427	FASN1	0,86971339	2,30E-08	1,11E-06
FBgn0037902	CG5281	1,01450627	2,83E-08	1,35E-06
FBgn0261266	zuc	0,59100256	4,51E-08	2,07E-06
FBgn0040001	FASN3	1,15849921	5,08E-08	2,32E-06
FBgn0039341	CG5112	0,52776631	9,83E-08	4,21E-06
FBgn0039938	Sox102F	0,96839303	1,34E-07	5,6477E-06
FBgn0051997	CG31997	1,08525441	1,72E-07	7,21E-06
FBgn0042696	Nfi	1,08171827	2,65E-07	1,07E-05
FBgn0263617	CR43626	1,0436084	3,50E-07	1,40E-05
FBgn0023535	arg	1,07140257	3,57E-07	1,42E-05
FBgn0039543	CG12428	0,51181318	3,79E-07	1,50E-05
FBgn0263660	CR43651	0,94475809	5,01E-07	1,94E-05
FBgn0033246	ACC	0,58306679	1,27E-06	4,62E-05
FBgn0265168	CR44237	0,75743644	2,18E-06	7,63E-05
FBgn0039927	CG11155	0,81040266	2,64E-06	9,00E-05
FBgn0260745	mfas	0,73309962	2,88E-06	9,71E-05
FBgn0260812	inaF-D	0,94838747	3,51E-06	1,17E-04
FBgn0027611	LManII	0,78767635	3,80E-06	1,27E-04
FBgn0002905	mus308	0,63117721	3,93E-06	1,30E-04
FBgn0004047	Yp3	0,86055593	4,75E-06	1,54E-04
FBgn0025629	CG4045	0,61428341	5,64E-06	1,80E-04
FBgn0264265	CR43765	0,89472755	7,33E-06	2,28E-04
FBgn0004895	Foxl1	0,94745812	8,43E-06	2,60E-04
FBgn0031703	CG12512	0,57709695	9,14E-06	2,79E-04
FBgn0041581	Att8	0,94032658	9,6168E-06	0,00029282
FBgn0025382	Rab27	0,84551951	1,32E-05	0,000398
FBgn0030583	CG14410	0,57134888	1,4142E-05	0,00042218
FBgn0263916	Ent2	0,54077834	1,78E-05	5,21E-04
FBgn0030660	CG8097	0,47918563	1,96E-05	5,64E-04
FBgn0016926	Pino	0,5721965	2,07E-05	5,92E-04
FBgn0267001	Ten-a	0,80076692	2,42E-05	6,84E-04
FBgn0037577	CG7443	0,82607808	2,8441E-05	0,00078987
FBgn0026361	Sep5	0,58579619	3,19E-05	8,77E-04
FBgn0085370	Pde11	0,4243612	3,21E-05	8,78E-04
FBgn0052702	Cuten	0,56358184	3,33E-05	0,00090215

S3 Table. Quantitative analysis of H3K4me3 differential enrichment in Control vs *lid* KD ovarian ChIP-Seq.

chromosome	start	end	Conc_WT	Conc_LidKD	Fold	p.value	FDR	Annotation	Detailed Annotation	Distance to TSS	Nearest PromoterID
chr2R	13409200	13409700	8,65	1,29	-7,35	4,80E-53	1,41E-49	TTS (FBgn0267026)	exon (NM_165983, exon 2 of 4)	437	FBgn0033836|FBtr0087716
chr2R	5108648	5109148	10,01	6,75	-3,26	2,10E-14	8,05E-12	Intergenic	NOMAD_I-int|LTR|Gypsy	13349	FBgn0026238|FBtr0300848
chrX	5312452	5312952	11,66	8,54	-3,11	5,62E-62	2,48E-58	promoter-TSS (FBgn0029752)	promoter-TSS (NM_131585)	349	FBgn0011761|FBtr0070749
chr2R	5106392	5106892	9,02	6,14	-2,89	2,69E-09	2,97E-07	Intergenic	FW2_DM|LINE|Jockey	14758	FBgn0033005|FBtr0101280
chr3R	10957890	10958390	9,47	6,85	-2,62	2,76E-13	8,13E-11	Intergenic	CpG	7057	FBgn0037857|FBtr0302326
chr2R	5105620	5106120	10,35	8,1	-2,25	8,30E-28	8,15E-25	Intergenic	NINA_I-int|LTR|Pao	13986	FBgn0033005|FBtr0101280
chr2L	20292285	20292785	9,44	7,36	-2,08	3,58E-14	1,27E-11	Intergenic	(CA)n|Simple_repeat|Simple_repeat	-2057	FBgn0040996|FBtr0081351
chr3L	18685896	18686396	10,01	7,94	-2,07	8,83E-13	2,36E-10	exon (FBgn0036806, exon 1 of 2)	exon (NM_140795, exon 1 of 2)	173	FBgn0036806|FBtr0345812
chr3L	13006940	13007440	10,57	9,1	-1,48	1,69E-09	1,99E-07	exon (FBgn0036330, exon 1 of 1)	exon (NM_001169964, exon 2 of 2)	374	FBgn0036330|FBtr0075873
chr2R	7681134	7681634	10,71	9,34	-1,38	1,97E-07	1,08E-05	promoter-TSS (FBgn0033212)	promoter-TSS (NM_001169675)	-334	FBgn0033212|FBtr0301780
chr3R	31196793	31197293	8,9	7,59	-1,3	1,03E-08	9,30E-07	exon (FBgn0039827, exon 1 of 12)	exon (NM_143592, exon 1 of 12)	128	FBgn0039827|FBtr0085755
chrX	12072279	12072779	10,45	9,3	-1,15	3,92E-08	2,86E-06	exon (FBgn0030373, exon 1 of 1)	exon (NM_132556, exon 1 of 1)	289	FBgn0030373|FBtr0078637
chr2L	17990861	17991361	9,1	7,95	-1,15	9,90E-07	4,10E-05	exon (FBgn0051742, exon 1 of 1)	exon (NM_165234, exon 1 of 1)	694	FBgn0051742|FBtr0081025
chr2L	7791670	7792170	9,08	7,94	-1,14	2,30E-08	1,80E-06	intron (FBgn0025687, intron 7 of 7)	CpG	-1363	FBgn0031948|FBtr0079496
chr3R	29925218	29925718	8,81	7,69	-1,12	4,83E-07	2,26E-05	promoter-TSS (FBgn0033356)	promoter-TSS (NM_079830)	721	FBgn0033358|FBtr0085511
chr2R	6022741	6023241	10,14	9,04	-1,11	9,50E-05	0,00162	exon (FBgn0033051, exon 1 of 3)	exon (NM_001273789, exon 1 of 3)	153	FBgn0033051|FBtr0335289
chr2R	4674779	4675279	9,36	8,25	-1,1	6,94E-05	0,00126	Intergenic	CpG	3177	FBgn0040005|FBtr0101291
chrX	18359008	18359508	9,3	8,21	-1,09	1,89E-05	0,000434	exon (FBgn0030914, exon 2 of 4)	exon (NM_133059, exon 2 of 4)	378	FBgn0030914|FBtr0074553
chr3L	1189844	1190344	10,23	9,15	-1,08	3,95E-08	2,86E-06	TTS (FBgn0035187)	TTS (NM_138216)	507	FBgn0035186|FBtr0072625
chr2L	9996097	9996597	9,91	8,88	-1,03	0,000117	0,0019	TTS (FBgn0051755)	TTS (NM_001273384)	225	FBgn0051875|FBtr0079973
chr2R	6769314	6769814	9,26	8,24	-1,02	0,00112	0,0106	exon (FBgn0085421, exon 1 of 16)	5' UTR (NM_001273808, exon 1 of 16)	194	FBgn0085421|FBtr0329851
chr3L	22901945	22902445	11,56	10,58	-0,98	9,65E-07	4,02E-05	exon (FBgn0037205, exon 1 of 1)	exon (NM_141173, exon 1 of 1)	284	FBgn0037205|FBtr0078559
chr4	946167	946667	8,4	7,45	-0,96	6,79E-06	0,00019	exon (FBgn0019985, exon 8 of 8)	exon (NM_001272347, exon 9 of 9)	9599	FBgn0019985|FBtr0332859
chrX	23222121	23222621	9,81	8,85	-0,96	0,00512	0,033	Intergenic	R2_DM|LINE|R2	7920	FBgn0267519|FBtr0346895
chr2R	4833428	4833928	9,12	8,19	-0,93	1,21E-05	0,000304	Intergenic	Baggins1|LINE|I.OA	4433	FBgn0033000|FBtr0299923
chr2R	4297886	4298386	9,7	8,77	-0,93	0,00224	0,0181	Intergenic	(TGGCGG)n|Simple_repeat|Simple_rep	-95202	FBgn0262117|FBtr0111268
chrX_DS483928v1_random	2011	2511	8,66	7,76	-0,91	0,000582	0,00667	NA	Intergenic	NA	NA
chr2L	16702472	16702972	9,38	8,49	-0,89	0,00813	0,0469	exon (FBgn0263745, exon 3 of 3)	Intergenic	475	FBgn0263745|FBtr0310392
chr2R	6716557	6717057	9,96	9,09	-0,87	0,00492	0,0321	promoter-TSS (FBgn0033095)	promoter-TSS (NM_136386)	900	FBgn0033096|FBtr0086139
chr3L	217378	217878	9,44	8,62	-0,82	5,78E-05	0,00109	promoter-TSS (FBgn0035112)	promoter-TSS (NM_138170)	259	FBgn0063923|FBtr0072488
chr2R	14910246	14910746	8,82	8,04	-0,78	0,00692	0,0416	exon (FBgn0027596, exon 3 of 10)	exon (NM_001103848, exon 4 of 11)	373	FBgn0027596|FBtr0080430
chr3L	19280205	19280705	8,74	7,97	-0,77	0,000339	0,00444	TTS (FBgn0036860)	TTS (NM_140845)	145	FBgn0036861|FBtr0075015
chrX	8035988	8036488	9,21	8,43	-0,77	0,000455	0,00555	exon (FBgn0029990, exon 4 of 5)	exon (NM_132705, exon 4 of 5)	1279	FBgn0029990|FBtr0078123
chrX	15676230	15676730	9,34	8,58	-0,75	0,00181	0,0153	exon (FBgn0030666, exon 2 of 2)	exon (NM_001144727, exon 2 of 2)	1005	FBgn0030666|FBtr0304052
chrX	22491784	22492284	9,72	9,01	-0,7	0,00135	0,0122	exon (FBgn0027779, exon 1 of 10)	exon (NM_176779, exon 1 of 11)	440	FBgn0027779|FBtr0299523
chr2R	12314643	12315143	8,97	8,27	-0,7	0,00675	0,0407	exon (FBgn0050046, exon 2 of 6)	exon (NM_165878, exon 2 of 6)	777	FBgn0050046|FBtr0082895
chrX_DS483892v1_random	617	1117	8,73	8,04	-0,69	0,00826	0,0475	NA	R1_DM|LINE|R1	NA	NA
chr2R	6705730	6706230	8,82	8,15	-0,68	0,00161	0,014	exon (FBgn0033095, exon 2 of 7)	5' UTR (NM_001169592, exon 2 of 7)	1267	FBgn0263518|FBtr0309587
chrX	22448695	22449195	10,38	9,71	-0,67	0,000683	0,00755	promoter-TSS (FBgn0014395)	promoter-TSS (NM_134616)	458	FBgn0031184|FBtr0319499
chr3L	218197	218697	9,2	8,54	-0,67	0,00455	0,0307	TTS (FBgn0063923)	TTS (NM_001031920)	287	FBgn0035112|FBtr0304058
chr3L	1755127	1755627	10,72	10,06	-0,65	0,00265	0,0206	promoter-TSS (FBgn0052508)	promoter-TSS (NM_001169853)	-305	FBgn0022702|FBtr0305966
chr2L	7789910	7790410	10,46	9,83	-0,63	0,00219	0,0178	exon (FBgn0031948, exon 1 of 9)	5' UTR (NM_135305, exon 1 of 8)	397	FBgn0031948|FBtr0079496
chr3L	14219569	14220069	8,81	8,17	-0,63	0,00416	0,0288	promoter-TSS (FBgn0013718)	promoter-TSS (NM_001038019)	78	FBgn0013718|FBtr0100043
chr3R	17059672	17060172	8,67	8,04	-0,63	0,00581	0,0363	intron (FBgn0020493, intron 3 of 7)	(CA)n|Simple_repeat|Simple_repeat	5026	FBgn0020493|FBtr0083394
chrX	7709187	7709687	8,44	7,83	-0,61	0,00521	0,0334	promoter-TSS (FBgn0029504)	promoter-TSS (NM_001272383)	-52	FBgn0029504|FBtr0310287
chr3L	20621817	20622317	8,99	8,42	-0,58	0,00481	0,0317	Intergenic	Intergenic	-1408	FBgn0001323|FBtr0078212
chr2L	6337817	6338317	11,39	11,69	0,29	0,006	0,0373	promoter-TSS (FBgn0015623)	promoter-TSS (NM_057810)	359	FBgn0031799|FBtr0079284
chr3R	4311476	4311976	11,7	12	0,29	0,00738	0,0435	promoter-TSS (FBgn0037231)	promoter-TSS (NM_001316578)	172	FBgn0037232|FBtr0273009
chr2R	24034534	24035034	11,64	11,94	0,3	0,00488	0,032	promoter-TSS (FBgn0013764)	promoter-TSS (NM_057734)	560	FBgn0034962|FBtr0072166
chr2R	13549543	13550043	11,23	11,53	0,3	0,00797	0,0463	exon (FBgn0033156, exon 2 of 4)	exon (NM_001103812, exon 2 of 4)	465	FBgn0033156|FBtr0080684
chr2L	6490282	6490782	11,72	12,01	0,3	0,00852	0,0484	promoter-TSS (FBgn0051638)	promoter-TSS (NM_001103629)	301	FBgn0031822|FBtr0079264
chr2R	18141277	18141777	11,39	11,7	0,31	0,00364	0,0261	exon (FBgn0265797, exon 2 of 5)	exon (NM_166765, exon 2 of 5)	153	FBgn0265797|FBtr0086740
chr3L	12534480	12534980	11,45	11,75	0,31	0,00402	0,0282	TTS (FBgn0085271)	TTS (NM_001104125)	141	FBgn0036300|FBtr0079561
chr3R	15834707	15835207	11,21	11,52	0,31	0,0045	0,0304	promoter-TSS (FBgn0263022)	promoter-TSS (NM_001144586)	-310	FBgn0038360|FBtr0310570
chr3L	9358969	9359469	11,17	11,48	0,31	0,00508	0,0329	promoter-TSS (FBgn0035978)	promoter-TSS (NM_001169928)	221	FBgn0052039|FBtr0076441
chrX	19730950	19731450	11,75	12,07	0,31	0,0056	0,0353	intron (FBgn0010380, intron 1 of 2)	intron (NM_078693, intron 1 of 2)	197	FBgn0010380|FBtr0074789
chrX	1899300	1899800	11,17	11,48	0,31	0,00612	0,0377	promoter-TSS (FBgn0000117)	promoter-TSS (NM_001272270)	-76	FBgn0000117|FBtr0089388
chr3R	8993122	8993622	11,73	12,05	0,31	0,00656	0,0398	promoter-TSS (FBgn0260243)	promoter-TSS (NM_141595)	120	FBgn0037648|FBtr0081960
chr3R	21017610	21018110	11,11	11,42	0,31	0,0068	0,0417	TTS (FBgn0038846)	TTS (NM_142675)	177	FBgn0026956|FBtr0084002
chr2L	13903602	13904102	11,23	11,54	0,31	0,00761	0,0446	exon (FBgn0039890, exon 2 of 6)	exon (NM_165263, exon 2 of 6)	395	FBgn0039890|FBtr0342669
chr3R	17686487	17686987	11,62	11,94	0,32	0,00296	0,0225	TTS (FBgn0053160)	TTS (NM_169773)	134	FBgn0053149|FBtr0084403
chr2L	21343327	21343827	11,38	11,7	0,32	0,00411	0,0285	promoter-TSS (FBgn0052436)	promoter-TSS (NM_168898)	139	FBgn0037074|FBtr0331797
chr2R	23698390	23698890	11,13	11,45	0,32	0,00433	0,0297	promoter-TSS (FBgn0050100)	promoter-TSS (NM_001144273)	536	FBgn0034893|FBtr0072084
chr2L	16258108	16258608	11,11	11,43	0,32	0,00456	0,0307	promoter-TSS (FBgn0024736)	promoter-TSS (NM_135936)	354	FBgn0028515|FBtr0080824
chr2R	18446572	18447072	11,82	12,14	0,32	0,00585	0,0365	TTS (FBgn0261119)	TTS (NM_079092)	225	FBgn0034350|FBtr0086694
chr2R	16291624	16292124	11,63	11,96	0,33	0,00234	0,0187	promoter-TSS (FBgn0263981)	promoter-TSS (NR_124571)	357	FBgn0050100|FBtr0340022
chrX	16440982	16441482	11,34	11,67	0,33	0,00233	0,0187	promoter-TSS (FBgn0030752)	promoter-TSS (NM_132901)	64	FBgn0030752|FBtr0343350
chr2L	8082353	8082853	11,23	11,56	0,33	0,00286	0,0218	promoter-TSS (FBgn0266795)	promoter-TSS (NM_164785)	-255	FBgn0266795|FBtr0345451
chr2L	4385471	4385971	11,64	11,97	0,33	0,00355	0,0257	TTS (FBgn0261976)	TTS (NM_001273093)	341	FBgn0031598|FBtr0077462
chr3L	6193522	6194022	11,37	11,7	0,33	0,00434	0,0297	promoter-TSS (FBgn0024921)	promoter-TSS (NM_168161)	77	FBgn0024921|FBtr0077002
chr3R	21364669	21365169	11,84	12,17	0,33	0,00471	0,0313	promoter-TSS (FBgn0261843)	promoter-TSS (NM_001202334)	371	FBgn0266172|FBtr0343748
chr2L	4850696	4851196	11,94	12,28	0,33	0,0052	0,0333	promoter-TSS (FBgn0031619)	promoter-TSS (NM_078749)	306	FBgn0031640|FBtr0077387
chrX	11454835	11455335	11,58	11,92	0,33	0,00541	0,0343	promoter-TSS (FBgn0262740)	promoter-TSS (NM_001169251)	300	FBgn0030301|FBtr0079500
chr2R	6213680	6214180	11,91	12,24	0,33	0,00602	0,0373	promoter-TSS (FBgn0263144)	promoter-TSS (NM_078907)	192	FBgn0021847|FBtr0086000
chr2L	15005806	15006306	11,16	11,49	0,33	0,00606	0,0374	TTS (FBgn0261881)	TTS (NM_135891)	324	FBgn0040228|FBtr0080693
chr3L	851243	851743	11,3	11,62	0,33	0,00603	0,0374	TTS (FBgn0035168)	TTS (NM_138220)	148	FBgn0035169|FBtr0072587
chr3R	29055857	29056357	11,5	11,83	0,33	0,00627	0,0384	promoter-TSS (FBgn0267776)	promoter-TSS (NR_133478)	181	FBgn0039631|FBtr0085364
chr3R	11237870	11238370	11,42	11,75	0,33	0,00691	0,0415	TTS (FBgn0051441)	TTS (NM_169382)	306	FBgn0051388|FBtr0082356
chrX	6225488	6225988	11,33	11,67	0,33	0,00734	0,0434	promoter-TSS (FBgn0003514)	promoter-TSS (NM_132077)	92	FBgn0262730|FBtr0307165
chr3L	15566221	15566721	11,08	11,42	0,33	0,00778	0,0453	TTS (FBgn0036510)	TTS (NM_140520)	459	FBgn0267390|FBtr0075562
chr3R	9412467	9412967	11,22	11,55	0,33	0,00876	0,0494	promoter-TSS (FBgn0037690)	promoter-TSS (NM_141634)	170	FBgn0011740|FBtr0082031
chrX	6266215	6266715	11,45	11,79	0,34	0,00131	0,012	exon (FBgn0040918, exon 1 of 6)	exon (NM_167063, exon 2 of 7)	763	FBgn0040918|FBtr0070937
chr2L	419073	419573	11,38	11,72	0,34	0,0017	0,0146	promoter-TSS (FBgn0002931)	promoter-TSS (NM_001272853)	329	FBgn0031752|FBtr0078090
chr2L	5519485	5519985	11,6	11,94	0,34	0,00211	0,0173	promoter-TSS (FBgn0000388)	promoter-TSS (NM_001273170)	161	FBgn0031708|FBtr0079130
chr2R	7793526	7794026	11,43	11,76	0,34	0,00215	0,0176	promoter-TSS (FBgn0001091)	promoter-TSS (NM_001038847)	152	FBgn0002891|FBtr0088831
chr3R	8726722	8727222	11,42	11,76	0,34	0,00215	0,0176	TTS (FBgn0037686)	TTS (NM_141565)	139	FBgn0037619|FBtr0301194
chr2L	10517255	10517755	11,58	11,92	0,34	0,00217	0,0177	promoter-TSS (FBgn0267828)	promoter-TSS (NM_001169469)	171	FBgn0010398|FBtr0080092
chr3L	5367427	5367927	11,9	12,24	0,34	0,00339	0,025	TTS (FBgn0260895)	TTS (NM_139703)	331	FBgn0035603|FBtr0077154
chr3R	8361993	8362493	11,32	11,66	0,34	0,00404	0,0282	promoter-TSS (FBgn0037584)	promoter-TSS (NM_141541)	311	FBgn0037583|FBtr0081853
chr3R	17802811	17803311	11,65	11,99	0,34	0,00451	0,0305	TTS (FBgn0038501)	TTS (NM_142402)	199	FBgn0038500|FBtr0082527
chr3R	19229577	19230077	11,75	12,1	0,34	0,00454	0,0306	promoter-TSS (FBgn0038691)	promoter-TSS (NM_142536)	365	FBgn0038692|FBtr0083737
chr3R	23986557	23987057	11,91	12,25	0,34	0,00483	0,0318	promoter-TSS (FBgn0039116)	promoter-TSS (NM_142943)	166	FBgn0039116|FBtr0084501
chr2L	2147454	2147954	11,43	11,77	0,34	0,00497	0,0324	promoter-TSS (FBgn0013291)	promoter-TSS (NM_001272577)	187	FBgn0027509|FBtr0077829
chrX	22454806	22455306	11,95	12,28	0,34	0,00511	0,033	promoter-TSS (FBgn0031187)	promoter-TSS (NM_167777)	366	FBgn0266848|FBtr0330498
chrX	2619468	2619968	11,28	11,61	0,34	0,00599	0,0372	promoter-TSS (FBgn0040334)	promoter-TSS (NM_130656)	20	FBgn0040334|FBtr0301159
chr3R	9053444	9053944	10,87	11,21	0,34	0,00604	0,0374	exon (FBgn0037693, exon 2 of 6)	exon (NM_141607, exon 2 of 6)	401	FBgn0037693|FBtr0336759
chr2L	2745133	2745633	11,9	12,24	0,34	0,0063	0,0386	promoter-TSS (FBgn0031451)	promoter-TSS (NM_001273026)	286	FBgn0031452|FBtr0077712
chr2L	12694470	12694970	10,91	11,25	0,34	0,00796	0,0462	promoter-TSS (FBgn0032447)	promoter-TSS (NM_135738)	268	FBgn0032446|FBtr0301273
chrX	11793180	11793680	11,49	11,85	0,35	0,00113	0,0107	intron (FBgn0000253, intron 1 of 6)	intron (NM_001258700, intron 1 of 6)	552	FBgn0000253|FBtr0073560
chrX	19495963	19496463	11,23	11,58	0,35	0,00197	0,0164	promoter-TSS (FBgn0027621)	promoter-TSS (NM_167656)	-317	FBgn0265428|FBtr0339739
chr2L	357349	357849	11,55	11,9	0,35	0,00223	0,0181	TTS (FBgn0266907)	TTS (NR_124001)	271	FBgn0266906|FBtr0345775
chr3R	10415624	10416124	11,78	12,13	0,35	0,00249	0,0197	exon (FBgn0037816, exon 1 of 1)	exon (NM_141745, exon 1 of 1)	172	FBgn0037816|FBtr0082258
chr3L	16590369	16590869	11,54	11,9	0,35	0,00253	0,0199	TTS (FBgn0072283)	TTS (NM_140649)	431	FBgn0031741|FBtr0075364
chr3R	16483669	16484169	11,84	12,19	0,35	0,00265	0,0206	TTS (FBgn0038439)	TTS (NM_142297)	304	FBgn0038438|FBtr0083307
chr2L	6566753	6566253	11,62	11,97	0,35	0,00282	0,0216	exon (FBgn0031834, exon 1 of 1)	exon (NM_135206, exon 1 of 1)	178	FBgn0031834|FBtr0341161
chr3L	7370380	7370880	10,97	11,33	0,35	0,00321	0,024	promoter-TSS (FBgn0082598)	promoter-TSS (NM_001274582)	-169	FBgn0082598|FBtr0332730
chr3L	11710826	11711326	11,8	12,14	0,35	0,00355	0,0258	TTS (FBgn0261953)	TTS (NM_206340)	310	FBgn0036198|FBtr0076123
chr3R	23927238	23927738	11,57	11,92	0,35	0,00439	0,0299	TTS (FBgn0264740)	TTS (NM_001043284)	146	FBgn0039126|FBtr0084522
chr2R	8913345	8913845	11,92	12,26	0,35	0,00457	0,0307	promoter-TSS (FBgn0002552)	promoter-TSS (NM_080076)	291	FBgn0003074|FBtr0088681
chr3R	8664294	8664794	11,67	12,02	0,35	0,00474	0,0314	promoter-TSS (FBgn0266679)	promoter-TSS (NM_141553)	220	FBgn0037606|FBtr0081880
chr3L	8998256	8998756	12,01	12,35	0,35	0,00548	0,0346	promoter-TSS (FBgn0036070)	promoter-TSS (NM_168309)	323	FBgn0035953|FBtr0076520
chr3L	19579984	19580484	11,5	11,85	0,35	0,00558	0,0352	TTS (FBgn0032812)	TTS (NM_001273664)	117	FBgn0032811|FBtr0081266
chr3L	22773591	22774091	11,55	11,89	0,35	0,00604	0,0374	promoter-TSS (FBgn0052451)	promoter-TSS (NM_001170025)	-195	FBgn0052451|FBtr0302134
chr2R	14239034	14239534	12,08	12,43	0,35	0,00657	0,0399	promoter-TSS (FBgn0033916)	promoter-TSS (NM_137099)	136	FBgn0033915|FBtr0082571
chr2R	17740000	17740500	11,93	12,28	0,35	0,00659	0,0399	promoter-TSS (FBgn0034270)	promoter-TSS (NM_137413)	350	FBgn0034271|FBtr0086864
chr3R	25097818	25098318	12,02	12,37	0,35	0,00669	0,0404	exon (FBgn0053095, exon 1 of 5)	exon (NM_001170248, exon 1 of 4)	197	FBgn0053096|FBtr0114464
chr3R	24584579	24585079	11,85	12,2	0,35	0,00891	0,05	promoter-TSS (FBgn0263491)	promoter-TSS (NM_001043289)	321	FBgn0039210|FBtr0086671
chr2R	16014947	16015447	11,51	11,87	0,36	0,00691	0,00759	promoter-TSS (FBgn0015901)	promoter-TSS (NM_143774)	293	FBgn0034065|FBtr0082206
chr3R	31669361	31669861	11,35	11,71	0,36	0,00819	0,00852	exon (FBgn0039863, exon 1 of 9)	5' UTR (NM_170563, exon 1 of 10)	147	FBgn0039863|FBtr0085823
chr3R	16186296	16186796	11,54	11,9	0,36	0,00824	0,00855	promoter-TSS (FBgn0086370)	promoter-TSS (NM_079654)	351	FBgn0024491|FBtr0083279
chr2R	21009036	21009536	11,64	12,01	0,36	0,00952	0,00944	TTS (FBgn0001133)	TTS (NM_176742)	290	FBgn0050291|FBtr0071549
chr2L	10858598	10859098	11,77	12,13	0,36	0,00119	0,0111	promoter-TSS (FBgn0024227)	promoter-TSS (NM_057888)	313	FBgn0027363|FBtr0080143
chr2R	20641046	20641546	11,73	12,09	0,36	0,00142	0,0127	promoter-TSS (FBgn0250801)	promoter-TSS (NM_137657)	321	FBgn0034534|FBtr0086230
chr3L	11061482	11061982	11,72	12,08	0,36	0,00147	0,013	promoter-TSS (FBgn0036137)	promoter-TSS (NM_140169)	162	FBgn0036118|FBtr0076202
chr3R	23061533	23062033	11,31	11,67	0,36	0,00191	0,016	promoter-TSS (FBgn0053131)	promoter-TSS (NM_176544)	291	FBgn0027526|FBtr0084347
chr2L	2574330	2574830	11,1	11,46	0,36	0,00211	0,0173	TTS (FBgn0031434)	TTS (NM_134846)	472	FBgn0026778|FBtr0077747
chr2L	3619194	3619694	11,03	11,39	0,36	0,00216	0,0177	exon (FBgn0015663, exon 1 of 3)	exon (NM_079947, exon 1 of 3)	167	FBgn0015663|FBtr0077532
chr2L	4462518	4463018	11,37	11,73	0,36	0,00232	0,0187	promoter-TSS (FBgn0031630)	promoter-TSS (NM_134996)	226	FBgn0031609|FBtr0077450

chr3R	24130383	24130883	11,83	12,19	0,36	0,00235	0,0188	promoter-TSS (FBgn0039153)	promoter-TSS (NM_142960)	327	FBgn0026317|FBtr0084546
chr2R	22174874	22175374	11,65	12,01	0,36	0,00247	0,0196	promoter-TSS (FBgn0034703)	promoter-TSS (NM_137802)	203	FBgn0034704|FBtr0071767
chr2R	24940004	24940504	10,91	11,27	0,36	0,0026	0,0203	TTS (FBgn0022343)	TTS (NM_001038885)	126	FBgn0035082|FBtr0345515
chr3L	18745922	18746422	11,72	12,08	0,36	0,00325	0,0242	TTS (FBgn0036810)	TTS (NM_140799)	317	FBgn0036811|FBtr0075054
chrX	529325	529825	11,89	12,26	0,36	0,00357	0,0259	promoter-TSS (FBgn0000108)	promoter-TSS (NM_057278)	274	FBgn0024983|FBtr0070089
chr3R	10042537	10043037	10,91	11,27	0,36	0,00416	0,0288	promoter-TSS (FBgn0053208)	promoter-TSS (NM_176450)	34	FBgn0053208|FBtr0082206
chr2R	13152101	13152601	11,66	12,02	0,36	0,00466	0,0311	TTS (FBgn0020370)	TTS (NM_165966)	326	FBgn0263998|FBtr0330329
chrX	13094411	13094911	11,84	12,2	0,36	0,00483	0,0318	TTS (FBgn0261524)	TTS (NM_057814)	194	FBgn0030447|FBtr0073721
chr3L	19589927	19590427	11,86	12,22	0,36	0,00647	0,0395	TTS (FBgn0005386)	TTS (NM_079436)	347	FBgn0036889|FBtr0074971
chr3R	10049257	10049757	11,88	12,24	0,36	0,00673	0,0407	promoter-TSS (FBgn0037779)	promoter-TSS (NM_141715)	309	FBgn0037780|FBtr0082174
chr2L	4876585	4977085	11,75	12,11	0,36	0,00695	0,0416	promoter-TSS (FBgn0031662)	promoter-TSS (NM_135045)	188	FBgn0031661|FBtr0079049
chr2R	15570964	15571464	11,54	11,91	0,36	0,00734	0,0434	promoter-TSS (FBgn0050466)	promoter-TSS (NM_166103)	203	FBgn0033762|FBtr0087350
chr2R	12692259	12692759	11,79	12,15	0,36	0,00812	0,0469	exon (FBgn0033769, exon 2 of 4)	exon (NM_136969, exon 2 of 4)	181	FBgn0033769|FBtr0087871
chr2L	11282009	11282509	11,01	11,38	0,36	0,0082	0,0473	TTS (FBgn0032358)	TTS (NM_135656)	170	FBgn0020270|FBtr0080213
chr3R	11407832	11408332	11,78	12,14	0,36	0,00828	0,0475	TTS (FBgn0264604)	TTS (NM_141810)	165	FBgn0037892|FBtr0082384
chr2R	19452653	19453153	12,14	12,5	0,36	0,00847	0,0482	exon (FBgn0034447, exon 2 of 4)	exon (NM_137578, exon 2 of 4)	400	FBgn0034447|FBtr0086535
chr3R	16452764	16453264	10,87	11,23	0,36	0,00884	0,0497	exon (FBgn0044826, exon 1 of 2)	5' UTR (NM_169719, exon 1 of 2)	807	FBgn0044826|FBtr0305003
chr2R	7698321	7698821	11,25	11,62	0,37	0,000457	0,00556	promoter-TSS (FBgn0050493)	promoter-TSS (NM_165551)	331	FBgn0033212|FBtr0332911
chr3R	31985153	31985653	11,26	11,64	0,37	0,000489	0,00586	exon (FBgn0011224, exon 1 of 14)	5' UTR (NM_001104524, exon 1 of 14)	365	FBgn0011224|FBtr0112866
chr2L	19533466	19533966	11,17	11,54	0,37	0,000598	0,00683	TTS (FBgn0032800)	TTS (NM_136137)	238	FBgn0053116|FBtr0081249
chr3R	8561149	8561649	11,33	11,7	0,37	0,000866	0,00891	TTS (FBgn0051450)	TTS (NM_169226)	365	FBgn0051453|FBtr0339330
chr3L	1303001	1303501	11,75	12,12	0,37	0,00095	0,00944	promoter-TSS (FBgn0010333)	promoter-TSS (NM_057602)	308	FBgn0035203|FBtr0072667
chr2L	16300406	16300906	11,37	11,75	0,37	0,000969	0,00958	promoter-TSS (FBgn0028375)	promoter-TSS (NM_078857)	443	FBgn0028895|FBtr0080829
chr2L	14362258	14362758	11,71	12,08	0,37	0,0014	0,0125	exon (FBgn0015546, exon 3 of 6)	exon (NM_001014482, exon 3 of 7)	440	FBgn0015546|FBtr0080630
chr2L	19759085	19759585	11,39	11,77	0,37	0,00206	0,017	promoter-TSS (FBgn0032818)	promoter-TSS (NM_136155)	457	FBgn0032819|FBtr0081290
chr2R	16170176	16170676	11,74	12,1	0,37	0,00235	0,0188	TTS (FBgn0034083)	TTS (NM_137249)	435	FBgn0034084|FBtr0087249
chr2R	6749577	6750077	11,75	12,12	0,37	0,00286	0,0218	TTS (FBgn0042083)	TTS (NM_144467)	312	FBgn0027066|FBtr0086129
chr3R	15361138	15361638	11,88	12,26	0,37	0,00376	0,0268	promoter-TSS (FBgn0038327)	promoter-TSS (NM_169650)	269	FBgn0026634|FBtr0083114
chr3L	5138981	5139481	11,52	11,89	0,37	0,00393	0,0277	promoter-TSS (FBgn0035589)	promoter-TSS (NM_139690)	164	FBgn0035590|FBtr0077180
chr3R	15274489	15274989	11,93	12,3	0,37	0,00421	0,029	promoter-TSS (FBgn0038313)	promoter-TSS (NM_169632)	51	FBgn0000283|FBtr0083127
chr2L	11807766	11808266	10,97	11,34	0,37	0,00428	0,0294	exon (FBgn0020309, exon 1 of 8)	5' UTR (NM_057897, exon 1 of 7)	956	FBgn0020309|FBtr0080262
chr2R	11223032	11223532	10,76	11,13	0,37	0,00481	0,0317	promoter-TSS (FBgn0033584)	promoter-TSS (NM_001299379)	-162	FBgn0033584|FBtr0339479
chrX	12611093	12611593	11,93	12,31	0,37	0,00488	0,032	promoter-TSS (FBgn0030407)	promoter-TSS (NM_132586)	265	FBgn0030406|FBtr0073657
chr3L	14786895	14787395	12,05	12,42	0,37	0,00498	0,0324	promoter-TSS (FBgn0036449)	promoter-TSS (NM_001169974)	355	FBgn0036450|FBtr0075691
chrX	1236282	1236782	11,31	11,67	0,37	0,00532	0,0339	TTS (FBgn0026876)	TTS (NM_130542)	152	FBgn0261444|FBtr0336978
chr2R	18421492	18421992	11,54	11,91	0,37	0,00682	0,0411	TTS (FBgn0027835)	TTS (NM_206164)	330	FBgn0034345|FBtr0301148
chrX	11869091	11869591	11,57	11,94	0,37	0,00693	0,0416	promoter-TSS (FBgn0030344)	promoter-TSS (NM_132529)	172	FBgn0030345|FBtr0073567
chr3L	3470696	3471196	11,27	11,64	0,37	0,00707	0,0422	TTS (FBgn0052267)	TTS (NM_168032)	363	FBgn0035449|FBtr0073143
chr3R	4387694	4388194	11,81	12,18	0,37	0,00747	0,044	TTS (FBgn0037240)	TTS (NM_141204)	203	FBgn0003882|FBtr0302338
chr2L	13782925	13783425	11,68	12,05	0,37	0,0078	0,0454	promoter-TSS (FBgn0028539)	promoter-TSS (NM_001042895)	285	FBgn0028932|FBtr0329825
chr3R	28812222	28812722	12,18	12,56	0,37	0,00842	0,048	promoter-TSS (FBgn0065070)	promoter-TSS (NR_002503)	-95	FBgn0065070|FBtr0091615
chr3R	7082279	7082779	11,29	11,66	0,37	0,00847	0,0482	TTS (FBgn0037470)	TTS (NM_169169)	348	FBgn0037469|FBtr0081638
chr2L	4459087	4459587	11,84	12,22	0,37	0,0085	0,0483	promoter-TSS (FBgn0031608)	promoter-TSS (NM_001201760)	265	FBgn0053002|FBtr0335135
chr3L	7356086	7356586	12,22	12,59	0,37	0,00881	0,0496	TTS (FBgn0035770)	TTS (NM_168209)	336	FBgn0267472|FBtr0346843
chr2R	17786200	17786700	11,68	12,06	0,38	0,000676	0,0075	exon (FBgn0026309, exon 2 of 3)	exon (NM_058065, exon 2 of 3)	316	FBgn0026309|FBtr0089549
chr2L	9575985	9576485	11,56	11,94	0,38	0,00109	0,0104	exon (FBgn0028479, exon 2 of 5)	5' UTR (NM_164860, exon 2 of 5)	534	FBgn0028479|FBtr0079857
chr3R	7073857	7074357	11,67	12,05	0,38	0,00151	0,0133	promoter-TSS (FBgn0037468)	promoter-TSS (NM_141434)	345	FBgn0037467|FBtr0081643
chr3L	16229251	16229751	10,92	11,3	0,38	0,00159	0,0138	promoter-TSS (FBgn0263605)	promoter-TSS (NM_140589)	402	FBgn0036579|FBtr0075457
chr3R	11620031	11620531	11,48	11,86	0,38	0,00188	0,0158	promoter-TSS (FBgn0051363)	promoter-TSS (NM_169406)	192	FBgn0037920|FBtr0299566
chr3L	19063069	19063569	10,8	11,18	0,38	0,00191	0,016	promoter-TSS (FBgn0036842)	promoter-TSS (NM_140828)	155	FBgn0036843|FBtr0075025
chr2R	15311626	15312126	11,46	11,83	0,38	0,00192	0,0161	promoter-TSS (FBgn0034008)	promoter-TSS (NM_137184)	367	FBgn0004608|FBtr0308700
chr3R	22462477	22462977	11,63	12,01	0,38	0,00195	0,0163	promoter-TSS (FBgn0028688)	promoter-TSS (NM_142791)	273	FBgn0263351|FBtr0084252
chr3L	13513559	13513059	11,64	12,03	0,38	0,00212	0,0173	promoter-TSS (FBgn0036376)	promoter-TSS (NM_168556)	303	FBgn0086785|FBtr0075818
chr3R	20550347	20550847	10,8	11,18	0,38	0,00211	0,0173	intron (FBgn0036917, intron 1 of 8)	intron (NM_001275830, intron 1 of 9)	510	FBgn0036917|FBtr0089484
chrX	8411211	8411711	10,89	11,28	0,38	0,0025	0,0197	exon (FBgn0262976, exon 1 of 4)	5' UTR (NM_001258650, exon 1 of 4)	197	FBgn0262976|FBtr0307286
chr3L	7976525	7977025	11,77	12,15	0,38	0,00256	0,0201	promoter-TSS (FBgn0035829)	promoter-TSS (NM_168247)	370	FBgn0035830|FBtr0076753
chr3L	19979228	19979728	11,84	12,22	0,38	0,00273	0,0211	exon (FBgn0036922, exon 2 of 2)	exon (NM_140906, exon 2 of 2)	334	FBgn0036922|FBtr0346534
chr3L	9887996	9888496	11,85	12,23	0,38	0,00324	0,0241	promoter-TSS (FBgn0025866)	promoter-TSS (NM_079292)	437	FBgn0011836|FBtr0076361
chr2R	24534711	24535211	11,37	11,74	0,38	0,00328	0,0244	exon (FBgn0035021, exon 2 of 4)	exon (NM_001038882, exon 4 of 6)	466	FBgn0035021|FBtr0072344
chr3R	9260852	9261352	12,11	12,49	0,38	0,00374	0,0266	TTS (FBgn0037670)	TTS (NM_141618)	465	FBgn0037671|FBtr0081978
chr3L	9457963	9458463	11,27	11,65	0,38	0,00424	0,0291	promoter-TSS (FBgn0035998)	promoter-TSS (NM_140061)	302	FBgn0035999|FBtr0076463
chr2R	21282667	21283167	10,72	11,1	0,38	0,00455	0,0307	promoter-TSS (FBgn0034611)	promoter-TSS (NM_001299742)	80	FBgn0034611|FBtr0342884
chr3L	22879287	22879787	11,93	12,31	0,38	0,0047	0,0312	promoter-TSS (FBgn0044324)	promoter-TSS (NM_168976)	292	FBgn0037202|FBtr0332051
chr3R	10143547	10144047	11,68	12,07	0,38	0,0047	0,0312	promoter-TSS (FBgn0086359)	promoter-TSS (NM_143815)	387	FBgn0032792|FBtr0333825
chr3L	1248092	1248592	12,12	12,5	0,38	0,0052	0,0333	promoter-TSS (FBgn0035194)	promoter-TSS (NM_138242)	323	FBgn0283500|FBtr0072652
chr3R	6405438	6405938	11,34	11,72	0,38	0,00601	0,0373	exon (FBgn0037443, exon 1 of 11)	5' UTR (NM_001170060, exon 1 of 11)	207	FBgn0037443|FBtr0289939
chr2R	20977097	20977597	11,21	11,6	0,38	0,00724	0,0429	TTS (FBgn0034565)	TTS (NM_001043099)	292	FBgn0034564|FBtr0071520
chr3R	14511927	14512427	11,42	11,8	0,38	0,00801	0,0464	promoter-TSS (FBgn0038233)	promoter-TSS (NM_142109)	340	FBgn0038234|FBtr0082953
chrX	23082875	23083375	12,14	12,52	0,38	0,00887	0,0499	promoter-TSS (FBgn0039942)	promoter-TSS (NM_001015255)	388	FBgn0039943|FBtr0113730
chrX	10010581	10011081	11,48	11,86	0,39	0,000238	0,00341	TTS (FBgn0053557)	TTS (NM_001014730)	351	FBgn0030170|FBtr0071415
chrX	12902720	12903220	11,21	11,6	0,39	0,000276	0,0038	TTS (FBgn0030432)	TTS (NM_132610)	192	FBgn0030431|FBtr0073696
chr3R	31743482	31743982	11,5	11,89	0,39	0,000564	0,0065	promoter-TSS (FBgn0039870)	promoter-TSS (NM_143629)	243	FBgn0039869|FBtr0085836
chrX	10365208	10365708	11,29	11,68	0,39	0,000564	0,0065	TTS (FBgn0052679)	TTS (NM_167225)	815	FBgn0028331|FBtr0347009
chr2L	106338	106838	11,45	11,84	0,39	0,000576	0,00662	promoter-TSS (FBgn0005278)	promoter-TSS (NM_205880)	144	FBgn0026787|FBtr0301452
chr3L	2553399	2553899	10,99	11,38	0,39	0,000666	0,00744	intron (FBgn0010905, intron 1 of 15)	intron (NM_001259641, intron 1 of 15)	643	FBgn0010905|FBtr0304614
chr3L	11164870	11165370	11,37	11,76	0,39	0,00071	0,00775	promoter-TSS (FBgn0264721)	promoter-TSS (NR_073923)	150	FBgn0052076|FBtr0076217
chr2R	23809307	23809807	11,72	12,11	0,39	0,000736	0,00795	promoter-TSS (FBgn0010278)	promoter-TSS (NM_079106)	322	FBgn0034908|FBtr0072124
chr2R	6971034	6971534	11,35	11,74	0,39	0,00074	0,00797	TTS (FBgn0033121)	TTS (NM_136408)	353	FBgn0053558|FBtr0332942
chr2L	19444310	19444810	11,8	12,2	0,39	0,000806	0,00843	promoter-TSS (FBgn0003346)	promoter-TSS (NM_001273649)	190	FBgn0024230|FBtr0081288
chr3L	17908182	17908682	11,63	12,02	0,39	0,000811	0,00847	promoter-TSS (FBgn0036770)	promoter-TSS (NM_140767)	290	FBgn0036771|FBtr0075144
chr2R	18133806	18134306	11,6	11,99	0,39	0,000834	0,00864	exon (FBgn0001222, exon 2 of 8)	exon (NM_001043092, exon 2 of 7)	578	FBgn0001222|FBtr0086782
chrX	2443372	2443872	11,56	11,95	0,39	0,00101	0,00988	TTS (FBgn0040388)	TTS (NM_001103398)	354	FBgn0003714|FBtr0070459
chr3R	8562850	8563350	11,56	11,95	0,39	0,00127	0,0117	promoter-TSS (FBgn0051450)	promoter-TSS (NM_169226)	265	FBgn0051460|FBtr0081873
chr3R	26052847	26053347	11,84	12,23	0,39	0,00137	0,0124	promoter-TSS (FBgn0266668)	promoter-TSS (NM_206576)	277	FBgn0039402|FBtr0084967
chr2L	13366526	13367026	11,82	12,21	0,39	0,00141	0,0126	promoter-TSS (FBgn0051852)	promoter-TSS (NM_165039)	330	FBgn0032509|FBtr0080465
chr2L	12722234	12722734	11,85	12,24	0,39	0,0023	0,0185	promoter-TSS (FBgn0032455)	promoter-TSS (NM_165019)	208	FBgn0032456|FBtr0090014
chr2L	2874063	2874563	11,43	11,82	0,39	0,00234	0,0188	promoter-TSS (FBgn0031478)	promoter-TSS (NM_134885)	176	FBgn0051694|FBtr0077685
chr2L	413987	414487	11,24	11,63	0,39	0,00243	0,0193	promoter-TSS (FBgn0263933)	promoter-TSS (NM_057981)	540	FBgn0264855|FBtr0089488
chr3L	4103634	4104134	11,62	12,01	0,39	0,00304	0,023	promoter-TSS (FBgn0035497)	promoter-TSS (NM_001163872)	321	FBgn0035498|FBtr0073209
chr3L	3303599	3304099	10,9	11,29	0,39	0,00331	0,0245	promoter-TSS (FBgn0035431)	promoter-TSS (NM_139543)	142	FBgn0035432|FBtr0073054
chr3R	20948891	20949391	10,76	11,15	0,39	0,0037	0,0265	intron (FBgn0002921, intron 1 of 9)	intron (NM_169936, intron 1 of 9)	362	FBgn0002921|FBtr0089510
chr2L	16827335	16827835	11,44	11,84	0,39	0,00376	0,0268	TTS (FBgn0004797)	TTS (NM_206002)	227	FBgn0051739|FBtr0331623
chrX	1669508	1670008	11,62	12,01	0,39	0,00388	0,0275	promoter-TSS (FBgn0023530)	promoter-TSS (NM_130576)	189	FBgn0001189|FBtr0070270
chr3L	17849754	17850254	11,66	12,06	0,39	0,004	0,0281	TTS (FBgn0036762)	TTS (NM_140760)	278	FBgn0036763|FBtr0331811
chr3R	16349458	16349958	11,52	11,91	0,39	0,00504	0,0327	promoter-TSS (FBgn0038419)	promoter-TSS (NM_169714)	305	FBgn0027095|FBtr0083283
chr2R	9839568	9840068	10,82	11,21	0,39	0,00582	0,0363	promoter-TSS (FBgn0033451)	promoter-TSS (NM_136679)	43	FBgn0033451|FBtr0088478
chr3R	9791393	9791893	11,52	11,9	0,39	0,00626	0,0384	promoter-TSS (FBgn0037755)	promoter-TSS (NM_001104262)	161	FBgn0037756|FBtr0082140
chr2L	19063466	19063966	11,87	12,26	0,39	0,00631	0,0386	TTS (FBgn0032749)	TTS (NM_001273629)	422	FBgn0032750|FBtr0081150
chr3L	9624329	9624829	11,46	11,85	0,39	0,00656	0,0398	TTS (FBgn0267348)	TTS (NM_079282)	343	FBgn0036018|FBtr0076383
chr3R	26875129	26875629	11,96	12,35	0,39	0,00761	0,0446	promoter-TSS (FBgn0002838)	promoter-TSS (NM_143253)	363	FBgn0004903|FBtr0085093
chrX	19847269	19847769	10,49	10,87	0,39	0,0083	0,0476	intron (FBgn0261811, intron 1 of 3)	CpG	959	FBgn0261811|FBtr0074805
chr3L	20521027	20521527	11,32	11,72	0,4	0,000279	0,00384	promoter-TSS (FBgn0037008)	promoter-TSS (NM_140983)	269	FBgn0037009|FBtr0078209
chr3L	7654002	7654502	11,46	11,86	0,4	0,000324	0,00428	intron (FBgn0035807, intron 1 of 2)	intron (NM_139889, intron 1 of 2)	500	FBgn0035807|FBtr0076821
chr3L	6755854	6756354	11,73	12,13	0,4	0,000419	0,00522	TTS (FBgn0052392)	TTS (NM_168180)	393	FBgn0035715|FBtr0076949
chr3R	12009876	12010376	11,6	12	0,4	0,000536	0,00626	promoter-TSS (FBgn0037979)	promoter-TSS (NM_001104285)	308	FBgn0037978|FBtr0335434
chrX	11572041	11572541	11,05	11,44	0,4	0,000555	0,00643	promoter-TSS (FBgn0030313)	promoter-TSS (NM_001272523)	151	FBgn0027259|FBtr0073541
chr2R	16010867	16011367	11,64	12,03	0,4	0,00069	0,00759	promoter-TSS (FBgn0034063)	promoter-TSS (NM_166132)	321	FBgn0034062|FBtr0087263
chr2R	22074747	22075247	11,3	11,69	0,4	0,000698	0,00765	promoter-TSS (FBgn0067102)	promoter-TSS (NM_137792)	311	FBgn0034689|FBtr0071800
chr2L	19032935	19033435	11,5	11,91	0,4	0,000705	0,00772	TTS (FBgn0051800)	TTS (NM_165272)	313	FBgn0001202|FBtr0081180
chrX	13336074	13336574	11,34	11,74	0,4	0,000732	0,00792	exon (FBgn0010198, exon 3 of 3)	exon (NM_001169267, exon 3 of 3)	1314	FBgn0010198|FBtr0073794
chr2L	11107069	11107569	11,39	11,79	0,4	0,000768	0,00816	promoter-TSS (FBgn0032341)	promoter-TSS (NM_135643)	377	FBgn0261983|FBtr0080197
chr3R	30177070	30177570	11,02	11,42	0,4	0,00077	0,00816	promoter-TSS (FBgn0039752)	promoter-TSS (NM_170475)	380	FBgn0039751|FBtr0339185
chr2R	15511978	15512478	11,52	11,92	0,4	0,00087	0,00893	exon (FBgn0034025, exon 2 of 4)	exon (NM_166099, exon 1 of 3)	417	FBgn0034025|FBtr0087332
chr2R	17761066	17761566	10,81	11,22	0,4	0,00101	0,00986	TTS (FBgn0022740)	TTS (NM_057954)	377	FBgn0027572|FBtr0089548
chr3L	22872435	22872935	11,79	12,19	0,4	0,00118	0,011	promoter-TSS (FBgn0010348)	promoter-TSS (NM_001104198)	428	FBgn0032200|FBtr0078553
chr3L	7641161	7641661	11,83	12,23	0,4	0,0012	0,0112	promoter-TSS (FBgn0053276)	promoter-TSS (NM_206296)	237	FBgn0035805|FBtr0076822
chr3R	23157396	23157896	11,37	11,77	0,4	0,00135	0,0123	TTS (FBgn0039058)	TTS (NM_142871)	216	FBgn0004395|FBtr0337052
chr3R	22689719	22690219	11,56	11,96	0,4	0,00137	0,0124	promoter-TSS (FBgn0039004)	promoter-TSS (NM_142823)	411	FBgn0039003|FBtr0084334
chr2L	10361996	10362496	11,6	12	0,4	0,00195	0,0163	promoter-TSS (FBgn0003087)	promoter-TSS (NM_001273405)	461	FBgn0027568|FBtr0332198
chrX	18136378	18136878	11,5	11,89	0,4	0,00205	0,0169	exon (FBgn0017418, exon 2 of 8)	exon (NM_001272743, exon 2 of 8)	511	FBgn0017418|FBtr0089507
chr3L	6495568	6496068	10,88	11,29	0,4	0,00302	0,0228	promoter-TSS (FBgn0035704)	promoter-TSS (NM_139791)	139	FBgn0020251|FBtr0076968
chr3L	21335294	21335794	12,16	12,56	0,4	0,00338	0,0249	TTS (FBgn0086913)	TTS (NM_001300213)	330	FBgn0037073|FBtr0078342
chrX	15889202	15889702	10,86	11,26	0,4	0,00341	0,0251	exon (FBgn0031703, exon 2 of 4)	exon (NM_001169294, exon 3 of 5)	657	FBgn0030703|FBtr0074166
chr2L	13393232	13393732	10,96	11,36	0,4	0,0036	0,0259	TTS (FBgn0032518)	TTS (NM_135805)	1610	FBgn0032518|FBtr0342637
chr3L	18681800	18681800	11,73	12,13	0,4	0,00359	0,0259	promoter-TSS (FBgn0052202)	promoter-TSS (NM_168774)	286	FBgn0036804|FBtr0113179
chr3L	14785737	14786237	10,89	11,29	0,4	0,00401	0,0281	promoter-TSS (FBgn0036450)	promoter-TSS (NM_140467)	425	FBgn0036449|FBtr0075699
chr3L	12471799	12472299	11,61	12,01	0,4	0,00422	0,0291	exon (FBgn0036286, exon 2 of 5)	exon (NM_140319, exon 2 of 5)	322	FBgn0036286|FBtr0075956
chr3L	4135373	4135873	12,04	12,44	0,4	0,0049	0,0321	TTS (FBgn0004574)	TTS (NM_001274475)	415	FBgn0260985|FBtr0073264
chr2R	24560647	24561147	11,38	11,78	0,4	0,00506	0,0328	promoter-TSS (FBgn0035024)	promoter-TSS (NM_138088)	156	FBgn0036687|FBtr0273253
chr2R	22212976	22213476	11,56	11,96	0,4	0,00605	0,0374	TTS (FBgn0034713)	TTS (NM_137812)	392	FBgn0025186|FBtr0071774
chr2R	13482527	13483027	11,88	12,28	0,4	0,00646	0,0394	TTS (FBgn0033842)	TTS (NM_137032)	452	FBgn0000119|FBtr0087702

chr2R	12430527	12431027	11,93	12,34	0,4	0,00649	0,0395	TTS (FBgn0033738)	TTS (NM_165900)	183	FBgn0262840	FBtr0306082
chr3R	25262806	25263306	11,46	11,87	0,41	0,00012	0,00194	promoter-TSS (FBgn0039304)	promoter-TSS (NM_143106)	316	FBgn0039305	FBtr0084815
chrX	20429002	20429502	11,67	12,08	0,41	0,00023	0,00333	promoter-TSS (FBgn0002641)	promoter-TSS (NM_078699)	421	FBgn0031115	FBtr0309682
chr3L	2651246	2651746	11,59	12,01	0,41	0,000256	0,00359	promoter-TSS (FBgn0259199)	promoter-TSS (NM_001144405)	354	FBgn0027082	FBtr0072948
chr3L	15576795	15577295	11,6	12,01	0,41	0,000274	0,00378	TTS (FBgn0267390)	TTS (NM_140521)	476	FBgn0036512	FBtr0075563
chrX	11493454	11493954	10,82	11,23	0,41	0,000533	0,00624	promoter-TSS (FBgn0265749)	promoter-TSS (NM_206685)	-114	FBgn0052666	FBtr0310295
chr2R	9122293	9122793	10,95	11,36	0,41	0,000739	0,00797	TTS (FBgn0027561)	TTS (NM_145873)	220	FBgn0033381	FBtr0085579
chr3L	9364380	9364880	11,82	12,23	0,41	0,0011	0,0105	exon (FBgn0035980, exon 1 of 1)	exon (NM_140045, exon 1 of 1)	281	FBgn0035980	FBtr0076444
chrX	7902201	7902701	11,82	12,23	0,41	0,00117	0,0109	exon (FBgn0010292, exon 3 of 5)	exon (NM_078519, exon 3 of 5)	572	FBgn0010292	FBtr0071090
chr3R	31616386	31616886	11,56	11,97	0,41	0,00131	0,012	promoter-TSS (FBgn0039859)	promoter-TSS (NM_143620)	334	FBgn0039860	FBtr0085819
chr3L	3035517	3036017	10,9	11,31	0,41	0,00135	0,0123	intron (FBgn0035388, intron 1 of 9)	(ACA)n|Simple_repeat|Simple_repeat	572	FBgn0035388	FBtr0072981
chr2L	5096469	5096969	11,46	11,87	0,41	0,00142	0,0126	TTS (FBgn0031682)	TTS (NM_001273156)	349	FBgn0031683	FBtr0309382
chr3L	19099712	19100212	11,66	12,07	0,41	0,00153	0,0135	TTS (FBgn0036849)	TTS (NM_140834)	393	FBgn0036850	FBtr0075032
chr3R	19876884	19877384	11,83	12,24	0,41	0,00164	0,0142	promoter-TSS (FBgn0038742)	promoter-TSS (NM_142583)	380	FBgn0038741	FBtr0083858
chrX	16886915	16887415	11,53	11,94	0,41	0,0018	0,0153	promoter-TSS (FBgn0030802)	promoter-TSS (NM_001272701)	348	FBgn0030803	FBtr0310519
chrX	5673862	5674362	10,66	11,07	0,41	0,00223	0,0181	TTS (FBgn0029785)	TTS (NM_167043)	1379	FBgn0029785	FBtr0070801
chr2L	18695772	18696272	11,61	12,02	0,41	0,00255	0,02	promoter-TSS (FBgn0032699)	promoter-TSS (NM_136052)	292	FBgn0032700	FBtr0081096
chr2R	12652964	12653464	11,93	12,35	0,41	0,00259	0,0202	promoter-TSS (FBgn0033761)	promoter-TSS (NM_136961)	410	FBgn0033762	FBtr0087844
chr2L	21102780	21103280	11,85	12,26	0,41	0,00319	0,0239	promoter-TSS (FBgn0284251)	promoter-TSS (NM_136242)	288	FBgn0032916	FBtr0081465
chr3L	8522871	8523371	11,36	11,77	0,41	0,0032	0,0239	TTS (FBgn0035907)	TTS (NM_139980)	380	FBgn0035906	FBtr0076654
chr3R	22380199	22380699	11,7	12,11	0,41	0,00346	0,0253	promoter-TSS (FBgn0263047)	promoter-TSS (NM_001260309)	322	FBgn0053985	FBtr0113489
chr2R	18095234	18095734	11,6	12,02	0,41	0,00367	0,0263	promoter-TSS (FBgn0034300)	promoter-TSS (NM_001103893)	80	FBgn0034300	FBtr0113092
chr2L	4971737	4972237	12,1	12,51	0,41	0,00377	0,0268	promoter-TSS (FBgn0010607)	promoter-TSS (NM_164605)	286	FBgn0031659	FBtr0078995
chr3R	13263526	13264026	11,89	12,3	0,41	0,00396	0,0279	promoter-TSS (FBgn0003595)	promoter-TSS (NM_001170130)	286	FBgn0038128	FBtr0082779
chr3R	24048389	24048889	11,48	11,89	0,41	0,00403	0,0282	promoter-TSS (FBgn0005649)	promoter-TSS (NM_170119)	342	FBgn0043455	FBtr0321261
chr3L	13043266	13043766	11,83	12,24	0,41	0,00436	0,0298	promoter-TSS (FBgn0036341)	promoter-TSS (NM_079330)	146	FBgn0086601	FBtr0091754
chr3L	20392892	20393392	11,17	11,57	0,41	0,00489	0,032	exon (FBgn0053969, exon 2 of 3)	exon (NM_001038946, exon 2 of 3)	411	FBgn0053969	FBtr0100010
chr3R	13964881	13965381	11,81	12,22	0,41	0,00489	0,032	promoter-TSS (FBgn0038191)	promoter-TSS (NM_142067)	247	FBgn0015270	FBtr0052866
chr2L	6062897	6063397	11,45	11,86	0,41	0,00555	0,035	promoter-TSS (FBgn0031771)	promoter-TSS (NM_135143)	159	FBgn0031772	FBtr0343122
chr3L	15144281	15144781	11,78	12,19	0,41	0,00563	0,0354	promoter-TSS (FBgn0047178)	promoter-TSS (NM_168616)	177	FBgn0036484	FBtr0075640
chr3L	21030861	21031361	10,86	11,26	0,41	0,00688	0,0413	promoter-TSS (FBgn0028402)	promoter-TSS (NM_001170015)	249	FBgn0037045	FBtr0078327
chr2R	9292558	9293058	10,45	10,86	0,41	0,00739	0,0436	promoter-TSS (FBgn0028408)	promoter-TSS (NM_001273891)	-800	FBgn0028408	FBtr0332998
chr3L	19913085	19913585	11,91	12,33	0,41	0,00767	0,0448	TTS (FBgn0036915)	TTS (NM_168825)	320	FBgn0036916	FBtr0074918
chr3L	5358883	5359383	11,9	12,31	0,41	0,00859	0,0487	exon (FBgn0004380, exon 1 of 1)	exon (NM_079210, exon 1 of 1)	259	FBgn0004380	FBtr0077157
chr2R	16149239	16149739	11,8	12,21	0,41	0,00888	0,0499	promoter-TSS (FBgn0029175)	promoter-TSS (NM_166150)	150	FBgn0034081	FBtr0344527
chr2R	6042723	6043223	11,41	11,83	0,42	9,11E-05	0,00156	exon (FBgn0033055, exon 1 of 5)	exon (NM_206025, exon 1 of 5)	319	FBgn0033055	FBtr0085974
chr3R	15350321	15350821	11,19	11,61	0,42	9,30E-05	0,00159	promoter-TSS (FBgn0038324)	promoter-TSS (NM_142194)	424	FBgn0266722	FBtr0083116
chrX	15075602	15076102	11,04	11,47	0,42	0,000145	0,00229	exon (FBgn0030608, exon 1 of 4)	exon (NM_001042812, exon 1 of 4)	368	FBgn0030608	FBtr0346060
chr3R	15277500	15278000	11,65	12,07	0,42	0,000173	0,00266	TTS (FBgn0011476)	TTS (NM_142186)	359	FBgn0027378	FBtr0083125
chrX	16303935	16304435	11,56	11,99	0,42	0,000185	0,0028	TTS (FBgn0030735)	TTS (NM_001103529)	316	FBgn0027521	FBtr0074222
chrX	6742782	6743282	11,42	11,84	0,42	0,00021	0,00309	promoter-TSS (FBgn0086668)	promoter-TSS (NR_003729)	-31	FBgn0083013	FBtr0113560
chrX	2180424	2180924	11,7	12,13	0,42	0,000281	0,00385	promoter-TSS (FBgn0003116)	promoter-TSS (NM_057336)	142	FBgn0265901	FBtr0342773
chr2L	21180297	21180797	11,72	12,14	0,42	0,000377	0,00483	promoter-TSS (FBgn0000239)	promoter-TSS (NM_138759)	675	FBgn0032929	FBtr0081475
chr2R	24195663	24196163	11,62	12,04	0,42	0,000392	0,00494	TTS (FBgn0266083)	TTS (NM_138050)	416	FBgn0034988	FBtr0072261
chrX	10220331	10220831	11,28	11,7	0,42	0,000504	0,00601	exon (FBgn0085437, exon 1 of 14)	exon (NM_001103468, exon 1 of 15)	472	FBgn0085437	FBtr0071439
chr2R	17716633	17717133	10,81	11,22	0,42	0,000669	0,00745	promoter-TSS (FBgn0028494)	promoter-TSS (NM_137405)	387	FBgn0028494	FBtr0340273
chr3L	19805662	19806162	11,56	11,98	0,42	0,00096	0,0095	promoter-TSS (FBgn0036909)	promoter-TSS (NM_168819)	124	FBgn0083952	FBtr0110816
chr2R	12037377	12037877	12,02	12,44	0,42	0,000992	0,00974	promoter-TSS (FBgn0262820)	promoter-TSS (NM_001259343)	330	FBgn0010339	FBtr0087976
chr3L	17622039	17622539	11,49	11,91	0,42	0,00117	0,0109	promoter-TSS (FBgn0036740)	promoter-TSS (NM_140740)	466	FBgn0036741	FBtr0075182
chr3L	8524310	8524810	11,08	11,5	0,42	0,00155	0,0136	promoter-TSS (FBgn0024236)	promoter-TSS (NM_079250)	306	FBgn0035907	FBtr0076652
chr3L	12849562	12850062	10,89	11,31	0,42	0,00188	0,0158	promoter-TSS (FBgn0036318)	promoter-TSS (NM_001144473)	-21	FBgn0036317	FBtr0273237
chr3R	5216930	5217430	11,66	12,08	0,42	0,0023	0,0185	TTS (FBgn0037296)	TTS (NM_141758)	276	FBgn0259217	FBtr0347363
chr3R	21855610	21856110	12,01	12,44	0,42	0,0025	0,0197	exon (FBgn0015229, exon 1 of 2)	exon (NM_079719, exon 1 of 2)	406	FBgn0015229	FBtr0084157
chrX	6597354	6597854	11,33	11,75	0,42	0,00258	0,0202	TTS (FBgn0029878)	TTS (NM_001272357)	422	FBgn0029879	FBtr0070947
chr3R	5375059	5375559	11,92	12,34	0,42	0,00316	0,0238	promoter-TSS (FBgn0086695)	promoter-TSS (NM_001316495)	298	FBgn0037317	FBtr0100433
chr3L	16105087	16105587	11,34	11,75	0,42	0,00327	0,0243	promoter-TSS (FBgn0262987)	promoter-TSS (NM_001259859)	290	FBgn0036570	FBtr0075495
chr3L	18867821	18868321	11,83	12,25	0,42	0,00356	0,0258	TTS (FBgn0036818)	TTS (NM_001259897)	301	FBgn0036819	FBtr0333708
chr2L	8196379	8196879	11,38	11,8	0,42	0,0043	0,0295	promoter-TSS (FBgn0031996)	promoter-TSS (NM_135346)	289	FBgn0031995	FBtr0335186
chrX	15710947	15711447	11,6	12,02	0,42	0,00441	0,03	promoter-TSS (FBgn0030672)	promoter-TSS (NM_132829)	141	FBgn0030673	FBtr0074055
chrX	5689047	5689547	11,72	12,14	0,42	0,00447	0,0303	promoter-TSS (FBgn0000394)	promoter-TSS (NM_080525)	176	FBgn0029789	FBtr0070847
chr2R	10074941	10075441	12,12	12,54	0,42	0,00449	0,0304	exon (FBgn0033487, exon 2 of 6)	exon (NM_136707, exon 2 of 6)	454	FBgn0033487	FBtr0088428
chr3R	11628848	11629348	11,86	12,28	0,42	0,00464	0,031	TTS (FBgn0042205)	TTS (NM_144455)	340	FBgn0037524	FBtr0082418
chr2R	16017704	16018204	10,99	11,41	0,42	0,00479	0,0317	promoter-TSS (FBgn0034066)	promoter-TSS (NM_137234)	218	FBgn0034067	FBtr0087207
chr3L	7320286	7320786	11,75	12,17	0,42	0,00505	0,0328	TTS (FBgn0035761)	TTS (NM_168199)	469	FBgn0035760	FBtr0076837
chr3R	18241602	18242102	11,85	12,27	0,42	0,00525	0,0336	promoter-TSS (FBgn0020238)	promoter-TSS (NM_169799)	307	FBgn0038588	FBtr0083606
chr2L	8514222	8514722	12,18	12,59	0,42	0,00567	0,0356	promoter-TSS (FBgn0032052)	promoter-TSS (NM_135394)	396	FBgn0032051	FBtr0079697
chr3L	654427	654927	11,07	11,48	0,42	0,00809	0,0468	promoter-TSS (FBgn0035149)	promoter-TSS (NM_138202)	335	FBgn0035150	FBtr0072557
chr3R	14125967	14126467	11,81	12,24	0,43	0,000243	0,00346	promoter-TSS (FBgn0010340)	promoter-TSS (NM_057603)	427	FBgn0262955	FBtr0082892
chrX	16586554	16587054	10,8	11,23	0,43	0,000593	0,00678	promoter-TSS (FBgn0267912)	promoter-TSS (NM_167524)	-139	FBgn0267912	FBtr0305198
chr3L	9073188	9073688	11,51	11,95	0,43	0,000659	0,00739	promoter-TSS (FBgn0035959)	promoter-TSS (NM_140028)	334	FBgn0035960	FBtr0076524
chr3L	1312719	1313219	11,63	12,06	0,43	0,000768	0,00816	promoter-TSS (FBgn0035207)	promoter-TSS (NM_167868)	236	FBgn0035206	FBtr0072728
chr3L	5780160	5780660	11,71	12,13	0,43	0,000842	0,0087	promoter-TSS (FBgn0040298)	promoter-TSS (NM_139730)	147	FBgn0260458	FBtr0091709
chr2L	21101727	21102227	11,65	12,08	0,43	0,000921	0,00929	promoter-TSS (FBgn0032916)	promoter-TSS (NM_136743)	452	FBgn0284251	FBtr0114615
chrX	13617175	13617675	10,91	11,34	0,43	0,000944	0,0094	promoter-TSS (FBgn0030502)	promoter-TSS (NM_001298287)	437	FBgn0030503	FBtr0308644
chr2R	9860156	9860656	10,97	11,41	0,43	0,00112	0,0106	promoter-TSS (FBgn0265339)	promoter-TSS (NR_124490)	353	FBgn0027580	FBtr0088456
chr3L	22727248	22727748	11,91	12,34	0,43	0,00119	0,0111	promoter-TSS (FBgn0037185)	promoter-TSS (NM_141355)	291	FBgn0037184	FBtr0078537
chrX	13821615	13822115	10,97	11,4	0,43	0,00131	0,012	promoter-TSS (FBgn0027537)	promoter-TSS (NM_132701)	442	FBgn0030529	FBtr0073835
chr2L	1166477	1166977	11,07	11,5	0,43	0,00204	0,0169	TTS (FBgn0024314)	TTS (NM_134735)	222	FBgn0031315	FBtr0077964
chr3L	2773446	2773946	11,72	12,15	0,43	0,00207	0,0171	promoter-TSS (FBgn0044452)	promoter-TSS (NM_139491)	311	FBgn0035372	FBtr0073015
chrX	20422638	20423138	10,54	10,97	0,43	0,0022	0,0179	exon (FBgn0023177, exon 2 of 3)	5' UTR (NM_167703, exon 2 of 3)	118	FBgn0023177	FBtr0345017
chr3R	13994790	13995290	11,83	12,26	0,43	0,00238	0,019	exon (FBgn0250848, exon 2 of 3)	exon (NM_138985, exon 2 of 3)	810	FBgn0250848	FBtr0075766
chr3R	21887069	21887569	11,56	12	0,43	0,00241	0,0192	promoter-TSS (FBgn0038916)	promoter-TSS (NM_142738)	36	FBgn0038916	FBtr0084151
chr3R	7907580	7908080	11,65	12,08	0,43	0,00275	0,0212	promoter-TSS (FBgn0037530)	promoter-TSS (NM_141490)	193	FBgn0024909	FBtr0114520
chrX	23106049	23106549	11,56	11,99	0,43	0,00275	0,0212	intron (FBgn0039946, intron 1 of 1)	intron (NM_001111011, intron 1 of 1)	297	FBgn0039946	FBtr0301978
chr3L	14071948	14072448	11,46	11,89	0,43	0,00331	0,0245	TTS (FBgn0267795)	TTS (NM_001144476)	307	FBgn0013563	FBtr0075777
chr3R	21101178	21101678	11,68	12,1	0,43	0,00332	0,0245	promoter-TSS (FBgn0038855)	promoter-TSS (NM_142684)	290	FBgn0038854	FBtr0084035
chr3R	26058595	26059095	12,16	12,58	0,43	0,00342	0,0251	promoter-TSS (FBgn0260224)	promoter-TSS (NM_001170272)	422	FBgn0039406	FBtr0084972
chr2L	7409115	7409615	11,31	11,75	0,43	0,0041	0,0285	TTS (FBgn0031908)	TTS (NM_001273262)	444	FBgn0031909	FBtr0079467
chrX	8463934	8464434	11,51	11,94	0,43	0,00464	0,031	TTS (FBgn0023506)	TTS (NM_132257)	254	FBgn0014032	FBtr0071241
chr2R	17406407	17406907	10,79	11,22	0,43	0,00614	0,0378	exon (FBgn0034210, exon 2 of 3)	exon (NM_137360, exon 3 of 4)	493	FBgn0034210	FBtr0340144
chrX	8719607	8720107	12,03	12,45	0,43	0,00757	0,0444	promoter-TSS (FBgn0030063)	promoter-TSS (NM_132276)	420	FBgn0027330	FBtr0071280
chr3L	15977048	15977548	10,84	11,28	0,43	0,00833	0,0476	TTS (FBgn0036550)	TTS (NM_140563)	266	FBgn0036551	FBtr0075514
chr2R	9583760	9584260	11,69	12,13	0,43	0,00852	0,0484	promoter-TSS (FBgn0033428)	promoter-TSS (NM_136657)	272	FBgn0033427	FBtr0339393
chr3R	17682701	17683201	11,59	12,04	0,44	0,000159	0,00247	promoter-TSS (FBgn0038535)	promoter-TSS (NM_206505)	293	FBgn0038536	FBtr0083479
chr2R	11984680	11985180	11,46	11,89	0,44	0,000195	0,00292	exon (FBgn0011704, exon 2 of 3)	exon (NM_080372, exon 2 of 3)	463	FBgn0011704	FBtr0088046
chr2R	16783742	16784242	11,33	11,77	0,44	0,000289	0,00393	TTS (FBgn0034157)	TTS (NM_206138)	322	FBgn0034158	FBtr0087027
chr3R	11581570	11582070	11,31	11,76	0,44	0,000395	0,00497	TTS (FBgn0037916)	TTS (NM_141831)	245	FBgn0037917	FBtr0082413
chr3L	692297	692797	11,8	12,24	0,44	0,000503	0,00601	TTS (FBgn0035155)	TTS (NM_138210)	372	FBgn0260862	FBtr0072607
chr3L	19818542	19819042	11,8	12,24	0,44	0,000524	0,00618	promoter-TSS (FBgn0036911)	promoter-TSS (NM_206401)	-309	FBgn0013799	FBtr0310476
chrX	11851903	11852403	11,98	12,42	0,44	0,000601	0,00686	TTS (FBgn0030342)	TTS (NM_167310)	377	FBgn0030341	FBtr0073604
chr2R	21518536	21519036	11,32	11,76	0,44	0,000677	0,0075	TTS (FBgn0050288)	TTS (NM_001103928)	320	FBgn0034634	FBtr0071699
chr2L	15255757	15256257	12,02	12,46	0,44	0,00082	0,00853	promoter-TSS (FBgn0259982)	promoter-TSS (NM_001273535)	297	FBgn0283467	FBtr0303164
chr2R	19141500	19142000	10,84	11,28	0,44	0,000891	0,00909	TTS (FBgn0034419)	TTS (NM_166328)	119	FBgn0000578	FBtr0100174
chr3R	18220584	18221084	11,67	12,11	0,44	0,000925	0,00932	promoter-TSS (FBgn0038583)	promoter-TSS (NM_142435)	-135	FBgn0038583	FBtr0083610
chr2R	16185390	16185890	11,61	12,04	0,44	0,000989	0,00973	promoter-TSS (FBgn0034087)	promoter-TSS (NM_137251)	392	FBgn0034086	FBtr0087747
chrX	7013126	7013626	11,81	12,25	0,44	0,00102	0,00995	promoter-TSS (FBgn0029929)	promoter-TSS (NM_132149)	286	FBgn0029928	FBtr0071032
chr3R	18184509	18185009	10,61	11,06	0,44	0,00107	0,0103	promoter-TSS (FBgn0038576)	promoter-TSS (NM_142427)	638	FBgn0038575	FBtr0083618
chr3R	19877844	19878344	11,37	11,81	0,44	0,00108	0,0104	promoter-TSS (FBgn0038741)	promoter-TSS (NM_142582)	358	FBgn0038742	FBtr0083817
chrX	11092609	11093109	11,54	11,98	0,44	0,00112	0,0106	TTS (FBgn0030263)	TTS (NM_132453)	368	FBgn0027498	FBtr0073429
chr3L	11992454	11992954	11,53	11,97	0,44	0,00156	0,0136	TTS (FBgn0036736)	TTS (NM_140280)	475	FBgn0036737	FBtr0076062
chrX	5671115	5671615	11,87	12,32	0,44	0,00158	0,0138	TTS (FBgn0028474)	TTS (NM_132014)	447	FBgn0015794	FBtr0070849
chr3L	3941944	3942444	10,79	11,23	0,44	0,00166	0,0143	promoter-TSS (FBgn0035477)	promoter-TSS (NM_139584)	271	FBgn0027552	FBtr0073171
chr3R	19643418	19643918	11,89	12,33	0,44	0,00169	0,0146	promoter-TSS (FBgn0038721)	promoter-TSS (NM_142563)	718	FBgn0283536	FBtr0346100
chr3L	16351290	16351790	11,82	12,25	0,44	0,0018	0,0153	promoter-TSS (FBgn0283681)	promoter-TSS (NM_140623)	411	FBgn0036614	FBtr0075428
chr2L	8220022	8220522	11,65	12,09	0,44	0,00372	0,0266	TTS (FBgn0032006)	TTS (NM_001169440)	469	FBgn0032005	FBtr0079631
chrX	11709295	11709795	12	12,44	0,44	0,00403	0,0282	TTS (FBgn0030328)	TTS (NM_167299)	406	FBgn0030327	FBtr0073620
chrX	13721385	13721885	12,02	12,45	0,44	0,00405	0,0282	promoter-TSS (FBgn0002578)	promoter-TSS (NM_080170)	342	FBgn0030514	FBtr0073843
chr3R	22465111	22465611	10,7	11,14	0,44	0,00446	0,0303	promoter-TSS (FBgn0038973)	promoter-TSS (NM_142794)	377	FBgn0038972	FBtr0084254
chr3R	22448231	22448731	11,63	12,07	0,44	0,00456	0,0307	exon (FBgn0085405, exon 1 of 3)	exon (NM_001104402, exon 1 of 3)	383	FBgn0085405	FBtr0112608
chr2L	19426071	19426571	10,9	11,35	0,44	0,0047	0,0312	promoter-TSS (FBgn0032780)	promoter-TSS (NM_001273646)	24	FBgn0032779	FBtr0334164
chr3L	15159151	15159651	12,09	12,53	0,44	0,00474	0,0314	promoter-TSS (FBgn0036486)	promoter-TSS (NM_140498)	302	FBgn0036487	FBtr0075642
chr3L	1307714	1308214	12,1	12,55	0,44	0,00485	0,0319	promoter-TSS (FBgn0035204)	promoter-TSS (NM_138251)	417	FBgn0035205	FBtr0072669
chr2R	24514347	24514847	11,22	11,66	0,44	0,00502	0,0326	exon (FBgn0284252, exon 1 of 4)	exon (NM_166675, exon 1 of 4)	400	FBgn0284252	FBtr0072349
chr3R	5555281	5555781	11,7	12,14	0,44	0,00648	0,0395	exon (FBgn0037338, exon 1 of 3)	exon (NM_141291, exon 1 of 3)	448	FBgn0037338	FBtr0078688
chr2L	8212350	8212850	12,13	12,57	0,44	0,00704	0,042	promoter-TSS (FBgn0032001)	promoter-TSS (NM_001273303)	302	FBgn0032000	FBtr0079633
chrX	11135593	11136093	10,17	10,62	0,44	0,00768	0,0449	exon (FBgn0030268, exon 2 of 5)	exon (NM_167269, exon 2 of 5)	580	FBgn0030268	FBtr0073479
chr2R	7965792	7966292	10,25	10,69	0,44	0,00804	0,0466	TTS (FBgn0033243)	TTS (NM_136496)	1982	FBgn0033243	FBtr0339127
chr3L	6494719	6495219	11,94	12,38	0,44	0,00808	0,0468	promoter-TSS (FBgn0020251)	promoter-TSS (NM_001169883)	328	FBgn0035704	FBtr0076986
chr2R	24796935	24797435	11,84	12,28	0,44	0,00843	0,0481	promoter-TSS (FBgn0035068)	promoter-TSS (NM_138125)	229	FBgn0023181	FBtr0072425
chr2R	17426929	17427429	11,96	12,39	0,44	0,00867	0,049	promoter-TSS (FBgn0034215)	promoter-TSS (NM_001274120)	332	FBgn0034214	FBtr0086961
chr3R	26059684	26060184	11,44	11,89	0,45	1,89E-05	0,000434	promoter-TSS (FBgn0039406)	promoter-TSS (NM_170257)	427	FBgn0039407	FBtr0346731

chrX	6036631	6037131	11,46	11,91	0,45	3,92E-05	0,000787	exon (FBgn0003302, exon 3 of 3)	exon (NM_078498, exon 2 of 2)	381	FBgn0003302	FBtr0070899
chrX	20430219	20430719	11,27	11,73	0,45	4,35E-05	0,000858	promoter-TSS (FBgn0031115)	promoter-TSS (NM_167704)	335	FBgn0002641	FBtr0077306
chr2R	16150071	16150571	11,16	11,61	0,45	5,09E-05	0,000976	promoter-TSS (FBgn0034081)	promoter-TSS (NM_001032251)	199	FBgn0034083	FBtr0302084
chr3L	8514309	8514809	11,09	11,55	0,45	7,98E-05	0,00139	exon (FBgn0035902, exon 2 of 2)	exon (NM_139975, exon 2 of 2)	362	FBgn0035902	FBtr0076655
chr3R	5793722	5794222	11,78	12,23	0,45	0,000119	0,00192	promoter-TSS (FBgn0037379)	promoter-TSS (NM_141334)	345	FBgn0037378	FBtr0078668
chr3R	24817674	24818174	11,84	12,3	0,45	0,000118	0,00192	promoter-TSS (FBgn0027617)	promoter-TSS (NM_143034)	461	FBgn0039229	FBtr0084700
chr3L	20375338	20375838	11,71	12,16	0,45	0,000215	0,00314	promoter-TSS (FBgn0036980)	promoter-TSS (NM_140959)	308	FBgn0001247	FBtr0273273
chr3L	3937452	3937952	11,82	12,28	0,45	0,000334	0,00439	TTS (FBgn0035476)	TTS (NM_139582)	290	FBgn0035475	FBtr0345342
chr3L	22877459	22877959	11,08	11,54	0,45	0,00034	0,00444	exon (FBgn0044324, exon 3 of 6)	exon (NM_168976, exon 3 of 6)	475	FBgn0044324	FBtr0078570
chr3R	29123473	29123973	11,35	11,81	0,45	0,000344	0,00448	exon (FBgn0039637, exon 1 of 3)	promoter-TSS (NM_057545)	308	FBgn0039637	FBtr0085372
chr3R	16435923	16436423	11,65	12,1	0,45	0,000473	0,0057	TTS (FBgn0038427)	TTS (NM_001038969)	424	FBgn0038426	FBtr0083316
chr3R	19863776	19864276	11,91	12,37	0,45	0,000514	0,0061	promoter-TSS (FBgn0038739)	promoter-TSS (NM_142580)	367	FBgn0038738	FBtr0083860
chr3L	19261554	19262054	11,62	12,07	0,45	0,000584	0,00668	TTS (FBgn0017578)	TTS (NM_140840)	411	FBgn0260857	FBtr0074989
chrX	17421350	17421850	11,77	12,22	0,45	0,00105	0,0102	TTS (FBgn0040877)	TTS (NM_144231)	545	FBgn0027602	FBtr0074440
chr3L	13929484	13929984	12,13	12,58	0,45	0,00115	0,0109	promoter-TSS (FBgn0036386)	promoter-TSS (NM_140412)	348	FBgn0001108	FBtr0075756
chr2R	13941505	13942005	10,89	11,34	0,45	0,00126	0,0116	TTS (FBgn0033885)	TTS (NM_137072)	355	FBgn0033733	FBtr0087616
chr2R	19310057	19310557	11,5	11,95	0,45	0,00141	0,0126	TTS (FBgn0264753)	TTS (NM_001274158)	358	FBgn0034433	FBtr0086558
chr3L	14001153	14001653	11,01	11,46	0,45	0,0018	0,0153	promoter-TSS (FBgn0036398)	promoter-TSS (NM_140424)	406	FBgn0036397	FBtr0333025
chr2L	18709003	18709503	11,57	12,02	0,45	0,00192	0,0161	promoter-TSS (FBgn0025608)	promoter-TSS (NM_058040)	408	FBgn0032705	FBtr0081099
chr2R	13197504	13198004	11,82	12,27	0,45	0,00208	0,0171	exon (FBgn0053182, exon 2 of 7)	5' UTR (NM_001169668, exon 2 of 7)	583	FBgn0053182	FBtr0087770
chr3R	13970746	13971246	11,08	11,53	0,45	0,00223	0,0181	promoter-TSS (FBgn0263414)	promoter-TSS (NR_043888)	-736	FBgn0263414	FBtr0305198
chr2L	7026537	7027037	11,82	12,27	0,45	0,00251	0,0198	promoter-TSS (FBgn0031881)	promoter-TSS (NM_135749)	500	FBgn0051908	FBtr0079429
chr3R	5613441	5613941	11,92	12,37	0,45	0,00261	0,0204	promoter-TSS (FBgn0017550)	promoter-TSS (NM_169080)	334	FBgn0019637	FBtr0078704
chr3L	7348350	7348850	10,93	11,38	0,45	0,00271	0,0209	promoter-TSS (FBgn0015798)	promoter-TSS (NM_057787)	288	FBgn0019662	FBtr0076846
chr3L	19792989	19793489	10,72	11,17	0,45	0,00273	0,0211	promoter-TSS (FBgn0261293)	promoter-TSS (NM_168816)	330	FBgn0261360	FBtr0302278
chr2R	20622767	20623267	12,14	12,6	0,45	0,0031	0,0234	promoter-TSS (FBgn0034529)	promoter-TSS (NM_137652)	412	FBgn0034528	FBtr0086254
chr3R	23957678	23958178	12,1	12,55	0,45	0,00322	0,024	promoter-TSS (FBgn0039132)	promoter-TSS (NM_142941)	463	FBgn0005674	FBtr0084511
chr2R	13133212	13133712	11,74	12,19	0,45	0,00352	0,0256	exon (FBgn0259876, exon 1 of 5)	exon (NM_001169664, exon1 of 5)	321	FBgn0259876	FBtr0299507
chr3L	15836660	15837160	10,84	11,29	0,45	0,00387	0,0275	TTS (FBgn0052150)	TTS (NM_168635)	572	FBgn0036538	FBtr0306854
chrX	5916001	5916501	10,7	11,15	0,45	0,00406	0,0283	promoter-TSS (FBgn0029823)	promoter-TSS (NM_001144690)	66	FBgn0029823	FBtr0345317
chr2L	143372	143872	11,78	12,23	0,45	0,00634	0,0388	promoter-TSS (FBgn0051974)	promoter-TSS (NM_001272871)	300	FBgn0031224	FBtr0078116
chrX	10745535	10746035	11,86	12,31	0,45	0,00674	0,0407	promoter-TSS (FBgn0052676)	promoter-TSS (NM_001272497)	352	FBgn0003204	FBtr0071494
chr2R	15482036	15482536	11,12	11,57	0,45	0,00682	0,0411	exon (FBgn0034021, exon 1 of 5)	exon (NM_137195, exon 1 of 5)	548	FBgn0034021	FBtr0345392
chr2L	9782678	9783178	11,39	11,84	0,45	0,00722	0,0429	exon (FBgn0032147, exon 1 of 4)	exon (NM_135469, exon 1 of 4)	545	FBgn0032147	FBtr0079869
chr3R	26966818	26967318	11,24	11,7	0,45	0,00793	0,0462	promoter-TSS (FBgn0041224)	promoter-TSS (NM_176570)	139	FBgn0039466	FBtr0085069
chrX	17710050	17710550	10,13	10,58	0,45	0,00826	0,0475	promoter-TSS (FBgn0030864)	promoter-TSS (NM_133011)	157	FBgn0261570	FBtr0302935
chrX	5419768	5420268	11,36	11,81	0,45	0,00877	0,0495	promoter-TSS (FBgn0263987)	promoter-TSS (NM_167033)	318	FBgn0263987	FBtr0070795
chr2L	2760006	2760506	12,03	12,48	0,45	0,00889	0,0499	promoter-TSS (FBgn0031455)	promoter-TSS (NM_001032050)	333	FBgn0031456	FBtr0077715
chr3L	22071345	22071845	11,36	11,82	0,46	2,02E-05	0,000457	promoter-TSS (FBgn0264727)	promoter-TSS (NR_073973)	253	FBgn0027532	FBtr0078486
chr3R	8032590	8033090	11,22	11,67	0,46	4,17E-05	0,000825	promoter-TSS (FBgn0010812)	promoter-TSS (NM_001316496)	169	FBgn0037544	FBtr0347360
chr2R	18706189	18706689	11,26	11,71	0,46	8,33E-05	0,00144	TTS (FBgn0262103)	TTS (NM_001103899)	463	FBgn0034379	FBtr0086607
chrX	6347453	6347953	11,57	12,03	0,46	0,000136	0,00216	exon (FBgn0029857, exon 1 of 1)	exon (NM_132089, exon 1 of 1)	601	FBgn0029857	FBtr0070905
chr2R	21292880	21293380	11,37	11,82	0,46	0,000163	0,00251	promoter-TSS (FBgn0016726)	promoter-TSS (NM_166438)	311	FBgn0050390	FBtr0071617
chrX	15784785	15785285	11,89	12,35	0,46	0,000239	0,00342	exon (FBgn0025809, exon 1 of 2)	exon (NM_167461, exon 1 of 2)	548	FBgn0025809	FBtr0074190
chr2R	24611874	24612374	11,43	11,89	0,46	0,000282	0,00386	promoter-TSS (FBgn0035040)	promoter-TSS (NM_001299921)	243	FBgn0035039	FBtr0343487
chr3L	12571810	12572310	11,48	11,93	0,46	0,000425	0,00526	exon (FBgn0036302, exon 2 of 13)	exon (NM_001144471, exon2 of 10)	482	FBgn0036302	FBtr0300857
chr2L	21237280	21237780	10,83	11,29	0,46	0,00075	0,00802	promoter-TSS (FBgn0051626)	promoter-TSS (NM_165362)	281	FBgn0261239	FBtr0081478
chr3L	10637255	10637755	11,22	11,68	0,46	0,000786	0,00829	promoter-TSS (FBgn0036090)	promoter-TSS (NM_168415)	374	FBgn0000629	FBtr0273338
chr2R	14993315	14993815	11,45	11,92	0,46	0,00127	0,0117	promoter-TSS (FBgn0264378)	promoter-TSS (NR_073877)	270	FBgn0033990	FBtr0332259
chr2R	16955558	16956058	11,83	12,3	0,46	0,00134	0,0122	promoter-TSS (FBgn0085444)	promoter-TSS (NM_001103882)	351	FBgn0265174	FBtr0339071
chr3R	19904120	19904620	11,8	12,25	0,46	0,00154	0,0136	promoter-TSS (FBgn0038745)	promoter-TSS (NM_169880)	498	FBgn0038746	FBtr0083854
chr3R	23758424	23758924	11,7	12,16	0,46	0,00197	0,0164	promoter-TSS (FBgn0039111)	promoter-TSS (NM_170090)	67	FBgn0039111	FBtr0084454
chr2R	12589749	12590249	10,93	11,39	0,46	0,00327	0,0243	promoter-TSS (FBgn0022764)	promoter-TSS (NM_001259353)	233	FBgn0050055	FBtr0345021
chr2L	10423554	10424054	12,12	12,58	0,46	0,00393	0,0278	exon (FBgn0032246, exon 3 of 7)	exon (NM_135556, exon 2 of 6)	471	FBgn0032246	FBtr0080020
chr2R	12515432	12515932	11,64	12,11	0,46	0,00395	0,0278	promoter-TSS (FBgn0033749)	promoter-TSS (NM_165912)	308	FBgn0033750	FBtr0087939
chrX	2603322	2603822	11,61	12,07	0,46	0,00641	0,0392	promoter-TSS (FBgn0004643)	promoter-TSS (NM_080162)	331	FBgn0011606	FBtr0340093
chr2L	15270835	15271335	10,85	11,31	0,46	0,00705	0,0421	promoter-TSS (FBgn0261268)	promoter-TSS (NM_165112)	543	FBgn0261268	FBtr0302158
chr3L	22263471	22263971	11,82	12,28	0,46	0,00772	0,045	promoter-TSS (FBgn0028500)	promoter-TSS (NM_001275276)	353	FBgn0015075	FBtr0078492
chr2L	10412870	10413370	11,24	11,7	0,46	0,00797	0,0463	promoter-TSS (FBgn0032243)	promoter-TSS (NM_001169466)	343	FBgn0032242	FBtr0080047
chr3L	9722587	9723087	11,73	12,19	0,46	0,00812	0,0469	promoter-TSS (FBgn0036038)	promoter-TSS (NM_140095)	357	FBgn0261530	FBtr0306039
chr3R	4813575	4814075	10,81	11,27	0,46	0,0085	0,0483	exon (FBgn0037279, exon 2 of 4)	exon (NM_169021, exon 2 of 4)	187	FBgn0037279	FBtr0345174
chr2R	10051544	10052044	11,58	12,04	0,47	2,09E-05	0,00047	promoter-TSS (FBgn0262169)	promoter-TSS (NM_001103784)	373	FBgn0263260	FBtr0088433
chr2R	17027272	17027772	11,37	11,84	0,47	2,45E-05	0,000539	promoter-TSS (FBgn0265540)	promoter-TSS (NR_124587)	333	FBgn0023172	FBtr0086969
chrX	7967574	7968074	11,02	11,49	0,47	2,60E-05	0,000563	exon (FBgn0003656, exon 1 of 11)	5' UTR (NM_167140, exon 1 of 11)	412	FBgn0003656	FBtr0071125
chr3R	16646364	16646864	11,06	11,53	0,47	3,68E-05	0,000749	promoter-TSS (FBgn0015019)	promoter-TSS (NM_169277)	390	FBgn0038454	FBtr0083356
chr3L	9863660	9864160	11,21	11,68	0,47	3,89E-05	0,000783	promoter-TSS (FBgn0027567)	promoter-TSS (NM_168386)	439	FBgn0036053	FBtr0076362
chrX	16287975	16288475	11,01	11,49	0,47	5,49E-05	0,00104	promoter-TSS (FBgn0011571)	promoter-TSS (NM_001272673)	308	FBgn0052576	FBtr0074245
chr3L	7347319	7347819	11,61	12,08	0,47	5,82E-05	0,00109	promoter-TSS (FBgn0019662)	promoter-TSS (NM_001169899)	-446	FBgn0035768	FBtr0076890
chr3R	24134938	24135438	11,62	12,09	0,47	5,91E-05	0,0011	TTS (FBgn0026317)	TTS (NM_058067)	358	FBgn0266673	FBtr0084547
chr3L	18900835	18901335	11,37	11,85	0,47	6,98E-05	0,00127	promoter-TSS (FBgn0036727)	promoter-TSS (NM_140815)	469	FBgn0036726	FBtr0075075
chrX	477461	477961	11,17	11,64	0,47	7,52E-05	0,00133	exon (FBgn0029523, exon 3 of 3)	exon (NM_001103388, exon2 of 3)	344	FBgn0029522	FBtr0070076
chr3R	10761423	10761923	11,68	12,16	0,47	8,04E-05	0,0014	promoter-TSS (FBgn0051390)	promoter-TSS (NM_206471)	-98	FBgn0037831	FBtr0082273
chr2L	1704977	1705477	11,53	11,99	0,47	0,000176	0,00268	promoter-TSS (FBgn0011570)	promoter-TSS (NM_001272948)	97	FBgn0011570	FBtr0331630
chr3R	24851805	24852305	11,71	12,18	0,47	0,000182	0,00276	TTS (FBgn0039233)	TTS (NM_143039)	455	FBgn0039234	FBtr0084705
chr3L	11122718	11123218	11,84	12,31	0,47	0,000283	0,00386	promoter-TSS (FBgn0260795)	promoter-TSS (NM_140184)	248	FBgn0036136	FBtr0076223
chr3L	1517963	1518463	11,77	12,24	0,47	0,000287	0,00391	promoter-TSS (FBgn0011204)	promoter-TSS (NM_138269)	363	FBgn0261243	FBtr0072702
chr3R	30056983	30057483	11,92	12,39	0,47	0,000317	0,00423	TTS (FBgn0039744)	TTS (NM_143512)	375	FBgn0260468	FBtr0085563
chrX	1901532	1902032	11,18	11,65	0,47	0,000319	0,00425	promoter-TSS (FBgn0264446)	promoter-TSS (NR_123771)	129	FBgn0052803	FBtr0070356
chr2R	13484775	13485275	11,82	12,3	0,47	0,00034	0,00444	promoter-TSS (FBgn0040477)	promoter-TSS (NM_079006)	366	FBgn0033842	FBtr0087701
chr3L	21839709	21840209	10,71	11,18	0,47	0,00035	0,00453	intron (FBgn0037135, intron 1 of 7)	intron (NM_168942, intron 1 of 7)	168	FBgn0037135	FBtr0078446
chr2R	15370933	15371433	11,12	11,59	0,47	0,00052	0,00616	promoter-TSS (FBgn0265651)	promoter-TSS (NR_124562)	337	FBgn0011650	FBtr0087388
chr3L	6958476	6958976	11,28	11,75	0,47	0,00053	0,00623	promoter-TSS (FBgn0035722)	promoter-TSS (NM_139807)	381	FBgn0029117	FBtr0076897
chr2L	8311431	8311931	11,62	12,09	0,47	0,000616	0,00699	promoter-TSS (FBgn0032017)	promoter-TSS (NM_135362)	283	FBgn0032018	FBtr0079600
chr3R	7247258	7247758	11,45	11,92	0,47	0,00066	0,00739	promoter-TSS (FBgn0037489)	promoter-TSS (NM_141453)	293	FBgn0037490	FBtr0081576
chr3R	8001669	8002169	11,71	12,18	0,47	0,000666	0,00744	promoter-TSS (FBgn0266598)	promoter-TSS (NM_001170075)	358	FBgn0037536	FBtr0081784
chr2L	11129579	11130079	11,68	12,15	0,47	0,000718	0,00782	promoter-TSS (FBgn0032348)	promoter-TSS (NM_135651)	488	FBgn0028700	FBtr0080225
chrX	4113001	4113501	11,95	12,41	0,47	0,000749	0,00802	promoter-TSS (FBgn0026085)	promoter-TSS (NM_001272303)	-449	FBgn0026085	FBtr0333184
chr3L	12149280	12149780	11,82	12,29	0,47	0,000754	0,00805	exon (FBgn0052099, exon 1 of 1)	exon (NM_168492, exon 1 of 1)	258	FBgn0052099	FBtr0076000
chr2L	10211414	10211914	12,04	12,5	0,47	0,000782	0,00827	promoter-TSS (FBgn0032193)	promoter-TSS (NM_135511)	495	FBgn0032194	FBtr0079947
chr3L	8297032	8297532	11,32	11,78	0,47	0,00109	0,0104	exon (FBgn0015793, exon 1 of 4)	exon (NM_079246, exon 1 of 4)	114	FBgn0015793	FBtr0076705
chr3R	14307758	14308258	10,51	10,98	0,47	0,0012	0,0112	intron (FBgn0003567, intron 1 of 6)	intron (NM_079625, intron 1 of 6)	581	FBgn0003567	FBtr0082945
chr3R	4645972	4646864	11,44	11,91	0,47	0,00138	0,0125	promoter-TSS (FBgn0040466)	promoter-TSS (NM_079500)	438	FBgn0022981	FBtr0078859
chrX	19353442	19353942	10,64	11,1	0,47	0,00248	0,0197	intron (FBgn0031016, intron 1 of 7)	intron (NM_001258317, intron 1 of 4)	512	FBgn0031016	FBtr0074707
chr3R	4228666	4229166	11,86	12,32	0,47	0,00374	0,0266	exon (FBgn0261436, exon 2 of 5)	exon (NM_141182, exon 2 of 5)	322	FBgn0261436	FBtr0078986
chr2R	24132932	24133432	11,83	12,3	0,47	0,00413	0,0286	promoter-TSS (FBgn0021875)	promoter-TSS (NM_138046)	369	FBgn0041582	FBtr0072281
chr2R	21298145	21298645	11,1	11,57	0,47	0,00419	0,0289	promoter-TSS (FBgn0261554)	promoter-TSS (NM_001144254)	100	FBgn0265937	FBtr0342901
chr2L	19493654	19494154	11,62	12,09	0,47	0,00482	0,0318	promoter-TSS (FBgn0032793)	promoter-TSS (NM_001273656)	337	FBgn0002044	FBtr0331326
chr2R	23908394	23908894	10,62	11,09	0,47	0,00529	0,0337	exon (FBgn0266041, exon 1 of 1)	non-coding (NR_124719, exon 1 of 1)	231	FBgn0266041	FBtr0343261
chr2R	24744181	24744681	11,78	12,25	0,47	0,00608	0,0375	exon (FBgn0050421, exon 1 of 6)	exon (NM_138115, exon 1 of 7)	683	FBgn0050421	FBtr0343495
chr3R	17391842	17392342	11,13	11,61	0,47	0,0062	0,0381	promoter-TSS (FBgn0265043)	promoter-TSS (NM_001170165)	81	FBgn0265043	FBtr0336488
chr3R	13029845	13030345	11,25	11,72	0,47	0,00832	0,0476	promoter-TSS (FBgn0002354)	promoter-TSS (NM_080203)	212	FBgn0283438	FBtr0445183
chr2L	16730491	16730991	11,39	11,87	0,48	4,11E-06	0,00013	TTS (FBgn0032596)	TTS (NM_001273582)	298	FBgn0032595	FBtr0080937
chr3R	18198251	18198751	10,97	11,44	0,48	2,01E-05	0,000454	intron (FBgn0011481, intron 1 of 1)	intron (NM_169794, intron 1 of 1)	1094	FBgn0011481	FBtr0083612
chr3R	7887203	7887703	11,58	12,06	0,48	2,83E-05	0,000604	promoter-TSS (FBgn0037525)	promoter-TSS (NM_001170070)	409	FBgn0037526	FBtr0081752
chr3R	9771011	9771511	11,19	11,67	0,48	3,09E-05	0,00064	TTS (FBgn0037750)	TTS (NM_001043234)	230	FBgn0037749	FBtr0113211
chr2L	7023387	7023887	11,39	11,87	0,48	4,95E-05	0,000959	exon (FBgn0000053, exon 1 of 7)	exon (NM_001014477, exon1 of 4)	261	FBgn0000053	FBtr0339663
chr2R	18183491	18183991	11,6	12,08	0,48	5,92E-05	0,0011	TTS (FBgn0053958)	TTS (NM_001038869)	349	FBgn0034315	FBtr0086771
chr3R	13088838	13089338	10,97	11,45	0,48	5,97E-05	0,00111	promoter-TSS (FBgn0085337)	promoter-TSS (NM_001104300)	-153	FBgn0085337	FBtr0445441
chr4	865901	866401	10,81	11,29	0,48	0,000108	0,00179	exon (FBgn0039936, exon 2 of 9)	exon (NM_001169357, exon2 of 10)	874	FBgn0039936	FBtr0300886
chr2L	10970710	10971210	11	11,49	0,48	0,000141	0,00223	promoter-TSS (FBgn0053129)	promoter-TSS (NM_176009)	518	FBgn0032321	FBtr0080146
chr2L	16327184	16327684	11,83	12,32	0,48	0,000176	0,00268	TTS (FBgn0001995)	TTS (NM_080200)	366	FBgn0014092	FBtr0080834
chrX	15333886	15334386	10,77	11,25	0,48	0,000268	0,00372	promoter-TSS (FBgn0026428)	promoter-TSS (NM_167437)	-83	FBgn0026428	FBtr0307383
chrX	16390778	16391278	11,61	12,09	0,48	0,000374	0,0048	promoter-TSS (FBgn0004367)	promoter-TSS (NM_078645)	410	FBgn0010416	FBtr0074305
chr2L	16311042	16311542	11,16	11,64	0,48	0,000405	0,00507	promoter-TSS (FBgn0000339)	promoter-TSS (NM_001273566)	337	FBgn0001086	FBtr0080833
chrX	18858372	18858872	11,95	12,43	0,48	0,000466	0,00564	promoter-TSS (FBgn0030968)	promoter-TSS (NM_001258487)	420	FBgn0030969	FBtr0074643
chr2L	20091518	20092018	11,55	12,02	0,48	0,000539	0,00629	promoter-TSS (FBgn0032845)	promoter-TSS (NM_001273689)	157	FBgn0032846	FBtr0081333
chr3R	9756634	9757134	11,21	11,69	0,48	0,000939	0,00939	promoter-TSS (FBgn0037742)	promoter-TSS (NM_169308)	-374	FBgn0037742	FBtr0332172
chr2L	21261152	21261652	11,61	12,09	0,48	0,00107	0,0103	intron (FBgn0021856, intron 1 of 3)	CpG	235	FBgn0021856	FBtr0081482
chr3R	26716698	26717198	11,63	12,12	0,48	0,00178	0,0151	promoter-TSS (FBgn0039450)	promoter-TSS (NM_170285)	441	FBgn0039449	FBtr0085047
chr3L	6957553	6958053	11,45	11,92	0,48	0,00281	0,0215	promoter-TSS (FBgn0029117)	promoter-TSS (NM_080019)	305	FBgn0035722	FBtr0076939
chrX	17842247	17842747	11,94	12,43	0,48	0,0035	0,0256	TTS (FBgn0030870)	TTS (NM_133017)	337	FBgn0000617	FBtr0074463
chr2R	20244834	20245334	11,36	11,84	0,48	0,00358	0,0259	TTS (FBgn0034489)	TTS (NM_137617)	304	FBgn0034488	FBtr0086322
chr3L	17428254	17428754	11,75	12,24	0,48	0,0036	0,0259	TTS (FBgn0052174)	TTS (NM_001144490)	332	FBgn0053052	FBtr0075229
chrX	4120406	4120906	11,43	11,92	0,48	0,00391	0,0277	exon (FBgn0026083, exon 5 of 8)	exon (NM_001169189, exon3 of 6)	559	FBgn0026083	FBtr0305185
chr2R	8106530	8106130	11,98	12,46	0,48	0,00411	0,0285	promoter-TSS (FBgn0033261)	promoter-TSS (NM_001316410)	434	FBgn0033260	FBtr0301355
chr3R	9767061	9767561	12,14	12,62	0,48	0,00436	0,0298	promoter-TSS (FBgn0037747)	promoter-TSS (NM_001014612)	504	FBgn0037330	FBtr0339719
chr3R	29936011	29936511	11,96	12,44	0,48	0,00574	0,036	promoter-TSS (FBgn0039726)	promoter-TSS (NM_143495)	284	FBgn0039727	FBtr0300825
chr3R	19403704	19404204	10,73	11,22	0,48	0,00694	0,0416	promoter-TSS (FBgn0086613)	promoter-TSS (NM_169854)	487	FBgn0038704	FBtr0083759
chr3L	8298994	8299494	11,41	11,89	0,48	0,00723	0,0429	promoter-TSS (FBgn0035867)	promoter-TSS (NM_139945)	595	FBgn0035866	FBtr0076715
chr3L	10638203	10638703	11,29	11,77	0,48	0,00738	0,0435	promoter-TSS (FBgn0000629)	promoter-TSS (NM_001144460)	308	FBgn0036090	FBtr0076254
chrX	4100267	4100767	11,42	11,91	0,49	3,24E-06	0,000106	promoter-TSS (FBgn0029694)	promoter-TSS (NM_131921)	514	FBgn0029693	FBtr0343297

chr3R	8806560	8807060	11,52	12,01	0,49	4,53E-06	0,000139	TTS (FBgn0037632)	TTS (NM_141578)	489	FBgn0037634|FBtr0081919
chr3R	7919439	7919939	11,01	11,51	0,49	7,23E-06	0,000201	promoter-TSS (FBgn0002542)	promoter-TSS (NM_080111)	422	FBgn0037531|FBtr0300685
chr3L	8340995	8341495	11,41	11,9	0,49	8,22E-06	0,000221	TTS (FBgn0035876)	TTS (NM_139953)	461	FBgn0035877|FBtr076604
chrX	54093	54593	11,44	11,94	0,49	1,58E-05	0,000376	Intergenic	HETA|LINE:Jockey	-68149	FBgn0058469|FBtr0307364
chr3L	13411941	13412441	11,67	12,16	0,49	1,74E-05	0,000406	promoter-TSS (FBgn0260049)	promoter-TSS (NM_168543)	262	FBgn0036356|FBtr0345341
chr3R	15857076	15857576	11,51	12	0,49	1,87E-05	0,000433	TTS (FBgn0051183)	TTS (NM_142248)	144	FBgn0038376|FBtr0083188
chr3L	19259925	19260425	11,22	11,71	0,49	2,10E-05	0,00047	exon (FBgn0026630, exon 2 of 4)	exon (NM_176349, exon 2 of 4)	136	FBgn0266787|FBtr0345237
chrX	15908598	15909098	11,54	12,03	0,49	3,18E-05	0,000655	exon (FBgn0010315, exon 2 of 6)	exon (NM_167473, exon 1 of 5)	828	FBgn0010315|FBtr0300391
chr2R	10880200	10880700	11,18	11,67	0,49	5,68E-05	0,00107	promoter-TSS (FBgn0010356)	promoter-TSS (NM_057609)	477	FBgn0033564|FBtr0339471
chr3R	8663253	8663753	11,88	12,37	0,49	6,81E-05	0,00124	promoter-TSS (FBgn0037606)	promoter-TSS (NM_141554)	396	FBgn0038679|FBtr0081887
chr3L	5751294	5751794	11,64	12,13	0,49	6,89E-05	0,00126	exon (FBgn0263106, exon 1 of 1)	exon (NM_168128, exon 1 of 1)	645	FBgn0263106|FBtr0077123
chr3R	8344822	8345322	11,13	11,62	0,49	7,53E-05	0,00133	TTS (FBgn0037579)	TTS (NM_141536)	673	FBgn0037580|FBtr0081840
chr3R	27112672	27113172	11,85	12,34	0,49	8,94E-05	0,00154	promoter-TSS (FBgn0039487)	promoter-TSS (NM_001316513)	357	FBgn0027574|FBtr0085106
chr2R	11453220	11453720	11,18	11,67	0,49	9,77E-05	0,00166	exon (FBgn0000581, exon 2 of 10)	5' UTR (NM_001273968, exon 2 of 11)	702	FBgn0000581|FBtr0088140
chr3R	16443318	16443818	11,63	12,12	0,49	0,00017	0,00261	promoter-TSS (FBgn0038428)	promoter-TSS (NM_142286)	325	FBgn0038429|FBtr0083289
chr3R	27227363	27274263	11,39	11,87	0,49	0,000333	0,00437	promoter-TSS (FBgn0046247)	promoter-TSS (NM_001104477)	309	FBgn0039505|FBtr0085158
chr2R	23356490	23356990	11,33	11,81	0,49	0,000441	0,00541	promoter-TSS (FBgn0034850)	promoter-TSS (NM_001169791)	651	FBgn0034849|FBtr0329860
chr2R	9290849	9291449	11,61	12,1	0,49	0,000453	0,00554	promoter-TSS (FBgn0028408)	promoter-TSS (NM_136634)	366	FBgn0026326|FBtr0088599
chr3R	25292521	25293021	10,92	11,41	0,49	0,000453	0,00554	TTS (FBgn0051102)	TTS (NM_170213)	206	FBgn0051098|FBtr0084863
chr2R	20644166	20644666	11,82	12,31	0,49	0,000604	0,00687	promoter-TSS (FBgn0061361)	promoter-TSS (NM_001032273)	381	FBgn0034537|FBtr0086232
chr3R	14662572	14663072	11,77	12,26	0,49	0,000665	0,00744	promoter-TSS (FBgn0038252)	promoter-TSS (NM_142126)	325	FBgn0025808|FBtr0082974
chr2L	20797873	20798373	10,44	10,92	0,49	0,000731	0,00792	exon (FBgn0032886, exon 1 of 3)	5' UTR (NM_165344, exon 1 of 3)	409	FBgn0032886|FBtr0081415
chr3L	16419643	16420143	11,95	12,44	0,49	0,000971	0,00959	promoter-TSS (FBgn0027080)	promoter-TSS (NM_140638)	297	FBgn0053158|FBtr0075390
chr2L	4459895	4460395	11,81	12,3	0,49	0,00103	0,01	promoter-TSS (FBgn0053002)	promoter-TSS (NM_001273099)	276	FBgn0031608|FBtr0077441
chr2R	23382474	23382974	11,44	11,93	0,49	0,00109	0,0105	promoter-TSS (FBgn0266011)	promoter-TSS (NR_124713)	700	FBgn0040660|FBtr0072033
chr3R	23762634	23763134	12,03	12,52	0,49	0,00109	0,0105	promoter-TSS (FBgn0039114)	promoter-TSS (NM_142926)	379	FBgn0039113|FBtr0084464
chr2R	8950319	8950819	12,04	12,53	0,49	0,0012	0,0111	exon (FBgn0033356, exon 2 of 3)	exon (NM_165638, exon 2 of 2)	517	FBgn0053199|FBtr0307344
chr2L	4969220	4969720	12,17	12,66	0,49	0,00128	0,0118	promoter-TSS (FBgn0262467)	promoter-TSS (NM_135040)	467	FBgn0031657|FBtr0078994
chr3R	24187998	24188498	11,93	12,43	0,49	0,00149	0,0132	TTS (FBgn0029503)	TTS (NM_142971)	451	FBgn0039163|FBtr0345215
chr2R	17733502	17734002	11,45	11,94	0,49	0,00168	0,0145	TTS (FBgn0034269)	TTS (NM_001169712)	515	FBgn0085224|FBtr0112388
chr3L	15512053	15512553	10,52	11,01	0,49	0,00183	0,0155	exon (FBgn0000565, exon 2 of 4)	exon (NM_206371, exon 2 of 4)	415	FBgn0000565|FBtr0330176
chr3R	29869566	29870066	11,79	12,29	0,49	0,0023	0,0185	promoter-TSS (FBgn0039714)	promoter-TSS (NM_170444)	452	FBgn0083969|FBtr0310888
chrX	9142768	9143268	11,69	12,19	0,49	0,00332	0,0246	exon (FBgn0030091, exon 2 of 3)	exon (NM_132301, exon 2 of 3)	526	FBgn0030091|FBtr0071299
chr3R	19085388	19085888	11,52	12,01	0,49	0,00444	0,0302	exon (FBgn0036844, exon 1 of 5)	exon (NM_140830, exon 1 of 5)	788	FBgn0036844|FBtr0333220
chr2L	18831434	18831934	10,97	11,47	0,49	0,00548	0,0346	promoter-TSS (FBgn0032715)	promoter-TSS (NM_001299137)	456	FBgn0015808|FBtr0081109
chr3L	21633723	21634223	12,23	12,71	0,49	0,00698	0,0417	exon (FBgn0037109, exon 2 of 4)	exon (NM_141084, exon 2 of 4)	473	FBgn0037109|FBtr0078464
chr3R	17671866	17672366	9,75	10,24	0,49	0,00732	0,0433	exon (FBgn0000063, exon 2 of 4)	exon (NM_142387, exon 2 of 4)	846	FBgn0000063|FBtr0083478
chr3R	16456267	16456767	11,34	11,84	0,5	2,13E-06	7,80E-05	TTS (FBgn0038431)	TTS (NM_001043252)	466	FBgn0038432|FBtr0083291
chr2R	17569013	17569513	11,44	11,94	0,5	3,06E-06	0,000102	promoter-TSS (FBgn0034243)	promoter-TSS (NM_137388)	532	FBgn0040294|FBtr0086828
chr3R	10045508	10046008	11,61	12,11	0,5	3,50E-06	0,000113	promoter-TSS (FBgn0037777)	promoter-TSS (NM_141713)	185	FBgn0037778|FBtr0082173
chr2L	20925542	20926042	11,39	11,88	0,5	4,94E-06	0,000147	TTS (FBgn0032907)	TTS (NM_136234)	355	FBgn0032906|FBtr0081438
chr3R	14328092	14328592	11,05	11,56	0,5	5,10E-06	0,00015	TTS (FBgn0038224)	TTS (NM_169579)	292	FBgn0003480|FBtr0082933
chr3L	12536602	12537102	11,57	12,06	0,5	5,52E-06	0,00016	TTS (FBgn0036302)	TTS (NM_001144471)	463	FBgn0036301|FBtr0075965
chr2R	13593843	13594343	11,71	12,22	0,5	8,66E-06	0,000227	promoter-TSS (FBgn0027581)	promoter-TSS (NM_001274029)	450	FBgn0033859|FBtr0087623
chr2R	8168111	8168611	11,21	11,71	0,5	9,76E-06	0,000253	TTS (FBgn0021995)	TTS (NM_143713)	414	FBgn0033273|FBtr0088789
chr3L	20426982	20427482	11,35	11,85	0,5	2,82E-05	0,000604	TTS (FBgn0036988)	TTS (NM_140966)	392	FBgn0036987|FBtr0078232
chr3R	5606001	5606501	11,69	12,18	0,5	2,90E-05	0,000614	exon (FBgn0261004, exon 2 of 3)	exon (NM_141300, exon 2 of 3)	292	FBgn0261004|FBtr0078743
chr3R	10043306	10043806	11,57	12,07	0,5	6,07E-05	0,00112	promoter-TSS (FBgn0053208)	promoter-TSS (NM_001316573)	287	FBgn0027524|FBtr0082172
chr3L	19092658	19093158	11,37	11,87	0,5	7,19E-05	0,00129	exon (FBgn0036846, exon 1 of 3)	exon (NM_079430, exon 1 of 2)	239	FBgn0036846|FBtr0075026
chr2R	12935752	12936252	11,63	12,13	0,5	0,000103	0,00172	promoter-TSS (FBgn0033785)	promoter-TSS (NM_176160)	533	FBgn0033784|FBtr0087803
chr2L	271009	271509	10,75	11,25	0,5	0,000184	0,00279	TTS (FBgn0086912)	TTS (NM_134667)	485	FBgn0031288|FBtr0078140
chr2L	277773	278273	11,88	12,38	0,5	0,00025	0,00355	promoter-TSS (FBgn0086855)	promoter-TSS (NM_001272882)	211	FBgn0086855|FBtr0330650
chr2R	9712774	9713274	11,46	11,96	0,5	0,00048	0,00577	exon (FBgn0010316, exon 1 of 3)	exon (NM_057600, exon 1 of 3)	704	FBgn0010316|FBtr0088469
chr3R	16433085	16433585	11,86	12,36	0,5	0,000686	0,00758	TTS (FBgn0051279)	TTS (NM_001170159)	338	FBgn0038424|FBtr0083286
chr3L	1731078	1731578	10,49	10,99	0,5	0,000801	0,00838	promoter-TSS (FBgn0027594)	promoter-TSS (NM_167911)	-221	FBgn0027594|FBtr0072798
chr3R	21130471	21130971	11,63	12,13	0,5	0,00106	0,0103	exon (FBgn0038860, exon 1 of 1)	exon (NM_142689, exon 1 of 1)	506	FBgn0038860|FBtr0084015
chr3L	11065187	11065687	11,41	11,91	0,5	0,00116	0,0109	promoter-TSS (FBgn0052075)	promoter-TSS (NM_140171)	447	FBgn0025355|FBtr0076203
chr2L	16287275	16287775	10,93	11,43	0,5	0,00118	0,011	promoter-TSS (FBgn0040079)	promoter-TSS (NM_135939)	205	FBgn0001994|FBtr0343814
chr2R	14161465	14161965	11,68	12,19	0,5	0,00135	0,0122	promoter-TSS (FBgn0033900)	promoter-TSS (NM_137086)	286	FBgn0033901|FBtr0087520
chr2L	9430500	9431000	10,25	10,75	0,5	0,0014	0,0126	promoter-TSS (FBgn0032117)	promoter-TSS (NM_080166)	302	FBgn0032117|FBtr0346623
chr2R	20618774	20619274	11,39	11,89	0,5	0,00239	0,0191	promoter-TSS (FBgn0050147)	promoter-TSS (NM_166402)	396	FBgn0034527|FBtr0086225
chr3R	9401579	9402079	11,59	12,09	0,5	0,00279	0,0214	promoter-TSS (FBgn0037686)	promoter-TSS (NM_169277)	335	FBgn0037687|FBtr0082029
chrX	4319756	4320256	11,8	12,3	0,5	0,00323	0,0241	exon (FBgn0266570, exon 2 of 2)	exon (NM_167007, exon 2 of 2)	569	FBgn0266570|FBtr0070648
chr3R	22042895	22043395	11,1	11,6	0,5	0,0033	0,0244	exon (FBgn0264491, exon 2 of 9)	exon (NM_001170213, exon 2 of 9)	955	FBgn0264491|FBtr0084178
chr2L	10488062	10488562	11,99	12,49	0,5	0,00348	0,0254	promoter-TSS (FBgn0032259)	promoter-TSS (NM_001038806)	310	FBgn0032258|FBtr0080038
chr2L	10427068	10427568	12,28	12,78	0,5	0,00366	0,0263	promoter-TSS (FBgn0262601)	promoter-TSS (NM_001201851)	432	FBgn0267330|FBtr0080021
chrX	16654426	16654926	12,01	12,51	0,5	0,00464	0,031	promoter-TSS (FBgn0003189)	promoter-TSS (NM_078653)	339	FBgn0003268|FBtr0074376
chrX	21027902	21028402	11	11,5	0,5	0,00478	0,0316	TTS (FBgn0031144)	TTS (NM_001144751)	209	FBgn0031143|FBtr0339633
chr3L	1546300	1546800	11,61	12,12	0,5	0,00495	0,0323	promoter-TSS (FBgn0052313)	promoter-TSS (NM_167894)	459	FBgn0041342|FBtr0072738
chr2R	17683771	17683271	11,13	11,63	0,5	0,00611	0,0377	promoter-TSS (FBgn0036059)	promoter-TSS (NM_206157)	-27	FBgn0036059|FBtr0086891
chr2L	6922813	6922313	10,7	11,2	0,5	0,00718	0,0427	intron (FBgn0004838, intron 1 of 4)	intron (NM_164720, intron 1 of 4)	425	FBgn0004838|FBtr0301404
chr2R	10478058	10478558	10,31	10,81	0,5	0,00823	0,0473	TTS (FBgn0033528)	TTS (NM_136747)	259	FBgn0261862|FBtr0088307
chr2R	17444193	17444693	11,59	12,09	0,5	0,0087	0,0491	TTS (FBgn0034219)	TTS (NM_176214)	495	FBgn0027506|FBtr0086958
chr2R	9959977	9960477	11,45	11,95	0,51	3,40E-06	0,000111	promoter-TSS (FBgn0033467)	promoter-TSS (NM_136694)	150	FBgn0283510|FBtr0339422
chr3R	5623641	5624141	11,03	11,54	0,51	4,81E-06	0,000146	promoter-TSS (FBgn0037351)	promoter-TSS (NM_141303)	234	FBgn0044823|FBtr0078739
chr3R	22025026	22025526	11,09	11,61	0,51	5,28E-06	0,000155	TTS (FBgn0038923)	TTS (NM_142746)	230	FBgn0038924|FBtr0084186
chr3R	16650490	16650990	11,47	11,98	0,51	6,03E-06	0,000172	TTS (FBgn0015019)	TTS (NM_169727)	417	FBgn0015351|FBtr0336486
chr2L	10387013	10387513	11,49	11,99	0,51	8,29E-06	0,000221	promoter-TSS (FBgn0267821)	promoter-TSS (NM_001273412)	602	FBgn0032716|FBtr0080007
chr2R	15217474	15217974	11,82	12,32	0,51	1,97E-05	0,000447	TTS (FBgn0265656)	TTS (NM_137177)	393	FBgn0034001|FBtr0087400
chr2R	12593846	12594346	10,77	11,28	0,51	2,89E-05	0,000613	promoter-TSS (FBgn0266817)	promoter-TSS (NR_124527)	-269	FBgn0266817|FBtr0345538
chr3R	9591280	9591780	11	11,51	0,51	4,40E-05	0,000864	promoter-TSS (FBgn0037719)	promoter-TSS (NM_001014611)	222	FBgn0037720|FBtr0082075
chr3L	8891824	8892324	11,16	11,67	0,51	4,88E-05	0,000948	TTS (FBgn0263930)	TTS (NM_001259756)	429	FBgn0020633|FBtr0076585
chr3L	12277653	12278153	11,43	11,94	0,51	5,92E-05	0,0011	promoter-TSS (FBgn0036272)	promoter-TSS (NM_168496)	249	FBgn0036273|FBtr0076007
chr3R	31804733	31805233	11,29	11,8	0,51	0,000113	0,00185	promoter-TSS (FBgn0039881)	promoter-TSS (NM_170578)	295	FBgn0250755|FBtr0290135
chr2L	8308590	8309090	11,52	12,03	0,51	0,000122	0,00195	promoter-TSS (FBgn0032015)	promoter-TSS (NM_135360)	414	FBgn0032016|FBtr0079599
chr3R	9741090	9741590	11,4	11,91	0,51	0,000147	0,00231	exon (FBgn0037737, exon 2 of 2)	exon (NM_001104257, exon 2 of 3)	442	FBgn0037737|FBtr0082126
chr2L	10331715	10332215	11,83	12,34	0,51	0,000201	0,003	promoter-TSS (FBgn0032221)	promoter-TSS (NM_001103669)	495	FBgn0032222|FBtr0079992
chr2R	21141667	21142167	10,6	11,12	0,51	0,000253	0,00357	promoter-TSS (FBgn0034592)	promoter-TSS (NM_137708)	47	FBgn0034590|FBtr0342873
chr3L	9972913	9973413	10,67	11,19	0,51	0,000298	0,00402	exon (FBgn0259932, exon 3 of 3)	exon (NM_001169935, exon 3 of 3)	408	FBgn0263251|FBtr0076351
chr2L	15057453	15057953	10,77	11,28	0,51	3,00E-04	0,00404	promoter-TSS (FBgn0053679)	promoter-TSS (NM_001032102)	159	FBgn0000317|FBtr0080723
chr2L	4187062	4187562	11,33	11,84	0,51	0,000377	0,00483	promoter-TSS (FBgn0040102)	promoter-TSS (NM_144384)	481	FBgn0051961|FBtr0077484
chr3R	20293468	20293968	11,2	11,71	0,51	0,000392	0,00494	exon (FBgn0262582, exon 2 of 13)	exon (NM_001104373, exon 2 of 13)	475	FBgn0262582|FBtr0305026
chr2R	7512197	7512697	11,76	12,27	0,51	0,000493	0,0059	exon (FBgn0025185, exon 1 of 3)	exon (NM_136445, exon 1 of 3)	302	FBgn0025185|FBtr0088980
chr3R	13305149	13306138	10,55	11,06	0,51	0,000784	0,00827	intron (FBgn0052473, intron 1 of 6)	intron (NM_169504, intron 1 of 6)	881	FBgn0052473|FBtr0082743
chr3L	7974605	7975105	11,21	11,73	0,51	0,000862	0,00888	TTS (FBgn0035829)	TTS (NM_168247)	136	FBgn0027554|FBtr0076766
chr2R	22483434	22483934	11,88	12,39	0,51	0,000891	0,00909	TTS (FBgn0034733)	TTS (NM_137831)	382	FBgn0034734|FBtr0071833
chr3L	21031893	21032393	11,91	12,42	0,51	0,000914	0,00928	promoter-TSS (FBgn0037045)	promoter-TSS (NM_141021)	319	FBgn0028402|FBtr0078288
chr3R	13963282	13963782	11,77	12,28	0,51	0,00109	0,0105	exon (FBgn0038191, exon 2 of 5)	exon (NM_142067, exon 2 of 5)	642	FBgn0038191|FBtr0082876
chr3L	6750969	6751469	10,39	10,9	0,51	0,00142	0,0126	exon (FBgn0035713, exon 3 of 9)	exon (NM_206286, exon 3 of 9)	1533	FBgn0035713|FBtr0076950
chr3L	18866237	18866737	11,6	12,1	0,51	0,0017	0,0146	promoter-TSS (FBgn0267572)	promoter-TSS (NR_133274)	263	FBgn0036818|FBtr0308812
chrX	18504443	18504943	10,39	10,9	0,51	0,00172	0,0147	exon (FBgn0010194, exon 1 of 1)	exon (NM_057576, exon 1 of 1)	712	FBgn0010194|FBtr0343046
chr2R	9599029	9599529	11,51	12,01	0,51	0,00263	0,0205	TTS (FBgn0050340)	TTS (NM_165686)	453	FBgn0261016|FBtr0305178
chr3R	11963263	11963763	11,35	11,87	0,51	0,00269	0,0208	promoter-TSS (FBgn0260741)	promoter-TSS (NM_141875)	390	FBgn0000147|FBtr0082483
chr3R	20990066	20990566	10,13	10,64	0,51	0,00277	0,0213	intron (FBgn0013995, intron 1 of 8)	intron (NM_169941, intron 1 of 8)	267	FBgn0013995|FBtr0309202
chr3R	19029007	19029507	11,81	12,32	0,51	0,00339	0,025	promoter-TSS (FBgn0260779)	promoter-TSS (NM_142518)	327	FBgn0015781|FBtr0083713
chr3R	6379494	6379994	11,79	12,3	0,51	0,00497	0,0324	promoter-TSS (FBgn0030282)	promoter-TSS (NM_079522)	463	FBgn0027514|FBtr0332175
chr3R	29146410	29146910	11,63	12,15	0,51	0,00686	0,0413	TTS (FBgn0039640)	TTS (NM_170398)	233	FBgn0039641|FBtr0085412
chr2L	6447592	6448092	11,2	11,71	0,51	0,00751	0,0441	promoter-TSS (FBgn0031813)	promoter-TSS (NM_001144328)	20	FBgn0031813|FBtr0114603
chr3L	16111485	16111985	12,05	12,56	0,51	0,0083	0,0476	exon (FBgn0263603, exon 3 of 6)	exon (NM_176332, exon 3 of 6)	675	FBgn0263603|FBtr0075493
chr2R	7699583	7700083	11,93	12,44	0,51	0,00856	0,0486	promoter-TSS (FBgn0033212)	promoter-TSS (NM_001169606)	334	FBgn0050496|FBtr0088926
chr3R	31588808	31589308	11,41	11,93	0,52	8,89E-07	3,81E-05	TTS (FBgn0034268)	TTS (NM_057357)	386	FBgn0039854|FBtr0085796
chr3R	27679343	27679843	11,41	11,93	0,52	1,54E-06	5,87E-05	TTS (FBgn0033330)	TTS (NM_143321)	303	FBgn0039538|FBtr0085216
chr2R	9911219	9911719	11,22	11,75	0,52	2,13E-06	7,80E-05	exon (FBgn0033465, exon 2 of 5)	exon (NM_136692, exon 2 of 5)	577	FBgn0033465|FBtr0088384
chr3L	8308228	8308728	11,09	11,61	0,52	3,75E-06	0,00012	TTS (FBgn0266958)	TTS (NR_124832)	463	FBgn0035871|FBtr0076711
chr2R	17026193	17026693	11,03	11,55	0,52	4,94E-06	0,000147	promoter-TSS (FBgn0023172)	promoter-TSS (NM_206147)	550	FBgn0265540|FBtr0340132
chr2L	1128307	1128807	11,49	12	0,52	8,11E-06	0,00022	promoter-TSS (FBgn0031304)	promoter-TSS (NM_134725)	396	FBgn0016926|FBtr0072987
chr2L	9330861	9331361	11,23	11,76	0,52	8,58E-06	0,000227	TTS (FBgn0032109)	TTS (NM_001273358)	349	FBgn0010314|FBtr0079799
chr3R	17149762	17150262	11,32	11,84	0,52	1,23E-05	0,000309	promoter-TSS (FBgn0038490)	promoter-TSS (NM_142352)	346	FBgn0264291|FBtr0083408
chr3L	5563797	5564297	11,6	12,11	0,52	1,45E-05	0,00035	promoter-TSS (FBgn0029118)	promoter-TSS (NM_143706)	274	FBgn0029117|FBtr0072083
chr3L	17420891	17421391	10,68	11,2	0,52	7,63E-05	0,00134	TTS (FBgn0266669)	TTS (NM_140719)	373	FBgn0027660|FBtr0305232
chr3L	15968221	15968721	11,61	12,13	0,52	0,000112	0,00184	promoter-TSS (FBgn0263599)	promoter-TSS (NM_140561)	268	FBgn0036549|FBtr0075512
chr3R	15228575	15229075	11,98	12,5	0,52	0,000128	0,00205	promoter-TSS (FBgn0038307)	promoter-TSS (NM_169624)	583	FBgn0038306|FBtr0083134
chr2L	5944058	5944558	11,39	11,9	0,52	0,000656	0,00737	exon (FBgn0001128, exon 2 of 7)	exon (NM_001273184, exon 2 of 7)	344	FBgn0001128|FBtr0079148
chr3R	9532215	9532715	10,84	11,36	0,52	0,000765	0,00815	exon (FBgn0000244, exon 1 of 2)	exon (NM_001170099, exon 1 of 1)	546	FBgn0000244|FBtr0082119
chr2L	2977148	2977648	11,01	11,53	0,52	0,00092	0,00929	promoter-TSS (FBgn0031483)	promoter-TSS (NM_164518)	277	FBgn0031484|FBtr0343781
chr3L	19992280	19992780	11,69	12,21	0,52	0,00197	0,0164	intron (FBgn0036926, intron 1 of 3)	intron (NM_001300195, intron 1 of 5)	644	FBgn0036926|FBtr0074901
chr3R	31592920	31593420	10,97	11,49	0,52	0,00394	0,0278	TTS (FBgn0039855)	TTS (NM_001104521)	239	FBgn0039856|FBtr0344003
chrX	908615	909115	10,45	10,97	0,52	0,00406	0,0283	exon (FBgn0264449, exon 1 of 12)	5' UTR (NM_001272178, exon 1 of 12)	329	FBgn0264449|FBtr0332604
chrX	5330005	5330505	11,59	12,1	0,52	0,00508	0,0328	promoter-TSS (FBgn0029756)	promoter-TSS (NM_131988)	380	FBgn0026751|FBtr0070763
chr2L	11498406	11498906	12,06	12,57	0,52	0,00539	0,0342	exon (FBgn0032361, exon 2 of 5)	exon (NM_135659, exon 2 of 5)	292	FBgn0032361|FBtr0080248
chr3R	11430001	11430501	10,67	11,19	0,52	0,00579	0,0363	TTS (FBgn0037899)	TTS (NM_169389)	191	FBgn0037898|FBtr0300901

chr2L	568439	568939	12,09	12,6	0,52	0,00659	0,0399	promoter-TSS (FBgn0021874)	promoter-TSS (NM_057946)	350	FBgn0031266|FBtr0078068
chrX	18409490	18409990	10,92	11,44	0,52	0,00802	0,0465	intron (FBgn0052549, intron 1 of 9)	intron (NM_206786, intron 1 of 9)	404	FBgn0052549|FBtr0074570
chr3L	18998416	18998916	9,24	9,76	0,52	0,00836	0,0478	promoter-TSS (FBgn0036837)	promoter-TSS (NM_176346)	-383	FBgn0036837|FBtr0075043
chr3R	5733772	5734272	11,96	12,48	0,52	0,00841	0,048	TTS (FBgn0037369)	TTS (NM_001170041)	510	FBgn0037368|FBtr0078720
chr2L	2740373	2740873	11,22	11,75	0,53	9,39E-07	3,93E-05	promoter-TSS (FBgn0031450)	promoter-TSS (NM_164497)	-371	FBgn0031450|FBtr0089749
chr3L	13966631	13967131	10,94	11,47	0,53	2,48E-06	8,66E-05	exon (FBgn0263232, exon 2 of 5)	exon (NM_168566, exon 2 of 5)	1679	FBgn0036389|FBtr0075759
chrX	19605348	19605848	11,05	11,58	0,53	5,75E-06	0,000165	exon (FBgn0031037, exon 1 of 4)	exon (NM_167669, exon 1 of 5)	400	FBgn0031037|FBtr0074733
chr3L	3466574	3467074	11,49	12,03	0,53	9,25E-06	0,000242	TTS (FBgn0041164)	TTS (NM_001014556)	397	FBgn0010317|FBtr0073127
chr3L	19834565	19835065	11,55	12,08	0,53	1,34E-05	0,000327	promoter-TSS (FBgn0003744)	promoter-TSS (NM_079446)	146	FBgn0052221|FBtr0301008
chrX	16942262	16942762	11,87	12,4	0,53	2,64E-05	0,000569	promoter-TSS (FBgn0030808)	promoter-TSS (NM_001042817)	359	FBgn0030806|FBtr0074417
chr2R	6015060	6015560	11,35	11,89	0,53	2,65E-05	0,000571	exon (FBgn0000043, exon 2 of 2)	exon (NM_078901, exon 2 of 2)	379	FBgn0000043|FBtr0086029
chr2L	18943230	18943730	10,88	11,41	0,53	2,98E-05	0,000625	exon (FBgn0032723, exon 1 of 11)	5'UTR (NM_136073, exon 1 of 11)	480	FBgn0032723|FBtr0342929
chr2R	24767202	24767702	11,06	11,6	0,53	3,08E-05	0,00064	TTS (FBgn0035060)	TTS (NM_166687)	255	FBgn0027590|FBtr0343496
chr3L	12193004	12193504	11,68	12,21	0,53	0,00012	0,00193	TTS (FBgn0000594)	TTS (NM_176323)	434	FBgn0036263|FBtr0346911
chr2R	22421070	22421570	11,5	12,04	0,53	0,00016	0,00248	promoter-TSS (FBgn0034727)	promoter-TSS (NM_079087)	308	FBgn0034728|FBtr0301668
chr2L	13829987	13830487	11,79	12,32	0,53	0,00023	0,00333	promoter-TSS (FBgn0001961)	promoter-TSS (NM_165063)	401	FBgn0015271|FBtr0080543
chr3R	9015608	9016108	11,59	12,12	0,53	0,000237	0,00341	promoter-TSS (FBgn0037655)	promoter-TSS (NM_001170091)	413	FBgn0037656|FBtr0081967
chr3L	18819945	18820445	10,96	11,49	0,53	0,00039	0,00494	promoter-TSS (FBgn0036815)	promoter-TSS (NM_168777)	480	FBgn0036814|FBtr0075084
chr2L	7222445	7222945	12,08	12,61	0,53	0,000527	0,00621	TTS (FBgn0259111)	TTS (NM_001273254)	386	FBgn0263133|FBtr0079413
chrX	2704802	2705302	12,06	12,59	0,53	0,000554	0,00642	exon (FBgn0024996, exon 3 of 5)	exon (NM_130664, exon 3 of 5)	482	FBgn0024996|FBtr0070479
chr2R	17431148	17431648	11,37	11,9	0,53	0,00093	0,00934	promoter-TSS (FBgn0025716)	promoter-TSS (NM_137365)	367	FBgn0034217|FBtr0086917
chr2L	9790963	9791463	11,88	12,41	0,53	0,000976	0,00963	promoter-TSS (FBgn0042174)	TTS (NM_001273372)	317	FBgn0032349|FBtr0079870
chr3L	835901	836401	11,76	12,3	0,53	0,00109	0,0104	TTS (FBgn0260755)	TTS (NM_138217)	469	FBgn0260756|FBtr0301253
chr2R	6613924	6614424	11,56	12,08	0,53	0,00122	0,0113	exon (FBgn0086655, exon 2 of 7)	exon (NM_001103730, exon 2 of 7)	407	FBgn0086655|FBtr0301636
chr2R	10782458	10782958	11,19	11,72	0,53	0,00137	0,0124	promoter-TSS (FBgn0265345)	promoter-TSS (NR_124506)	161	FBgn0053144|FBtr0088254
chr2L	13219080	13219580	11,58	12,11	0,53	0,00168	0,0145	promoter-TSS (FBgn0032486)	promoter-TSS (NM_135773)	593	FBgn0032485|FBtr0080484
chr3R	29033410	29033910	12	12,53	0,53	0,00346	0,0254	promoter-TSS (FBgn0027873)	promoter-TSS (NM_143401)	348	FBgn0039625|FBtr0085419
chr2L	1610735	1611235	11,37	11,91	0,53	0,00366	0,0263	promoter-TSS (FBgn0031351)	promoter-TSS (NM_134765)	172	FBgn0051935|FBtr0077916
chr2R	9139167	9139667	10,55	11,08	0,53	0,00367	0,0263	exon (FBgn0265313, exon 2 of 3)	5'UTR (NM_001299303, exon 2 of 3)	336	FBgn0265313|FBtr0344468
chr3R	25126967	25127467	11,21	11,74	0,53	0,00392	0,0277	promoter-TSS (FBgn0259152)	promoter-TSS (NM_001170250)	142	FBgn0039280|FBtr0084782
chr3R	15837321	15837821	11,08	11,6	0,53	0,00507	0,0328	promoter-TSS (FBgn0017567)	promoter-TSS (NM_079980)	153	FBgn0004883|FBtr0083183
chr2L	4882066	4882566	11,59	12,12	0,53	0,00597	0,0372	promoter-TSS (FBgn0031643)	promoter-TSS (NM_135027)	791	FBgn0000286|FBtr0304887
chr3R	9629823	9630323	12,01	12,54	0,53	0,00724	0,0429	exon (FBgn0005585, exon 3 of 4)	exon (NM_079569, exon 3 of 4)	778	FBgn0005585|FBtr0334618
chr2R	24786678	24787178	10,96	11,5	0,54	1,71E-06	6,45E-05	exon (FBgn0041205, exon 2 of 6)	exon (NM_079132, exon 2 of 6)	483	FBgn0041205|FBtr0072428
chrX	496681	497181	11,47	12,01	0,54	2,89E-06	9,79E-05	TTS (FBgn0023534)	TTS (NM_130490)	443	FBgn0266196|FBtr0343793
chr3L	18901669	18902169	11,73	12,27	0,54	3,01E-06	0,000101	promoter-TSS (FBgn0036826)	promoter-TSS (NM_140814)	326	FBgn0036827|FBtr0075067
chr2L	7800638	7801138	11,17	11,71	0,54	3,17E-06	0,000105	promoter-TSS (FBgn0031950)	promoter-TSS (NM_135307)	507	FBgn0031951|FBtr0301329
chr2R	13230559	13231059	11,38	11,92	0,54	3,90E-06	0,000124	promoter-TSS (FBgn0033812)	promoter-TSS (NM_137006)	227	FBgn0033813|FBtr0087742
chr3R	17001628	17002128	11,11	11,65	0,54	8,32E-06	0,000221	promoter-TSS (FBgn0038465)	promoter-TSS (NM_142327)	477	FBgn0266917|FBtr0083374
chr3L	21317322	21317822	11,77	12,31	0,54	4,85E-05	0,000946	TTS (FBgn0267234)	TTS (NR_125033)	448	FBgn0000147|FBtr0078405
chr3R	29933378	29933878	11,64	12,17	0,54	6,25E-05	0,00115	promoter-TSS (FBgn0051040)	promoter-TSS (NM_143493)	342	FBgn0260759|FBtr0301256
chr3L	4826006	4826506	12,06	12,59	0,54	0,000131	0,00208	promoter-TSS (FBgn0261797)	promoter-TSS (NM_168103)	404	FBgn0027085|FBtr0073348
chr2R	13509669	13510169	11,03	11,56	0,54	0,000161	0,00248	TTS (FBgn0024556)	TTS (NM_001169673)	302	FBgn0033846|FBtr0301388
chr3R	8805066	8805566	11,17	11,71	0,54	0,000272	0,00377	exon (FBgn0037633, exon 2 of 3)	exon (NM_141579, exon 1 of 2)	283	FBgn0037633|FBtr0081934
chr2R	8939142	8939642	11	11,55	0,54	0,000284	0,00388	exon (FBgn0033354, exon 2 of 13)	exon (NM_136585, exon 2 of 13)	397	FBgn0033354|FBtr0088675
chr2R	8444632	8445132	10,32	10,86	0,54	0,00044	0,00541	exon (FBgn0044469, exon 2 of 7)	promoter-TSS (NR_048064)	-117	FBgn0262316|FBtr0304480
chrX	11887455	11887955	11,99	12,53	0,54	0,000562	0,0065	promoter-TSS (FBgn0030349)	promoter-TSS (NM_001272545)	422	FBgn0030350|FBtr0073570
chr3R	14730541	14731041	10,27	10,82	0,54	0,00062	0,00702	exon (FBgn0038256, exon 1 of 5)	5'UTR (NM_142130, exon 1 of 5)	483	FBgn0038256|FBtr0083021
chr3R	18301005	18301505	11,61	12,15	0,54	0,000731	0,00792	TTS (FBgn0038602)	TTS (NM_142452)	473	FBgn0038601|FBtr0083594
chrX	19601253	19601753	11,89	12,43	0,54	0,000944	0,0094	exon (FBgn0031036, exon 2 of 4)	exon (NM_134481, exon 2 of 4)	348	FBgn0031036|FBtr0307162
chr3R	28337137	28337637	10,68	11,22	0,54	0,00117	0,0109	promoter-TSS (FBgn0261618)	promoter-TSS (NM_170365)	499	FBgn0262773|FBtr0347337
chr2R	6675204	6675704	11,55	12,08	0,54	0,00154	0,0136	promoter-TSS (FBgn0033092)	promoter-TSS (NM_165484)	351	FBgn0033089|FBtr0307502
chr2R	20258031	20258531	11,29	11,84	0,54	0,00271	0,0209	promoter-TSS (FBgn0025720)	promoter-TSS (NM_001274172)	289	FBgn0034491|FBtr0086272
chr2R	10820131	10820631	12,25	12,79	0,54	0,0043	0,0295	promoter-TSS (FBgn0086898)	promoter-TSS (NM_165800)	404	FBgn0029134|FBtr0088224
chr2R	19496158	19496658	12,24	12,78	0,54	0,00456	0,0307	exon (FBgn0261456, exon 1 of 2)	exon (NM_001274163, exon 1 of 2)	448	FBgn0261456|FBtr0331920
chrX	18099932	18100432	9,33	9,88	0,54	0,00512	0,033	promoter-TSS (FBgn0030894)	promoter-TSS (NM_167602)	79	FBgn0030894|FBtr0310272
chr2L	6065408	6065908	12,02	12,55	0,54	0,00536	0,034	promoter-TSS (FBgn0031774)	promoter-TSS (NM_164680)	295	FBgn0031773|FBtr0079215
chr3R	20328980	20329480	10,21	10,75	0,54	0,00542	0,0344	exon (FBgn0038788, exon 4 of 4)	exon (NM_142623, exon 4 of 4)	766	FBgn0038788|FBtr0083882
chrX	10890154	10890654	9,69	10,23	0,54	0,00566	0,0356	exon (FBgn0017561, exon 1 of 7)	5'UTR (NM_078557, exon 1 of 7)	416	FBgn0017561|FBtr0073404
chr2L	245546	246046	9,23	9,77	0,54	0,00759	0,0445	intron (FBgn0266557, intron 1 of 16)	intron (NM_001258891, intron 1 of 16)	-2720	FBgn0262752|FBtr0304344
chrX	15577347	15577847	11,23	11,78	0,55	9,94E-07	4,10E-05	promoter-TSS (FBgn0030658)	promoter-TSS (NM_132816)	401	FBgn0030657|FBtr0089702
chr2R	9093883	9094383	11,44	11,98	0,55	1,06E-06	4,33E-05	exon (FBgn0033374, exon 2 of 3)	exon (NM_176109, exon 2 of 3)	525	FBgn0033374|FBtr0088632
chr2R	7924303	7924803	11,24	11,79	0,55	2,67E-06	9,17E-05	intron (FBgn0033233, intron 2 of 3)	intron (NM_001259265, intron 2 of 3)	435	FBgn0033233|FBtr0088886
chr3R	18659727	18660227	11,8	12,35	0,55	2,66E-06	9,17E-05	promoter-TSS (FBgn0051224)	promoter-TSS (NM_169826)	360	FBgn0027841|FBtr0083660
chr2R	14871627	14872127	10,86	11,41	0,55	5,29E-06	0,000155	promoter-TSS (FBgn0264962)	promoter-TSS (NM_001169683)	190	FBgn0013773|FBtr0087450
chrX	2713351	2713851	11,66	12,22	0,55	8,26E-06	0,000221	promoter-TSS (FBgn0024991)	promoter-TSS (NM_166949)	359	FBgn0024998|FBtr0070499
chr2R	14163736	14164236	11,74	12,29	0,55	1,10E-05	0,000281	TTS (FBgn0033901)	TTS (NM_001299477)	635	FBgn0033902|FBtr0339964
chrX	15984036	15984536	11,38	11,93	0,55	4,09E-05	0,000814	exon (FBgn0030717, exon 3 of 4)	exon (NM_132868, exon 3 of 4)	515	FBgn0030717|FBtr0074134
chr3R	9555865	9556365	11,76	12,3	0,55	4,14E-05	0,000821	promoter-TSS (FBgn0037708)	promoter-TSS (NM_141647)	331	FBgn0037709|FBtr0082067
chr2R	10124932	10125432	11,12	11,67	0,55	5,10E-05	0,000977	promoter-TSS (FBgn0050011)	promoter-TSS (NM_165750)	-313	FBgn0050011|FBtr0089759
chr3R	24161787	24162287	11,5	12,05	0,55	7,17E-05	0,00129	promoter-TSS (FBgn0039157)	promoter-TSS (NM_001032037)	311	FBgn0039158|FBtr0084551
chr3L	20226638	20227138	11,32	11,87	0,55	0,000135	0,00214	exon (FBgn0260397, exon 2 of 4)	exon (NM_168835, exon 2 of 4)	508	FBgn0260397|FBtr0074825
chr3R	27929793	27930293	11,82	12,38	0,55	0,000178	0,027	exon (FBgn0027579, exon 3 of 8)	exon (NM_170359, exon 2 of 7)	419	FBgn0027579|FBtr0085251
chr3R	12691934	12692434	11,94	12,49	0,55	0,00021	0,00309	promoter-TSS (FBgn0005355)	promoter-TSS (NM_080502)	413	FBgn0051347|FBtr0082664
chr3R	25686503	25687003	11,95	12,5	0,55	0,000244	0,00347	exon (FBgn0039360, exon 2 of 5)	exon (NM_170238, exon 2 of 5)	396	FBgn0039360|FBtr0084930
chr2R	23063627	23064127	11,71	12,26	0,55	0,000784	0,00827	promoter-TSS (FBgn0261363)	promoter-TSS (NM_080021)	383	FBgn0034814|FBtr0071084
chr2R	14852832	14853332	11,32	11,87	0,55	0,00101	0,00984	promoter-TSS (FBgn0027783)	promoter-TSS (NM_137151)	142	FBgn0028434|FBtr0087448
chr3R	31805711	31806211	11,23	11,78	0,55	0,00136	0,0124	promoter-TSS (FBgn0250755)	promoter-TSS (NM_143642)	283	FBgn0039881|FBtr0305131
chr2L	17496710	17497210	10,37	10,93	0,55	0,0018	0,0153	promoter-TSS (FBgn0267229)	promoter-TSS (NR_124331)	-50	FBgn0267279|FBtr0346495
chr3R	5735764	5736264	11,66	12,2	0,55	0,00199	0,0165	promoter-TSS (FBgn0037370)	promoter-TSS (NM_141322)	341	FBgn0037369|FBtr0301574
chrX	15761496	15761996	11,76	12,32	0,55	0,00204	0,0169	exon (FBgn0030686, exon 3 of 4)	exon (NM_078611, exon 3 of 4)	499	FBgn0030686|FBtr0074090
chr3L	440300	440800	10,17	10,72	0,55	0,00279	0,0214	exon (FBgn0001316, exon 1 of 4)	exon (NM_001103992, exon 1 of 4)	546	FBgn0001316|FBtr0112807
chrX	10475019	10475519	12,1	12,65	0,55	0,00279	0,0214	promoter-TSS (FBgn0261710)	promoter-TSS (NM_167231)	554	FBgn0030206|FBtr0307487
chr3L	9460923	9461423	9,76	10,31	0,55	0,00291	0,0221	promoter-TSS (FBgn0036000)	promoter-TSS (NM_140063)	124	FBgn0266301|FBtr0343555
chrX	5963593	5964093	11,75	12,3	0,55	0,00402	0,0281	exon (FBgn0005390, exon 1 of 7)	exon (NM_132056, exon 1 of 7)	404	FBgn0005390|FBtr0070892
chr3L	19922020	19922520	9,78	10,33	0,55	0,00409	0,0284	exon (FBgn0020887, exon 3 of 7)	exon (NM_168826, exon 3 of 6)	1192	FBgn0020887|FBtr0074916
chr3R	24718715	24719215	12,14	12,69	0,55	0,00411	0,0285	promoter-TSS (FBgn0004885)	promoter-TSS (NM_170168)	399	FBgn0039219|FBtr0084745
chr3R	22749910	22750410	11,77	12,32	0,55	0,00459	0,0308	promoter-TSS (FBgn0039026)	promoter-TSS (NM_001044410)	437	FBgn0086253|FBtr0084320
chrX	19866610	19867110	11	11,55	0,55	0,00511	0,033	exon (FBgn0052529, exon 2 of 9)	5'UTR (NM_001272807, exon 2 of 9)	667	FBgn0052529|FBtr0306520
chr2L	22168025	22168525	11,02	11,57	0,55	0,00517	0,0332	exon (FBgn0032979, exon 3 of 7)	exon (NM_001014498, exon 3 of 7)	868	FBgn0032979|FBtr0100407
chr3R	11231273	11231773	11,83	12,38	0,55	0,00535	0,034	promoter-TSS (FBgn0037881)	promoter-TSS (NM_141798)	356	FBgn0037882|FBtr0082365
chr2L	12427220	12427720	11,35	11,91	0,55	0,00624	0,0383	promoter-TSS (FBgn0032430)	promoter-TSS (NM_135722)	239	FBgn0032429|FBtr0333094
chr3R	20818342	20818842	11,58	12,13	0,55	0,00712	0,0424	TTS (FBgn0038825)	TTS (NM_001043269)	337	FBgn0038828|FBtr0083994
chr3L	349129	349629	8,92	9,47	0,55	0,00864	0,0489	intron (FBgn0261985, intron 1 of 9)	CpG	-1695	FBgn0261985|FBtr0306559
chr2L	16261017	16261517	11,4	11,96	0,56	8,25E-07	3,56E-05	promoter-TSS (FBgn0028897)	promoter-TSS (NM_135938)	497	FBgn0000673|FBtr0331445
chr3L	2376891	2377391	11,47	12,03	0,56	1,51E-06	5,78E-05	promoter-TSS (FBgn0266696)	promoter-TSS (NM_001274398)	415	FBgn0035337|FBtr0072899
chr3R	16481232	16481732	11,38	11,95	0,56	4,88E-06	0,000147	promoter-TSS (FBgn0267693)	promoter-TSS (NR_133407)	249	FBgn0004087|FBtr0083295
chr3L	15987264	15987764	11,71	12,27	0,56	8,16E-06	0,00022	promoter-TSS (FBgn0259824)	promoter-TSS (NM_140567)	-269	FBgn0266995|FBtr0345917
chr2L	16307547	16308047	11,76	12,32	0,56	1,19E-05	3,00E-04	promoter-TSS (FBgn0015338)	promoter-TSS (NM_135945)	452	FBgn0011708|FBtr0080831
chrX	18646729	18647229	10,78	11,35	0,56	1,24E-05	0,000309	intron (FBgn0027335, intron 1 of 5)	CpG	588	FBgn0027335|FBtr0074616
chr3R	19161604	19162104	12,1	12,66	0,56	7,10E-05	0,00128	exon (FBgn0259705, exon 2 of 2)	exon (NM_142530, exon 2 of 4)	446	FBgn0259704|FBtr0299957
chr2R	13989710	13990210	10,9	11,45	0,56	7,55E-05	0,00133	exon (FBgn0020620, exon 2 of 7)	promoter-TSS (NM_001201996)	440	FBgn0020620|FBtr0330626
chr3R	27925598	27926098	10,73	11,29	0,56	7,88E-05	0,00138	promoter-TSS (FBgn0267126)	promoter-TSS (NR_125280)	184	FBgn0027579|FBtr0335011
chr3L	20347486	20347986	11,3	11,86	0,56	9,46E-05	0,00162	promoter-TSS (FBgn0036974)	promoter-TSS (NM_168848)	206	FBgn0036973|FBtr0078242
chr3R	27111386	27111886	11,53	12,08	0,56	0,000202	0,00301	promoter-TSS (FBgn0027574)	promoter-TSS (NM_170317)	189	FBgn0039487|FBtr0345216
chr3R	25247959	25248459	11,9	12,45	0,56	0,000383	0,00488	promoter-TSS (FBgn0039300)	promoter-TSS (NM_143102)	339	FBgn0039301|FBtr0084812
chr3L	19632125	19632625	10,16	10,72	0,56	0,000677	0,0075	exon (FBgn0036896, exon 1 of 7)	exon (NM_001202203, exon 1 of 7)	721	FBgn0036896|FBtr0302513
chr2R	22805560	22806060	11,35	11,91	0,56	0,00147	0,013	exon (FBgn0000405, exon 3 of 5)	exon (NM_166558, exon 2 of 4)	493	FBgn0000405|FBtr0071914
chr2R	11288080	11288580	10,47	11,03	0,56	0,00156	0,0136	exon (FBgn0033609, exon 2 of 9)	exon (NM_165816, exon 2 of 9)	1442	FBgn0033609|FBtr0088178
chr3R	10389021	10389521	11,2	11,76	0,56	0,0025	0,0197	exon (FBgn0259938, exon 1 of 3)	5'UTR (NM_080036, exon 1 of 4)	1014	FBgn0259938|FBtr0082246
chr3L	19817100	19817600	11,02	11,58	0,56	0,00281	0,0215	promoter-TSS (FBgn0013799)	promoter-TSS (NM_001038944)	440	FBgn0036911|FBtr0332727
chr2R	10420575	10421075	9,54	10,11	0,56	0,00354	0,0257	promoter-TSS (FBgn0053474)	promoter-TSS (NM_206078)	244	FBgn0033519|FBtr0088316
chrX	18500029	18500529	10,71	11,27	0,56	0,00449	0,0304	promoter-TSS (FBgn0030930)	promoter-TSS (NM_167623)	153	FBgn0030931|FBtr0074592
chrX	12759559	12760059	10,43	11	0,56	0,00462	0,031	TTS (FBgn0030420)	TTS (NM_001298238)	808	FBgn0020513|FBtr0333799
chr2R	7964994	7965494	11,24	11,8	0,56	0,00522	0,0334	TTS (FBgn0033243)	TTS (NM_001299247)	2780	FBgn0033243|FBtr0339127
chrX	8563117	8563617	9,24	9,8	0,56	0,00591	0,0368	exon (FBgn0030049, exon 2 of 5)	5'UTR (NM_001103444, exon 2 of 6)	1673	FBgn0030049|FBtr0331723
chr2L	478161	478661	9,32	9,88	0,56	0,00624	0,0383	exon (FBgn0043364, exon 1 of 1)	5'UTR (NM_134685, exon 1 of 1)	1277	FBgn0043364|FBtr0078083
chr2R	8086265	8086765	8,59	9,15	0,56	0,00661	0,04	promoter-TSS (FBgn0028562)	promoter-TSS (NM_079993)	-880	FBgn0028562|FBtr0088778
chrX	1617075	1617575	9,34	9,9	0,56	0,00713	0,0424	intron (FBgn0283451, intron 2 of 8)	intron (NM_166895, intron 1 of 7)	830	FBgn0025390|FBtr0303587
chr2L	3515617	3516117	9,35	9,9	0,56	0,00817	0,0471	exon (FBgn0031544, exon 2 of 4)	exon (NM_001273069, exon 2 of 4)	996	FBgn0031544|FBtr0077525
chr2R	8132151	8132651	11,56	12,12	0,56	0,00821	0,0473	exon (FBgn0005648, exon 3 of 5)	exon (NM_165589, exon 3 of 5)	971	FBgn0005648|FBtr0088786
chr2L	2972991	2973491	11,13	11,71	0,57	1,40E-06	5,47E-05	promoter-TSS (FBgn0004584)	promoter-TSS (NM_001144304)	351	FBgn0260639|FBtr0077641
chr2L	13367868	13368368	11,36	11,93	0,57	1,44E-06	5,61E-05	TTS (FBgn0032509)	TTS (NM_135797)	502	FBgn0051852|FBtr0080466
chr2R	9871721	9872221	11,77	12,34	0,57	2,25E-06	8,19E-05	exon (FBgn0033458, exon 1 of 7)	exon (NM_136685, exon 1 of 2)	502	FBgn0033458|FBtr0088376
chr2R	7219424	7219924	10,73	11,31	0,57	4,39E-06	0,000138	promoter-TSS (FBgn0266324)	promoter-TSS (NR_124131)	359	FBgn0031897|FBtr0330197
chr2R	10821445	10821945	10,77	11,34	0,57	7,51E-06	0,000207	promoter-TSS (FBgn0033555)	promoter-TSS (NM_136772)	20	FBgn0033555|FBtr0088226
chr2R	10422144	10422644	11,47	12,03	0,57	2,94E-05	0,000619	promoter-TSS (FBgn0032246)	promoter-TSS (NM_135556)	386	FBgn0005683|FBtr0333490
chr2R	5698292	5698792	11,04	11,61	0,57	2,94E-05	0,000619	promoter-TSS (FBgn0259979)	promoter-TSS (NM_001299213)	85	FBgn0259979|FBtr0345358
chr2L	13548477	13548977	10,45	11,02	0,57	6,28E-05	0,00115	promoter-TSS (FBgn0023407)	promoter-TSS (NM_165046)	601	FBgn0023407|FBtr0332509
chr2R	17580759	17581259	10,48	11,05	0,57	0,00026	0,00363	TTS (FBgn0034247)	TTS (NM_137390)	516	FBgn0034246|FBtr0086904
chr2L	10729205	10729705	11,05	11,62	0,57	0,00032	0,00425	promoter-TSS (FBgn0032291)	promoter-TSS (NM_164941)	478	FBgn0032290|FBtr0080110

chrX	19750996	19751496	11,08	11,65	0,57	0,000995	0,00975	exon (FBgn0031069, exon 1 of 8)	5' UTR (NM_001272805, exon 1 of 8)	477	FBgn0031069	FBtr0074795
chr3L	16379878	16380832	10,57	11,13	0,57	0,00158	0,0138	intron (FBgn0036622, intron 2 of 4)	intron (NM_001275013, intron 2 of 4)	826	FBgn0036622	FBtr0075422
chrX	2187087	2187587	10,7	11,27	0,57	0,00173	0,0148	promoter-TSS (FBgn0024984)	promoter-TSS (NM_130629)	-482	FBgn0024984	FBtr0070392
chr2L	20084416	20084916	11,6	12,17	0,57	0,00184	0,0156	exon (FBgn0263773, exon 1 of 2)	exon (NM_001273688, exon 1 of 2)	404	FBgn0263773	FBtr0310560
chrX	8689514	8690014	11,58	12,15	0,57	0,00192	0,0161	promoter-TSS (FBgn0027864)	promoter-TSS (NM_132271)	282	FBgn0030057	FBtr0071225
chr3R	30783554	30784054	10,24	10,8	0,57	0,00211	0,0173	promoter-TSS (FBgn0266699)	promoter-TSS (NR_125303)	-159	FBgn0266699	FBtr0345123
chr2L	20680929	20681429	11,42	12	0,57	0,00301	0,0228	exon (FBgn0032876, exon 1 of 1)	exon (NM_165338, exon 1 of 1)	447	FBgn0032876	FBtr0081401
chr2L	3037623	3038123	12,02	12,59	0,57	0,00351	0,0256	promoter-TSS (FBgn0031497)	promoter-TSS (NM_001273053)	368	FBgn0031498	FBtr0335478
chr2L	6051377	6051877	10,4	10,97	0,57	0,00382	0,0271	exon (FBgn0031769, exon 2 of 4)	5' UTR (NM_164679, exon 2 of 4)	789	FBgn0031769	FBtr0079185
chr3L	14762801	14763301	8,8	9,37	0,57	0,00464	0,031	intron (FBgn0036446, intron 1 of 3)	intron (NM_001274918, intron 1 of 3)	1024	FBgn0036446	FBtr0075690
chr3R	10887776	10888276	10	10,57	0,57	0,00478	0,0316	exon (FBgn0042094, exon 2 of 2)	exon (NM_169373, exon 2 of 2)	1255	FBgn0042094	FBtr0339379
chr3L	3053082	3053582	9,36	9,94	0,57	0,00606	0,0374	exon (FBgn0035392, exon 3 of 7)	exon (NM_167973, exon 3 of 7)	674	FBgn0035392	FBtr0072987
chr2R	12917919	12918419	10,05	10,62	0,57	0,00707	0,0422	exon (FBgn0010488, exon 2 of 4)	5' UTR (NM_001038854, exon 2 of 4)	312	FBgn0010488	FBtr0087787
chr2L	7027637	7028137	11,47	12,04	0,57	0,00771	0,045	promoter-TSS (FBgn0051908)	promoter-TSS (NM_164727)	362	FBgn0031881	FBtr0079389
chr2L	16039162	16039662	9,09	9,66	0,57	0,00794	0,0462	exon (FBgn0028644, exon 8 of 8)	exon (NM_078856, exon 8 of 8)	-2634	FBgn0000182	FBtr0080803
chr2R	18850823	18851323	11,44	12,02	0,58	6,03E-07	2,69E-05	promoter-TSS (FBgn0034401)	promoter-TSS (NM_137538)	230	FBgn0034402	FBtr0086619
chr3L	9968474	9968974	10,96	11,54	0,58	6,15E-07	2,72E-05	promoter-TSS (FBgn0036062)	promoter-TSS (NM_140119)	246	FBgn0026404	FBtr0076347
chr2L	4883510	4884010	11,51	12,09	0,58	1,14E-06	4,56E-05	promoter-TSS (FBgn0000286)	promoter-TSS (NM_001273128)	463	FBgn0031643	FBtr0077389
chr3L	12267595	12268095	11,4	11,98	0,58	1,26E-06	4,98E-05	exon (FBgn0052100, exon 2 of 2)	exon (NM_168495, exon 2 of 2)	318	FBgn0052100	FBtr0076006
chr3L	2373956	2374456	11,53	12,11	0,58	1,46E-06	5,64E-05	promoter-TSS (FBgn0035335)	promoter-TSS (NM_001144401)	479	FBgn0035336	FBtr0072890
chr2L	10223016	10223516	10,67	11,25	0,58	2,46E-06	8,61E-05	TTS (FBgn0250843)	TTS (NM_078805)	610	FBgn0032195	FBtr0079949
chr3L	21515408	21515908	10,76	11,34	0,58	1,16E-05	0,000294	promoter-TSS (FBgn0037093)	promoter-TSS (NM_168912)	229	FBgn0026371	FBtr0078387
chr2L	12027500	12028000	10,49	11,07	0,58	2,60E-05	0,000563	exon (FBgn0010497, exon 1 of 5)	5' UTR (NM_138760, exon 1 of 5)	313	FBgn0010497	FBtr0080292
chrX	7109448	7109948	10,99	11,57	0,58	2,82E-05	0,000604	exon (FBgn0027342, exon 2 of 4)	5' UTR (NM_167119, exon 2 of 4)	623	FBgn0027342	FBtr0071017
chr3L	19487911	19488411	11,47	12,05	0,58	2,91E-05	0,000614	exon (FBgn0062928, exon 1 of 4)	exon (NM_168799, exon 2 of 2)	278	FBgn0062928	FBtr0091951
chr3R	10144967	10145467	10,59	11,17	0,58	9,98E-05	0,00168	exon (FBgn0086359, exon 1 of 9)	5' UTR (NM_143815, exon 1 of 9)	550	FBgn0086359	FBtr0082181
chr2R	11899751	11900251	11,59	12,17	0,58	0,000118	0,00192	exon (FBgn0033665, exon 1 of 1)	exon (NM_136868, exon 1 of 1)	485	FBgn0033665	FBtr0088038
chr2L	1981225	1981725	11,47	12,05	0,58	0,000301	0,00404	promoter-TSS (FBgn0031377)	promoter-TSS (NM_134791)	300	FBgn0031378	FBtr0077814
chrX	1874083	1874583	12,02	12,59	0,58	0,000421	0,00522	promoter-TSS (FBgn0023517)	promoter-TSS (NM_130595)	481	FBgn0014411	FBtr0070311
chr2L	8522287	8522787	10,14	10,72	0,58	0,000457	0,00556	TTS (FBgn0032055)	TTS (NM_001273328)	605	FBgn0016122	FBtr0079685
chr3L	11215639	11216139	9,98	10,56	0,58	0,00102	0,00995	exon (FBgn0261553, exon 1 of 7)	5' UTR (NM_001300099, exon 1 of 8)	111	FBgn0261553	FBtr0302696
chr3R	15351315	15351815	11,66	12,24	0,58	0,00117	0,0109	promoter-TSS (FBgn0266722)	promoter-TSS (NM_142193)	341	FBgn0038324	FBtr0083089
chr2R	9414594	9415094	11,33	11,91	0,58	0,00141	0,0126	exon (FBgn0041087, exon 1 of 6)	5' UTR (NM_080252, exon 1 of 6)	503	FBgn0041087	FBtr0088506
chr3R	10863289	10863789	10,44	11,02	0,58	0,00286	0,0219	promoter-TSS (FBgn0037846)	promoter-TSS (NM_141772)	-551	FBgn0037846	FBtr0082297
chr2R	17460302	17460802	9,52	10,11	0,58	0,00291	0,0221	promoter-TSS (FBgn0028953)	promoter-TSS (NM_137370)	-45	FBgn0028953	FBtr0086922
chr2R	6742865	6743365	9,43	10,01	0,58	0,00306	0,0231	exon (FBgn0028579, exon 4 of 8)	exon (NM_136388, exon 4 of 8)	1217	FBgn0028579	FBtr0086125
chr3R	9019314	9019814	12,06	12,64	0,58	0,00404	0,0282	TTS (FBgn0002932)	TTS (NM_169257)	458	FBgn0264075	FBtr0082005
chr2R	19437856	19438356	10,37	10,95	0,58	0,00476	0,0315	promoter-TSS (FBgn0020440)	promoter-TSS (NM_001169736)	624	FBgn0040273	FBtr0086531
chr2L	108447	108947	11,54	12,12	0,58	0,00506	0,0328	promoter-TSS (FBgn0005278)	promoter-TSS (NM_164362)	565	FBgn0005278	FBtr0089434
chrX	8895119	8895619	8,98	9,55	0,58	0,00517	0,0332	intron (FBgn0011661, intron 1 of 8)	intron (NM_001277432, intron 1 of 8)	-1174	FBgn0011661	FBtr0071273
chrX	21043014	21043514	9,15	9,73	0,58	0,0053	0,0338	TTS (FBgn0265613)	TTS (NR_123873)	195	FBgn0025834	FBtr0077243
chr3L	18999800	19000300	11,38	11,97	0,59	5,73E-08	3,75E-06	TTS (FBgn0036839)	TTS (NM_140827)	558	FBgn0036838	FBtr0075041
chr3R	6659621	6660121	10,86	11,45	0,59	3,25E-07	1,64E-05	TTS (FBgn0262801)	TTS (NM_143419)	229	FBgn0024912	FBtr0347362
chr3R	17040948	17041448	11,67	12,26	0,59	5,94E-07	2,67E-05	promoter-TSS (FBgn0038470)	promoter-TSS (NM_142332)	517	FBgn0038471	FBtr0083391
chrX	9272333	9272833	11,66	12,26	0,59	1,24E-06	4,90E-05	promoter-TSS (FBgn0030122)	promoter-TSS (NM_132329)	377	FBgn0030121	FBtr0071327
chr2L	10270241	10270741	11,51	12,1	0,59	3,72E-06	0,00012	TTS (FBgn0032205)	TTS (NM_135522)	441	FBgn0260750	FBtr0079986
chr3R	15794549	15795049	11,06	11,65	0,59	4,63E-06	0,000142	intron (FBgn0262527, intron 1 of 8)	intron (NM_001170151, intron 1 of 8)	1018	FBgn0262527	FBtr0301726
chr2L	13780891	13781391	11,77	12,36	0,59	4,79E-06	0,000146	promoter-TSS (FBgn0028540)	promoter-TSS (NM_165055)	453	FBgn0024846	FBtr0080534
chrX	3375116	3375616	10,98	11,57	0,59	7,57E-06	0,000208	exon (FBgn0262656, exon 2 of 3)	exon (NM_001272275, exon 2 of 3)	2208	FBgn0262656	FBtr0070525
chrX	16271305	16271805	10,75	11,33	0,59	7,65E-06	0,000209	exon (FBgn0030731, exon 1 of 2)	exon (NM_132881, exon 2 of 3)	152	FBgn0030731	FBtr0340442
chr3R	29253830	29254330	10,41	11	0,59	2,51E-05	0,000549	intron (FBgn0003525, intron 1 of 1)	intron (NM_001276137, intron 1 of 1)	1245	FBgn0003525	FBtr0085397
chr2L	5325752	5326252	11,09	11,68	0,59	2,99E-05	0,000625	promoter-TSS (FBgn0266320)	promoter-TSS (NR_124075)	-501	FBgn0266320	FBtr0344050
chr2R	12880531	12881031	11,54	12,13	0,59	3,15E-05	0,000651	promoter-TSS (FBgn0013305)	promoter-TSS (NM_165959)	350	FBgn0002069	FBtr0339391
chr3R	13647828	13648328	11,06	11,65	0,59	4,92E-05	0,000954	promoter-TSS (FBgn0015778)	promoter-TSS (NM_169531)	-743	FBgn0015778	FBtr0346346
chr2R	11198823	11199323	10,5	11,09	0,59	0,000104	0,00172	intron (FBgn0003396, intron 1 of 6)	intron (NM_134279, intron 1 of 6)	798	FBgn0003396	FBtr0088099
chr3R	5788344	5788844	11,28	11,87	0,59	0,00015	0,00234	promoter-TSS (FBgn0028690)	promoter-TSS (NM_141331)	480	FBgn0037376	FBtr0078670
chr3R	24582142	24582642	10,62	11,2	0,59	0,000288	0,00391	TTS (FBgn0039210)	TTS (NM_143015)	472	FBgn0039209	FBtr0084672
chr2R	9399063	9399563	11,56	12,15	0,59	0,000344	0,00448	promoter-TSS (FBgn0028473)	promoter-TSS (NM_136640)	234	FBgn0016970	FBtr0088505
chr3R	17545766	17546266	11,36	11,95	0,59	0,00099	0,00973	TTS (FBgn0025571)	TTS (NM_079915)	515	FBgn0038519	FBtr0083503
chr2L	2769227	2769727	12	12,59	0,59	0,00111	0,0106	promoter-TSS (FBgn0031459)	promoter-TSS (NM_001273035)	589	FBgn0019830	FBtr0077734
chr2L	19132507	19133007	11,86	12,45	0,59	0,0047	0,0312	promoter-TSS (FBgn0086443)	promoter-TSS (NM_001273632)	435	FBgn0086446	FBtr0081157
chr2L	16349154	16349654	8,89	9,48	0,59	0,00502	0,0326	exon (FBgn0000307, exon 2 of 2)	exon (NM_001273570, exon 2 of 2)	879	FBgn0000307	FBtr0321313
chrX	7969644	7970144	10,01	10,6	0,59	0,00595	0,0371	exon (FBgn0003447, exon 1 of 6)	5' UTR (NM_001169226, exon 1 of 6)	192	FBgn0003447	FBtr0301677
chr2R	25268998	25269498	8,23	8,82	0,59	0,0065	0,0396	Intergenic	TAHRE | LINE | Jockey	-13930	FBgn0035094	FBtr0333172
chr3L	18622739	18623239	11,3	11,89	0,59	0,00877	0,0495	promoter-TSS (FBgn0013717)	promoter-TSS (NM_079416)	298	FBgn0259791	FBtr0075108
chr3R	9632267	9632767	10,99	11,58	0,6	1,08E-07	6,24E-06	TTS (FBgn0003334)	TTS (NM_169299)	559	FBgn0266413	FBtr0344394
chr2R	14877688	14878188	10,95	11,56	0,6	1,56E-07	8,77E-06	TTS (FBgn0033978)	TTS (NM_137156)	153	FBgn0033979	FBtr0087453
chr3R	11235326	11235826	11,09	11,69	0,6	3,92E-07	1,92E-05	promoter-TSS (FBgn0051441)	promoter-TSS (NM_169382)	194	FBgn0037885	FBtr0304707
chr2R	15931355	15931855	11,16	11,75	0,6	4,90E-07	2,26E-05	TTS (FBgn0015247)	TTS (NM_176182)	330	FBgn0034049	FBtr0087298
chr2R	10111204	10111704	10,83	11,43	0,6	1,08E-06	4,40E-05	exon (FBgn0003071, exon 1 of 8)	exon (NM_165747, exon 1 of 8)	585	FBgn0003071	FBtr0088421
chr3R	4381718	4382218	10,73	11,33	0,6	1,29E-05	0,000318	TTS (FBgn0037239)	TTS (NM_164347)	663	FBgn0037240	FBtr0078917
chr3L	10631372	10631872	11,51	12,11	0,6	1,71E-05	0,000402	promoter-TSS (FBgn0260643)	promoter-TSS (NM_001169941)	281	FBgn0001179	FBtr0114599
chr3L	16779039	16779539	11,34	11,94	0,6	1,71E-05	0,000402	promoter-TSS (FBgn0036661)	promoter-TSS (NM_168683)	447	FBgn0036660	FBtr0075346
chr2R	21482123	21482623	11,52	12,12	0,6	0,000256	0,00359	exon (FBgn0026369, exon 2 of 8)	exon (NM_079990, exon 2 of 8)	447	FBgn0026369	FBtr0071641
chr3L	4289079	4289579	10,83	11,43	0,6	0,000389	0,00494	TTS (FBgn0015829)	TTS (NM_001169875)	385	FBgn0041630	FBtr0333567
chr2R	22940228	22940728	10,59	11,19	0,6	0,000885	0,00905	exon (FBgn0034804, exon 3 of 4)	exon (NM_001274217, exon 3 of 4)	468	FBgn0034804	FBtr0071933
chr3R	24258919	24259419	9,61	10,21	0,6	0,00122	0,0113	exon (FBgn0011225, exon 2 of 13)	exon (NM_001014649, exon 2 of 13)	319	FBgn0011225	FBtr0084636
chr3L	17533778	17534278	9,79	10,39	0,6	0,00138	0,0124	intron (FBgn0259174, intron 1 of 16)	intron (NM_206394, intron 1 of 16)	278	FBgn0259174	FBtr0299642
chr2R	12570599	12571099	10,51	11,11	0,6	0,00144	0,0128	exon (FBgn0003527, exon 2 of 4)	exon (NM_057404, exon 2 of 4)	483	FBgn0003527	FBtr0087825
chr2L	8892022	8892522	11,7	12,3	0,6	0,00156	0,0136	promoter-TSS (FBgn0033337)	promoter-TSS (NM_001273893)	441	FBgn0021825	FBtr0088641
chr3R	11742240	11742740	11,49	12,09	0,6	0,00162	0,014	promoter-TSS (FBgn0002906)	promoter-TSS (NM_079595)	601	FBgn0037943	FBtr0082431
chr4	1304145	1304645	9,13	9,73	0,6	0,00221	0,0179	Intergenic	HETA | LINE | Jockey	72513	FBgn0053653	FBtr0093630
chr2R	13821258	13821758	9,35	9,95	0,6	0,00229	0,0185	exon (FBgn0000662, exon 3 of 5)	exon (NM_166010, exon 3 of 5)	3045	FBgn0000662	FBtr0087647
chr3R	5736828	5737328	11,88	12,48	0,6	0,00239	0,019	promoter-TSS (FBgn0037369)	promoter-TSS (NM_001170041)	331	FBgn0037370	FBtr0078721
chrX	2122297	2122797	10,19	10,79	0,6	0,00254	0,02	promoter-TSS (FBgn0004860)	promoter-TSS (NM_080055)	739	FBgn0004860	FBtr0112843
chr2R	11358051	11358551	9,91	10,5	0,6	0,00555	0,035	promoter-TSS (FBgn0011987)	TTS (NM_078971)	-651	FBgn0011987	FBtr0088156
chr3R	29593080	29593580	9,42	10,02	0,6	0,00883	0,0497	exon (FBgn0086361, exon 2 of 7)	5' UTR (NM_170419, exon 2 of 7)	228	FBgn0086361	FBtr0085446
chr3R	31581019	31581519	11,34	11,95	0,61	4,59E-09	4,62E-07	promoter-TSS (FBgn0043900)	promoter-TSS (NM_143615)	319	FBgn0003268	FBtr0085795
chr2L	7783070	7783570	11,04	11,66	0,61	4,65E-08	3,13E-06	TTS (FBgn0031946)	TTS (NM_135303)	456	FBgn0031947	FBtr0079488
chr3L	6174483	6174983	11,26	11,87	0,61	4,86E-07	2,26E-05	promoter-TSS (FBgn0035688)	promoter-TSS (NM_139776)	486	FBgn0035689	FBtr0076998
chr2R	18971980	18972480	11,49	12,1	0,61	5,98E-07	2,68E-05	promoter-TSS (FBgn0267351)	promoter-TSS (NM_001274154)	307	FBgn0041702	FBtr0086600
chrX	3967952	3968452	11,7	12,32	0,61	7,84E-07	3,41E-05	promoter-TSS (FBgn0267037)	promoter-TSS (NR_123785)	453	FBgn0029689	FBtr0070625
chr2L	5721090	5721590	11,56	12,17	0,61	1,17E-06	4,68E-05	promoter-TSS (FBgn0031732)	promoter-TSS (NM_001169419)	290	FBgn0024191	FBtr0079134
chr3L	22075267	22075767	11,25	11,86	0,61	5,61E-06	0,000162	promoter-TSS (FBgn0000100)	promoter-TSS (NM_141122)	239	FBgn0037151	FBtr0078484
chr3L	8339290	8339790	10,48	11,08	0,61	1,35E-05	0,000328	promoter-TSS (FBgn0011762)	promoter-TSS (NM_079748)	490	FBgn0035876	FBtr0076602
chrX	634835	635335	11,87	12,49	0,61	1,75E-05	0,000409	promoter-TSS (FBgn0003575)	promoter-TSS (NM_057406)	460	FBgn0020381	FBtr0114559
chr2L	18703675	18704175	11,16	11,77	0,61	6,98E-05	0,00127	promoter-TSS (FBgn0032702)	promoter-TSS (NM_136055)	453	FBgn0032703	FBtr0081098
chr2R	21633674	21634174	10,22	10,83	0,61	9,86E-05	0,00167	promoter-TSS (FBgn0034643)	promoter-TSS (NM_001274195)	116	FBgn0260720	FBtr0301177
chr3L	21532897	21533397	11,77	12,38	0,61	0,000144	0,00227	exon (FBgn0029152, exon 2 of 4)	5' UTR (NM_168922, exon 2 of 4)	566	FBgn0029152	FBtr0078383
chr2R	21719218	21719718	11,71	12,32	0,61	0,000215	0,00314	TTS (FBgn0050398)	TTS (NM_164853)	377	FBgn0050404	FBtr0071747
chr2R	11295499	11295999	10,66	11,27	0,61	0,00032	0,00425	promoter-TSS (FBgn0259238)	promoter-TSS (NM_001144172)	-395	FBgn0259238	FBtr0299854
chr2R	17793433	17793933	10,51	11,12	0,61	0,000323	0,00428	exon (FBgn0028743, exon 1 of 7)	5' UTR (NM_137427, exon 1 of 7)	814	FBgn0028743	FBtr0301142
chr3R	11622730	11623230	9,98	10,59	0,61	0,00038	0,00485	promoter-TSS (FBgn0037922)	promoter-TSS (NM_141837)	117	FBgn0037921	FBtr0307351
chr3L	8973966	8974466	11,92	12,53	0,61	0,00094	0,00939	promoter-TSS (FBgn0035947)	promoter-TSS (NM_140016)	201	FBgn0086706	FBtr0076558
chr2L	2217413	2217913	11,91	12,52	0,61	0,0014	0,0125	promoter-TSS (FBgn0040715)	promoter-TSS (NM_001144295)	374	FBgn0031399	FBtr0077835
chr3L	5768325	5768825	11,74	12,35	0,61	0,00154	0,0136	promoter-TSS (FBgn0260936)	promoter-TSS (NM_168132)	219	FBgn0035632	FBtr0077120
chr3L	16408989	16409489	9,26	9,87	0,61	0,00175	0,0149	promoter-TSS (FBgn0014163)	promoter-TSS (NM_001014586)	-790	FBgn0014163	FBtr0075413
chrX	13111609	13112109	10,82	11,43	0,61	0,00194	0,0162	exon (FBgn0263005, exon 1 of 6)	5' UTR (NM_132625, exon 1 of 6)	603	FBgn0263005	FBtr0346130
chrX	9212656	9213156	9,44	10,05	0,61	0,00207	0,0171	exon (FBgn0035969, exon 3 of 6)	exon (NM_140036, exon 3 of 6)	1027	FBgn0035969	FBtr0076429
chr2R	12878343	12878843	9,11	9,72	0,61	0,00245	0,0194	exon (FBgn0013305, exon 2 of 4)	exon (NM_001274000, exon 1 of 3)	213	FBgn0013305	FBtr0332883
chr2R	6611033	6611533	9,62	10,23	0,61	0,00291	0,0221	intron (FBgn0086655, intron 1 of 6)	intron (NM_136371, intron 1 of 6)	797	FBgn0086655	FBtr0114364
chr2L	12054988	12055488	10,76	11,36	0,61	0,00377	0,0268	exon (FBgn0028425, exon 2 of 8)	exon (NM_164988, exon 2 of 8)	349	FBgn0028425	FBtr0305089
chr3R	7185928	7186428	12,1	12,72	0,61	0,00617	0,038	promoter-TSS (FBgn0086372)	promoter-TSS (NM_001170067)	495	FBgn0037482	FBtr0081605
chrX	10847547	10848047	12	12,61	0,61	0,00834	0,0477	promoter-TSS (FBgn0030240)	promoter-TSS (NM_132429)	360	FBgn0030239	FBtr0073379
chr3R	25124789	25125289	10,5	11,11	0,61	0,00866	0,049	TTS (FBgn0039280)	TTS (NM_001170249)	1595	FBgn0046214	FBtr0084776
chr2L	19127307	19127807	11,17	11,79	0,62	6,36E-08	4,07E-06	promoter-TSS (FBgn0086444)	promoter-TSS (NM_136102)	298	FBgn0086445	FBtr0081156
chrX	15713858	15714358	11,03	11,65	0,62	6,44E-08	4,09E-06	exon (FBgn0030674, exon 2 of 20)	5' UTR (NM_132831, exon 2 of 19)	468	FBgn0030674	FBtr0339686
chr2R	18156106	18156606	10,83	11,45	0,62	2,22E-07	1,17E-05	promoter-TSS (FBgn0022238)	promoter-TSS (NM_001169715)	23	FBgn0022238	FBtr0300484
chrX	8591232	8591732	11,64	12,25	0,62	3,29E-07	1,65E-05	promoter-TSS (FBgn0025864)	promoter-TSS (NM_001169739)	247	FBgn0040929	FBtr0332627
chr2R	22182161	22182661	11,05	11,68	0,62	6,36E-06	0,000179	promoter-TSS (FBgn0034707)	promoter-TSS (NM_137806)	468	FBgn0034705	FBtr0071786
chr3L	11966853	11967353	11,84	12,45	0,62	3,04E-05	0,000632	promoter-TSS (FBgn0260743)	promoter-TSS (NM_141877)	354	FBgn0260742	FBtr0113223
chr2R	17422168	17422668	10,51	11,13	0,62	0,000188	0,00282	intron (FBgn0022029, intron 1 of 6)	intron (NM_166224, intron 1 of 6)	1042	FBgn0022029	FBtr0086915
chr2L	9697585	9698085	9,97	10,59	0,62	0,000323	0,00428	exon (FBgn0000273, exon 2 of 3)	5' UTR (NM_205950, exon 2 of 3)	1462	FBgn0000273	FBtr0079851
chr2R	18820050	18820550	10,65	11,26	0,62	0,000735	0,00795	exon (FBgn0010551, exon 2 of 5)	exon (NM_001103903, exon 2 of 5)	834	FBgn0010551	FBtr0086614
chr3R	27958378	27958878	11,58	12,21	0,62	0,00109	0,0104	promoter-TSS (FBgn0039565)	promoter-TSS (NM_143347)	-482	FBgn0039565	FBtr0085264
chr2R	24188293	24188793	9,45	10,07	0,62	0,00173	0,0148	exon (FBgn0266083, exon 2 of 6)	exon (NM_138050, exon 2 of 6)	267	FBgn0266083	FBtr0343436
chr2R	24186604	24187104	8,99	9,61	0,62	0,00188	0,0158	promoter-TSS (FBgn0266083)	promoter-TSS (NM_138050)	152	FBgn0266083	FBtr0303783
chr2L	5008994	5009494	11,43	12,05	0,62	0,00219	0,0178	TTS (FBgn0031668)	TTS (NM_001144319)	476	FBgn0053113	FBtr0079038
chrX	6221291	6221791	8,92	9,54	0,62	0,00228	0,0184	exon (FBgn0029849, exon 2 of 2)	exon (NM_167062, exon 3 of 3)	1287	FBgn0029849	FBtr0070875
chr2L	21167739	21168239	11,78	12,4	0,62	0,00251	0,0198	promoter-TSS (FBgn0010100)	promoter-TSS (NM_001103716)	360	FBgn0263050	FBtr0306974
chr3R	9344432	9344932	8,95	9,57	0,62	0,00298	0,0226	intron (FBgn0266410, intron 2 of 5)	CpG	2816	FBgn0266410	FBtr0344368

chr2L	10857543	10858043	11,41	12,03	0,62	0,00416	0,0288	promoter-TSS (FBgn0027363)	promoter-TSS (NM_058100)	301	FBgn0024227|FBtr0080180
chr2R	23987938	23988438	10,53	11,15	0,62	0,0077	0,045	promoter-TSS (FBgn0034950)	promoter-TSS (NM_138020)	267	FBgn0283509|FBtr0072203
chrX	11855190	11855690	12,1	12,71	0,62	0,00828	0,0475	promoter-TSS (FBgn0030342)	promoter-TSS (NM_167310)	419	FBgn0030343|FBtr0273257
chrX	11892890	11893390	10,57	11,19	0,62	0,00846	0,0482	promoter-TSS (FBgn0260780)	promoter-TSS (NM_132538)	-802	FBgn0260780|FBtr0073573
chr3L	11117650	11118150	10,17	10,79	0,62	0,00868	0,0491	exon (FBgn0036134, exon 2 of 9)	exon (NM_168446, exon 2 of 9)	566	FBgn0036134|FBtr0300785
chr3L	19447247	19447747	11,6	12,23	0,63	4,09E-08	2,91E-06	exon (FBgn0023395, exon 1 of 1)	exon (NM_140854, exon 1 of 1)	325	FBgn0023395|FBtr0074998
chr2R	12587015	12587515	10,31	10,94	0,63	4,69E-05	0,000916	intron (FBgn0022764, intron 1 of 11)	intron (NM_165916, intron 1 of 11)	1887	FBgn0022764|FBtr0303565
chrX	8101130	8101630	10,62	11,25	0,63	0,000101	0,0017	promoter-TSS (FBgn0029997)	promoter-TSS (NM_001298071)	74	FBgn0029997|FBtr0340140
chr2L	2752157	2752657	10,47	11,1	0,63	0,000151	0,00236	promoter-TSS (FBgn0031453)	promoter-TSS (NM_001273031)	-37	FBgn0031453|FBtr0335125
chr3L	21432519	21433019	11,18	11,81	0,63	0,000219	0,00318	promoter-TSS (FBgn0005694)	promoter-TSS (NM_168904)	365	FBgn0037081|FBtr0078399
chrX	9552453	9552953	10,14	10,77	0,63	0,000522	0,00617	exon (FBgn0028327, exon 2 of 2)	exon (NM_132339, exon 2 of 2)	958	FBgn0028327|FBtr0343412
chr3L	9366424	9366924	11	11,63	0,63	0,000527	0,00621	promoter-TSS (FBgn0035981)	promoter-TSS (NM_140046)	277	FBgn0004379|FBtr0076499
chr2L	5987521	5988021	9,58	10,21	0,63	0,00113	0,0107	exon (FBgn0001941, exon 2 of 2)	exon (NM_057246, exon 2 of 2)	694	FBgn0001941|FBtr0332599
chrX	15845445	15845945	9,87	10,5	0,63	0,0019	0,016	exon (FBgn0030699, exon 3 of 7)	exon (NM_132854, exon 3 of 7)	1059	FBgn0030699|FBtr0340116
chrX	6869281	6869781	11,91	12,54	0,63	0,00254	0,02	exon (FBgn0263993, exon 2 of 4)	exon (NM_001272369, exon 2 of 5)	1024	FBgn0263993|FBtr0330262
chr2R	9185416	9185916	11,26	11,89	0,63	0,00267	0,0207	exon (FBgn0002567, exon 2 of 5)	exon (NM_165660, exon 2 of 5)	676	FBgn0002567|FBtr0089932
chr2L	17385480	17385980	8,66	9,29	0,63	0,00291	0,0221	promoter-TSS (FBgn0020503)	promoter-TSS (NM_001273598)	-415	FBgn0020503|FBtr0332451
chrX	20426563	20427063	11,6	12,24	0,63	0,00306	0,0231	TTS (FBgn0031115)	TTS (NM_167704)	229	FBgn0040650|FBtr0340402
chr3L	19898509	19899009	8,27	8,9	0,63	0,00348	0,0254	intron (FBgn0014037, intron 1 of 4)	intron (NM_140898, intron 1 of 4)	-2368	FBgn0052218|FBtr0304110
chr2R	12149675	12150175	11,25	11,88	0,63	0,00748	0,044	exon (FBgn0027504, exon 2 of 5)	exon (NM_001273984, exon 2 of 5)	681	FBgn0027504|FBtr0333063
chrX	9195717	9196217	11,14	11,77	0,64	1,99E-09	2,31E-07	TTS (FBgn0030100)	TTS (NM_167187)	447	FBgn0030101|FBtr0071339
chr3R	29858358	29858858	11,3	11,94	0,64	4,95E-09	4,85E-07	TTS (FBgn0051032)	exon (NM_143481, exon 2 of 2)	328	FBgn0039711|FBtr0089927
chr2L	21164125	21164625	11,79	12,44	0,64	2,44E-06	8,61E-05	promoter-TSS (FBgn0266215)	promoter-TSS (NR_124409)	-104	FBgn0266215|FBtr0343876
chr3L	5812323	5812823	11,02	11,66	0,64	4,13E-06	0,00013	TTS (FBgn0003984)	TTS (NM_001014565)	520	FBgn0035640|FBtr0077113
chr3R	9763910	9764410	11,36	12	0,64	5,08E-06	0,00015	exon (FBgn0037746, exon 2 of 4)	exon (NM_001170105, exon 2 of 4)	407	FBgn0037746|FBtr0301870
chr3L	11070655	11071155	10,65	11,29	0,64	1,32E-05	0,000323	exon (FBgn0263241, exon 1 of 4)	exon (NM_176317, exon 1 of 4)	342	FBgn0263241|FBtr0076204
chr3R	18169579	18170079	10,06	10,69	0,64	0,000162	0,00251	exon (FBgn0042693, exon 2 of 9)	exon (NM_001144599, exon 2 of 9)	1052	FBgn0042693|FBtr0305034
chr3R	29248106	29248606	10,36	11	0,64	0,000278	0,00383	exon (FBgn0263236, exon 2 of 7)	exon (NM_170406, exon 2 of 7)	548	FBgn0263236|FBtr0085400
chrX	653705	654205	11,22	11,86	0,64	0,000391	0,00494	exon (FBgn0025639, exon 2 of 3)	exon (NM_130497, exon 2 of 3)	983	FBgn0025639|FBtr0308652
chr3R	28634589	28635089	10,82	11,46	0,64	0,000441	0,00541	exon (FBgn0039590, exon 1 of 6)	5' UTR (NM_143367, exon 1 of 6)	260	FBgn0039590|FBtr0085319
chr3R	9627884	9628384	10,12	10,76	0,64	0,000533	0,00624	TTS (FBgn0005585)	TTS (NM_079569)	814	FBgn0037722|FBtr0082077
chr2L	18707513	18708013	10	10,63	0,64	0,000616	0,00699	exon (FBgn0025608, exon 2 of 3)	exon (NM_058040, exon 2 of 3)	836	FBgn0025608|FBtr0341115
chrX	2121256	2121756	11	11,65	0,64	0,000624	0,00706	exon (FBgn0004860, exon 2 of 5)	exon (NM_080055, exon 2 of 5)	286	FBgn0004860|FBtr0070433
chrX	6997609	6998109	9,74	10,37	0,64	0,000838	0,00867	promoter-TSS (FBgn0027108)	promoter-TSS (NM_001169213)	-60	FBgn0263485|FBtr0332282
chr2R	7458406	7458906	10,48	11,13	0,64	0,000954	0,00945	exon (FBgn0025885, exon 1 of 5)	exon (NM_058057, exon 1 of 5)	218	FBgn0025885|FBtr0080329
chr2L	8404104	8404604	11,58	12,23	0,64	0,00104	0,0101	promoter-TSS (FBgn0266326)	promoter-TSS (NR_124146)	-430	FBgn0266326|FBtr0344057
chr2R	9548329	9548829	9,07	9,71	0,64	0,00173	0,0148	promoter-TSS (FBgn0033421)	promoter-TSS (NM_001273898)	-444	FBgn0033421|FBtr0310031
chr2L	19790079	19790579	8,58	9,22	0,64	0,00253	0,0199	intron (FBgn0032821, intron 1 of 6)	intron (NM_136158, intron 1 of 6)	1553	FBgn0032821|FBtr0332179
chrX	8907982	8908482	9,01	9,65	0,64	0,00264	0,0206	exon (FBgn0261549, exon 2 of 18)	exon (NM_001042799, exon 2 of 17)	1165	FBgn0261549|FBtr0302662
chrX	3296546	3297046	7,79	8,43	0,64	0,00266	0,0207	intron (FBgn0000479, intron 5 of 15)	intron (NM_166969, intron 1 of 11)	1516	FBgn0000479|FBtr0070518
chrX	7681014	7681514	8,09	8,73	0,64	0,00315	0,0237	promoter-TSS (FBgn0267225)	promoter-TSS (NR_123832)	14	FBgn0267225|FBtr0346397
chr3L	11112521	11113021	11,2	11,84	0,64	0,00319	0,0239	TTS (FBgn0036133)	TTS (NM_140187)	969	FBgn0003462|FBtr0076229
chr3L	14053666	14054166	10,92	11,56	0,64	0,00351	0,0256	promoter-TSS (FBgn0036406)	promoter-TSS (NM_140433)	388	FBgn0267736|FBtr0347296
chr2R	6502135	6502635	9,51	10,15	0,64	0,0036	0,0259	promoter-TSS (FBgn0267744)	promoter-TSS (NR_133106)	380	FBgn0086655|FBtr0114365
chrX	5736261	5736761	9,1	9,74	0,64	0,00389	0,0275	intron (FBgn0052758, intron 1 of 5)	intron (NM_167045, intron 1 of 5)	1520	FBgn0052758|FBtr0070843
chr2R	13337902	13338402	8,47	9,11	0,64	0,0042	0,029	promoter-TSS (FBgn0265104)	promoter-TSS (NR_133117)	-817	FBgn0265104|FBtr0346709
chr3L	5901709	5902209	9,93	10,57	0,64	0,00432	0,0296	TTS (FBgn0052413)	TTS (NM_001140451)	497	FBgn0052412|FBtr0077080
chr2L	22033	22533	8,3	8,93	0,64	0,00516	0,0332	promoter-TSS (FBgn0002121)	promoter-TSS (NM_001272858)	332	FBgn0263584|FBtr0309810
chrX	12597193	12597693	9,66	10,31	0,64	0,00531	0,0338	exon (FBgn0052654, exon 2 of 13)	exon (NM_001103494, exon 2 of 8)	543	FBgn0052654|FBtr0113445
chr3R	31794844	31795344	9,81	10,45	0,64	0,00756	0,0444	exon (FBgn0027620, exon 2 of 6)	exon (NM_080486, exon 2 of 6)	1114	FBgn0027620|FBtr0085845
chr3L	18683354	18683854	11,65	12,29	0,65	2,13E-07	1,13E-05	TTS (FBgn0036806)	TTS (NM_168774)	457	FBgn0036805|FBtr0345383
chr2L	19114712	19115212	10,56	11,21	0,65	4,58E-07	2,19E-05	TTS (FBgn0000075)	TTS (NM_165278)	562	FBgn0002036|FBtr0081155
chr3R	5646858	5647358	10,41	11,06	0,65	3,82E-06	0,000122	exon (FBgn0027951, exon 1 of 11)	exon (NM_001144539, exon 1 of 11)	802	FBgn0027951|FBtr0290206
chrX	6999109	6999609	11,93	12,57	0,65	3,80E-05	0,000767	exon (FBgn0027108, exon 1 of 1)	exon (NM_001169213, exon 1 of 1)	688	FBgn0027108|FBtr0301860
chr2L	19577872	19578372	11,26	11,92	0,65	4,52E-05	0,000887	promoter-TSS (FBgn0005672)	promoter-TSS (NM_134291)	422	FBgn0027949|FBtr0081258
chr3L	12733669	12734169	9,8	10,46	0,65	0,000235	0,00339	exon (FBgn0261933, exon 2 of 2)	exon (NM_080035, exon 2 of 2)	692	FBgn0261933|FBtr0075952
chr2R	21501041	21501541	11,5	12,16	0,65	0,000245	0,00348	promoter-TSS (FBgn0043070)	promoter-TSS (NM_206194)	441	FBgn0034631|FBtr0071701
chr2R	24022641	24023141	11,7	12,35	0,65	0,00043	0,00531	promoter-TSS (FBgn0034958)	promoter-TSS (NM_166647)	549	FBgn0034959|FBtr0072162
chr3R	26462113	26462613	9,21	9,86	0,65	0,000917	0,00928	intron (FBgn0039430, intron 1 of 6)	intron (NM_143224, intron 1 of 6)	837	FBgn0039430|FBtr0085015
chr2L	8277233	8277733	10	10,65	0,65	0,00124	0,0114	exon (FBgn0003502, exon 1 of 10)	5' UTR (NM_164805, exon 1 of 10)	219	FBgn0003502|FBtr0079618
chr2R	14619874	14620374	9,61	10,26	0,65	0,0014	0,0126	TTS (FBgn0010638)	TTS (NM_143780)	1196	FBgn0033948|FBtr0087500
chr2R	13550610	13551110	10,71	11,36	0,65	0,00185	0,0156	promoter-TSS (FBgn0053156)	promoter-TSS (NM_176167)	590	FBgn0053156|FBtr0087683
chr2L	15744780	15745280	8,69	9,34	0,65	0,00349	0,0255	intron (FBgn0010382, intron 1 of 5)	intron (NM_165125, intron 1 of 5)	-1226	FBgn0266309|FBtr0344038
chrX	15046410	15046910	7,52	8,17	0,65	0,0037	0,0265	intron (FBgn0030603, intron 1 of 4)	intron (NM_206715, intron 1 of 4)	-2267	FBgn0030603|FBtr0073959
chr3L	9376778	9377278	11,71	12,36	0,65	0,00524	0,0335	TTS (FBgn0035982)	TTS (NM_140047)	347	FBgn0001225|FBtr0076496
chr2R	23812258	23812758	10,2	10,85	0,65	0,00552	0,0349	promoter-TSS (FBgn0028411)	promoter-TSS (NM_137589)	324	FBgn0266042|FBtr0343262
chr2L	16698867	16699367	9,48	10,13	0,65	0,00576	0,0361	TTS (FBgn0263744)	TTS (NR_047974)	360	FBgn0262413|FBtr0304346
chr2L	3353016	3353516	9,71	10,35	0,65	0,00653	0,0397	exon (FBgn0020445, exon 2 of 9)	exon (NM_205900, exon 2 of 9)	1563	FBgn0020445|FBtr0089979
chr3R	19158394	19158894	10,54	11,19	0,65	0,00698	0,0417	exon (FBgn0002962, exon 3 of 4)	exon (NM_057310, exon 2 of 3)	1234	FBgn0038683|FBtr0083749
chr2L	2235559	2236059	9,91	10,55	0,65	0,00729	0,0432	promoter-TSS (FBgn0264946)	promoter-TSS (NR_073696)	-537	FBgn0264946|FBtr0335158
chr3L	9694021	9694521	10,95	11,61	0,66	3,94E-09	4,10E-07	promoter-TSS (FBgn0266596)	promoter-TSS (NR_124838)	186	FBgn0036030|FBtr0345032
chr3L	5927784	5928284	10,84	11,51	0,66	1,12E-08	9,93E-07	promoter-TSS (FBgn0053523)	promoter-TSS (NM_001014568)	253	FBgn0053523|FBtr0091477
chr2R	21385813	21386313	10,66	11,32	0,66	4,15E-08	2,92E-06	promoter-TSS (FBgn0034628)	promoter-TSS (NM_079078)	158	FBgn0034627|FBtr0071608
chr2R	23972508	23973008	11,11	11,77	0,66	2,10E-07	1,12E-05	TTS (FBgn0034946)	TTS (NM_166643)	328	FBgn0002791|FBtr0072156
chrX	16597946	16598446	11,69	12,35	0,66	2,68E-06	9,18E-05	exon (FBgn0030761, exon 2 of 2)	exon (NM_001272695, exon 2 of 2)	300	FBgn0030761|FBtr0074289
chr2R	12916545	12917045	11,17	11,84	0,66	3,20E-06	0,000105	intron (FBgn0010488, intron 1 of 3)	intron (NM_165961, intron 1 of 3)	802	FBgn0010488|FBtr0087786
chr3R	25739096	25739596	11,55	12,2	0,66	1,51E-05	0,000362	TTS (FBgn0267771)	TTS (NR_133454)	1119	FBgn0051092|FBtr0113384
chr3R	27069647	27070147	10,24	10,91	0,66	1,89E-05	0,000434	exon (FBgn0003495, exon 1 of 5)	5' UTR (NM_001144644, exon 1 of 6)	173	FBgn0003495|FBtr0112834
chr2L	12460324	12460824	10,16	10,81	0,66	8,16E-05	0,00142	intron (FBgn0259176, intron 2 of 2)	promoter-TSS (NR_047945)	-484	FBgn0262203|FBtr0304239
chr2R	9091287	9091787	10,24	10,9	0,66	9,16E-05	0,00157	TTS (FBgn0033374)	TTS (NM_176109)	248	FBgn0033373|FBtr0310146
chr2L	20675233	20675733	11,98	12,65	0,66	0,000116	0,0019	promoter-TSS (FBgn0088657)	promoter-TSS (NM_165337)	458	FBgn0051678|FBtr0290059
chrX	15703030	15703530	11,45	12,12	0,66	0,000127	0,00203	promoter-TSS (FBgn0030671)	promoter-TSS (NM_132828)	490	FBgn0030670|FBtr0074058
chr3R	22638627	22639127	11,22	11,88	0,66	0,000408	0,00509	promoter-TSS (FBgn0266418)	promoter-TSS (NM_001300541)	510	FBgn0020278|FBtr0084273
chr2L	10985729	10986229	9,82	10,48	0,66	0,000505	0,00601	exon (FBgn0004872, exon 2 of 8)	exon (NM_057527, exon 2 of 8)	1441	FBgn0004872|FBtr0080166
chr2R	22942097	22942597	10,3	10,96	0,66	0,000536	0,00626	promoter-TSS (FBgn0261584)	promoter-TSS (NM_001202065)	471	FBgn0261584|FBtr0334011
chr3R	13010641	13011141	11,6	12,27	0,66	0,000562	0,0065	promoter-TSS (FBgn0020496)	promoter-TSS (NM_001014617)	419	FBgn0038110|FBtr0082719
chr3L	18870487	18870987	10,68	11,34	0,66	0,000648	0,0073	TTS (FBgn0036820)	TTS (NM_001104169)	514	FBgn0085284|FBtr0112449
chr3R	14918689	14919189	10,58	11,23	0,66	0,000936	0,00939	exon (FBgn0038279, exon 1 of 7)	exon (NM_142151, exon 1 of 7)	312	FBgn0038279|FBtr0083004
chr3R	30005959	30006459	10,08	10,74	0,66	0,000995	0,00975	exon (FBgn0039736, exon 8 of 8)	exon (NM_143504, exon 8 of 8)	1259	FBgn0016685|FBtr0334701
chr2L	7427881	7428381	9,14	9,8	0,66	0,00113	0,0107	exon (FBgn0283658, exon 2 of 7)	exon (NM_001273267, exon 2 of 7)	404	FBgn0283658|FBtr0079445
chr2R	18441361	18441861	11,08	11,74	0,66	0,00164	0,0142	exon (FBgn0261477, exon 1 of 3)	exon (NM_166289, exon 1 of 3)	647	FBgn0261477|FBtr0331958
chr3L	3327224	3327724	8,77	9,43	0,66	0,00167	0,0144	exon (FBgn0035438, exon 2 of 4)	exon (NM_168025, exon 2 of 4)	1210	FBgn0035438|FBtr0073066
chr2R	5673000	5673500	8,17	8,84	0,66	0,00208	0,0171	TTS (FBgn0038372)	TTS (NM_136335)	1510	FBgn0038372|FBtr0086037
chr3L	3218170	3218670	11,25	11,91	0,66	0,00318	0,0238	promoter-TSS (FBgn0035421)	promoter-TSS (NM_139533)	500	FBgn0035420|FBtr0302302
chrX	1897662	1898162	9,16	9,82	0,66	0,00322	0,024	intron (FBgn0000117, intron 2 of 6)	intron (NM_057317, intron 2 of 6)	1612	FBgn0000117|FBtr0089988
chrX	9929474	9929974	8,8	9,45	0,66	0,0046	0,0308	TTS (FBgn0086044)	TTS (NR_003732)	282	FBgn0086044|FBtr0114320
chr3L	23279580	23280080	9,28	9,94	0,66	0,00773	0,0451	intron (FBgn0266347, intron 10 of 10)	Gypsy/B_LTR (LTR) Gypsy	30802	FBgn0266347|FBtr0308331
chr2L	2882552	2883052	10,78	11,45	0,67	3,11E-08	2,34E-06	exon (FBgn0024947, exon 2 of 4)	exon (NM_001273043, exon 2 of 3)	324	FBgn0024947|FBtr0077682
chr2R	18624619	18625119	10,77	11,43	0,67	4,17E-08	2,92E-06	promoter-TSS (FBgn0266671)	promoter-TSS (NM_137507)	175	FBgn0034366|FBtr0086711
chr3L	648771	649271	11,27	11,94	0,67	9,86E-08	5,84E-06	exon (FBgn0035147, exon 1 of 4)	5' UTR (NM_138200, exon 1 of 4)	248	FBgn0035147|FBtr0306917
chr2R	9841761	9842261	10,69	11,35	0,67	2,70E-06	9,19E-05	promoter-TSS (FBgn0033453)	promoter-TSS (NM_136681)	491	FBgn0266186|FBtr0089394
chr3R	6373107	6373607	10,43	11,1	0,67	5,47E-06	0,000159	exon (FBgn0037440, exon 2 of 5)	exon (NM_001043219, exon 2 of 5)	217	FBgn0037440|FBtr0110774
chrX	2468981	2469481	10,33	11	0,67	1,35E-05	0,000328	intron (FBgn0040388, intron 2 of 8)	intron (NM_166940, intron 2 of 8)	812	FBgn0040388|FBtr0070457
chr2R	1263494	1263994	9,99	10,67	0,67	0,000111	0,00184	promoter-TSS (FBgn0058191)	promoter-TSS (NM_001110883)	-395	FBgn0058191|FBtr0113827
chrX	11610430	11610930	9,96	10,63	0,67	0,000196	0,00293	exon (FBgn0030320, exon 2 of 8)	exon (NM_132507, exon 2 of 9)	972	FBgn0030320|FBtr0073536
chr3L	16413078	16413578	10,71	11,38	0,67	0,000281	0,00385	exon (FBgn0028399, exon 2 of 7)	exon (NM_140636, exon 2 of 7)	607	FBgn0028399|FBtr0075389
chr3R	24922617	24923117	10,87	11,53	0,67	0,00039	0,00494	TTS (FBgn0039249)	TTS (NM_001170244)	395	FBgn0039250|FBtr0084716
chrX	9049059	9049559	9,82	10,48	0,67	0,000438	0,0054	promoter-TSS (FBgn0264384)	promoter-TSS (NR_073643)	-318	FBgn0264384|FBtr0332279
chr3R	10351607	10352107	9,36	10,03	0,67	0,000687	0,00759	intron (FBgn0015396, intron 1 of 2)	intron (NM_079578, intron 1 of 2)	1676	FBgn0015396|FBtr0082237
chr2R	7491172	7491672	10,9	11,57	0,67	0,000791	0,00831	promoter-TSS (FBgn0263967)	promoter-TSS (NR_073855)	890	FBgn0263240|FBtr0329876
chr3R	13781179	13781679	11,34	12,01	0,67	0,00132	0,012	promoter-TSS (FBgn0000454)	promoter-TSS (NM_169558)	466	FBgn0038183|FBtr0082830
chr3R	14817323	14817823	10,15	10,82	0,67	0,00156	0,0136	exon (FBgn0266756, exon 8 of 14)	exon (NM_001014624, exon 1 of 7)	373	FBgn0266756|FBtr0334287
chr2R	11634089	11634589	8,91	9,58	0,67	0,00264	0,0206	intron (FBgn0033638, intron 1 of 7)	intron (NM_001259338, intron 1 of 7)	-1824	FBgn0033638|FBtr0300945
chr3R	18739412	18739912	9,74	10,41	0,67	0,00363	0,0261	exon (FBgn0024329, exon 1 of 7)	5' UTR (NM_142493, exon 1 of 7)	434	FBgn0024329|FBtr0331353
chr3R	18658210	18658710	11,23	11,91	0,68	1,14E-09	1,48E-07	intron (FBgn0051224, intron 1 of 5)	intron (NM_001300467, intron 1 of 5)	849	FBgn0051224|FBtr0083691
chrX	1047430	1047930	10,83	11,51	0,68	1,31E-09	1,61E-07	TTS (FBgn0266569)	TTS (NM_001047791)	439	FBgn0266005|FBtr0343175
chr3L	15587345	15587845	10,81	11,5	0,68	4,42E-08	3,00E-06	exon (FBgn0036516, exon 1 of 2)	5' UTR (NM_168628, exon 2 of 3)	272	FBgn0036516|FBtr0332095
chrX	8059698	8060198	10,57	11,25	0,68	1,26E-07	7,23E-06	exon (FBgn0004656, exon 2 of 8)	5' UTR (NM_001169228, exon 2 of 8)	1026	FBgn0004656|FBtr0071121
chrX	6771575	6772075	10,9	11,58	0,68	4,72E-06	0,000144	exon (FBgn0003390, exon 7 of 8)	exon (NM_132121, exon 7 of 8)	601	FBgn0029502|FBtr0070963
chr2R	7623473	7623973	10,28	10,96	0,68	1,04E-05	0,000269	intron (FBgn0263077, intron 1 of 14)	intron (NM_001259256, intron 1 of 14)	482	FBgn0263077|FBtr0306933
chr2R	10097193	10097693	11,69	12,38	0,68	2,55E-05	0,000553	exon (FBgn0001291, exon 3 of 3)	exon (NM_001273915, exon 2 of 2)	516	FBgn0001291|FBtr0088411
chrX	15320978	15321478	10,95	11,63	0,68	5,06E-05	0,000973	exon (FBgn0004924, exon 2 of 8)	exon (NM_001014742, exon 2 of 8)	860	FBgn0004924|FBtr0308699
chr2R	20319616	20320116	10,04	10,72	0,68	0,000333	0,00437	promoter-TSS (FBgn0027529)	promoter-TSS (NM_137630)	-629	FBgn0027529|FBtr0086281
chr2L	7425367	7425867	10,61	11,28	0,68	0,000469	0,00566	exon (FBgn0264439, exon 2 of 2)	promoter-TSS (NR_047918)	-235	FBgn0264253|FBtr0304473
chr3L	14036109	14036609	10,21	10,89	0,68	0,000506	0,00601	promoter-TSS (FBgn0026418)	promoter-TSS (NM_168574)	477	FBgn0265295|FBtr0304128
chrX	8114596	8115096	9,44	10,12	0,68	0,000603	0,00686	intron (FBgn0040319, intron 1 of 4)	intron (NM_001298072, intron 1 of 4)	1301	FBgn0040319|FBtr0340138
chrX	2170599	2171099	10,55	11,23	0,68	0,000746	0,00801	exon (FBgn0023540, exon 2 of 3)	promoter-TSS (NR_047736)	-236	FBgn0263630|FBtr0309629
chrX	5964365	5964865	8,7	9,38	0,68	0,000816	0,00851	promoter-TSS (FBgn0005390)	promoter-TSS (NM_132056)	-368	FBgn0005390|FBtr0070892
chrX	9102735	9103235	9,93	10,61	0,68	0,000938	0,00939	TTS (FBgn0004856)	TTS (NM_001272441)	754	FBgn0030087|FBtr0071351
chr2R	21158413	21158913	9,05	9,73	0,68	0,00125	0,0115	promoter-TSS (FBgn0050389)	promoter-TSS (NM_137712)	-646	FBgn0050389|FBtr0071633
chr3R	4379293	4379793	10,29	10,97	0,68	0,00129	0,0118	exon (FBgn0037239, exon 1 of 6)	exon (NM_164347, exon 2 of 7)	237	FBgn0037239|FBtr0078916

chr3R	24924606	24925106	10,39	11,07	0,68	0,00169	0,0146	promoter-TSS (FBgn0039251)	promoter-TSS (NM_143056)	-359	FBgn0039251 | FBtr0084718
chrX	6969903	6970403	10,22	10,9	0,68	0,00171	0,0147	exon (FBgn0029924, exon 1 of 2)	exon (NM_132143, exon 1 of 2)	236	FBgn0029924 | FBtr0071003
chr2L	1731574	1732074	10,7	11,38	0,68	0,00174	0,0148	promoter-TSS (FBgn0264494)	promoter-TSS (NM_164436)	532	FBgn0031361 | FBtr0333543
chr2L	20311605	20312105	11,62	12,3	0,68	0,00195	0,0163	exon (FBgn0003475, exon 1 of 16)	exon (NM_001169549, exon 1 of 16)	637	FBgn0003475 | FBtr0307894
chr2R	9439931	9440431	9,96	10,63	0,68	0,00316	0,0237	intron (FBgn0029092, intron 1 of 6)	intron (NM_001258296, intron 1 of 6)	705	FBgn0029092 | FBtr0088550
chr2R	6758341	6758841	11,58	12,27	0,68	0,00394	0,0278	exon (FBgn0033101, exon 1 of 1)	exon (NM_136391, exon 1 of 1)	312	FBgn0033101 | FBtr0086134
chr3R	19890928	19891428	9,71	10,39	0,68	0,00442	0,0301	exon (FBgn0038744, exon 1 of 9)	5' UTR (NM_142585, exon 1 of 9)	331	FBgn0038744 | FBtr0301117
chrX	5965319	5965819	9,34	10,02	0,68	0,00825	0,0474	promoter-TSS (FBgn0029830)	promoter-TSS (NM_132057)	-709	FBgn0029830 | FBtr0070865
chr2R	14160653	14161153	11,16	11,85	0,69	2,42E-09	2,78E-07	promoter-TSS (FBgn0033901)	promoter-TSS (NM_137087)	359	FBgn0033900 | FBtr0339965
chr2R	8902133	8902633	10,5	11,19	0,69	2,84E-07	1,46E-05	exon (FBgn0004921, exon 2 of 2)	exon (NM_165532, exon 2 of 2)	951	FBgn0004921 | FBtr0088646
chr3R	5792117	5792617	11,31	12	0,69	7,59E-06	0,00208	TTS (FBgn0037378)	TTS (NM_141333)	489	FBgn0037377 | FBtr0078630
chr3L	20139894	20140394	9,94	10,64	0,69	0,000299	0,0043	exon (FBgn0036942, exon 1 of 1)	exon (NM_140524, exon 1 of 1)	483	FBgn0036942 | FBtr0074864
chrX	10803761	10804749	9,24	9,92	0,69	0,000578	0,0063	intron (FBgn0285926, intron 2 of 6)	intron (NM_001258687, intron 2 of 6)	2601	FBgn0285926 | FBtr0073418
chr2L	6337024	6337524	9,9	10,59	0,69	0,000646	0,0072	intron (FBgn0031799, intron 1 of 6)	intron (NM_135169, intron 1 of 6)	1352	FBgn0031799 | FBtr0079284
chr2R	24043915	24044415	9,69	10,38	0,69	0,000706	0,0077	TTS (FBgn0011726)	TTS (NM_057686)	2640	FBgn0011726 | FBtr0072188
chr3R	5658334	5658834	10,26	10,96	0,69	0,00075	0,0080	promoter-TSS (FBgn0264902)	promoter-TSS (NR_073985)	-892	FBgn0264902 | FBtr0334945
chr2R	4471777	4472277	9,4	10,09	0,69	0,000789	0,0083	promoter-TSS (FBgn0260798)	promoter-TSS (NM_001042973)	-967	FBgn0260798 | FBtr0345363
chr2R	24258522	24259022	9,76	10,45	0,69	0,00121	0,0113	intron (FBgn0034997, intron 1 of 6)	intron (NM_001299904, intron 1 of 6)	760	FBgn0034997 | FBtr0072766
chr3R	14696526	14697026	10,33	11,01	0,69	0,0015	0,0133	TTS (FBgn0262127)	TTS (NM_001300400)	516	FBgn0265140 | FBtr0301498
chrX	6268604	6269104	9,61	10,31	0,69	0,00293	0,0222	exon (FBgn0028982, exon 3 of 6)	exon (NM_143705, exon 3 of 6)	1058	FBgn0028982 | FBtr0340027
chr2L	11999837	12000337	11,3	11,99	0,69	0,00317	0,0238	promoter-TSS (FBgn0042125)	promoter-TSS (NM_144407)	434	FBgn0032393 | FBtr0080290
chrX	3721602	3722102	8,31	9	0,69	0,00335	0,0248	intron (FBgn0283657, intron 2 of 7)	intron (NM_001272292, intron 2 of 7)	1846	FBgn0283657 | FBtr0301659
chrX	16003567	16004067	8,33	9,01	0,69	0,00358	0,0259	exon (FBgn0003969, exon 4 of 11)	exon (NM_206759, exon 4 of 11)	1995	FBgn0003969 | FBtr0340415
chr2L	16686417	16686917	8,83	9,52	0,69	0,004	0,0281	intron (FBgn0261278, intron 1 of 6)	intron (NM_057663, intron 1 of 6)	1278	FBgn0261278 | FBtr0080886
chr2L	183691	184191	10,68	11,38	0,69	0,00434	0,0297	exon (FBgn0016977, exon 2 of 11)	exon (NM_001272876, exon 2 of 11)	1122	FBgn0016977 | FBtr0332337
chr3R	5672555	5673055	9,2	9,89	0,69	0,00472	0,0313	intron (FBgn0037363, intron 2 of 5)	CpG-13261	3093	FBgn0037363 | FBtr0078716
chr3L	16730084	16730584	11,13	11,81	0,69	0,00502	0,0326	exon (FBgn0004556, exon 2 of 3)	exon (NM_057485, exon 2 of 3)	484	FBgn0004556 | FBtr0075347
chr3L	9062073	9062573	10,9	11,58	0,69	0,00544	0,0345	exon (FBgn0000116, exon 3 of 4)	exon (NM_168311, exon 3 of 4)	625	FBgn0000116 | FBtr0076544
chrX	8063754	8064254	10,22	10,91	0,69	0,00562	0,0354	exon (FBgn0004657, exon 2 of 7)	exon (NM_080054, exon 2 of 7)	2360	FBgn0004657 | FBtr0071105
chr2L	12975987	12976487	9,64	10,33	0,69	0,00581	0,0363	exon (FBgn0263598, exon 3 of 5)	exon (NM_001273496, exon 3 of 5)	836	FBgn0263598 | FBtr0336613
chr3R	9684458	9684958	10,12	10,81	0,69	0,00589	0,0367	promoter-TSS (FBgn0037730)	promoter-TSS (NM_141670)	-444	FBgn0037730 | FBtr0333194
chrX	12044569	12045069	8,4	9,09	0,69	0,00598	0,0372	intron (FBgn0267001, intron 1 of 19)	intron (NR_073650, intron 1 of 2)	1122	FBgn0264675 | FBtr0333769
chr2L	13810823	13811323	11,52	12,22	0,7	7,57E-09	7,11E-07	promoter-TSS (FBgn0029919)	promoter-TSS (NM_001273522)	401	FBgn0029858 | FBtr0080573
chr2L	8070771	8071271	11,45	12,14	0,7	8,80E-09	8,13E-07	TTS (FBgn0013531)	TTS (NM_001273294)	603	FBgn0011230 | FBtr0079545
chr3L	8121980	8122480	11,12	11,83	0,7	8,47E-06	0,00225	TTS (FBgn0026252)	TTS (NM_080041)	404	FBgn0035838 | FBtr0076687
chr3R	25250166	25250666	10,82	11,52	0,7	1,55E-05	0,00037	exon (FBgn0039302, exon 2 of 7)	exon (NM_143104, exon 2 of 7)	1069	FBgn0039302 | FBtr0084813
chr3L	12203352	12203852	10,05	10,75	0,7	2,86E-05	0,00609	TTS (FBgn0036766)	TTS (NM_140302)	333	FBgn0022709 | FBtr0076017
chrX	6090420	6090920	9,68	10,38	0,7	0,000144	0,0022	promoter-TSS (FBgn0029840)	promoter-TSS (NM_132066)	-469	FBgn0029840 | FBtr0345895
chrX	7891161	7891661	10,73	11,44	0,7	0,000243	0,0036	exon (FBgn0029970, exon 1 of 1)	exon (NM_132187, exon 1 of 1)	235	FBgn0029970 | FBtr0071142
chr2R	24187504	24188004	9,77	10,47	0,7	0,000403	0,0050 5	promoter-TSS (FBgn0266083)	promoter-TSS (NM_001299902)	116	FBgn0266083 | FBtr0072260
chr3L	8441149	8441649	9,13	9,83	0,7	0,000514	0,0061	exon (FBgn0263352, exon 1 of 9)	5' UTR (NM_001144440, exon 1 of 9)	308	FBgn0263352 | FBtr0345595
chr2R	16729556	16730056	8,33	9,03	0,7	0,000853	0,0088	intron (FBgn0050463, intron 1 of 11)	intron (NM_165188, intron 1 of 11)	1578	FBgn0050463 | FBtr0087113
chr3R	10856943	10857443	11,41	12,11	0,7	0,00173	0,0148	TTS (FBgn0037843)	TTS (NM_001170114)	387	FBgn0037844 | FBtr0082287
chr3R	10309955	10310455	9,09	9,78	0,7	0,00429	0,0294	exon (FBgn0037807, exon 2 of 4)	exon (NM_141737, exon 2 of 4)	1408	FBgn0037807 | FBtr0337051
chr2L	10430365	10430865	11,25	11,95	0,7	0,00708	0,0422	promoter-TSS (FBgn0004915)	promoter-TSS (NM_001273420)	303	FBgn0032248 | FBtr0080044
chrX	587330	587830	8,27	8,97	0,7	0,0075	0,0441	promoter-TSS (FBgn0267827)	promoter-TSS (NR_144661)	-467	FBgn0267827 | FBtr0347397
chr3R	18403476	18403976	11,29	12	0,71	1,04E-10	1,83E-08	exon (FBgn0264816, exon 3 of 4)	exon (NM_169814, exon 3 of 4)	405	FBgn0264816 | FBtr0334146
chr3R	31225184	31225684	10,6	11,31	0,71	1,55E-07	8,75E-06	exon (FBgn0039831, exon 1 of 6)	5' UTR (NM_170545, exon 1 of 6)	518	FBgn0039831 | FBtr0113312
chr2L	9570375	9570875	10,52	11,23	0,71	1,66E-06	6,30E-05	exon (FBgn0032130, exon 1 of 4)	5' UTR (NM_135454, exon 1 of 4)	355	FBgn0032130 | FBtr0078835
chr2R	12170955	12171455	10,39	11,1	0,71	1,86E-06	6,96E-05	promoter-TSS (FBgn0014184)	promoter-TSS (NM_165864)	80	FBgn0014184 | FBtr0088014
chr4	1295421	1295921	6,89	7,6	0,71	0,000332	0,00437	Intergenic	HETA | LINE | Jockey	63789	FBgn0053653 | FBtr0091630
chr3R	14124495	14124995	9,71	10,41	0,71	0,000349	0,00453	TTS (FBgn0038206)	TTS (NM_142081)	803	FBgn0010340 | FBtr0337095
chr3R	22034715	22035215	11,62	12,33	0,71	0,000391	0,00494	promoter-TSS (FBgn0038927)	promoter-TSS (NM_142748)	511	FBgn0038928 | FBtr0084176
chr3L	15109490	15109990	9,32	10,03	0,71	0,000657	0,00737	promoter-TSS (FBgn0264702)	promoter-TSS (NR_073936)	-805	FBgn0264702 | FBtr0333936
chr2R	17028681	17029181	9,5	10,2	0,71	0,000677	0,0075	exon (FBgn0023172, exon 2 of 24)	5' UTR (NM_206147, exon 2 of 23)	1412	FBgn0023172 | FBtr0086969
chr2R	19488122	19488622	9	9,71	0,71	0,000893	0,00909	exon (FBgn0034452, exon 7 of 9)	exon (NM_137582, exon 7 of 9)	-1535	FBgn0034451 | FBtr0086502
chr2L	8367028	8367528	10,25	10,95	0,71	0,00123	0,0114	intron (FBgn0260439, intron 2 of 6)	CpG	1241	FBgn0260439 | FBtr0005088
chrX	2292223	2292723	10,91	11,62	0,71	0,00156	0,0137	exon (FBgn0023526, exon 2 of 3)	exon (NM_001272255, exon 2 of 3)	938	FBgn0023526 | FBtr0332962
chr3R	25128025	25128525	9,92	10,63	0,71	0,00181	0,0153	promoter-TSS (FBgn0039280)	promoter-TSS (NM_001170249)	646	FBgn0259152 | FBtr0301277
chrX	6655042	6655542	11,86	12,57	0,71	0,00221	0,018	exon (FBgn0028360, exon 2 of 4)	exon (NM_167080, exon 2 of 4)	634	FBgn0028360 | FBtr0343377
chr3L	20779717	20780217	9,52	10,23	0,71	0,00225	0,0182	TTS (FBgn0037021)	TTS (NM_140997)	1369	FBgn0037020 | FBtr0078251
chr2R	24765443	24765943	10,39	11,1	0,71	0,0034	0,025	exon (FBgn0035059, exon 2 of 4)	exon (NM_138119, exon 2 of 4)	2014	FBgn0027590 | FBtr0343496
chr3R	8342289	8342789	9,82	10,53	0,71	0,00457	0,0307	TTS (FBgn0004908)	TTS (NM_057538)	977	FBgn0037578 | FBtr0081854
chr2L	3143308	3143808	8,59	9,29	0,71	0,00484	0,0318	intron (FBgn0015600, intron 1 of 10)	intron (NM_057805, intron 1 of 10)	1228	FBgn0015600 | FBtr0077662
chr2R	17004391	17004891	10,85	11,55	0,71	0,00491	0,0321	promoter-TSS (FBgn0034179)	promoter-TSS (NM_137334)	508	FBgn0026402 | FBtr0087058
chrX	657006	657506	10,67	11,38	0,71	0,00747	0,044	exon (FBgn0025637, exon 2 of 2)	exon (NM_001038729, exon 1 of 1)	183	FBgn0025637 | FBtr0345314
chr3R	12711596	12712096	11,8	12,52	0,72	4,16E-09	4,27E-07	exon (FBgn0002905, exon 1 of 7)	exon (NM_079609, exon 1 of 7)	453	FBgn0002905 | FBtr0086662
chr2R	18845666	18846166	11,2	11,92	0,72	7,34E-09	7,05E-07	TTS (FBgn0034401)	TTS (NM_137538)	703	FBgn0034400 | FBtr0086628
chr2L	6724665	6725165	10,7	11,42	0,72	1,84E-08	1,49E-06	exon (FBgn0046704, exon 2 of 15)	exon (NM_001173226, exon 2 of 15)	1013	FBgn0046704 | FBtr0079300
chrX	15851914	15852414	10,94	11,66	0,72	5,91E-08	3,82E-06	exon (FBgn0026076, exon 2 of 5)	exon (NM_001169292, exon 2 of 5)	1011	FBgn0026076 | FBtr0074174
chr2R	6630130	6630630	10,36	11,09	0,72	2,66E-06	9,17E-05	intron (FBgn0262736, intron 2 of 3)	intron (NM_057453, intron 2 of 3)	2004	FBgn0262736 | FBtr0086151
chrX	17126147	17126647	10,04	10,76	0,72	3,47E-05	0,00071	exon (FBgn0260748, exon 3 of 10)	exon (NM_132967, exon 4 of 11)	520	FBgn0260748 | FBtr0302375
chrX	17626894	17627394	11,31	12,02	0,72	5,02E-05	0,00967	exon (FBgn0030850, exon 2 of 4)	exon (NM_001144745, exon 2 of 3)	751	FBgn0030850 | FBtr0074487
chr3R	26882113	26882613	9,77	10,49	0,72	7,77E-05	0,00136	intron (FBgn0004359, intron 1 of 2)	intron (NM_001276070, intron 1 of 2)	630	FBgn0004359 | FBtr0085065
chr3R	8671563	8672063	10,42	11,15	0,72	9,70E-05	0,00165	exon (FBgn0037607, exon 2 of 3)	exon (NM_169232, exon 2 of 3)	-1129	FBgn0086679 | FBtr0347576
chr2R	17633005	17633505	10,26	10,99	0,72	0,000101	0,0017	TTS (FBgn0034255)	TTS (NM_137396)	261	FBgn0004400 | FBtr0086897
chr3L	17655072	17655572	9,36	10,08	0,72	0,000169	0,00259	exon (FBgn0036745, exon 3 of 3)	exon (NM_140743, exon 3 of 3)	706	FBgn0036745 | FBtr0075184
chr3L	9130214	9130714	8,4	9,13	0,72	0,000347	0,00451	promoter-TSS (FBgn0011206)	promoter-TSS (NM_079265)	-109	FBgn0011206 | FBtr0331858
chrX	13331041	13331541	10,77	11,49	0,72	0,000422	0,00522	exon (FBgn0040309, exon 2 of 2)	exon (NM_167359, exon 2 of 2)	273	FBgn0040309 | FBtr0345161
chr2R	7824667	7825167	9,15	9,87	0,72	0,000467	0,00565	promoter-TSS (FBgn0003082)	promoter-TSS (NM_165564)	224	FBgn0050383 | FBtr0088897
chr3R	27254347	27254847	9,85	10,56	0,72	0,00075	0,00802	exon (FBgn0011289, exon 2 of 7)	exon (NM_057648, exon 2 of 6)	1368	FBgn0011289 | FBtr0085155
chr3L	20454845	20455345	9,54	10,27	0,72	0,000759	0,00809	TTS (FBgn0033120)	TTS (NR_033163)	600	FBgn0082947 | FBtr0113615
chr3R	5661447	5661947	9,55	10,27	0,72	0,000795	0,00834	exon (FBgn0046222, exon 3 of 9)	exon (NM_169092, exon 3 of 9)	1063	FBgn0046222 | FBtr0078713
chrX	19616840	19617340	10,08	10,8	0,72	0,000865	0,0089	TTS (FBgn0031040)	TTS (NM_134484)	895	FBgn0031040 | FBtr0344070
chr2R	11843282	11843782	10,17	10,89	0,72	0,000881	0,00903	promoter-TSS (FBgn0262819)	promoter-TSS (NM_001259341)	708	FBgn0033656 | FBtr0088063
chrX	1045515	1046015	10,38	11,11	0,72	9,00E-04	0,00916	promoter-TSS (FBgn0266569)	promoter-TSS (NM_001042791)	-458	FBgn0266569 | FBtr0299571
chr3R	18759338	18759838	9,25	9,96	0,72	0,000907	0,00922	promoter-TSS (FBgn0038651)	promoter-TSS (NM_142495)	-715	FBgn0038651 | FBtr0273382
chr2R	14764991	14765491	8,73	9,45	0,72	0,00115	0,0109	intron (FBgn0020767, intron 2 of 5)	CpG	4182	FBgn0020767 | FBtr0329880
chr2L	21238780	21239758	8,87	9,59	0,72	0,00399	0,0281	intron (FBgn0261239, intron 2 of 7)	TTS (NR_144677)	931	FBgn0283561 | FBtr0445491
chr2R	9438762	9439262	8,82	9,54	0,72	0,00447	0,0303	intron (FBgn0029092, intron 1 of 6)	intron (NM_001259296, intron 1 of 6)	1874	FBgn0029092 | FBtr0088550
chr3L	16384161	16384661	8,86	9,59	0,72	0,0058	0,0363	promoter-TSS (FBgn0036623)	promoter-TSS (NM_168662)	-40	FBgn0036623 | FBtr0075419
chrX	20172675	20173175	10,37	11,09	0,72	0,00656	0,0398	exon (FBgn0000084, exon 2 of 4)	exon (NM_001169333, exon 2 of 5)	589	FBgn0000084 | FBtr0070025
chr3L	22073847	22074347	11,4	12,13	0,73	8,39E-11	1,51E-08	TTS (FBgn0037151)	TTS (NM_141123)	426	FBgn0037150 | FBtr0078485
chr3R	5601720	5602220	11,15	11,88	0,73	2,05E-07	1,10E-05	promoter-TSS (FBgn0250753)	promoter-TSS (NM_169074)	538	FBgn0037347 | FBtr0273377
chr2R	13168707	13169207	11,02	11,75	0,73	1,22E-05	0,00307	promoter-TSS (FBgn0033799)	promoter-TSS (NM_001274011)	134	FBgn0086532 | FBtr0087730
chrX	21518719	21519219	10,74	11,47	0,73	0,000146	0,0023	exon (FBgn0031182, exon 1 of 1)	exon (NM_134613, exon 1 of 1)	249	FBgn0031182 | FBtr0077212
chrX	10069795	10070295	9,62	10,36	0,73	0,00016	0,00248	intron (FBgn0030174, intron 2 of 6)	intron (NM_001258674, intron 2 of 6)	823	FBgn0030174 | FBtr0071423
chr2L	16680595	16681095	11,01	11,74	0,73	0,000218	0,00317	TTS (FBgn0051807)	TTS (NM_165170)	276	FBgn0267347 | FBtr0305565
chr2R	17428062	17428562	11,59	12,32	0,73	0,000234	0,00338	promoter-TSS (FBgn0034214)	promoter-TSS (NM_137363)	360	FBgn0034215 | FBtr0086916
chr3L	11126168	11126668	10,1	10,83	0,73	0,000366	0,00471	intron (FBgn0260795, intron 1 of 6)	CpG	-2983	FBgn0260795 | FBtr0332705
chr2L	2736900	2737400	8,42	9,15	0,73	0,000396	0,00498	exon (FBgn0031449, exon 3 of 11)	promoter-TSS (NR_047877)	-417	FBgn0263564 | FBtr0309710
chr2R	22120975	22121475	8,45	9,19	0,73	0,00047	0,00566	promoter-TSS (FBgn0002715)	promoter-TSS (NM_057286)	-875	FBgn0002715 | FBtr0071761
chr2L	1911586	1912086	9,63	10,36	0,73	0,000811	0,00847	promoter-TSS (FBgn0031374)	promoter-TSS (NM_001103828)	95	FBgn0031374 | FBtr0309828
chrX	15334711	15335211	9,29	10,02	0,73	0,00124	0,0114	promoter-TSS (FBgn0026428)	promoter-TSS (NM_001169289)	-179	FBgn0026428 | FBtr0301774
chr2R	18400818	18401318	8,99	9,72	0,73	0,00172	0,0147	promoter-TSS (FBgn0263770)	TTS (NM_137480)	356	FBgn0063497 | FBtr0086671
chr3L	18671325	18671825	9,44	10,17	0,73	0,00219	0,0178	exon (FBgn0042134, exon 2 of 4)	exon (NM_144414, exon 2 of 4)	1585	FBgn0042134 | FBtr0075098
chrX	18091793	18092293	11,68	12,41	0,73	0,00493	0,0322	exon (FBgn0021765, exon 2 of 2)	exon (NM_078672, exon 2 of 2)	786	FBgn0021765 | FBtr0074511
chr3R	31057537	31058037	9,14	9,87	0,73	0,00521	0,0334	exon (FBgn0002413, exon 3 of 3)	exon (NM_170536, exon 4 of 4)	3423	FBgn0002413 | FBtr0334548
chr3L	11756706	11757206	8,24	8,96	0,73	0,00567	0,0356	intron (FBgn0017581, intron 1 of 5)	intron (NM_143729, intron 1 of 5)	3123	FBgn0017581 | FBtr0082535
chrX	7946315	7946815	10,87	11,62	0,74	5,45E-11	1,00E-08	exon (FBgn0027280, exon 1 of 5)	exon (NM_132199, exon 1 of 5)	343	FBgn0027280 | FBtr0071129
chr3L	16142883	16143383	10,81	11,55	0,74	1,25E-10	2,05E-08	exon (FBgn0052152, exon 1 of 4)	exon (NM_168553, exon 1 of 4)	599	FBgn0036576 | FBtr0307519
chr2R	6672619	6673119	11,23	11,97	0,74	6,48E-08	4,09E-06	promoter-TSS (FBgn0033085)	promoter-TSS (NM_165482)	503	FBgn0033087 | FBtr0086145
chr3L	21537266	21537766	11,84	12,58	0,74	1,49E-07	8,48E-06	TTS (FBgn0053289)	TTS (NM_206416)	451	FBgn0015283 | FBtr0333453
chr2R	12260104	12260604	10,7	11,44	0,74	8,92E-07	3,81E-05	exon (FBgn0264501, exon 3 of 3)	non-coding (NR_073871, exon 3 of 3)	323	FBgn0000253 | FBtr0345018
chr3L	7434200	7434700	11,17	11,91	0,74	4,53E-06	0,00139	exon (FBgn0014011, exon 1 of 1)	exon (NM_139864, exon 1 of 1)	740	FBgn0014011 | FBtr0332800
chrX	18783795	18784295	11,29	12,03	0,74	5,01E-06	0,00149	promoter-TSS (FBgn0030956)	promoter-TSS (NM_133096)	-551	FBgn0030956 | FBtr0074661
chr3L	1860885	1861385	11,3	12,04	0,74	5,65E-05	0,00107	exon (FBgn0004636, exon 1 of 1)	exon (NM_057509, exon 2 of 2)	681	FBgn0004636 | FBtr0332671
chr3L	1515821	1516321	10,03	10,77	0,74	0,000325	0,0043	intron (FBgn0011204, intron 1 of 3)	intron (NM_138269, intron 1 of 3)	1200	FBgn0011204 | FBtr0072706
chr3R	30278767	30279267	10,97	11,71	0,74	0,000349	0,00453	exon (FBgn0010113, exon 1 of 6)	exon (NM_176591, exon 1 of 6)	1086	FBgn0010113 | FBtr0085619
chr2L	10425638	10426138	11,62	12,36	0,74	0,000351	0,00454	promoter-TSS (FBgn0267330)	promoter-TSS (NM_164928)	739	FBgn0262601 | FBtr0304118
chr3R	11242707	11243207	10,17	10,91	0,74	0,000449	0,0055	TTS (FBgn0037889)	TTS (NM_141805)	1042	FBgn0037890 | FBtr0082360
chr3L	11831095	11831595	8,58	9,32	0,74	0,000821	0,00853	TTS (FBgn0036214)	TTS (NM_140258)	1969	FBgn0036214 | FBtr0332130
chr2L	20825670	20826170	10,99	11,73	0,74	0,00108	0,0104	exon (FBgn0032889, exon 3 of 6)	exon (NM_206015, exon 2 of 5)	385	FBgn0032889 | FBtr0081418
chr2R	15999592	16000092	10,59	11,33	0,74	0,00257	0,0201	exon (FBgn0020236, exon 2 of 9)	exon (NM_001144202, exon 2 of 9)	445	FBgn0020236 | FBtr0300598
chr2R	15921458	15921958	8,93	9,67	0,74	0,00283	0,0216	exon (FBgn0264089, exon 1 of 21)	5' UTR (NM_001103863, exon 1 of 20)	430	FBgn0264089 | FBtr0330732
chr2L	4463804	4464304	10,51	11,25	0,74	0,00452	0,0305	promoter-TSS (FBgn0031609)	promoter-TSS (NM_001273100)	444	FBgn0031610 | FBtr0077442
chr3L	21024550	21025050	9,24	9,98	0,74	0,00647	0,0395	intron (FBgn0003415, intron 2 of 13)	intron (NM_001275205, intron 2 of 12)	1404	FBgn0003415 | FBtr0333284
chr3R	17117306	17117806	8,54	9,29	0,74	0,0068	0,041	intron (FBgn0014141, intron 1 of 15)	intron (NM_001202309, intron 1 of 15)	1526	FBgn0014141 | FBtr0089471
chr3L	3194620	3195120	10,66	11,41	0,75	1,61E-08	1,33E-06	exon (FBgn0001233, exon 2 of 2)	exon (NM_079175, exon 2 of 2)	1655	FBgn0001233 | FBtr0073040
chr2L	4847981	4848481	11,68	12,43	0,75	6,81E-08	4,19E-06	promoter-TSS (FBgn0031637)	promoter-TSS (NM_001169403)	466	FBgn0031638 | FBtr0077386
chr2R	14169621	14170121	10,52	11,28	0,75	9,86E-08	5,84E-06	promoter-TSS (FBgn0033906)	promoter-TSS (NM_137092)	427	FBgn0265499 | FBtr0339963

chr3R	15329053	15329553	11,05	11,8	0,75	8,66E-06	0,000227	exon (FBgn0000533, exon 2 of 3)	exon (NM_079638, exon 2 of 3)	575	FBgn0000533	FBtr0083083
chr2L	12038828	12039328	9,99	10,75	0,75	9,75E-06	0,000253	promoter-TSS (FBgn0032397)	promoter-TSS (NM_164986)	-567	FBgn0032397	FBtr0080309
chr2L	12098296	12098796	10,25	11	0,75	2,24E-05	5,00E-04	TTS (FBgn0028707)	TTS (NM_001042890)	709	FBgn0032409	FBtr0080330
chr3R	31591762	31592262	10,16	10,91	0,75	3,02E-05	0,000631	promoter-TSS (FBgn0039856)	promoter-TSS (NM_143618)	-790	FBgn0039856	FBtr0085798
chrX	19164293	19164793	9,38	10,13	0,75	0,00014	0,00222	exon (FBgn0261461, exon 2 of 6)	exon (NM_001144749, exon 2 of 6)	804	FBgn0261461	FBtr0299622
chr3R	17400240	17400740	10,14	10,89	0,75	0,000217	0,00317	intron (FBgn0038504, intron 1 of 2)	(CCACCCA)n|Simple_repeat|Simple_rep	964	FBgn0038504	FBtr0083448
chr3R	17448375	17448875	8,56	9,31	0,75	0,000312	0,00417	promoter-TSS (FBgn0260632)	promoter-TSS (NM_001169530)	-115	FBgn0260632	FBtr0301384
chr2R	11983921	11984421	10,38	11,13	0,75	0,000717	0,00781	exon (FBgn0011704, exon 3 of 3)	exon (NM_080372, exon 3 of 3)	-1215	FBgn0053145	FBtr0088047
chrX	9281010	9281510	9,28	10,03	0,75	0,00447	0,0303	exon (FBgn0040236, exon 3 of 9)	exon (NM_144349, exon 3 of 9)	1857	FBgn0040236	FBtr0343368
chrX	2065330	2065830	11,31	12,07	0,76	6,65E-08	4,13E-06	promoter-TSS (FBgn0025626)	promoter-TSS (NM_130617)	126	FBgn0265531	FBtr0340110
chrX	621761	622261	10,97	11,73	0,76	1,07E-07	6,24E-06	promoter-TSS (FBgn0029529)	promoter-TSS (NM_130493)	206	FBgn0016038	FBtr0089723
chrX	8062184	8062684	9,95	10,72	0,76	1,05E-05	0,000271	intron (FBgn0004657, intron 1 of 6)	promoter-TSS (NM_206647)	790	FBgn0004657	FBtr0071105
chr3R	20587192	20587692	10,49	11,25	0,76	1,44E-05	0,00035	promoter-TSS (FBgn0267711)	promoter-TSS (NR_133475)	-560	FBgn0267711	FBtr0347751
chr3R	22133745	22134245	10,03	10,79	0,76	1,45E-05	0,00035	TTS (FBgn0259736)	TTS (NM_206540)	161	FBgn0051163	FBtr0084197
chr3R	15289997	15290497	9,62	10,38	0,76	0,000114	0,00186	promoter-TSS (FBgn0003721)	promoter-TSS (NM_079636)	552	FBgn0266745	FBtr0345248
chrX	3447601	3448101	8,07	8,83	0,76	0,000211	0,00309	intron (FBgn0029657, intron 2 of 6)	intron (NM_001272276, intron 2 of 6)	1092	FBgn0029657	FBtr0344078
chr2L	2584076	2584576	9,64	10,4	0,76	0,000258	0,00361	exon (FBgn0026479, exon 2 of 8)	exon (NM_001273017, exon 2 of 8)	1104	FBgn0026479	FBtr0335173
chr2R	25262610	25263110	8,09	8,85	0,76	0,000267	0,00371	Intergenic	HETA|LINE|Rodrey	-7542	FBgn0035094	FBtr0333172
chr2R	12514615	12515115	10,07	10,83	0,76	0,000373	0,00479	promoter-TSS (FBgn0033750)	promoter-TSS (NM_136949)	197	FBgn0033749	FBtr0087942
chr2R	17591098	17591598	11,43	12,19	0,76	0,000407	0,00509	promoter-TSS (FBgn0034249)	promoter-TSS (NM_001274131)	385	FBgn0029079	FBtr0086832
chrX	2146596	2147096	10,27	11,04	0,76	0,000891	0,00909	intron (FBgn0004654, intron 2 of 2)	intron (NM_057512, intron 2 of 2)	1484	FBgn0004654	FBtr0331410
chr2R	12146652	12147152	9,49	10,25	0,76	0,000917	0,00928	exon (FBgn0027504, exon 5 of 5)	exon (NM_001273984, exon 5 of 5)	1193	FBgn0033686	FBtr0087984
chrX	16799231	16799731	9,95	10,7	0,76	0,00122	0,0113	exon (FBgn0030791, exon 1 of 3)	exon (NM_206768, exon 1 of 3)	253	FBgn0030791	FBtr0074353
chrX	9354806	9355306	9,09	9,86	0,76	0,00125	0,0115	exon (FBgn0085478, exon 2 of 11)	5' UTR (NM_001103452, exon 2 of 10)	1171	FBgn0085478	FBtr0112753
chr2R	17395514	17396014	8,8	9,56	0,76	0,00162	0,0141	intron (FBgn0010620, intron 1 of 1)	intron (NM_079973, intron 1 of 1)	1172	FBgn0010620	FBtr0086909
chr3L	11196636	11197136	9,86	10,61	0,76	0,00808	0,0468	intron (FBgn0036144, intron 1 of 7)	intron (NM_001259785, intron 1 of 7)	650	FBgn0036144	FBtr0076189
chr3L	8357618	8358118	9,22	9,99	0,76	0,0086	0,0487	exon (FBgn0001248, exon 2 of 2)	exon (NM_001144439, exon 3 of 3)	257	FBgn0001248	FBtr0076671
chr3L	21173387	21173887	11,51	12,28	0,77	2,09E-11	4,68E-09	exon (FBgn0270926, exon 1 of 1)	exon (NM_206410, exon 1 of 1)	520	FBgn0270926	FBtr0089463
chr2R	23994299	23994799	11,06	11,84	0,77	1,11E-09	1,47E-07	TTS (FBgn0053519)	TTS (NM_001014545)	506	FBgn0034951	FBtr0072201
chr3R	16051946	16052446	10,21	10,99	0,77	6,28E-07	2,76E-05	exon (FBgn0027948, exon 2 of 15)	exon (NM_001170156, exon 2 of 15)	319	FBgn0027948	FBtr0304803
chr2R	13952647	13953147	9,99	10,76	0,77	1,03E-05	0,000267	intron (FBgn0262739, intron 3 of 7)	intron (NM_001259385, intron 3 of 7)	1128	FBgn0262739	FBtr0087614
chr3R	10265184	10265684	9,35	10,13	0,77	0,000113	0,00185	intron (FBgn0262617, intron 1 of 11)	intron (NM_001260090, intron 1 of 13)	1129	FBgn0262617	FBtr0305354
chr3R	18747098	18747598	9,6	10,37	0,77	0,000176	0,00268	exon (FBgn0260399, exon 2 of 5)	exon (NM_080121, exon 2 of 6)	979	FBgn0260399	FBtr0083674
chrX	8419511	8420011	9,13	9,9	0,77	0,000192	0,00288	intron (FBgn0261793, intron 3 of 9)	intron (NM_206654, intron 3 of 9)	-1603	FBgn0261793	FBtr0330105
chrX	2157080	2157580	9,87	10,64	0,77	0,000295	0,004	exon (FBgn0004655, exon 2 of 8)	exon (NM_080303, exon 2 of 8)	-1428	FBgn0004655	FBtr0070430
chr2L	8161804	8162304	10,23	11	0,77	0,000414	0,00516	TTS (FBgn0261064)	TTS (NM_135342)	364	FBgn0031992	FBtr0079640
chr3L	18626350	18626850	9,9	10,68	0,77	0,00077	0,00816	intron (FBgn0036801, intron 1 of 8)	intron (NM_001275088, intron 1 of 8)	642	FBgn0036801	FBtr0075049
chr3R	15294441	15295439	9,61	10,38	0,77	0,000943	0,0094	intron (FBgn0003721, intron 1 of 7)	intron (NM_001260191, intron 1 of 7)	3995	FBgn0003721	FBtr0305656
chrX	8142743	8143243	11,9	12,67	0,77	0,00159	0,0139	promoter-TSS (FBgn0025800)	promoter-TSS (NM_078524)	612	FBgn0030006	FBtr0071191
chr3L	1964852	1965352	9,54	10,31	0,77	0,00362	0,026	promoter-TSS (FBgn0265988)	promoter-TSS (NM_139424)	644	FBgn0035298	FBtr0072844
chr2R	21495626	21496126	8,71	9,48	0,77	0,00661	0,04	promoter-TSS (FBgn0010470)	promoter-TSS (NM_001299751)	-352	FBgn0010470	FBtr0342897
chr2L	12270149	12270649	8,2	8,97	0,77	0,00714	0,0424	promoter-TSS (FBgn0000114)	promoter-TSS (NM_001169492)	-532	FBgn0000114	FBtr0300567
chr2L	6069884	6070384	11,17	11,95	0,78	9,44E-13	2,45E-10	promoter-TSS (FBgn0266449)	promoter-TSS (NM_078766)	512	FBgn0031777	FBtr0079213
chr3R	11821495	11821995	11,25	12,03	0,78	1,16E-09	1,48E-07	TTS (FBgn0037956)	TTS (NM_001144565)	332	FBgn0037955	FBtr0082521
chr3L	2598639	2599139	10,05	10,83	0,78	2,38E-06	8,47E-05	promoter-TSS (FBgn0035355)	promoter-TSS (NM_139473)	-407	FBgn0035355	FBtr0072929
chr3R	29200641	29201141	11,54	12,32	0,78	2,45E-06	8,61E-05	TTS (FBgn0039650)	TTS (NM_143425)	438	FBgn0014427	FBtr0085390
chrX	6353086	6353586	9,94	10,72	0,78	5,43E-05	0,00103	intron (FBgn0261955, intron 1 of 2)	intron (NM_132091, intron 1 of 2)	1055	FBgn0261955	FBtr0070907
chr2L	6371603	6372103	9,32	10,1	0,78	7,66E-05	0,00135	promoter-TSS (FBgn0043854)	promoter-TSS (NM_135176)	-534	FBgn0043854	FBtr0290281
chr3R	25070142	25070642	10,61	11,38	0,78	8,55E-05	0,00147	promoter-TSS (FBgn0039272)	promoter-TSS (NM_001170247)	466	FBgn0039272	FBtr0304718
chr3L	22774569	22775069	9,33	10,12	0,78	0,000185	0,00279	exon (FBgn0052451, exon 2 of 5)	5' UTR (NM_001170025, exon 2 of 5)	783	FBgn0052451	FBtr0302134
chrX	9683125	9683625	11,58	12,37	0,78	0,000292	0,00396	exon (FBgn0261617, exon 2 of 14)	5' UTR (NM_001201647, exon 2 of 14)	2292	FBgn0261617	FBtr0071402
chr3L	11293716	11294216	10,82	11,6	0,78	0,000304	0,00408	exon (FBgn0036152, exon 1 of 3)	exon (NM_140200, exon 1 of 3)	822	FBgn0036152	FBtr0076183
chr3R	15804317	15804817	10,19	10,97	0,78	0,000796	0,00834	TTS (FBgn0038365)	TTS (NM_142236)	320	FBgn0026616	FBtr0083179
chr3R	13013732	13014232	9,67	10,45	0,78	0,000918	0,00928	intron (FBgn0020496, intron 1 of 5)	intron (NM_169491, intron 1 of 5)	2334	FBgn0020496	FBtr0082699
chr3L	7156497	7156997	8,24	9,03	0,78	0,00367	0,0263	exon (FBgn0259173, exon 1 of 8)	5' UTR (NM_168193, exon 1 of 8)	326	FBgn0259173	FBtr0299641
chrX	15856855	15857355	11,14	11,93	0,79	4,51E-11	8,66E-09	exon (FBgn0002914, exon 2 of 3)	5' UTR (NM_206734, exon 2 of 3)	738	FBgn0002914	FBtr0074171
chr3R	23363070	23363570	10,73	11,52	0,79	2,46E-09	2,79E-07	exon (FBgn0039073, exon 1 of 1)	exon (NM_142884, exon 1 of 1)	248	FBgn0039073	FBtr0339619
chrX	16357850	16358350	11,08	11,88	0,79	1,10E-08	9,80E-07	exon (FBgn0005411, exon 2 of 5)	exon (NM_057543, exon 2 of 5)	353	FBgn0005411	FBtr0307176
chr2R	23895284	23895784	10,77	11,56	0,79	4,34E-08	3,00E-06	promoter-TSS (FBgn0034923)	promoter-TSS (NM_166629)	472	FBgn0034924	FBtr0072133
chrX	18083713	18084213	10,38	11,17	0,79	4,41E-08	3,00E-06	intron (FBgn0030890, intron 1 of 6)	CpG	1444	FBgn0030890	FBtr0343317
chr3R	25244418	25244918	10,19	10,99	0,79	2,34E-06	8,41E-05	exon (FBgn0000158, exon 1 of 3)	exon (NM_057452, exon 1 of 3)	389	FBgn0000158	FBtr0084869
chrX	20166773	20167273	11,46	12,25	0,79	6,22E-06	0,000176	exon (FBgn0031092, exon 2 of 4)	exon (NM_134531, exon 2 of 4)	351	FBgn0031092	FBtr0070007
chr2R	10416336	10416836	9,75	10,54	0,79	7,37E-06	0,000204	exon (FBgn0261698, exon 1 of 28)	5' UTR (NM_001273935, exon 1 of 28)	430	FBgn0261698	FBtr0303083
chrX	12655108	12655608	9,61	10,4	0,79	1,54E-05	0,000368	intron (FBgn0015024, intron 2 of 3)	CpG	659	FBgn0015024	FBtr0073682
chr2L	16043928	16044428	9,59	10,38	0,79	2,22E-05	0,000495	promoter-TSS (FBgn0000182)	promoter-TSS (NM_165145)	-373	FBgn0000182	FBtr0080805
chr2R	17847294	17847794	11,28	12,07	0,79	3,75E-05	0,00076	exon (FBgn0015522, exon 1 of 1)	exon (NM_137428, exon 1 of 1)	846	FBgn0015522	FBtr0086799
chrX	20658222	20658722	11,01	11,79	0,79	5,01E-05	0,000967	promoter-TSS (FBgn0267022)	promoter-TSS (NR_123969)	-794	FBgn0267022	FBtr0345968
chr3R	5255582	5256082	9,18	9,97	0,79	6,19E-05	0,00114	TTS (FBgn0037304)	TTS (NM_141265)	849	FBgn0037305	FBtr0078821
chr2L	1156937	1157437	10	10,78	0,79	7,49E-05	0,00133	promoter-TSS (FBgn0261458)	promoter-TSS (NM_001038781)	-876	FBgn0261458	FBtr0100023
chrX	5880787	5881287	10,02	10,81	0,79	7,94E-05	0,00139	exon (FBgn0029820, exon 2 of 6)	5' UTR (NM_132047, exon 2 of 6)	219	FBgn0029820	FBtr0345313
chr2L	19574180	19574680	9,3	10,09	0,79	8,17E-05	0,00142	intron (FBgn0005672, intron 1 of 2)	intron (NM_134291, intron 1 of 2)	1157	FBgn0005672	FBtr0100597
chr3L	12806803	12807303	9,96	10,75	0,79	0,000231	0,00833	exon (FBgn0262714, exon 2 of 10)	exon (NM_168519, exon 2 of 10)	868	FBgn0262714	FBtr0114506
chr3R	30013316	30013816	8,87	9,66	0,79	0,000309	0,00413	intron (FBgn0039737, intron 1 of 3)	CpG	1599	FBgn0039737	FBtr0334706
chr3L	222232	222732	9,39	10,18	0,79	0,000691	0,00759	exon (FBgn0085113, exon 2 of 9)	exon (NM_138171, exon 2 of 9)	587	FBgn0035113	FBtr0072524
chr2R	14171673	14172173	9,44	10,23	0,79	0,00074	0,00797	exon (FBgn0033906, exon 1 of 4)	5' UTR (NM_001201998, exon 1 of 4)	135	FBgn0033906	FBtr0302452
chr2R	19670663	19671163	11,76	12,56	0,79	0,00115	0,0108	promoter-TSS (FBgn0028372)	promoter-TSS (NM_166373)	-249	FBgn0028372	FBtr0086474
chrX	12582123	12582623	11,97	12,77	0,79	0,00243	0,0193	exon (FBgn0030400, exon 1 of 4)	exon (NM_001144720, exon 1 of 4)	820	FBgn0030400	FBtr0331718
chr2L	2376995	2377495	9,61	10,41	0,79	0,00437	0,0298	exon (FBgn0031420, exon 2 of 3)	exon (NM_001273004, exon 2 of 3)	913	FBgn0031420	FBtr0331437
chr2L	18696457	18696957	9,84	10,63	0,79	0,00514	0,0331	exon (FBgn0032700, exon 2 of 4)	exon (NM_136053, exon 2 of 4)	977	FBgn0032700	FBtr0081096
chr3R	14291044	14291544	7,63	8,42	0,79	0,00531	0,0338	intron (FBgn0285913, intron 2 of 4)	intron (NM_001260168, intron 2 of 4)	894	FBgn0285913	FBtr0082922
chr3R	25594963	25595463	11,94	12,73	0,79	0,00764	0,0447	exon (FBgn0011666, exon 1 of 3)	exon (NM_170229, exon 5 of 7)	739	FBgn0011666	FBtr0084882
chr3L	21304970	21305470	11,13	11,93	0,8	3,08E-08	2,34E-06	promoter-TSS (FBgn0037070)	promoter-TSS (NM_168896)	524	FBgn0037071	FBtr0078339
chr2L	9891314	9891814	10,33	11,13	0,8	5,40E-08	3,56E-06	promoter-TSS (FBgn0085212)	promoter-TSS (NM_001103664)	680	FBgn0032153	FBtr0113031
chr2R	11631883	11632383	9,66	10,46	0,8	7,12E-05	0,00128	exon (FBgn0033638, exon 1 of 8)	5' UTR (NM_001169647, exon 1 of 8)	382	FBgn0033638	FBtr0300945
chr2L	10203199	10203699	10,39	11,19	0,8	7,23E-05	0,00129	exon (FBgn0085188, exon 2 of 3)	exon (NM_001103667, exon 2 of 3)	868	FBgn0085188	FBtr0112350
chr2R	11825752	11826252	10,26	11,06	0,8	0,000159	0,00247	exon (FBgn0033653, exon 2 of 3)	exon (NM_136858, exon 2 of 3)	658	FBgn0033653	FBtr0088031
chr3L	9679762	9680262	9,46	10,26	0,8	0,000257	0,0036	promoter-TSS (FBgn0016081)	promoter-TSS (NM_168357)	832	FBgn0036028	FBtr0076392
chr2R	5411914	5412414	7,54	8,34	0,8	0,000409	0,0051	Intergenic	TC1_DM1|DNA|TcMar-Tc1	-1579	FBgn0259247	FBtr0299918
chr2R	9294546	9295046	9,55	10,36	0,8	0,000522	0,00617	promoter-TSS (FBgn0028408)	promoter-TSS (NM_001103768)	2	FBgn0028408	FBtr0112930
chr2L	4196297	4196797	8,15	8,96	0,8	0,000572	0,00659	exon (FBgn0031589, exon 2 of 12)	exon (NM_001103607, exon 3 of 13)	833	FBgn0031589	FBtr0077483
chr2R	13860930	13861430	10,42	11,23	0,8	0,000775	0,0082	promoter-TSS (FBgn0033884)	promoter-TSS (NM_001032745)	750	FBgn0033883	FBtr0339954
chr3L	18993632	18994132	9,99	10,78	0,8	0,00141	0,0126	promoter-TSS (FBgn0036837)	promoter-TSS (NM_176348)	111	FBgn0036837	FBtr0075044
chr2L	12273324	12273824	8,93	9,74	0,8	0,006	0,0373	intron (FBgn0000114, intron 2 of 8)	intron (NM_165002, intron 3 of 11)	2643	FBgn0000114	FBtr0300567
chr2R	18854720	18855220	10,04	10,85	0,81	9,05E-07	3,84E-05	TTS (FBgn0034405)	TTS (NM_176233)	117	FBgn0010053	FBtr0086625
chr3L	14274883	14275383	9,31	10,12	0,81	5,37E-05	0,00102	exon (FBgn0001085, exon 1 of 5)	exon (NM_080073, exon 1 of 5)	791	FBgn0001085	FBtr0075743
chr2L	12274455	12274955	8,4	9,21	0,81	0,000121	0,00195	intron (FBgn0000114, intron 2 of 8)	intron (NM_165002, intron 3 of 11)	3774	FBgn0000114	FBtr0300567
chr3R	25889493	25889993	10,24	11,05	0,81	0,000264	0,00367	exon (FBgn0028717, exon 2 of 4)	5' UTR (NM_170247, exon 2 of 4)	1202	FBgn0028717	FBtr0084935
chr3R	18225266	18225766	10,87	11,67	0,81	0,000272	0,00377	promoter-TSS (FBgn0262559)	promoter-TSS (NM_142439)	566	FBgn0038586	FBtr0083608
chr2L	5537375	5537875	9,26	10,07	0,81	0,000297	0,00401	promoter-TSS (FBgn0031715)	promoter-TSS (NM_135092)	-867	FBgn0031715	FBtr0079127
chr2L	3805452	3805952	9,54	10,35	0,81	0,000744	0,008	promoter-TSS (FBgn0021800)	promoter-TSS (NM_164561)	21	FBgn0021800	FBtr0077498
chr2R	2857223	2857723	7,53	8,33	0,81	0,00113	0,0107	Intergenic	MAX_I-int|LTR|Pao	-10765	FBgn0085638	FBtr0301792
chr3R	29952300	29952800	7,94	8,75	0,81	0,00139	0,0125	intron (FBgn0004622, intron 7 of 9)	CpG	16573	FBgn0039727	FBtr0300825
chr3L	7719911	7720411	10,64	11,46	0,81	0,00155	0,0136	exon (FBgn0035812, exon 5 of 5)	exon (NM_139892, exon 2 of 3)	832	FBgn0035811	FBtr0076808
chr2R	12591043	12591543	9,26	10,07	0,81	0,00534	0,034	TTS (FBgn0050055)	TTS (NR_037739)	1527	FBgn0050055	FBtr0345021
chr3L	21955138	21955638	10,83	11,65	0,82	1,87E-12	4,60E-10	exon (FBgn0037144, exon 1 of 6)	exon (NM_141117, exon 1 of 6)	270	FBgn0037144	FBtr0078475
chr3L	8177306	8177806	10	10,82	0,82	1,38E-06	5,43E-05	exon (FBgn0020392, exon 2 of 2)	exon (NM_079245, exon 2 of 2)	873	FBgn0020392	FBtr0076728
chrX	19320712	19321212	9,77	10,59	0,82	2,76E-06	9,38E-05	intron (FBgn0259834, intron 1 of 4)	intron (NM_001298506, intron 1 of 4)	1144	FBgn0259834	FBtr0344324
chr3L	1306526	1307026	11,15	11,97	0,82	5,21E-06	0,000153	promoter-TSS (FBgn0035205)	promoter-TSS (NM_176271)	336	FBgn0035204	FBtr0345006
chr2R	21313407	21313907	10,67	11,49	0,82	5,35E-06	0,000156	promoter-TSS (FBgn0034618)	promoter-TSS (NM_137733)	-214	FBgn0034618	FBtr0071601
chr2R	17567386	17567886	10	10,82	0,82	2,28E-05	0,000504	exon (FBgn0034243, exon 2 of 3)	exon (NM_137888, exon 2 of 3)	820	FBgn0034243	FBtr0086906
chr3R	22421792	22422292	9,68	10,5	0,82	2,49E-05	0,000546	promoter-TSS (FBgn0038964)	promoter-TSS (NM_142783)	718	FBgn0038965	FBtr0345205
chrX	19636009	19636509	10,64	11,46	0,82	6,24E-05	0,00115	exon (FBgn0087008, exon 2 of 12)	exon (NM_001272792, exon 3 of 13)	2110	FBgn0087008	FBtr0334278
chr3R	30449546	30450046	10,3	11,13	0,82	0,000101	0,0017	intron (FBgn0028646, intron 2 of 9)	CpG	630	FBgn0028646	FBtr0085694
chr2L	7574410	7574910	7,89	8,71	0,82	0,000188	0,00283	intron (FBgn0264895, intron 1 of 5)	intron (NM_144299, intron 1 of 5)	1353	FBgn0264895	FBtr0334850
chr3L	13389464	13389964	11,3	12,12	0,82	0,000263	0,00366	exon (FBgn0036354, exon 1 of 2)	exon (NM_140383, exon 1 of 2)	292	FBgn0036354	FBtr0075863
chr2L	11000354	11000854	9,85	10,67	0,82	0,000729	0,00792	exon (FBgn0000146, exon 3 of 9)	exon (NM_001103674, exon 2 of 8)	504	FBgn0000146	FBtr0112793
chr3R	13304054	13304554	9,27	10,1	0,82	0,000884	0,00905	promoter-TSS (FBgn0052473)	promoter-TSS (NM_169504)	-459	FBgn0052473	FBtr0082743
chr2R	24941115	24941615	11,26	12,09	0,83	3,60E-14	1,27E-11	promoter-TSS (FBgn0035082)	promoter-TSS (NM_138138)	755	FBgn0035083	FBtr0100389
chr2R	6714110	6714610	9,58	10,41	0,83	1,29E-05	0,000319	intron (FBgn0033095, intron 1 of 6)	intron (NM_001299217, intron 1 of 6)	1532	FBgn0033095	FBtr0086140
chr2L	20082695	20083195	10,53	11,35	0,83	1,96E-05	0,000445	exon (FBgn0263773, exon 2 of 2)	exon (NM_080713, exon 2 of 2)	2125	FBgn0263773	FBtr0310560
chr3L	5928544	5929044	9,11	9,95	0,83	4,05E-05	0,000808	exon (FBgn0053523, exon 7 of 8)	exon (NM_001014569, exon 6 of 7)	379	FBgn0053523	FBtr0091476
chr3R	10389671	10390171	8,67	9,5	0,83	4,18E-05	0,000826	intron (FBgn0259938, intron 1 of 2)	intron (NM_001260095, intron 1 of 2)	1664	FBgn0259938	FBtr0082246
chr3R	4171126	4171626	8,64	9,47	0,83	8,50E-05	0,00147	exon (FBgn0261274, exon 2 of 5)	exon (NM_139608, exon 2 of 5)	973	FBgn0261274	FBtr0073217
chr3R	22368954	22369454	9,27	10,1	0,83	0,000104	0,00172	promoter-TSS (FBgn0267385)	promoter-TSS (NM_079724)	-77	FBgn0267385	FBtr0084214
chr3L	14027977	14028477	10,18	11	0,83	0,000198	0,00295	exon (FBgn0052133, exon 2 of 7)	exon (NM_168571, exon 2 of 7)	894	FBgn0052133	FBtr0075784
chr3L	4320120	4320620	9,19	10,02	0,83	0,000689	0,00759	TTS (FBgn0035532)	TTS (NM_139635)	1616	FBgn0052250	FBtr0073287
chr2R	24945575	24946075	11,06	11,89	0,83	0,000927	0,00932	promoter-TSS (FBgn0035084)	promoter-TSS (NM_001299934)	161	FBgn0035085	FBtr0343502
chr2R	6713452	6713952	8,11	8,94	0,83	0,00095	0,00944	intron (FBgn0033095, intron 1 of 6)	intron (NM_001299217, intron 1 of 6)	-1418	FBgn0033095	FBtr0336659
chrX	10323700	10324200	9,81	10,64	0,83	0,00144	0,0128	exon (FBgn0259170, exon 2 of 7)	exon (NM_206676, exon 2 of 7)	2008	FBgn0259170	FBtr0300511
chr3R	10047638	10048138	10,61	11,45	0,84	2,61E-11	5,35E-09	TTS (FBgn0037778)	TTS (NM_141714)	909	FBgn0037779	FBtr0082204
chr2L	6675830	6676330	10,4	11,23	0,84	1,71E-07	9,43E-06	TTS (FBgn0031848)	TTS (NM_001273216)	487	FBgn0000351	FBtr0333350

chr3L	15162476	15162976	10,06	10,91	0,84	2,42E-07	1,26E-05	TTS (FBgn0036488)	TTS (NM_140500)	902	FBgn0036489 | FBtr0075645
chr3R	25051130	25051630	10,6	11,44	0,84	1,24E-05	0,000309	exon (FBgn0039266, exon 2 of 3)	exon (NM_001104437, exon 2 of 3)	1138	FBgn0039266 | FBtr0084763
chrX	18566494	18566994	10,08	10,92	0,84	1,25E-05	0,000501	TTS (FBgn0052546)	exon (NM_001272759, exon 3 of 5)	439	FBgn0265598 | FBtr0340365
chr2R	18407821	18408321	9,83	10,67	0,84	3,41E-05	0,000701	promoter-TSS (FBgn0063491)	promoter-TSS (NM_166279)	238	FBgn0063492 | FBtr0086676
chr2R	11614930	11615430	9,76	10,59	0,84	6,25E-05	0,00115	intron (FBgn0033636, intron 1 of 16)	intron (NM_078977, intron 1 of 16)	865	FBgn0033686 | FBtr0088091
chr3L	16043981	16044481	8,91	9,75	0,84	0,000102	0,00171	intron (FBgn0260635, intron 1 of 2)	intron (NM_001274988, intron 1 of 2)	1661	FBgn0260635 | FBtr0075501
chrX	8151641	8152141	10,25	11,1	0,84	0,00304	0,023	exon (FBgn0030011, exon 1 of 3)	exon (NM_132224, exon 1 of 3)	384	FBgn0030011 | FBtr0071189
chr2L	6481870	6482370	10,79	11,64	0,85	4,81E-11	9,04E-09	exon (FBgn0031820, exon 2 of 4)	exon (NM_135191, exon 2 of 4)	-1190	FBgn0267019 | FBtr0345975
chr2R	16692226	16692726	10,66	11,51	0,85	2,91E-07	1,48E-05	exon (FBgn0013763, exon 2 of 3)	exon (NM_057733, exon 2 of 3)	776	FBgn0013763 | FBtr0087111
chrX	5905635	5906135	10,38	11,23	0,85	9,18E-07	3,88E-05	promoter-TSS (FBgn0029821)	promoter-TSS (NM_132048)	4	FBgn0029821 | FBtr0070824
chr3L	24535054	24535554	8,63	9,48	0,85	0,00013	0,00208	exon (FBgn0040045, exon 2 of 2)	CpG	1215	FBgn0040045 | FBtr0307117
chr3L	11121452	11121952	10,14	10,99	0,85	0,000227	0,0033	promoter-TSS (FBgn0036134)	promoter-TSS (NM_168443)	856	FBgn0036135 | FBtr0076211
chr2R	18397116	18397616	8,55	9,4	0,85	0,000297	0,00401	exon (FBgn0063499, exon 1 of 1)	exon (NM_137478, exon 1 of 1)	160	FBgn0063499 | FBtr0086726
chr3R	29766889	29767389	9,02	9,87	0,85	0,000428	0,00528	exon (FBgn0001297, exon 1 of 3)	exon (NM_001032408, exon 1 of 3)	1145	FBgn0001297 | FBtr0099588
chrX	19781974	19782474	11,4	12,25	0,85	0,000458	0,00557	exon (FBgn0259789, exon 2 of 3)	exon (NM_167685, exon 2 of 2)	919	FBgn0259789 | FBtr0345014
chr2L	3630814	3631314	9,41	10,26	0,85	0,000502	0,00601	intron (FBgn0000721, intron 1 of 7)	intron (NM_001163387, intron 1 of 7)	1090	FBgn0000721 | FBtr0089306
chr2R	18287383	18287883	10,12	10,97	0,85	0,000542	0,0063	exon (FBgn0285917, exon 4 of 11)	exon (NM_001169739, exon 5 of 5)	-1062	FBgn0034321 | FBtr0301546
chr2R	18128533	18129033	9,86	10,7	0,85	0,000981	0,00967	TTS (FBgn0028983)	TTS (NM_080214)	290	FBgn0040465 | FBtr0086734
chr2R	9293515	9294015	9,98	10,85	0,86	1,63E-07	9,06E-06	intron (FBgn0028408, intron 1 of 2)	intron (NM_001273891, intron 1 of 2)	157	FBgn0028408 | FBtr0332958
chrX	492231	492731	11,46	12,32	0,86	1,31E-05	0,000322	exon (FBgn0025537, exon 2 of 2)	exon (NM_166344, exon 2 of 2)	542	FBgn0025537 | FBtr0070093
chr3R	15198453	15198953	9,39	10,25	0,86	1,80E-05	0,000417	intron (FBgn0260659, intron 1 of 5)	intron (NM_001170145, intron 1 of 5)	1762	FBgn0260659 | FBtr0301102
chrX	16067455	16067955	7,06	7,92	0,86	2,71E-05	0,000582	exon (FBgn0030723, exon 5 of 9)	exon (NM_132874, exon 5 of 9)	3968	FBgn0030723 | FBtr0074206
chrUn_DS484009v1	1823	2323	8,85	9,71	0,86	0,000531	0,00623	NA	TART1 (LINE) Jockey	NA	NA
chr2R	13556794	13557294	10,22	11,08	0,86	0,00144	0,0128	TTS (FBgn0263459)	TTS (NR_048104)	642	FBgn0083006 | FBtr0113500
chrX	1477670	1478170	11,93	12,79	0,86	0,00328	0,0244	promoter-TSS (FBgn0025381)	promoter-TSS (NM_166888)	-631	FBgn0025381 | FBtr0070259
chr3R	27272631	27273131	10,15	11,02	0,87	1,60E-07	8,96E-06	promoter-TSS (FBgn0039505)	promoter-TSS (NM_143295)	392	FBgn0002441 | FBtr0085175
chrX	8713710	8714210	10,88	11,75	0,87	4,93E-06	0,000147	promoter-TSS (FBgn0030061)	promoter-TSS (NM_132274)	213	FBgn0030060 | FBtr0312960
chr3R	11195144	11195644	7,16	8,03	0,87	1,78E-05	0,000414	promoter-TSS (FBgn0037870)	promoter-TSS (NM_141787)	-697	FBgn0037870 | FBtr0082341
chr2L	8410850	8411350	10,4	11,26	0,87	3,73E-05	0,000757	exon (FBgn0014417, exon 2 of 2)	exon (NM_001273322, exon 2 of 2)	508	FBgn0014417 | FBtr0331991
chr3R	12373064	12373564	9,32	10,2	0,87	5,90E-05	0,0011	promoter-TSS (FBgn0010040)	promoter-TSS (NM_080174)	247	FBgn0010039 | FBtr0082570
chrX	7138036	7138536	9,08	9,94	0,87	0,000119	0,00192	intron (FBgn0029939, intron 1 of 4)	intron (NM_132157, intron 1 of 4)	564	FBgn0029939 | FBtr0339835
chrX	21043635	21044135	9,4	10,28	0,87	0,00314	0,0237	exon (FBgn0025814, exon 2 of 2)	exon (NM_167724, exon 2 of 2)	139	FBgn0265613 | FBtr0340490
chrX	20252037	20252537	9,53	10,4	0,87	0,00353	0,0257	exon (FBgn0015789, exon 2 of 4)	exon (NM_078695, exon 2 of 4)	950	FBgn0015789 | FBtr0077337
chr3L	1477801	1478301	10,43	11,31	0,88	3,56E-12	8,50E-10	exon (FBgn0028567, exon 1 of 1)	3' UTR (NM_138266, exon 1 of 1)	433	FBgn0028567 | FBtr0332695
chr3L	3162507	3163007	11,27	12,15	0,88	4,31E-07	2,08E-05	TTS (FBgn0035405)	TTS (NM_167991)	578	FBgn0024194 | FBtr0073029
chr2R	11853385	11853885	9,86	10,74	0,88	4,99E-07	2,28E-05	exon (FBgn0013756, exon 2 of 5)	exon (NM_001273974, exon 2 of 5)	1019	FBgn0013756 | FBtr0088033
chrX	13717259	13717759	10,26	11,14	0,88	7,24E-06	0,000201	exon (FBgn0265726, exon 15 of 15)	exon (NM_001298298, exon 15 of 15)	776	FBgn0030512 | FBtr0073844
chrX	468935	469435	8,75	9,63	0,88	1,09E-05	0,000279	exon (FBgn0010019, exon 1 of 1)	exon (NM_080292, exon 1 of 1)	150	FBgn0010019 | FBtr0070099
chr3R	29040851	29041351	9,88	10,76	0,88	7,11E-05	0,00128	exon (FBgn0003093, exon 2 of 11)	5' UTR (NM_001170296, exon 2 of 10)	1272	FBgn0003093 | FBtr0339150
chrX	15708559	15709059	10,55	11,43	0,88	0,000215	0,00314	exon (FBgn0030672, exon 2 of 5)	exon (NM_167458, exon 1 of 4)	235	FBgn0030672 | FBtr0074057
chr3R	31808020	31808520	9,72	10,6	0,88	0,000399	0,005	exon (FBgn0039882, exon 2 of 2)	exon (NM_143644, exon 2 of 2)	1916	FBgn0039882 | FBtr0085852
chrX	22538334	22538834	8,94	9,82	0,88	0,00463	0,031	exon (FBgn0031194, exon 2 of 3)	exon (NM_001272851, exon 2 of 3)	1799	FBgn0031194 | FBtr0333716
chr2R	12138682	12139182	10,55	11,44	0,89	7,78E-13	2,15E-10	TTS (FBgn0026176)	TTS (NM_136885)	146	FBgn0033683 | FBtr0087982
chrX	16656232	16656732	10,33	11,22	0,89	1,07E-10	1,85E-08	exon (FBgn0003189, exon 2 of 8)	exon (NM_078653, exon 2 of 8)	392	FBgn0003189 | FBtr0340155
chr3R	24231688	24232188	11,51	12,4	0,89	7,46E-10	1,03E-07	promoter-TSS (FBgn0266744)	promoter-TSS (NR_125242)	-574	FBgn0266744 | FBtr0345246
chr3L	1473790	1474290	8,36	9,25	0,89	2,53E-05	0,000551	exon (FBgn0267487, exon 3 of 8)	5' UTR (NM_001274324, exon 3 of 8)	1217	FBgn0267487 | FBtr0310161
chr2L	2749623	2750123	11,01	11,89	0,89	0,000209	0,00308	promoter-TSS (FBgn0250906)	promoter-TSS (NM_001273030)	274	FBgn0250906 | FBtr0330716
chr2R	25281169	25281669	10,03	10,93	0,89	0,000382	0,00487	intergenic	HETA (LINE) Jockey	-26101	FBgn0035094 | FBtr0333172
chr3L	11685472	11685972	9,07	9,95	0,89	0,00203	0,0169	intron (FBgn0036191, intron 1 of 5)	intron (NM_140236, intron 1 of 4)	1743	FBgn0036191 | FBtr0273362
chr3R	24627304	24627804	9,97	10,86	0,89	0,0024	0,0191	exon (FBgn0046685, exon 3 of 3)	exon (NM_170155, exon 3 of 3)	1884	FBgn0039213 | FBtr0084656
chr2L	4183850	4184350	8,73	9,62	0,89	0,0034	0,025	intergenic	intergenic	-1300	FBgn0264866 | FBtr0334786
chr3L	9715688	9716188	10,24	11,12	0,89	0,00343	0,0251	promoter-TSS (FBgn0065081)	promoter-TSS (NR_002482)	-864	FBgn0065081 | FBtr0091797
chr3L	7591537	7592037	8,84	9,73	0,89	0,00517	0,0332	promoter-TSS (FBgn0035800)	promoter-TSS (NM_139882)	-789	FBgn0035800 | FBtr0076824
chr3R	29675872	29676372	10,67	11,57	0,9	1,14E-10	1,93E-08	promoter-TSS (FBgn0025457)	promoter-TSS (NM_058033)	472	FBgn0039680 | FBtr0085452
chr2R	16582939	16583439	10,34	11,24	0,9	6,62E-09	6,42E-07	exon (FBgn0265525, exon 1 of 1)	non-coding (NR_124526, exon 1 of 1)	180	FBgn0265525 | FBtr0340074
chr3L	15140142	15140642	9,41	10,31	0,9	3,34E-06	0,000109	intron (FBgn0014002, intron 1 of 1)	intron (NM_001300141, intron 1 of 1)	-1738	FBgn0266945 | FBtr0345844
chr3L	682998	683498	9,6	10,5	0,9	8,25E-06	0,000221	promoter-TSS (FBgn0035152)	promoter-TSS (NM_001274288)	-778	FBgn0035152 | FBtr0333378
chr3L	9764773	9765273	9,26	10,16	0,9	1,28E-05	0,000318	intron (FBgn0036043, intron 1 of 12)	intron (NM_001274724, intron 1 of 13)	1480	FBgn0036043 | FBtr0076318
chr4	1302084	1302584	7,89	8,79	0,9	0,00393	0,0277	intergenic	HETA (LINE) Jockey	70452	FBgn0053653 | FBtr0091630
chr3R	18591830	18592330	9,85	10,76	0,91	1,18E-06	4,69E-05	TTS (FBgn0038629)	TTS (NM_001144608)	1054	FBgn0263974 | FBtr0329922
chr2L	6049920	6050420	10,27	11,18	0,91	1,51E-06	5,78E-05	promoter-TSS (FBgn0031769)	promoter-TSS (NM_164679)	-629	FBgn0031769 | FBtr0346135
chrX	18844328	18844828	9,93	10,84	0,91	2,94E-06	9,91E-05	exon (FBgn0085451, exon 2 of 5)	exon (NM_133102, exon 2 of 5)	916	FBgn0085451 | FBtr0310440
chrX	7284612	7285112	9,51	10,42	0,91	2,98E-06	9,99E-05	promoter-TSS (FBgn0029941)	promoter-TSS (NM_001298047)	15	FBgn0029941 | FBtr0339819
chr2L	21308406	21308906	11,06	11,97	0,91	4,48E-06	0,000139	exon (FBgn0032940, exon 2 of 12)	exon (NM_001169568, exon 2 of 12)	833	FBgn0032940 | FBtr0301461
chrX	14836974	14837474	9,17	10,09	0,91	0,000176	0,00268	TTS (FBgn0030582)	TTS (NM_206713)	500	FBgn0030583 | FBtr0073948
chr2R	18613835	18614335	10,19	11,09	0,91	0,000356	0,00458	promoter-TSS (FBgn0034362)	promoter-TSS (NM_137502)	933	FBgn0034361 | FBtr0086714
chr2R	12338281	12338781	10,22	11,14	0,92	1,24E-10	2,05E-08	TTS (FBgn0054021)	TTS (NM_001038853)	232	FBgn0033716 | FBtr0301874
chr3L	3811858	3812358	10,11	11,03	0,92	3,54E-09	3,72E-07	promoter-TSS (FBgn0052263)	promoter-TSS (NM_168041)	846	FBgn0035464 | FBtr0073149
chr2L	5005351	5005851	10,93	11,85	0,92	1,15E-08	1,00E-06	promoter-TSS (FBgn0053113)	promoter-TSS (NM_001169407)	-673	FBgn0053113 | FBtr0079040
chr2L	15065052	15065552	9,27	10,19	0,92	2,50E-06	8,70E-05	exon (FBgn0024183, exon 3 of 4)	exon (NM_165102, exon 3 of 4)	2776	FBgn0024183 | FBtr0080721
chrX	12908340	12908840	10,2	11,12	0,92	1,48E-05	0,000356	TTS (FBgn0030433)	TTS (NM_132611)	1032	FBgn0030434 | FBtr0073698
chr3L	11821058	11821558	9,89	10,82	0,92	7,51E-05	0,00133	exon (FBgn0036212, exon 2 of 2)	exon (NM_001043137, exon 3 of 3)	897	FBgn0036211 | FBtr0302136
chr3R	23052651	23053151	9,19	10,11	0,92	0,000111	0,00184	promoter-TSS (FBgn0267758)	promoter-TSS (NR_133437)	-14	FBgn0267758 | FBtr0347322
chrX	3866226	3866726	8,75	9,67	0,92	0,000155	0,00241	intron (FBgn0265575, intron 3 of 5)	intron (NM_001297915, intron 3 of 5)	241	FBgn0265575 | FBtr0340205
chrX	13843389	13843889	7,98	8,91	0,92	0,000205	0,00304	intron (FBgn0052626, intron 1 of 9)	intron (NM_001258730, intron 1 of 8)	2227	FBgn0052626 | FBtr0309245
chrX	15885422	15885922	10,93	11,86	0,93	1,06E-09	1,42E-07	exon (FBgn0260938, exon 2 of 14)	exon (NM_001272657, exon 2 of 14)	1639	FBgn0260938 | FBtr0310065
chr2R	7987992	7988492	10,37	11,3	0,93	9,24E-08	5,63E-06	promoter-TSS (FBgn0033247)	promoter-TSS (NM_165583)	-219	FBgn0033247 | FBtr0088860
chr3L	15100260	15100760	8,81	9,74	0,93	4,87E-06	0,000147	exon (FBgn0264703, exon 2 of 2)	CpG	-1008	FBgn0264704 | FBtr0333938
chr2L	19439667	19440167	8,9	9,83	0,93	8,08E-06	0,000219	promoter-TSS (FBgn0032783)	promoter-TSS (NM_001273648)	-951	FBgn0032783 | FBtr0081209
chr3R	18411364	18411864	8,66	9,6	0,93	2,31E-05	0,00051	promoter-TSS (FBgn0038621)	promoter-TSS (NM_142469)	17	FBgn0038621 | FBtr0083654
chr3L	15556674	15557174	7,41	8,34	0,93	3,44E-05	0,000705	exon (FBgn0087035, exon 1 of 6)	exon (NM_168626, exon 2 of 7)	102	FBgn0087035 | FBtr0331933
chr2R	10157576	10158076	11,23	12,16	0,93	3,85E-05	0,000775	exon (FBgn0265512, exon 1 of 1)	exon (NM_001273924, exon 1 of 1)	758	FBgn0265512 | FBtr0331945
chrY_CP007111v1_random	14507	15007	7,54	8,47	0,93	0,000207	0,00307	NA	TART_B1 (LINE) Jockey	NA	NA
chr2L	21675292	21675792	7,97	8,9	0,93	0,000462	0,0056	intron (FBgn0032957, intron 1 of 11)	FB4_DM (DNA) TcMar-Tc1	685	FBgn0032957 | FBtr0085914
chrX	530142	530642	9,53	10,46	0,93	0,000708	0,00774	promoter-TSS (FBgn0000108)	promoter-TSS (NM_001038728)	-101	FBgn0024983 | FBtr0100476
chr3R	7248734	7249234	10,69	11,63	0,94	4,81E-14	1,57E-11	promoter-TSS (FBgn0037492)	promoter-TSS (NM_141456)	513	FBgn0037491 | FBtr0339736
chr2R	18856000	18856500	9,91	10,85	0,94	1,62E-08	1,33E-06	exon (FBgn0034405, exon 4 of 4)	exon (NM_176233, exon 4 of 4)	-1163	FBgn0010053 | FBtr0086625
chr2R	13414020	13414520	9,8	10,73	0,94	6,65E-08	4,13E-06	TTS (FBgn0259221)	TTS (NM_001144183)	350	FBgn0260475 | FBtr0087735
chr3L	11090926	11091426	9,69	10,63	0,94	6,11E-06	0,000174	exon (FBgn0020412, exon 2 of 8)	exon (NM_168439, exon 1 of 7)	680	FBgn0020412 | FBtr0076237
chr2L	7573424	7573924	8,19	9,13	0,94	8,01E-06	0,000218	exon (FBgn0264895, intron 1 of 5)	CpG	2339	FBgn0264895 | FBtr0334850
chrX	17108773	17109273	7,86	8,8	0,94	2,37E-05	0,000522	intron (FBgn0260748, intron 1 of 10)	intron (NM_132967, intron 1 of 10)	1442	FBgn0260748 | FBtr0074386
chrX	15474877	15475377	10,56	11,5	0,94	0,000237	0,0034	promoter-TSS (FBgn0030647)	promoter-TSS (NM_132805)	273	FBgn0267977 | FBtr0074074
chr2R	21479270	21479770	8,4	9,33	0,94	0,000251	0,00355	intron (FBgn0010415, intron 2 of 6)	intron (NM_057617, intron 2 of 6)	1656	FBgn0010415 | FBtr0342838
chr2L	21657729	21658229	8,01	8,95	0,94	0,000845	0,00872	promoter-TSS (FBgn0032956)	promoter-TSS (NM_165390)	321	FBgn0262620 | FBtr0342855
chr2R	21710175	21710675	10,01	10,96	0,95	2,73E-09	2,97E-07	promoter-TSS (FBgn0265962)	promoter-TSS (NR_124682)	-830	FBgn0265962 | FBtr0342964
chrX	10471806	10472306	9,79	10,74	0,95	1,15E-07	6,61E-06	exon (FBgn0261710, exon 2 of 6)	5' UTR (NM_001272480, exon 2 of 6)	1531	FBgn0261710 | FBtr0332953
chr3R	23182794	23183294	9,88	10,83	0,95	5,87E-06	0,000168	exon (FBgn0265042, exon 3 of 5)	exon (NM_001170226, exon 2 of 4)	125	FBgn0265042 | FBtr0336475
chr2L	20430120	20430620	9,84	10,79	0,95	1,12E-05	0,000285	intron (FBgn0263355, intron 1 of 4)	intron (NM_136191, intron 1 of 4)	1346	FBgn0263355 | FBtr0273378
chr3L	18995274	18995774	10,33	11,28	0,95	0,000211	0,00309	exon (FBgn0036837, exon 1 of 2)	5' UTR (NM_140825, exon 1 of 2)	285	FBgn0036837 | FBtr0075042
chrX	12731021	12731521	9,08	10,04	0,95	0,000648	0,0073	promoter-TSS (FBgn0264678)	promoter-TSS (NR_073653)	-318	FBgn0264678 | FBtr0333774
chr2R	17265741	17266241	8,96	9,91	0,95	0,000927	0,00932	exon (FBgn0265487, exon 1 of 4)	5' UTR (NM_001144217, exon 1 of 6)	474	FBgn0265487 | FBtr0086991
chr2R	6215184	6215684	8,76	9,7	0,95	0,0011	0,0105	TTS (FBgn0265044)	TTS (NR_073841)	867	FBgn0263144 | FBtr0085992
chr3L	12144784	12145284	10,05	11,01	0,96	1,87E-08	1,50E-06	exon (FBgn0036258, exon 2 of 4)	exon (NM_140296, exon 2 of 4)	1063	FBgn0036258 | FBtr0076022
chr3R	14653334	14653834	9,86	10,82	0,96	2,06E-06	7,60E-05	intron (FBgn0086686, intron 1 of 5)	intron (NM_142122, intron 1 of 5)	1613	FBgn0086686 | FBtr0344158
chr3R	2133888	2134388	7,51	8,47	0,96	1,76E-05	0,00041	intron (FBgn0267431, intron 16 of 21)	Gypsy12A_ETR (LTR) Gypsy	23068	FBgn0058182 | FBtr0302347
chr2R	15929744	15930244	9,54	10,5	0,96	2,10E-05	0,00047	intron (FBgn0034049, intron 1 of 7)	intron (NM_001299540, intron 1 of 7)	-1664	FBgn0034049 | FBtr0087299
chrX	4610817	4611317	7,92	8,88	0,96	2,26E-05	0,000502	exon (FBgn0052773, exon 1 of 5)	non-coding (NR_123790, exon 1 of 5)	318	FBgn0052773 | FBtr0344480
chr2R	9589218	9589718	11,36	12,32	0,96	4,02E-05	0,000804	exon (FBgn0033431, exon 2 of 2)	exon (NM_136660, exon 2 of 2)	419	FBgn0033431 | FBtr0339392
chr2R	7456525	7457025	10,08	11,04	0,96	9,69E-05	0,00165	exon (FBgn0025885, exon 2 of 5)	exon (NM_058057, exon 2 of 5)	2099	FBgn0025885 | FBtr0089329
chrX	15321748	15322248	9,63	10,59	0,96	0,00095	0,00944	promoter-TSS (FBgn0004924)	promoter-TSS (NM_167435)	-847	FBgn0004924 | FBtr0074006
chrX	15796366	15796866	9,42	10,38	0,96	0,00116	0,0109	promoter-TSS (FBgn0030693)	promoter-TSS (NM_206726)	140	FBgn0265533 | FBtr0340112
chrX	248432	248932	9,44	10,39	0,96	0,0014	0,0126	exon (FBgn0040372, exon 2 of 10)	exon (NM_001272159, exon 2 of 9)	2705	FBgn0040372 | FBtr0070063
chrX	9154710	9155210	10,13	11,1	0,97	1,34E-10	2,15E-08	promoter-TSS (FBgn0004828)	promoter-TSS (NM_167180)	52	FBgn0004828 | FBtr0071346
chrX	5677306	5677806	9,76	10,72	0,97	2,23E-08	1,77E-06	promoter-TSS (FBgn0046687)	promoter-TSS (NM_001258605)	-598	FBgn0046687 | FBtr0308339
chr3R	26799760	26800260	9,39	10,35	0,97	4,30E-07	2,08E-05	intron (FBgn0262473, intron 1 of 3)	intron (NM_001276066, intron 1 of 3)	970	FBgn0262473 | FBtr0330155
chr3R	29217279	29217779	10,45	11,43	0,97	1,95E-06	7,24E-05	exon (FBgn0051044, exon 2 of 3)	TTS (NR_048510)	286	FBgn0262404 | FBtr0304320
chr3R	9349452	9349952	8,55	9,52	0,97	0,00109	0,0105	intron (FBgn0266410, intron 2 of 5)	intron (NM_001300317, intron 2 of 5)	-4565	FBgn0086053 | FBtr0114329
chr2L	21699837	21700337	7,41	8,38	0,97	0,00116	0,0109	intron (FBgn0051619, intron 3 of 15)	intron (NM_001259399, intron 3 of 19)	35982	FBgn0051619 | FBtr0085902
chr2R	18398559	18399059	10,45	11,44	0,98	3,07E-16	1,51E-13	promoter-TSS (FBgn0063499)	promoter-TSS (NM_137480)	-290	FBgn0063499 | FBtr0344195
chr2R	24943959	24944459	11,05	12,03	0,98	6,92E-07	3,03E-05	promoter-TSS (FBgn0035085)	promoter-TSS (NM_138141)	391	FBgn0035084 | FBtr0072430
chr3R	17117854	17118354	9,13	10,11	0,98	1,06E-06	4,33E-05	intron (FBgn0014141, intron 1 of 15)	CpG	978	FBgn0014141 | FBtr0089471
chr2R	13493438	13493938	8,98	9,96	0,98	2,37E-06	8,46E-05	intron (FBgn0033844, intron 1 of 5)	CpG	1174	FBgn0033844 | FBtr0087699
chr3L	3320370	3320870	9,51	10,5	0,98	1,07E-05	0,000274	exon (FBgn0035436, exon 2 of 2)	exon (NM_001169867, exon 2 of 2)	284	FBgn0035436 | FBtr0073064
chr3R	11560858	11561358	9,71	10,69	0,98	7,53E-05	0,00133	exon (FBgn0037912, exon 3 of 4)	exon (NM_001032008, exon 3 of 4)	1188	FBgn0037912 | FBtr0100462
chr3R	25640191	25640691	8,81	9,79	0,98	0,00024	0,00343	intron (FBgn0039350, intron 1 of 5)	intron (NM_170234, intron 1 of 5)	649	FBgn0039350 | FBtr0084889
chr2L	3157914	3158414	7,84	8,82	0,98	0,000675	0,0075	intron (FBgn0011648, intron 1 of 3)	intron (NM_057669, intron 1 of 3)	1479	FBgn0011648 | FBtr0077636
chrX	18833999	18834499	9,4	10,4	0,99	9,94E-08	5,85E-06	intron (FBgn0030964, intron 1 of 5)	intron (NM_001169321, intron 1 of 5)	1568	FBgn0030964 | FBtr0074640
chrX	18510910	18511410	10,02	11,01	0,99	2,26E-07	1,19E-05	intron (FBgn0030932, intron 1 of 3)	intron (NM_001298479, intron 1 of 3)	1177	FBgn0030932 | FBtr0340368
chrX	11718242	11718742	9,52	10,51	0,99	1,14E-06	4,56E-05	exon (FBgn0030329, exon 3 of 4)	exon (NM_001201655, exon 3 of 4)	1481	FBgn0030329 | FBtr0332954
chr3L	10223892	10224392	9,22	10,21	0,99	3,87E-06	0,000123	promoter-TSS (FBgn0052056)	promoter-TSS (NM_168404)	-882	FBgn0052056 | FBtr0076302
chr3R	29492366	29492866	10,06	11,05	0,99	1,95E-05	0,000444	exon (FBgn0039665, exon 2 of 4)	exon (NM_170411, exon 2 of 4)	902	FBgn0039665 | FBtr0085433

chrX	3074350	3074850	8,13	9,13	1	1,77E-06	6,64E-05	intron (FBgn0028369, intron 7 of 12)	intron (NM_080320, intron 7 of 12)	-7038	FBgn0029649 | FBtr0070561
chr3R	9345830	9346330	8,85	9,85	1	1,87E-06	6,96E-05	intron (FBgn0266410, intron 2 of 5)	intron (NM_001300317, intron 2 of 5)	4214	FBgn0266410 | FBtr0344368
chrX	15813903	15814403	9,53	10,54	1	4,04E-05	0,000806	exon (FBgn0003345, exon 3 of 12)	5' UTR (NM_001103522, exon 2 of 11)	601	FBgn0003345 | FBtr0308130
chr2L	16824116	16824616	9,69	10,69	1,01	3,44E-06	0,000112	exon (FBgn0022213, exon 2 of 7)	exon (NM_078864, exon 2 of 7)	841	FBgn0022213 | FBtr0080930
chr3L	21881613	21882113	7,51	8,52	1,01	0,00406	0,0283	intron (FBgn0262737, intron 1 of 9)	intron (NM_001259945, intron 1 of 9)	2287	FBgn0262737 | FBtr0301364
chr3R	30598876	30599376	10	11,02	1,02	2,60E-08	2,01E-06	exon (FBgn0051019, exon 4 of 4)	exon (NM_170512, exon 4 of 4)	1197	FBgn0039790 | FBtr0085676
chr3L	11490065	11490565	7,84	8,86	1,02	1,25E-05	0,000311	intron (FBgn0036165, intron 1 of 3)	intron (NM_140213, intron 1 of 3)	2766	FBgn0036165 | FBtr0076093
chr3L	3908183	3908683	9,42	10,44	1,02	0,000641	0,00725	TTS (FBgn0041147)	TTS (NM_139580)	1159	FBgn0085473 | FBtr0073176
chr2L	4977718	4978218	10,6	11,62	1,03	4,48E-19	3,60E-16	promoter-TSS (FBgn0031661)	promoter-TSS (NM_135044)	657	FBgn0031662 | FBtr0078997
chr3L	1330766	1331266	9,67	10,7	1,03	3,67E-07	1,82E-05	promoter-TSS (FBgn0035209)	promoter-TSS (NM_138256)	-727	FBgn0085209 | FBtr0072678
chrX	12762762	12763262	10,62	11,65	1,03	8,65E-06	0,000227	exon (FBgn0030420, exon 1 of 1)	exon (NM_132599, exon 1 of 1)	599	FBgn0030420 | FBtr0346120
chr2L	16690845	16691345	9,09	10,12	1,03	1,72E-05	0,000404	exon (FBgn0261278, exon 2 of 7)	exon (NM_165172, exon 3 of 8)	4428	FBgn0261278 | FBtr0100459
chr3R	8347697	8348197	10,07	11,1	1,03	5,49E-05	0,00104	TTS (FBgn0037580)	TTS (NM_169218)	229	FBgn0037581 | FBtr0081842
chr3L	2636877	2637377	9,79	10,83	1,04	1,80E-08	1,47E-06	exon (FBgn0035357, exon 2 of 7)	5' UTR (NM_001144403, exon 3 of 8)	223	FBgn0035357 | FBtr0072936
chrX	3968884	3969384	10,07	11,11	1,04	4,83E-08	3,23E-06	promoter-TSS (FBgn0029689)	promoter-TSS (NM_130732)	202	FBgn0267037 | FBtr0346011
chr2R	18852138	18852638	10,6	11,64	1,04	1,51E-06	5,78E-05	TTS (FBgn0034402)	TTS (NM_137539)	655	FBgn0034403 | FBtr0273238
chr3L	16956935	16957435	8,2	9,24	1,04	4,42E-06	0,000138	promoter-TSS (FBgn0010357)	promoter-TSS (NM_001104159)	-253	FBgn0010357 | FBtr0075269
chr2L	10977804	10978304	9,94	10,98	1,04	3,35E-05	0,000689	exon (FBgn0041781, exon 2 of 5)	exon (NM_001273440, exon 2 of 5)	1283	FBgn0041781 | FBtr0080148
chr3L	19634087	19634587	9,39	10,44	1,05	2,86E-08	2,20E-06	exon (FBgn0036896, exon 2 of 8)	exon (NM_176363, exon 2 of 8)	-1241	FBgn0036896 | FBtr0302513
chr2L	22983725	22984225	7,43	8,48	1,05	4,73E-07	2,22E-05	intron (FBgn0000384, intron 1 of 5)	intron (NM_001273767, intron 1 of 5)	2160	FBgn0000384 | FBtr0111126
chr2R	15479517	15480017	8,97	10,02	1,05	7,13E-06	0,000199	intron (FBgn0034021, intron 1 of 4)	intron (NM_001299529, intron 1 of 4)	3067	FBgn0034021 | FBtr0345392
chr2R	21830190	21830690	7,2	8,25	1,05	3,51E-05	0,000715	intron (FBgn0003866, intron 1 of 2)	intron (NM_078891, intron 1 of 2)	1848	FBgn0003866 | FBtr0085906
chr2R	21314277	21314777	8,73	9,78	1,05	0,000255	0,00359	exon (FBgn0034618, exon 2 of 8)	exon (NM_001169764, exon 2 of 8)	656	FBgn0034618 | FBtr0071601
chr2L	18858109	18858609	10,04	11,1	1,06	8,85E-09	8,13E-07	promoter-TSS (FBgn0032721)	promoter-TSS (NM_165269)	-680	FBgn0032721 | FBtr0089314
chr2L	2976277	2976777	11,22	12,28	1,06	1,86E-07	1,02E-05	promoter-TSS (FBgn0031484)	promoter-TSS (NM_134888)	335	FBgn0031483 | FBtr0077676
chr2L	18967104	18967604	9,46	10,52	1,06	1,99E-07	1,08E-05	intron (FBgn0015772, intron 1 of 6)	intron (NM_001299146, intron 1 of 7)	1367	FBgn0015772 | FBtr0081189
chr3L	7361658	7362158	10,28	11,35	1,06	4,08E-06	0,000129	exon (FBgn0267485, exon 1 of 1)	exon (NM_139854, exon 2 of 4)	1348	FBgn0035771 | FBtr0076847
chr3L	14415323	14415823	9,14	10,2	1,06	1,66E-05	0,000393	exon (FBgn0087007, exon 3 of 7)	exon (NM_001144481, exon 3 of 7)	-4875	FBgn0266768 | FBtr0345393
chr2L	12028733	12029233	8,32	9,38	1,06	0,00655	0,0398	intron (FBgn0010497, intron 1 of 4)	intron (NM_138760, intron 1 of 4)	1546	FBgn0010497 | FBtr0080292
chr2R	7624073	7624573	8,2	9,26	1,06	0,00879	0,0495	intron (FBgn0263077, intron 1 of 14)	intron (NM_001259256, intron 1 of 14)	1082	FBgn0263077 | FBtr0306933
chr2L	19123998	19124498	10,05	11,11	1,07	3,77E-07	1,86E-05	promoter-TSS (FBgn0002031)	promoter-TSS (NM_001169541)	-379	FBgn0002031 | FBtr0346428
chrX	5278292	5278792	8,17	9,24	1,07	2,42E-06	8,57E-05	Intergenic	Intergenic	-17523	FBgn0261803 | FBtr0303278
chr2R	7956802	7957302	9,63	10,71	1,08	5,67E-05	0,00107	exon (FBgn0033240, exon 3 of 5)	exon (NM_001103755, exon 3 of 5)	903	FBgn0033240 | FBtr0113052
chrX	2274004	2274504	9,68	10,77	1,09	1,11E-06	4,49E-05	exon (FBgn0023529, exon 2 of 3)	exon (NM_001169174, exon 2 of 3)	524	FBgn0023529 | FBtr0300792
chrX	22457563	22458063	9,68	10,78	1,09	2,28E-06	8,24E-05	exon (FBgn0031187, exon 3 of 11)	exon (NM_167776, exon 3 of 11)	923	FBgn0031187 | FBtr0077348
chr3R	727707	728207	8,28	9,38	1,1	6,83E-08	4,19E-06	intron (FBgn0267431, intron 1 of 21)	Gypsy12_ETR|LTR|Gypsy	-5336	FBgn0085804 | FBtr0114258
chr2L	21170039	21170539	9,86	10,96	1,1	9,77E-08	5,84E-06	exon (FBgn0010100, exon 2 of 4)	exon (NM_001103716, exon 2 of 4)	1639	FBgn0010100 | FBtr0081473
chr2R	18406055	18406555	10,25	11,35	1,1	0,000546	0,00634	promoter-TSS (FBgn0063493)	promoter-TSS (NM_137485)	295	FBgn0063494 | FBtr0086674
chr3R	27905196	27905696	7,85	8,95	1,11	5,92E-08	3,82E-06	exon (FBgn0085382, exon 1 of 12)	5' UTR (NM_001104479, exon 1 of 12)	397	FBgn0085382 | FBtr0305292
chr3R	15805855	15806355	8,3	9,41	1,11	5,04E-07	2,29E-05	intron (FBgn0026616, intron 1 of 4)	intron (NM_142237, intron 1 of 4)	1858	FBgn0026616 | FBtr0083179
chr2L	588855	589355	7,68	8,8	1,12	3,55E-08	2,63E-06	TTS (FBgn0267827)	TTS (NR_144661)	958	FBgn0267827 | FBtr0445834
chr3L	18627723	18628223	9,07	10,18	1,12	2,76E-07	1,43E-05	intron (FBgn0036801, intron 2 of 8)	CpG	2015	FBgn0036801 | FBtr0075049
chr3R	7809299	7809799	9,48	10,6	1,13	3,11E-10	4,57E-08	promoter-TSS (FBgn0051472)	promoter-TSS (NM_169195)	465	FBgn0037521 | FBtr0331691
chr2R	998184	998684	9,22	10,35	1,13	5,35E-08	3,55E-06	Intergenic	Intergenic	-47182	FBgn0069969 | FBtr0308892
chr3R	21272495	21272995	9,39	10,53	1,13	1,95E-05	0,000444	exon (FBgn0038877, exon 2 of 4)	exon (NM_142706, exon 2 of 4)	1072	FBgn0038877 | FBtr0084102
chrX	3290979	3291479	9,02	10,15	1,13	5,37E-05	0,00102	promoter-TSS (FBgn0000479)	promoter-TSS (NM_166967)	-14	FBgn0000479 | FBtr0070517
chr2R	15481016	15481516	9,19	10,32	1,13	0,00478	0,0316	intron (FBgn0034021, intron 1 of 4)	intron (NM_001299529, intron 1 of 4)	1568	FBgn0034021 | FBtr0345392
chr3R	15546532	15547032	9,6	10,74	1,14	1,17E-09	1,48E-07	exon (FBgn0038349, exon 4 of 9)	exon (NM_001316510, exon 4 of 9)	954	FBgn0038349 | FBtr0083151
chr2L	9915914	9916414	9,88	11,02	1,14	2,34E-06	8,41E-05	exon (FBgn0040064, exon 3 of 4)	exon (NM_078804, exon 3 of 4)	912	FBgn0040064 | FBtr0079876
chr3R	29765807	29766307	8,96	10,1	1,14	4,44E-06	0,000138	promoter-TSS (FBgn0001297)	promoter-TSS (NM_001032408)	63	FBgn0001297 | FBtr0099988
chr2L	5341671	5342171	9,33	10,47	1,14	0,00102	0,00991	intron (FBgn0031703, intron 1 of 2)	intron (NM_135080, intron 1 of 2)	313	FBgn0031703 | FBtr0079077
chr2R	18170891	18171391	9,71	10,85	1,15	2,66E-09	2,97E-07	exon (FBgn0027836, exon 2 of 5)	exon (NM_166274, exon 2 of 5)	329	FBgn0027836 | FBtr0086774
chrX	626405	626905	10,6	11,75	1,15	2,91E-09	3,13E-07	TTS (FBgn0267031)	TTS (NR_123763)	1114	FBgn0025635 | FBtr0070116
chr3R	21066756	21067256	8,76	9,91	1,15	2,29E-08	1,80E-06	intron (FBgn0000083, intron 1 of 4)	CpG	1124	FBgn0000083 | FBtr0336797
chr3R	11436057	11436557	10,31	11,47	1,15	3,67E-08	2,70E-06	promoter-TSS (FBgn0037901)	promoter-TSS (NM_141818)	458	FBgn0037902 | FBtr0082391
chr3R	29148859	29149359	10,66	11,81	1,15	3,41E-07	1,70E-05	promoter-TSS (FBgn0039642)	promoter-TSS (NM_143419)	748	FBgn0014869 | FBtr0100482
chr3R	863786	864286	7,88	9,02	1,15	4,70E-07	2,22E-05	intron (FBgn0267431, intron 2 of 21)	Gypsy12_ETR|LTR|Gypsy	-141415	FBgn0085804 | FBtr0114258
chr4	1305651	1306151	7,36	8,51	1,15	2,25E-06	8,19E-05	Intergenic	HETA|LINE|Jockey	74019	FBgn0053653 | FBtr0091630
chr2R	18853439	18853939	10,11	11,28	1,16	2,17E-10	3,36E-08	promoter-TSS (FBgn0034403)	promoter-TSS (NM_137540)	-646	FBgn0034403 | FBtr0273238
chr3R	31670624	31671124	8,9	10,06	1,16	3,10E-06	0,000103	exon (FBgn0039863, exon 3 of 9)	exon (NM_170563, exon 3 of 10)	1410	FBgn0039863 | FBtr0085823
chr2L	19794691	19795191	9,46	10,62	1,16	1,56E-05	0,00037	exon (FBgn0004811, exon 2 of 3)	exon (NM_001273673, exon 2 of 3)	910	FBgn0004811 | FBtr0081316
chr2L	6945702	6946202	9,98	11,14	1,16	4,66E-05	0,000911	promoter-TSS (FBgn0031871)	promoter-TSS (NM_001273242)	-663	FBgn0031871 | FBtr0332325
chr3R	18295667	18296167	8,59	9,76	1,17	0,00042	0,00522	intron (FBgn0010877, intron 1 of 3)	intron (NM_143794, intron 1 of 3)	-1191	FBgn0010877 | FBtr0334314
chr3L	1479055	1479555	9,57	10,75	1,18	5,83E-10	8,17E-08	promoter-TSS (FBgn0020248)	promoter-TSS (NM_176273)	-364	FBgn0020248 | FBtr0077313
chrX	3448211	3448711	7,97	9,15	1,18	1,31E-08	1,13E-06	intron (FBgn0029657, intron 1 of 6)	intron (NM_001272276, intron 1 of 6)	482	FBgn0029657 | FBtr0344078
chr3L	9695175	9695675	9,76	10,95	1,19	2,46E-11	5,16E-09	promoter-TSS (FBgn0036030)	promoter-TSS (NM_168360)	16	FBgn0036030 | FBtr0076416
chr3L	6977484	6977984	8,5	9,69	1,19	0,000253	0,00357	exon (FBgn0047205, exon 3 of 3)	non-coding (NR_001944, exon 3 of 3)	1413	FBgn0047205 | FBtr0076899
chr2R	16338012	16338512	9,79	10,99	1,2	2,37E-10	3,60E-08	promoter-TSS (FBgn0010611)	promoter-TSS (NM_166168)	-39	FBgn0010611 | FBtr0087146
chr2L	15064476	15064976	10,36	11,56	1,2	9,80E-08	5,84E-06	exon (FBgn0024183, exon 4 of 4)	exon (NM_165102, exon 4 of 4)	3071	FBgn0283440 | FBtr0445188
chr2R	5784731	5785231	7,51	8,71	1,2	4,17E-07	2,03E-05	Intergenic	Gypsy12A_ETR|LTR|Gypsy	-2123	FBgn0025693 | FBtr0086053
chr3L	1646189	1646689	10,02	11,23	1,2	6,13E-06	0,000174	TTS (FBgn0035248)	TTS (NM_139380)	973	FBgn0035248 | FBtr0072759
chrX	2352784	2353284	8,75	9,95	1,2	0,00278	0,0214	intron (FBgn0003159, intron 1 of 3)	intron (NM_001258559, intron 1 of 3)	1234	FBgn0003159 | FBtr0070403
chrY_CP007111v1_random	13407	13907	7,46	8,68	1,21	0,000356	0,00458	NA	TART_B1|LINE|Jockey	NA	NA
chrX	11568961	11569461	9,8	11,02	1,22	1,57E-10	2,47E-08	exon (FBgn0003277, exon 2 of 4)	exon (NM_078569, exon 2 of 4)	1115	FBgn0003277 | FBtr0073542
chr3L	15564210	15564710	9,6	10,82	1,22	7,46E-09	7,08E-07	exon (FBgn0036510, exon 3 of 3)	exon (NM_140520, exon 2 of 2)	1034	FBgn0036510 | FBtr0306154
chrUn_DS484314v1	1878	2378	8,09	9,3	1,22	4,07E-08	2,91E-06	NA	TART_B1|LINE|Jockey	NA	NA
chr3R	27927665	27928165	10,21	11,44	1,23	2,55E-07	1,32E-05	exon (FBgn0051053, exon 1 of 1)	exon (NM_170357, exon 1 of 1)	259	FBgn0051053 | FBtr0085268
chr3R	12368181	12368681	10,97	12,2	1,23	5,65E-07	2,56E-05	promoter-TSS (FBgn0038020)	promoter-TSS (NM_141924)	837	FBgn0001149 | FBtr0082607
chr2R	18408955	18409455	9,32	10,56	1,24	4,07E-11	7,98E-09	TTS (FBgn0063492)	TTS (NM_137486)	158	FBgn0063491 | FBtr0086677
chrY	2900094	2900594	6,73	7,97	1,24	1,56E-09	1,86E-07	Intergenic	TART|LINE|Jockey	-121944	FBgn0265047 | FBtr0302230
chrX	7679798	7680298	7,9	9,13	1,24	1,33E-08	1,14E-06	promoter-TSS (FBgn0267227)	promoter-TSS (NR_123829)	-427	FBgn0267227 | FBtr0346400
chr3L	5182902	5183402	8,28	9,52	1,24	4,49E-07	2,15E-05	intron (FBgn0052423, intron 3 of 11)	intron (NM_168111, intron 3 of 10)	1645	FBgn0052423 | FBtr0333288
chr3R	14899814	14900314	10,35	11,6	1,25	3,36E-09	3,57E-07	TTS (FBgn0038277)	TTS (NM_142150)	213	FBgn0262514 | FBtr0290022
chr3L	1567122	1567622	10,21	11,47	1,25	2,86E-07	1,46E-05	exon (FBgn0035234, exon 2 of 2)	exon (NM_139368, exon 2 of 2)	1236	FBgn0085235 | FBtr0072826
chr2L	19734784	19735284	8,55	9,8	1,25	7,23E-05	0,00129	exon (FBgn0032815, exon 3 of 8)	exon (NM_001038826, exon 2 of 7)	686	FBgn0032815 | FBtr0100352
chr2R	22939529	22940029	9,92	11,18	1,26	5,61E-13	1,60E-10	TTS (FBgn0034803)	TTS (NM_137896)	1167	FBgn0034804 | FBtr0071993
chrX	1476449	1476949	10,68	11,93	1,26	9,19E-09	8,36E-07	promoter-TSS (FBgn0260986)	promoter-TSS (NM_130566)	275	FBgn0025382 | FBtr0070293
chr3R	20817457	20817957	8,87	10,13	1,26	1,52E-08	1,29E-06	exon (FBgn0038828, exon 2 of 5)	exon (NM_142658, exon 2 of 5)	1222	FBgn0038828 | FBtr0083994
chrX	2739098	2739598	8,74	10	1,26	9,25E-07	3,89E-05	promoter-TSS (FBgn0000376)	promoter-TSS (NM_166951)	-575	FBgn0000376 | FBtr0070495
chr3L	2174746	2175246	7,4	8,66	1,26	0,000186	0,00281	promoter-TSS (FBgn0035312)	promoter-TSS (NM_139439)	-664	FBgn0035312 | FBtr0072913
chr2R	2956001	2956501	6,96	8,22	1,26	0,00054	0,00629	intron (FBgn0020908, intron 3 of 5)	Copia2_I-int|LTR|Copia	11093	FBgn0020908 | FBtr0113713
chrX	11729510	11730010	8,91	10,2	1,29	4,70E-07	2,22E-05	promoter-TSS (FBgn0260812)	promoter-TSS (NM_001103488)	-661	FBgn0260812 | FBtr0301267
chr3L	382152	382652	8,36	9,66	1,3	3,26E-10	4,71E-08	intron (FBgn0262139, intron 4 of 17)	intron (NM_001274280, intron 4 of 12)	-5086	FBgn0262139 | FBtr0304120
chr3L	22749543	22750043	11	12,3	1,3	9,62E-10	1,31E-07	exon (FBgn0052451, exon 1 of 5)	exon (NM_168961, exon 1 of 5)	350	FBgn0052451 | FBtr0078533
chrX	15583611	15584111	10,49	11,79	1,3	4,84E-09	4,80E-07	promoter-TSS (FBgn0030659)	promoter-TSS (NM_132817)	703	FBgn0030660 | FBtr0074047
chr2R	7960740	7961240	10,88	12,17	1,3	1,55E-08	1,30E-06	promoter-TSS (FBgn0033241)	promoter-TSS (NM_165577)	931	FBgn0026361 | FBtr0088876
chr3L	642721	643221	8,78	10,1	1,32	4,60E-09	4,62E-07	TTS (FBgn0263039)	TTS (NR_073905)	713	FBgn0262451 | FBtr0304469
chr3L	18811811	18812311	7,16	8,48	1,32	6,25E-06	0,000176	intron (FBgn0036814, intron 2 of 5)	intron (NM_001275093, intron 2 of 5)	8614	FBgn0036814 | FBtr0075084
chr2R	17096283	17096783	8,72	10,03	1,32	0,000102	0,00171	intron (FBgn0010226, intron 1 of 4)	intron (NM_079043, intron 1 of 4)	444	FBgn0010226 | FBtr0087006
chr3R	9283924	9284424	9,63	10,97	1,33	4,91E-16	2,28E-13	Intergenic	Intergenic	17156	FBgn0285911 | FBtr0081979
chr2R	11368542	11369042	9,32	10,65	1,33	1,92E-11	4,46E-09	exon (FBgn0033627, exon 3 of 3)	exon (NM_165827, exon 3 of 3)	507	FBgn0033627 | FBtr0088129
chr2R	7470979	7471479	8,44	9,8	1,35	2,12E-11	4,68E-09	intron (FBgn0010548, intron 3 of 11)	intron (NM_136441, intron 5 of 13)	2901	FBgn0010548 | FBtr0088993
chrX	13209660	13210160	9,03	10,38	1,35	2,65E-10	3,97E-08	intron (FBgn0265630, intron 1 of 12)	intron (NM_078589, intron 1 of 11)	1764	FBgn0265630 | FBtr0340488
chr4	1306341	1306841	6,75	8,12	1,37	0,000109	0,00181	Intergenic	HETA|LINE|Jockey	74709	FBgn0053653 | FBtr0091630
chrY_CP007111v1_random	27530	28030	9,54	10,91	1,38	3,16E-08	2,36E-06	NA	TART_B1|LINE|Jockey	NA	NA
chrX	5278911	5279411	7,03	8,42	1,39	0,000106	0,00175	Intergenic	Intergenic	-16904	FBgn0261803 | FBtr0303278
chrX	2246141	2246641	9,75	11,17	1,42	1,25E-13	3,93E-11	TTS (FBgn0000810)	TTS (NM_058143)	161	FBgn0023523 | FBtr0070397
chr3L	13450814	13451314	9,91	11,32	1,42	1,36E-09	1,64E-07	promoter-TSS (FBgn0036366)	promoter-TSS (NM_140394)	295	FBgn0036368 | FBtr0302487
chr3R	30563935	30564435	7,86	9,29	1,43	0,000477	0,00573	intron (FBgn0082582, intron 1 of 6)	intron (NM_057633, intron 1 of 6)	1006	FBgn0082582 | FBtr0085662
chr3L	7651018	7651518	9,54	11	1,46	2,78E-11	5,58E-09	promoter-TSS (FBgn0035806)	promoter-TSS (NM_139888)	89	FBgn0035806 | FBtr0076807
chr3L	8238708	8239208	8,87	10,35	1,48	1,90E-13	5,78E-11	intron (FBgn0263219, intron 1 of 31)	intron (NM_001274642, intron 1 of 31)	312	FBgn0263219 | FBtr0299841
chr2L	17497930	17498430	10,19	11,69	1,49	7,83E-33	1,38E-29	promoter-TSS (FBgn0003187)	promoter-TSS (NM_165222)	641	FBgn0032645 | FBtr0080995
chr2R	12474705	12475205	9,14	10,65	1,51	1,62E-15	6,82E-13	TTS (FBgn0033742)	TTS (NM_136943)	532	FBgn0033744 | FBtr0087936
chr2R	11206571	11207071	8,53	10,04	1,51	1,26E-09	1,57E-07	intron (FBgn0003396, intron 1 of 6)	intron (NM_057376, intron 1 of 6)	2193	FBgn0003396 | FBtr0088100
chr2L	12043121	12043621	9,03	10,55	1,52	1,22E-15	5,41E-13	promoter-TSS (FBgn0032399)	promoter-TSS (NM_001298332)	-262	FBgn0032399 | FBtr0342596
chr3L	22061898	22062398	8,62	10,16	1,54	8,27E-07	3,56E-05	exon (FBgn0004514, exon 3 of 4)	exon (NM_001170023, exon 3 of 4)	-3758	FBgn0037149 | FBtr0078480
chrX	3074946	3075446	7,74	9,3	1,56	6,07E-07	2,69E-05	intron (FBgn0028369, intron 7 of 12)	intron (NM_080320, intron 7 of 12)	-7634	FBgn0029649 | FBtr0070561
chrX	11728381	11728881	8,81	10,39	1,58	3,68E-10	5,25E-08	exon (FBgn0260812, exon 1 of 2)	exon (NM_001103488, exon 1 of 2)	468	FBgn0260812 | FBtr0301267
chrX	10807855	10808355	8,84	10,45	1,61	6,68E-17	3,68E-14	intron (FBgn0285926, intron 2 of 6)	CpG	-1249	FBgn0285926 | FBtr0073418
chr3L	16091430	16091930	10,06	11,67	1,62	3,46E-17	2,04E-14	exon (FBgn0036566, exon 2 of 11)	exon (NM_168650, exon 2 of 10)	1225	FBgn0036566 | FBtr0075444
chr3R	27705441	27705941	9,8	11,42	1,62	2,01E-15	8,07E-13	exon (FBgn0039543, exon 2 of 6)	exon (NM_170354, exon 2 of 6)	637	FBgn0039543 | FBtr0085239
chr3R	15792054	15792554	8,51	10,14	1,63	4,33E-08	3,00E-06	promoter-TSS (FBgn0038363)	promoter-TSS (NM_142234)	275	FBgn0000246 | FBtr0083194
chrX	801779	802279	8,94	10,62	1,68	1,93E-18	1,42E-15	promoter-TSS (FBgn0015799)	promoter-TSS (NM_080297)	-550	FBgn0015799 | FBtr0070146
chr3R	31812880	31813380	8,88	10,59	1,7	1,34E-12	3,37E-10	promoter-TSS (FBgn0266268)	promoter-TSS (NM_001170314)	56	FBgn0039883 | FBtr0302179
chr2R	14755687	14756187	9,69	11,44	1,75	3,53E-31	3,90E-28	promoter-TSS (FBgn0033960)	promoter-TSS (NM_137141)	159	FBgn0033960 | FBtr0087472
chr3L	11489426	11489926	8,58	10,37	1,79	2,41E-18	1,64E-15	intron (FBgn0036165, intron 1 of 3)	intron (NM_140213, intron 1 of 3)	2127	FBgn0036165 | FBtr0076093
chr3R	29758078	29758578	9,03	10,97	1,93	4,34E-14	1,47E-11	intron (FBgn0266258, intron 1 of 3)	(CACGCAG)n|Simple_repeat|Simple_rep	712	FBgn0266258 | FBtr0343925
chr3L	2173258	2173758	9,79	11,74	1,95	5,49E-32	6,93E-29	promoter-TSS (FBgn0035311)	exon (NM_139439, exon 2 of 7)	-735	FBgn0035311 | FBtr0072914
chrY_CP007111v1_random	11447	11947	9,83	11,91	2,08	1,77E-32	2,61E-29	NA	TART|LINE|Jockey	NA	NA
chr3L	4188997	4189497	8,41	10,56	2,15	1,12E-27	9,88E-25	intron (FBgn0003710, intron 1 of 2)	intron (NM_079196, intron 1 of 2)	749	FBgn0003710 | FBtr0073219
chr2L	21691163	21691663	6,59	8,75	2,17	4,92E-07	2,26E-05	intron (FBgn0051619, intron 3 of 15)	intron (NM_001259199, intron 3 of 19)	7308	FBgn0051619 | FBtr0085902

chr3L	22999735	23000235	6,26	8,5	2,25	2,68E-16	1,39E-13	intron (FBgn0262509, intron 1 of 23)	DNAREP1_DM|RC|Helitron	1614	FBgn0262509|FBtr0304830
chr3L	1474669	1475169	8,81	11,14	2,33	2,74E-18	1,73E-15	TTS (FBgn0020248)	TTS (NM_176273)	338	FBgn0267487|FBtr0310161
chr3L	22997396	22997896	5,51	7,92	2,41	2,24E-11	4,82E-09	promoter-TSS (FBgn0262509)	promoter-TSS (NM_001043156)	-725	FBgn0262509|FBtr0304830
chr3L	22998072	22998572	7,55	10,21	2,66	3,15E-35	6,95E-32	promoter-TSS (FBgn0262509)	promoter-TSS (NM_001043156)	-49	FBgn0262509|FBtr0304830
chr3R	27961166	27961666	-0,18	10,05	10,23	2,83E-116	2,50E-112	promoter-TSS (FBgn0051253)	promoter-TSS (NM_170364)	405	FBgn0267308|FBtr0346202

II. The concerted activity of epigenomic effectors is essential to establish transcriptional programs during oogenesis

1. Article Presentation

In our first study, a genetic screen allowed us to identify Lid and Sin3A as essential regulators of *dhd* expression. These factors have been found in a repressive complex (Moshkin et al., 2009), which made us wonder if other chromatin complexes were involved in *dhd* regulation. Broadening our analysis to other knockdowns led us to identify two additional factors, essential for *dhd* expression: Snr1, a subunit of the chromatin remodeler Swi/Snf and the chromatin factor Mod(mdg4) mainly known for its insulator role. We thus wondered how are all of these factors promoting the hyperactivation of *dhd*?

To tackle this question, in this second article, I investigated the impact of these different knockdowns on the epigenome, using the chromatin profiling method Cut&Run. I also used a dedicated data analysis strategy to identify potential regulatory elements associated to histone marks.

Of note, this revised version of the article has been accepted by PLOS Genetics.

Three classes of epigenomic regulators converge to hyperactivate the essential maternal gene *deadhead* within a heterochromatin mini-domain.

Daniela Torres-Campana[1] , Béatrice Horard[1] , Sandrine Denaud[2] , Gérard Benoit[1] , Benjamin Loppin[1,*] & Guillermo A. Orsi[1,3*].

[1] : Laboratoire de Biologie et Modélisation de la Cellule, CNRS UMR5239, École Normale Supérieure de Lyon, University of Lyon, France.

[2] : Institute of Human Genetics, UMR 9002, CNRS–University of Montpellier, 34396 Montpellier, France.

[3]: Current address: Institute for Advanced Biosciences, INSERM U1209, CNRS, Université Grenoble Alpes, France.

[*] : correspondence: benjamin.loppin@ens-lyon.fr; guillermo.orsi@inserm.fr

Abstract

The formation of a diploid zygote is a highly complex cellular process that is entirely controlled by maternal gene products stored in the egg cytoplasm. This highly specialized transcriptional program is tightly controlled at the chromatin level in the female germline. As an extreme case in point, the massive and specific ovarian expression of the essential thioredoxin Deadhead (DHD) is critically regulated in *Drosophila* by the histone demethylase Lid and its partner, the histone deacetylase complex Sin3A/Rpd3, via yet unknown mechanisms. Here, we identified Snr1 and Mod(mdg4) as essential for *dhd* expression and investigated how these epigenomic effectors act with Lid and Sin3A to hyperactivate *dhd*. Using Cut&Run chromatin profiling with a dedicated data analysis procedure, we found that *dhd* is intriguingly embedded in an H3K27me3/H3K9me3-enriched mini-domain flanked by DNA regulatory elements, including a *dhd* promoter-proximal element essential for its expression. Surprisingly, Lid, Sin3a, Snr1 and Mod(mdg4) impact H3K27me3 and this regulatory element in distinct manners. However, we show that these effectors activate *dhd* independently of H3K27me3/H3K9me3, and that *dhd* remains silent in the absence of these marks. Together, our study demonstrates an atypical and critical role for chromatin regulators Lid, Sin3A, Snr1 and Mod(mdg4) to trigger tissue-specific hyperactivation within a unique heterochromatin mini-domain.

Author Summary

Multicellular development depends on a tight control of gene expression in each cell type. This relies on the coordinated activities of nuclear proteins that interact with DNA or its histone scaffold to promote or restrict gene transcription. For example, we previously showed that the histone modifying enzymes Lid and Sin3A/Rpd3 are required in *Drosophila* ovaries for the massive expression of *deadhead (dhd),* a gene encoding for a thioredoxin that is essential for fertility. In this paper, we have further identified two additional *dhd* regulators, Snr1 and Mod(mdg4) and dissected the mechanism behind hyperactivation of this gene. Using the epigenomic profiling method Cut&Run with a dedicated data analysis approach, we unexpectedly found that *dhd* is embedded in an unusual chromatin mini-domain featuring repressive histone modifications H3K27me3 and H3K9me3 and flanked by two regulatory elements. However, we further showed that Lid, Sin3A, Snr1 and Mod(mdg4) behave like obligatory activators of *dhd* independently of this mini-domain. Our study unveils how multiple broad-acting epigenomic effectors operate in non-canonical manners to ensure a critical and specialized gene activation event. These findings challenge our knowledge on these regulatory mechanisms and their roles in development and pathology.

Introduction

Gene expression is tightly controlled in eukaryotic cells by the composition, organization and dynamics of nucleosomes, consisting of an octamer of histone proteins wrapped in ~146bp of DNA. The concerted activity of protein complexes including histone chaperones, readers and writers as well as nucleosome remodelers, defines the positioning, composition and post-translational modifications of nucleosomes [1–3]. The resulting chromatin landscape is further organized by insulator proteins that delimit tridimensional contacts along the genome, forming sub-nuclear domains and guiding contacts between promoters and their cognate regulatory elements [4]. This tightly regulated epigenomic environment profoundly influences RNA Polymerase access to DNA and transcriptional activity.

Tremendous efforts in the past decades aimed at dissecting the roles of these epigenomic effectors *in vivo*. A privileged method is ablation or dosage manipulation of each component to measure its impact on gene expression. While these approaches can yield precious functional insight, the ubiquitous expression and wide range of activities of these factors, as well as redundancies in their interactions, make it difficult to infer their precise function. Understanding their function therefore requires identifying biologically relevant situations where disrupting these effectors impacts transcription in a critical and specific manner. We previously described one of such cases, where perturbation of the histone H3K4 demethylase Lid/KDM5 or the histone deacetylase complex Sin3A/Rpd3 in *Drosophila* ovaries dramatically abrogated the expression of the maternal gene *deadhead (dhd)*, which is essential for female fertility [5].

The *Drosophila* egg is loaded with maternal gene products synthesized by germline nurse cells that enable early embryonic development in the absence of zygotic

transcription [6]. An extreme example of this specialized transcriptome, *dhd* is among the most highly expressed genes in adult ovaries, while it is almost completely silent in any other tissue and developmental stage [5,7–9]. The DHD protein is a thioredoxin involved in regulating the general redox state in oocytes [10,11]. In addition, DHD plays a critical role at fertilization to reduce cysteine-cysteine disulfide bonds on the Protamine-like proteins that replace histones on chromatin during spermiogenesis [9,12]. In the absence of DHD, paternal chromosomes fail to decondense and are excluded from the first zygotic nucleus, leading to haploid gynogenetic development and embryonic lethality. The *dhd* locus, which produces a single, short (952bp), intronless transcript is packed within a 1369bp region that separates its flanking genes *Trx-T* and *CG4198*. Remarkably, these two genes are expressed exclusively in the male germline, thereby constituting an apparently unfavorable environment for *dhd* transcription in ovaries. In addition, we showed that a 4305bp transgene spanning only *Trx-T, dhd* and part of *CG4198* largely recapitulates the expression of *dhd* [5,9], indicating that regulatory elements sufficient for *dhd* activation are contained within this restricted region. Our previous study further found that Lid and Sin3A are essential activators of *dhd* in *Drosophila* ovaries, in striking contrast to their otherwise relatively modest impact on the rest of the transcriptome. Considering these unusual features, we postulated that the exquisite sensitivity of *dhd* to these broad-acting chromatin effectors revealed a singular mode of epigenomic regulation that enables its massive and specific ovarian expression [5].

Here, we exploited this singular model locus to understand how multiple classes of epigenomic effectors converge to achieve programmed transcriptional hyperactivation. We identified the Brahma chromatin remodeler component Snr1 [13] and the BTB/POZ-domain protein Mod(mdg4) [14] as factors that share with Lid and

Sin3A a critical and highly specific role in activating *dhd*. By exploiting the chromatin profiling method Cut&Run [15] and an adapted data analysis strategy, we found that *dhd* is unexpectedly embedded within a heterochromatin mini-domain flanked by two border regulatory elements. One of these is a *dhd*-proximal element, which encompasses a DNA Replication-related Element (DRE-box) motif [16] that is essential for *dhd* expression. Yet, exploiting knockdown and transgenic tools, we found that Lid, Sin3A, Snr1 and Mod(mdg4) activate *dhd* independently of the associated heterochromatin mini-domain. Furthermore, this mini-domain is not required to restrict *dhd* expression to ovaries. Together, our results put into perspective our understanding on these epigenomic regulators by revealing how they exert a biologically essential control of *dhd* via non-canonical mechanisms.

Results

Mod(mdg4) and Snr1 are essential for *dhd* expression

We previously performed a female germline RNA interference screen to identify chromatin factors required for paternal chromosome incorporation into the zygote at fertilization. As part of that screen, the histone H3K4 demethylase Lid, Sin3A and Rpd3, which participate in deacetylase complexes targeting various lysine residues in H3 and H4 [17,18], were identified as essential regulators of *dhd* expression. Because Lid and Sin3A can interact within a co-repressor complex [19,20], we asked whether other chromatin regulatory complexes might also be involved in *dhd* regulation. We therefore broadened our analysis to other knockdowns that caused maternal effect sterility associated with a *dhd*-like mutant phenotype, i.e. defective sperm nuclear decompaction

at fertilization. Among these, we focused on two additional UAS-controlled small hairpin RNA (shRNA) constructs from the TRiP collection [21], respectively targeting *mod(mdg4)* and *Snr1*. Snr1 is an essential subunit of the Brahma chromatin remodeler that mediates protein-protein interactions within this complex as well as with external interacting partners [13,22]. The *mod(mdg4)* gene codes for up to 31 isoforms [23], all of which are targeted by the shRNA construct. Among these, the most well characterized, Mod(mdg4)67.2 is a common component of boundary insulators in the *Drosophila* genome [24], but other non-insulating isoforms exhibiting activator functions have also been identified [4,25,26]. These two candidates belonged to two classes of epigenomic effectors distinct from Lid and Sin3A, and we thus decided to investigate their function during the oocyte to zygote transition.

When activated by the Maternal Triple Driver (MTD) Gal4 source, these shRNAs efficiently reduced the levels of *mod(mdg4)* and *Snr1* transcripts (FigS1-A). Previous studies reported defective oogenesis and diminished egg production in *mod(mdg4)* as well as *Snr1* mutant females [22,25]. Consistently, females with ovarian knockdown of *mod(mdg4)* or *Snr1* (hereby referred to as *mod(mdg4)* KD or *Snr1* KD females) were almost completely sterile (Table 1). Indeed, while KD females were able to lay more eggs than mutants, these almost systematically failed to hatch. Focusing on paternal chromatin organization at fertilization in these embryos, we found that both *mod(mdg4)* and *Snr1* ovarian KDs systematically led to failure of male pronucleus decondensation, which remained elongated (Fig1-A). Concomitantly, these eggs exhibited retention of the protamine fluorescent marker Mst35Ba::GFP (ProtA::GFP) [27] in paternal chromatin, as observed in *dhd* loss of function mutants [9,12].

Table 1. Embryo hatching rates.

The w^{1118} strain is used as reference.

Knockdowns			
Female Genotype	Male Genotype	Number of eggs	Hatch. rate (%)
Control	w^{1118}	1561	98.27%
Snr1 KD	w^{1118}	791	0.00%
mod(mdg4) KD	w^{1118}	1589	1.01%
lid KD (val22)	w^{1118}	1403	2.14%
lid KD (val*21*)	w^{1118}	1144	1.05%
Sin3a KD	w^{1118}	1221	0.25%
E(z) KD	w^{1118}	843	0.00%
Rescue with WT or ΔDRE mutant transgene			
w^{1118}	w^{1118}	344	97.67%
dhd^{J5}	w^{1118}	375	0.00%
dhd^{J5};;$pW8\text{-}dhd^{WT}$	w^{1118}	663	85.67%
dhd^{J5};;$pW8\text{-}dhd^{\Delta DRE}$	w^{1118}	475	2.15%
dhd^{J5};;$pW8\text{-}dhd^{FD}$	w^{1118}	410	87.80%
Knockdown rescue with the WT transgene			
dhd^{J5};; *lid KD(val21),* $pW8\text{-}dhd^{WT}$	w^{1118}	175	1.92%
dhd^{J5};; *Sin3a KD,* $pW8\text{-}dhd^{WT}$	w^{1118}	271	0.37%
dhd^{J5};; *Snr1 KD,* $pW8\text{-}dhd^{WT}$	w^{1118}	247	0.00%
dhd^{J5};; *mod(mdg4) KD,* $pW8\text{-}dhd^{WT}$	w^{1118}	462	0.43%

The above results suggest that Mod(mdg4) and Snr1 could regulate *dhd* expression. RNA-sequencing on *mod(mdg4)* and *Snr1* KD ovaries indeed revealed that *dhd* is dramatically downregulated in both KDs, with a fold reduction of almost two orders of magnitude (Fig1-B,C, and FigS1-B,E). *dhd* was the first most strongly affected gene in *mod(mdg4)* KD ovaries in terms of fold-change in expression, and the 14th most affected gene in *Snr1* KD ovaries. Consistently, DHD protein levels assessed by Western Blot in KD ovaries were also dramatically reduced (Fig1-D). This was in contrast to a more modest impact of both KDs on the rest of the transcriptome and the limited overlap in their effects (Fig S1-B,C,D). In particular, genes in the vicinity of *dhd* were not significantly affected by the KDs (Fig1-C and FigS1-B). Therefore, despite the packed

genomic organization of the *dhd* locus, its expression strictly and singularly depends on multiple epigenomic effectors.

Cut&Run with dedicated analysis reveals both the distribution of histone modifications and their associated regulatory elements

To more precisely characterize the chromatin landscape at the *dhd* locus, we next implemented the Cut&Run epigenomic profiling method [15]. In Cut&Run, histone modifications of interest are targeted *in situ* by a specific antibody following tissue permeabilization. Target-bound antibodies are subsequently coupled to a fusion between the bacterial Protein A and Micrococcal Nuclease (ProteinA-MNase) that cleaves exposed DNA in the vicinity of the antibody, releasing target nucleosomal particles into solution. Importantly, MNase is expected to also cleave exposed DNA in the immediate spatial vicinity of the nucleosome-bound antibody, causing the release of DNA particles bound by other proteins such as polymerases or DNA sequence-specific transcription factors (Fig2-A). In particular, DNA regulatory elements occupied by sequence-specific transcription factors are typically associated with MNase footprints distinctly shorter than nucleosomes [28–30]. Partially unwrapped dynamic nucleosomes typically associated with regulatory elements can also produce such distinctly short footprints [31]. Following paired-end sequencing, such released DNA fragments can be distinguished and separated by their size, yielding a map of nucleosomes (>146bp) and sub-nucleosomal particles, putatively corresponding to

regulatory elements (<120bp). A single Cut&Run experiment should thus identify DNA regulatory elements that are in physical proximity of target histone modifications.

With this in mind, we conducted H3K27me3 Cut&Run in *Drosophila* ovaries. Using only 12 pairs of ovaries per sample, we robustly revealed H3K27me3 domains. Remarkably, visualization of Cut&Run fragments shorter than 120bp (which excludes fully wrapped octameric nucleosomes) revealed that these were enriched at discrete peaks within H3K27me3 domains. Genome-wide analysis identified 679 peaks of fragments <120bp (hereon referred to as "short fragment peaks") that were ~250bp-wide in average (Fig2-B,D). We hypothesized that short fragment peaks represented H3K27me3-associated regulatory elements occupied by transcription factors. Within H3K27me3 domains, we expected these to include Polycomb Response Elements (PREs) as well as insulators. For example, short fragment peaks corresponded to several well-described PREs and insulators in the Bithorax complex H3K27me3 domain [26,32,33] (Fig2-C), consistent with observations in larval tissue [34]. To ask whether this reflects a broader genome-wide trend, we compared short fragment peaks with PRE and insulator markers genome-wide. Although there is scarce genome-wide data available for *Drosophila* ovaries, H3K27me3 domains are generally present in most cell types. We thus exploited datasets from embryonic-derived S2 and Kc cell lines. Consistent with their occupancy by transcription factors, ATAC-seq peaks [35] -revealing hyper-accessible DNA- coincide with Polycomb regulatory elements in flies and mice [35,36]. Genome-wide, our small fragment peaks identified in ovaries were enriched for ATAC-seq signal, arguing that these indeed correspond to DNA regulatory elements (Fig2-D). Enrichment at these peaks of the Polycomb protein [37] and the insulator protein CP190 [38] further argues that these elements often correspond to functional PREs or insulators. Accordingly, at the borders of H3K27me3 domains, short fragment peaks

were more frequently associated with CP190, confirming previous reports that this factor is associated with H3K27me3 domain boundaries [24,39] (Fig2-D). Instead, Polycomb was rather enriched at peaks localized internally within these domains. Our Cut&Run analysis strategy can therefore be used to reveal not only the breadth of histone modification domains in ovaries but also their associated DNA regulatory elements.

dhd lies within an H3K27me3/H3K9me3 mini-domain flanked by DNA regulatory elements.

To gain insight on *dhd* regulation, we next sought to analyze its associated chromatin configuration. We previously showed that the active transcription modification H3K4me3 is enriched at the *dhd* promoter and that this mark is lost in *lid* KD ovaries [5](FigS2-A). Using available ChIP-seq datasets from embryonic derived S2 cells, we further observed that that *dhd* lies within a ~5kbp mini-domain featuring two types of repressive histone modifications: H3K27me3 and H3K9me3 (FigS2-A) [40]. H3K27me3 is the hallmark of Polycomb-based repression [41,42], whereas H3K9me3 dictates Heterochromatin Protein 1 (HP1)-based repression [43,44]. Interestingly, this mini-domain was also found in ChIP-seq data from fly ovaries (FigS2-A) [45]. Potentially regulating this chromatin environment, Lid and Sin3A were described as participating in a co-repressor complex [20], but their global impact on repressive histone modifications is unclear. In turn, previous reports showed that depletion of insulator proteins Mod(mdg4), as well as CTCF, Su(Hw), CP190 or BEAF-32, did not affect the spread of Polycomb-associated domains but instead caused a general decrease in H3K27me3 levels [24]. In contrast, the Brahma/BAF complex is typically considered as

counteracting Polycomb repression based on work in mammals [46], but this interplay has not been analyzed in Drosophila.

Based on these observations, we sought to better characterize the distribution of H3K27me3 and H3K9me3 in ovaries at the *dhd* locus. Using our Cut&Run approach, we confirmed that *dhd* is included in a ~5450bp heterochromatic H3K27me3/H3K9me3 mini-domain that extends from the promoter region of *dhd* to the promoter of the next gene active in ovaries, *Sas10* (Fig3-A). While our whole-tissue Cut&Run approach cannot distinguish which cells harbor this domain, published H3K27me3 ChIP-seq profiles from either somatic or germline cells in ovaries indicate that this mark is present in both (Figure S2-A). We segmented the Cut&Run H3K27me3 signal in control ovaries and identified 278 discrete H3K27me3 domains, ranging from 3 to 240kb in width. The *dhd* H3K27me3 domain stood out when considering its enrichment in this mark relative to its length, compared to other domains (Fig3-B). Our analyses indicate that despite its reduced size, the *dhd* locus is capable of accumulating proportionately high amounts of this repressive modification. While we also identified other previously described H3K9me3 domains lodged in euchromatic regions (FigS3), the signal is, as expected, largely dominated by pericentric heterochromatin. We could thus not robustly call such euchromatic H3K9me3 domains, preventing us from conducting an analogous analysis for *dhd* on this mark.

Surprisingly, short fragment peak analysis revealed two putative DNA regulatory elements associated with both histone marks, precisely at the mini-domain borders, with no internal peaks present (Fig3-A). ATAC-seq data from S2 cell lines confirmed presence of only these two border elements (FigS2-B). In addition, in Kc cells, *dhd* border elements are occupied by CP190 and Mod(mdg4), both of which can be found at the boundaries of *Drosophila* H3K27me3 domains [24,47]. However, the insulating

isoform Mod(mdg4)67.2 is not found at the *dhd* locus (FigS2-B), suggesting that a different isoform playing an activator function is responsible for *dhd* regulation. Finally, the *dhd*-proximal 5' border element featured a significant, although very modest enrichment for PRE markers Polycomb and Polyhomeotic (Fig-S2-B). This regulatory architecture was quite unusual, as we could not find any other H3K27me3 domain in the genome sharing this particular organization with two border elements and no internal elements. Together, these results revealed that *dhd* lies within a unique H3K27me3/H3K9me3 mini-domain featuring only border elements.

Sin3A, Snr1 and Mod(mdg4) control the regulatory architecture of the *dhd* mini-domain.

We next aimed at evaluating the potential role for Lid, Sin3A, Mod(mdg4) and Snr1 in regulating this heterochromatin mini-domain. We used KD ovaries for these factors and included as a control a KD for the H3K27 methyltransferase Enhancer of zeste (E(z)), induced in germ cells by the MTD-Gal4 driver. While *E(z)* KD females were sterile as previously described [48,49] (Table1), they were able to lay eggs and displayed only a moderate effect on *dhd* expression (a 25% reduction compared to controls) (FigS4-A). Immunofluorescence staining on dissected control ovaries showed that H3K27me3 marks follicle cell nuclei, the karyosome (i.e the oocyte nucleus) and nurse cell nuclei, although nurse cell staining was relatively weaker (FigS3-B), consistent with previous reports [48]. As expected, H3K27me3 was undetectable in the karyosome and in nurse cells of *E(z)* KD ovaries, whereas follicle cells (which do not express MTD-driven shRNAs) still carried this mark at normal levels. While *lid*, *Sin3a* and *mod(mdg4)* KD ovaries displayed normal H3K27me3 staining, we observed a

moderate reduction in H3K27me3 levels in nurse cells in *Snr1* KD ovaries, even while H3K27me3 levels were not affected on the karyosome (FigS4-B).

We next carried out H3K27me3 Cut&Run on ovaries from all KDs. Within our 278 identified H3K27me3 domains (see above), we compared the average enrichment in H3K27me3 signal in control and KD ovaries (Fig3-C). In *E(z)* KD ovaries, Cut&Run experiments revealed only a moderate loss of H3K27me3 signal (35% average reduction at these domains compared to controls) (Fig3-C), contrasting with the strong global reduction in H3K27me3 immunofluorescence signal. This difference is likely to reflect the fact that the H3K27me3 signal from Cut&Run experiments originates from both germline and somatic cells. Accordingly, *E(z)* KD completely abrogated H3K27me3 signal at the *spen*, *Corto* or *ptc* loci, all of which are decorated with H3K27me3 in nurse cells but not in follicle cells (FigS4-C) [50]. In contrast, the *gl, dpp,* or *repo* loci, which show stronger H3K27me3 in follicle cells compared to nurse cells, were only slightly affected in *E(z)* KD ovaries (FigS4-C). Together, these results show that our Cut&Run strategy detects H3K27me3 signal from both germline and somatic cells and is able to detect quantitative differences in the averaged signal when nurse cells are strongly affected. Consistent with immunofluorescence experiments, *lid, Sin3a* and *mod(mdg4)* KDs had only a modest global impact on average H3K27me3 levels (5% reduction compared to controls), and no effect on the spread of H3K27me3 domains (Fig3-C). Also consistent with our immunofluorescence experiments, *Snr1* KD led to a more severe average reduction of H3K27me3 Cut&Run signal compared to controls (20%), although not as dramatic as *E(z)* KD.

In agreement with genome-wide observations, the levels of H3K27me3 in the *dhd* mini-domain were reduced in *E(z)* KD ovaries and unaffected in *Sin3a* or *mod(mdg4)* KD ovaries. More surprisingly, the domain was not measurably affected in

Snr1 KD ovaries, despite the fact that H3K27me3 is globally impacted by this knockdown (Fig3-D and FigS5-A). Within the sensitivity limits of our approach, these results indicate that *Sin3a, Snr1* and *mod(mdg4)* KDs have little if any impact on H3K27me3 at the *dhd* locus. Conversely, in *lid* KD ovaries, in which global H3K27me3 levels were unaffected, we detected an increase in H3K27me3 levels at the *dhd* mini-domain (Fig3-C,D and FigS5-A). This raised the possibility that Lid could facilitate *dhd* expression by counteracting Polycomb-mediated repression.

Since the *dhd* mini-domain also featured H3K9me3, we next turned to Cut&Run followed by qPCR to evaluate its status in KD ovaries. H3K27me3 Cut&Run-qPCR measures the expected enrichments at H3K27me3 domains and detects variations in the signal coherent with Cut&Run-seq results (Fig3-E and FigS5-B). To validate the H3K9me3 Cut&Run-qPCR approach in ovaries, we exploited the *CG12239* gene as a positive control [45], and detected an expected enrichment in H3K9me3 signal at this locus (Fig3-E and FigS5-B). At the *dhd* locus, H3K9me3 was enriched as expected from ChIP-seq results. Importantly, knockdown of *lid, Sin3a, mod(mdg4) or Snr1* had no effect on this enrichment. (Fig3-E). The *dhd* heterochromatin mini-domain including H3K27me3 and H3K9me3 is thus independent of Sin3A, Snr1, whereas Lid counteracts H3K27me3.

We next evaluated the impact of different KDs on the *dhd* mini-domain short fragment peaks at border regions. We first analyzed the effect of our different knockdowns on the full set of 679 peaks previously defined (Fig2-B). Both *E(z)* and *Snr1* KD led to a strong (~63%) decrease in short fragment peak average counts genome-wide (Fig4-A). Since these KDs also affect global H3K27me3 levels, this reduction could result from a general absence of histone modification-targeted MNase on chromatin. Remarkably, *Sin3a* KD led to a similarly strong effect on short fragment peak counts that

could not be attributed to its global impact on H3K27me3. Instead, this data suggests that Sin3A is required to ensure proper occupancy and organization of transcription factors and/or nucleosomes at DNA regulatory elements associated with H3K27me3. In contrast, *lid* or *mod(mdg4)* KD did not globally affect short fragment peak counts, indicating that these factors do not play such a role (Fig4-A).

Consistent with their effects genome-wide, short fragment counts at the *dhd* mini-domain border elements were strongly diminished upon *E(z)* and *Sin3a* KDs (Fig4-B and FigS5-C). Intriguingly, *mod(mdg4)* KD led to a similar impact on these border elements (particularly the *dhd*-proximal one), even though it did not globally affect H3K27me3-associated elements genome-wide (Fig4-B and FigS5-C). This observation could indicate that the *dhd* border elements become less frequently occupied by transcription factors, that these factors become less frequently associated with H3K27me3, and/or that their nucleosomal organization is compromised. In all cases, this suggests that Mod(mdg4) is required to ensure chromatin organization of the border DNA regulatory elements at the *dhd* mini-domain. Remarkably, *Snr1* KD led to a similar effect on border elements without affecting H3K27me3 levels at the *dhd* mini-domain, suggesting that Snr1 is also required for the proper organization of the *dhd* border elements. In striking contrast, *lid* KD had no detectable effect on these regulatory elements (Fig4-B and FigS5-C). We concluded that Lid, although essential for *dhd* expression, was not required to ensure the proper organization of *dhd* border elements.

Altogether our results, summarized in Fig4-C, indicate that Lid, Sin3A, Snr1 and Mod(mdg4), impact H3K27me3 or its associated regulatory elements genome-wide and/or at the *dhd* mini-domain in four distinct manners.

The *dhd* promoter-proximal DNA regulatory element is required for dhd expression independently of its heterochromatin mini-domain.

We next performed sequence analysis of the *dhd* mini-domain border elements, screening against the flyreg.v2 transcription factor DNA binding motif database [51,52]. At the 5' border element, which mapped to the *dhd* promoter region, we identified four perfect matches for the DNA replication-related element (DRE) motif, TATCGATA (Fig5-A). This motif is recognized by the insulator-associated factor BEAF-32 [53] and the core-promoter factor DREF [16]. These four DRE motifs overlap in the palindromic sequence TATCGATATCGATA, 37bp upstream of the *dhd* transcription start site. Consistently, BEAF-32 and DREF both occupy this element in Kc cells (FigS6) [38]. Previous studies showed that BEAF-32 null females are partially fertile (~40% hatching rate) [54], indicating that this factor is not essential for *dhd* expression. In turn, DREF is essential in a cell-autonomous manner and indeed *dref* mutations cause oogenesis defects [55]. Accordingly, we observed severe atrophy and failure to produce oocytes in *dref* KD ovaries. Because this precluded studying the role of DREF in *dhd* regulation, we instead sought to probe the importance of the DRE motifs themselves.

The dhd^{J5} null allele is a 1.4 kb deletion affecting the entire promoter region including the promoter-proximal regulatory element, and part of the coding region of *dhd* [7,9] (Fig5-A). A $pW8\text{-}dhd^{WT}$ transgenic construct, bearing the entire *dhd* gene -including its promoter region-, restores *dhd* expression as well as fertility in dhd^{J5} mutants [9] (Fig5-A,B, Table1). We now constructed a second rescue transgene based on the $pW8\text{-}dhd^{WT}$, where the 14bp carrying the DRE motifs were deleted ($pW8\text{-}dhd^{\Delta DRE}$)

(Fig5-A). These constructs were inserted into the same genomic location as *pW8-dhd^{WT}* (62E1) and combined with the *dhd^{J5}* deficiency. In striking contrast to *pW8-dhd^{WT}*, the *pW8-dhd$^{\Delta DRE}$* construct was unable to rescue *dhd* expression, or substantially improve fertility in *dhd^{J5}* deficient flies (Fig5-B, Table1). The DRE motifs are thus essential to ensure *dhd* expression.

To test a role for this regulatory element and its DRE motifs in regulating the H3K27me3/H3K9me3 mini-domain, we performed Cut&Run-seq and Cut&Run-qPCR on homozygous *dhd^{J5}* ovaries, as well as rescue *dhd^{J5};;pW8-dhd^{WT}* and non-rescued *dhd^{J5};;pW8-dhd$^{\Delta DRE}$* ovaries. Strikingly, the 5.4kbp *dhd* H3K27me3 mini-domain was completely lost in *dhd^{J5}* ovaries (Fig5-C,D and FigS7), despite the fact that 90% of this mini-domain were intact in the deficient chromosome. This indicates that the *dhd*-proximal border of this mini-domain is essential for establishment and/or maintenance of H3K27me3. Furthermore, H3K27me3 signal was absent within the mini-domain in *dhd^{J5};;pW8-dhd^{WT}* rescue ovaries (Fig5-C,D and FigS7), suggesting that the 5'-most 2.8kbp of the domain are also insufficient to establish and/or maintain H3K27me3. This result further confirms that *dhd* can be expressed at high levels in the absence of H3K27me3, consistent with results from *E(z)* KD ovaries (FigS4-A). Finally, the H3K27me3 mini-domain was also completely absent in *dhd^{J5};;pW8-dhd$^{\Delta DRE}$* ovaries (Fig5-C), indicating that the DRE motifs are required for *dhd* expression independently of H3K27me3.

Based on these observations, we hypothesized that the complete mini-domain sequence, including both border regulatory elements, might be necessary for restoring heterochromatin marks. We thus constructed a transgene containing the full domain sequence of the *dhd* heterochromatin domain (*pW8-dhd^{FD}*)(Fig5-A), inserted at the same genomic location as the *pW8-dhd^{WT}* transgene. Interestingly, this transgene

restored *dhd* expression (Fig5-B) and rescued fertility (Table 1) but was unable to restore H3K27me3 (Fig5-D and FigS7). These results indicate that the border-to-border mini-domain is not autonomous and suggest that its genomic location impacts its chromatin configuration.

We next focused on the H3K9me3 mark. In contrast to H3K27me3, Cut&Run analysis in dhd^{J5} mutants showed that H3K9me3 was lost at the *dhd*-proximal half of the domain, while this mark was maintained at the *dhd*-distal part (Fig5-C). Cut&Run-qPCR using primers across the *dhd* domain revealed that H3K9me3 was not restored at the *dhd*-proximal part of the H3K9me3 domain in dhd^{J5};;*pW8-*dhd^{WT} or dhd^{J5};;*pW8-*dhd^{FD} ovaries (Fig5-D and FigS7). Together, these results indicate that the border-to-border mini-domain is not autonomous to establish its own heterochromatin configuration, and that *dhd* expression can proceed at near normal levels independently of these marks.

Lid, Sin3A, Snr1 and Mod(mdg4) activate *dhd* independently of its heterochromatin mini-domain.

The fact that the *pW8-*dhd^{WT} transgene restored most of *dhd* expression without re-establishment of the heterochromatin mini-domain at this locus provided an opportunity to clarify the role of our set of *dhd* regulators. KD of lid is associated with increased H3K27me3 at the *dhd* mini-domain, suggesting that Lid may operate as an anti-repressor by counteracting heterochromatinization of the locus. However, we have previously found that *dhd* expression is not re-established in *lid* KD ovaries carrying a *pW8-*dhd^{WT} rescue transgene [5]. Lid is thus required for *dhd* expression not only at its endogenous locus but also from the rescue transgene not decorated by H3K27me3

(Fig5). Therefore, Lid activates *dhd* independently of heterochromatin, suggesting that it does not operate strictly as an anti-repressor.

To discriminate between anti-repressive or activating roles of Sin3A, Mod(mdg4) and Snr1, we generated flies combining a dhd^{J5} deficiency, the $pW8\text{-}dhd^{WT}$ transgene and an shRNA targeting *lid*, *Sin3a, Snr1 or mod(mdg4)*, driven in germ cells by a *nos-Gal4* driver (Fig6-A). We confirmed by RT-qPCR that knockdowns were still efficient when using this driver (Fig-S8-A). Remarkably, all of these flies were almost completely sterile, and showed strong downregulation of *dhd* revealed by RT-qPCR (Fig6-B and Table1). Using Cut&Run-qPCR at the *dhd* locus, we further confirmed that these knockdowns had no effect on H3K27me3, which remained depleted in all conditions (Fig6-C and FigS8-B). Lid, Sin3A, Snr1 and Mod(mdg4) therefore stimulate *dhd* transcription in the absence of its heterochromatin mini-domain.

Our results indicate that the *dhd* heterochromatin mini-domain does not play a repressive role in ovaries, but do not exclude that it might maintain *dhd* silent in other tissues. RT-qPCR analysis on dissected ovaries, testes and male and female carcasses from transgenic lines expressing dhd^{J5};;$pW8\text{-}dhd^{WT}$ revealed *dhd* expression uniquely from ovaries (Fig6-D). Because this transgene rescues *dhd* expression without restoring heterochromatin marks, these results suggest that the *dhd* heterochromatin mini-domain is not essential to repress ectopic *dhd* expression in adults. We note, however, that we cannot exclude that *dhd* was weakly and/or transiently expressed in certain cell types in these conditions, or that the rescue transgene could accumulate repressive marks in tissues other than ovaries.

Discussion

The ovarian hyperactivation of *dhd*

Here, we sought to understand how the genomic and epigenomic environments of *dhd* contributed to its remarkable regulation, its expression being both among the highest in Drosophila, and absolutely specific to adult ovaries [5,9]. Lid, Sin3A, Snr1 and Mod(mdg4) all shared a critical and rather specific role in ensuring *dhd* expression. Yet, these four broadly expressed proteins play multiple roles other than *dhd* regulation. For example, transcriptomic analyses following individual depletion of Lid, Sin3A or Snr1 in S2 cells, wing discs or pupae shows activation or repression of hundreds of targets [19,22,56]. ChIP-seq data further indicates that Mod(mdg4), Sin3A and Lid each target several thousand sites in the genome [24,26,57,58]. Consistently, our RNA-seq analyses did reveal that each of these knockdowns were associated to up- or down-regulation of 407 to 2020 genes in ovaries, with *dhd* being in every case among the most strongly dependent on these factors. We propose that *dhd* is a hypersensitive gene that reacts radically to epigenome imbalances.

The key question is therefore what is the formula for *dhd* ovarian hyperactivation. One reasonable hypothesis was that *dhd* could be highly regulated by distal enhancers. This would be notably consistent with the previously described role of Mod(mdg4) in organizing 3D contacts between regulatory elements and promoters [26]. It would also be consistent with recent findings that H3K27me3 micro-domains may reflect such contacts [59]. However, no interaction between *dhd* and any other locus can be found in Hi-C data, and our rescue transgene experiments show that a small, ectopic genomic segment almost fully recapitulates its expression, arguing that

the genomic and epigenomic environment at the endogenous *dhd* region may play only a minor role in its ovary-specific hyperactivation.

We indeed found a key regulatory element containing a tandem DRE motif, known to recruit the DREF core promoter factor. The minimal DRE motif (TATCGATA) is found in thousands of gene promoters [60], while multiple genes were individually shown to require this motif for proper activation. These include genes with ovarian expression, and, accordingly, DREF mutations cause oogenesis defects and female sterility [55]. In contrast, the particular tandem DRE motif in the *dhd* regulatory sequence is uncommon, being only found in 9 other gene promoters. Yet, among these 9 genes, only 4 displayed an expression bias in ovaries, and none were nearly as highly transcribed as *dhd*. Therefore, this motif does not seem to be autonomously sufficient for ovarian hyperexpression.

Another unusual feature of *dhd* is its surrounding heterochromatin mini-domain bearing both H3K27me3 and H3K9me3 marks, as well as H3K4me3. The co-occurrence of these active and repressive modifications at an ensemble of developmentally regulated genes in mammals led to the concept of bivalent promoters [61]. It is speculated that such promoters may be poised for rapid activation or repression upon differentiation. In *Drosophila*, bivalent chromatin is associated with genes that can be strongly activated in a tissue-specific manner [62,63]. Our experiments showed that *dhd* is expressed at ~60-70% of its normal levels in *E(z)* KD ovaries, as well as in rescue transgenes - conditions in which the H3K27me3/H3K9me3 mini-domain is impaired. We thus cannot exclude that these heterochromatin marks play a positive role in *dhd* activation to ensure its transcription at maximum capacity, perhaps via establishment of a bivalent configuration. We also note that our whole-tissue experiments leave the

possibility open that these histone modifications may decorate *dhd* in different cell types and/or at different times during gametogenesis.

Altogether, we uncovered multiple unusual genomic and epigenomic characteristics at the *dhd* locus, but failed to identify any single feature that was truly defining. The dramatic regulation of *dhd* may rely not on any individual trait but rather on a unique combination of such rare features. Further work will be needed to elucidate how these different components may together achieve ovarian hyperexpression.

A non-canonical chromatin domain

The unique properties of *dhd* led us to uncover interesting features of its epigenomic regulators. First, *dhd* is embedded in an H3K27me3 mini-domain flanked by regulatory elements. A recent report suggested that H3K27me3 domain borders may be established independently of PREs or border elements, provided that an immediately neighboring active gene instead delimits H3K27me3 spreading [47]. The case of *dhd* is however peculiar in that the H3K27me3 domain border overlaps with this highly active gene, a scenario that was not found in other domains. The coincidence of H3K27me3 and H3K9me3 is also uncommon and, in fact, we could not find any other such dual domain in ovaries. Our result favors the view that this heterochromatin domain does not silence *dhd* expression. Nonetheless, H3K9me3 was always maintained at the *dhd*-distal portion of the domain. We therefore cannot exclude that this mark represses *dhd* neighbors.

An intriguing question is then how this heterochromatin mini-domain is formed. We found that a transgene containing the full mini-domain sequence is unable to restore H3K27me3 or H3K9me3, suggesting that genomic location of this domain is a

critical determinant of *dhd* heterochromatin. From this perspective, the border elements may act as weak PREs, as described in other contexts [64]. Interestingly, we also showed that H3K9me3 can be partially maintained at the distal part of the domain in dhd^{J5} mutants while H3K27me3 is completely lost. This indicates that these marks are not necessarily inter-dependent at this locus, and H3K9me3 may benefit from additional mechanisms ensuring its deposition. While not much is known on highly localized euchromatic deposition of H3K9me3, Smolko and colleagues suggested that Setdb1-dependent accumulation of H3K9me3 at certain target genes is dependent on the RNA-binding protein Sxl [45]. At the *dhd* domain, different mechanisms could thus ensure H3K27me3 and H3K9me deposition, both of which would depend on the endogenous genomic location.

Along these lines, another recent study reported the existence of H3K27me3 micro-domains (typically 2-8 nucleosomes wide) that depend on 3D contacts with larger H3K27me3 domains, mediated, in particular, by BEAF-32 and CP190 [59]. The *dhd* mini-domain is wider and much more strongly enriched in H3K27me3 than typical micro-domains. Nonetheless, our data is consistent with a model whereby H3K27me3 could be deposited via such looping interactions. First, BEAF-32 and CP190 are indeed found at the border elements of the *dhd* mini-domain. Second, this mini-domain does not feature internal PREs and border elements are only weakly if at all bound by Polycomb proteins, arguing against an autonomous recruitment of E(z). Finally, a deletion of the BEAF-32/CP190-bearing regulatory element in the dhd^{J5} mutant, or its displacement to an ectopic genomic location in rescue transgenes both abrogate H3K27me3 deposition. Consistent with such a model, data from Heurteau *et al.* show a modest reduction of H3K27me3 enrichment at the *dhd* mini-domain upon BEAF-32 depletion. Of note, BEAF-32 was also previously shown to facilitate H3K9me3

deposition at sites featuring multiple instances of the CGATA motif, analogous to those found at the *dhd* promoter [65]. Other studies found that ATCGAT motifs recognized by BEAF-32, also found at the *dhd* promoter, are more broadly enriched at the promoters of Lid-activated genes [66], which is the case of *dhd*. Thus, it is possible that a BEAF-32-mediated looping mechanism is responsible for H3K27me3 enrichment at the *dhd* mini-domain. However, our results also show that this mark is not strictly required to repress nor to activate *dhd* in adults, and that Lid, Sin3A, Snr1 and Mod(mdg4) activate *dhd* independently of it.

Scrutiny of *dhd* regulation further uncovered how its four regulators have convergent yet distinct roles. This was particularly intriguing for Lid and Sin3A, which can be found in a co-repressor complex [20], at odds with their positive impact on *dhd*. Indeed, their dual depletion in cultured cells causes the misregulation of hundreds of genes [19]. Interestingly, in that study, only 55 out of 849 affected genes were similarly impacted by individual and dual knockdowns, indicating that Lid and Sin3A functionally cooperate only at a minor subset of their common targets. This seems to be the case at the *dhd* locus, where individual KD of these factors caused an equally catastrophic collapse of transcriptional activity, suggesting a cooperative activity. Yet, Lid, but not Sin3A, acted as a negative regulator of H3K27me3 at the *dhd* locus, revealing at least partially independent functions. In contrast, Sin3A, but not Lid, controlled the stability of regulatory elements associated with this H3K27me3, not only at the *dhd* domain but also genome-wide.

Our results further show a critical role for Mod(mdg4) as a transcriptional activator. In cell lines, ChIP-seq experiments specifically mapping the insulating Mod(mdg4)67.2 isoform or total Mod(mdg4) showed that additional isoforms are recruited to DNA [24]. Isoforms other than the 67.2 were found in particular at gene

promoters in ovaries and female heads [4]. Such is the case at the *dhd* promoter, where total Mod(mdg4) is found but not the 67.2 isoform (FigS2-B). Non-insulating roles of Mod(mdg4) were previously discussed in the context of the Polycomb-repressed Bithorax complex where the close binding of Mod(mdg4) to *Abd-B* transcription start sites suggested a role in transcription activation [26]. While we cannot rule out indirect effects, these observations argue that an activating isoform of Mod(mdg4) operates directly at the *dhd* promoter. In agreement, Mod(mdg4) appears to be essential to activate *dhd* within its H3K27me3 mini-domain, seemingly by stabilizing the *dhd* promoter regulatory element, although its function is equally essential in the absence of heterochromatin marks in the *dhd* transgenic rescue construct.

The Snr1-containing Brahma complex is required for activation of target genes in *Drosophila in vivo*, notably during immune responses [60] and tissue regeneration [56]. In ovaries, while Snr1 has a global impact on nuclear integrity and architecture, previous immunostaining experiments interestingly showed that this factor is only expressed during a restricted time in early oogenesis [22]. This underlines the fact that *dhd* may be dynamically regulated during oogenesis, with different regulatory components intervening at particular times. Considering that *Snr1* KD causes a disruption of the *dhd* promoter-proximal regulatory element associated with H3K27me3, this would suggest that its associated DNA-binding transcription factors also intervene during a restricted time in oogenesis. A precise dissection of the timing of *dhd* transcription, and determining whether these factors target *dhd* directly and simultaneously, would be essential to understand the cascade of events leading to its massive expression.

The case of *dhd* indeed illustrates the complexity of understanding the chromatin landscape at cell type-specific genes, when the starting material is a complex tissue. In

this context, the Cut&Run analysis implemented in our study allowed us to reveal the co-occupancy of H3K27me3 nucleosomes and associated transcription factors. While this approach cannot identify the cell of origin of each individual DNA molecule, it can be used to make important deductions on the combinatorial co-occupancy on DNA of different chromatin components. This approach joins other recent methods comparable in their principle, namely the DNA methyl-transferase single-molecule footprinting (dSMF) method [67] and the low-salt antibody-targeted tagmentation (CUTAC) approach [68]. Together with single-cell methodologies, these approaches hold the potential to begin uncovering complex epigenomic regulation processes, such as that of *dhd*, that were until recently inaccessible.

Acknowledgements

We thank Dr. Kami Ahmad for sharing reagents and advice on Cut&Run. We are grateful to the TRiP projects and Bloomington Drosophila Stock Center for fly stocks. We acknowledge the contribution of SFR Biosciences (UAR3444/CNRS, US8/Inserm, ENS de Lyon, UCBL) facilities PLATIM and Arthro-tools. Sequencing was performed by the GenomEast platform, a member of the 'France Génomique' consortium. We would like to thank Raphaëlle Dubruille and Francesca Palladino for critical reading of the manuscript. We also warmly thank them, as well as Lucas Waltzer and all members of the Loppin lab for their input throughout this project. This work was supported by an Association pour la Recherche sur le Cancer (ARC) Foundation grant (PJA20191209671) to BL. DTC was supported by a PhD fellowship from the Ministère de l'Enseignement supérieur, de la Recherche et de l'Innovation and from the ARC (ARCDOC42020020001727).

Competing Interests Statement:

The authors declare no competing interests.

Author Contributions

Conceptualization: Daniela Torres-Campana, Benjamin Loppin, Guillermo A. Orsi.

Funding acquisition: Benjamin Loppin, Guillermo A. Orsi.

Investigation: Daniela Torres-Campana, Béatrice Horard, Sandrine Denaud, Benjamin Loppin, Guillermo A. Orsi.

Data curation and formal analysis: Daniela Torres-Campana, Gérard Benoit, Guillermo A. Orsi.

Methodology: Daniela Torres-Campana, Guillermo A. Orsi

Supervision: Béatrice Horard, Benjamin Loppin, Guillermo A. Orsi.

Validation: Daniela Torres-Campana, Guillermo A. Orsi.

Writing – original draft: Daniela Torres-Campana, Guillermo A. Orsi.

Writing – review & editing: Daniela Torres-Campana, Béatrice Horard, Gérard Benoit, Benjamin Loppin and Guillermo A. Orsi.

Materials & Methods

Drosophila strains

Flies were raised at 25°C on standard medium. The following stocks were obtained from the Bloomington *Drosophila* Stock Center (simplified genotypes are given):

P{TRiP.HMS00849}attP2 (*mod(mdg4)* shRNA; #33907), *P{TRiP. HMS00363}attP2* (*Snr1* shRNA; #32372), *P{TRiP.GL00612}attP40* (*lid* shRNA; #36652), *P{TRiP.GLV21071}attP2* (*lid* shRNA; #35706), *P{TRiP.HMS00359}attP2* (*Sin3a* shRNA; #32368), *P{TRiP.HMS00066}attP2* (*E(z)* shRNA; #*33659), P{y[+t7.7]=CaryP}attP2* (Control line for TRiP RNAi lines; #B36303), *P{otu-GAL4::VP16.R}1; P{GAL4-nos.NGT}40; P{GAL4::VP16-nos.UTR}MVD1* (Maternal Triple Driver or "MTD-Gal4"; #31777), *P{GAL4::VP16-nos.UTR}MVD1* ("nos-Gal4"; #4937). Other stocks are: w^{1118}, *Df(1)J5/FM7c* (Salz et al., 1994), *P[Mst35Ba-EGFP]* (Manier et al., 2010), *pW8-dhd*^{WT} (Tirmarche et al., 2016). TRiP lines target all predicted isoforms of their respective target genes. "Control" in shRNA experiments refers to the offspring of the control line for TRiP lines crossed with the MTD-Gal4 line.

For the *pW8-dhd*$^{\Delta DRE}$ mutant, two fragments were amplified by PCR from w^{1118} genomic DNA using the primers ΔDRE-1-for/ ΔDRE-1-rev and ΔDRE-2-for/ ΔDRE-2-rev (Table S1). PCR products were assembled and cloned into the *pW8-dhd*^{WT} vector (Tirmarche et al., 2016) previously digested by KpnI and BamHI using the NEBuilder HiFi DNA Assembly Cloning Kit (NEB, #E5520S). *dhd*$^{\Delta DRE}$ transgene was integrated in the *PBac{attP-3B}VK00031* platform (62E1) using PhiC31-mediated transformation (Bischof et al., 2007) and flies were generated by The Best Gene (TheBestGene.com).

Germline knock-down and fertility tests

To obtain *KD* females, virgin shRNA transgenic females were mass crossed with transgenic Gal4 males at 25°C and females of the desired genotype were recovered in the F1 progeny. All RNAi experiments were carried at 25°C. To measure fertility, virgin

females of different genotypes were mated to males in a 1:1 ratio and placed for 2 days at 25˚C. They were then transferred to a new vial and allowed to lay eggs for 24 hours. Embryos were counted and then let to develop for at least 36 hours at 25˚C. Unhatched embryos were counted to determine hatching rates.

Gene expression analysis by RT-QPCR

Total RNA was extracted from ovaries of 3-day-old females using the NucleoSpin RNA isolation kit (Macherey-Nagel), following the instructions of the manufacturer. 1µg of total RNA was reverse transcribed using the SuperScript II Reverse Trancriptase kit (Invitrogen) with oligo (dT) primers. RT-qPCR reactions were performed in duplicates as described previously (Torres-Campana et al., 2020). Primer sets used are provided in Table S1. Statistical tests were performed using GraphPad Prism version 9.2.0 for Mac OS (GraphPad Software).

Immunofluorescence and imaging

Early (0–30 min) embryos laid by females of the indicated genotypes were collected on agar plates. Embryos were dechorionated in bleach, fixed in a 1:1 heptane:methanol mixture and stored at -20˚C. Embryos were washed three times (10 min each) with PBS 0.1%, Triton X-100 (PBS-T) and then incubated with primary antibodies in the same buffer on a wheel overnight at 4˚C. They were then washed three times (20 min each) with PBS-T. Incubations with secondary antibodies were performed identically. Embryos were mounted in DAKO mounting medium containing DAPI.

Ovaries were dissected in PBS-T and fixed at room temperature in 4% formaldehyde in PBS for 25 minutes. Immunofluorescence was performed as for embryos. Ovaries were then mounted as described above.

Antibodies used are provided in Table S2. Images were acquired on an LSM 800 confocal microscope (Carl Zeiss). Images were processed with Zen imaging software (Carl Zeiss) and ImageJ software.

Western blotting

Ovaries from 30 females were collected and homogenized in lysis buffer (20mM Hepes pH7.9, 100mM KCl, 0.1mM EDTA, 0.1mM EGTA, 5% Glycerol, 0.05% Igepal and protease inhibitors (Roche)). Protein extracts were cleared by centrifugation and purified with Pierce GST Spin Purification Kit (ThermoFisher Scientific, #16106). Western analysis was performed using standard procedures and used antibodies and concentrations are presented in Table S2.

Ovarian RNA sequencing and analysis

Samples were processed as previously described (Torres-Campana et al., 2020).

Sequencing was completed on two biological replicates of the following genotypes:

mod(mdg4) KD (*MTD-Gal4>shRNA mod(mdg4)*), i.e

P{w[+mC] = otu-GAL4::VP16.R}1, w[*]/y[1] sc[*] v[1]; P{w[+mC] = GAL4-nos.NGT}40/+;

P{w[+mC] = GAL4::VP16-nos.UTR}CG6325[MVD1]/P{y[+t7.7] v[+t1.8] = TRiP.

HMS00849} attP2

Snr1 KD (*MTD-Gal4>shRNA Snr1*), i.e

P{w[+mC] = otu-GAL4::VP16.R}1, w[*]/y[1] sc[*] v[1];P{w[+mC] = GAL4-nos.NGT}40/+;

P{w [+mC] = GAL4::VP16-nos.UTR}CG6325[MVD1]/P{y[+t7.7] v[+t1.8] = TRiP. HMS00363}attP2

Chromatin profiling by CUT&RUN

Cut&Run in *Drosophila* tissues was previously described [37]. Briefly, ovaries from 3-day-old flies were dissected in Wash+ Buffer (20 mM HEPES pH 7.5, 150 mM NaCl, 0.9 mM spermidine, 0.1% BSA with cOmplete protease inhibitor, Roche) and were bound to BioMag Plus Concanavalin-A-conjugated magnetic beads (ConA beads, Polysciences, Inc). Tissues were then permeabilized for 10min in dbe+ Buffer (20 mM HEPES pH 7.5, 150 mM NaCl, 0.9 mM spermidine, 2 mM EDTA, 0.1% BSA, 0.05% digitonin and protease inhibitors). Samples were then incubated with gentle rocking overnight at 4°C with primary antibody solution in dbe+ buffer (see Table S2 for antibody concentrations). Protein A fused to micrococcal nuclease (p-AMNase) was added in dbe+ buffer and samples were incubated with rotation at room temperature for 1 hour. Cleavage was done in WashCa+ buffer (20 mM HEPES pH 7.5, 150 mM NaCl, 0.9 mM spermidine, 0.1% BSA, 2 mM CaCl2 with and protease inhibitors) at 0˚ for 30 minutes. Digestion was stopped with addition of 2XSTOP Buffer (200mM NaCl, 20mM EDTA, 4mM EGTA, 62.5µg/mL RNaseA). Samples were incubated at 37°C for 30 min to digest RNA and release DNA fragments. Cleaved DNA was then recovered with Ampure XP beads (Beckman Coulter) immediately after protease treatment. Antibodies used for CUT&RUN are listed in Table S2. Retrieved DNA was used either for qPCR or for library preparation followed by deep sequencing. Sequencing libraries for each sample were synthesized using Diagenode MicroPlex Library Preparation kit according to supplier recommendations (version 2.02.15) and were sequenced on Illumina Hiseq 4000

sequencer as Paired-End 100 base reads following Illumina's instructions (GenomEast platform, IGBM, Strasbourg, France). Image analysis and base calling were performed using RTA 2.7.7 and bcl2fastq 2.17.1.14. Adapter dimer reads were removed using DimerRemover.

Cut&Rut-qPCR

0,1 ng of retrieved DNA in Cut&Run were used as template in a real time quantitative PCR assay using SYBR Premix Ex Taq II (Tli RNaseH Plus) (Takara). All qPCR reactions were performed in duplicates using Bio-Rad CFX-96 Connect system with the following conditions: 95˚C for 30s followed by 40 cycles of denaturation at 95˚C for 5s and annealing and extension at 59˚C for 30s. As a normalization control, we processed ovary samples from each studied genotype as for Cut&Run, except the antibody and pA-MNase incubation steps were omitted and instead we incubated tissue with 10U of Micrococcal Nuclease for 30min at 37°C (ThermoFisher Scientific, #88216). Fold change in histone mark enrichment was determined relative to this whole MNase control and relative to the *Sas10* gene, which was depleted in the histone marks tested in this study. Primer sets used are provided in Table S1.

Sequencing data processing

Paired-end reads were mapped to the release 6 of the *D. melanogaster* genome using Bowtie2 (v. 2.4.2). To compare samples with identical readcount for genome coverage quantifications, we employed Downsample SAM/BAM (Galaxy Version 2.18.2.1). To obtain short fragment datasets for DNA regulatory element identification, peak calling and visualization, we selected fragments shorter than 120 bp from SAM files. These

were typically a small minority of all fragments, as our Cut&Run datasets were largely dominated by nucleosome-sized fragments (150-250bp). We therefore could separately analyze modification-bearing nucleosome coverage (for which the complete Cut&Run dataset, "All fragments", was a good approximation) or putative regulatory element coverage (<120bp fragments). For genomic track visualization, we used bamCoverage from deepTools 2.0 (Galaxy Version 3.3.2.0.0) to calculate read coverage per 25bp bin for all fragments or 10bp bin for short fragments, with paired-end extension. Peak calling was done on sorted short fragments (<120 bp) with MACS2 (v. 2.1.1.20160309) with the following parameters: –nomodel, –p-value =0.0001, –keep-dup=all and the rest by default. To establish a high-confidence short fragment peak list we retained peaks that were present in biological replicates from the control genotype. Genome browser views screenshots were produced with the IGV software, for Cut&Run we used a 25bp bin for all fragments and a 10bp bin for short fragments (<120bp). For the midpoint-plot of fragment sizes around short fragment peaks, the length of each fragment was plotted as a function of the distance from the fragment midpoint to the summit of the peak identified by MACS2. For signal quantification at the *dhd* locus , normalized read counts were counted within the domain (Coordinates [5,312,054-5,317,465]) or within border element peaks (5' element: [5,312,120-5,312,211], *3'* element: [5,317,300-5,317,447])

Heatmaps were generated with RStudio (RStudio Team (2016). RStudio: Integrated Development for R. RStudio, Inc., Boston, MA URL) and the packages 'gplots' (v.3.1.1) and 'plyr' (Wickham, 2011).

Data Availability:

Original sequencing data from this publication have been deposited to the Gene Expression Omnibus with identifiers GSE174263 (RNA-seq) and GSE174250 (Cut&Run).

Additional sequencing data used in this study are available from GEO under the following accession numbers: GSE151981 (ATAC-seq), GSE37444 and GSE146993 (H3K27me3 ChIP-seq), GSE99027 (H3K9me3 ChIP-seq), GSE36393 (Mod(mdg4) ChIP-seq), GSE62904 (CP190, Beaf-32 and Dref ChIP-seq) and GSE24521 (Polycomb and Polyohomeotic ChIP-seq).

Motif scanning

Motif scanning on the *pW8-dhd^{WT}* transgene sequence was done with FIMO (v. 5.3.3) [69] using the flyreg v.2 motif database with default parameters.

Figure Legends

Figure 1. Mod(mdg4) and Snr1 are required for *dhd* expression.

A—Maternal Mod(mdg4) and Snr1 are required for protamine removal and sperm nuclear decompaction at fertilization. Top: Confocal images of pronuclear apposition in eggs from Control (*MTD>+*), *dhd^{J5}*, *mod(mdg4)* KD or *Snr1* KD females mated with transgenic *ProtA::GFP* males. The sperm nucleus in *dhd^{J5}*, *mod(mdg4)* KD and *Snr1* KD eggs retains ProtA::GFP (green) and has a needle-shape morphology. Bottom: zoom on the sperm nucleus. Scale bars: 5µm.

B— *dhd* is strongly downregulated in *mod(mdg4)* KD and *Snr1* KD ovaries. RNA-seq normalized reads per gene (in RPKM) are shown for *mod(mdg4)* KD vs Control (top) and *Snr1* KD vs Control (bottom). Genes downregulated (green) or upregulated (red) in KD ovaries are highlighted.

C— Genome Browser view of Control, *dhd^{J5}*, *lid* KD, *Sin3a* KD, *mod(mdg4)* KD and *Snr1* KD ovarian RNA-seq signal at the *dhd* region showing dramatic downregulation in all KD conditions. Note that the Control track is represented at two different scales to fit

the high read count for *dhd* (top track) or the low read count for its neighboring genes (bottom track).

D— The DHD protein is undetectable in KD ovaries. Western blot analysis using an anti-DHD antibody on ovary extracts of the indicated genotypes. Alpha-tubulin is used as a loading control.

Figure 2. A single Cut&Run experiment maps both histone modifications and their associated regulatory elements.

A— Schematic overview of the Cut&Run procedure for dissected *Drosophila* ovaries. After tissue permeabilization and antibody targeting, ProteinA-MNase cleaves nearby exposed DNA allowing the solubilization and retrieval of both nucleosomal particles carrying the targeted histone modification and DNA particles occupied by transcription factors in the immediate vicinity.

B—Cut&Run reveals nucleosomes and transcription factor binding sites. Mid-point plot of ovarian H3K27me3 Cut&Run data centered at peaks identified by MACS2 from short fragments (<120bp) in the same experiment. This plot represents all paired-end sequenced fragments as their middle point coordinate in the X-axis, and their size in the Y-axis, revealing a class of clustered short fragments (50-130bp) flanked by nucleosome-sized fragments (>140bp).

C— H3K27me3 Cut&Run at the bithorax complex (BX-C) in *Drosophila* ovaries reveals its regulatory architecture. Genome browser track displaying all Cut&Run fragments and <120 bp fragments separately. Multiple well-described Polycomb Response Elements (PRE) and insulators within the Bithorax complex detected as short fragment peaks are indicated (arrows).

D— Cut&Run re-discovers regulatory elements associated with H3K27me3 genome-wide. Upper panels: short fragment peaks read density heatmaps of ovarian H3K27me3 Cut&Run (all fragments and <120bp fragments), ATAC-seq (from S2 cells, [35]), CP190 ChIP-seq (from Kc cells, [38]) and Polycomb ChIP-seq (Pc, from S2 cells, [37]) plotted at ±1kb around peak summit. Data is sorted by the ratio of H3K27me3 Cut&Run total reads at the 3' versus 5' flanks to reveal short fragment peaks at the borders or within H3K27me3 domains (dashed lines). Lower panels: average profiles corresponding to the top heatmaps, distinguishing 5' border peaks, 3' border peaks and peaks embedded within domains. Cut&Run short fragment peaks are enriched for ATAC-seq signal as well as CP190 (particularly at border peaks) and Polycomb (particularly at middle peaks).

Figure 3. *dhd* is embedded in an H3K27me3/H3K9me3 mini-domain flanked by regulatory elements.

A— The *dhd* region features an H3K27me3 and H3K9me3 mini-domain. Genome browser snapshots showing the distribution of all fragments and <120 bp fragments in the *dhd* region, revealing that *dhd* lies within a ~5450bp heterochromatin mini-domain

flanked by border regulatory elements associated with both H3K27me3 and H3K9me3. Arrows indicate direction of transcription.

B-The *dhd* mini-domain is highly enriched in H3K27me3 relative to its size. Scatter plot of our 278 ovarian H3K27me3 domains identified in Cut&Run, representing their average read counts normalized to domain size in the Y-axis versus domain size in the X-axis. C– Effect of the KDs on H3K27me3 enrichment genome-wide. Average normalized counts of H3K27me3 Cut&Run (all fragments) in H3K27me3 domains (plotted as meta-domains and including ±3kb from domain borders) in Control (*MTD>+*), *lid* KD, *Sin3a* KD, *mod(mdg4)* KD, *Snr1* KD and *E(z)* KD (arrows).

D– *lid* KD, but not *Sin3a*, *Snr1* or *mod(mdg4)*, impacts H3K27me3 enrichment at the *dhd* mini-domain. Left: genome browser plots of normalized H3K27me3 Cut&Run signal (all fragments) at the *dhd* genomic region in Control and KD ovaries. Right: Quantification of normalized read counts for the same samples. Data in this figure is for one representative replicate: other replicates are shown in FigS5-A.

E- Weak impact of KDs on heterochromatic marks at *dhd*. H3K27me3 and H3K9me3 Cut&Run-qPCR in Control and KD ovaries using the *Sas10* gene as negative control and *Ubx* and *CG12239* as positive controls for H3K27me3 and H3K9me3 respectively. Fold enrichment was calculated relative to *Sas10.* Error bars show technical variability from a representative replicate. Data in this figure is for one representative replicate: other replicates are shown in FigS5-B. P values indicate one-way ANOVA with Dunnett's multiple comparisons test to a control (* $P < 0.0001$; n.s = not significant).

Figure 4. Sin3A, Snr1 and Mod(mdg4) control the regulatory architecture of the *dhd* H3K27me3 mini-domain

A– *Sin3a* and *Snr1* KD, but not *lid* or *mod(mdg4)*, impact H3K27me3-associated regulatory elements genome-wide. Left: H3K27me3 Cut&Run <120 bp fragments normalized counts in Control and KD ovaries, plotted at ±1kb around the summit of short fragment peaks. Right: Heatmaps displaying H3K27me3 Cut&Run short fragment peaks normalized read counts ±1kb around peak center in Control and KD ovaries.

B- Sin3A, Snr1 and Mod(mdg4), but not Lid, impact the organization of regulatory elements at the borders of the *dhd* H3K27me3 mini-domain. Left: genome browser plots of normalized Control H3K27me3 Cut&Run signal (all fragments, top) and of normalized signal from <120bp fragments retrieved in H3K27me3 Cut&Run in Control and KD ovaries. Right: Quantification of <120bp fragments normalized read counts for the same samples. 5' and 3' border elements are plotted separately. Data in this figure is for one representative replicate: other replicates are shown in FigS4-C.

C- Table recapitulating the effect of the different KDs on H3K27me3 and H3K27me3-associated regulatory elements (H3K27me3-RE) genome-wide and at the *dhd* locus. "≈" indicates modest or no change, "↗" indicates an increase and "↘" a decrease in average read counts compared to Control. "?" indicates inability to conclude.

Figure 5. The *dhd* promoter-proximal DRE motifs are required for its expression.

A– Schematic representation of the genotypes studied in this figure. Upper panels: genomic browser views recapitulating the Control distribution of H3K27me3 Cut&Run signal (all fragments and <120bp fragments) as well as RNA-seq signal from Figures 1 and 2 at the *dhd* locus and showing lack of signal at the transgene insertion locus in the absence of any transgenic construct. Middle panel: schematic representation of the genomic composition of w^{1118} (reference strain), mutant and rescue flies, indicating the status of the *dhd* locus and the composition of the rescue transgene. Dashed lines indicate the targeted region by primer couples (primers R and 1-5) used for RT- and Cut&Run-qPCR in panels B and D. Bottom panel: sequence of the *dhd* promoter at the endogenous location (left) and in the ΔDRE mutant transgene where the 14bp containing the DRE motifs were deleted.

B- The DRE motifs at the *dhd* promoter are necessary for its expression. RT-qPCR quantification of *dhd* mRNA levels in ovaries from wild-type w^{1118} flies, dhd^{J5} mutants or dhd^{J5} mutants carrying either a WT ($pW8\text{-}dhd^{WT}$) or a mutant ($pW8\text{-}dhd^{\Delta DRE}$) or a full domain ($pW8\text{-}dhd^{FD}$) transgene (measured using the R primers, normalized to *rp49* and relative to expression in w^{1118}). Data from biological duplicates analyzed in technical duplicates are presented as mean ± SEM. P values indicate one-way ANOVA with Tukey's multiple comparisons test (* $P < 0.0001$; n.s = not significant).

C- The *dhd* heterochromatin domain is affected in *dhd*-containing transgenic constructs. Genome browser plots of normalized ovarian H3K27me3 and H3K9me3 Cut&Run signal at the *dhd* genomic region in the indicated genotypes. The H3K27me3 domain is abolished in all transgenic rescues. The H3K9me3 domain is partly affected in the dhd^{J5} mutant, being lost the *dhd*-proximal end but maintained in the *dhd*-distal end. Dashed lines and numbers (1 to 5) indicate the targeted region by primer couples used for qPCR in panel D.

D- A transgene containing the full *dhd* domain does not restore heterochromatin marks. H3K27me3 and H3K9me3 Cut&Run-qPCR in Control, dhd^{J5}, $dhd^{J5};;pW8\text{-}dhd^{WT}$ *and* $dhd^{J5};;pW8\text{-}dhd^{FD}$ ovaries. Fold enrichment was calculated relative to *Sas10.* Error bars show technical variability from a representative replicate. Data in this figure is for one representative replicate: other replicates are shown in FigS7.

Figure 6. Lid, Sin3A, Mod(mdg4) and Snr1 are necessary for *dhd* expression in the absence of its heterochromatin domain.

A–Schematic representation of the genomic composition of w^{1118} (reference strain) and mutant flies carrying a rescue transgene and shRNA constructs controlled by the female germline specific nanos-Gal4 driver, respectively inserted at the platforms *attP 3B-62E1* and *attP 2- 68A4*.

B-The rescue transgene does not restore *dhd* expression in KD ovaries. RT-qPCR quantification of *dhd* mRNA levels in ovaries of the indicated genotypes (normalized to *rp49* and relative to expression in w^{1118} ovaries). Data from biological duplicates analyzed in technical duplicates are presented as mean ± SEM. P value indicates one-way ANOVA with Tukey's multiple comparisons test (* $P < 0.0001$),

C-H3K27me3 is absent from the *dhd* rescue transgene. H3K27me3 Cut&Run-qPCR in the indicated genotypes. The *Sas10* gene was used as negative control and *Ubx* as positive control. Fold enrichment was calculated relative to *Sas10.* Error bars show technical variability from a representative replicate. Error bars show technical variability from a representative replicate. Data in this figure is for one representative replicate: other replicates are shown in FigS8.

D- *dhd* is not ectopically expressed in adult tissues in the absence of its heterochromatin domain. RT-qPCR quantification of *dhd* mRNA levels in dissected ovaries or corresponding female carcasses as well as testes or corresponding male carcasses, in all indicated genotypes (normalized to *rp49* and relative to expression in ovaries in w^{1118}). Data from biological duplicates analyzed in technical duplicates are presented as mean ± SEM. P value indicates one-way ANOVA with Tukey's multiple comparisons test (* $P < 0.0001$).

REFERENCES

1. Bannister AJ, Kouzarides T. Regulation of chromatin by histone modifications. Cell Res. 2011;21: 381–395. doi:10.1038/cr.2011.22

2. Hammond CM, Strømme CB, Huang H, Patel DJ, Groth A. Histone chaperone networks shaping chromatin function. Nat Rev Mol Cell Biol. 2017;18: 141–158. doi:10.1038/nrm.2016.159

3. Tyagi M, Imam N, Verma K, Patel AK. Chromatin remodelers: We are the drivers!! Nucleus. 2016;7: 388–404. doi:10.1080/19491034.2016.1211217

4. Melnikova LS, Georgiev PG, Golovnin AK. The Functions and Mechanisms of Action of Insulators in the Genomes of Higher Eukaryotes. Acta Naturae. 2020;12: 15–33. doi:10.32607/actanaturae.11144

5. Torres-Campana D, Kimura S, Orsi GA, Horard B, Benoit G, Loppin B. The Lid/KDM5 histone demethylase complex activates a critical effector of the oocyte-to-zygote transition. Bosco G, editor. PLoS Genet. 2020;16: e1008543. doi:10.1371/journal.pgen.1008543

6. Spradling A. The development of Drosophila melanogaster. 1993.

7. Salz HK, Flickinger TW, Mittendorf E, Pellicena-Palle A, Petschek JP, Albrecht EB. The Drosophila maternal effect locus deadhead encodes a thioredoxin homolog required for female meiosis and early embryonic development. Genetics. 1994;136: 1075–1086. doi:10.1093/genetics/136.3.1075

8. Svensson MJ, Chen JD, Pirrotta V, Larsson J. The ThioredoxinT and deadhead gene pair encode testis- and ovary-specific thioredoxins in Drosophila melanogaster. Chromosoma. 2003;112: 133–143. doi:10.1007/s00412-003-0253-5

9. Tirmarche S, Kimura S, Dubruille R, Horard B, Loppin B. Unlocking sperm chromatin at fertilization requires a dedicated egg thioredoxin in Drosophila. Nat Commun. 2016;7: 13539. doi:10.1038/ncomms13539

10. Petrova B, Liu K, Tian C, Kitaoka M, Freinkman E, Yang J, et al. Dynamic redox balance directs the oocyte-to-embryo transition via developmentally controlled reactive cysteine changes. Proc Natl Acad Sci USA. 2018;115: E7978–E7986. doi:10.1073/pnas.1807918115

11. Freier R, Aragón E, Bagiński B, Pluta R, Martin-Malpartida P, Ruiz L, et al. Structures of the germline-specific Deadhead and thioredoxin T proteins from *Drosophila melanogaster* reveal unique features among thioredoxins. IUCrJ. 2021;8: 281–294. doi:10.1107/S2052252521000221

12. Emelyanov AV, Fyodorov DV. Thioredoxin-dependent disulfide bond reduction is required for protamine eviction from sperm chromatin. Genes Dev. 2016;30: 2651–2656. doi:10.1101/gad.290916.116

13. Dingwall AK, Beek SJ, McCallum CM, Tamkun JW, Kalpana GV, Goff SP, et al. The Drosophila snr1 and brm proteins are related to yeast SWI/SNF proteins and are components of a large protein complex. MBoC. 1995;6: 777–791. doi:10.1091/mbc.6.7.777

14. Gerasimova TI, Gdula DA, Gerasimov DV, Simonova O, Corces VG. A drosophila protein that imparts directionality on a chromatin insulator is an enhancer of position-effect variegation. Cell. 1995;82: 587–597. doi:10.1016/0092-8674(95)90031-4

15. Skene PJ, Henikoff S. An efficient targeted nuclease strategy for high-resolution mapping of DNA binding sites. eLife. 2017;6: e21856. doi:10.7554/eLife.21856

16. Hirose F, Yamaguchi M, Handa H, Inomata Y, Matsukage A. Novel 8-base pair sequence (Drosophila DNA replication-related element) and specific binding factor involved in the expression of Drosophila genes for DNA polymerase alpha and proliferating cell nuclear antigen. J Biol Chem. 1993;268: 2092–2099.

17. Spain MM, Caruso JA, Swaminathan A, Pile LA. Drosophila SIN3 isoforms interact with distinct proteins and have unique biological functions. J Biol Chem. 2010;285: 27457–27467. doi:10.1074/jbc.M110.130245

18. Das TK, Sangodkar J, Negre N, Narla G, Cagan RL. Sin3a acts through a multi-gene module to regulate invasion in Drosophila and human tumors. Oncogene. 2013;32: 3184–3197. doi:10.1038/onc.2012.326

19. Gajan A, Barnes VL, Liu M, Saha N, Pile LA. The histone demethylase dKDM5/LID interacts with the SIN3 histone deacetylase complex and shares functional

similarities with SIN3. Epigenetics & Chromatin. 2016;9: 4. doi:10.1186/s13072-016-0053-9

20. Moshkin YM, Kan TW, Goodfellow H, Bezstarosti K, Maeda RK, Pilyugin M, et al. Histone Chaperones ASF1 and NAP1 Differentially Modulate Removal of Active Histone Marks by LID-RPD3 Complexes during NOTCH Silencing. Molecular Cell. 2009;35: 782–793. doi:10.1016/j.molcel.2009.07.020

21. Ni J-Q, Zhou R, Czech B, Liu L-P, Holderbaum L, Yang-Zhou D, et al. A genome-scale shRNA resource for transgenic RNAi in Drosophila. Nat Methods. 2011;8: 405–407. doi:10.1038/nmeth.1592

22. Zraly CB, Marenda DR, Nanchal R, Cavalli G, Muchardt C, Dingwall AK. SNR1 is an essential subunit in a subset of Drosophila brm complexes, targeting specific functions during development. Dev Biol. 2003;253: 291–308. doi:10.1016/s0012-1606(02)00011-8

23. Dorn R, Reuter G, Loewendorf A. Transgene analysis proves mRNA trans-splicing at the complex mod(mdg4) locus in Drosophila. Proc Natl Acad Sci U S A. 2001;98: 9724–9729. doi:10.1073/pnas.151268698

24. Van Bortle K, Ramos E, Takenaka N, Yang J, Wahi JE, Corces VG. Drosophila CTCF tandemly aligns with other insulator proteins at the borders of H3K27me3 domains. Genome Res. 2012;22: 2176–2187. doi:10.1101/gr.136788.111

25. Büchner K, Roth P, Schotta G, Krauss V, Saumweber H, Reuter G, et al. Genetic and Molecular Complexity of the Position Effect Variegation Modifier *mod(mdg4)* in Drosophila. Genetics. 2000;155: 141–157. doi:10.1093/genetics/155.1.141

26. Savitsky M, Kim M, Kravchuk O, Schwartz YB. Distinct Roles of Chromatin Insulator Proteins in Control of the *Drosophila* Bithorax Complex. Genetics. 2016;202: 601–617. doi:10.1534/genetics.115.179309

27. Manier MK, Belote JM, Berben KS, Novikov D, Stuart WT, Pitnick S. Resolving mechanisms of competitive fertilization success in Drosophila melanogaster. Science. 2010;328: 354–357. doi:10.1126/science.1187096

28. Henikoff JG, Belsky JA, Krassovsky K, MacAlpine DM, Henikoff S. Epigenome characterization at single base-pair resolution. Proceedings of the National Academy of Sciences. 2011;108: 18318–18323. doi:10.1073/pnas.1110731108

29. Kasinathan S, Orsi GA, Zentner GE, Ahmad K, Henikoff S. High-resolution mapping of transcription factor binding sites on native chromatin. Nat Methods. 2014;11: 203–209. doi:10.1038/nmeth.2766

30. Orsi GA, Kasinathan S, Hughes KT, Saminadin-Peter S, Henikoff S, Ahmad K. High-resolution mapping defines the cooperative architecture of Polycomb response elements. Genome Research. 2014;24: 809–820. doi:10.1101/gr.163642.113

31. Ramachandran S, Ahmad K, Henikoff S. Transcription and Remodeling Produce Asymmetrically Unwrapped Nucleosomal Intermediates. Molecular Cell. 2017;68: 1038-1053.e4. doi:10.1016/j.molcel.2017.11.015

32. Cleard F, Wolle D, Taverner AM, Aoki T, Deshpande G, Andolfatto P, et al. Different Evolutionary Strategies To Conserve Chromatin Boundary Function in the Bithorax Complex. Genetics. 2017;205: 589–603. doi:10.1534/genetics.116.195586

33. Kyrchanova O, Mogila V, Wolle D, Deshpande G, Parshikov A, Cléard F, et al. Functional Dissection of the Blocking and Bypass Activities of the Fab-8 Boundary in the Drosophila Bithorax Complex. Sánchez-Herrero E, editor. PLoS Genet. 2016;12: e1006188. doi:10.1371/journal.pgen.1006188

34. Ahmad K, Spens AE. Separate Polycomb Response Elements control chromatin state and activation of the vestigial gene. Cavalli G, editor. PLoS Genet. 2019;15: e1007877. doi:10.1371/journal.pgen.1007877

35. Jain SU, Rashoff AQ, Krabbenhoft SD, Hoelper D, Do TJ, Gibson TJ, et al. H3 K27M and EZHIP Impede H3K27-Methylation Spreading by Inhibiting Allosterically Stimulated PRC2. Mol Cell. 2020;80: 726-735.e7. doi:10.1016/j.molcel.2020.09.028

36. Minoux M, Holwerda S, Vitobello A, Kitazawa T, Kohler H, Stadler MB, et al. Gene bivalency at Polycomb domains regulates cranial neural crest positional identity. Science. 2017;355: eaal2913. doi:10.1126/science.aal2913

37. Enderle D, Beisel C, Stadler MB, Gerstung M, Athri P, Paro R. Polycomb preferentially targets stalled promoters of coding and noncoding transcripts. Genome Res. 2011;21: 216–226. doi:10.1101/gr.114348.110

38. Li L, Lyu X, Hou C, Takenaka N, Nguyen HQ, Ong C-T, et al. Widespread Rearrangement of 3D Chromatin Organization Underlies Polycomb-Mediated Stress-Induced Silencing. Molecular Cell. 2015;58: 216–231. doi:10.1016/j.molcel.2015.02.023

39. Bartkuhn M, Straub T, Herold M, Herrmann M, Rathke C, Saumweber H, et al. Active promoters and insulators are marked by the centrosomal protein 190. EMBO J. 2009;28: 877–888. doi:10.1038/emboj.2009.34

40. Colmenares SU, Swenson JM, Langley SA, Kennedy C, Costes SV, Karpen GH. Drosophila Histone Demethylase KDM4A Has Enzymatic and Non-enzymatic Roles in Controlling Heterochromatin Integrity. Developmental Cell. 2017;42: 156-169.e5. doi:10.1016/j.devcel.2017.06.014

41. Kassis JA, Kennison JA, Tamkun JW. Polycomb and Trithorax Group Genes in *Drosophila*. Genetics. 2017;206: 1699–1725. doi:10.1534/genetics.115.185116

42. Schuettengruber B, Bourbon H-M, Di Croce L, Cavalli G. Genome Regulation by Polycomb and Trithorax: 70 Years and Counting. Cell. 2017;171: 34–57. doi:10.1016/j.cell.2017.08.002

43. Brower-Toland B, Riddle NC, Jiang H, Huisinga KL, Elgin SCR. Multiple SET methyltransferases are required to maintain normal heterochromatin domains in the genome of Drosophila melanogaster. Genetics. 2009;181: 1303–1319. doi:10.1534/genetics.108.100271

44. Ninova M, Fejes Tóth K, Aravin AA. The control of gene expression and cell identity by H3K9 trimethylation. Development. 2019;146: dev181180. doi:10.1242/dev.181180

45. Smolko AE, Shapiro-Kulnane L, Salz HK. The H3K9 methyltransferase SETDB1 maintains female identity in Drosophila germ cells. Nat Commun. 2018;9: 4155. doi:10.1038/s41467-018-06697-x

46. Kadoch C, Williams RT, Calarco JP, Miller EL, Weber CM, Braun SMG, et al. Dynamics of BAF–Polycomb complex opposition on heterochromatin in normal and oncogenic states. Nat Genet. 2017;49: 213–222. doi:10.1038/ng.3734

47. De S, Gehred ND, Fujioka M, Chan FW, Jaynes JB, Kassis JA. Defining the Boundaries of Polycomb Domains in *Drosophila*. Genetics. 2020;216: 689–700. doi:10.1534/genetics.120.303642

48. Iovino N, Ciabrelli F, Cavalli G. PRC2 controls Drosophila oocyte cell fate by repressing cell cycle genes. Dev Cell. 2013;26: 431–439. doi:10.1016/j.devcel.2013.06.021

49. Phillips MD, Shearn A. Mutations in polycombeotic, a Drosophila polycomb-group gene, cause a wide range of maternal and zygotic phenotypes. Genetics. 1990;125: 91–101.

50. DeLuca SZ, Ghildiyal M, Pang L-Y, Spradling AC. Differentiating Drosophila female germ cells initiate Polycomb silencing by regulating PRC2-interacting proteins. eLife. 2020;9: e56922. doi:10.7554/eLife.56922

51. Bergman CM, Carlson JW, Celniker SE. Drosophila DNase I footprint database: a systematic genome annotation of transcription factor binding sites in the fruitfly, Drosophila melanogaster. Bioinformatics. 2005;21: 1747–1749. doi:10.1093/bioinformatics/bti173

52. Daniel Avery Pollard. Drosophila Sequence Specific Transcription Factor Binding Site Matrices. Available: http://www.danielpollard.com/matrices.html

53. Zhao K, Hart CM, Laemmli UK. Visualization of chromosomal domains with boundary element-associated factor BEAF-32. Cell. 1995;81: 879–889. doi:10.1016/0092-8674(95)90008-X

54. Roy S, Gilbert MK, Hart CM. Characterization of *BEAF* Mutations Isolated by Homologous Recombination in Drosophila. Genetics. 2007;176: 801–813. doi:10.1534/genetics.106.068056

55. Park J-S, Choi Y-J, Thao DTP, Kim Y-S, Yamaguchi M, Yoo M-A. DREF is involved in the steroidogenesis via regulation of shadow gene. Am J Cancer Res. 2012;2: 714–725.

56. Tian Y, Smith-Bolton RK. Regulation of growth and cell fate during tissue regeneration by the two SWI/SNF chromatin-remodeling complexes of *Drosophila*. Duronio R, editor. Genetics. 2021;217: 1–16. doi:10.1093/genetics/iyaa028

57. Liu X, Secombe J. The Histone Demethylase KDM5 Activates Gene Expression by Recognizing Chromatin Context through Its PHD Reader Motif. Cell Reports. 2015;13: 2219–2231. doi:10.1016/j.celrep.2015.11.007

58. Saha N, Liu M, Gajan A, Pile LA. Genome-wide studies reveal novel and distinct biological pathways regulated by SIN3 isoforms. BMC Genomics. 2016;17: 111. doi:10.1186/s12864-016-2428-5

59. Heurteau A, Perrois C, Depierre D, Fosseprez O, Humbert J, Schaak S, et al. Insulator-based loops mediate the spreading of H3K27me3 over distant micro-domains repressing euchromatin genes. Genome Biol. 2020;21: 193. doi:10.1186/s13059-020-02106-z

60. Gurudatta B, Yang J, Van Bortle K, Donlin-Asp P, Corces V. Dynamic changes in the genomic localization of DNA replication-related element binding factor during the cell cycle. Cell Cycle. 2013;12: 1605–1615. doi:10.4161/cc.24742

61. Bernstein BE, Mikkelsen TS, Xie X, Kamal M, Huebert DJ, Cuff J, et al. A bivalent chromatin structure marks key developmental genes in embryonic stem cells. Cell. 2006;125: 315–326. doi:10.1016/j.cell.2006.02.041

62. Akmammedov A, Geigges M, Paro R. Bivalency in Drosophila embryos is associated with strong inducibility of Polycomb target genes. Fly (Austin). 2019;13: 42–50. doi:10.1080/19336934.2019.1619438

63. Schertel C, Albarca M, Rockel-Bauer C, Kelley NW, Bischof J, Hens K, et al. A large-scale, in vivo transcription factor screen defines bivalent chromatin as a key property of regulatory factors mediating Drosophila wing development. Genome Res. 2015;25: 514–523. doi:10.1101/gr.181305.114

64. De S, Mitra A, Cheng Y, Pfeifer K, Kassis JA. Formation of a Polycomb-Domain in the Absence of Strong Polycomb Response Elements. Bantignies F, editor. PLoS Genet. 2016;12: e1006200. doi:10.1371/journal.pgen.1006200

65. Emberly E, Blattes R, Schuettengruber B, Hennion M, Jiang N, Hart CM, et al. BEAF Regulates Cell-Cycle Genes through the Controlled Deposition of H3K9 Methylation Marks into Its Conserved Dual-Core Binding Sites. Misteli T, editor. PLoS Biology. 2008;6: e327. doi:10.1371/journal.pbio.0060327

66. Zamurrad S, Hatch HAM, Drelon C, Belalcazar HM, Secombe J. A Drosophila Model of Intellectual Disability Caused by Mutations in the Histone Demethylase KDM5. Cell Rep. 2018;22: 2359–2369. doi:10.1016/j.celrep.2018.02.018

67. Krebs AR, Imanci D, Hoerner L, Gaidatzis D, Burger L, Schübeler D. Genome-wide Single-Molecule Footprinting Reveals High RNA Polymerase II Turnover at Paused Promoters. Molecular Cell. 2017;67: 411-422.e4. doi:10.1016/j.molcel.2017.06.027

68. Henikoff S, Henikoff JG, Kaya-Okur HS, Ahmad K. Efficient chromatin accessibility mapping *in situ* by nucleosome-tethered tagmentation. Genomics; 2020 Apr. doi:10.1101/2020.04.15.043083

69. Grant CE, Bailey TL, Noble WS. FIMO: scanning for occurrences of a given motif. Bioinformatics. 2011;27: 1017–1018. doi:10.1093/bioinformatics/btr064

Supporting Information Captions:

Figure S1. *mod(mdg4)* KD and *Snr1* KD downregulate *dhd*

A-*mod(mdg4)* KD and *Snr1* KD are efficient in the female germline. Left: RT-qPCR quantification of *mod(mdg4)* (top) or *Snr1* (bottom) mRNA levels in Control and KD ovaries (normalized to *rp49* and relative to expression in Control ovaries). Data from biological duplicates analyzed in technical duplicates are presented as mean ± SEM. Right: Quantification of *mod(mdg4)* (top) and *Snr1*(bottom) counts in RNA-seq data from Fig1B. Both duplicates are shown.

B-*lid, Sin3a, Snr1 and mod(mdg4)* KDs downregulate *dhd* but do not significantly affect its neighboring genes. Quantification of counts in RNA-seq data for *dhd* and its neighboring genes in Control, *lid, Sin3a, Snr1* and *mod(mdg4)* KD show that low-expressing genes in the *dhd* region are not or only modestly impacted by the KDs. Both duplicates are shown.

C-Limited overlap in the effects of *mod(mdg4)* and *Snr1* KDs. Hierarchical clustering of sample distance heatmap of RNA-seq samples.

D-Principal component analysis for RNA-seq samples.

E- *lid, Sin3a, mod(mdg4) and Snr1* KD severely downregulate *dhd* expression. RT-qPCR quantification of *dhd* mRNA levels in ovaries of indicated genotypes (normalized to *rp49* and relative to expression in Control ovaries). Two different shRNA constructs (val21 and val22) against *lid* were tested. Data from biological duplicates analyzed in technical duplicates are presented as mean ± SEM.

Figure S2. Cut&Run is consistent with ChIP-seq data.

A—Histone modification profiles at the *dhd* region in cultured embryonic cells and ovaries. ChIP-seq data showing the active mark H3K4me3 (yellow) [5], and the repressive marks H3K9me3 (green) [40,45] and H3K27me3 (blue) (accession number GSE146993, [50]).

B—Short fragment peaks align with known regulatory elements. Genome browser views of the bithorax complex (BX-C) (left) and the *dhd* region (right). Display of H3K27me3 Cut&Run (from Control ovaries, all fragments and <120bp fragments), ATAC-seq (from S2 cells, [35]), CP190 ChIP-seq (from Kc cells, [38]), Mod(mdg4) (all isoforms) and Mod(mdg4)67.2 isoform ChIP-seq (from Kc cells, [24]) Polycomb (Pc) and Polyhomeotic (Ph) ChIP-seq (from S2 cells, [37]). Cut&Run short fragments largely overlap with peaks from the other tracks displayed.

Figure S3. Cut&Run maps H3K9me3 in ovaries.

A- Cut&Run shows the expected enrichment of H3K9me3 at pericentromeric heterochromatin. Genome browser views of H3K9me3 ChIP-seq [45] and Cut&Run signal in all chromosomes.

B- Cut&Run detects a previously identified H3K9me3 peak over a testis-specific TSS [45]. Genome browser view of *phf7* and neighboring genes. Blue arrow indicates testis-specific TSS and magenta arrow indicates ovary-specific TSS.

Figure S4. Whole-ovary experiments yield signal from both somatic follicle cells and germline cells.

A-*E(z)* KD does not severely affect *dhd* expression. RT-qPCR quantification of *dhd* mRNA levels in Control and *E(z)* KD ovaries (normalized to *rp49* and relative to expression in Control ovaries). Data from biological duplicates analyzed in technical duplicates are presented as mean ± SEM.

B- *E(z)* KD and *Snr1* KD affect H3K27me3 levels in nurse cells. Confocal images of representative egg chambers in Control, *E(z)* KD, *lid* KD, *Sin3a* KD, *mod(mdg4)* KD and *Snr1* KD. In control ovaries, H3K27me3 staining marks somatic follicle cell nuclei, the karyosome and germline nurse cell nuclei. In *E(z)* KD ovaries the karyosome and nurse cells loose staining of the histone mark but follicle cells are marked normally. No notable change is observed in *lid* KD, *Sin3a* KD or *mod(mdg4)* KD while in *Snr1* KD nurse cells staining is less intense. Scale bar 10μm.

C- Cut&Run in whole ovaries captures signal from both somatic and germline cells. Genome browser views of H3K27me3 Cut&Run signal in Control and *E(z)* KD ovaries and H3K27me3 ChIP-seq from FACS sorted nurse cells and somatic follicle cells [50]. Upper panels show representative loci enriched for the mark solely in nurse cells (germline) and absent in *E(z)* KD ovaries. Lower panels show H3K27me3 domains where the signal comes almost exclusively from follicle cells and is not significantly affected in the germline *E(z)* KD.

Figure S5. Cut&Run is reproducible among replicates.

A—H3K27me3 Cut&Run signal at the *dhd* locus from Control and KD ovaries. Left: Dotplot showing normalized read counts of H3K27me3 Cut&Run at the *dhd* domain from independent biological triplicates of the indicated genotypes (duplicates for *E(z)* KD).

B— Cut&Run qPCR yields reproducible data among replicates. Biological replicates from H3K27me3 and H3K9me3 Cut&Run-qPCR in Control and KD ovaries shown in Fig3-E. The Sas10 gene was used as negative control and Ubx and CG12239 as positive controls for H3K27me3 and H3K9me3 respectively. Fold enrichment was calculated relative to Sas10. Error bars show technical variability.

C— *Sin3a* KD, *Snr1* KD and *mod(mdg4)* KD affect the stability of the H3K27me3-associated regulatory elements at the *dhd* mini-domain. Dotplot showing normalized read counts of H3K27me3 Cut&Run <120bp fragments at *dhd* regulatory elements from independent biological triplicates of the indicated genotypes (duplicates for *E(z)* KD). 5' and 3' border elements are plotted separately.

Figure S6. Dref and Beaf-32 are found at *dhd* regulatory elements.

Genome browser views of ovarian H3K27me3 Cut&Run (all fragments and <120bp fragments) and Dref and Beaf-32 ChIP-seq (from Kc cells, [38]). <120 bp fragment peaks at the *dhd* domain borders align with DREF and Beaf-32 peaks.

Figure S7. Cut&Run qPCR generates reproducible data from transgenes

Biological replicates of H3K27me3 and H3K9me3 Cut&Run-qPCR in Control, dhd^{J5}, dhd^{J5};;$pW8\text{-}dhd^{WT}$ and dhd^{J5};;$pW8\text{-}dhd^{FD}$ ovaries shown in Fig5-D. Fold enrichment was calculated relative to Sas10. Error bars show technical variability.

Figure S8. In *lid* KD, *Sin3a* KD, *mod(mdg4)* KD and *Snr1* KD rescue flies, H3K27me3 is absent from the *dhd* rescue transgene

A— *lid* KD, *Sin3a* KD, *mod(mdg4)* KD and *Snr1* KD are efficient in the female germline of rescue flies. From left to right: RT-qPCR quantification of *lid*, *Sin3a*, *mod(mdg4)* and *Snr1* mRNA levels in ovaries of the indicated genotypes (normalized to *rp49* and relative to expression in w^{1118} ovaries). Data from biological duplicates analyzed in technical duplicates are presented as mean ± SEM.

B— The *dhd* rescue transgene does not restore H3K27me3 in KD flies. Biological replicates of H3K27me3 Cut&Run-qPCR in the indicated genotypes shown in Fig6-C. The *Sas10* gene was used as negative control and Ubx as positive control. Fold enrichment was calculated relative to *Sas10*. Error bars show technical variability.

Table S1. List of primers used in this paper.

Table S2. List of antibodies used in this paper.

Figure 1

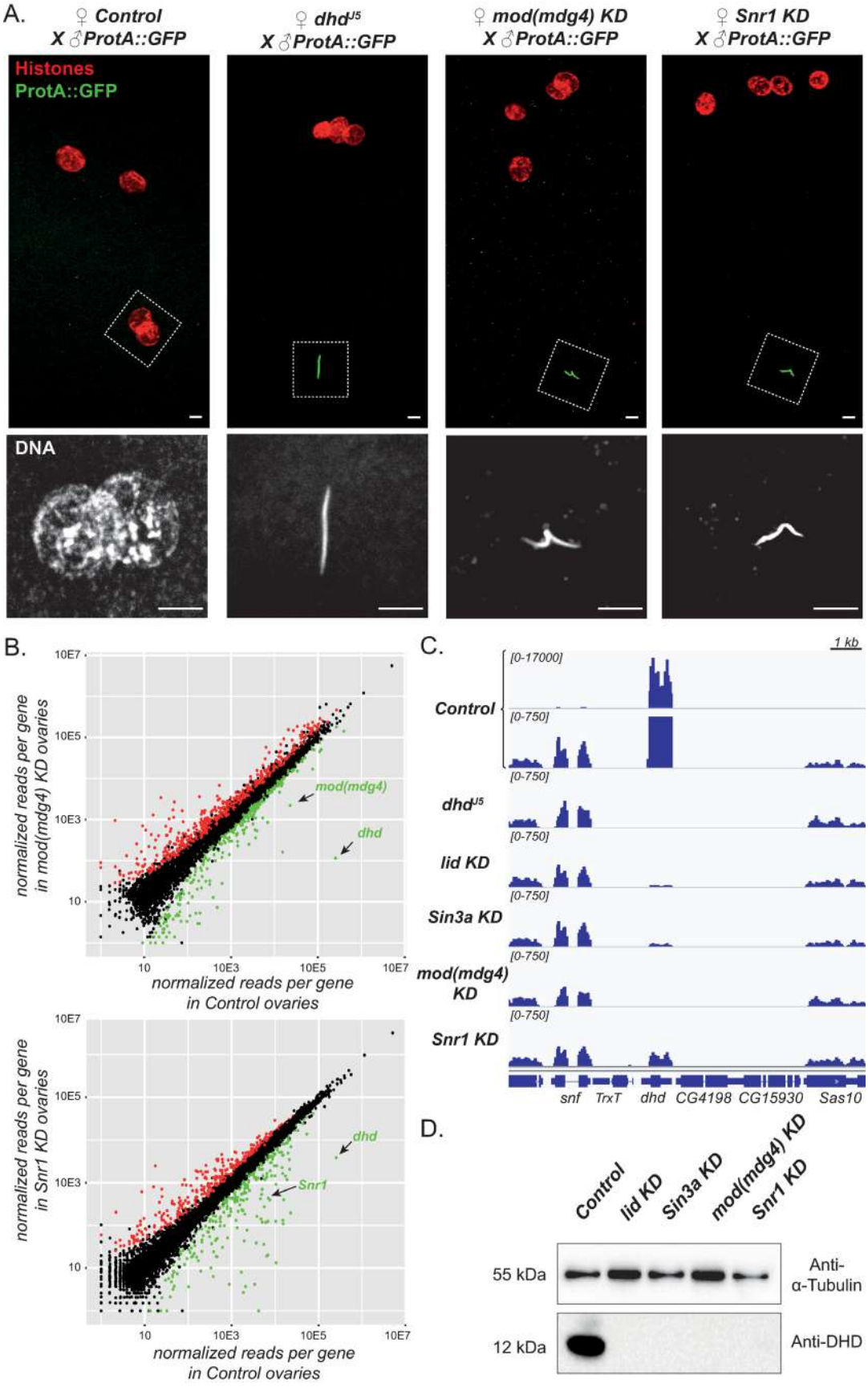
A.
♀ Control X ♂ProtA::GFP
♀ dhd^J5 X ♂ProtA::GFP
♀ mod(mdg4) KD X ♂ProtA::GFP
♀ Snr1 KD X ♂ProtA::GFP
Histones
ProtA::GFP
DNA
B.
normalized reads per gene in mod(mdg4) KD ovaries
normalized reads per gene in Control ovaries
mod(mdg4)
dhd
normalized reads per gene in Snr1 KD ovaries
normalized reads per gene in Control ovaries
dhd
Snr1
10E7
10E5
10E3
10
C.
1 kb
Control
dhd^J5
lid KD
Sin3a KD
mod(mdg4) KD
Snr1 KD
[0-17000]
[0-750]
snf
TrxT
dhd
CG4198
CG15930
Sas10
D.
Control
lid KD
Sin3a KD
mod(mdg4) KD
Snr1 KD
55 kDa
Anti-α-Tubulin
12 kDa
Anti-DHD

Figure 2

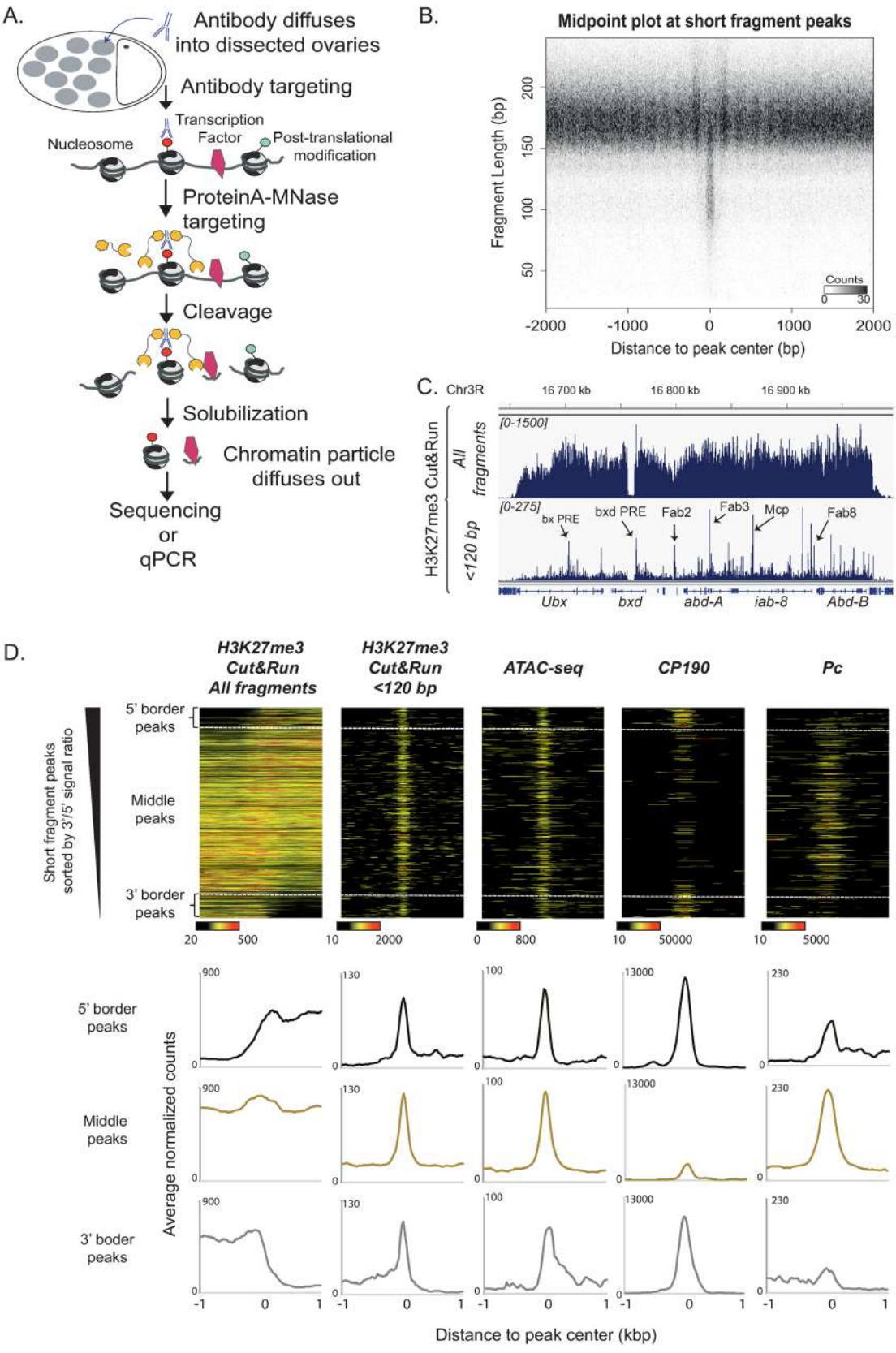
A.
Antibody diffuses into dissected ovaries
Antibody targeting
Transcription Factor
Post-translational modification
Nucleosome
ProteinA-MNase targeting
Cleavage
Solubilization
Chromatin particle diffuses out
Sequencing or qPCR
B.
Midpoint plot at short fragment peaks
Fragment Length (bp)
Counts
Distance to peak center (bp)
C.
Chr3R
16 700 kb
16 800 kb
16 900 kb
H3K27me3 Cut&Run
All fragments
<120 bp
[0-1500]
[0-275]
bx PRE
bxd PRE
Fab2
Fab3
Mcp
Fab8
Ubx
bxd
abd-A
iab-8
Abd-B
D.
H3K27me3 Cut&Run All fragments
H3K27me3 Cut&Run <120 bp
ATAC-seq
CP190
Pc
Short fragment peaks sorted by 3'/5' signal ratio
5' border peaks
Middle peaks
3' border peaks
Average normalized counts
Distance to peak center (kbp)

Figure 3

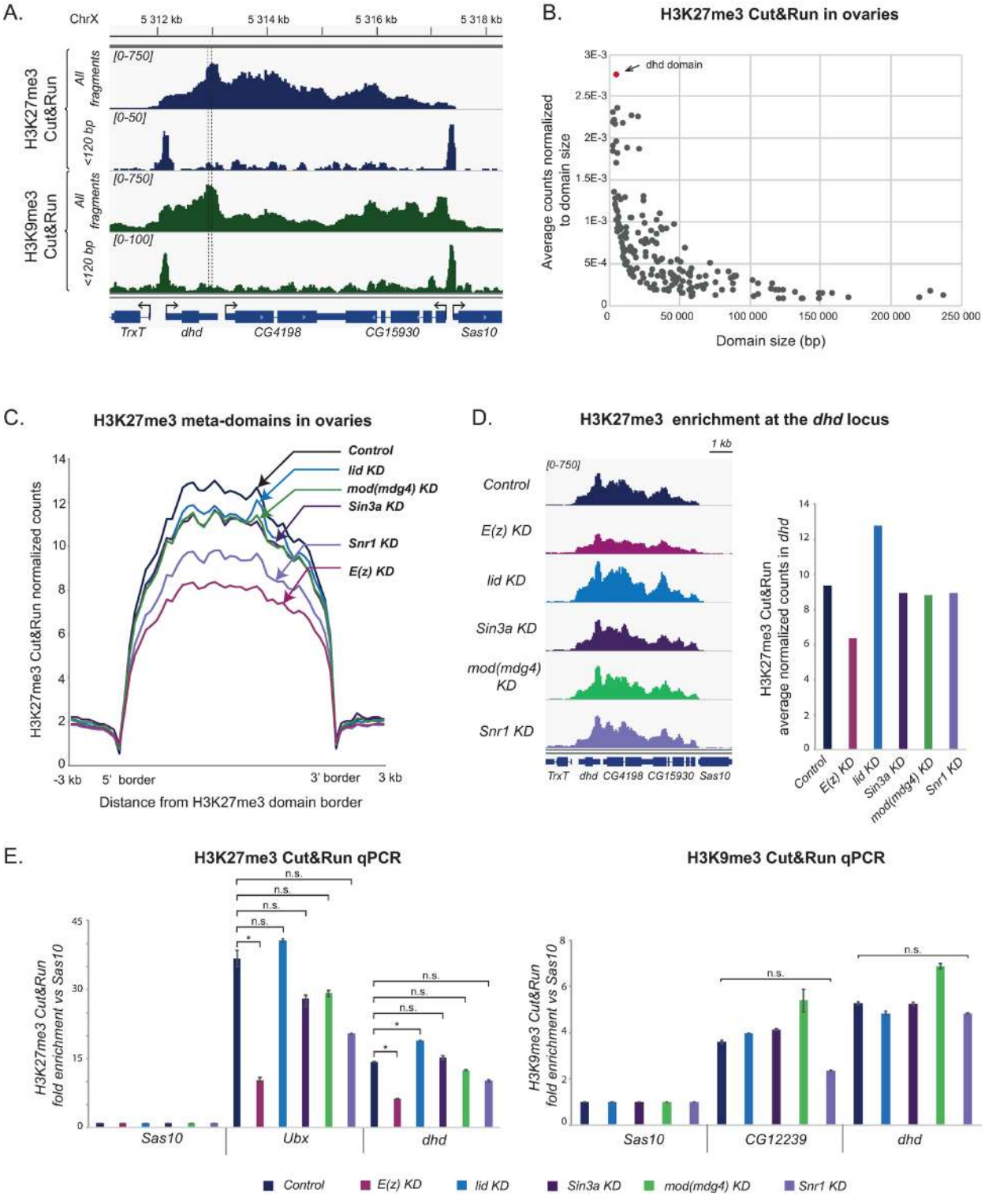
A.
ChrX
5 312 kb
5 314 kb
5 316 kb
5 318 kb
H3K27me3 Cut&Run
All fragments
<120 bp
[0-750]
[0-50]
H3K9me3 Cut&Run
[0-750]
[0-100]
TrxT
dhd
CG4198
CG15930
Sas10
B.
H3K27me3 Cut&Run in ovaries
dhd domain
Average counts normalized to domain size
Domain size (bp)
C.
H3K27me3 meta-domains in ovaries
Control
lid KD
mod(mdg4) KD
Sin3a KD
Snr1 KD
E(z) KD
H3K27me3 Cut&Run normalized counts
-3 kb
5' border
3' border
3 kb
Distance from H3K27me3 domain border
D.
H3K27me3 enrichment at the dhd locus
1 kb
[0-750]
Control
E(z) KD
lid KD
Sin3a KD
mod(mdg4) KD
Snr1 KD
TrxT
dhd
CG4198
CG15930
Sas10
H3K27me3 Cut&Run average normalized counts in dhd
E.
H3K27me3 Cut&Run qPCR
H3K27me3 Cut&Run fold enrichment vs Sas10
Sas10
Ubx
dhd
H3K9me3 Cut&Run qPCR
H3K9me3 Cut&Run fold enrichment vs Sas10
Sas10
CG12239
dhd
Control
E(z) KD
lid KD
Sin3a KD
mod(mdg4) KD
Snr1 KD

Figure 4

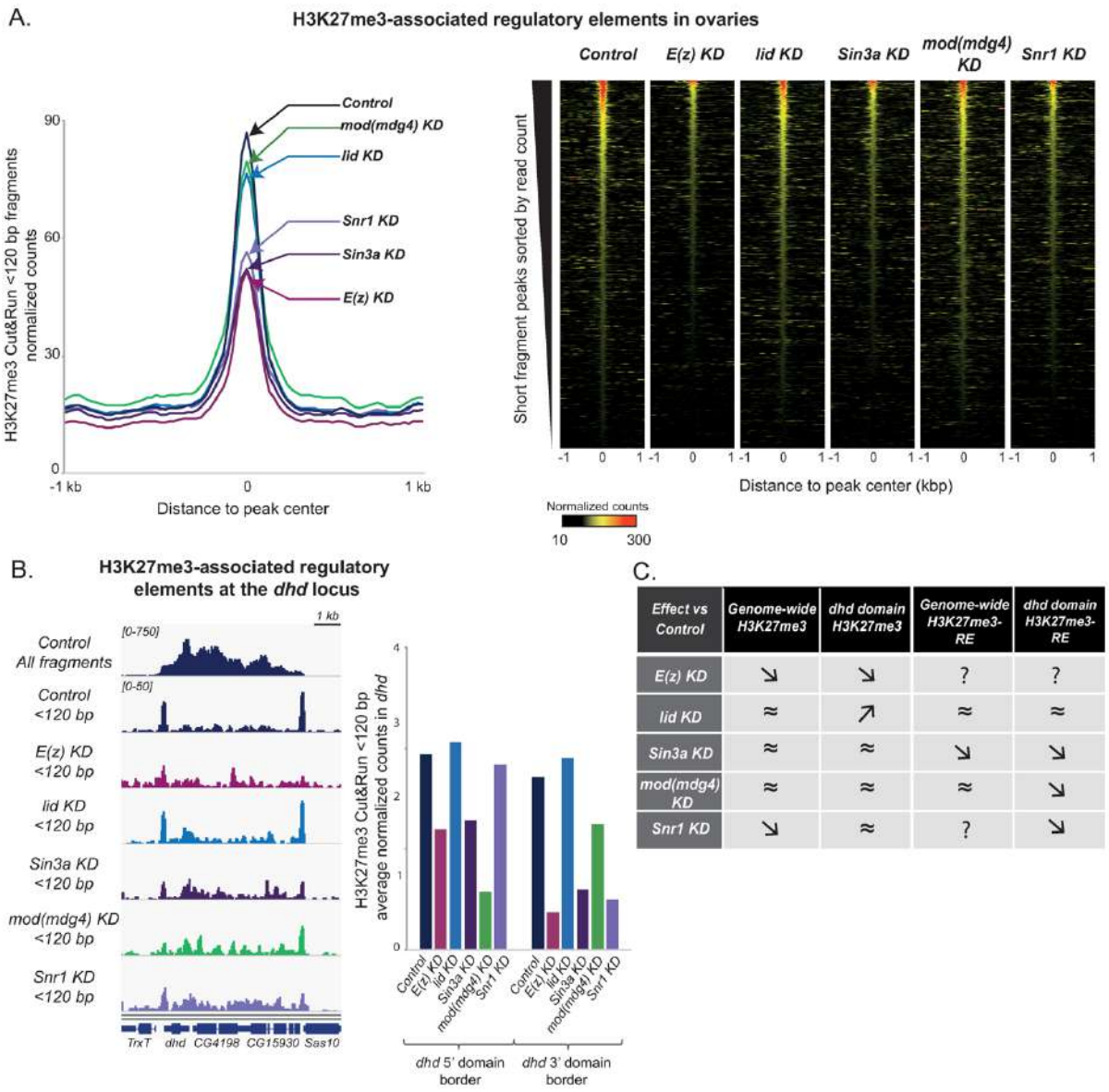

Effect vs Control	Genome-wide H3K27me3	dhd domain H3K27me3	Genome-wide H3K27me3-RE	dhd domain H3K27me3-RE
E(z) KD	↘	↘	?	?
lid KD	≈	↗	≈	≈
Sin3a KD	≈	≈	↘	↘
mod(mdg4) KD	≈	≈	≈	↘
Snr1 KD	↘	≈	?	↘

Figure 5

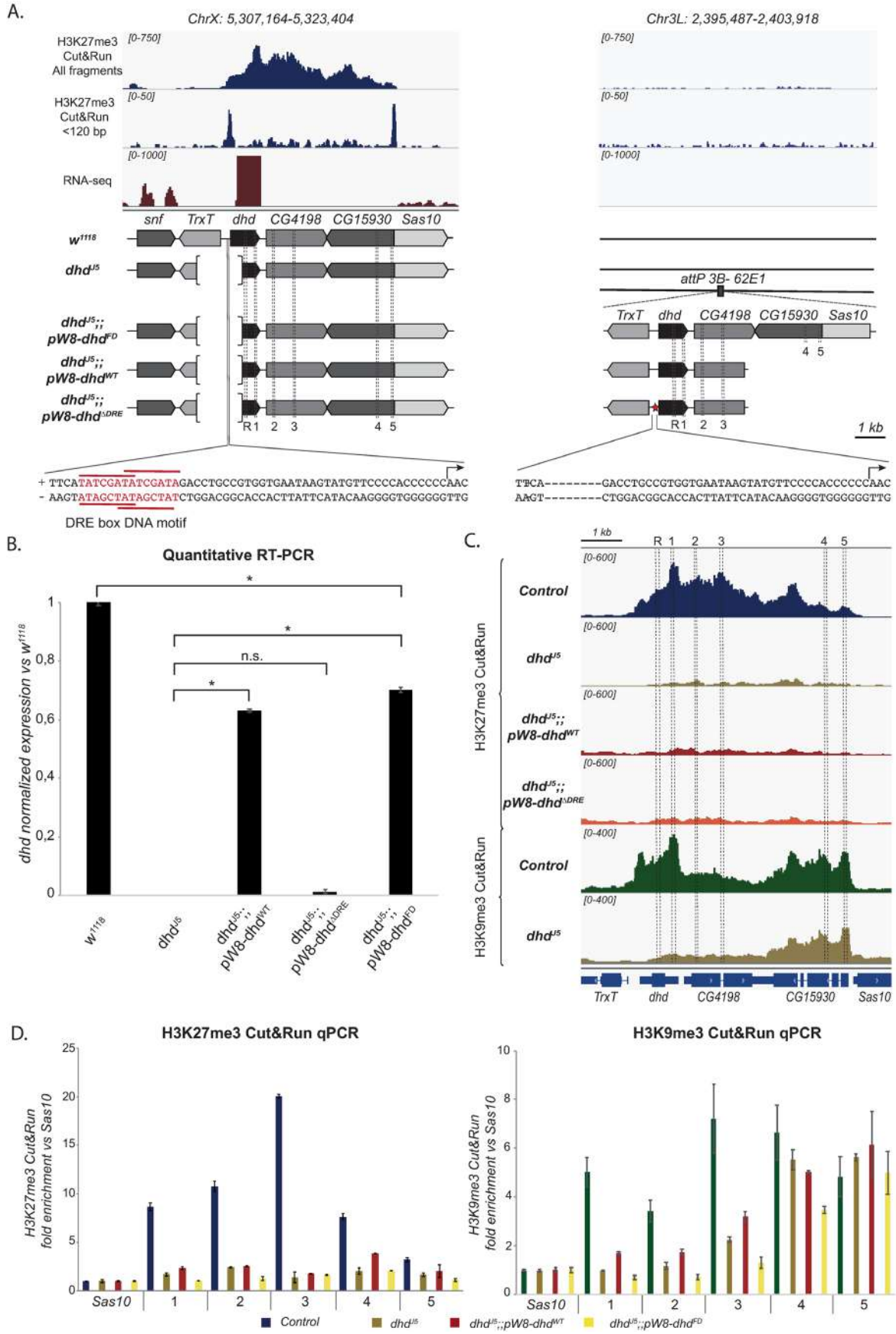
A.
ChrX: 5,307,164-5,323,404
Chr3L: 2,395,487-2,403,918
H3K27me3 Cut&Run All fragments
H3K27me3 Cut&Run <120 bp
RNA-seq
snf TrxT dhd CG4198 CG15930 Sas10
attP 3B- 62E1
1 kb
DRE box DNA motif
B.
Quantitative RT-PCR
dhd normalized expression vs w1118
n.s.
C.
H3K27me3 Cut&Run
H3K9me3 Cut&Run
Control
TrxT dhd CG4198 CG15930 Sas10
D.
H3K27me3 Cut&Run qPCR
H3K9me3 Cut&Run qPCR
H3K27me3 Cut&Run fold enrichment vs Sas10
H3K9me3 Cut&Run fold enrichment vs Sas10
Control

Figure 6

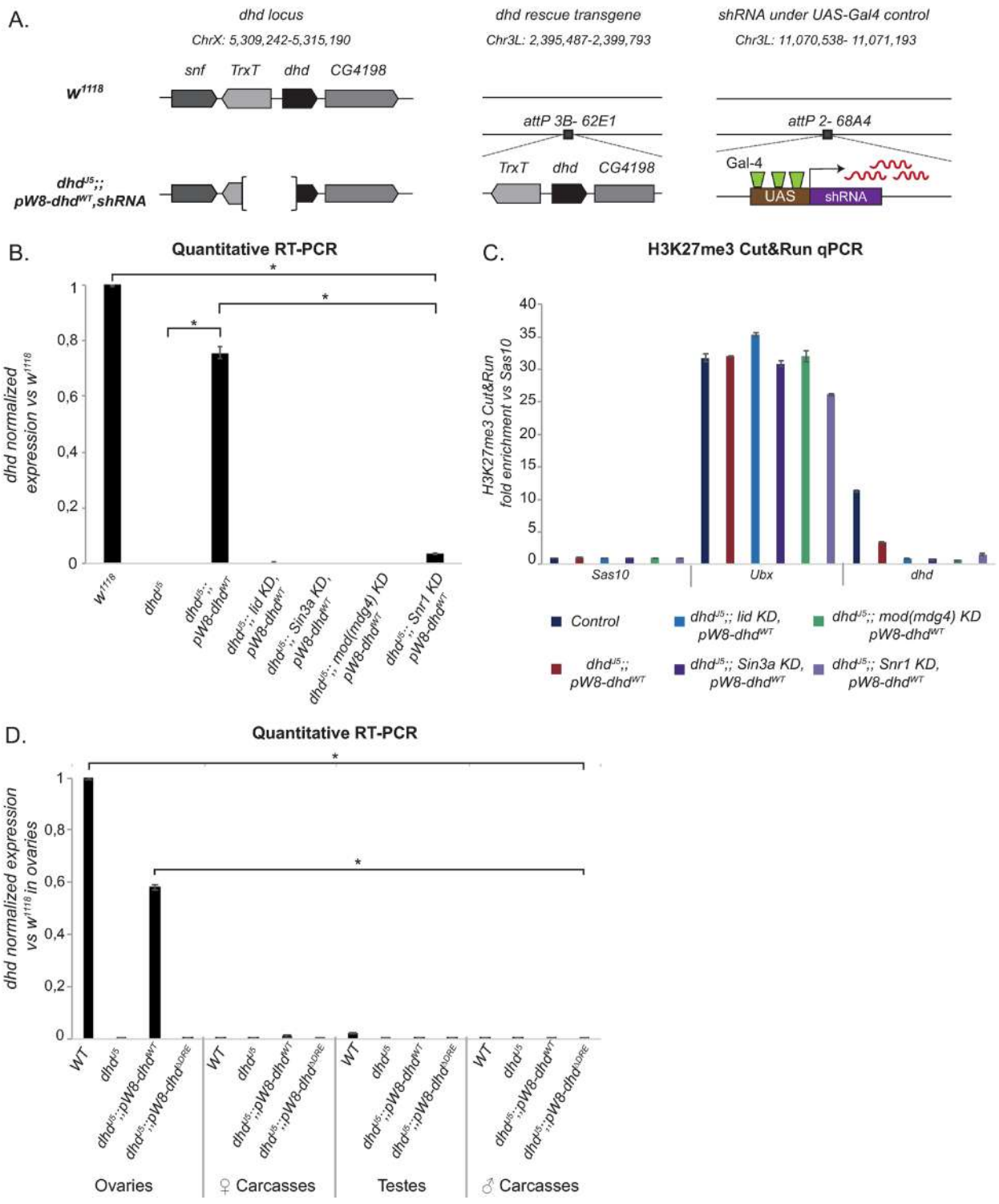
A.
dhd locus
ChrX: 5,309,242-5,315,190
snf
TrxT
dhd
CG4198
w1118
dhdJ5;;
pW8-dhdWT,shRNA
dhd rescue transgene
Chr3L: 2,395,487-2,399,793
attP 3B- 62E1
TrxT
dhd
CG4198
shRNA under UAS-Gal4 control
Chr3L: 11,070,538- 11,071,193
attP 2- 68A4
Gal-4
UAS
shRNA
B.
Quantitative RT-PCR
dhd normalized expression vs w1118
w1118
dhdJ5
dhdJ5;; pW8-dhdWT
dhdJ5;; lid KD, pW8-dhdWT
dhdJ5;; Sin3a KD, pW8-dhdWT
dhdJ5;; mod(mdg4) KD pW8-dhdWT
dhdJ5;; Snr1 KD pW8-dhdWT
C.
H3K27me3 Cut&Run qPCR
H3K27me3 Cut&Run fold enrichment vs Sas10
Sas10
Ubx
dhd
Control
dhdJ5;; pW8-dhdWT
dhdJ5;; lid KD, pW8-dhdWT
dhdJ5;; Sin3a KD, pW8-dhdWT
dhdJ5;; mod(mdg4) KD pW8-dhdWT
dhdJ5;; Snr1 KD, pW8-dhdWT
D.
Quantitative RT-PCR
dhd normalized expression vs w1116 in ovaries
WT
dhdJ5
dhdJ5;;pW8-dhdWT
dhdJ5;;pW8-dhdΔDRE
Ovaries
♀ Carcasses
Testes
♂ Carcasses

Figure S1

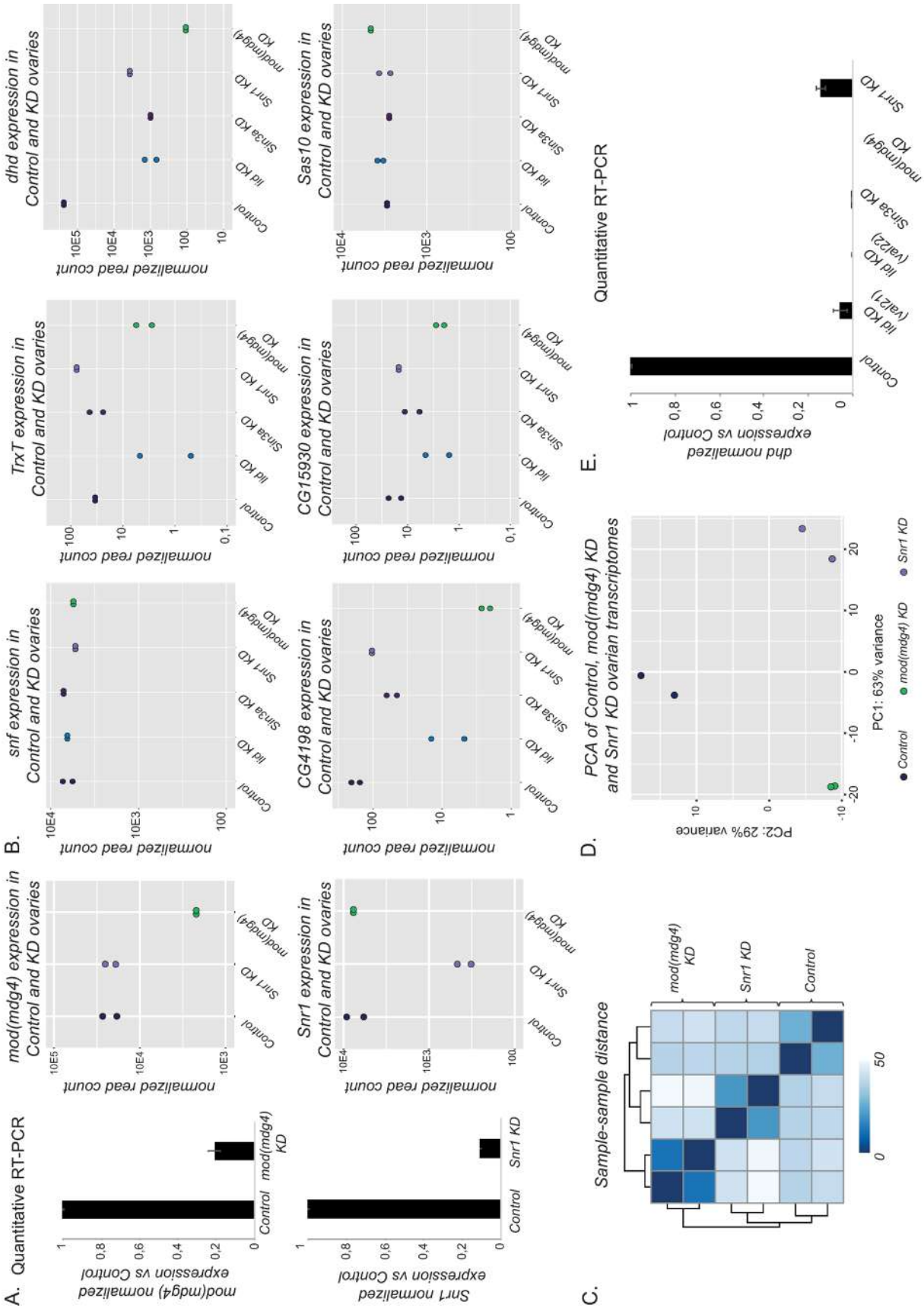
A. Quantitative RT-PCR
mod(mdg4) normalized expression vs Control
Control
mod(mdg4) KD
Snr1 normalized expression vs Control
Snr1 KD
mod(mdg4) expression in Control and KD ovaries
Snr1 expression in Control and KD ovaries
B.
snf expression in Control and KD ovaries
CG4198 expression in Control and KD ovaries
TrxT expression in Control and KD ovaries
CG15930 expression in Control and KD ovaries
dhd expression in Control and KD ovaries
Sas10 expression in Control and KD ovaries
normalized read count
Control
lid KD
Sin3a KD
Snr1 KD
mod(mdg4) KD
C.
Sample-sample distance
D.
PCA of Control, mod(mdg4) KD and Snr1 KD ovarian transcriptomes
PC1: 63% variance
PC2: 29% variance
E.
Quantitative RT-PCR
dhd normalized expression vs Control
lid KD (val21)
lid KD (val22)

Figure S2

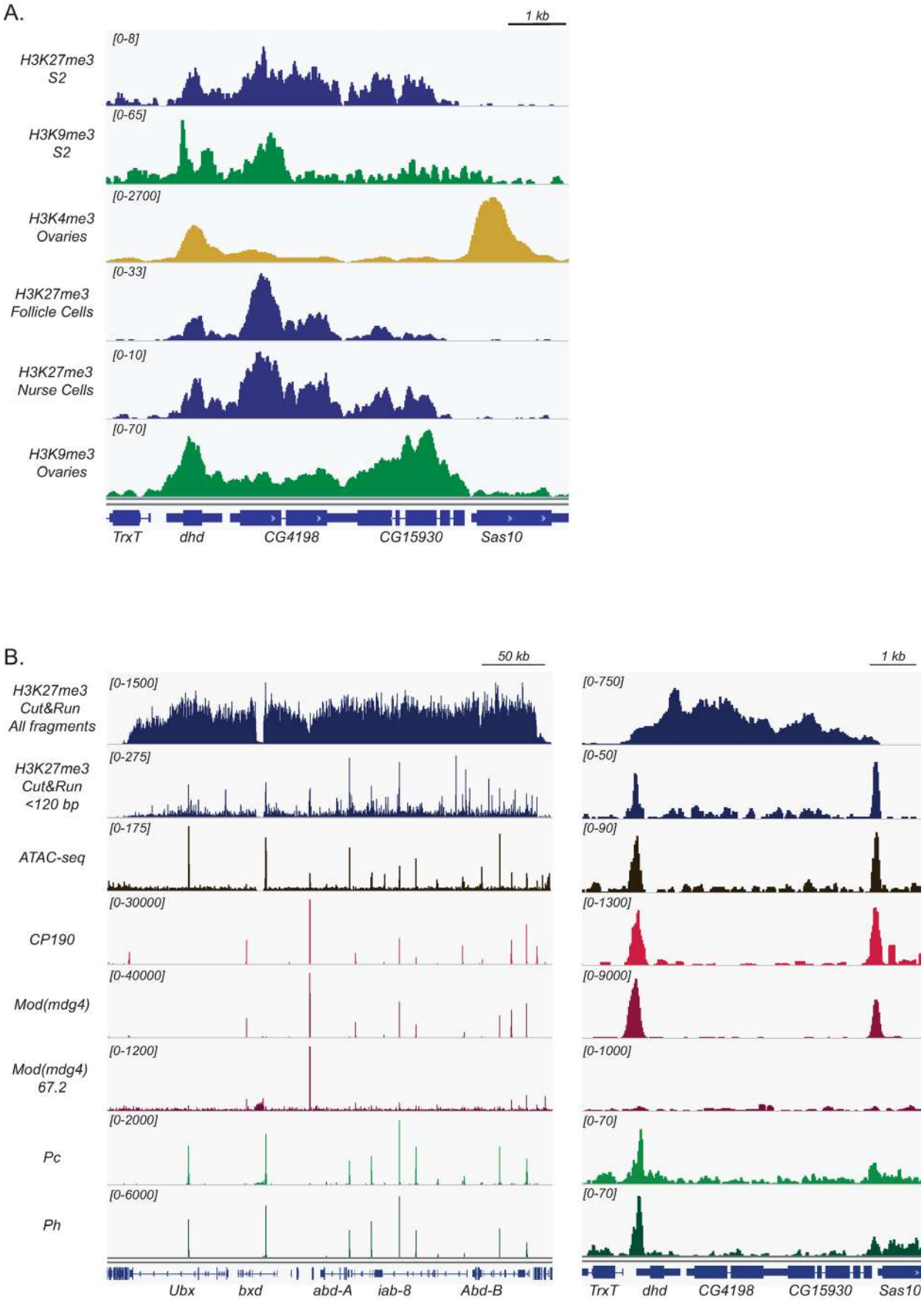
A.
1 kb
[0-8]
H3K27me3
S2
[0-65]
H3K9me3
S2
[0-2700]
H3K4me3
Ovaries
[0-33]
H3K27me3
Follicle Cells
[0-10]
H3K27me3
Nurse Cells
[0-70]
H3K9me3
Ovaries
TrxT
dhd
CG4198
CG15930
Sas10
B.
50 kb
1 kb
[0-1500]
H3K27me3
Cut&Run
All fragments
[0-750]
[0-275]
H3K27me3
Cut&Run
<120 bp
[0-50]
[0-175]
ATAC-seq
[0-90]
[0-30000]
CP190
[0-1300]
[0-40000]
Mod(mdg4)
[0-9000]
[0-1200]
Mod(mdg4)
67.2
[0-1000]
[0-2000]
Pc
[0-70]
[0-6000]
Ph
[0-70]
Ubx
bxd
abd-A
iab-8
Abd-B
TrxT
dhd
CG4198
CG15930
Sas10

Figure S3

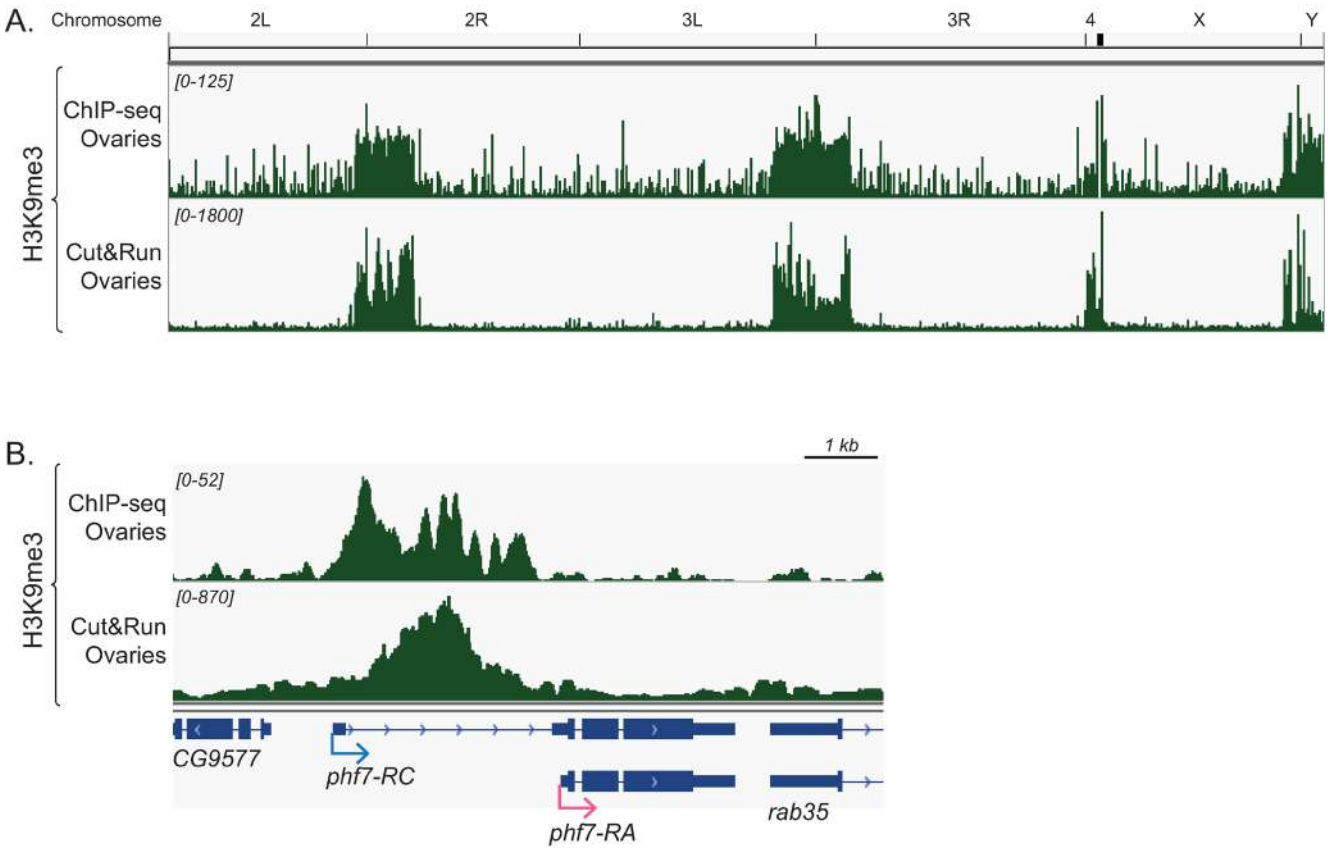
A.
Chromosome
2L
2R
3L
3R
4
X
Y
H3K9me3
ChIP-seq Ovaries
[0-125]
Cut&Run Ovaries
[0-1800]
B.
1 kb
H3K9me3
ChIP-seq Ovaries
[0-52]
Cut&Run Ovaries
[0-870]
CG9577
phf7-RC
phf7-RA
rab35

Figure S4

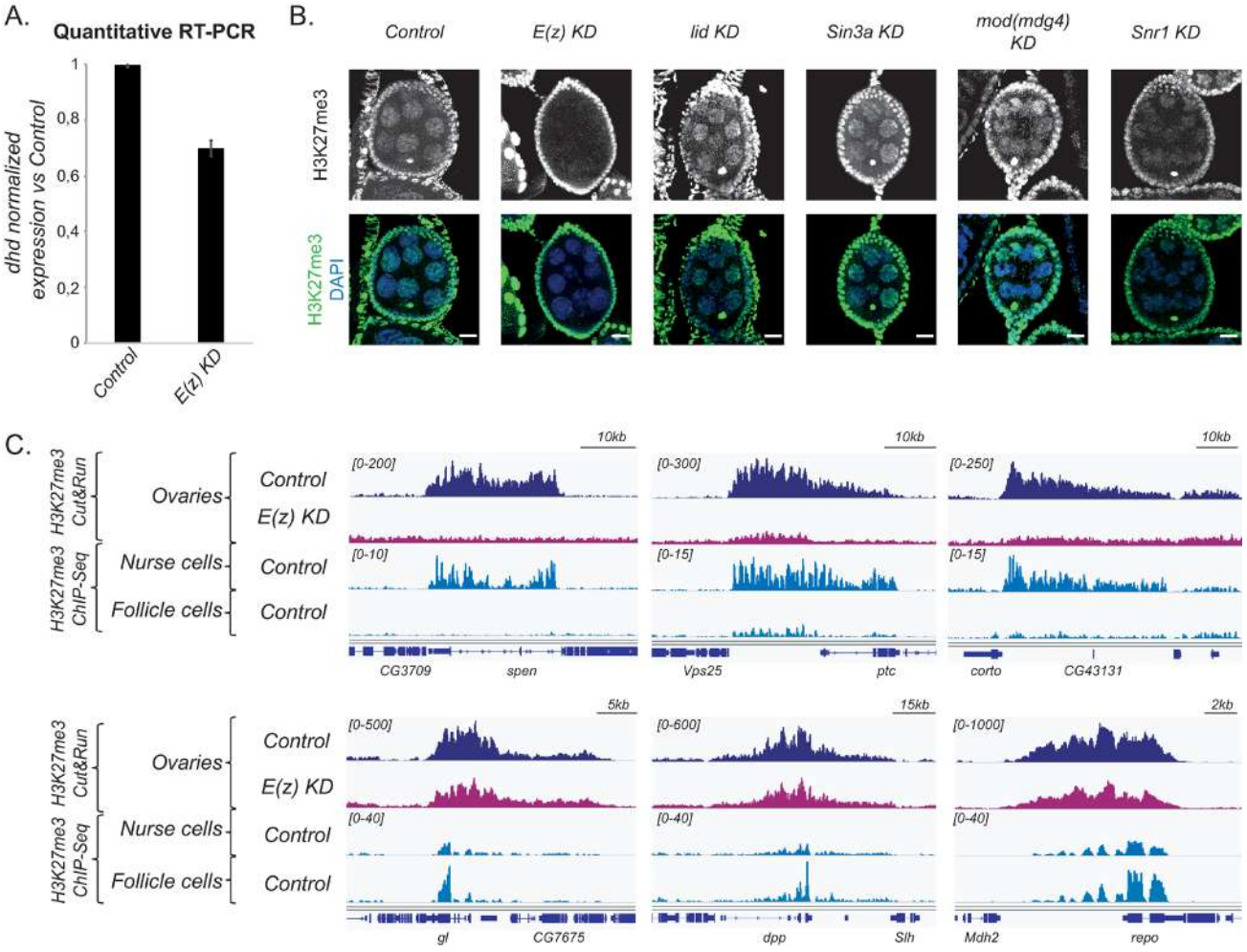
A.
Quantitative RT-PCR
dhd normalized expression vs Control
1
0,8
0,6
0,4
0,2
0
Control
E(z) KD
B.
Control
E(z) KD
lid KD
Sin3a KD
mod(mdg4) KD
Snr1 KD
H3K27me3
H3K27me3 DAPI
C.
H3K27me3 Cut&Run
H3K27me3 ChIP-Seq
Ovaries
Nurse cells
Follicle cells
Control
E(z) KD
Control
Control
10kb
[0-200]
[0-300]
[0-250]
[0-10]
[0-15]
[0-15]
CG3709
spen
Vps25
ptc
corto
CG43131
5kb
15kb
2kb
[0-500]
[0-600]
[0-1000]
[0-40]
[0-40]
[0-40]
gl
CG7675
dpp
Slh
Mdh2
repo

Figure S5

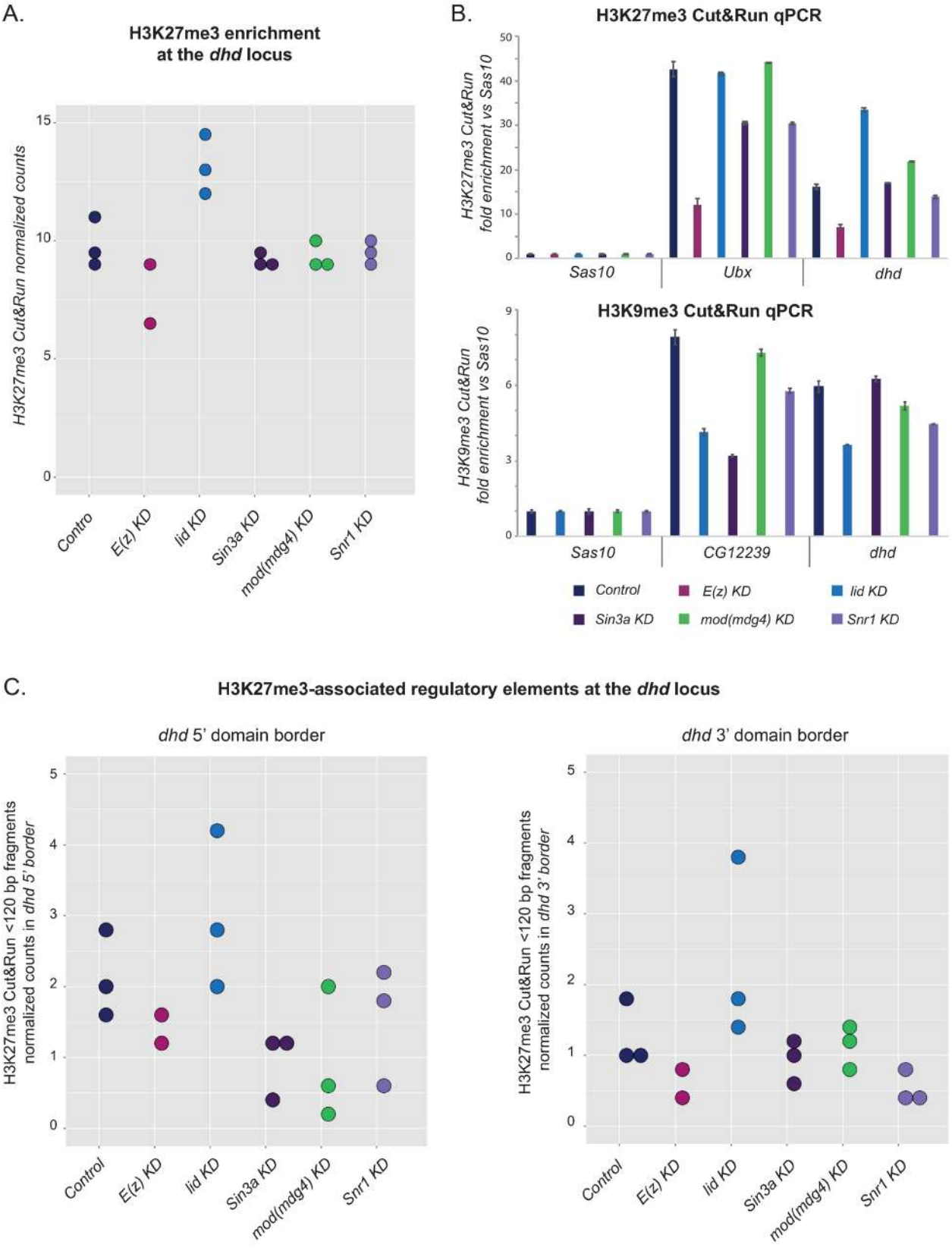
A.
H3K27me3 enrichment at the dhd locus
H3K27me3 Cut&Run normalized counts
Contro
E(z) KD
lid KD
Sin3a KD
mod(mdg4) KD
Snr1 KD
B.
H3K27me3 Cut&Run qPCR
H3K27me3 Cut&Run fold enrichment vs Sas10
Sas10
Ubx
dhd
H3K9me3 Cut&Run qPCR
H3K9me3 Cut&Run fold enrichment vs Sas10
Sas10
CG12239
dhd
Control
E(z) KD
lid KD
Sin3a KD
mod(mdg4) KD
Snr1 KD
C.
H3K27me3-associated regulatory elements at the dhd locus
dhd 5' domain border
H3K27me3 Cut&Run <120 bp fragments normalized counts in dhd 5' border
dhd 3' domain border
H3K27me3 Cut&Run <120 bp fragments normalized counts in dhd 3' border
Control
E(z) KD
lid KD
Sin3a KD
mod(mdg4) KD
Snr1 KD

Figure S6

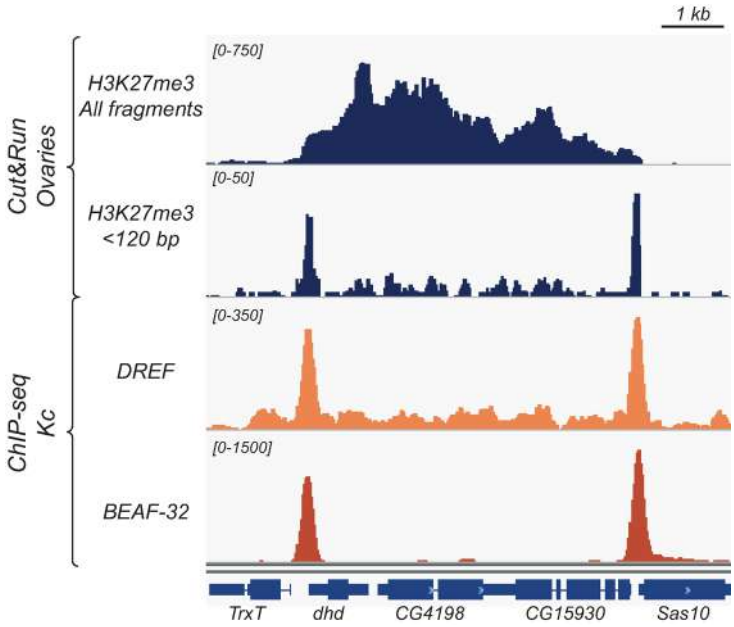

Figure S7

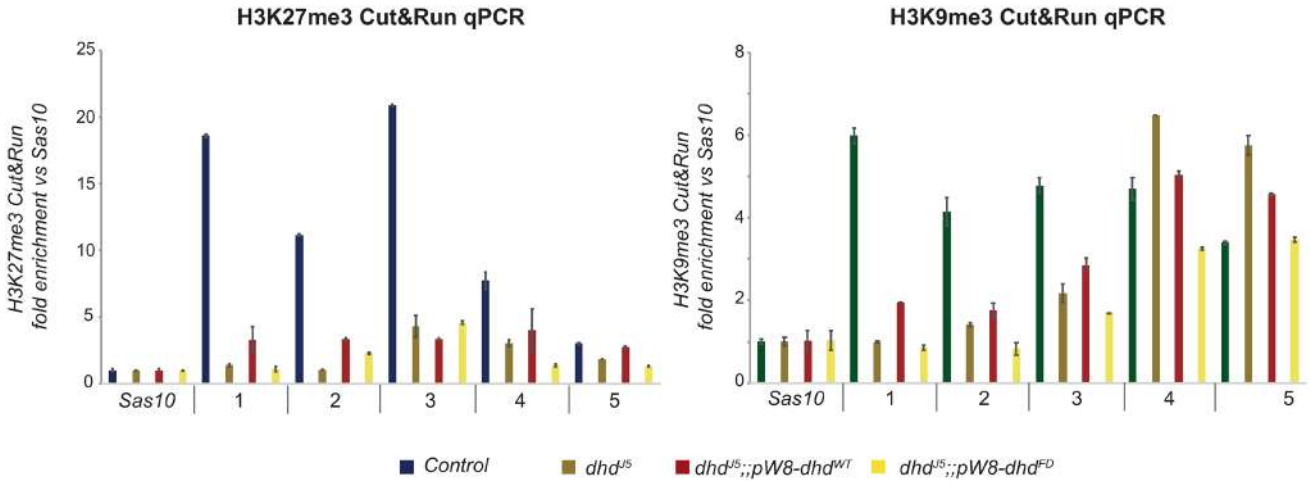

Figure S8

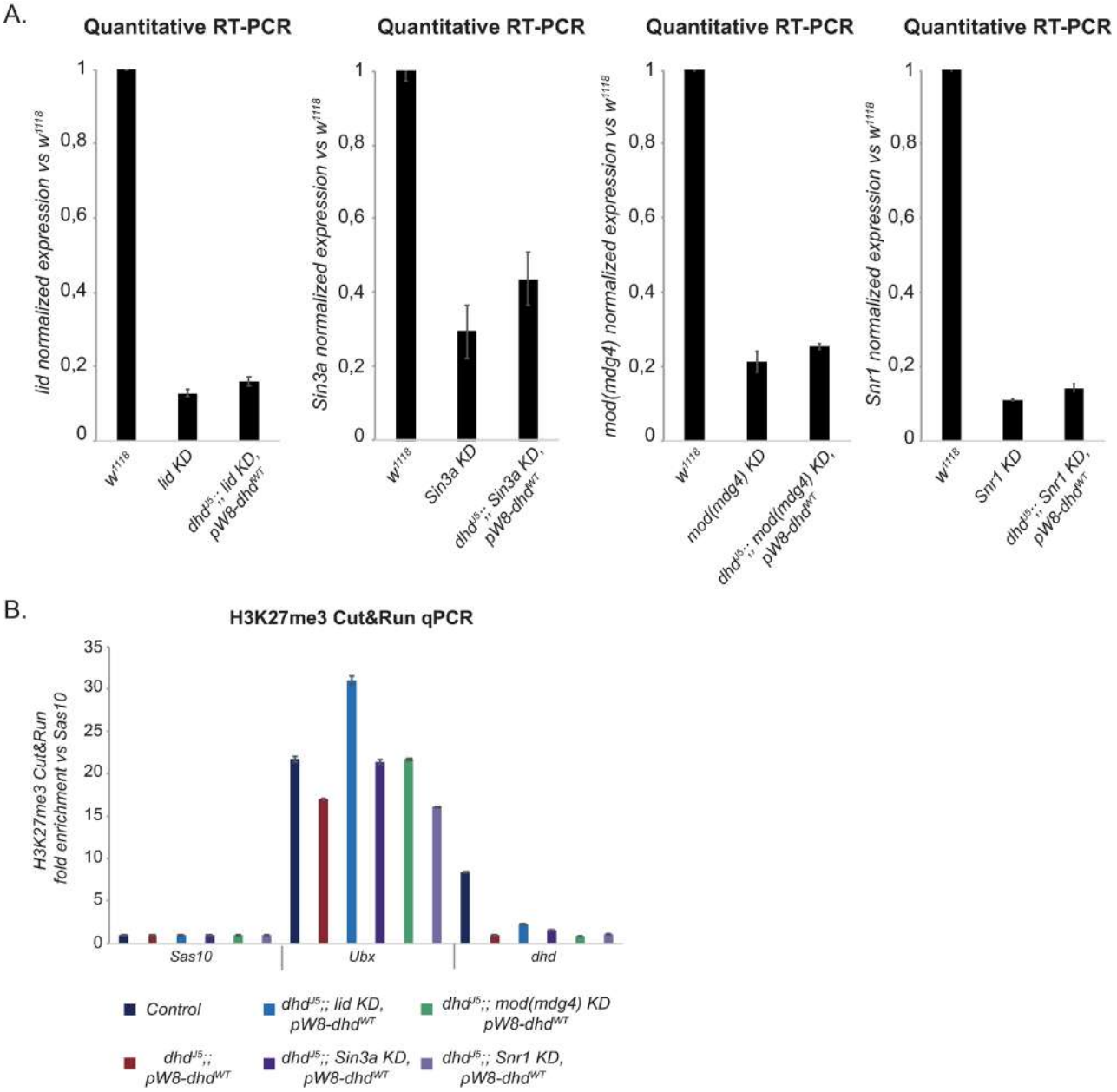
A.
Quantitative RT-PCR
lid normalized expression vs w1118
w1118
lid KD
dhdJ5;; lid KD, pW8-dhdWT
Quantitative RT-PCR
Sin3a normalized expression vs w1118
w1118
Sin3a KD
dhdJ5;; Sin3a KD, pW8-dhdWT
Quantitative RT-PCR
mod(mdg4) normalized expression vs w1118
w1118
mod(mdg4) KD
dhdJ5;; mod(mdg4) KD, pW8-dhdWT
Quantitative RT-PCR
Snr1 normalized expression vs w1118
w1118
Snr1 KD
dhdJ5;; Snr1 KD, pW8-dhdWT
B.
H3K27me3 Cut&Run qPCR
H3K27me3 Cut&Run fold enrichment vs Sas10
Sas10
Ubx
dhd
Control
dhdJ5;; lid KD, pW8-dhdWT
dhdJ5;; mod(mdg4) KD pW8-dhdWT
dhdJ5;; pW8-dhdWT
dhdJ5;; Sin3a KD, pW8-dhdWT
dhdJ5;; Snr1 KD, pW8-dhdWT

Table S1. List of primers used in this paper.

Primer	Sequence (5' —> 3')	Purpose
dhd-for	TCTATGCGACATGGTGTGGT	RT-qPCR
dhd-rev	TCCACATCGATCTTGAGCAC	RT-qPCR
lid-for	ATTGGTTTCACGAGGATTGC	RT-qPCR
lid-rev	CATAGCCACTTGGGTCGATT	RT-qPCR
Sin3a-for	CGACAAATGGGTATCGTTCC	RT-qPCR
Sin3a-rev	GACCAGGTCCAGCTCGAAT	RT-qPCR
mod(mdg4)-for	CAACAGATCACCGTGCAAAC	RT-qPCR
mod(mdg4)-rev	GTTCAGATTTCGTGGGCAAT	RT-qPCR
Snr1-for	TCAGCTCCCACATCTTAGCC	RT-qPCR
Snr1-rev	ACTGGCGTATCGGAAGTGTT	RT-qPCR
Rp49-for	AAGATCGTGAAGAAGCGCAC	RT-qPCR
Rp49-rev	GATACTGTCCCTTGAAGCGG	RT-qPCR
Ubx-for	AAAATTCCTCGGCCTGATTC	Cut&Run-qPCR
Ubx-rev	AAAAATGGGCGTAGCTCAGA	Cut&Run-qPCR
Sas10-for	AGGAGGAGCAGCAGGATGT	Cut&Run-qPCR
Sas10-rev	AGATCGCGGTCATCGTCTT	Cut&Run-qPCR
CG12239-for	AGATGAGGGACGAAGGATTG	Cut&Run-qPCR
CG12239-rev	TTCCTCGGTACGTTCAGCTT	Cut&Run-qPCR
dhd-3UTR-for	GTTTAGCTTGTAAGCGCGAGA	Cut&Run-qPCR
dhd-3UTR-rev	ATATCATCTGGTCACTGCTGTTG	Cut&Run-qPCR
CG4198-1-for	GAGCAAGAAGAATGGCCAAC	Cut&Run-qPCR
CG4198-1-rev	CGATCGTTGAACTCCTGGAT	Cut&Run-qPCR
CG4198-2-for	GTGTCCATAGCGCAGCAG	Cut&Run-qPCR
CG4198-2-for	AAGGTGAACATAACCCCACAA	Cut&Run-qPCR
CG15930-1-for	ACCTGGACATCGGCTACATC	Cut&Run-qPCR
CG15930-1-rev	ACCATGTGCGAATTTTCGAT	Cut&Run-qPCR

CG15930-2-for	TTATTCCGCATTTTGGCACT	Cut&Run-qPCR
CG15930-2-for	GGAAGAAGCCGAGGATAACA	Cut&Run-qPCR
ΔDRE-1-for	GAGCAGCAGCCGAATTCGGTACCCCCATATCCCTCCCATATCC	ΔDRE-transgene
ΔDRE-1-rev	CACGGCAGGTCTGAATATTATTATCGTAATTATGGCAAAATAATGGC	ΔDRE-transgene
ΔDRE-2-for	GATAATAATATTCAGACCTGCCGTGGTGAATAAG	ΔDRE-transgene
ΔDRE-2-rev	CACAGGGATGCCACCCGGGATCCGCTAATGGAATCGCAATCGT	ΔDRE-transgene
FD-for	GATTGCGATTCCATTAGCGAATGCGGACGATATGCCAACGC	FD-transgene
FD-rev	GTCACAGGGATGCCACCCGGGATCCACAAAGAGAAAAACTGTTGTAA	FD-transgene

Table S2. List of antibodies used in this paper.

Antibody	Host animal	Dilution	Experiment	Company (Catalog#)
Anti-Histones	mouse, monoclonal	1:1000	Immunofluorescence	Merck (#F152.C25.WJJ)
Anti-GFP	mouse, monoclonal	1:200	Immunofluorescence	Roche (#118144600001)
Anti-H3K27me3	rabbit, polyclonal	1:500	Immunofluorescence	Merck (#07-449)
Anti-H3K27me3	rabbit, monoclonal	1:100	Cut&Run	Cell Signalling Technology (#9733)
Anti-H3K9me3	rabbit, polyclonal	1:50	Cut&Run	Abcam (#8898)
Anti-DHD	rabbit, polyclonal	1:1000	Western Blot	*Tirmarche et al., 2016*
Anti-α-tubulin	mouse, monoclonal	1:500	Western Blot	Merck (#T9026)

III. Additional Results and Discussion

The oocyte-to-zygote transition involves a series of complex nuclear and cellular events, including completion of meiosis, selective translation of maternal RNAs and formation of male and female pronuclei. These events are mainly controlled by maternal factors present in the oocyte at the moment of fertilization. For example, the maternal HIRA histone chaperone complex is essential for the assembly of paternal chromatin at fertilization (Bonnefoy et al., 2007), hinting thus on the importance of chromatin factors involved in zygote formation. This opened the question of what other maternal chromatin factors are required for the integration of paternal chromosomes into the zygote. To answer this, we performed a female germline specific shRNA genetic screen. Remarkably, among the 8 genes causing paternal chromosome loss (among 380 targets tested), 3 belonged to the HIRA complex and the rest were found to abolish *dhd* expression on a rather specific manner. This result revealed a complex network of epigenomic effectors dedicated to the hyperactivation of this small gene. I thus investigated the molecular mechanisms underlying this regulation.

1. Is there an "ovarian hyperactivation code"?

My work led me to discover a series of epigenomic effectors that play general roles in gene regulation but are critical for *dhd* expression in ovaries. I focused thus on the mechanisms mediated by: (i) the H3K4me3 demethylase Lid, (ii) the deacetylase complex scaffold Sin3A, (iii) the Snr1 subunit of the remodeler Swi/Snf complex and (iv) the chromatin factor Mod(mdg4). Available data in other cell contexts showed that depletion of Lid/dKDM5, Sin3A and Snr1 affects hundreds or even thousands of genes (Gajan et al., 2016; Liu and Secombe, 2015; Saha et al., 2016; Xie et al., 2017; Zamurrad et al., 2018). Genome-wide impact on transcription after for Mod(mdg4) depletion has not been studied. Nonetheless, this factor has also been involved in gene regulation (Gerasimova et al., 1995; Savitsky et al., 2016). Strikingly our RNA-seq data analysis showed that *dhd* is hypersensitive to the loss of any of these factors, suggesting that these ubiquitous regulators of gene expression have a specificity for *dhd* in ovaries.

A hypothesis we considered to explain *dhd* hyperactivation was the control of *dhd* by specific distal regulatory elements and/or its positioning in a genomic environment favorable to high transcription levels. There is more and more evidence that links the 3D folding of the genome to transcription. Indeed, the eukaryotic genome is constrained in the nucleus and it has been observed that it is partitioned in domains with similar transcriptional state (Szabo et al., 2019). An emerging hypothesis is that this can favor gene activation by creating compartments containing the necessary factors to favor transcription (Cho et al., 2018; Cramer, 2019; Sabari et al., 2018). Many factors are required for gene transcription, this could be thus a way to deliver quickly and in sufficient amount the necessary proteins at sites of high transcription activity. At a lower scale, eukaryotic genomes, including *Drosophila*'s are organized in self-interacting regions: TADs (Schwartz and Cavalli, 2017; Szabo et al., 2019). This means that DNA sequences within a TAD physically interact with each other more frequently than with sequences outside the TAD. It was reasonable therefore to consider that the 3D organization of the genome could favor *dhd* interaction with specific regulatory regions. However, using available Hi-C data in embryonic fly cells we did not identify any particular contacts at the *dhd* locus (Fig24). The expression of *dhd* is strictly restricted to ovaries, it is thus possible that specific contacts are only established in the germline at a precise developmental stage and are thus undetectable in other cells. Nevertheless, our *pW8-attB-dhd*^{WT} transgene inserted in the chromosome III is capable of restoring *dhd* expression to high levels, arguing against *dhd* endogenous genomic environment as a key feature for its hyperactivation. This suggests that, at least in some specific cases, a gene can be massively expressed quite independently of its genomic context and putative 3D contacts.

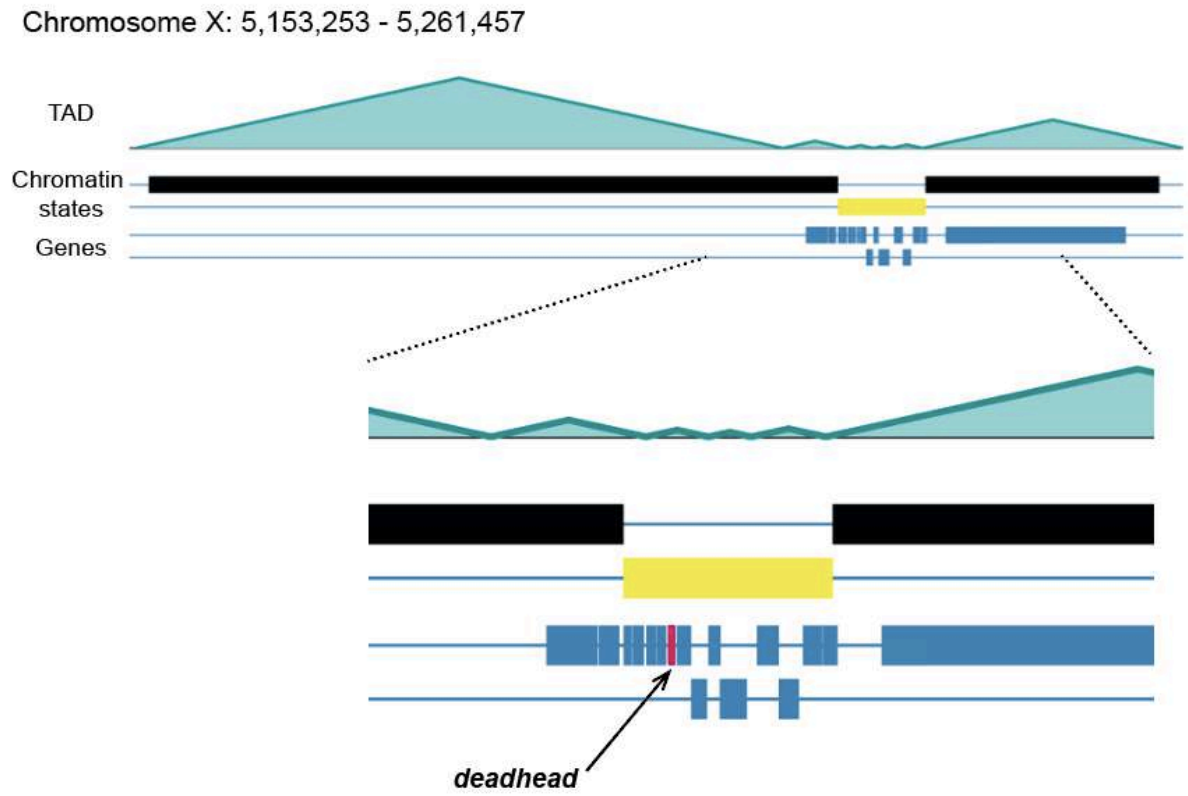

Fig24: *dhd* does not show contacts with other loci in cultured cells.
Representation of Hi-C datasets from *Drosophila* Kc embryonic cell using the Chorogenome Navigator (Ramírez et al., 2018), showing TADs, chromatin state and genes at the indicated coordinates and a zoom on the *dhd* region. Yellow corresponds to active chromatin and black to inactive chromatin.

To explain *dhd* hyperactivation we can also look at the gene itself. Indeed, *dhd* gene architecture, short and intronless, could contribute to explain its hyperactivation. The process of eliminating introns is energy- and time-consuming. Therefore, *dhd* structure could provide an advantage in transcription and translation efficiency, resulting in its high expression. In humans, shorter gene length is associated with high expression, smaller proteins, and little intronic content. It was hypothesized that, due to the great levels of expression in smaller genes, there is a selective pressure to maximize protein synthesis efficiency (Urrutia, 2003). Also, the main fraction of intronless genes correspond to those coding for histones and G protein-coupled receptors and both of this gene families are abundantly expressed (Bryson-Richardson et al., 2004; Doenecke and Albig, 2005; Louhichi et al., 2011). Genes with longer transcripts are mostly associated with functions in the early development stages, while genes with smaller transcripts have important roles in more general functions (Lopes et al., 2021). A correlation between gene length and function has therefore been established. Shorter genes tend to be associated with housekeeping functions, however *dhd* is required only at a very

specific time and contrary to housekeeping genes, it does not need to be constitutively expressed. While *dhd* length could confer an advantage for high expression, the latter must be precisely regulated. Notably, the *dhd* transcribed region would correspond to ~4 nucleosomes. Nucleosomes represent a barrier for RNA Pol II progression, requiring thus a coordinated dance of nucleosomes sliding, evicting, assembling, among others. It is then possible that this low number of nucleosomes favors transcriptional efficiency.

Promoter-enhancer communication is a key point in transcriptional regulation. Both of these elements are bound by transcription factors recognizing specific DNA motifs. Motif scanning at the *dhd* promoter identified a tandem DRE motif. Remarkably, only 4 other gene promoters in the genome presented this motif with ovary-bias expression but none had high levels of expression, similar to *dhd*. DRE motifs are enriched at core promoters of highly expressed housekeeping genes (FitzGerald et al., 2006; Ohler et al., 2002). Additionally, DRE-binding factor Dref, preferentially binds to and activates housekeeping enhancers that are located closely to ubiquitously expressed genes with specificity to its core promoter, and suggests that the DRE motif is required and sufficient for housekeeping enhancer function (Zabidi et al., 2015). Although we were not able to identify any obvious candidate enhancer element in the vicinity of the *dhd* gene region we cannot exclude that this tandem DRE motif plays an important role in *dhd* hyperactivation by recruiting a still unknown enhancer. Nonetheless, this motif by its own, is not sufficient for ovarian hyperactivation.

As mentioned before, *dhd* is a short gene, it was then reasonable to consider that in order to optimize this retrained space, regulatory elements could be present within the coding sequence (CDS). During my PhD I used a rescue transgene, *pW8-attB-dhd*^{WT}, capable of restoring *dhd* expression to ~70% of its endogenous level. I also had at my disposal a transgenic line with a construct identical to the *pW8-attB-dhd*^{WT} transgene except that *dhd* CDS had been replaced by the similar in size CDS of the ubiquitous thioredoxin *Trx2* (Fig25-A) (Tirmarche, 2016). I thus sought to establish if the *pW8-attB-dhd>Trx2* transgene was able to induce similar *Trx2* levels to those found for *dhd* with the *pW8-attB-dhd*^{WT} transgene. Along with a master student, we tackled this question by measuring by RT-qPCR in ovaries transcripts emerging either from the *pW8-attB-dhd*^{WT} or the *pW8-attB-dhd>Trx2* transgene in a *dhd*^{J5} null mutant context. For this, we used primers targeting *dhd* 3'UTR region allowing us to measure endogenous *dhd* expression in the control as well as transcripts originating from both transgenes. We used the same method as described in (Torres-Campana et al.,

2020). Our preliminary results indicated that as previously observed, the *dhd* transgene is able to restore high *dhd* expression. However, transcripts emerging from the *pW8-attB-dhd>Trx2* transgene were weakly expressed. Indeed, they represented ~10% of the endogenous *dhd* levels and ~15% of the *dhd* levels retrieved with the *pW8-attB-dhd*^{WT} transgene (Fig25-B). Replacing the CDS of *dhd* by the CDS of *Trx2* does not suffice to induce high transcript levels of *Trx2*, comparable to those of *dhd*. These results suggest that *dhd* CDS is important to achieve high levels of transcription.

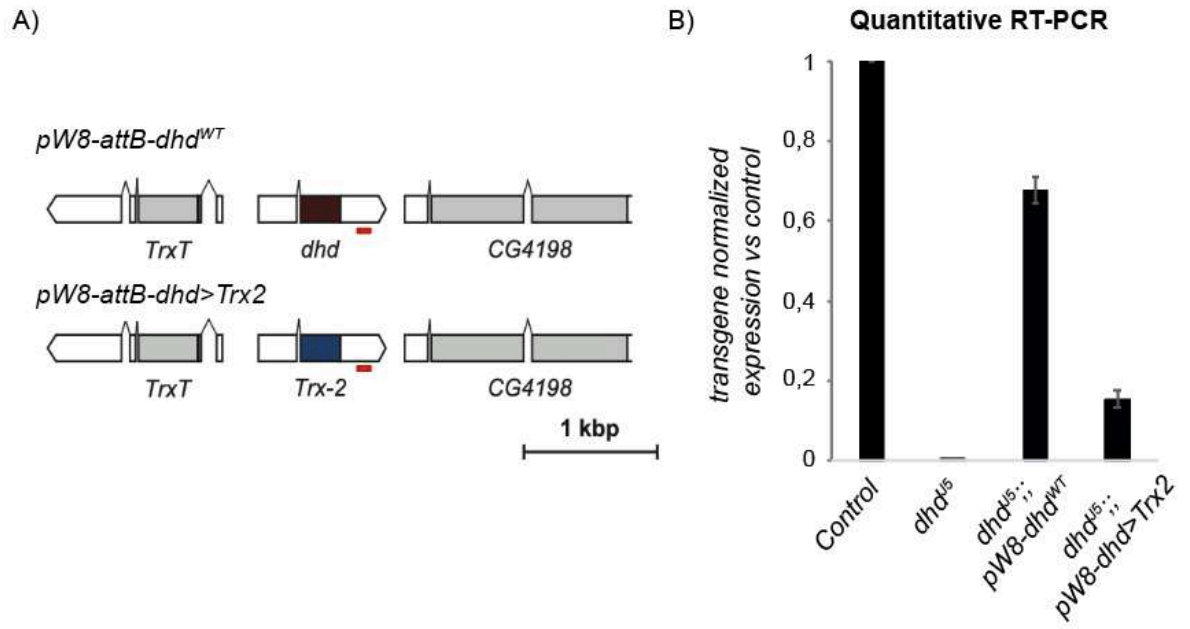

Fig 25-Replacement of *dhd* coding sequence does not replicate its highly expressed levels

(A) Schematic representation of the *pW8-attB-dhd*^{WT} and *pW8-attB-dhd>Trx2* transgenes. The *pW8-attB-dhd*^{WT} contains a genomic region of 4.3 kb containing the *dhd* gene. In the *pW8-attB-dhd>Trx2* transgene, the coding sequence of *dhd* (brown) was replaced by the one of *Trx2* (blue), to place it under the control of the *dhd* promoter. The red line indicates the region covered by the primers used in (B) (Tirmarche, 2016). (B) RT-qPCR quantification of *pW8-attB-dhd*^{WT} and *pW8-attB-dhd>Trx2* mRNA levels in ovaries from control flies, *dhd*^{J5} mutants or *dhd*^{J5} mutants carrying one of the two transgenes (normalized to *Rp49* and relative to expression in control). Data from biological duplicates analyzed in technical duplicates are presented as mean ± SEM.

How can a sequence be optimized for high transcription? Codon usage bias, the preference for certain synonymous codons, is a feature of eukaryotic and prokaryotic genomes that plays an important role in gene expression levels. It has been observed that this is, at least in part,

due to codon usage influence on translation rates (Duret and Mouchiroud, 1999; Weinberg et al., 2016; Yu et al., 2015; Zhao et al., 2017). Recent studies have also found a correlation between codon usage on mRNA levels due to changes in transcription in *Neurospora* (Zhou et al., 2016), suggesting that codon optimization could also play a role at the transcriptional level. It is thus reasonable, to hypothesize that *dhd* sequence contributes to its hyperactivation by this mechanism. It could thus be interesting to determine if *dhd* shows codon usage bias and if so, assess the impact on expression level when such codons are replaced by synonym codons. Also, the comparison of codon usage between *dhd* and other highly transcribed genes could shed light into the optimization of the CDS for transcriptional efficiency.

Finally, the peculiar genomic landscape of *dhd* is also worth considering in the recipe for hyperactivation. I found that *dhd* is embedded within a heterochromatic domain harboring both H3K27me3 and H3K9me3 while also being enriched for H3K4me3. The type of promoters carrying both active and repressive marks *i.e*., bivalent promoters are associated to developmental genes in mammals (Bernstein et al., 2006; Lesch et al., 2013). When carrying both marks genes are repressed or weakly transcribed and upon cell differentiation, these bivalent regions undergo either full activation or stable silencing (Gaertner et al., 2012; Mikkelsen et al., 2007; Pan et al., 2007; Zhao et al., 2007). Recently, this kind of domains were identified in *Drosophila* embryos at a handful of *Hox* genes (Akmammedov et al., 2019). If these domains represent promoters poised for activation or repression has not been investigated yet. However, our *dhd* rescue transgene is expressed to high levels even in the absence of both heterochromatic marks indicating that this epigenetic configuration is not necessary for *dhd* massive expression. Importantly, our data comes from whole ovaries, that is a mix of germ cells and somatic cells at various stages of differentiation. Due to technical limitations in our study, we cannot exclude that these marks are not cell-type and oogenesis-stage-specific.

In conclusion, I uncovered a series of specific features at the *dhd* gene. However, none of them alone seems to define an “ovarian hyperactivation code”. It is more likely that the ensemble of the particular characteristics of *dhd* are necessary to achieve its massive expression.

2. An unusual heterochromatic domain

Both H3K9me3 and H3K27me3 are commonly found in large extended domains however we uncovered an H3K27me3/H3K9me3 mini-domain flanked by regulatory elements.

How can this be achieved? In *Drosophila*, insulators and active transcription have been found important for Polycomb/H3K27me3 domain boundaries (De et al., 2020; Fujioka et al., 2013). CP190 is a protein common to most insulators (Ahanger et al., 2013) and in embryonic fly cells it binds both borders of the *dhd* H3K27me3 domain. The study by *De et al.*, reported different categories of Polycomb boundaries in fly larvae (De et al., 2020). 22% of the boundaries analyzed corresponded to an insulator and an active promoter next to the Polycomb domain, transcribing away from the domain. This is the case observed at the *Sas10*-proximal boundary of the mini-domain we identified. However, the scenario of a gene transcribing towards the H3K27me3 domain, as is the case at the *dhd*-proximal border, was not observed in this study. Although the case of *dhd* transcribing within the heterochromatic domain is peculiar, both borders of the domain show active transcription and insulator proteins. It is thus possible that the presence of these two elements helps define these boundaries.

One of the features of heterochromatic H3K9me3 domains it's their ability to spread. However, we and others observe in the female germline a highly localized deposition of H3K9me3 [Smolko et al., 2018]. To target H3K9me3 deposition, RNA-based mechanisms or DNA-binding proteins mechanisms have been described. In their study, Smolko and colleagues found that H3K9me3 deposition by the histone methyltransferase dSETDB1 depended on Sxl, an RNA binding protein. It is thus possible that an RNA-based mechanism is at play. Of the three Drosophila enzymes known to methylate H3K9, only dSETDB1 is required for germline development. It is thus possible that this methyltransferase achieves a localized deposition of H3K9me3 through specific features and interactions with determined partners such as Sxl. In some cases, H3K9me3 is permissive to – or even required for – transcription (Lu et al., 2000; Smolko et al., 2018; Wakimoto and Hearn, 1990). Active heterochromatic genes have H3K9me3 on their bodies but not their TSSs, it is tempting to speculate that H3K9me3 is repressive only at promoter regions, while being compatible with, or even promoting, transcription on gene bodies.

Both H3K27me3 and H3K9me3 are known as important to mediate gene repression. The role they play at the *dhd* locus is thus intriguing. First, as suggested by the *dhd* rescue transgene, these marks are not necessary to achieve high levels of expression. Next, we did

not detect an ectopic expression of *dhd* in adult tissues when these marks were absent, arguing thus against a repressive role outside of ovarian tissue. Nonetheless, we cannot exclude a repressive role at other developmental stages.

H3K27me3 and H3K9me3 are compatible with transcription (Ahmad and Spens, 2019; Lu et al., 2000; Smolko et al., 2018; Wakimoto and Hearn, 1990) we can thus wonder if they could actually play a role in promoting transcription of *dhd*. It is also possible that this mini-domain has a role in repressing the other two genes present within it, *CG4198*, which is testis-specific, and *CG15930*, which shows low expression in larval imaginal discs (http://flybase.org). Of note, these two hypotheses are not mutually exclusive. Further studies will be necessary to elucidate the role of this heterochromatic mini-domain and shed light on the roles played by these marks on transcription regulation.

3. Different roles for epigenomic regulators

Lid, Sin3A, Snr1 and Mod(mdg4) are essential for *dhd* expression. They regulate *dhd* without significantly impacting H3K27me3 enrichment in the *dhd* domain, except for Lid who slightly counteracts it. This suggests that depletion of epigenomic effectors can alter transcription without major changes in the surrounding epigenomic landscape. In agreement, a recent study reported that depletion of the H3K4me1/2 demethylase dLsd1 in the female germline results in both up and down-regulation of gene expression in similar proportions, with a subset of misregulated genes directly bound by dLsd1 (Lepesant et al., 2020). In this study, they assessed histone marks in fly embryonic cells at four dLsd1-bound genes, two up-regulated and two down-regulated. The mark targeted by dLsd1, H3K4me2, increased upon its depletion. Interestingly, none of the other marks tested, H3K4me3, H3K9me2 and H3K27me3 were significantly affected. However, contrary to the case of *dhd*, low-transcribed genes in ovaries were enriched for the H3K27me3 mark while active ones were not, highlighting the enigmatic role of H3K27me3 at the *dhd* locus.

Snr1 is part of the *Drosophila* Swi/Snf remodeler complex, known to oppose Polycomb repression (Kassis et al., 2017; Kingston and Tamkun, 2014; Schuettengruber et al., 2017). In mammalian cells it has been found that mSWI/SNF can actively remove PRC complexes form chromatin thereby counteracting its repression (Kadoch et al., 2017). Surprisingly, we found that upon *snr1* knockdown there is a genome-wide decrease on H3K27me3, suggesting thus that Snr1 could play a role favoring this mark. Interestingly, a

recent study described a role for the mSWI/SNF complex in promoting polycomb repression (Weber et al., 2021). Their model proposes that in the absence of mSWI/SNF, PRC complexes accumulate where mSWI/SNF normally evicts them, thereby causing their redistribution away from heavily occupied sites and causing derepression at these sites. This result illustrates a mechanism where control of one locus can be exerted by effectively maintaining a certain amount of soluble repressive complexes in the cell. It would thus be interesting to measure the composition of soluble regulatory complexes in our knockdown conditions. This could help identify a putative regulator of *dhd* that becomes altered upon our knockdown conditions.

Another level of complexity in the study of the molecular mechanisms promoted by a single factor, comes from the fact that the latter can have different isoforms with different effects. Therefore, the impact on transcription can vary. This is particularly relevant for Mod(mdg4) since ~ 30 isoforms have been identified to date with a common N-Terminal domain (Büchner et al., 2000). Little is known about the impact of Mod(mdg4) depletion on genome-wide transcription. Nonetheless, it has been found that it promotes *Hox* gene activation (Gerasimova et al., 1995; Savitsky et al., 2016). Isoforms other than the insulator isoform 67.2 were found at gene promoters (Melnikova et al., 2019), as is the case for *dhd*, indicating potential targets regulated by specific Mod(mdg4) isoforms. We can wonder if there is a functional significance in having a single gene encoding for such a large number of isoforms. Gabler and colleagues compared *mod(mdg4)* orthologous loci from *D. melanogaster* and *D. virilis* and found and evolutionary conservation of all Mod(mdg4) isoforms (Gabler et al., 2005). The large number of isoforms is thus functionally important in both *Drosophila* species. Additionally, they observed the conservation of the unique C-terminal regions pointing towards a functional differentiation between single isoforms. It would therefore be interesting to assess if, as in *D. melanogaster,* in other species, Mod(mdg4) isoforms can play distinct roles such as insulation and activation.

Emerging evidence, including my study, suggest that the influence of epigenomic effectors on transcriptional outcomes cannot just be categorized as activating or repressing. Most of these factors have pivotal roles depending on cellular context, interactors and targets.

4. An approach to profile regulatory architecture of chromatin domains.

Due to heterogenous cell populations in complex tissues, the study of the chromatin landscape at cell-type specific genes is a major challenge. Great efforts have thus been deployed in the development of single-cell profiling technologies (Lee et al., 2020), opening the possibility to profile chromatin in isolated single cells. Clustering analysis can then be used to retrospectively assign identities to individual cells and give an insight into the epigenomic features of individual cell types. Yet, these approaches suffer from low per-cell throughput, leading to relatively low resolution, high false-negative rates and therefore complicating the interpretations.

Alternatively, the dual-enzyme single-molecule footprinting (dSMF) allows to measure protein-DNA contacts at the level of single molecules (Krebs et al., 2017). This method uses both GpC and CpG DNA methyltransferases to methylate exposed DNA *in vivo*, followed by bisulfite long-read sequencing. With this approach, the occupation of chromatin by nucleosomes, transcription factors and polymerases can be resolved on individual DNA molecules at the scale of several kilobases. While this approach cannot identify the cell of origin of each individual DNA molecule, it can be used to make deductions on the co-occupancy on DNA of different chromatin components. Analogously, the Cut&Run analysis I implemented revealed the co-occupancy on DNA of H3K27me3 nucleosomes and transcription factors at their associated insulators and PREs. This was possible because in Cut&Run, antibody-bound MNase does not restrict its activity to its sole protein target but can rather cleave DNA in spatial proximity of the affected nucleosome.

Similarly, a recent study described the CUTAC method (Henikoff et al., 2020). Authors showed that lowering salt concentrations during antibody tethering in Cut&Tag can reveal H3K4me3-associated DNA regulatory elements (*i.e.*, associated with active chromatin). A relative advantage to our strategy is that histone modifications and regulatory elements can be mapped simultaneously, under a single experimental condition. Yet, compared to CUTAC, our approach presents two likely caveats. First, DNA regulatory inference from Cut&Run is likely to be more difficult to apply to lower input samples, as small cleavage fragments are quite rare compared to nucleosome-sized fragments (1 in 10

approximately). Second, DNA regulatory elements which transcription factor footprint is at least as large as a nucleosome are likely to be missed.

Further exploration of how combination of these approaches may help circumvent the issues associated to each approach. For example, a recent study has combined high-resolution nuclease footprinting with single-molecule methylation profiling (MNase-seq, ORGANIC ChIP, CUT&RUN, and dSMF) to study transcription factor cooperativity at active enhancers on a genome-wide scale in Drosophila embryonic cells. This shows how the combination of different approaches can yield valuable insight on the chromatin regulatory landscape. These are thus promising methods, as they hold the potential to universally map the regulatory landscape around histone modifications, which are universal, opening the possibility to implement them in any tissue or species.

General Conclusion

In almost every animal, the first stages of life depend almost exclusively on maternal products contained in the mature oocyte. Preparation of a competent egg represents an extreme cellular differentiation process where complex transcriptional programs must be tightly regulated. Emerging evidence has highlighted the importance of epigenetic mechanisms in the establishment of the molecular basis of the crucial and complex oocyte-to-zygote transition.

Indeed, the work I presented focused on the intricate regulatory network of epigenomic effectors to achieve hyperactivation of the oocyte-to-zygote effector: the maternal thioredoxin Deadhead. Interestingly, the *dhd* gene can achieve massive levels of transcription with a short regulatory sequence, surrounded by silenced genes, without apparent particular 3D contacts and embedded in a heterochromatic mini-domain. While in different cellular contexts, *dhd* regulators, Lid, Sin3A, Snr1 and Mod(mdg4) have broad effects on transcription, in ovaries, the *dhd* gene represents a hypersensitive target to the loss of any of these factors. The example of *dhd* is thus an illustration of how the activation of a single gene in the right place, at the right time and in the right amount, requires a unique recipe involving a series of factors, that at first glance might not be expected to cooperate.

This study also raises the question of the role of non-canonical heterochromatin domains. Although *dhd* was embedded in an H3K27me3/H3K9me3 mini-domain, these marks were not necessary for its expression in ovaries, nor for its repression in adult tissues. Further studies will be needed to understand the role of these marks, usually mediating transcriptional repression, at actively transcribed genes.

Altogether, my work identified a series of chromatin factors necessary for the establishment of specific transcriptional programs during oogenesis. Importantly, it showed how mechanisms underlying chromatin-based gene regulation are highly dependent on cellular context, interactors of effectors and targeted genes.

References:

Adam M, Robert F, Larochelle M, Gaudreau L. H2A.Z Is Required for Global Chromatin Integrity and for Recruitment of RNA Polymerase II under Specific Conditions. Mol Cell Biol 2001;21:6270–9. https://doi.org/10.1128/MCB.21.18.6270-6279.2001.

Agarwal N, Ansari A. Enhancement of Transcription by a Splicing-Competent Intron Is Dependent on Promoter Directionality. PLoS Genet 2016;12:e1006047. https://doi.org/10.1371/journal.pgen.1006047.

Ahanger SH, Shouche YS, Mishra RK. Functional sub-division of the Drosophila genome via chromatin looping: The emerging importance of CP190. Nucleus 2013;4:115–22. https://doi.org/10.4161/nucl.23389.

Ahmad K, Henikoff S. The Histone Variant H3.3 Marks Active Chromatin by Replication-Independent Nucleosome Assembly. Molecular Cell 2002;9:1191–200. https://doi.org/10.1016/S1097-2765(02)00542-7.

Ahmad K, Spens AE. Separate Polycomb Response Elements control chromatin state and activation of the vestigial gene. PLoS Genet 2019;15:e1007877. https://doi.org/10.1371/journal.pgen.1007877.

Ahn SH, Kim M, Buratowski S. Phosphorylation of Serine 2 within the RNA Polymerase II C-Terminal Domain Couples Transcription and 3′ End Processing. Molecular Cell 2004;13:67–76. https://doi.org/10.1016/S1097-2765(03)00492-1.

Akkouche A, Mugat B, Barckmann B, Varela-Chavez C, Li B, Raffel R, et al. Piwi Is Required during Drosophila Embryogenesis to License Dual-Strand piRNA Clusters for Transposon Repression in Adult Ovaries. Molecular Cell 2017;66:411-419.e4. https://doi.org/10.1016/j.molcel.2017.03.017.

Akmammedov A, Geigges M, Paro R. Bivalency in Drosophila embryos is associated with strong inducibility of Polycomb target genes. Fly (Austin) 2019;13:42–50. https://doi.org/10.1080/19336934.2019.1619438.

Albert B, Léger-Silvestre I, Normand C, Ostermaier MK, Pérez-Fernández J, Panov KI, et al. RNA polymerase I–specific subunits promote polymerase clustering to enhance the rRNA gene transcription cycle. Journal of Cell Biology 2011;192:277–93. https://doi.org/10.1083/jcb.201006040.

Allshire RC, Madhani HD. Ten principles of heterochromatin formation and function. Nat Rev Mol Cell Biol 2018;19:229–44. https://doi.org/10.1038/nrm.2017.119.

Andersen PR, Tirian L, Vunjak M, Brennecke J. A heterochromatin-dependent transcription machinery drives piRNA expression. Nature 2017;549:54–9. https://doi.org/10.1038/nature23482.

Aravin AA, Naumova NM, Tulin AV, Vagin VV, Rozovsky YM, Gvozdev VA. Double-stranded RNA-mediated silencing of genomic tandem repeats and transposable elements in the D. melanogaster germline. Current Biology 2001;11:1017–27. https://doi.org/10.1016/S0960-9822(01)00299-8.

Ardehali MB, Mei A, Zobeck KL, Caron M, Lis JT, Kusch T. *Drosophila* Set1 is the major histone H3 lysine 4 trimethyltransferase with role in transcription: dSet1 is the major H3K4 trimethyltransferase. The EMBO Journal 2011;30:2817–28. https://doi.org/10.1038/emboj.2011.194.

Arents G, Burlingame RW, Wang BC, Love WE, Moudrianakis EN. The nucleosomal core histone octamer at 3.1 A resolution: a tripartite protein assembly and a left-handed superhelix. Proceedings of the National Academy of Sciences 1991;88:10148–52. https://doi.org/10.1073/pnas.88.22.10148.

Arimbasseri AG, Maraia RJ. RNA Polymerase III Advances: Structural and tRNA Functional Views. Trends in Biochemical Sciences 2016;41:546–59. https://doi.org/10.1016/j.tibs.2016.03.003.

Arnér ESJ, Holmgren A. Physiological functions of thioredoxin and thioredoxin reductase: Thioredoxin and thioredoxin reductase. European Journal of Biochemistry 2000;267:6102–9. https://doi.org/10.1046/j.1432-1327.2000.01701.x.

Arnold CD, Gerlach D, Stelzer C, Boryn LM, Rath M, Stark A. Genome-Wide Quantitative Enhancer Activity Maps Identified by STARR-seq. Science 2013;339:1074–7. https://doi.org/10.1126/science.1232542.

Avilés-Pagán EE, Kang ASW, Orr-Weaver TL. Identification of New Regulators of the Oocyte-to-Embryo Transition in *Drosophila*. G3 2020;10:2989–98. https://doi.org/10.1534/g3.120.401415.

Avilés-Pagán EE, Orr-Weaver TL. Activating embryonic development in Drosophila. Seminars in Cell & Developmental Biology 2018;84:100–10. https://doi.org/10.1016/j.semcdb.2018.02.019.

Ayyanathan K. Regulated recruitment of HP1 to a euchromatic gene induces mitotically heritable, epigenetic gene silencing: a mammalian cell culture model of gene variegation. Genes & Development 2003;17:1855–69. https://doi.org/10.1101/gad.1102803.

Banerji J, Rusconi S, Schaffner W. Expression of a β-globin gene is enhanced by remote SV40 DNA sequences. Cell 1981;27:299–308. https://doi.org/10.1016/0092-8674(81)90413-X.

Bannister AJ, Kouzarides T. Regulation of chromatin by histone modifications. Cell Res 2011;21:381–95. https://doi.org/10.1038/cr.2011.22.

Bastock R, St Johnston D. Drosophila oogenesis. Curr Biol 2008;18:R1082-1087. https://doi.org/10.1016/j.cub.2008.09.011.

Becker PB, Workman JL. Nucleosome Remodeling and Epigenetics. Cold Spring Harbor Perspectives in Biology 2013;5:a017905–a017905. https://doi.org/10.1101/cshperspect.a017905.

Bernstein BE, Kamal M, Lindblad-Toh K, Bekiranov S, Bailey DK, Huebert DJ, et al. Genomic Maps and Comparative Analysis of Histone Modifications in Human and Mouse. Cell 2005;120:169–81. https://doi.org/10.1016/j.cell.2005.01.001.

Bernstein BE, Mikkelsen TS, Xie X, Kamal M, Huebert DJ, Cuff J, et al. A bivalent chromatin structure marks key developmental genes in embryonic stem cells. Cell 2006;125:315–26. https://doi.org/10.1016/j.cell.2006.02.041.

Bernstein BE, Tong JK, Schreiber SL. Genomewide studies of histone deacetylase function in yeast. Proceedings of the National Academy of Sciences 2000;97:13708–13. https://doi.org/10.1073/pnas.250477697.

Beuchle D, Struhl G, Muller J. Polycomb group proteins and heritable silencing of Drosophila Hox genes. Development 2001;128:993–1004. https://doi.org/10.1242/dev.128.6.993.

Biswas S, Rao CM. Epigenetic tools (The Writers, The Readers and The Erasers) and their implications in cancer therapy. European Journal of Pharmacology 2018;837:8–24. https://doi.org/10.1016/j.ejphar.2018.08.021.

Blastyák A, Mishra RK, Karch F, Gyurkovics H. Efficient and Specific Targeting of Polycomb Group Proteins Requires Cooperative Interaction between Grainyhead and Pleiohomeotic. Mol Cell Biol 2006;26:1434–44. https://doi.org/10.1128/MCB.26.4.1434-1444.2006.

Boettiger AN, Bintu B, Moffitt JR, Wang S, Beliveau BJ, Fudenberg G, et al. Super-resolution imaging reveals distinct chromatin folding for different epigenetic states. Nature 2016;529:418–22. https://doi.org/10.1038/nature16496.

Bolzer A, Kreth G, Solovei I, Koehler D, Saracoglu K, Fauth C, et al. Three-Dimensional Maps of All Chromosomes in Human Male Fibroblast Nuclei and Prometaphase Rosettes. PLoS Biol 2005;3:e157. https://doi.org/10.1371/journal.pbio.0030157.

Bonev B, Mendelson Cohen N, Szabo Q, Fritsch L, Papadopoulos GL, Lubling Y, et al. Multiscale 3D Genome Rewiring during Mouse Neural Development. Cell 2017;171:557-572.e24. https://doi.org/10.1016/j.cell.2017.09.043.

Bonnefoy E, Orsi GA, Couble P, Loppin B. The Essential Role of Drosophila HIRA for De Novo Assembly of Paternal Chromatin at Fertilization. PLoS Genet 2007;3:e182. https://doi.org/10.1371/journal.pgen.0030182.

Bowman SK, Deaton AM, Domingues H, Wang PI, Sadreyev RI, Kingston RE, et al. H3K27 modifications define segmental regulatory domains in the Drosophila bithorax complex. ELife 2014;3:e02833. https://doi.org/10.7554/eLife.02833.

Brent MM, Anand R, Marmorstein R. Structural Basis for DNA Recognition by FoxO1 and Its Regulation by Posttranslational Modification. Structure 2008;16:1407–16. https://doi.org/10.1016/j.str.2008.06.013.

Brown JL, Kassis JA. Spps, a *Drosophila* Sp1/KLF family member, binds to PREs and is required for PRE activity late in development. Development 2010;137:2597–602. https://doi.org/10.1242/dev.047761.

Bryson-Richardson RJ, Logan DW, Currie PD, Jackson IJ. Large-scale analysis of gene structure in rhodopsin-like GPCRs: evidence for widespread loss of an ancient intron. Gene 2004;338:15–23. https://doi.org/10.1016/j.gene.2004.05.001.

Buchenau P, Hodgson J, Strutt H, Arndt-Jovin DJ. The Distribution of Polycomb-Group Proteins During Cell Division and Development in Drosophila Embryos: Impact on Models for Silencing. Journal of Cell Biology 1998;141:469–81. https://doi.org/10.1083/jcb.141.2.469.

Büchner K, Roth P, Schotta G, Krauss V, Saumweber H, Reuter G, et al. Genetic and Molecular Complexity of the Position Effect Variegation Modifier *mod(mdg4)* in Drosophila. Genetics 2000;155:141–57. https://doi.org/10.1093/genetics/155.1.141.

Bulut-Karslioglu A, Perrera V, Scaranaro M, de la Rosa-Velazquez IA, van de Nobelen S, Shukeir N, et al. A transcription factor–based mechanism for mouse heterochromatin formation. Nat Struct Mol Biol 2012;19:1023–30. https://doi.org/10.1038/nsmb.2382.

Buratowski S. Progression through the RNA Polymerase II CTD Cycle. Molecular Cell 2009;36:541–6. https://doi.org/10.1016/j.molcel.2009.10.019.

Burke TW, Kadonaga JT. Drosophila TFIID binds to a conserved downstream basal promoter element that is present in many TATA-box-deficient promoters. Genes & Development 1996;10:711–24. https://doi.org/10.1101/gad.10.6.711.

Burton A, Brochard V, Galan C, Ruiz-Morales ER, Rovira Q, Rodriguez-Terrones D, et al. Heterochromatin establishment during early mammalian development is regulated by pericentromeric RNA and characterized by non-repressive H3K9me3. Nat Cell Biol 2020;22:767–78. https://doi.org/10.1038/s41556-020-0536-6.

Cairns BR. The logic of chromatin architecture and remodelling at promoters. Nature 2009;461:193–8. https://doi.org/10.1038/nature08450.

Cammas F. Association of the transcriptional corepressor TIF1 with heterochromatin protein 1 (HP1): an essential role for progression through differentiation. Genes & Development 2004;18:2147–60. https://doi.org/10.1101/gad.302904.

Cano-Rodriguez D, Gjaltema RAF, Jilderda LJ, Jellema P, Dokter-Fokkens J, Ruiters MHJ, et al. Writing of H3K4Me3 overcomes epigenetic silencing in a sustained but context-dependent manner. Nat Commun 2016;7:12284. https://doi.org/10.1038/ncomms12284.

Cao R, Wang L, Wang H, Xia L, Erdjument-Bromage H, Tempst P, et al. Role of Histone H3 Lysine 27 Methylation in Polycomb-Group Silencing. Science 2002;298:1039–43. https://doi.org/10.1126/science.1076997.

Carey M, Li B, Workman JL. RSC Exploits Histone Acetylation to Abrogate the Nucleosomal Block to RNA Polymerase II Elongation. Molecular Cell 2006;24:481–7. https://doi.org/10.1016/j.molcel.2006.09.012.

Carrozza MJ, Li B, Florens L, Suganuma T, Swanson SK, Lee KK, et al. Histone H3 Methylation by Set2 Directs Deacetylation of Coding Regions by Rpd3S to Suppress Spurious Intragenic Transcription. Cell 2005;123:581–92. https://doi.org/10.1016/j.cell.2005.10.023.

Cattoni DI, Cardozo Gizzi AM, Georgieva M, Di Stefano M, Valeri A, Chamousset D, et al. Single-cell absolute contact probability detection reveals chromosomes are organized by multiple low-frequency yet specific interactions. Nat Commun 2017;8:1753. https://doi.org/10.1038/s41467-017-01962-x.

Cesarini E, Mozzetta C, Marullo F, Gregoretti F, Gargiulo A, Columbaro M, et al. Lamin A/C sustains PcG protein architecture, maintaining transcriptional repression at target genes. Journal of Cell Biology 2015;211:533–51. https://doi.org/10.1083/jcb.201504035.

Chaubal A, Pile LA. Same agent, different messages: insight into transcriptional regulation by SIN3 isoforms. Epigenetics & Chromatin 2018;11:17. https://doi.org/10.1186/s13072-018-0188-y.

Cho W-K, Spille J-H, Hecht M, Lee C, Li C, Grube V, et al. Mediator and RNA polymerase II clusters associate in transcription-dependent condensates. Science 2018;361:412–5. https://doi.org/10.1126/science.aar4199.

Chubb JR, Trcek T, Shenoy SM, Singer RH. Transcriptional Pulsing of a Developmental Gene. Current Biology 2006;16:1018–25. https://doi.org/10.1016/j.cub.2006.03.092.

Clapier CR, Cairns BR. The Biology of Chromatin Remodeling Complexes. Annu Rev Biochem 2009;78:273–304. https://doi.org/10.1146/annurev.biochem.77.062706.153223.

Claycomb J, Orrweaver T. Developmental gene amplification: insights into DNA replication and gene expression. Trends in Genetics 2005;21:149–62. https://doi.org/10.1016/j.tig.2005.01.009.

Cramer P. Organization and regulation of gene transcription. Nature 2019;573:45–54. https://doi.org/10.1038/s41586-019-1517-4.

Cubeñas-Potts C, Rowley MJ, Lyu X, Li G, Lei EP, Corces VG. Different enhancer classes in Drosophila bind distinct architectural proteins and mediate unique chromatin interactions and 3D architecture. Nucleic Acids Research 2017;45:1714–30. https://doi.org/10.1093/nar/gkw1114.

Curry E, Zeller C, Masrour N, Patten DK, Gallon J, Wilhelm-Benartzi CS, et al. Genes Predisposed to DNA Hypermethylation during Acquired Resistance to Chemotherapy Are Identified in Ovarian Tumors by Bivalent Chromatin Domains at Initial Diagnosis. Cancer Res 2018;78:1383–91. https://doi.org/10.1158/0008-5472.CAN-17-1650.

Czermin B, Melfi R, McCabe D, Seitz V, Imhof A, Pirrotta V. Drosophila Enhancer of Zeste/ESC Complexes Have a Histone H3 Methyltransferase Activity that Marks Chromosomal Polycomb Sites. Cell 2002;111:185–96. https://doi.org/10.1016/S0092-8674(02)00975-3.

van Daal A, White EM, Gorovsky MA, Elgin CR. *Drosophila* has a single copy of the gene encoding a highly conserved histone H2A variant of the H2A. F/Z type. Nucl Acids Res 1988;16:7487–97. https://doi.org/10.1093/nar/16.15.7487.

Das TK, Sangodkar J, Negre N, Narla G, Cagan RL. Sin3a acts through a multi-gene module to regulate invasion in Drosophila and human tumors. Oncogene 2013;32:3184–97. https://doi.org/10.1038/onc.2012.326.

Davidson, E. Gene Activity in Early Development. Academic Press, Orlando, FL; 1986.
De S, Gehred ND, Fujioka M, Chan FW, Jaynes JB, Kassis JA. Defining the Boundaries of Polycomb Domains in *Drosophila*. Genetics 2020;216:689–700. https://doi.org/10.1534/genetics.120.303642.

Deal RB, Henikoff JG, Henikoff S. Genome-Wide Kinetics of Nucleosome Turnover Determined by Metabolic Labeling of Histones. Science 2010;328:1161–4. https://doi.org/10.1126/science.1186777.

Deaton AM, Gómez-Rodríguez M, Mieczkowski J, Tolstorukov MY, Kundu S, Sadreyev RI, et al. Enhancer regions show high histone H3.3 turnover that changes during differentiation. ELife 2016;5:e15316. https://doi.org/10.7554/eLife.15316.

Dej KJ, Spradling AC. Nurse cell chromosome reorganization 1999:11.
Déjardin J, Rappailles A, Cuvier O, Grimaud C, Decoville M, Locker D, et al. Recruitment of Drosophila Polycomb group proteins to chromatin by DSP1. Nature 2005;434:533–8. https://doi.org/10.1038/nature03386.

Delattre M, Spierer A, Tonka CH, Spierer P. The genomic silencing of position-effect variegation in Drosophila melanogaster: interaction between the heterochromatin-associated proteins Su(var)3-7 and HP1. J Cell Sci 2000;113 Pt 23:4253–61.

DeLuca SZ, Ghildiyal M, Niu W, Pang L-Y, Spradling AC. Differentiating Drosophila female germ cells initiate Polycomb silencing by altering PRC2 sampling. Developmental Biology; 2020. https://doi.org/10.1101/2020.02.03.932582.

Deng WM, Althauser C, Ruohola-Baker H. Notch-Delta signaling induces a transition from mitotic cell cycle to endocycle in Drosophila follicle cells. Development 2001;128:4737–46.
de Wit E, Vos ESM, Holwerda SJB, Valdes-Quezada C, Verstegen MJAM, Teunissen H, et al. CTCF Binding Polarity Determines Chromatin Looping. Molecular Cell 2015;60:676–84. https://doi.org/10.1016/j.molcel.2015.09.023.

Di Stefano L, Walker JA, Burgio G, Corona DFV, Mulligan P, Naar AM, et al. Functional antagonism between histone H3K4 demethylases in vivo. Genes & Development 2011;25:17–28. https://doi.org/10.1101/gad.1983711.

Dingwall AK, Beek SJ, McCallum CM, Tamkun JW, Kalpana GV, Goff SP, et al. The Drosophila snr1 and brm proteins are related to yeast SWI/SNF proteins and are components of a large protein complex. MBoC 1995;6:777–91. https://doi.org/10.1091/mbc.6.7.777.

Dixon JR, Selvaraj S, Yue F, Kim A, Li Y, Shen Y, et al. Topological domains in mammalian genomes identified by analysis of chromatin interactions. Nature 2012;485:376–80. https://doi.org/10.1038/nature11082.

Doenecke D, Albig W. Intronless Genes. In: John Wiley & Sons, Ltd, editor. Encyclopedia of Life Sciences, Chichester: John Wiley & Sons, Ltd; 2005, p. a0005022. https://doi.org/10.1038/npg.els.0005022.

Dorafshan E, Kahn TG, Schwartz YB. Hierarchical recruitment of Polycomb complexes revisited. Nucleus 2017;8:496–505. https://doi.org/10.1080/19491034.2017.1363136.

Dorn R, Krauss V, Reuter G, Saumweber H. The enhancer of position-effect variegation of Drosophila, E(var)3-93D, codes for a chromatin protein containing a conserved domain common to several transcriptional regulators. PNAS 1993;90:11376–80. https://doi.org/10.1073/pnas.90.23.11376.

Douillet D, Sze CC, Ryan C, Piunti A, Shah AP, Ugarenko M, et al. Uncoupling histone H3K4 trimethylation from developmental gene expression via an equilibrium of COMPASS, Polycomb and DNA methylation. Nat Genet 2020;52:615–25. https://doi.org/10.1038/s41588-020-0618-1.

Drelon C, Belalcazar HM, Secombe J. The Histone Demethylase KDM5 Is Essential for Larval Growth in *Drosophila*. Genetics 2018:genetics.301004.2018. https://doi.org/10.1534/genetics.118.301004.

Drouin S, Laramée L, Jacques P-É, Forest A, Bergeron M, Robert F. DSIF and RNA Polymerase II CTD Phosphorylation Coordinate the Recruitment of Rpd3S to Actively Transcribed Genes. PLoS Genet 2010;6:e1001173. https://doi.org/10.1371/journal.pgen.1001173.

Du Z, Zheng H, Huang B, Ma R, Wu J, Zhang Xianglin, et al. Allelic reprogramming of 3D chromatin architecture during early mammalian development. Nature 2017;547:232–5. https://doi.org/10.1038/nature23263.

Duret L, Mouchiroud D. Expression pattern and, surprisingly, gene length shape codon usage in Caenorhabditis, Drosophila, and Arabidopsis. Proceedings of the National Academy of Sciences 1999;96:4482–7. https://doi.org/10.1073/pnas.96.8.4482.

Dwyer K, Agarwal N, Pile L, Ansari A. Gene Architecture Facilitates Intron-Mediated Enhancement of Transcription. Front Mol Biosci 2021;8:669004. https://doi.org/10.3389/fmolb.2021.669004.

Ecco G, Cassano M, Kauzlaric A, Duc J, Coluccio A, Offner S, et al. Transposable Elements and Their KRAB-ZFP Controllers Regulate Gene Expression in Adult Tissues. Developmental Cell 2016;36:611–23. https://doi.org/10.1016/j.devcel.2016.02.024.

Egloff S, Dienstbier M, Murphy S. Updating the RNA polymerase CTD code: adding gene-specific layers. Trends in Genetics 2012;28:333–41. https://doi.org/10.1016/j.tig.2012.03.007.

Egloff S, O'Reilly D, Chapman RD, Taylor A, Tanzhaus K, Pitts L, et al. Serine-7 of the RNA Polymerase II CTD Is Specifically Required for snRNA Gene Expression. Science 2007;318:1777–9. https://doi.org/10.1126/science.1145989.

Eichhorn SW, Subtelny AO, Kronja I, Kwasnieski JC, Orr-Weaver TL, Bartel DP. mRNA poly(A)-tail changes specified by deadenylation broadly reshape translation in Drosophila oocytes and early embryos. ELife 2016;5:e16955. https://doi.org/10.7554/eLife.16955.

Emelyanov AV, Fyodorov DV. Thioredoxin-dependent disulfide bond reduction is required for protamine eviction from sperm chromatin. Genes Dev 2016;30:2651–6. https://doi.org/10.1101/gad.290916.116.

Erceg J, Pakozdi T, Marco-Ferreres R, Ghavi-Helm Y, Girardot C, Bracken AP, et al. Dual functionality of *cis* -regulatory elements as developmental enhancers and Polycomb response elements. Genes Dev 2017;31:590–602. https://doi.org/10.1101/gad.292870.116.

Eskeland R, Eberharter A, Imhof A. HP1 Binding to Chromatin Methylated at H3K9 Is Enhanced by Auxiliary Factors. Mol Cell Biol 2007;27:453–65. https://doi.org/10.1128/MCB.01576-06.

Esnault C, Ghavi-Helm Y, Brun S, Soutourina J, Van Berkum N, Boschiero C, et al. Mediator-Dependent Recruitment of TFIIH Modules in Preinitiation Complex. Molecular Cell 2008;31:337–46. https://doi.org/10.1016/j.molcel.2008.06.021.

Eychenne T, Novikova E, Barrault M-B, Alibert O, Boschiero C, Peixeiro N, et al. Functional interplay between Mediator and TFIIB in preinitiation complex assembly in relation to promoter architecture. Genes Dev 2016;30:2119–32. https://doi.org/10.1101/gad.285775.116.

Ferreira H, Flaus A, Owen-Hughes T. Histone Modifications Influence the Action of Snf2 Family Remodelling Enzymes by Different Mechanisms. Journal of Molecular Biology 2007;374:563–79. https://doi.org/10.1016/j.jmb.2007.09.059.

Fischer T, Cui B, Dhakshnamoorthy J, Zhou M, Rubin C, Zofall M, et al. Diverse roles of HP1 proteins in heterochromatin assembly and functions in fission yeast. Proceedings of the National Academy of Sciences 2009;106:8998–9003. https://doi.org/10.1073/pnas.0813063106.

FitzGerald PC, Sturgill D, Shyakhtenko A, Oliver B, Vinson C. Comparative genomics of Drosophila and human core promoters. Genome Biol 2006;7:R53. https://doi.org/10.1186/gb-2006-7-7-r53.

Flavahan WA, Drier Y, Liau BB, Gillespie SM, Venteicher AS, Stemmer-Rachamimov AO, et al. Insulator dysfunction and oncogene activation in IDH mutant gliomas. Nature 2016;529:110–4. https://doi.org/10.1038/nature16490.

Franke M, Ibrahim DM, Andrey G, Schwarzer W, Heinrich V, Schöpflin R, et al. Formation of new chromatin domains determines pathogenicity of genomic duplications. Nature 2016;538:265–9. https://doi.org/10.1038/nature19800.

Freier R, Aragón E, Bagiński B, Pluta R, Martin-Malpartida P, Ruiz L, et al. Structures of the germline-specific Deadhead and thioredoxin T proteins from *Drosophila melanogaster* reveal unique features among thioredoxins. IUCrJ 2021;8:281–94. https://doi.org/10.1107/S2052252521000221.

Fudenberg G, Abdennur N, Imakaev M, Goloborodko A, Mirny LA. Emerging Evidence of Chromosome Folding by Loop Extrusion. Cold Spring Harb Symp Quant Biol 2017;82:45–55. https://doi.org/10.1101/sqb.2017.82.034710.

Fudenberg G, Imakaev M, Lu C, Goloborodko A, Abdennur N, Mirny LA. Formation of Chromosomal Domains by Loop Extrusion. Cell Reports 2016;15:2038–49. https://doi.org/10.1016/j.celrep.2016.04.085.

Fujioka M, Sun G, Jaynes JB. The Drosophila eve Insulator Homie Promotes eve Expression and Protects the Adjacent Gene from Repression by Polycomb Spreading. PLoS Genet 2013;9:e1003883. https://doi.org/10.1371/journal.pgen.1003883.

Fukaya T, Lim B, Levine M. Enhancer Control of Transcriptional Bursting. Cell 2016;166:358–68. https://doi.org/10.1016/j.cell.2016.05.025.

Furger A, O'Sullivan JM, Binnie A, Lee BA, Proudfoot NJ. Promoter proximal splice sites enhance transcription. Genes Dev 2002;16:2792–9. https://doi.org/10.1101/gad.983602.

Gabler M, Volkmar M, Weinlich S, Herbst A, Dobberthien P, Sklarss S, et al. Trans-splicing of the mod(mdg4) Complex Locus Is Conserved Between the Distantly Related Species Drosophila melanogaster and D. virilis. Genetics 2005;169:723–36. https://doi.org/10.1534/genetics.103.020842.

Gaertner B, Johnston J, Chen K, Wallaschek N, Paulson A, Garruss AS, et al. Poised RNA Polymerase II Changes over Developmental Time and Prepares Genes for Future Expression. Cell Reports 2012;2:1670–83. https://doi.org/10.1016/j.celrep.2012.11.024.

Gajan A, Barnes VL, Liu M, Saha N, Pile LA. The histone demethylase dKDM5/LID interacts with the SIN3 histone deacetylase complex and shares functional similarities with SIN3. Epigenetics & Chromatin 2016;9:4. https://doi.org/10.1186/s13072-016-0053-9.

Ganapathi M, Srivastava P, Sutar S, Kumar K, Dasgupta D, Pal Singh G, et al. Comparative analysis of chromatin landscape in regulatory regions of human housekeeping and tissue specific genes. BMC Bioinformatics 2005;6:126. https://doi.org/10.1186/1471-2105-6-126.

Garcia JF, Dumesic PA, Hartley PD, El-Samad H, Madhani HD. Combinatorial, site-specific requirement for heterochromatic silencing factors in the elimination of nucleosome-free regions. Genes & Development 2010;24:1758–71. https://doi.org/10.1101/gad.1946410.

Gates LA, Foulds CE, O'Malley BW. Histone Marks in the 'Driver's Seat': Functional Roles in Steering the Transcription Cycle. Trends in Biochemical Sciences 2017;42:977–89. https://doi.org/10.1016/j.tibs.2017.10.004.

Georgiev PG, Gerasimova TI. Novel genes influencing the expression of the yellow locus and mdg4 (gypsy) in Drosophila melanogaster. Molec Gen Genet 1989;220:121–6. https://doi.org/10.1007/BF00260865.

Gerasimova TI, Corces VG. Polycomb and Trithorax Group Proteins Mediate the Function of a Chromatin Insulator. Cell 1998;92:511–21. https://doi.org/10.1016/S0092-8674(00)80944-7.

Gerasimova TI, Gdula DA, Gerasimov DV, Simonova O, Corces VG. A drosophila protein that imparts directionality on a chromatin insulator is an enhancer of position-effect variegation. Cell 1995;82:587–97. https://doi.org/10.1016/0092-8674(95)90031-4.

Ghosh SK, Jost D. How epigenome drives chromatin folding and dynamics, insights from efficient coarse-grained models of chromosomes. PLoS Comput Biol 2018;14:e1006159. https://doi.org/10.1371/journal.pcbi.1006159.

Goldberg AD, Banaszynski LA, Noh K-M, Lewis PW, Elsaesser SJ, Stadler S, et al. Distinct Factors Control Histone Variant H3.3 Localization at Specific Genomic Regions. Cell 2010;140:678–91. https://doi.org/10.1016/j.cell.2010.01.003.

Gorgoni B. The roles of cytoplasmic poly(A)-binding proteins in regulating gene expression: A developmental perspective. Briefings in Functional Genomics and Proteomics 2004;3:125–41. https://doi.org/10.1093/bfgp/3.2.125.

Gu B, Lee M. Histone H3 lysine 4 methyltransferases and demethylases in self-renewal and differentiation of stem cells. Cell Biosci 2013;3:39. https://doi.org/10.1186/2045-3701-3-39.

Guenther MG, Levine SS, Boyer LA, Jaenisch R, Young RA. A Chromatin Landmark and Transcription Initiation at Most Promoters in Human Cells. Cell 2007;130:77–88. https://doi.org/10.1016/j.cell.2007.05.042.

Guillemette B, Bataille AR, Gévry N, Adam M, Blanchett

e M, Robert F, et al. Variant Histone H2A.Z Is Globally Localized to the Promoters of Inactive Yeast Genes and Regulates Nucleosome Positioning. PLoS Biol 2005;3:e384. https://doi.org/10.1371/journal.pbio.0030384.

Guo Y, Xu Q, Canzio D, Shou J, Li J, Gorkin DU, et al. CRISPR Inversion of CTCF Sites Alters Genome Topology and Enhancer/Promoter Function. Cell 2015;162:900–10. https://doi.org/10.1016/j.cell.2015.07.038.

Gurudatta BV, Corces VG. Chromatin insulators: lessons from the fly. Briefings in Functional Genomics and Proteomics 2009;8:276–82. https://doi.org/10.1093/bfgp/elp032.
Haberle V, Stark A. Eukaryotic core promoters and the functional basis of transcription initiation. Nat Rev Mol Cell Biol 2018;19:621–37. https://doi.org/10.1038/s41580-018-0028-8.

Hall AW, Battenhouse AM, Shivram H, Morris AR, Cowperthwaite MC, Shpak M, et al. Bivalent Chromatin Domains in Glioblastoma Reveal a Subtype-Specific Signature of Glioma Stem Cells. Cancer Res 2018;78:2463–74. https://doi.org/10.1158/0008-5472.CAN-17-1724.

Hall IM. Establishment and Maintenance of a Heterochromatin Domain. Science 2002;297:2232–7. https://doi.org/10.1126/science.1076466.

Hammond CM. Histone chaperone networks shaping chromatin function 2017:18.
Hammond MP, Laird CD. Chromosome structure and DNA replication in nurse and follicle cells of Drosophila melanogaster. Chromosoma 1985;91:267–78. https://doi.org/10.1007/BF00328222.

Harvey AJ, Bidwai AP, Miller LK. Doom, a product of the Drosophila mod(mdg4) gene, induces apoptosis and binds to baculovirus inhibitor-of-apoptosis proteins. Mol Cell Biol 1997;17:2835–43. https://doi.org/10.1128/MCB.17.5.2835.

Heintzman ND, Stuart RK, Hon G, Fu Y, Ching CW, Hawkins RD, et al. Distinct and predictive chromatin signatures of transcriptional promoters and enhancers in the human genome. Nat Genet 2007;39:311–8. https://doi.org/10.1038/ng1966.

Henikoff S, Henikoff JG, Kaya-Okur HS, Ahmad K. Efficient chromatin accessibility mapping *in situ* by nucleosome-tethered tagmentation. Genomics; 2020. https://doi.org/10.1101/2020.04.15.043083.

Henikoff S, Henikoff JG, Sakai A, Loeb GB, Ahmad K. Genome-wide profiling of salt fractions maps physical properties of chromatin. Genome Research 2008;19:460–9. https://doi.org/10.1101/gr.087619.108.

Henry KW. Transcriptional activation via sequential histone H2B ubiquitylation and deubiquitylation, mediated by SAGA-associated Ubp8. Genes & Development 2003;17:2648–63. https://doi.org/10.1101/gad.1144003.

Hödl M, Basler K. Transcription in the Absence of Histone H3.2 and H3K4 Methylation. Current Biology 2012;22:2253–7. https://doi.org/10.1016/j.cub.2012.10.008.

Hoffmann NA, Jakobi AJ, Moreno-Morcillo M, Glatt S, Kosinski J, Hagen WJH, et al. Molecular structures of unbound and transcribing RNA polymerase III. Nature 2015;528:231–6. https://doi.org/10.1038/nature16143.

Horard B, Loppin B. Fécondation: Le noyau spermatique déverrouillé par une thiorédoxine ultraspécialisée. Med Sci (Paris) 2017;33:585–7. https://doi.org/10.1051/medsci/20173306009.

Horner VL, Wolfner MF. Transitioning from egg to embryo: Triggers and mechanisms of egg activation. Dev Dyn 2008;237:527–44. https://doi.org/10.1002/dvdy.21454.

Hornung G, Bar-Ziv R, Rosin D, Tokuriki N, Tawfik DS, Oren M, et al. Noise-mean relationship in mutated promoters. Genome Research 2012;22:2409–17. https://doi.org/10.1101/gr.139378.112.

Howe FS, Fischl H, Murray SC, Mellor J. Is H3K4me3 instructive for transcription activation? BioEssays 2017;39:e201600095. https://doi.org/10.1002/bies.201600095.

Hsin J-P, Manley JL. The RNA polymerase II CTD coordinates transcription and RNA processing. Genes & Development 2012;26:2119–37. https://doi.org/10.1101/gad.200303.112.

Hug CB, Grimaldi AG, Kruse K, Vaquerizas JM. Chromatin Architecture Emerges during Zygotic Genome Activation Independent of Transcription. Cell 2017;169:216-228.e19. https://doi.org/10.1016/j.cell.2017.03.024.

Imbeault M, Helleboid P-Y, Trono D. KRAB zinc-finger proteins contribute to the evolution of gene regulatory networks. Nature 2017;543:550–4. https://doi.org/10.1038/nature21683.

Iovino N, Ciabrelli F, Cavalli G. PRC2 controls Drosophila oocyte cell fate by repressing cell cycle genes. Dev Cell 2013;26:431–9. https://doi.org/10.1016/j.devcel.2013.06.021.

Ito H, Sato K, Koganezawa M, Ote M, Matsumoto K, Hama C, et al. Fruitless Recruits Two Antagonistic Chromatin Factors to Establish Single-Neuron Sexual Dimorphism. Cell 2012;149:1327–38. https://doi.org/10.1016/j.cell.2012.04.025.

Ivanov AV, Peng H, Yurchenko V, Yap KL, Negorev DG, Schultz DC, et al. PHD Domain-Mediated E3 Ligase Activity Directs Intramolecular Sumoylation of an Adjacent Bromodomain Required for Gene Silencing. Molecular Cell 2007;28:823–37. https://doi.org/10.1016/j.molcel.2007.11.012.

J. Svensson M, Larsson J. Thioredoxin-2 affects lifespan and oxidative stress in Drosophila: Thioredoxins in Drosophila. Hereditas 2007;144:25–32. https://doi.org/10.1111/j.2007.0018-0661.01990.x.

Jacobs SA, Taverna SD, Zhang Y, Briggs SD, Li J, Eissenberg JC, et al. Specificity of the HP1 chromo domain for the methylated N-terminus of histone H3. EMBO J 2001;20:5232–41. https://doi.org/10.1093/emboj/20.18.5232.

Jiang C, Pugh BF. Nucleosome positioning and gene regulation: advances through genomics. Nat Rev Genet 2009;10:161–72. https://doi.org/10.1038/nrg2522.

Jiang Z, Zhang B. On the role of transcription in positioning nucleosomes. PLoS Comput Biol 2021;17:e1008556. https://doi.org/10.1371/journal.pcbi.1008556.

Jost D, Carrivain P, Cavalli G, Vaillant C. Modeling epigenome folding: formation and dynamics of topologically associated chromatin domains. Nucleic Acids Research 2014;42:9553–61. https://doi.org/10.1093/nar/gku698.

Kadamb R, Mittal S, Bansal N, Batra H, Saluja D. Sin3: Insight into its transcription regulatory functions. European Journal of Cell Biology 2013;92:237–46. https://doi.org/10.1016/j.ejcb.2013.09.001.

Kadoch C, Crabtree GR. Mammalian SWI/SNF chromatin remodeling complexes and cancer: Mechanistic insights gained from human genomics. Sci Adv 2015;1:e1500447. https://doi.org/10.1126/sciadv.1500447.

Kadoch C, Williams RT, Calarco JP, Miller EL, Weber CM, Braun SMG, et al. Dynamics of BAF–Polycomb complex opposition on heterochromatin in normal and oncogenic states. Nat Genet 2017;49:213–22. https://doi.org/10.1038/ng.3734.

Kahn TG, Dorafshan E, Schultheis D, Zare A, Stenberg P, Reim I, et al. Interdependence of PRC1 and PRC2 for recruitment to Polycomb Response Elements. Nucleic Acids Res 2016:gkw701. https://doi.org/10.1093/nar/gkw701.

Kahn TG, Schwartz YB, Dellino GI, Pirrotta V. Polycomb Complexes and the Propagation of the Methylation Mark at the Drosophila Ubx Gene. Journal of Biological Chemistry 2006;281:29064–75. https://doi.org/10.1074/jbc.M605430200.

Kao C-F. Rad6 plays a role in transcriptional activation through ubiquitylation of histone H2B. Genes & Development 2004;18:184–95. https://doi.org/10.1101/gad.1149604.

Karimi MM, Goyal P, Maksakova IA, Bilenky M, Leung D, Tang JX, et al. DNA Methylation and SETDB1/H3K9me3 Regulate Predominantly Distinct Sets of Genes, Retroelements, and Chimeric Transcripts in mESCs. Cell Stem Cell 2011;8:676–87. https://doi.org/10.1016/j.stem.2011.04.004.

Kassis JA, Brown JL. Polycomb Group Response Elements in Drosophila and Vertebrates. Advances in Genetics, vol. 81, Elsevier; 2013, p. 83–118. https://doi.org/10.1016/B978-0-12-407677-8.00003-8.

Kassis JA, Kennison JA, Tamkun JW. Polycomb and Trithorax Group Genes in *Drosophila*. Genetics 2017;206:1699–725. https://doi.org/10.1534/genetics.115.185116.

Ke Y, Xu Y, Chen X, Feng S, Liu Z, Sun Y, et al. 3D Chromatin Structures of Mature Gametes and Structural Reprogramming during Mammalian Embryogenesis. Cell 2017;170:367-381.e20. https://doi.org/10.1016/j.cell.2017.06.029.

Keller C, Adaixo R, Stunnenberg R, Woolcock KJ, Hiller S, Bühler M. HP1Swi6 Mediates the Recognition and Destruction of Heterochromatic RNA Transcripts. Molecular Cell 2012;47:215–27. https://doi.org/10.1016/j.molcel.2012.05.009.

King, RC. Ovarian development in Drosophila melanogaster. New York. Academic.; 1970.
Kingston RE, Tamkun JW. Transcriptional Regulation by Trithorax-Group Proteins. Cold Spring Harbor Perspectives in Biology 2014;6:a019349–a019349. https://doi.org/10.1101/cshperspect.a019349.

Klattenhoff C, Xi H, Li C, Lee S, Xu J, Khurana JS, et al. The Drosophila HP1 Homolog Rhino Is Required for Transposon Silencing and piRNA Production by Dual-Strand Clusters. Cell 2009;138:1137–49. https://doi.org/10.1016/j.cell.2009.07.014.

Klymenko T, Müller J. The histone methyltransferases Trithorax and Ash1 prevent transcriptional silencing by Polycomb group proteins. EMBO Rep 2004;5:373–7. https://doi.org/10.1038/sj.embor.7400111.

Kochetov AV, Ponomarenko MP, Frolov AS, Kisselev LL, Kolchanov NA. Prediction of eukaryotic mRNA translational properties. Bioinformatics 1999;15:704–12. https://doi.org/10.1093/bioinformatics/15.7.704.

Krebs AR, Imanci D, Hoerner L, Gaidatzis D, Burger L, Schübeler D. Genome-wide Single-Molecule Footprinting Reveals High RNA Polymerase II Turnover at Paused Promoters. Molecular Cell 2017;67:411-422.e4. https://doi.org/10.1016/j.molcel.2017.06.027.

Kronja I, Whitfield ZJ, Yuan B, Dzeyk K, Kirkpatrick J, Krijgsveld J, et al. Quantitative proteomics reveals the dynamics of protein changes during *Drosophila* oocyte maturation and the oocyte-to-embryo transition. Proc Natl Acad Sci USA 2014;111:16023–8. https://doi.org/10.1073/pnas.1418657111.

Kubik S, Bruzzone MJ, Jacquet P, Falcone J-L, Rougemont J, Shore D. Nucleosome Stability Distinguishes Two Different Promoter Types at All Protein-Coding Genes in Yeast. Molecular Cell 2015;60:422–34. https://doi.org/10.1016/j.molcel.2015.10.002.

Kusch T, Mei A, Nguyen C. Histone H3 lysine 4 trimethylation regulates cotranscriptional H2A variant exchange by Tip60 complexes to maximize gene expression. Proc Natl Acad Sci USA 2014;111:4850–5. https://doi.org/10.1073/pnas.1320337111.

Kutach AK, Kadonaga JT. The Downstream Promoter Element DPE Appears To Be as Widely Used as the TATA Box in *Drosophila* Core Promoters. Mol Cell Biol 2000;20:4754–64. https://doi.org/10.1128/MCB.20.13.4754-4764.2000.

Kuzmichev A. Histone methyltransferase activity associated with a human multiprotein complex containing the Enhancer of Zeste protein. Genes & Development 2002;16:2893–905. https://doi.org/10.1101/gad.1035902.

Kyrchanova O, Georgiev P. Chromatin insulators and long-distance interactions in *Drosophila*. FEBS Letters 2014;588:8–14. https://doi.org/10.1016/j.febslet.2013.10.039.

Larson AG, Elnatan D, Keenen MM, Trnka MJ, Johnston JB, Burlingame AL, et al. Liquid droplet formation by HP1α suggests a role for phase separation in heterochromatin. Nature 2017;547:236–40. https://doi.org/10.1038/nature22822.

Lauberth SM, Nakayama T, Wu X, Ferris AL, Tang Z, Hughes SH, et al. H3K4me3 Interactions with TAF3 Regulate Preinitiation Complex Assembly and Selective Gene Activation. Cell 2013;152:1021–36. https://doi.org/10.1016/j.cell.2013.01.052.

Lavarone E, Barbieri CM, Pasini D. Dissecting the role of H3K27 acetylation and methylation in PRC2 mediated control of cellular identity. Nat Commun 2019;10:1679. https://doi.org/10.1038/s41467-019-09624-w.

Lee C-K, Shibata Y, Rao B, Strahl BD, Lieb JD. Evidence for nucleosome depletion at active regulatory regions genome-wide. Nat Genet 2004;36:900–5. https://doi.org/10.1038/ng1400.

Lee J, Hyeon DY, Hwang D. Single-cell multiomics: technologies and data analysis methods. Exp Mol Med 2020;52:1428–42. https://doi.org/10.1038/s12276-020-0420-2.

Lepesant JMJ, Iampietro C, Galeota E, Augé B, Aguirrenbengoa M, Mercé C, et al. A dual role of dLsd1 in oogenesis: regulating developmental genes and repressing transposons. Nucleic Acids Research 2020;48:1206–24. https://doi.org/10.1093/nar/gkz1142.

Lesch BJ, Dokshin GA, Young RA, McCarrey JR, Page DC. A set of genes critical to development is epigenetically poised in mouse germ cells from fetal stages through completion of meiosis. Proceedings of the National Academy of Sciences 2013;110:16061–6. https://doi.org/10.1073/pnas.1315204110.

Lhoumaud P, Hennion M, Gamot A, Cuddapah S, Queille S, Liang J, et al. Insulators recruit histone methyltransferase dMes4 to regulate chromatin of flanking genes. The EMBO Journal 2014;33:1599–613. https://doi.org/10.15252/embj.201385965.

Li B, Gogol M, Carey M, Lee D, Seidel C, Workman JL. Combined Action of PHD and Chromo Domains Directs the Rpd3S HDAC to Transcribed Chromatin. Science 2007;316:1050–4. https://doi.org/10.1126/science.1139004.

Li H, Liefke R, Jiang J, Kurland JV, Tian W, Deng P, et al. Polycomb-like proteins link the PRC2 complex to CpG islands. Nature 2017;549:287–91. https://doi.org/10.1038/nature23881.

Li L, Greer C, Eisenman RN, Secombe J. Essential Functions of the Histone Demethylase Lid. PLoS Genetics 2010;6:e1001221. https://doi.org/10.1371/journal.pgen.1001221.

Lianoglou S, Garg V, Yang JL, Leslie CS, Mayr C. Ubiquitously transcribed genes use alternative polyadenylation to achieve tissue-specific expression. Genes & Development 2013;27:2380–96. https://doi.org/10.1101/gad.229328.113.

Lieberman-Aiden E, van Berkum NL, Williams L, Imakaev M, Ragoczy T, Telling A, et al. Comprehensive Mapping of Long-Range Interactions Reveals Folding Principles of the Human Genome. Science 2009;326:289–93. https://doi.org/10.1126/science.1181369.

Lim J, Lee M, Son A, Chang H, Kim VN. mTAIL-seq reveals dynamic poly(A) tail regulation in oocyte-to-embryo development. Genes Dev 2016;30:1671–82. https://doi.org/10.1101/gad.284802.116.

Liu X, Greer C, Secombe J. KDM5 Interacts with Foxo to Modulate Cellular Levels of Oxidative Stress. PLoS Genetics 2014;10:e1004676. https://doi.org/10.1371/journal.pgen.1004676.

Liu X, Secombe J. The Histone Demethylase KDM5 Activates Gene Expression by Recognizing Chromatin Context through Its PHD Reader Motif. Cell Reports 2015;13:2219–31. https://doi.org/10.1016/j.celrep.2015.11.007.

Lloret-Llinares M, Pérez-Lluch S, Rossell D, Morán T, Ponsa-Cobas J, Auer H, et al. dKDM5/LID regulates H3K4me3 dynamics at the transcription-start site (TSS) of actively transcribed developmental genes. Nucleic Acids Res 2012;40:9493–505. https://doi.org/10.1093/nar/gks773.

Lobanenkov VV, Nicolas RH, Adler VV, Paterson H, Klenova EM, Polotskaja AV, et al. A novel sequence-specific DNA binding protein which interacts with three regularly spaced direct repeats of the CCCTC-motif in the 5'-flanking sequence of the chicken c-myc gene. Oncogene 1990;5:1743–53.

Lopes I, Altab G, Raina P, de Magalhães JP. Gene Size Matters: An Analysis of Gene Length in the Human Genome. Front Genet 2021;12:559998. https://doi.org/10.3389/fgene.2021.559998.

Loppin B, Dubruille R, Horard B. The intimate genetics of *Drosophila* fertilization. Open Biol 2015;5:150076. https://doi.org/10.1098/rsob.150076.

Loubiere V, Delest A, Thomas A, Bonev B, Schuettengruber B, Sati S, et al. Coordinate redeployment of PRC1 proteins suppresses tumor formation during Drosophila development. Nat Genet 2016;48:1436–42. https://doi.org/10.1038/ng.3671.

Louhichi A, Fourati A, Rebaï A. IGD: A resource for intronless genes in the human genome. Gene 2011;488:35–40. https://doi.org/10.1016/j.gene.2011.08.013.

Lu BY, Emtage PC, Duyf BJ, Hilliker AJ, Eissenberg JC. Heterochromatin protein 1 is required for the normal expression of two heterochromatin genes in Drosophila. Genetics 2000;155:699–708.

Lucas T, Ferraro T, Roelens B, De Las Heras Chanes J, Walczak AM, Coppey M, et al. Live Imaging of Bicoid-Dependent Transcription in Drosophila Embryos. Current Biology 2013;23:2135–9. https://doi.org/10.1016/j.cub.2013.08.053.

Luger K, Mäder AW, Richmond RK, Sargent DF, Richmond TJ. Crystal structure of the nucleosome core particle at 2.8 Å resolution. Nature 1997;389:251–60. https://doi.org/10.1038/38444.

Lupiáñez DG, Kraft K, Heinrich V, Krawitz P, Brancati F, Klopocki E, et al. Disruptions of Topological Chromatin Domains Cause Pathogenic Rewiring of Gene-Enhancer Interactions. Cell 2015;161:1012–25. https://doi.org/10.1016/j.cell.2015.04.004.

Luzhin AV, Flyamer IM, Khrameeva EE, Ulianov SV, Razin SV, Gavrilov AA. Quantitative differences in TAD border strength underly the TAD hierarchy in *Drosophila* chromosomes. J Cell Biochem 2019;120:4494–503. https://doi.org/10.1002/jcb.27737.

Lynch MD, Smith AJH, De Gobbi M, Flenley M, Hughes JR, Vernimmen D, et al. An interspecies analysis reveals a key role for unmethylated CpG dinucleotides in vertebrate Polycomb complex recruitment: An interspecies analysis of chromatin bivalency. The EMBO Journal 2012;31:317–29. https://doi.org/10.1038/emboj.2011.399.

Mahowald AP, Tiefert M. Fine structural changes in theDrosophila oocyte nucleus during a short period of RNA synthesis: An autoradiographic and ultrastructural study of RNA synthesis in the oocyte nucleus ofDrosophila. W Roux' Archiv f Entwicklungsmechanik 1970;165:8–25. https://doi.org/10.1007/BF00576994.

Malone CD, Brennecke J, Dus M, Stark A, McCombie WR, Sachidanandam R, et al. Specialized piRNA Pathways Act in Germline and Somatic Tissues of the Drosophila Ovary. Cell 2009;137:522–35. https://doi.org/10.1016/j.cell.2009.03.040.

Mangus DA, Evans MC, Jacobson A. Poly(A)-binding proteins: multifunctional scaffolds for the post-transcriptional control of gene expression. Genome Biol 2003;4:223. https://doi.org/10.1186/gb-2003-4-7-223.

Margaritis T, Oreal V, Brabers N, Maestroni L, Vitaliano-Prunier A, Benschop JJ, et al. Two Distinct Repressive Mechanisms for Histone 3 Lysine 4 Methylation through Promoting 3′-End Antisense Transcription. PLoS Genet 2012;8:e1002952. https://doi.org/10.1371/journal.pgen.1002952.

Martire S, Banaszynski LA. The roles of histone variants in fine-tuning chromatin organization and function. Nat Rev Mol Cell Biol 2020;21:522–41. https://doi.org/10.1038/s41580-020-0262-8.

Marullo F, Cesarini E, Antonelli L, Gregoretti F, Oliva G, Lanzuolo C. Nucleoplasmic Lamin A/C and Polycomb group of proteins: An evolutionarily conserved interplay. Nucleus 2016;7:103–11. https://doi.org/10.1080/19491034.2016.1157675.

Matharu N, Ahituv N. Minor Loops in Major Folds: Enhancer–Promoter Looping, Chromatin Restructuring, and Their Association with Transcriptional Regulation and Disease. PLoS Genet 2015;11:e1005640. https://doi.org/10.1371/journal.pgen.1005640.

Matsui T, Leung D, Miyashita H, Maksakova IA, Miyachi H, Kimura H, et al. Proviral silencing in embryonic stem cells requires the histone methyltransferase ESET. Nature 2010;464:927–31. https://doi.org/10.1038/nature08858.

Matsui T, Segall J, Weil PA, Roeder RG. Multiple factors required for accurate initiation of transcription by purified RNA polymerase II. J Biol Chem 1980;255:11992–6.

Mavrich TN, Jiang C, Ioshikhes IP, Li X, Venters BJ, Zanton SJ, et al. Nucleosome organization in the Drosophila genome. Nature 2008;453:358–62. https://doi.org/10.1038/nature06929.

Mayer A, Heidemann M, Lidschreiber M, Schreieck A, Sun M, Hintermair C, et al. CTD Tyrosine Phosphorylation Impairs Termination Factor Recruitment to RNA Polymerase II. Science 2012;336:1723–5. https://doi.org/10.1126/science.1219651.

Mayer A, Lidschreiber M, Siebert M, Leike K, Söding J, Cramer P. Uniform transitions of the general RNA polymerase II transcription complex. Nat Struct Mol Biol 2010;17:1272–8. https://doi.org/10.1038/nsmb.1903.

McClelland S, Shrivastava R, Medh JD. Regulation of Translational Efficiency by Disparate 5 ′ -UTRs of PPAR γ Splice Variants. PPAR Research 2009;2009:1–8. https://doi.org/10.1155/2009/193413.

McCracken S., Fong N, Rosonina E, Yankulov K, Brothers G, Siderovski D, et al. 5'-Capping enzymes are targeted to pre-mRNA by binding to the phosphorylated carboxy-terminal domain of RNA polymerase II. Genes & Development 1997;11:3306–18. https://doi.org/10.1101/gad.11.24.3306.

McCracken Susan, Fong N, Yankulov K, Ballantyne S, Pan G, Greenblatt J, et al. The C-terminal domain of RNA polymerase II couples mRNA processing to transcription. Nature 1997;385:357–61. https://doi.org/10.1038/385357a0.

McDonel P, Costello I, Hendrich B. Keeping things quiet: Roles of NuRD and Sin3 co-repressor complexes during mammalian development. The International Journal of Biochemistry & Cell Biology 2009;41:108–16. https://doi.org/10.1016/j.biocel.2008.07.022.

McLaughlin JM, Bratu DP. Drosophila melanogaster Oogenesis: An Overview. In: Bratu DP, McNeil GP, editors. Drosophila Oogenesis, vol. 1328, New York, NY: Springer New York; 2015, p. 1–20. https://doi.org/10.1007/978-1-4939-2851-4_1.

Melnikova L, Elizar'ev P, Erokhin M, Molodina V, Chetverina D, Kostyuchenko M, et al. The same domain of Su(Hw) is required for enhancer blocking and direct promoter repression. Sci Rep 2019;9:5314. https://doi.org/10.1038/s41598-019-41761-6.

Melnikova L, Juge F, Gruzdeva N, Mazur A, Cavalli G, Georgiev P. Interaction between the GAGA factor and Mod(mdg4) proteins promotes insulator bypass in Drosophila. Proceedings of the National Academy of Sciences 2004;101:14806–11. https://doi.org/10.1073/pnas.0403959101.

Melnikova L, Kostyuchenko M, Molodina V, Parshikov A, Georgiev P, Golovnin A. Multiple interactions are involved in a highly specific association of the Mod(mdg4)-67.2

isoform with the Su(Hw) sites in *Drosophila*. Open Biol 2017;7:170150. https://doi.org/10.1098/rsob.170150.

Melnikova LS, Georgiev PG, Golovnin AK. The Functions and Mechanisms of Action of Insulators in the Genomes of Higher Eukaryotes. Acta Naturae 2020;12:15–33. https://doi.org/10.32607/actanaturae.11144.

Mendenhall EM, Koche RP, Truong T, Zhou VW, Issac B, Chi AS, et al. GC-Rich Sequence Elements Recruit PRC2 in Mammalian ES Cells. PLoS Genet 2010;6:e1001244. https://doi.org/10.1371/journal.pgen.1001244.

Messmer S, Franke A, Paro R. Analysis of the functional role of the Polycomb chromo domain in Drosophila melanogaster. Genes & Development 1992;6:1241–54. https://doi.org/10.1101/gad.6.7.1241.

Mikkelsen TS, Ku M, Jaffe DB, Issac B, Lieberman E, Giannoukos G, et al. Genome-wide maps of chromatin state in pluripotent and lineage-committed cells. Nature 2007;448:553–60. https://doi.org/10.1038/nature06008.

Miller D, Brinkworth M, Iles D. Paternal DNA packaging in spermatozoa: more than the sum of its parts? DNA, histones, protamines and epigenetics. REPRODUCTION 2010;139:287–301. https://doi.org/10.1530/REP-09-0281.

Minsky N, Shema E, Field Y, Schuster M, Segal E, Oren M. Monoubiquitinated H2B is associated with the transcribed region of highly expressed genes in human cells. Nat Cell Biol 2008;10:483–8. https://doi.org/10.1038/ncb1712.

Mito Y, Henikoff JG, Henikoff S. Histone Replacement Marks the Boundaries of cis-Regulatory Domains. Science 2007;315:1408–11. https://doi.org/10.1126/science.1134004.
Mohan M, Herz H-M, Smith ER, Zhang Y, Jackson J, Washburn MP, et al. The COMPASS Family of H3K4 Methylases in Drosophila. Mol Cell Biol 2011;31:4310–8. https://doi.org/10.1128/MCB.06092-11.

Mohrmann L, Langenberg K, Krijgsveld J, Kal AJ, Heck AJR, Verrijzer CP. Differential Targeting of Two Distinct SWI/SNF-Related Drosophila Chromatin-Remodeling Complexes. MCB 2004;24:3077–88. https://doi.org/10.1128/MCB.24.8.3077-3088.2004.

Moshkin YM, Kan TW, Goodfellow H, Bezstarosti K, Maeda RK, Pilyugin M, et al. Histone Chaperones ASF1 and NAP1 Differentially Modulate Removal of Active Histone Marks by LID-RPD3 Complexes during NOTCH Silencing. Molecular Cell 2009;35:782–93. https://doi.org/10.1016/j.molcel.2009.07.020.

Müller J, Hart CM, Francis NJ, Vargas ML, Sengupta A, Wild B, et al. Histone Methyltransferase Activity of a Drosophila Polycomb Group Repressor Complex. Cell 2002;111:197–208. https://doi.org/10.1016/S0092-8674(02)00976-5.

Nagano T, Lubling Y, Stevens TJ, Schoenfelder S, Yaffe E, Dean W, et al. Single-cell Hi-C reveals cell-to-cell variability in chromosome structure. Nature 2013;502:59–64. https://doi.org/10.1038/nature12593.

Navarro-Costa P, McCarthy A, Prudêncio P, Greer C, Guilgur LG, Becker JD, et al. Early programming of the oocyte epigenome temporally controls late prophase I transcription and chromatin remodelling. Nat Commun 2016;7:12331. https://doi.org/10.1038/ncomms12331.

Nègre N, Brown CD, Shah PK, Kheradpour P, Morrison CA, Henikoff JG, et al. A Comprehensive Map of Insulator Elements for the Drosophila Genome. PLoS Genet 2010;6:e1000814. https://doi.org/10.1371/journal.pgen.1000814.

Neri F, Rapelli S, Krepelova A, Incarnato D, Parlato C, Basile G, et al. Intragenic DNA methylation prevents spurious transcription initiation. Nature 2017;543:72–7. https://doi.org/10.1038/nature21373.

Nilsen TW, Graveley BR. Expansion of the eukaryotic proteome by alternative splicing. Nature 2010;463:457–63. https://doi.org/10.1038/nature08909.

Nojima T, Gomes T, Grosso ARF, Kimura H, Dye MJ, Dhir S, et al. Mammalian NET-Seq Reveals Genome-wide Nascent Transcription Coupled to RNA Processing. Cell 2015;161:526–40. https://doi.org/10.1016/j.cell.2015.03.027.

Nora EP, Goloborodko A, Valton A-L, Gibcus JH, Uebersohn A, Abdennur N, et al. Targeted Degradation of CTCF Decouples Local Insulation of Chromosome Domains from Genomic Compartmentalization. Cell 2017;169:930-944.e22. https://doi.org/10.1016/j.cell.2017.05.004.

Nordman J, Orr-Weaver TL. Regulation of DNA replication during development. Development 2012;139:455–64. https://doi.org/10.1242/dev.061838.
Nott A. A quantitative analysis of intron effects on mammalian gene expression. RNA 2003;9:607–17. https://doi.org/10.1261/rna.5250403.

van Oevelen C, Wang J, Asp P, Yan Q, Kaelin WG, Kluger Y, et al. A Role for Mammalian Sin3 in Permanent Gene Silencing. Molecular Cell 2008;32:359–70. https://doi.org/10.1016/j.molcel.2008.10.015.

Ogienko AA, Fedorova SA, Baricheva EM. Basic aspects of ovarian development in Drosophila melanogaster. Russ J Genet 2007;43:1120–34. https://doi.org/10.1134/S1022795407100055.

Ohler U, Liao G, Niemann H, Rubin GM. Computational analysis of core promoters in the Drosophila genome 2002:12.

Orphanides G, Lagrange T, Reinberg D. The general transcription factors of RNA polymerase II. Genes & Development 1996;10:2657–83. https://doi.org/10.1101/gad.10.21.2657.

Orsi GA, Kasinathan S, Hughes KT, Saminadin-Peter S, Henikoff S, Ahmad K. High-resolution mapping defines the cooperative architecture of Polycomb response elements. Genome Research 2014;24:809–20. https://doi.org/10.1101/gr.163642.113.

Ozata DM, Gainetdinov I, Zoch A, O'Carroll D, Zamore PD. PIWI-interacting RNAs: small RNAs with big functions. Nat Rev Genet 2019;20:89–108. https://doi.org/10.1038/s41576-018-0073-3.

Özdemir, Gambetta. The Role of Insulation in Patterning Gene Expression. Genes 2019;10:767. https://doi.org/10.3390/genes10100767.

Pai C-Y, Lei EP, Ghosh D, Corces VG. The Centrosomal Protein CP190 Is a Component of the gypsy Chromatin Insulator. Molecular Cell 2004;16:737–48. https://doi.org/10.1016/j.molcel.2004.11.004.

Pan G, Tian S, Nie J, Yang C, Ruotti V, Wei H, et al. Whole-Genome Analysis of Histone H3 Lysine 4 and Lysine 27 Methylation in Human Embryonic Stem Cells. Cell Stem Cell 2007;1:299–312. https://doi.org/10.1016/j.stem.2007.08.003.

Parisi M, Nuttall R, Edwards P, Minor J, Naiman D, Lü J, et al. A survey of ovary-, testis-, and soma-biased gene expression in Drosophila melanogaster adults. Genome Biology 2004:18.

Pascucci T, Perrino J, Mahowald AP, Waring GL. Eggshell Assembly in Drosophila: Processing and Localization of Vitelline Membrane and Chorion Proteins. Developmental Biology 1996;177:590–8. https://doi.org/10.1006/dbio.1996.0188.

Pavri R, Zhu B, Li G, Trojer P, Mandal S, Shilatifard A, et al. Histone H2B Monoubiquitination Functions Cooperatively with FACT to Regulate Elongation by RNA Polymerase II. Cell 2006;125:703–17. https://doi.org/10.1016/j.cell.2006.04.029.

Pengelly AR, Copur O, Jackle H, Herzig A, Muller J. A Histone Mutant Reproduces the Phenotype Caused by Loss of Histone-Modifying Factor Polycomb. Science 2013;339:698–9. https://doi.org/10.1126/science.1231382.

Pengelly AR, Kalb R, Finkl K, Müller J. Transcriptional repression by PRC1 in the absence of H2A monoubiquitylation. Genes Dev 2015;29:1487–92. https://doi.org/10.1101/gad.265439.115.

Perino M, van Mierlo G, Karemaker ID, van Genesen S, Vermeulen M, Marks H, et al. MTF2 recruits Polycomb Repressive Complex 2 by helical-shape-selective DNA binding. Nat Genet 2018;50:1002–10. https://doi.org/10.1038/s41588-018-0134-8.

Petrova B, Liu K, Tian C, Kitaoka M, Freinkman E, Yang J, et al. Dynamic redox balance directs the oocyte-to-embryo transition via developmentally controlled reactive cysteine changes. Proc Natl Acad Sci USA 2018;115:E7978–86. https://doi.org/10.1073/pnas.1807918115.

Pherson M, Misulovin Z, Gause M, Mihindukulasuriya K, Swain A, Dorsett D. Polycomb repressive complex 1 modifies transcription of active genes. Sci Adv 2017;3:e1700944. https://doi.org/10.1126/sciadv.1700944.

Phillips-Cremins JE, Sauria MEG, Sanyal A, Gerasimova TI, Lajoie BR, Bell JSK, et al. Architectural Protein Subclasses Shape 3D Organization of Genomes during Lineage Commitment. Cell 2013;153:1281–95. https://doi.org/10.1016/j.cell.2013.04.053.

Plath K. Role of Histone H3 Lysine 27 Methylation in X Inactivation. Science 2003;300:131–5. https://doi.org/10.1126/science.1084274.

Prudêncio P, Guilgur LG, Sobral J, Becker JD, Martinho RG, Navarro-Costa P. The Trithorax group protein dMLL3/4 instructs the assembly of the zygotic genome at fertilization. EMBO Rep 2018;19. https://doi.org/10.15252/embr.201845728.

Raab JR, Chiu J, Zhu J, Katzman S, Kurukuti S, Wade PA, et al. Human tRNA genes function as chromatin insulators: Human tRNA genes function as chromatin insulators. The EMBO Journal 2012;31:330–50. https://doi.org/10.1038/emboj.2011.406.

Rach EA, Winter DR, Benjamin AM, Corcoran DL, Ni T, Zhu J, et al. Transcription Initiation Patterns Indicate Divergent Strategies for Gene Regulation at the Chromatin Level. PLoS Genet 2011;7:e1001274. https://doi.org/10.1371/journal.pgen.1001274.

Racko D, Benedetti F, Goundaroulis D, Stasiak A. Chromatin Loop Extrusion and Chromatin Unknotting. Polymers 2018;10:1126. https://doi.org/10.3390/polym10101126.

Raj A, Peskin CS, Tranchina D, Vargas DY, Tyagi S. Stochastic mRNA Synthesis in Mammalian Cells. PLoS Biol 2006;4:e309. https://doi.org/10.1371/journal.pbio.0040309.

Ramakrishnan S, Pokhrel S, Palani S, Pflueger C, Parnell TJ, Cairns BR, et al. Counteracting H3K4 methylation modulators Set1 and Jhd2 co-regulate chromatin dynamics and gene transcription. Nat Commun 2016;7:11949. https://doi.org/10.1038/ncomms11949.

Ramírez F, Bhardwaj V, Arrigoni L, Lam KC, Grüning BA, Villaveces J, et al. High-resolution TADs reveal DNA sequences underlying genome organization in flies. Nat Commun 2018;9:189. https://doi.org/10.1038/s41467-017-02525-w.

Rangan P, Malone CD, Navarro C, Newbold SP, Hayes PS, Sachidanandam R, et al. piRNA Production Requires Heterochromatin Formation in Drosophila. Current Biology 2011;21:1373–9. https://doi.org/10.1016/j.cub.2011.06.057.

Rao SSP, Huang S-C, Glenn St Hilaire B, Engreitz JM, Perez EM, Kieffer-Kwon K-R, et al. Cohesin Loss Eliminates All Loop Domains. Cell 2017;171:305-320.e24. https://doi.org/10.1016/j.cell.2017.09.026.

Rao SSP, Huntley MH, Durand NC, Stamenova EK, Bochkov ID, Robinson JT, et al. A 3D Map of the Human Genome at Kilobase Resolution Reveals Principles of Chromatin Looping. Cell 2014;159:1665–80. https://doi.org/10.1016/j.cell.2014.11.021.

Ray P, De S, Mitra A, Bezstarosti K, Demmers JAA, Pfeifer K, et al. Combgap contributes to recruitment of Polycomb group proteins in *Drosophila*. Proc Natl Acad Sci USA 2016;113:3826–31. https://doi.org/10.1073/pnas.1520926113.

Reddington JP, Perricone SM, Nestor CE, Reichmann J, Youngson NA, Suzuki M, et al. Redistribution of H3K27me3 upon DNA hypomethylation results in de-repression of Polycomb target genes. Genome Biol 2013;14:R25. https://doi.org/10.1186/gb-2013-14-3-r25.

Rennie S, Dalby M, van Duin L, Andersson R. Transcriptional decomposition reveals active chromatin architectures and cell specific regulatory interactions. Nat Commun 2018;9:487. https://doi.org/10.1038/s41467-017-02798-1.

Ringrose L, Paro R. Epigenetic Regulation of Cellular Memory by the Polycomb and Trithorax Group Proteins. Annu Rev Genet 2004;38:413–43. https://doi.org/10.1146/annurev.genet.38.072902.091907.

Rodriguez J, Munoz M, Vives L, Frangou CG, Groudine M, Peinado MA. Bivalent domains enforce transcriptional memory of DNA methylated genes in cancer cells. Proceedings of the National Academy of Sciences 2008;105:19809–14. https://doi.org/10.1073/pnas.0810133105.

Roelens B, Clémot M, Leroux-Coyau M, Klapholz B, Dostatni N. Maintenance of Heterochromatin by the Large Subunit of the CAF-1 Replication-Coupled Histone Chaperone

Requires Its Interaction with HP1a Through a Conserved Motif. Genetics 2017;205:125–37. https://doi.org/10.1534/genetics.116.190785.

Royzman I, Orr-Weaver TL. S phase and differential DNA replication during *Drosophila* oogenesis: Endo cell cycle in Drosophila oogenesis. Genes to Cells 1998;3:767–76. https://doi.org/10.1046/j.1365-2443.1998.00232.x.

Sabari BR, Dall'Agnese A, Boija A, Klein IA, Coffey EL, Shrinivas K, et al. Coactivator condensation at super-enhancers links phase separation and gene control. Science 2018;361:eaar3958. https://doi.org/10.1126/science.aar3958.

Saha N, Liu M, Gajan A, Pile LA. Genome-wide studies reveal novel and distinct biological pathways regulated by SIN3 isoforms. BMC Genomics 2016;17:111. https://doi.org/10.1186/s12864-016-2428-5.

Sahu SC, Swanson KA, Kang RS, Huang K, Brubaker K, Ratcliff K, et al. Conserved Themes in Target Recognition by the PAH1 and PAH2 Domains of the Sin3 Transcriptional Corepressor. Journal of Molecular Biology 2008;375:1444–56. https://doi.org/10.1016/j.jmb.2007.11.079.

Sakai A, Schwartz BE, Goldstein S, Ahmad K. Transcriptional and Developmental Functions of the H3.3 Histone Variant in Drosophila. Current Biology 2009;19:1816–20. https://doi.org/10.1016/j.cub.2009.09.021.

Salz HK, Flickinger TW, Mittendorf E, Pellicena-Palle A, Petschek JP, Albrecht EB. The Drosophila maternal effect locus deadhead encodes a thioredoxin homolog required for female meiosis and early embryonic development. Genetics 1994;136:1075–86. https://doi.org/10.1093/genetics/136.3.1075.

Santaguida S, Musacchio A. The life and miracles of kinetochores. EMBO J 2009;28:2511–31. https://doi.org/10.1038/emboj.2009.173.

Sanz AB, García R, Rodríguez-Peña JM, Nombela C, Arroyo J. Cooperation between SAGA and SWI/SNF complexes is required for efficient transcriptional responses regulated by the yeast MAPK Slt2. Nucleic Acids Res 2016:gkw324. https://doi.org/10.1093/nar/gkw324.

Savitsky M, Kim M, Kravchuk O, Schwartz YB. Distinct Roles of Chromatin Insulator Proteins in Control of the *Drosophila* Bithorax Complex. Genetics 2016;202:601–17. https://doi.org/10.1534/genetics.115.179309.

Schmitges FW, Prusty AB, Faty M, Stützer A, Lingaraju GM, Aiwazian J, et al. Histone Methylation by PRC2 Is Inhibited by Active Chromatin Marks. Molecular Cell 2011;42:330–41. https://doi.org/10.1016/j.molcel.2011.03.025.

Schuettengruber B, Bourbon H-M, Di Croce L, Cavalli G. Genome Regulation by Polycomb and Trithorax: 70 Years and Counting. Cell 2017;171:34–57. https://doi.org/10.1016/j.cell.2017.08.002.

Schuettengruber B, Ganapathi M, Leblanc B, Portoso M, Jaschek R, Tolhuis B, et al. Functional Anatomy of Polycomb and Trithorax Chromatin Landscapes in Drosophila Embryos. PLoS Biol 2009;7:e1000013. https://doi.org/10.1371/journal.pbio.1000013.

Schultz DC. SETDB1: a novel KAP-1-associated histone H3, lysine 9-specific methyltransferase that contributes to HP1-mediated silencing of euchromatic genes by KRAB zinc-finger proteins. Genes & Development 2002;16:919–32. https://doi.org/10.1101/gad.973302.

Schwabish MA, Struhl K. The Swi/Snf Complex Is Important for Histone Eviction during Transcriptional Activation and RNA Polymerase II Elongation In Vivo. Mol Cell Biol 2007;27:6987–95. https://doi.org/10.1128/MCB.00717-07.

Schwabish MA, Struhl K. Evidence for Eviction and Rapid Deposition of Histones upon Transcriptional Elongation by RNA Polymerase II. Mol Cell Biol 2004;24:10111–7. https://doi.org/10.1128/MCB.24.23.10111-10117.2004.

Schwartz YB, Cavalli G. Three-Dimensional Genome Organization and Function in *Drosophila*. Genetics 2017;205:5–24. https://doi.org/10.1534/genetics.115.185132.

Schwartz YB, Kahn TG, Nix DA, Li X-Y, Bourgon R, Biggin M, et al. Genome-wide analysis of Polycomb targets in Drosophila melanogaster. Nat Genet 2006;38:700–5. https://doi.org/10.1038/ng1817.

Schwartz YB, Kahn TG, Stenberg P, Ohno K, Bourgon R, Pirrotta V. Alternative Epigenetic Chromatin States of Polycomb Target Genes. PLoS Genet 2010;6:e1000805. https://doi.org/10.1371/journal.pgen.1000805.

Schwartz YB, Linder-Basso D, Kharchenko PV, Tolstorukov MY, Kim M, Li H-B, et al. Nature and function of insulator protein binding sites in the Drosophila genome. Genome Res 2012;22:2188–98. https://doi.org/10.1101/gr.138156.112.

Scott KC, Merrett SL, Willard HF. A Heterochromatin Barrier Partitions the Fission Yeast Centromere into Discrete Chromatin Domains. Current Biology 2006;16:119–29. https://doi.org/10.1016/j.cub.2005.11.065.

Secombe J, Li L, Carlos L, Eisenman RN. The Trithorax group protein Lid is a trimethyl histone H3K4 demethylase required for dMyc-induced cell growth. Genes & Development 2007;21:537–51. https://doi.org/10.1101/gad.1523007.

Segal E, Widom J. What controls nucleosome positions? Trends in Genetics 2009;25:335–43. https://doi.org/10.1016/j.tig.2009.06.002.

Sentenac A. Eukaryotic RNA Polymerase. Critical Reviews in Biochemistry 1985;18:31–90. https://doi.org/10.3109/10409238509082539.

Sexton T, Yaffe E, Kenigsberg E, Bantignies F, Leblanc B, Hoichman M, et al. Three-Dimensional Folding and Functional Organization Principles of the Drosophila Genome. Cell 2012;148:458–72. https://doi.org/10.1016/j.cell.2012.01.010.

Shaul O. How introns enhance gene expression. The International Journal of Biochemistry & Cell Biology 2017;91:145–55. https://doi.org/10.1016/j.biocel.2017.06.016.

Shlyueva D, Stampfel G, Stark A. Transcriptional enhancers: from properties to genome-wide predictions. Nat Rev Genet 2014;15:272–86. https://doi.org/10.1038/nrg3682.

Silverstein RA, Ekwall K. Sin3: a flexible regulator of global gene expression and genome stability. Curr Genet 2005;47:1–17. https://doi.org/10.1007/s00294-004-0541-5.

Simon JA, Kingston RE. Occupying chromatin: Polycomb mechanisms for getting to genomic targets, stopping transcriptional traffic, and staying put. Mol Cell 2013;49:808–24. https://doi.org/10.1016/j.molcel.2013.02.013.

Smolko AE, Shapiro-Kulnane L, Salz HK. The H3K9 methyltransferase SETDB1 maintains female identity in Drosophila germ cells. Nat Commun 2018;9:4155. https://doi.org/10.1038/s41467-018-06697-x.

Spellman PT, Rubin GM. Evidence for large domains of similarly expressed genes in the Drosophila genome. J Biol 2002;1:5. https://doi.org/10.1186/1475-4924-1-5.

Spradling A. The development of Drosophila melanogaster. 1993.

Stevens TJ, Lando D, Basu S, Atkinson LP, Cao Y, Lee SF, et al. 3D structures of individual mammalian genomes studied by single-cell Hi-C. Nature 2017;544:59–64. https://doi.org/10.1038/nature21429.

Stitzel ML, Seydoux G. Regulation of the Oocyte-to-Zygote Transition. Science 2007;316:407–8. https://doi.org/10.1126/science.1138236.

Strahl BD, Ohba R, Cook RG, Allis CD. Methylation of histone H3 at lysine 4 is highly conserved and correlates with transcriptionally active nuclei in Tetrahymena. Proceedings of the National Academy of Sciences 1999;96:14967–72. https://doi.org/10.1073/pnas.96.26.14967.

Strom AR, Emelyanov AV, Mir M, Fyodorov DV, Darzacq X, Karpen GH. Phase separation drives heterochromatin domain formation. Nature 2017;547:241–5. https://doi.org/10.1038/nature22989.

Svensson MJ, Chen JD, Pirrotta V, Larsson J. The ThioredoxinT and deadhead gene pair encode testis- and ovary-specific thioredoxins in Drosophila melanogaster. Chromosoma 2003;112:133–43. https://doi.org/10.1007/s00412-003-0253-5.

Svensson MJ, Stenberg P, Larsson J. Organization and regulation of sex-specific thioredoxin encoding genes in the genus Drosophila. Dev Genes Evol 2007;217:639–50. https://doi.org/10.1007/s00427-007-0175-y.

Szabo Q, Bantignies F, Cavalli G. Principles of genome folding into topologically associating domains. Sci Adv 2019;5:eaaw1668. https://doi.org/10.1126/sciadv.aaw1668.

Szenker E, Lacoste N, Almouzni G. A Developmental Requirement for HIRA-Dependent H3.3 Deposition Revealed at Gastrulation in Xenopus. Cell Reports 2012;1:730–40. https://doi.org/10.1016/j.celrep.2012.05.006.

Tadros W, Goldman AL, Babak T, Menzies F, Vardy L, Orr-Weaver T, et al. SMAUG Is a Major Regulator of Maternal mRNA Destabilization in Drosophila and Its Translation Is Activated by the PAN GU Kinase. Developmental Cell 2007;12:143–55. https://doi.org/10.1016/j.devcel.2006.10.005.

Talbert PB, Henikoff S. Histone variants on the move: substrates for chromatin dynamics. Nat Rev Mol Cell Biol 2017;18:115–26. https://doi.org/10.1038/nrm.2016.148.

Tie F, Banerjee R, Fu C, Stratton CA, Fang M, Harte PJ. Polycomb inhibits histone acetylation by CBP by binding directly to its catalytic domain. Proc Natl Acad Sci USA 2016;113:E744–53. https://doi.org/10.1073/pnas.1515465113.

Tie F, Banerjee R, Stratton CA, Prasad-Sinha J, Stepanik V, Zlobin A, et al. CBP-mediated acetylation of histone H3 lysine 27 antagonizes *Drosophila* Polycomb silencing. Development 2009;136:3131–41. https://doi.org/10.1242/dev.037127.

Tirmarche S. Fonctions des thiorédoxines sexuelles et contrôle de l'état rédox des protamines chez la drosophile 2016:157.

Tirmarche S, Kimura S, Dubruille R, Horard B, Loppin B. Unlocking sperm chromatin at fertilization requires a dedicated egg thioredoxin in Drosophila. Nat Commun 2016;7:13539. https://doi.org/10.1038/ncomms13539.

Torné J, Ray-Gallet D, Boyarchuk E, Garnier M, Le Baccon P, Coulon A, et al. Two HIRA-dependent pathways mediate H3.3 de novo deposition and recycling during transcription. Nat Struct Mol Biol 2020;27:1057–68. https://doi.org/10.1038/s41594-020-0492-7.

Torres-Campana D, Kimura S, Orsi GA, Horard B, Benoit G, Loppin B. The Lid/KDM5 histone demethylase complex activates a critical effector of the oocyte-to-zygote transition. PLoS Genet 2020;16:e1008543. https://doi.org/10.1371/journal.pgen.1008543.

Ulianov SV, Khrameeva EE, Gavrilov AA, Flyamer IM, Kos P, Mikhaleva EA, et al. Active chromatin and transcription play a key role in chromosome partitioning into topologically associating domains. Genome Res 2016;26:70–84. https://doi.org/10.1101/gr.196006.115.

Urrutia AO. The Signature of Selection Mediated by Expression on Human Genes. Genome Research 2003;13:2260–4. https://doi.org/10.1101/gr.641103.

Van Bortle K, Nichols MH, Li L, Ong C-T, Takenaka N, Qin ZS, et al. Insulator function and topological domain border strength scale with architectural protein occupancy. Genome Biol 2014;15:R82. https://doi.org/10.1186/gb-2014-15-5-r82.

Van Bortle K, Ramos E, Takenaka N, Yang J, Wahi JE, Corces VG. Drosophila CTCF tandemly aligns with other insulator proteins at the borders of H3K27me3 domains. Genome Res 2012;22:2176–87. https://doi.org/10.1101/gr.136788.111.

Verdel A. RNAi-Mediated Targeting of Heterochromatin by the RITS Complex. Science 2004;303:672–6. https://doi.org/10.1126/science.1093686.

Vo ngoc L, Wang Y-L, Kassavetis GA, Kadonaga JT. The punctilious RNA polymerase II core promoter. Genes Dev 2017;31:1289–301. https://doi.org/10.1101/gad.303149.117.

Voigt P, LeRoy G, Drury WJ, Zee BM, Son J, Beck DB, et al. Asymmetrically Modified Nucleosomes. Cell 2012;151:181–93. https://doi.org/10.1016/j.cell.2012.09.002.

Voigt P, Tee W-W, Reinberg D. A double take on bivalent promoters. Genes & Development 2013;27:1318–38. https://doi.org/10.1101/gad.219626.113.

Volpe TA. Regulation of Heterochromatic Silencing and Histone H3 Lysine-9 Methylation by RNAi. Science 2002;297:1833–7. https://doi.org/10.1126/science.1074973.

Wakimoto BT, Hearn MG. The effects of chromosome rearrangements on the expression of heterochromatic genes in chromosome 2L of Drosophila melanogaster. Genetics 1990;125:141–54.

Wang C, Lin H. Roles of piRNAs in transposon and pseudogene regulation of germline mRNAs and lncRNAs. Genome Biol 2021;22:27. https://doi.org/10.1186/s13059-020-02221-x.

Wang H, Wang L, Erdjument-Bromage H, Vidal M, Tempst P, Jones RS, et al. Role of histone H2A ubiquitination in Polycomb silencing. Nature 2004;431:873–8. https://doi.org/10.1038/nature02985.

Wang Q, Sun Q, Czajkowsky DM, Shao Z. Sub-kb Hi-C in D. melanogaster reveals conserved characteristics of TADs between insect and mammalian cells. Nat Commun 2018;9:188. https://doi.org/10.1038/s41467-017-02526-9.

Weber CM, Hafner A, Kirkland JG, Braun SMG, Stanton BZ, Boettiger AN, et al. mSWI/SNF promotes Polycomb repression both directly and through genome-wide redistribution. Nat Struct Mol Biol 2021;28:501–11. https://doi.org/10.1038/s41594-021-00604-7.

Weinberg DE, Shah P, Eichhorn SW, Hussmann JA, Plotkin JB, Bartel DP. Improved Ribosome-Footprint and mRNA Measurements Provide Insights into Dynamics and Regulation of Yeast Translation. Cell Reports 2016;14:1787–99. https://doi.org/10.1016/j.celrep.2016.01.043.

Weiner A, Chen HV, Liu CL, Rahat A, Klien A, Soares L, et al. Systematic Dissection of Roles for Chromatin Regulators in a Yeast Stress Response. PLos Biol 2012;10:e1001369. https://doi.org/10.1371/journal.pbio.1001369.

Williams K, Christensen J, Pedersen MT, Johansen JV, Cloos PAC, Rappsilber J, et al. TET1 and hydroxymethylcytosine in transcription and DNA methylation fidelity. Nature 2011;473:343–8. https://doi.org/10.1038/nature10066.

Wolf G, Yang P, Füchtbauer AC, Füchtbauer E-M, Silva AM, Park C, et al. The KRAB zinc finger protein ZFP809 is required to initiate epigenetic silencing of endogenous retroviruses. Genes Dev 2015;29:538–54. https://doi.org/10.1101/gad.252767.114.

Wutz G, Várnai C, Nagasaka K, Cisneros DA, Stocsits RR, Tang W, et al. Topologically associating domains and chromatin loops depend on cohesin and are regulated by CTCF, WAPL, and PDS5 proteins. EMBO J 2017;36:3573–99. https://doi.org/10.15252/embj.201798004.

Xi Y, Yao J, Chen R, Li W, He X. Nucleosome fragility reveals novel functional states of chromatin and poises genes for activation. Genome Research 2011;21:718–24. https://doi.org/10.1101/gr.117101.110.

Xie G, Chen H, Jia D, Shu Z, Palmer WH, Huang Y-C, et al. The SWI/SNF Complex Protein Snr1 Is a Tumor Suppressor in *Drosophila* Imaginal Tissues. Cancer Res 2017;77:862–73. https://doi.org/10.1158/0008-5472.CAN-16-0963.

Yamada T, Fischle W, Sugiyama T, Allis CD, Grewal SIS. The Nucleation and Maintenance of Heterochromatin by a Histone Deacetylase in Fission Yeast. Molecular Cell 2005;20:173–85. https://doi.org/10.1016/j.molcel.2005.10.002.

Yu C-H, Dang Y, Zhou Z, Wu C, Zhao F, Sachs MS, et al. Codon Usage Influences the Local Rate of Translation Elongation to Regulate Co-translational Protein Folding. Molecular Cell 2015;59:744–54. https://doi.org/10.1016/j.molcel.2015.07.018.

Zabidi MA, Arnold CD, Schernhuber K, Pagani M, Rath M, Frank O, et al. Enhancer–core-promoter specificity separates developmental and housekeeping gene regulation. Nature 2015;518:556–9. https://doi.org/10.1038/nature13994.

Zamurrad S, Hatch HAM, Drelon C, Belalcazar HM, Secombe J. A Drosophila Model of Intellectual Disability Caused by Mutations in the Histone Demethylase KDM5. Cell Rep 2018;22:2359–69. https://doi.org/10.1016/j.celrep.2018.02.018.

Zhang H, Roberts DN, Cairns BR. Genome-Wide Dynamics of Htz1, a Histone H2A Variant that Poises Repressed/Basal Promoters for Activation through Histone Loss. Cell 2005;123:219–31. https://doi.org/10.1016/j.cell.2005.08.036.

Zhang K, Mosch K, Fischle W, Grewal SIS. Roles of the Clr4 methyltransferase complex in nucleation, spreading and maintenance of heterochromatin. Nat Struct Mol Biol 2008;15:381–8. https://doi.org/10.1038/nsmb.1406.

Zhao F, Yu C, Liu Y. Codon usage regulates protein structure and function by affecting translation elongation speed in Drosophila cells. Nucleic Acids Research 2017;45:8484–92. https://doi.org/10.1093/nar/gkx501.

Zhao XD, Han X, Chew JL, Liu J, Chiu KP, Choo A, et al. Whole-Genome Mapping of Histone H3 Lys4 and 27 Trimethylations Reveals Distinct Genomic Compartments in Human Embryonic Stem Cells. Cell Stem Cell 2007;1:286–98. https://doi.org/10.1016/j.stem.2007.08.004.

Zhaunova L, Ohkura H, Breuer M. Kdm5/Lid Regulates Chromosome Architecture in Meiotic Prophase I Independently of Its Histone Demethylase Activity. PLoS Genet 2016;12:e1006241. https://doi.org/10.1371/journal.pgen.1006241.

Zhou Z, Dang Y, Zhou M, Li L, Yu C, Fu J, et al. Codon usage is an important determinant of gene expression levels largely through its effects on transcription. Proc Natl Acad Sci USA 2016;113:E6117–25. https://doi.org/10.1073/pnas.1606724113.

Zraly CB, Dingwall AK. The chromatin remodeling and mRNA splicing functions of the Brahma (SWI/SNF) complex are mediated by the SNR1/SNF5 regulatory subunit. Nucleic Acids Research 2012;40:5975–87. https://doi.org/10.1093/nar/gks288.

Zraly CB, Marenda DR, Nanchal R, Cavalli G, Muchardt C, Dingwall AK. SNR1 is an essential subunit in a subset of Drosophila brm complexes, targeting specific functions during development. Dev Biol 2003;253:291–308. https://doi.org/10.1016/s0012-1606(02)00011-8.

Zraly CB, Middleton FA, Dingwall AK. Hormone-response genes are direct in vivo regulatory targets of Brahma (SWI/SNF) complex function. J Biol Chem 2006;281:35305–15. https://doi.org/10.1074/jbc.M607806200.